Anionic Ring-Opening Polymerization of Epoxides: Kinetics, Reactivity Ratios, and Renewable Monomer Strategies

Dissertation zur Erlangung des Grades

„Doktor der Naturwissenschaften“

im Promotionsfach Chemie

am Fachbereich Chemie, Pharmazie, Geographie und Geowissenschaften der Johannes Gutenberg-Universität Mainz

vorgelegt von

Gregor Michael Linden

geboren in Mainz

Mainz, Dezember 2024

JOHANNES GUTENBERG UNIVERSITÄT MAINZ

JG|U

Die als Dissertation vorgelegte Arbeit wurde in der Zeit vom Februar 2021 bis Dezember 2024 im Department Chemie der Johannes Gutenberg-Universität Mainz angefertigt.

Dekanin: [redacted]

1. Berichterstatter: [redacted]

2. Berichterstatter: [redacted]

Tag der mündlichen Prüfung: 30.01.2025

Eigenständigkeitserklärung

Hiermit erkläre ich, Gregor Michael Linden, dass ich die vorliegende Arbeit mit dem Titel:

„Anionic Ring-Opening Polymerization of Epoxides: Kinetics, Reactivity Ratios, and Renewable Monomer Strategies“

selbstständig verfasst und keine anderen als die angegebenen Quellen und Hilfsmittel benutzt habe. Sämtliche wörtlichen oder sinngemäßen Übernahmen und Zitate sind kenntlich gemacht und nachgewiesen. Ich versichere, dass ich keine Hilfsmittel verwendet habe, deren Nutzung die Prüferin oder der Prüfer explizit ausgeschlossen hat. Folgende KI-Tools habe ich wie entsprechend beschrieben verwendet:

KI-Tool	Genutzt für	Warum	Wann
Microsoft Word	Rechtschreibkorrektur, Grammatikprüfung, Formulierungsvorschläge	Sprachliche Korrektheit, Verständnis	Über die gesamte Arbeit hinweg
ChatGPT	Neuformulierung meiner Textentwürfe, Bereitstellung von Synonymen, Grammatikkorrektur, Übersetzungen von Englischen ins Deutsche	Sprachliche Korrektheit, Verständnis, bessere Lesbarkeit	Über die gesamte Arbeit hinweg
DeepL Translate	Übersetzung von Begriffen auf Englisch und auf Deutsch	Sprachliche Korrektheit, Verständnis, bessere Lesbarkeit	Über die gesamte Arbeit hinweg
DeepL Write	Neuformulierung meiner Textentwürfe	Sprachliche Korrektheit, Verständnis, bessere Lesbarkeit	Über die gesamte Arbeit hinweg
Grammarly	Rechtschreibkorrektur, Grammatikprüfung, Formulierungsvorschläge	Sprachliche Korrektheit, Verständnis, bessere Lesbarkeit	Über die gesamte Arbeit hinweg

Mit Abgabe der vorliegenden Leistung übernehme ich die Verantwortung für das eingereichte Gesamtprodukt. Ich verantworte damit auch jegliche KI-generierten Inhalte, die ich in meine Arbeit übernommen habe. Die Richtigkeit übernommener (KI-generierter) Aussagen und Inhalte habe ich nach bestem Wissen und Gewissen geprüft. Mir ist bekannt, dass ein Verstoß gegen die genannten Punkte prüfungsrechtliche Konsequenzen hat und insbesondere dazu führen kann, dass die

Promotionsleistung als mit „nicht bestanden“ bewertet wird. Die Einschreibung kann für bis zu zwei Jahre widerrufen werden, wenn Studierende zweimal oder häufiger bei Prüfungsleistungen täuschen (§ 69 Abs. 4 und 5 HochSchG).

Hiermit versichere ich gemäß § 10 Abs. 3d der Promotionsordnung vom 24. Juli 2007 in der Fassung vom 22. August 2012:

Ich habe die jetzt als Dissertation vorgelegte Arbeit selbst angefertigt und alle benutzten Hilfsmittel (Literatur, Apparaturen, Material, KI-Tools) in der Arbeit angegeben. Ich habe oder hatte die jetzt als Dissertation vorgelegte Arbeit nicht als Prüfungsarbeit für eine andere staatliche oder andere wissenschaftliche Prüfung eingereicht. Ich hatte weder die jetzt als Dissertation vorgelegte Arbeit noch Teile davon bei einer anderen Fakultät bzw. einem anderen Fachbereich als Dissertation eingereicht.

Mainz, 17.12.2024 _____

Gregor M. Linden

Für alle, die meinen Weg begleitet haben

[redacted]

- [redacted]

Danksagung

Author Contributions

Colleagues and collaborators provided essential scientific input that supported the content of the individual chapters.

Chapter 2 is an extension of the introduction regarding the topic of copolymerization. [redacted] and Gregor Linden equally contributed to this work; parts were used in [redacted] dissertation. Gregor Linden redrafted the original manuscript, changed the focus, and updated the content. Gregor Linden, [redacted], [redacted], and [redacted] contributed to the literature research. [redacted] discussed the role of the copolymerization model and [redacted] compared the structure relationships.

Chapter 3 was conceptualized, written, and conducted mainly by Gregor Linden. [redacted] supplied the monomer, [redacted] helped with the experimental part. [redacted] contributed to the evaluation. Parts of the results are included in a manuscript submitted to Science (**Chapter A1**).

Gregor Linden and [redacted] equally contributed to **Chapter 4**. Gregor Linden supervised the NMR kinetics studies and evaluation. [redacted] took on the experimental part, synthesizing the copolymers and investigating the properties. Both authors compiled the manuscript.

Chapter 5 is a result of the collaboration of Gregor Linden and [redacted]. Both authors contributed equally to the experimental part and writing process. A prequel version of the manuscript was issued in [redacted] dissertation. [redacted] designed the project, synthesized monomers, and polymers, and conducted and evaluated NMR kinetic studies. Gregor Linden conducted and evaluated NMR kinetic studies, addressed the side reaction in copolymerization, and performed and optimized the postpolymerization modifications. [redacted] helped with the experimental part by synthesizing monomers and performing postpolymerization reactions as a research module. [redacted] and [redacted] collaborated to synthesize terpenoid-derived monomers.

Chapter 6 was conceptualized by Gregor Linden, who conducted the experimental part and wrote the manuscript. [redacted] supervised the NMR kinetic study. In collaboration with the [redacted]group, [redacted] conducted and evaluated the DLS measurements.

Appendix chapters

Chapter A1 was equally conceptualized by [redacted] and [redacted]. Gregor Linden supplemented NMR kinetic studies, the detailed author contributions can be found in the chapter.

Chapter A2 was conceptualized by [redacted]. [redacted] conducted experiments and wrote the manuscript. Gregor Linden and [redacted] advised and performed parts of the analysis. [redacted] addressed mass spectronomy.

Chapter A3 is a result of the investigations by [redacted]. Gregor Linden supervised the NMR kinetic studies, [redacted] conducted fluorescence analysis, and [redacted] performed the DFT calculations.

Table of Contents

Motivation and Objectives

Poly(ethylene glycol) (PEG) is a well-known hydrophilic polyether, with its aqueous solubility being a rare feature among polyethers, which makes it indispensable for many everyday life and biomedical applications.[1] PEG is primarily synthesized via anionic ring-opening polymerization (AROP) of ethylene oxide (EO), yielding polymers with narrow molar mass distributions.[2] EO is often copolymerized with other epoxide comonomers, such as alkylene oxides and glycidyl ethers, to introduce functional groups into the polymer backbone. Since the copolymerization is a living process without transfer or termination reactions, the reactivity ratios of the monomers employed can be directly translated to monomer gradients in the polymer chains formed. The incorporation behavior depends on both comonomer structure and the particular copolymerization conditions.[3] The same comonomers can be incorporated randomly under conventional AROP or form gradient structures under monomer-activated anionic ring-opening polymerization (MAROP) conditions, resulting in markedly different polymer properties.[4] Understanding incorporation behavior is essential for controlling the microstructure of these copolymers. **Chapter 2** highlights the significance of distinguishing between random and gradient copolymers and addresses the following question:

"What are the incorporation preferences of literature-known epoxide comonomers in anionic ring-opening polymerization?"

The attachment of PEG to therapeutics or lipid nanoparticles (PEGylation) can significantly extend their blood circulation half-life to treat diseases in patients.[5] Conventional AROP gives narrowly distributed PEG suitable for pharmaceutical applications as side reactions seldom occur and no catalysts have to be removed.[1] Due to its use not only in biomedicine but also in many everyday applications in the last decades, most people in developed countries have developed anti-PEG antibodies (APAs) even if they were never treated with PEGylated drugs.[6,7] Random copolymers of EO with glycidyl methyl ether (GME) pose a promising alternative to PEG, while concurrently the oxygen-to-carbon ratio is unaltered, preserving hydrophilicity. Incorporating randomly distributed GME imperfections into the backbone can drastically diminish APA binding efficiency by preventing the specific binding motif for the APAs from occurring (**Chapter A1**). The incorporation preference has direct implications for the required comonomer composition. Copolymerization conditions regarding the used solvent and applied degree of deprotonation are usually disregarded, even though they are unexplored (Figure 1, top left). **Chapter 3** is subject to answering the following question:

"How do the solvent and degree of deprotonation influence the incorporation preferences of the comonomer pair ethylene oxide and glycidyl methyl ether?"

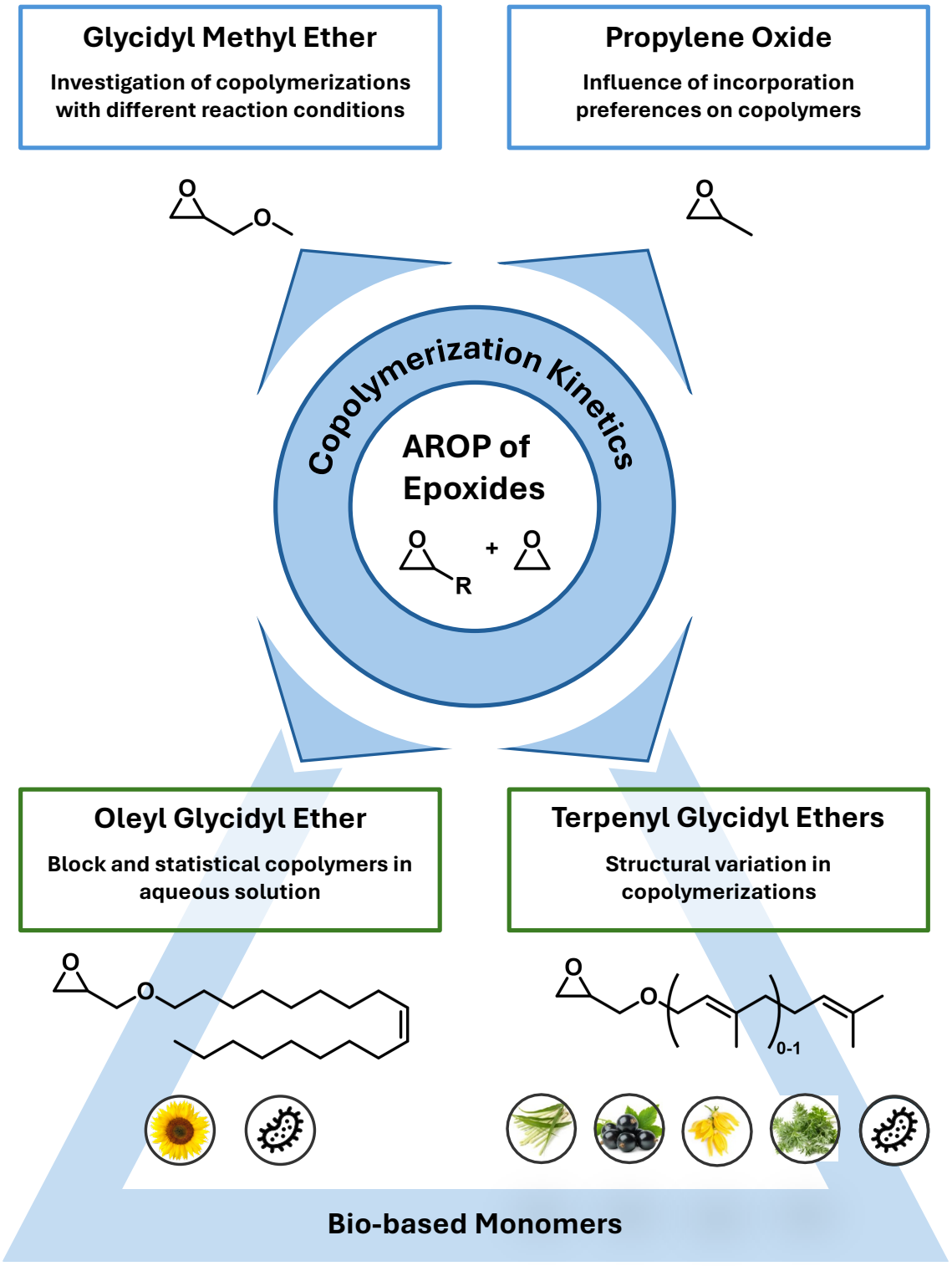

Figure 1: Objectives of this thesis by the anionic ring-opening polymerization of epoxides.

In contrast to GME, propylene oxide (PO) is commonly used to disable the crystallization of PEG. Block copolymers of EO and PO are widely used as nonionic surfactants. The copolymerization of PO reduces the aqueous solubility of PEG and lowers its cloud point temperature.[1] This property is utilized in drug delivery systems, in which polymer precipitation at body temperature releases hydrophobic drugs from lipid carriers, making them accessible to patients.[8] Copolymerizing EO with PO is a well-established method to reduce or disable PEG crystallization, making these copolymers attractive for use as solid polymer electrolytes. The copolymerization is unfortunately accompanied by a reduction in polarity, which is a key factor in enabling ion conductivity.[9–11] The incorporation preference of EO is significantly higher than PO, resulting in a monomer gradient along the polymer chains.[12] Consequently, larger amounts of PO are required to prevent long, crystalline PEG segments within the copolymer. Similar to the EO/GME comonomer pair, the impact of reaction conditions on this EO/PO system has often been overlooked, despite being known for decades (Figure 1, top right). **Chapter 4** will address the following question:

"How do the reaction conditions directly influence the incorporation preferences in the copolymerization of ethylene oxide and propylene oxide, and what are the resulting implications for material properties?"

Addressing global warming necessitates decarbonizing the chemical industry to reduce greenhouse gas emissions. In recent decades, extensive research has focused on renewable solvents and reagents.[13–15] A key requirement is that these renewable resources must not interfere with the food supply chain.[16,17] Terpenoids, which can be sourced either from industrial by-products or through genetically modified microbes with tailor-made synthesis profiles, offer a promising solution.[18–20] Terpenoid-derived glycidyl ether monomers have the potential to replace traditional petro-based hydrophobic monomers like PO, butylene oxide, or allyl glycidyl ether. Due to their structural diversity and modifiability, these monomers can be tailored for specialized applications. Statistical copolymers offer the advantage of tuning material properties by adjusting the comonomer ratio (Figure 1, bottom right). **Chapter 5** explores the following question:

"Do variations in the structure of linear terpenyl glycidyl ethers lead to different incorporation preferences in the copolymerization with EO?"

Bio-based triglycerides from fats and oils represent a valuable natural resource, much like terpenoids. These materials are already produced on a large scale from natural sources and waste streams[21–24] and can be used to synthesize linear hydrophobic glycidyl ethers from the corresponding fatty alcohols. Due to their highly hydrophobic nature and high molar mass, these

glycidyl ethers can introduce hydrophobicity into PEG even at low comonomer percentages.[25] Polymers made from long-chain saturated glycidyl ethers of fatty alcohols tend to crystallize at room temperature, while those made from medium-chain saturated glycidyl ethers remain liquid.[26] Block copolymers are of particular interest for surfactant applications, as small amounts can boost the efficiency of low molar mass surfactants.[27] Oleyl alcohol represents the unsaturated equivalent to the solid stearyl alcohol. After polymerization, the side chains could be partially hydrogenated to adjust the melting temperature into the physiological range, making these materials suitable for potential biomedical applications (Figure 1, bottom left). **Chapter 6** addresses the following question:

"How do block and statistical copolymers of ethylene oxide and oleyl glycidyl ether behave in both bulk and aqueous solutions?"

In summary, this thesis covers the copolymerization of epoxide comonomers mainly with EO for biomedical applications. Detailed knowledge regarding incorporation preference is crucial to predict the physical properties. Bio-based monomers will play an important role in the future for a broad variety of applications.

References

(1) Herzberger, J.; Niederer, K.; Pohlit, H.; Seiwert, J.; Worm, M.; Wurm, F. R.; Frey, H. Polymerization of Ethylene Oxide, Propylene Oxide, and Other Alkylene Oxides: Synthesis, Novel Polymer Architectures, and Bioconjugation. *Chem. Rev.* **2016**, *116* (4), 2170–2243. DOI: 10.1021/acs.chemrev.5b00441.

(2) Odian, G. *Principles of Polymerization*, 4th ed.; Wiley-Interscience, 2004. DOI: 10.1002/047147875X.

(3) Blankenburg, J.; Kersten, E.; Maciol, K.; Wagner, M.; Zarbakhsh, S.; Frey, H. The poly(propylene oxide-*co*-ethylene oxide) gradient is controlled by the polymerization method: determination of reactivity ratios by direct comparison of different copolymerization models. *Polym. Chem.* **2019**, *10* (22), 2863–2871. DOI: 10.1039/C9PY00500E.

(4) Herzberger, J.; Leibig, D.; Liermann, J. C.; Frey, H. Conventional Oxyanionic versus Monomer-Activated Anionic Copolymerization of Ethylene Oxide with Glycidyl Ethers: Striking Differences in Reactivity Ratios. *ACS Macro Lett.* **2016**, *5* (11), 1206–1211. DOI: 10.1021/acsmacrolett.6b00701.

(5) Milla, P.; Dosio, F.; Cattel, L. PEGylation of proteins and liposomes: a powerful and flexible strategy to improve the drug delivery. *Curr. Drug Metab.* **2012**, *13* (1), 105–119. DOI: 10.2174/138920012798356934.

(6) Yang, Q.; Jacobs, T. M.; McCallen, J. D.; Moore, D. T.; Huckaby, J. T.; Edelstein, J. N.; Lai, S. K. Analysis of Pre-existing IgG and IgM Antibodies against Polyethylene Glycol (PEG) in the General Population. *Anal. Chem.* **2016**, *88* (23), 11804–11812. DOI: 10.1021/acs.analchem.6b03437.

(7) Deuker, M. F. S.; Mailänder, V.; Morsbach, S.; Landfester, K. Anti-PEG antibodies enriched in the protein corona of PEGylated nanocarriers impact the cell uptake. *Nanoscale Horiz.* **2023**, *8* (10), 1377–1385. DOI: 10.1039/d3nh00198a.

(8) Mura, S.; Nicolas, J.; Couvreur, P. Stimuli-responsive nanocarriers for drug delivery. *Nat. Mater.* **2013**, *12* (11), 991–1003. DOI: 10.1038/nmat3776.

(9) Andrieu, X.; Fauvarque, J. F.; Goux, A.; Hamaide, T.; M'hamdi, R.; Vicedo, T. Solid polymer electrolytes based on statistical poly (ethylene oxide-propylene oxide) copolymers. *Electrochim. Acta* **1995**, *40* (13-14), 2295–2299. DOI: 10.1016/0013-4686(95)00181-D.

(10) Hamaide, T.; Goux, A.; Llauro, M.-F.; Spitz, R.; Guyot, A. Stat-poly(ethylene oxide-*co*-propylene oxide). Synthesis, NMR characterization and crystallinity studies. Correlation with monte carlo simulation. *Angew. Makromol. Chem.* **1996**, *237* (1), 55–77. DOI: 10.1002/apmc.1996.052370103.

(11) Louai, A.; Sarazin, D.; Pollet, G.; François, J.; Moreaux, F. Properties of ethylene oxide-propylene oxide statistical copolymers in aqueous solution. *Polymer* **1991**, *32* (4), 703–712. DOI: 10.1016/0032-3861(91)90484-Z.

(12) Heatley, F.; Yu, G.; Booth, C.; Blease, T. G. Determination of reactivity ratios for the anionic copolymerization of ethylene oxide and propylene oxide in bulk. *Eur. Polym. J.* **1991**, *27* (7), 573–579. DOI: 10.1016/0014-3057(91)90138-E.

(13) Allen, M. R.; Friedlingstein, P.; Girardin, C. A.; Jenkins, S.; Malhi, Y.; Mitchell-Larson, E.; Peters, G. P.; Rajamani, L. Net Zero: Science, Origins, and Implications. *Annu. Rev. Environ. Resour.* **2022**, *47* (1), 849–887. DOI: 10.1146/annurev-environ-112320-105050.

(14) Sustainable Development, Poverty Eradication and Reducing Inequalities. In *Global Warming of 1.5°C*; IPCC, Ed.; Cambridge University Press, 2022; pp 445–538. DOI: 10.1017/9781009157940.007.

(15) Jong, E. de; Higson, A.; Walsh, P.; Wellisch, M. *Bio-based Chemicals*:*Value Added Products from Biorefineries*. http://www.ieabioenergy.com/wp-content/uploads/2013/10/Task-42-Biobased-Chemicals-value-added-products-from-biorefineries.pdf.

(16) García-Franco, A.; Godoy, P.; La Torre, J. de; Duque, E.; Ramos, J. L. United Nations sustainability development goals approached from the side of the biological production of fuels. *Microb. Biotechnol.* **2021**, *14* (5), 1871–1877. DOI: 10.1111/1751-7915.13912.

(17) Hill, J.; Nelson, E.; Tilman, D.; Polasky, S.; Tiffany, D. Environmental, economic, and energetic costs and benefits of biodiesel and ethanol biofuels. *Proc. Natl. Acad. Sci. U.S.A* **2006**, *103* (30), 11206–11210. DOI: 10.1073/pnas.0604600103.

(18) Tetali, S. D. Terpenes and isoprenoids: a wealth of compounds for global use. *Planta* **2019**, *249* (1), 1–8. DOI: 10.1007/s00425-018-3056-x.

(19) Carsanba, E.; Pintado, M.; Oliveira, C. Fermentation Strategies for Production of Pharmaceutical Terpenoids in Engineered Yeast. *Pharmaceuticals (Basel, Switzerland)* **2021**, *14* (4). DOI: 10.3390/ph14040295.

(20) Ciriminna, R.; Lomeli-Rodriguez, M.; Demma Carà, P.; Lopez-Sanchez, J. A.; Pagliaro, M. Limonene: a versatile chemical of the bioeconomy. *Chem. Commun.* **2014**, *50* (97), 15288–15296. DOI: 10.1039/C4CC06147K.

(21) Biermann, U.; Bornscheuer, U.; Meier, M. A. R.; Metzger, J. O.; Schäfer, H. J. Oils and fats as renewable raw materials in chemistry. *Angew. Chem. Int. Ed.* **2011**, *50* (17), 3854–3871. DOI: 10.1002/anie.201002767.

(22) Biermann, U.; Bornscheuer, U. T.; Feussner, I.; Meier, M. A. R.; Metzger, J. O. Fatty Acids and their Derivatives as Renewable Platform Molecules for the Chemical Industry. *Angew. Chem. Int. Ed.* **2021**, *60*, 20144–20165. DOI: 10.1002/anie.202100778.

(23) Noweck, K.; Grafahrend, W. Fatty Alcohols. In *Ullmann's Encyclopedia of Industrial Chemistry*; Wiley-VCH Verlag GmbH & Co. KGaA, 2000. DOI: 10.1002/14356007.a10_277.pub2.

(24) Baumann, H.; Bühler, M.; Fochem, H.; Hirsinger, F.; Zoebelein, H.; Falbe, J. Natural Fats and Oils-Renewable Raw Materials for the Chemical Industry. *Angew. Chem. Int. Ed. Engl.* **1988**, *27* (1), 41–62. DOI: 10.1002/anie.198800411.

(25) Verkoyen, P.; Dreier, P.; Bros, M.; Hils, C.; Schmalz, H.; Seiffert, S.; Frey, H. "Dumb" pH-Independent and Biocompatible Hydrogels Formed by Copolymers of Long-Chain Alkyl Glycidyl Ethers and Ethylene Oxide. *Biomacromolecules* **2020**, *21* (8), 3152–3162. DOI: 10.1021/acs.biomac.0c00576.

(26) Verkoyen, P.; Johann, T.; Blankenburg, J.; Czysch, C.; Frey, H. Polymerization of long chain alkyl glycidyl ethers: a platform for micellar gels with tailor-made melting points. *Polym. Chem.* **2018**, *9* (44), 5327–5338. DOI: 10.1039/C8PY01312H.

(27) Schneider, K.; Verkoyen, P.; Krappel, M.; Gardiner, C.; Schweins, R.; Frey, H.; Sottmann, T. Efficiency Boosting of Surfactants with Poly(ethylene oxide)-Poly(alkyl glycidyl ether)s: A New Class of Amphiphilic Polymers. *Langmuir* **2020**, 9849–9866. DOI: 10.1021/acs.langmuir.0c01491.

Abstract

Anionic ring-opening polymerization (AROP) of epoxides is a fundamental method for developing innovative and customized materials. Established for more than a century, it is widely used in both industry and academia. Poly(ethylene oxide) (PEO) or poly(ethylene glycol) (PEG), with its exceptional aqueous solubility, enables the formation of amphiphilic block copolymers that compatibilize hydrophobic molecules with water. Hydrophobic and hydrophilic comonomers can be varied over a vast range towards the desired application. Statistical copolymerization of epoxides allows for combining the properties of different comonomers, with ethylene oxide commonly used due to its hydrophilic nature.

In recent years, the synthesis of bio-based compounds from renewable and abundant resources has gained significant attention. Terpenoids provide an accessible platform for synthesizing a variety of glycidyl ethers, offering structural diversity and modifiability for creating customized materials. Fatty alcohols complement this by providing linear hydrophobic monomers, which can be subsequently modified if a double bond is present. The copolymerization of epoxide monomers requires detailed investigations into incorporation preferences to understand the resulting structure-property relationships. This thesis presents a comprehensive review of the existing literature on epoxide copolymerization and explores the copolymerization of various monomers suited for developing innovative materials. Particular emphasis is placed on the synthesis and inquiry of bio-based monomers.

Chapter 2 provides a general introduction to copolymerization, focusing on the underlying kinetic aspects. It presents the official terminology for copolymers and reviews the commonly used but imprecise term "random copolymer", offering a more accurate definition. Distinct mathematical models applicable to describing copolymerization are discussed, along with recommendations for their use. Copolymers with a gradient distribution of comonomers are highlighted as a class at the boundary between random and block copolymers. Depending on the copolymerization method, conventional or monomer-activated anionic ring-opening polymerization, control over the incorporation preferences is allowed within certain limits. The centerpiece of this chapter represents the tables of copolymerization behavior of all available epoxide comonomer combinations gathered from the literature.

Chapter 3 investigates how polymerization conditions influence the incorporation preferences of ethylene oxide (EO) and glycidyl methyl ether (GME). Copolymers of EO and GME, a “dimeric isomer” of EO, are explored as a potential alternative to PEG for biomedical applications. Variables

such as solvent choice can shift the incorporation of preferences of EO and GME from a random copolymerization to one with a slight gradient. This shift is significant for synthesizing copolymers with specific monomer distributions, as anti-PEG antibodies bind to certain motifs of consecutive EO units. The crystallinity of the bulk material depends on the monomer distribution, which is crucial for applications requiring amorphous polymers, such as solid-state batteries.

Chapter 4 examines the influence of copolymerization conditions on the well-established EO and propylene oxide (PO) comonomer pair, which has been used industrially for decades. Despite its decades-long use, comprehensive data on melting points and aqueous solubility are unavailable. Even small variations in incorporation preferences impact aqueous properties. PO is incorporated slower than EO, leading to pronounced gradient formations. Copolymers with a steeper gradient were better soluble in water compared to those with a smoother gradient.

Chapter 5 explores bio-based terpenyl glycidyl ethers, which offer a renewable alternative to conventional petro-based monomers, contributing to the goal of decarbonizing the chemical industry. The copolymerization of short- to medium-chain acyclic terpenyl glycidyl ethers with EO was investigated. Despite the structural diversity of these monomers, similar incorporation preferences with EO were observed, although the more apolar compounds exhibited slower incorporation rates. The double bonds of the terpenyl glycidyl ethers were functionalized by thiol-ene click reaction using 2-mercaptoethanol as a model compound, making these materials suitable for introducing virtually any functional group for tailor-made applications. Reduction of the double bonds with diimide enabled subsequent saturation of the side chains, making these materials less prone to aging.

Chapter 6 focuses on synthesizing oleyl glycidyl ether (OlGE) from oleyl alcohol and epichlorohydrin. Similar to terpenyl glycidyl ethers, monomers derived from fatty alcohols serve as valuable resources for hydrophobic monomers. Their linear structure allows saturated long-chain variants to solidify at room temperature, while medium-chain or *cis*-unsaturated variants remain liquid. Despite its highly apolar and bulky side chain, OlGE exhibited only a slightly lower incorporation preference when copolymerized with EO. Block and statistical copolymers of OlGE and EO were investigated for their micellization behavior. By incorporating just a few mol% of this hydrophobic comonomer with a high molar mass, a wide range of hydrophilic-lipophilic balances could be achieved. Transmission electron microscopy (TEM) and dynamic light scattering (DLS) revealed the formation of micelles, which assembled into larger aggregates. The double bond in OlGE was accessible to thiol-ene click reactions and reduction via diimide, allowing partial or complete reduction of the side chains. This modification enabled the fine-tuning of melting points

to fall within the physiological range, offering customizable material properties for biomedical applications.

Appendix chapters

Chapter A1 is a collaboration with epoxide specialists from the [redacted] group and the University Medical Center of Mainz. It focuses on the synthesis of random copolymers composed of varying ratios of EO and GME as an alternative to PEG in biomedical applications. These copolymers were found to be biocompatible across a wide range of concentrations and were tested for their antigenicity against anti-PEG antibodies (APAs). When the GME content reached 50 mol%, the APAs were unable to bind to the polymer backbone. The equal incorporation preferences of the comonomers resulted in randomly distributed imperfections along the polyether chains. A simulation utilizing a kinetical Monte-Carlo approach visualized the negligible amount of copolymer chains carrying the binding motif of the APAs, explaining the low binding affinity of APAs to the copolymers.

Chapter A2 provides fundamental insights into “on water” catalysis of epoxide ROP at a static oil-alkaline water interface. Despite the usually water-sensitive reaction, styrene oxide, which exhibits a low reactivity under conventional AROP conditions, polymerized at the interface and yielded surprisingly high molar masses. Several reaction parameters, such as pH, solvent, initiator salt, etc. were investigated. The highest observable species in matrix-assisted laser desorption ionization by time-of-flight mass spectrometry (MALDI-ToF MS) had a molar mass of 8 000 g/mol.

Chapter A3 addresses the carbanionic polymerization of 1-phenyl isoprene and 4-phenyl isoprene. The disubstituted 1,3-dienes were synthesized using a Wittig reaction and polymerized in cyclohexane, and with different amounts of THF as a polar additive. The 1,4 incorporation of the phenyl isoprenes surprisingly decreased with small amounts of THF but increased again with larger amounts. Cationic cyclization in a postpolymerization modification, employing trifluoromethyl sulfonic acid, induced fluorescence properties and a pronounced increase in the glass transition temperature of 187 °C and 131 °C for P(1-phenyl isoprene) and P(4-phenyl isoprene), respectively. Copolymerizations of 1-phenyl isoprene with isoprene resulted in random copolymers but with styrene in gradient structures. The β-C shift in ^{13}C-NMR spectroscopy and density functional theory (DFT) calculations revealed a similar electronic structure to isoprene, which explains the comparable incorporation preference.

Zusammenfassung

Die anionische ringöffnende Polymerisation (AROP) von Epoxiden ist eine wichtige Methode zur Entwicklung innovativer und maßgeschneiderter Materialien. Seit mehr als einem Jahrhundert etabliert, findet sie sowohl in der Industrie als auch in der Wissenschaft breite Anwendung. Poly(ethylenglycol) (PEG) oder auch Poly(ethylenoxid) (PEO) zeichnet sich durch seine außergewöhnliche Wasserlöslichkeit aus und ermöglicht die Herstellung amphiphiler Blockcopolymere, die hydrophobe Moleküle mit Wasser kompatibilisieren. Hydrophobe und hydrophile Comonomere können in einem breiten Spektrum variiert werden, um den Anforderungen spezifischer Anwendungen gerecht zu werden. Die statistische Copolymerisation von Epoxiden erlaubt die Kombination der Eigenschaften verschiedener Comonomere, wobei Ethylenoxid aufgrund seiner hydrophilen Natur häufig eingesetzt wird.

In den letzten Jahren hat die Synthese biobasierter Verbindungen aus erneuerbaren und gut verfügbaren Ressourcen erheblich an Bedeutung gewonnen. Terpenoide bieten eine zugängliche Plattform zur Synthese einer Vielzahl von Glycidylethern, die durch ihre strukturelle Vielfalt und Modifizierbarkeit die Entwicklung maßgeschneiderter Polymere ermöglichen. Fettalkohole ergänzen dieses Spektrum durch lineare hydrophobe Monomere, die bei Vorhandensein einer Doppelbindung modifiziert werden können. Die Copolymerisation von Epoxid-Monomeren erfordert detaillierte Untersuchungen zu den Einbaupräferenzen, um die resultierenden Struktur-Eigenschafts-Beziehungen zu verstehen. Diese Dissertation bietet eine umfassende Übersicht über den aktuellen Stand der Literatur zur Epoxid-Copolymerisation und untersucht die Copolymerisation verschiedener Monomere, die sich für die Entwicklung innovativer Materialien eignen. Ein besonderer Schwerpunkt liegt auf der Synthese und Untersuchung biobasierter Monomere.

Kapitel 2 gibt eine allgemeine Einführung in die Copolymerisation mit Fokus auf die zugrunde liegenden kinetischen Aspekte. Es stellt die offizielle Terminologie für Copolymere vor und setzt sich kritisch mit dem häufig verwendeten, aber unpräzisen Begriff des „statistischen Copolymers“ auseinander, indem eine genauere Definition vorgeschlagen wird. Verschiedene mathematische Modelle, die zur Beschreibung der Copolymerisation anwendbar sind, werden diskutiert, ergänzt durch Empfehlungen für deren Einsatz. Copolymere mit einer Gradientenverteilung der Comonomere werden als Klasse hervorgehoben, die an der Grenze zwischen statistischen und Blockcopolymeren liegt. Je nach Copolymerisationsmethode, konventionelle oder monomeraktivierte anionische ringöffnende Polymerisation, ist eine Steuerung der

Einbaupräferenzen innerhalb bestimmter Grenzen möglich. Den Schwerpunkt dieses Kapitels bilden Tabellen mit dem Copolymerisationsverhalten aller verfügbaren Epoxid-Comonomer-Kombinationen, die aus der Literatur zusammengetragen wurden.

Kapitel 3 untersucht, wie Polymerisationsbedingungen die Einbaupräferenzen von Ethylenoxid (EO) und Glycidylmethylether (GME) beeinflussen. Copolymere aus EO und GME, ein „dimeres Isomer" von EO, werden als potenzielle Alternative zu PEG für biomedizinische Anwendungen erforscht. Variablen wie die Wahl des Lösungsmittels können die Einbaupräferenzen der Monomere EO und GME von einer statistischen Copolymerisation hin zu einer mit leichtem Gradienten verschieben. Diese Verschiebung ist besonders bedeutsam für die Synthese von Copolymeren mit spezifischen Monomerverteilungen, da Anti-PEG-Antikörper an bestimmte Motive aus aufeinanderfolgenden EO-Einheiten binden. Die Kristallinität des Polymers hängt von der Monomerverteilung ab, was entscheidend für Anwendungen ist, die amorphe Polymere erfordern, wie etwa Feststoffbatterien.

Kapitel 4 untersucht den Einfluss der Polymerisationsbedingungen auf das fest etablierte Comonomerpaar EO und Propylenoxid (PO), das seit Jahrzehnten industriell genutzt wird. Trotz seiner langjährigen Verwendung fehlen umfassende Daten zu Schmelzpunkten und Wasserlöslichkeit. Selbst geringe Variationen in den Einbaupräferenzen beeinflussen die wässrigen Eigenschaften. PO wird langsamer als EO eingebaut, was zu ausgeprägten Gradientenbildungen führt. Copolymere mit einem steileren Gradienten waren besser wasserlöslich als solche mit einem gleichmäßigeren Gradienten.

Kapitel 5 untersucht biobasierte Terpenylglycidylether, die eine erneuerbare Alternative zu konventionellen erdölbasierten Monomeren darstellen und somit zum Ziel der Dekarbonisierung der chemischen Industrie beitragen. Die Copolymerisation von kurz- bis mittelkettigen azyklischen Terpenylglycidylethern mit EO wurde analysiert. Trotz der strukturellen Vielfalt dieser Monomere wurden ähnliche Einbaupräferenzen mit EO beobachtet, wobei jedoch die apolareren Verbindungen langsamere Einbauraten zeigten. Die Doppelbindungen der Terpenylglycidylether wurden durch eine Thiol-En-Klick-Reaktion mit 2-Mercaptoethanol als Modellverbindung funktionalisiert, wodurch sich diese Materialien für die Einführung nahezu beliebiger funktioneller Gruppen für maßgeschneiderte Anwendungen eignen. Die Reduktion der Doppelbindungen mit Diimid ermöglichte die anschließende Sättigung der Seitenketten, wodurch diese Materialien weniger alterungsanfällig wurden.

Kapitel 6 konzentriert sich auf die Synthese von Oleylglycidylether (OlGE) aus Oleylalkohol und Epichlorhydrin. Ähnlich wie Terpenylglycidylether dienen Monomere, die aus Fettalkoholen

gewonnen werden, als wertvolle Ressourcen für hydrophobe Monomere. Ihre lineare Struktur ermöglicht es gesättigten langkettigen Varianten bei Raumtemperatur zu erstarren, während mittelkettige oder *cis*-ungesättigte Varianten flüssig bleiben. Trotz seiner stark apolaren und sterisch anspruchsvollen Seitenkette zeigte OlGE nur eine leicht geringere Einbaupräferenz in der Copolymerisation mit EO. Block- und statistische Copolymere aus OlGE und EO wurden auf ihr Mizellenverhalten hin untersucht. Durch den Einbau von nur wenigen mol% dieses hydrophoben Comonomers mit hoher molarer Masse konnte ein breites Spektrum an hydrophilen-lipophilen Verhältnissen erreicht werden. Die Transmissionselektronenmikroskopie (TEM) und dynamische Lichtstreuung (DLS) zeigten die Bildung von Mizellen, die sich zu größeren Aggregaten zusammenschlossen. Die Doppelbindung in OlGE war für Thiol-En-Klick-Reaktionen und die Reduktion mittels Diimid zugänglich, was eine teilweise oder vollständige Reduktion der Seitenketten ermöglichte. Diese Modifikation ermöglichte das Einstellen der Schmelzpunkte, sodass sie in den physiologischen Bereich fielen und anpassbare Materialeigenschaften für biomedizinische Anwendungen boten.

Anhang-Kapitel

Kapitel A1 ist eine Zusammenarbeit mit Epoxid-Spezialisten der [redacted]-Gruppe und des Universitätsklinikums Mainz. Es konzentriert sich auf die Synthese von statistischen Copolymeren, die aus unterschiedlichen Verhältnissen von EO und GME bestehen und als Alternative zu PEG in biomedizinischen Anwendungen dienen. Diese Copolymere erwiesen sich über einen breiten Konzentrationsbereich hinweg als biokompatibel und wurden auf ihre Antigenizität gegenüber Anti-PEG-Antikörpern (APAs) getestet. Sobald der GME-Anteil 50 mol% erreichte, konnten die APAs nicht mehr an das Polymerrückgrat binden. Die gleichen Einbaupräferenzen der Comonomere führten zu zufällig verteilten Störstellen entlang der Polyetherketten. Eine kinetische Monte-Carlo-Simulation visualisierte die vernachlässigbare Anzahl von Copolymerketten, die das Bindungsmotiv der APAs trugen, und erklärte so die niedrige Bindungsaffinität der APAs zu den Copolymeren.

Kapitel A2 bietet grundlegende Einblicke in die „auf Wasser“-Katalyse der ringöffnenden Polymerisation (ROP) von Epoxiden an einer statischen Öl-alkalischen Wassergrenze. Trotz der normalerweise wasserempfindlichen Reaktion polymerisierte Styroloxid, das unter konventionellen AROP-Bedingungen eine geringe Reaktivität aufweist, an der Grenzfläche und ergab überraschend hohe molare Massen. Verschiedene Reaktionsparameter, wie pH-Wert, Lösungsmittel, Initiatorsalz usw., wurden untersucht. Die höchste beobachtete Spezies in der Matrix-assistierten Laser-Desorptions/Ionisation-Flugzeit-Massenspektrometrie (MALDI-ToF MS) wies eine molare Masse von 8 000 g/mol auf.

Kapitel A3 befasst sich mit der carbanionischen Polymerisation von 1-Phenylisopren und 4-Phenylisopren. Die disubstituierten 1,3-Diene wurden durch eine Wittig-Reaktion synthetisiert und in Cyclohexan sowie mit unterschiedlichen Mengen an THF als polarem Additiv polymerisiert. Die 1,4-Inkorporation der Phenylisoprene nahm überraschenderweise bei geringen Mengen an THF ab, stieg jedoch wieder mit größeren Mengen an. Eine kationische Zyklisierung in einer Postpolymerisationsmodifikation unter Verwendung von Trifluormethylsulfonsäure induzierte Fluoreszenzeigenschaften und einen ausgeprägten Anstieg der Glasübergangstemperatur auf 187 °C für P(1-Phenylisopren) und 131 °C für P(4-Phenylisopren). Copolymerisationen von 1-Phenylisopren mit Isopren führten zu statistischen Copolymeren, während mit Styrol Gradientstrukturen entstanden. Die β-C-Verschiebung in der ^{13}C-NMR-Spektroskopie und Dichtefunktionaltheorie (DFT)-Berechnungen zeigten eine ähnliche elektronische Struktur wie Isopren, was die vergleichbare Einbaupräferenz erklärt.

Graphical Abstract

Chapter 2:

Anionic Copolymerization of Epoxides and their Reactivity Ratios

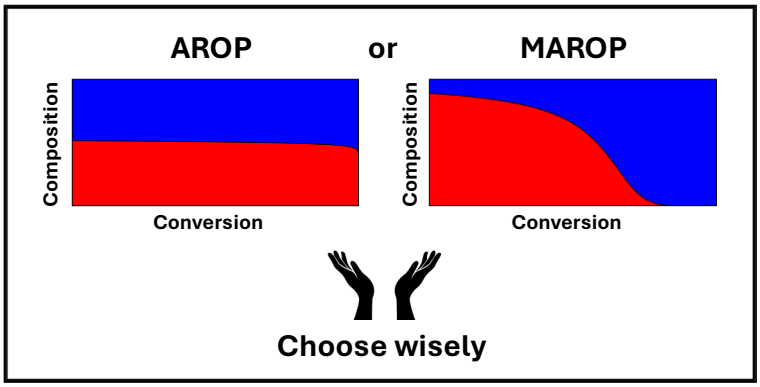

Chapter 3:

Influence of Solvent and Degree of Deprotonation on Reactivity Ratios and Reaction Rates in Ethylene Oxide/Glycidyl Methyl Ether Copolymerization

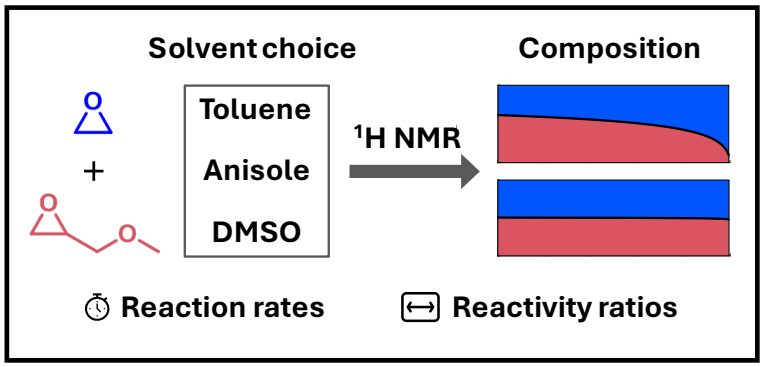

Chapter 4:

Reaction Temperature and Solvent Determine Reactivity Ratios in the Copolymerization of Ethylene Oxide and Propylene Oxide

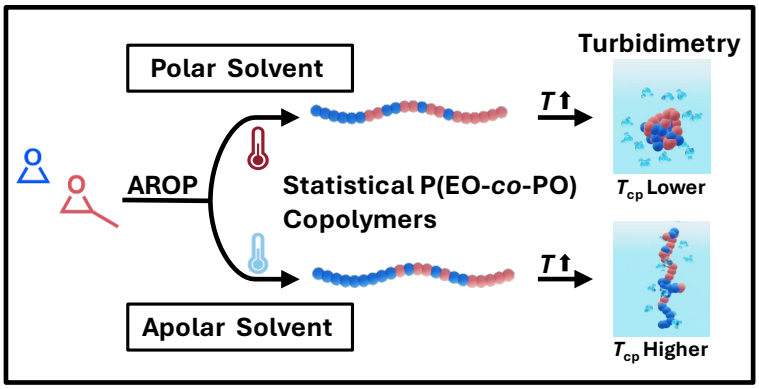

Chapter 5:

Poly(Terpenyl Glycidyl Ethers): Copolymerization with Ethylene Oxide, Properties, and Functionalization

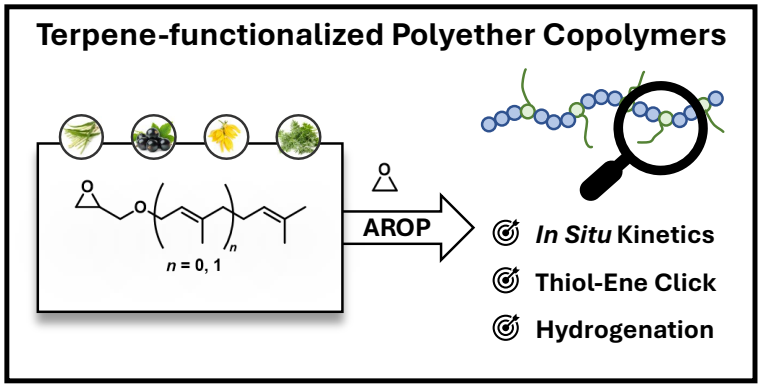

Chapter 6:

Polymers of Biobased Oleyl Glycidyl Ether: Insights into Copolymerization with Ethylene Oxide, Postmodification, Thermal Properties, and Micellization Behavior

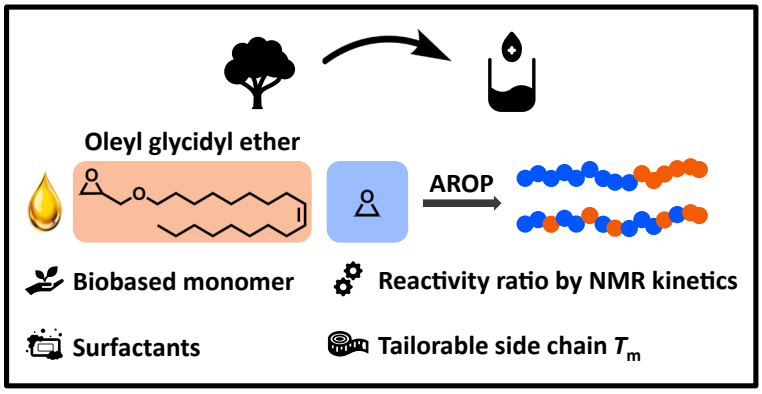

Chapter 1

Introduction

1 Introduction

The following section introduces poly(ethylene glycol) (PEG), widely regarded as a gold standard in pharmaceutical and medical applications.[1] PEG is produced in various GMP-grade (Good Manufacturing Practice) qualities tailored for these fields[2] and is primarily synthesized through anionic ring-opening polymerization (AROP), which will be discussed in detail in a later section. Catalytic and cationic ring-opening polymerization pathways are possible but exhibit several drawbacks.[3] These techniques are not used in this thesis and are therefore not discussed here. Several reviews have highlighted the aforementioned polymerization techniques in detail, *e.g*. by Penczek, Kubisa, and Matyjaszewski, Chen, or Frey *et al*.[1,4,5]

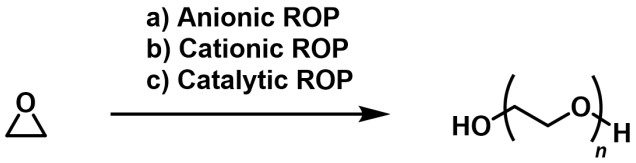

Figure 1: Synthesis of poly(ethylene glycol) from ethylene oxide (EO) by different ring-opening polymerization (ROP) pathways.

PEG itself is a nonfunctional material. However, ethylene oxide has been frequently copolymerized with functional epoxides (see **Chapter 2**). The resulting multifunctional PEGs feature incorporated hydrophobic segments and/or functional groups along the otherwise hydrophilic backbone. The comonomers are commonly derived from fossil-based resources. Introducing functional groups significantly broadens the application scope, especially for various biomedical uses.[1] Alongside this, the push for sustainable solutions has intensified the demand for renewable resources in materials science. The search for bio-based alternatives to fossil-based resources is imperative due to nowadays environmental challenges and climate change.[6,7] Bio-based comonomers, such as those derived from fatty alcohols and terpenoid alcohols, are presented as underrated yet promising building blocks. The monomer ethylene oxide is already available from renewable resources.[8]

Poly(Ethylene Glycol) (PEG)

In 1859, Wurtz described the synthesis of ethylene oxide (EO) from 2-chloroethanol and its reaction with aqueous sodium hydrogen sulfate, producing hygroscopic crystals with a “refreshing taste”.[9] He later systematically investigated the physical properties of the oligomers of EO.[10,11] Lourenco independently found similar results.[12,13] Staudinger and Schweitzer published a comprehensive overview on the polymerization of EO in 1929.[14] Today, EO is synthesized via the gas-phase oxidation of ethylene with oxygen at 220–300 °C, using Al_2O_3–supported silver catalysts (Figure 2).[15]

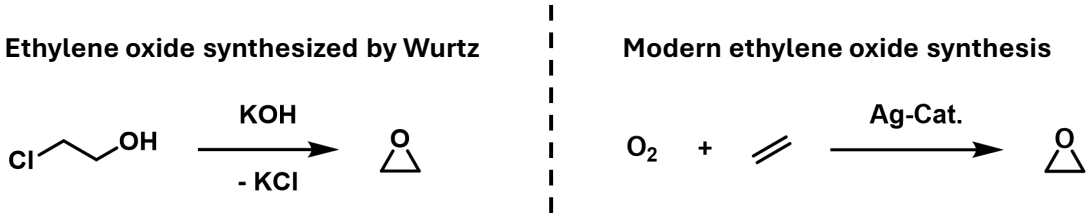

Figure 2: Ethylene oxide synthesis by Wurtz[9] and today's industrial-scale synthesis.[15]

PEG and poly(ethylene oxide) (PEO) refer to the same polymer, though PEG is typically used for molecular weights below 30 000 g/mol. Yet, in pharmaceutical and medical applications, the term PEG is used exclusively. Due to its highly regular helical structure,[16] PEG transitions from a viscous liquid to a waxy, semicrystalline state once its molar mass exceeds 1 000 g/mol. At molar masses above 6 000 g/mol, PEG typically is obtained as a crystalline powder and exhibits a melting point (T_m) around 65 °C.[17] Although the semicrystalline state can be beneficial in certain applications,[1] it poses significant limitations in solid-state batteries,[18,19] and membrane technology, where amorphous regions are crucial for molecular interactions and transport phenomena.[20,21] The glass transition temperature (T_g) of PEG is below -60 °C, attributed to the high flexibility of the polyether backbone.[22] PEG is highly water-soluble, even at high concentrations, particularly at low molar masses. While solubility decreases as the molar mass increases, preparation of 50% aqueous solutions is still possible at room temperature for PEG with a molar mass of up to 35 000 g/mol.[3] This feature is unique among the polyethers. The structurally related poly(oxymethylene), poly(acetaldehyde), poly(propylene oxide) (PPO), poly(trimethylene oxide), and poly(tetrahydrofuran) are insoluble in water.[23]

PEG is widely used in everyday applications, including skin care products, ointments, lubricants, and surfactants. It is commonly used when moisture retention or solubilization of hydrophobic molecules is required. Despite PEG's ether backbone without cleavable bonds, such as esters or amides, it is considered biodegradable, though this depends on the molar mass and the applied test criteria. Polymers with low molar mass degrade faster than their high molar mass analogs.[24] The high aqueous solubility, low toxicity, antigenicity, and immunogenicity, render PEG derivatives advantageous for coupling with lipids, drugs, and proteins in biomedical applications. In these so-called "PEGylated" compounds, PEG forms a highly hydrated polymer shell, significantly extending the half-lives of the compounds in the bloodstream. This is known as the stealth effect and results in greatly enhanced therapeutic effects.[1,25,26] The increased use of PEGylated therapeutics,[27] and other still unclear factors have led to the formation of anti-PEG antibodies (APAs). In the year 2023, approximately 83% of the German population tested positive for these antibodies (Figure 3).[28] Lai *et al*. conducted a detailed time-resolved analysis of APA prevalence across different age groups,

genders, and races. They confirmed the widespread prevalence of pre-existing APAs. The IgG levels correlated with the patient's age, but not with gender or race.[29] Despite this rise in APAs, the United States Food and Drug Administration (FDA) approved three PEGylated drugs in 2023, highlighting the benefits of this technology.[30]

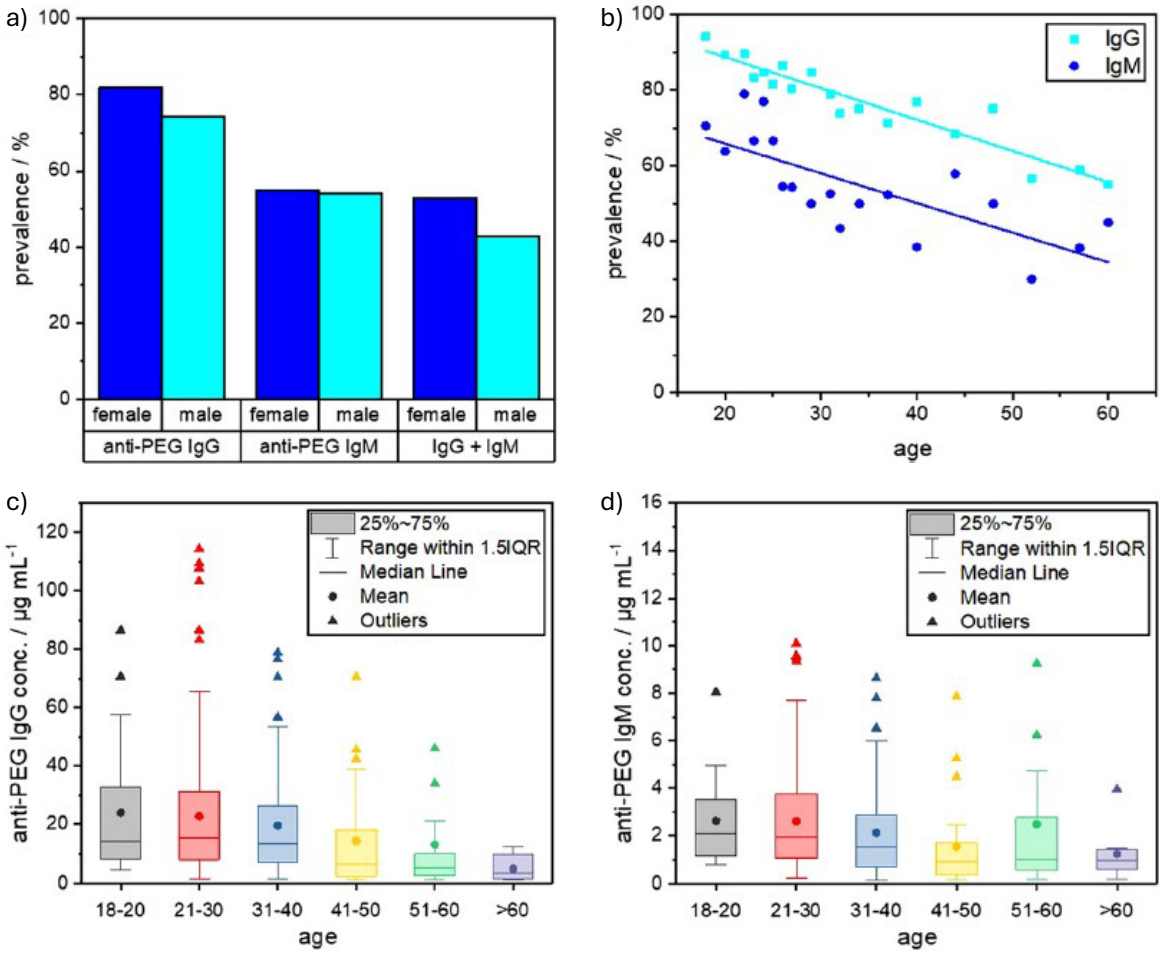

Figure 3: Plasma screening to analyze anti-PEG antibody prevalence and concentration in a sample of the German population (*n* = 500). a) Prevalence of anti-PEG IgG and IgM antibodies (blue: female, cyan: male samples). b) Prevalence distribution depending on age (cyan: IgG, blue: IgM), the line indicates the linear regression. c) Concentration of anti-PEG IgG antibodies in age groups. d) Concentration of anti-PEG IgM antibodies in age groups. Differences in average concentrations shown in c) and d) are not statistically significant due to outliers in the high concentration range. Reprinted and adapted with permission from Landfester *et al.*[28] Royal Society of Chemistry, © 2023.

There are several strategies to introduce additional functional groups into the polymer to broaden the applications of PEG. On the one hand, this can be achieved using a functional initiator (*α*-functionalization) and/or a functional terminating agent (*ω*-functionalization), resulting in mono- or (hetero)bifunctional polymers. On the other hand, postpolymerization modification can be employed to alter the terminal hydroxyl groups, though this method is challenging and restricted to the chain ends. In contrast, copolymerization of EO with functional epoxides allows for the

tailoring of PEG properties. Sequential polymerization yields block copolymers, while simultaneous copolymerization yields statistical copolymers. The polymer properties are altered depending on the comonomer incorporation statistics and its ratio. However, this approach is limited to epoxides withstanding the harsh conditions of the polymerization, such as high temperatures and strong bases.[1] **Chapter 2** comprehensively reviews the statistical copolymerization of a large variety of epoxide monomers, with a special emphasis on EO.

Ring-Opening Polymerization of Epoxides

The ring-opening polymerization (ROP) of epoxides can be achieved through one of three pathways: a) anionic, b) cationic, or c) catalytic. The monomer-activated anionic ROP (MAROP), pioneered by Carlotti and Deffieux,[31] represents a special subclass of the anionic ring-opening polymerization (AROP) and is briefly discussed in **Chapter 2**. The utilization of double metal cyanide (DMC) catalysis plays a large role in the polymerization of propylene oxide (PO) for the commercial production of PPO-based polyols for polyurethane applications.[32] Due to the need for elevated temperatures and pressures, as well as the nontrivial catalyst preparation, the use is mostly limited to a few industry purposes.[1] Cationic ring-opening polymerization suffers from low control over the polymerization, and transfer reactions broaden the molar mass distribution and reduce the targeted molar mass.[33] It furthermore produces several (toxic) cyclic side-products, such as 1,4-dioxane.[34] The industrially most relevant and conventional technique to polymerize epoxides is the AROP. The driving force for the EO polymerization is the ring strain release, which is around 110 kJ/mol.[35] The AROP is a living (no termination, no chain transfer) and controlled (fast initiation, low dispersity, controlled molar mass) polymerization. This requires rigorously purified chemicals and equipment, as protic compounds can impede the polymerization and/or initiate a growing polymer chain themselves.[36]

Anionic Ring-Opening Polymerization (AROP)

The AROP relies on highly nucleophilic alkali metal compounds in aprotic, polar solvents, such as tetrahydrofuran (THF), dimethyl sulfoxide (DMSO), and hexamethylphosphoric triamide (HMPTA). These solvents enable the separation of the countercation (mostly Na^+, K^+, Cs^+) from the active alkoxide chain end. Lithium as a counterion forms stable aggregates with the alkoxide chain ends and due to the rather covalent than ionic bond between lithium and the alkoxide, the polymerization cannot take place or is extremely decelerated.[1,37] This matches with the principles of “hard and soft acids and bases” developed by Pearson.[38] The reaction rate usually increases with increasing temperature, larger ionic radius of the counterion ($Na^+<K^+<Cs^+$), polarity of the solvent,[39] cation-chelating additives (crown-ethers, cryptands),[40] and by adding small amounts of alcohol to the mixture.[41] The chosen reaction conditions influence the equilibria between the different species

shown in Scheme 1. Reversibly aggregated ion pairs are dormant, and hence do not result in monomer propagation. In THF at 70 °C, living PEG forms trimers with potassium or cesium as counterions and tetramers with sodium. These aggregates disaggregate at very low concentrations, but in the case of sodium, they are present at all concentrations.[42] The term "aggregation" is often used interchangeably with "association" in the literature, but due to its similarity with "dissociation" and the related reverse reaction, this thesis will not adopt this usage.

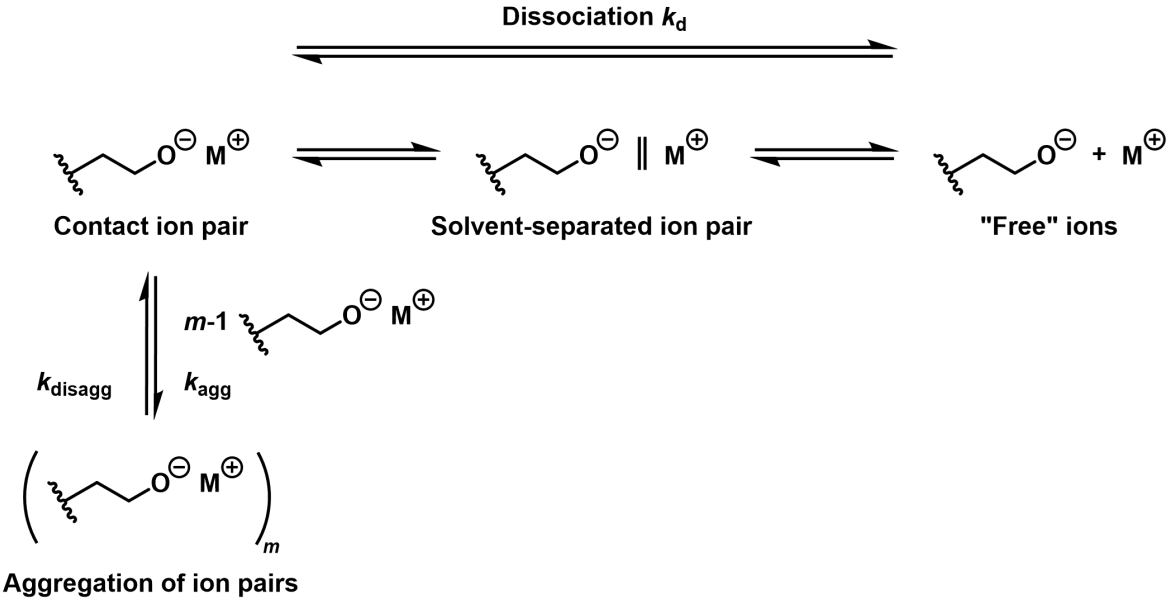

Scheme 1: Different species present in the AROP. The aggregates are dormant, whereas contact ion pairs, solvent-separated ion pairs, and free ions exhibit increasing polymerization rate constants. Reprinted and adapted from *Reference Module in Chemistry* 2016, Penczek, S.; Pretula, J.B., Ring-Opening Polymerization, Page 17, Copyright 2016, with permission from Elsevier.[33]

The aggregation of alkoxide ion pairs can even be observed in polar solvents like DMSO[42,43] or HMPTA.[44] In THF at 25 °C, the dissociation constant k_d is $1.8 \cdot 10^{-10}$ mol/L,[45] meaning propagation occurs almost exclusively by contact ion pairs. In some papers, the total concentration of active centers is determined incorrectly, if the capability of aggregation is ignored, as stated by Penczek and Pretula.[33] The contribution of the contact ion pairs and the free anions can be determined using the "Szwarc's plot":[46]

$$-\frac{\mathrm{d[M]}}{\mathrm{d}t} = k_{\mathrm{p}}^{-}[\mathrm{P}^{-}][\mathrm{M}] + k_{\mathrm{p}}^{\pm}[\mathrm{P}^{\pm}][\mathrm{M}] \quad (1)$$

With: [M] monomer concentration, t time, k_p^- propagation constant of the free anion, $[P^-]$ concentration of the free anion active chain end, $k_p^{\pm}$ propagation constant of the contact ion pair, $[P^{\pm}]$ concentration of the contact ion active chain end. $[P^{\pm}]$ and $[P^-]$ are steady for living polymerizations and equal to the initiator concentration $[I]_0$. The following equations can be made, with $[M^+]$ as the counter cation:

$$[\mathrm{P}^{\pm}] \rightleftharpoons [\mathrm{P}^{-}] + [\mathrm{M}^{+}] \tag{2}$$

$$k_{\mathrm{d}} = \frac{[\mathrm{P}^{-}][\mathrm{M}^{+}]}{[\mathrm{P}^{\pm}]} \tag{3}$$

Solving equation (1) and applying the equations (2)–(3) yields:

$$k_{\mathrm{p}}^{\mathrm{app}} = -\frac{\mathrm{d}[\mathrm{M}]}{[\mathrm{M}][\mathrm{I}]_0 \mathrm{d}t} = k_{\mathrm{p}}^{\pm} + (k_{\mathrm{p}}^{-} - k_{\mathrm{p}}^{\pm}) k_{\mathrm{d}}^{1/2} [\mathrm{I}]_0^{-1/2} \tag{4}$$

Duda and Penczek took aggregation into account and reported the following equation:[33,47]

$$r_{\mathrm{p}}^{1-m} = -\frac{m k_{\mathrm{agg}}}{k_{\mathrm{p}}^{m-1}} + k_{\mathrm{p}} [\mathrm{I}]_0 r_{\mathrm{p}}^{-m} \tag{5}$$

With:[48]

$$\mathrm{P}_n^{-} + \mathrm{M} \xrightarrow{k_{\mathrm{p}}} \mathrm{P}_{n+1}^{-} \equiv \mathrm{P}_n^{-} \tag{6}$$

$$m\mathrm{P}_n^{-} \underset{}{\overset{k_{\mathrm{agg}}}{\rightleftharpoons}} (\mathrm{P}_n^{-})_m \tag{7}$$

$$r_{\mathrm{p}} = \frac{\mathrm{d}[\mathrm{M}]}{[\mathrm{M}]\mathrm{d}t} = \ln\left(\frac{[\mathrm{M}]_0}{[\mathrm{M}]}\right) t^{-1} = -\frac{\mathrm{d}\ln[\mathrm{M}]}{\mathrm{d}t} \tag{8}$$

Fitting r_{p} and $[\mathrm{I}]_0$ to the following equation, the aggregation number *m* can be obtained.

$$\ln r_{\mathrm{p}} = \ln k_{\mathrm{p}} \left(m k_{\mathrm{agg}}\right)^{-1/m} + \frac{1}{m} \ln[\mathrm{I}]_0 \tag{9}$$

The propagation follows a simple scheme, due to the low solubility of alkoxides even in polar solvents, the initiator salts are in most cases partially deprotonated (Scheme 2). As can be seen in equation (7), this has a strong impact on the ratio of aggregates, pushing toward disaggregated species. This leads to a fast equilibrium between the dormant, protonated species and the active, deprotonated species and should not be viewed as a chain transfer reaction.

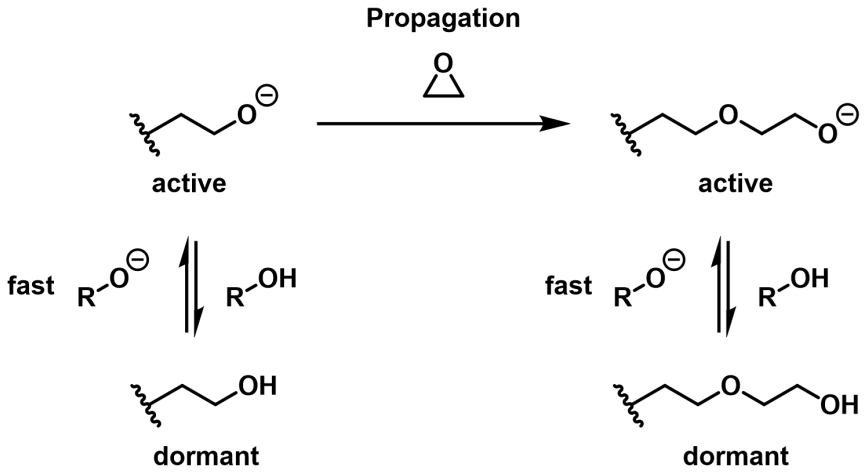

Scheme 2: Polymerization propagation of EO and the equilibrium with the dormant protonated species. ROH represents another dormant polymer chain end. Counterion omitted. Depending on the nature of the anion, different propagation constants are obtained.

Although the alcohol functionality is considered dormant, its presence accelerates the overall reaction rate by shifting the equilibrium from aggregated to active ion pairs. Additionally, the proton participates in epoxide activation, forming a ternary transition state involving the alkoxide, monomer, and alcohol. This occurs due to strong alcohol-alkoxide interaction. In the absence of a protic functional group, propagation is hindered. When the alkoxide to alcohol ratio falls below a threshold, the reaction rate decreases.[41,49–51] At the onset of polymerization, the reaction rate increases as the added EO units coordinate with the potassium counterion (Scheme 3). This shifts the equilibrium from contact ion pairs to separated ion pairs and/or enhances dissociation (compare to Scheme 1).[52] This effect can also be observed by conductometry, as the k_d of living PEG alkoxide in DMSO is over 10 times higher than that of potassium methoxide.[53]

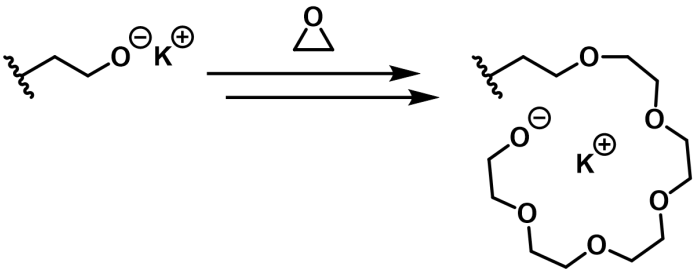

Scheme 3: Complexation of the counterion by the growing poly(ethylene oxide) chain. Reprinted and adapted from *Living ring-opening polymerizations of heterocyclic monomers* 2007, Penczek, S.; Cypryk, M.; *et al*., Ring-Opening Polymerization, Page 251, Copyright 2007, with permission from Elsevier.[52]

Due to the living nature of AROP, if no termination occurs via protic compounds (*e.g*. excess water) or electrophilic reagents and no transfer to monomer occurs, it is possible to proceed with the polymerization by sequentially adding a second monomer. Consequently, block copolymers can be formed, which combine the distinct properties by covalently bonding two homopolymers,

distinguishing them from polymer blends.[54] A well-known example are poloxamers, amphiphilic block copolymers composed of EO and PO, marketed under the brand name Pluronic®.[55]

Substituted epoxide monomers, such as PO, are prone to chain transfer from the chain end to the monomer. Under the strong basic AROP conditions, the active alkoxide chain end can abstract a proton from the methyl side group, forming an allylic alkoxide (Scheme 4). This initiates an additional chain and also results in an mostly undesired allylic chain end, limiting the achievable molar mass to around 6 000 g/mol.[56] This side reaction can be suppressed by adding crown ethers or using counterions with a larger ionic radius, such as Rb^+ or Cs^+.[57] Polymerization of racemic, substituted spoxide monomers is regioselective and produces atactic polymers, which are mainly connected by head-to-tail.[37,58,59]

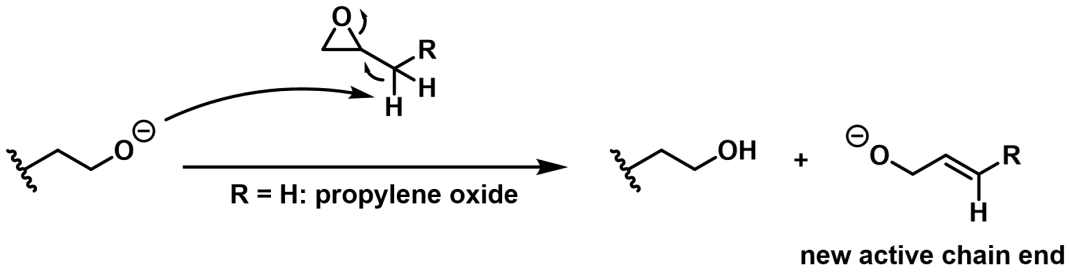

Scheme 4: Chain transfer reaction to the monomer. Counterion and the proton exchange equilibrium between active alkoxide and dormant alcohol species are omitted.

Flory predicted that the living and controlled polymerization of EO would result in a narrow molar mass distribution, mathematically following a Poisson distribution. For a number-average degree of polymerization (P_n), commonly referred to simply as the "degree of polymerization", the dispersity $Đ$ initially increases at a value of $P_n = 2$ but decreases thereafter. If P_n increases substantially, the dispersity approaches unity.[60]

$$P_n = \frac{M_n}{M_{Mono}} \tag{10}$$

$$Đ = \frac{M_w}{M_n} = 1 + \frac{1}{P_n} \tag{11}$$

M_{Mono} is the molar mass of the monomer, M_n is the number-average molar mass, defined by the total weight of all molecules in a polymer sample w, the number of repeating units i, and the number of moles N_i whose weight is M_i. N_i^{frac} is the mole or number fraction of molecules with the molar mass M_i.

$$M_n = \frac{w}{\sum N_i} = \frac{\sum N_i M_i}{\sum N_i} = \sum N_i^{frac} M_i \tag{12}$$

The mass-average molar mass (M_m or M_w, previously called the weight-average molar mass, with the abbreviation M_w still in use)[61] is calculated using the weight fraction w_i of molecules with molar mass M_i. The weight concentration c_i represents the concentration of molecules with molar mass M_i, while c is the total weight concentration of all polymer molecules.[62]

$$M_w = \sum w_i M_i = \frac{\sum c_i M_i}{\sum c_i} = \frac{\sum c_i M_i}{c} = \frac{\sum N_i {M_i}^2}{\sum N_i M_i} \quad (13)$$

$$w_i = \frac{c_i}{c} \quad (14)$$

$$c_i = N_i M_i \quad (15)$$

$$c = \sum c_i = \sum N_i M_i \quad (16)$$

Bio-Based Glycidyl Ethers from Renewable Resources and Polymers Thereof

The United Nations has committed to achieving net-zero carbon emissions by 2050 to limit global warming to well below 2 °C compared to the preindustrial level while pursuing efforts to keep the increase below 1.5 °C. This commitment necessitates the decarbonization of the chemical industry, and extensive research aimed at reducing greenhouse gas emissions.[6,7,63] Ethylene oxide can be sourced from bio-based materials via two main routes: bioethanol dehydration to ethylene, followed by oxidation,[64,65] or electrosynthesis directly from bioethanol.[66] Another feasible method is the electrochemical synthesis of ethylene oxide from CO_2 and water.[67] Glycidyl ether monomers can be prepared from various bio-based sources, especially from terpenoids and fatty alcohols. Some of the already described examples in the literature are depicted in Figure 4. Apart from polymerization to polyethers, the epoxide functionalities are also well-suited for the synthesis of polycarbonates with carbon dioxide or polyesters with anhydrides through ring-opening copolymerization.

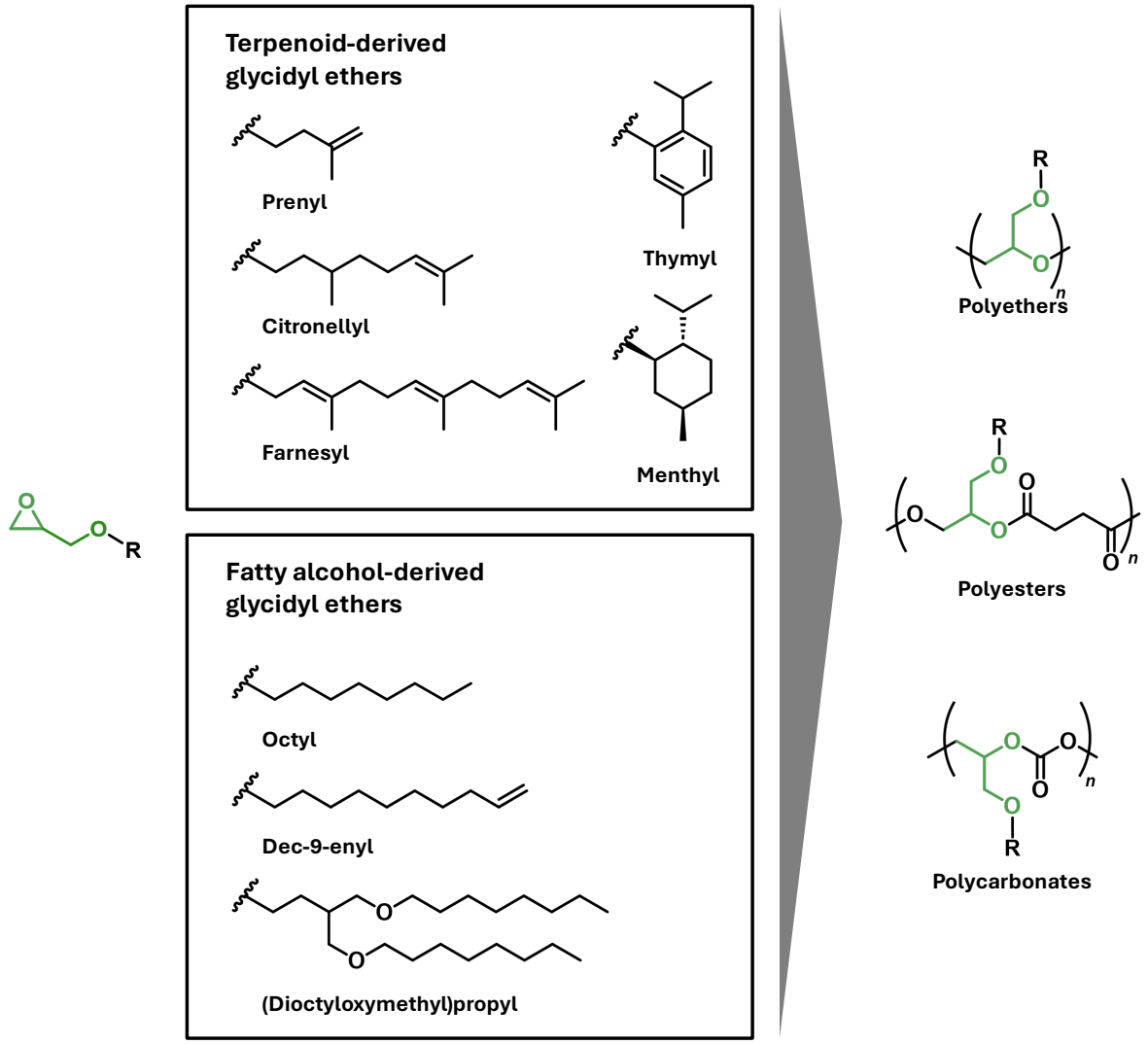

Figure 4: Examples of glycidyl ethers from bio-based alcohols polymerized to polyethers, polyesters, and/or polycarbonates.[68–75]

PEG lacks functional groups aside from those introduced by the initiators and terminating agents. To achieve further customization, incorporating additional comonomers is necessary. Glycidyl ethers (GEs) are promising candidates to obtain multifunctional PEG (mf-PEG). In theory, any functional group can be incorporated, provided it withstands the harsh reaction conditions. Alternatively, the functional groups can be released from protecting groups or introduced by postpolymerization modification. Glycidyl ethers can be conveniently synthesized by etherifying the respective alcohols and epichlorohydrin (ECH) (Scheme 5). Under basic conditions, the alcohol is deprotonated, attacking ECH's epoxide ring, which releases a chloride anion during ring closure.[76] Alternatively, epichlorohydrin can be activated by Lewis or Brönstedt acids, facilitating a nucleophilic attack. The resulting chlorohydrin is subsequently treated with a base to eliminate the chloride, forming the glycidyl ether.[73] Prileschajew oxidation permits access to glycidyl ethers from

the respective allyl ethers. The related α-alkylene oxides can be derived from the α-alkylenes in the same way.[77]

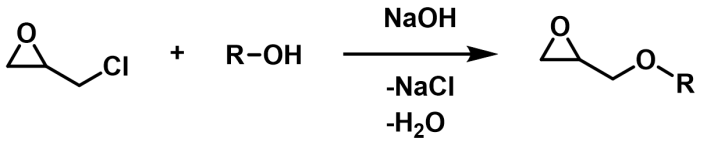

Scheme 5: Synthesis of glycidyl ethers by Williamson Ether Synthesis.

ECH can be produced from either propylene or bioderived glycerol (see section below), with the latter being available commercially as Epicerol® from Solvay company. In this process, glycerol undergoes two-step chlorination with HCl, followed by an elimination reaction to yield ECH (Scheme 6).[78–80]

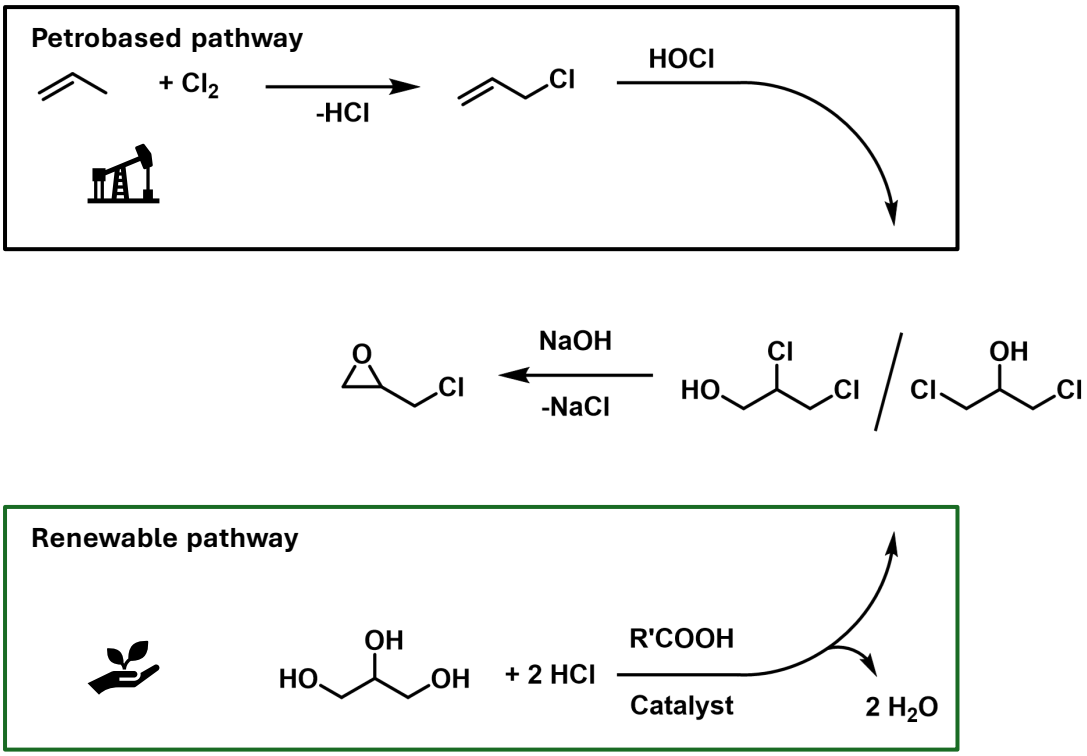

Scheme 6: Epichlorohydrin synthesis by fossil-based (top) and renewable (bottom) pathway.[79]

Fatty Alcohols from Triglycerides

Fats and oils serve as renewable feedstocks for the chemical industry. Their high production volume (208.1 Mt in 2019) facilitates the cost-effective generation of a wide variety of linear alkyl and alkenyl alcohols from triglycerides.[81–85] They can be produced from naturally occurring triglycerides in fats and oils and are already utilized in large quantities for fatty alcohol ethoxylate surfactants.[86] Most fatty alcohols are produced from oil plants (oil palm, coconut, soybean, rapeseed, cotton, sunflower, etc.) but genetically modified microbes are a space-efficient method to produce fatty

acids in reliable quantities and tailor-made compositions.[87–89] The fatty alcohol can be converted into the respective GEs, which represent an apolar comonomer class due to the side chain rich in methylene units.

The corresponding fatty acids are biosynthesized (see Scheme 7) starting from acetyl-coenzyme A (Acetyl-CoA), which is converted into malonyl-CoA via hydrogen carbonate and adenosine triphosphate (ATP). The CoA is then replaced by an acyl carrier protein (ACP), allowing chain elongation with acetyl-ACP through decarboxylation. Nicotinamide adenine dinucleotide phosphate (NADPH, reduced form) reduces acetoacetyl-ACP to D-3-hydroxybutyryl-ACP, followed by dehydration to form crotonyl-ACP. After the reduction of the double bond with NADPH, butyryl-ACP is obtained. This reacts with malonyl-ACP to form the respective C_6 building block, which can undergo further extension to form higher fatty acids. The fatty acids are then converted into triglycerides.[90]

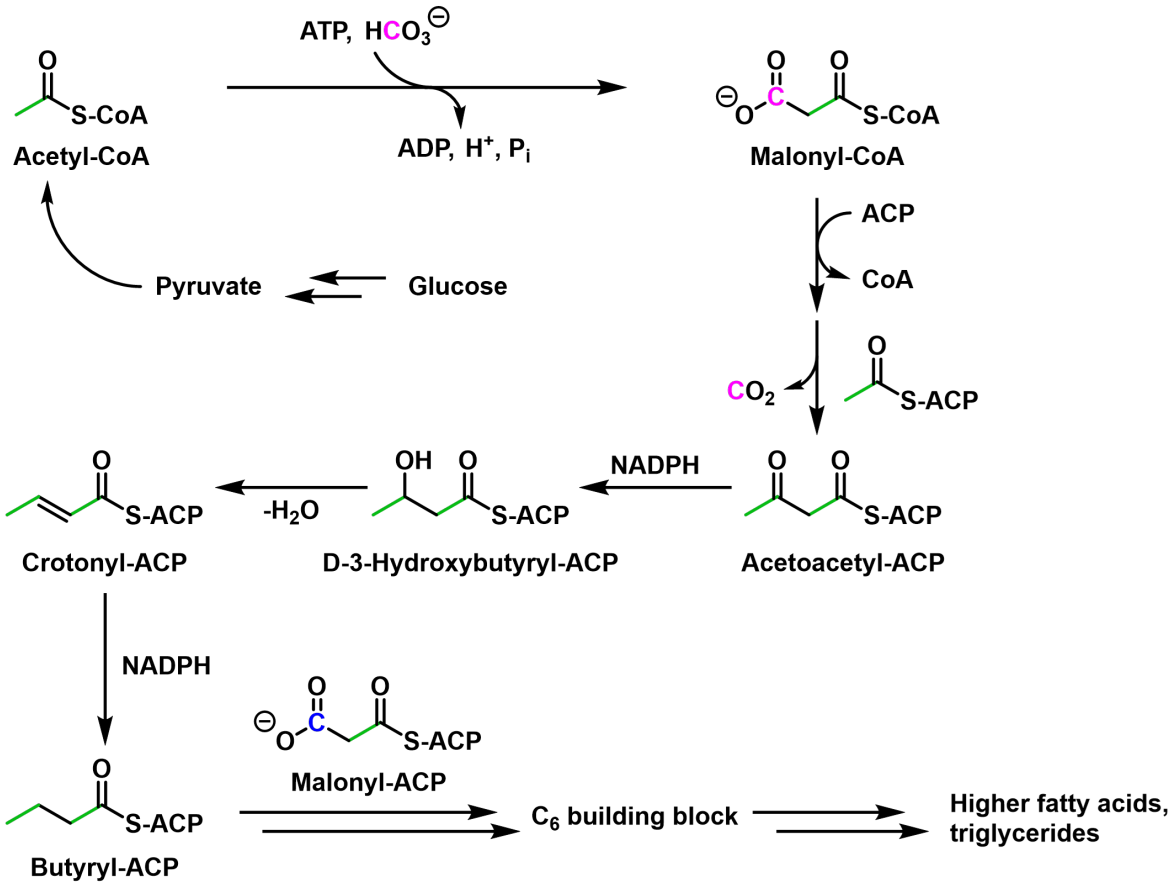

Scheme 7: Fatty acid biosynthesis.[90] Charges and atoms are not fully equated for clarity reasons.

In industry, triglycerides are transesterified with excess methanol under constant distillation to remove the products and shift the equilibrium to the methyl ester and glycerol. The methyl ester is hydrogenated to the respective fatty alcohol (Scheme 8).[83]

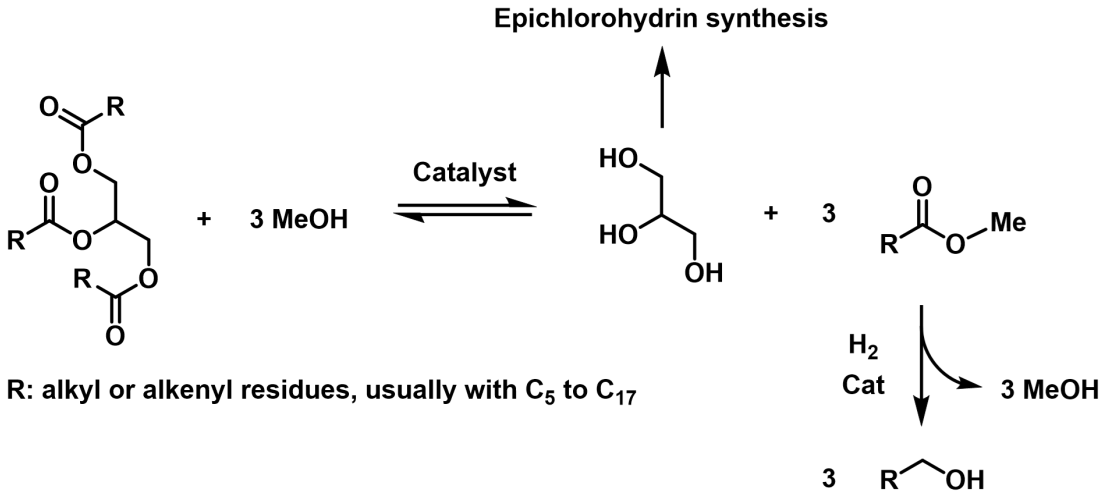

Scheme 8: Fatty alcohol synthesis from triglycerides. The first step is a transesterification, the second step is a catalytic reduction.[83] R is not necessarily equal.

Saturated, linear chains (C_{14} and higher) can crystallize at room temperature, whereas compounds with shorter chains are liquid. Unsaturated triglycerides with *cis* double bonds are liquid at room temperature. After polymerization of the fatty alcohol-based GE, the polymers can be further functionalized through thiol-ene click reactions,[91,92] (partially) hydrogenated to tailor the melting point (see Chapter 6), or crosslinked.[75,93] Ozonolysis of the double bond can yield primary alcohols, aldehydes, or carboxylic acids by partial cleavage of the side chains.[94,95] The ability to introduce functional groups allows researchers to adjust material properties beyond hydrophobicity, particularly when combined with hydrophilic PEG in block- or statistical copolymers. Subsequent coupling of the polymer, for instance with proteins, can further expand the range of potential applications. Thus, double bond modification enables the creation of tailor-made materials suited for a wide variety of uses.

With increasing focus on developing bio-based chemicals that do not interfere with the food supply chain[96,97] it is vital to highlight the efficient use of triglycerides from non-edible oil plants as an alternative to food crops.[98] Additionally, converting waste into chemicals is significantly more economical compared to the production of biofuels or electricity.[99]

Terpenoid Alcohols

Terpenes and terpenoids are a class of naturally occurring compounds, comprising over 38 000 known substances. These molecules play crucial roles in plant biology, including modulating cellular functions, attracting pollinators, repelling natural enemies, and regulating mutualistic interactions.[100] They are well-known for their distinctive scents and are often named after the fruits from which they were first extracted. Common examples are limonene from lemon, geraniol from geranium, perillyl alcohol from perilla, senecioic acid from senecio, isovaleric acid from valerian,

etc.[101] Terpenes are pure hydrocarbons, formally derived from isoprene (C_5) units. They are classified into the subclasses hemiterpenes (C_5), monoterpenes (C_{10}), sesquiterpenes (C_{15}), diterpenes (C_{20}), and so forth. Terpenoids are terpenes containing oxygen in various functional groups (alcohols, ethers, carboxylic acids, ketones, etc.) and can differ slightly from the isoprene derivation.[102] The biosynthesis proceeds via two initially different pathways, which is described in Scheme 9. One pathway is the synthesis of 2-C-Methyl-D-erythriol-4-phosphate (MEP) from pyruvic acid. The second pathway is the synthesis of mevalonic acid (MVA) from acetyl coenzyme A. Phosphorylation and dehydration of both MEP and MVA yields isoprenyl pyrophosphate (IPP) or dimethyl allyl pyrophosphate (DMAPP). Higher terpenoids, such as geranyl pyrophosphate (GPP) and farnesyl pyrophosphate (FPP), are synthesized through consecutive head-to-tail additions of the IPP and DMAPP building blocks.

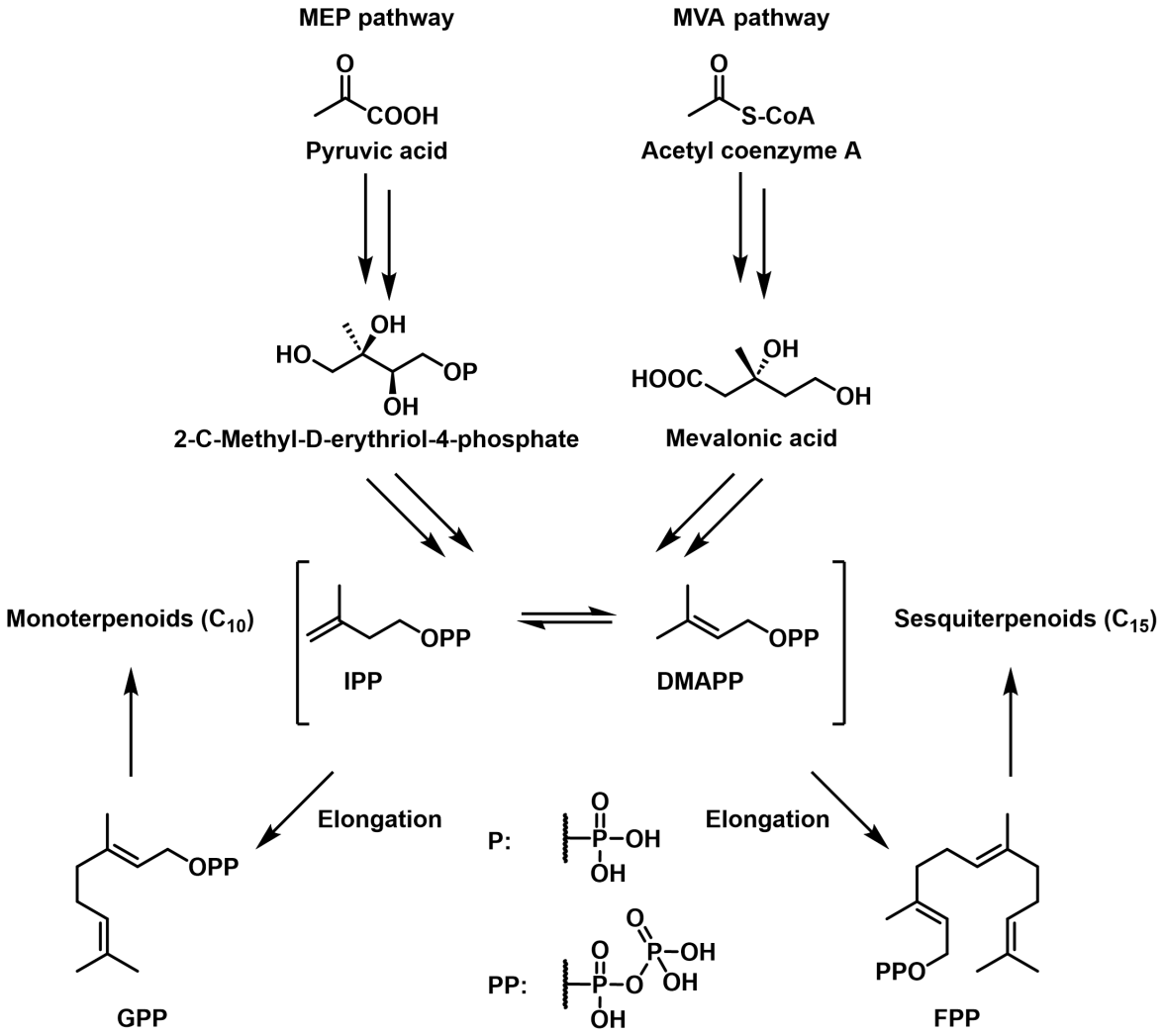

Scheme 9: Terpenoid biosynthesis. Reprinted and adapted from *Pharmacognosy*, Ludwiczuk, A.; Skalicka-Wozniak, K.; Georgiev, M. I., Terpenoids, Page 235, Copyright 2016, with permission from Elsevier.[101]

Direct extraction of terpenoids from plants is not always economically feasible, and it is important to avoid competition between their use for chemicals and food. Instead, microbial systems, using genetically modified fermentative organisms, offer an alternative by synthesizing terpenoids in cell factories. This approach enables large-scale production under controlled conditions, optimizing space efficiency and neutralizing dependence on seasonal or geographical factors. As a result, microbial production presents a sustainable, ecological, and cost-effective alternative to plant-based terpenoid extraction in the future.[103,104]

Nature offers a plethora of terpenoid structures, including saturated, unsaturated, cyclic, linear, and aromatic forms, many of which contain functional groups and vary in molar mass. This versatility can be utilized to create novel (multi)functional materials through AROP using bio-based monomers. Terpenyl glycidyl ethers represent a scarcely investigated monomer class that exhibits unexplored potential for polyethers. Farnesyl glycidyl ether (FarGE) was recently studied in depth for its copolymerization with EO. The properties of the resulting amphiphilic statistical and block copolymers were also thoroughly investigated.[74] Several commercially available terpenoid alcohols offer the potential for producing glycidyl ethers, positioning them as viable bio-based alternatives to PO.

Bio-based glycidyl ethers offer versatile, sustainable alternatives in polymer synthesis, reducing dependency on fossil-based resources. These renewable monomers enable the creation of tunable materials. Expanding their applications through copolymerization and modification marks a critical step toward a greener chemical industry and more sustainable materials.

References

(1) Herzberger, J.; Niederer, K.; Pohlit, H.; Seiwert, J.; Worm, M.; Wurm, F. R.; Frey, H. Polymerization of Ethylene Oxide, Propylene Oxide, and Other Alkylene Oxides: Synthesis, Novel Polymer Architectures, and Bioconjugation. *Chem. Rev.* **2016**, *116* (4), 2170–2243. DOI: 10.1021/acs.chemrev.5b00441.

(2) Souto, E. B.; Silva, G. F.; Dias-Ferreira, J.; Zielinska, A.; Ventura, F.; Durazzo, A.; Lucarini, M.; Novellino, E.; Santini, A. Nanopharmaceutics: Part I-Clinical Trials Legislation and Good Manufacturing Practices (GMP) of Nanotherapeutics in the EU. *Pharmaceutics* **2020**, *12* (2). DOI: 10.3390/pharmaceutics12020146.

(3) Dingels, C.; Schömer, M.; Frey, H. Die vielen Gesichter des Poly(ethylenglykol)s. *Chem. Unserer Zeit* **2011**, *45* (5), 338–349. DOI: 10.1002/ciuz.201100551.

(4) Penczek, S.; Kubisa, P.; Matyjaszewski, K. *Cationic ring-opening polymerization of hetero-cyclic monomers*; Advances in Polymer Science, Vol. 37; Springer.

(5) Chen, S.; Xu, N.; Shi, J. Structure and properties of polyether polyols catalyzed by Fe/Zn double metal cyanide complex catalyst. *Prog. Org. Coat.* **2004**, *49* (2), 125–129. DOI: 10.1016/j.porgcoat.2003.08.021.

(6) Sustainable Development, Poverty Eradication and Reducing Inequalities. In *Global Warming of 1.5°C*; IPCC, Ed.; Cambridge University Press, 2022; pp 445–538. DOI: 10.1017/9781009157940.007.

(7) Allen, M. R.; Friedlingstein, P.; Girardin, C. A.; Jenkins, S.; Malhi, Y.; Mitchell-Larson, E.; Peters, G. P.; Rajamani, L. Net Zero: Science, Origins, and Implications. *Annu. Rev. Environ. Resour.* **2022**, *47* (1), 849–887. DOI: 10.1146/annurev-environ-112320-105050.

(8) Clariant. *Clariant launches 100% bio-based surfactants range driving the transition towards renewable carbon*. https://www.clariant.com/en/Corporate/News/2022/02/Clariant-launches-100-biobased-surfactants-range-driving-the-transition-towards-renewable-carbon.

(9) Wurtz, A. Ueber das Aethylenoxyd. *Justus Liebigs Ann. Chem.* **1859**, *110* (1), 125–128. DOI: 10.1002/jlac.18591100116.

(10) Wurtz, A. Neue Untersuchungen über das Aethylenoxyd. *Justus Liebigs Ann. Chem.* **1860**, *116* (2), 249–252. DOI: 10.1002/jlac.18601160212.

(11) Wurtz, A. Synthese des Glycols aus Aethylenoxyd und Wasser. *Justus Liebigs Ann. Chem.* **1860**, *113* (2), 255–256. DOI: 10.1002/jlac.18601130218.

(12) Lourenço, A. V. Intermediäre Aether des Glykols. *J. Prakt. Chem.* **1860**, *79* (1), 212–213. DOI: 10.1002/prac.18600790130.

(13) Lourenço, A. V. Ueber die Polyäthylenalkohole. *J. Prakt. Chem.* **1862**, *85* (1), 389–392. DOI: 10.1002/prac.18620850149.

(14) Staudinger, H.; Schweitzer, O. Über hochpolymere Verbindungen, 20. Mitteil.: Über die Poly‐äthylenoxyde. *Ber. dtsch. Chem. Ges. A/B* **1929**, *62* (8), 2395–2405. DOI: 10.1002/cber.19290620879.

(15) Pinaeva, L. G.; Noskov, A. S. Prospects for the Development of Ethylene Oxide Production Catalysts and Processes (Review). *Pet. Chem.* **2020**, *60* (11), 1191–1206. DOI: 10.1134/S096554412011016X.

(16) French, A. C.; Thompson, A. L.; Davis, B. G. High-purity discrete PEG-oligomer crystals allow structural insight. *Angew. Chem. Int. Ed.* **2009**, *48* (7), 1248–1252. DOI: 10.1002/anie.200804623.

(17) Sedlák, M. Recent Advances in Chemistry and Applications of Substituted Poly(ethylene glycol)s. *Collect. Czech. Chem. Commun.* **2005**, *70* (3), 269–291. DOI: 10.1135/cccc20050269.

(18) Croce, F.; Appetecchi, G. B.; Persi, L.; Scrosati, B. Nanocomposite polymer electrolytes for lithium batteries. *Nature* **1998**, *394* (6692), 456–458. DOI: 10.1038/28818.

(19) Quartarone, E.; Mustarelli, P. Electrolytes for solid-state lithium rechargeable batteries: recent advances and perspectives. *Chem. Soc. Rev.* **2011**, *40* (5), 2525–2540. DOI: 10.1039/c0cs00081g.

(20) Lin, H.; Freeman, B. D. Materials selection guidelines for membranes that remove CO2 from gas mixtures. *J. Mol. Struct.* **2005**, *739* (1-3), 57–74. DOI: 10.1016/j.molstruc.2004.07.045.

(21) Juber, F. A. H.; Jawad, Z. A.; Chin, B. L. F.; Yeap, S. P.; Chew, T. L. The prospect of synthesis of PES/PEG blend membranes using blend NMP/DMF for CO2/N2 separation. *J. Polym. Res.* **2021**, *28* (5). DOI: 10.1007/s10965-021-02500-6.

(22) Brandrup, J., Ed. *Polymer handbook*, 4. ed.; Wiley, 1999.

(23) Kjellander, R.; Florin, E. Water structure and changes in thermal stability of the system poly(ethylene oxide)–water. *J. Chem. Soc., Faraday Trans. 1* **1981**, *77* (9), 2053. DOI: 10.1039/f19817702053.

(24) Menzies, J.; Wilcox, A.; Casteel, K.; McDonough, K. Water soluble polymer biodegradation evaluation using standard and experimental methods. *Sci. Total. Environ.* **2022**, *858* (Pt 3), 160006. DOI: 10.1016/j.scitotenv.2022.160006.

(25) Veronese, F. M.; Pasut, G. PEGylation, successful approach to drug delivery. *Drug Discov. Today* **2005**, *10* (21), 1451–1458. DOI: 10.1016/S1359-6446(05)03575-0.

(26) Lasic, D. D.; Needham, D. The "Stealth" Liposome: A Prototypical Biomaterial. *Chem. Rev.* **1995**, *95* (8), 2601–2628. DOI: 10.1021/cr00040a001.

(27) Verhoef, J. J. F.; Carpenter, J. F.; Anchordoquy, T. J.; Schellekens, H. Potential induction of anti-PEG antibodies and complement activation toward PEGylated therapeutics. *Drug Discov. Today* **2014**, *19* (12), 1945–1952. DOI: 10.1016/j.drudis.2014.08.015.

(28) Deuker, M. F. S.; Mailänder, V.; Morsbach, S.; Landfester, K. Anti-PEG antibodies enriched in the protein corona of PEGylated nanocarriers impact the cell uptake. *Nanoscale Horiz.* **2023**, *8* (10), 1377–1385. DOI: 10.1039/d3nh00198a.

(29) Yang, Q.; Jacobs, T. M.; McCallen, J. D.; Moore, D. T.; Huckaby, J. T.; Edelstein, J. N.; Lai, S. K. Analysis of Pre-existing IgG and IgM Antibodies against Polyethylene Glycol (PEG) in the General Population. *Anal. Chem.* **2016**, *88* (23), 11804–11812. DOI: 10.1021/acs.analchem.6b03437.

(30) Sivasankaran, R. P.; Snell, K.; Kunkel, G.; Georgiou, P. G.; Puente, E. G.; Maynard, H. D. Polymer-mediated protein/peptide therapeutic stabilization: Current progress and future directions. *Prog. Polym. Sci.* **2024**, *156*, 101867. DOI: 10.1016/j.progpolymsci.2024.101867.

(31) Brocas, A.-L.; Mantzaridis, C.; Tunc, D.; Carlotti, S. Polyether synthesis: From activated or metal-free anionic ring-opening polymerization of epoxides to functionalization. *Prog. Polym. Sci.* **2013**, *38* (6), 845–873. DOI: 10.1016/j.progpolymsci.2012.09.007.

(32) Pyatakov, D. A.; Nifant'ev, I. E. Double Metal Cyanide (DMC) Catalysts: Synthesis, Structure, and Action Mechanism (A Review). *Pet. Chem.* **2023**, *63* (10), 1170–1193. DOI: 10.1134/S0965544123090074.

(33) Penczek, S.; Pretula, J. B. Ring-Opening Polymerization. In *Reference Module in Chemistry, Molecular Sciences and Chemical Engineering*; Elsevier, 2016. DOI: 10.1016/B978-0-12-409547-2.11351-4.

(34) Kobayashi, S.; Morikawa, K.; Saegusa, T. Superacids and Their Derivatives. X. Mechanistic Studies of Selective Cyclodimerization of Ethylene Oxide by Superacid Ester Catalysts. *Polym. J.* **1979**, *11* (5), 405–412. DOI: 10.1295/polymj.11.405.

(35) Dudev, T.; Lim, C. Ring Strain Energies from ab Initio Calculations. *J. Am. Chem. Soc.* **1998**, *120* (18), 4450–4458. DOI: 10.1021/ja973895x.

(36) Penczek, S.; Pretula, J.; Lewiński, P. Dormant Polymers and Their Role in Living and Controlled Polymerizations; Influence on Polymer Chemistry, Particularly on the Ring Opening Polymerization. *Polymers* **2017**, *9* (12). DOI: 10.3390/polym9120646.

(37) Mark, H. F., Ed. *Encyclopedia of Polymer Science and Engineering*, 2. ed.; A Wiley Interscience publication; Wiley, 1985.

(38) Pearson, R. G. Hard and Soft Acids and Bases. *J. Am. Chem. Soc.* **1963**, *85* (22), 3533–3539. DOI: 10.1021/ja00905a001.

(39) Herman, M. F. *Encyclopedia of polymer science and technology*, 3rd ed.; Wiley-Interscience, 2004.

(40) Boileau, S. Use of Cryptates in Anionic Polymerization of Heterocyclic Compounds. In *Anionic Polymerization*:*Kinetics, Mechanisms, and Synthesis*; McGrath, J. E., Ed.; ACS symposium series; American Chemical Society, 1981; pp 283–305. DOI: 10.1021/bk-1981-0166.ch019.

(41) Wojtech, V. B. Zur Darstellung hochmolekularer Polyäthylenoxyde. *Makromol. Chem.* **1963**, *66* (1), 180–195. DOI: 10.1002/macp.1963.020660118.

(42) Kazanskii, K. S.; Solovyanov, A. A.; Entelis, S. G. Polymerization of ethylene oxide by alkali metal-naphthalene complexes in tetrahydrofuran. *Eur. Polym. J.* **1971**, *7* (10), 1421–1433. DOI: 10.1016/0014-3057(71)90036-X.

(43) Bessonov, V. A.; Alikhanov, P. P.; Gur'yanova, E. N.; Simonov, A. P.; Shapiro, I. O.; Yakovleva, E. A.; Shatenshtein, A. I. Studies of solvent capacity of ethers by means of hydrogen isotopic exchange:IV. Physicochemical properties of lithium and potassium tert.-butylates in dimethyl sulphoxides and hydrocarbons. *Zh. obshch. Khim.* **1967**, *37* (109).

(44) Figueruelo, J. E.; Worsfold, D. J. The anionic polymerization of ethylene oxide in hexamethyl phosphoramide. *Eur. Polym. J.* **1968**, *4* (4), 439–444. DOI: 10.1016/0014-3057(68)90062-1.

(45) Deffieux, A.; Carlotti, S.; Barrère, A. Anionic Ring-Opening Polymerization of Epoxides and Related Nucleophilic Polymerization Processes. In *Polymer Science*:*A comprehensive reference*; Matyjaszewski, K., Möller, M., Eds.; Elsevier, 2012; pp 117–140. DOI: 10.1016/B978-0-444-53349-4.00099-6.

(46) Szwarc, M. *Carbanions, living polymers, and electron transfer processes*; Interscience Publishers, 1968.

(47) Duda, A.; Penczek, S. Determination of the Absolute Propagation Rate Constants in Polymerization with Reversible Aggregation of Active Centers. *Macromolecules* **1994**, *27* (18), 4867–4870. DOI: 10.1021/ma00096a002.

(48) Duda, A.; Kowalski, A. Thermodynamics and Kinetics of Ring-Opening Polymerization. In *Handbook of Ring-Opening Polymerization*; Dubois, P., Coulembier, O., Raquez, J.-M., Eds.; Wiley, 2009; pp 1–51. DOI: 10.1002/9783527628407.ch1.

(49) Patat, V. F.; Wojtech, B. Die Kondensation von Äthylenoxyd an Phenol. *Makromol. Chem.* **1960**, *37* (1), 1–18. DOI: 10.1002/macp.1960.020370101.

(50) Gladkovskii, G. A.; Ryzhenkova, Y. Anionic copolymerization reactions of ethylene oxide and propylene oxide. *Polym. Sci. U.S.S.R.* **1971**, *13* (3), 723–730. DOI: 10.1016/0032-3950(71)90038-4.

(51) Lebedev, N. N.; Savel'yanov, V. P.; Baranov, Y. I.; Shvets, V. F. Reactivity and the role of specific solvation in the base-catalysis reactions of ethylene oxide. *Theor. Exp. Chem.* **1971**, *4* (2), 128–133. DOI: 10.1007/BF00525572.

(52) Penczek, S.; Cypryk, M.; Duda, A.; Kubisa, P.; Slomkowski, S. Living ring-opening polymerizations of heterocyclic monomers. *Prog. Polym. Sci.* **2007**, *32* (2), 247–282. DOI: 10.1016/j.progpolymsci.2007.01.002.

(53) Solov'yanov, A. A.; Kazanskii, K. S. Polymerization of ethylene oxide in dimethyl sulphoxide (DMS). *Polym. Sci. U.S.S.R.* **1972**, *14* (5), 1196–1206. DOI: 10.1016/0032-3950(72)90163-3.

(54) Matyjaszewski, K.; Möller, M., Eds. *Polymer Science*:*A comprehensive reference*; Elsevier, 2012.

(55) Fusco, S.; Borzacchiello, A.; Netti, P. A. Perspectives on: PEO-PPO-PEO Triblock Copolymers and their Biomedical Applications. *J. Bioact. Compat. Polym.* **2006**, *21* (2), 149–164. DOI: 10.1177/0883911506063207.

(56) Price, C. C. Polyethers. *Acc. Chem. Res.* **1974**, *7* (9), 294–301. DOI: 10.1021/ar50081a003.

(57) Quirk, R. P.; Lizarraga, G. M. Anionic synthesis of well-defined, poly[(styrene)-*block*-(propylene oxide)] block copolymers. *Macromol. Chem. Phys.* **2000**, *201* (13), 1395–1404. DOI: 10.1002/1521-3935(20000801)201:13<1395:AID-MACP1395>3.0.CO;2-H.

(58) Gee, G.; Higginson, W. C. E.; Levesley, P.; Taylor, K. J. 266. Polymerisation of epoxides. Part I. Some kinetic aspects of the addition of alcohols to epoxides catalysed by sodium alkoxides. *J. Chem. Soc.* **1959** (0), 1338. DOI: 10.1039/JR9590001338.

(59) Yu, G.-E.; Masters, A. J.; Heatley, F.; Booth, C.; Blease, T. G. Anionic polymerisation of propylene oxide. Investigation of double ‑ bond and head ‑ to ‑ head content by NMR spectroscopy. *Macromol. Chem. Phys.* **1994**, *195* (5), 1517–1538. DOI: 10.1002/macp.1994.021950506.

(60) Flory, P. J. Molecular Size Distribution in Ethylene Oxide Polymers. *J. Am. Chem. Soc.* **1940**, *62* (6), 1561–1565. DOI: 10.1021/ja01863a066.

(61) Luscombe, C. K.; Moad, G.; Hiorns, R. C.; Jones, R. G.; Keddie, D. J.; Matson, J. B.; Merna, J.; Nakano, T.; Russell, G. T.; Topham, P. D. A brief guide to polymerization terminology (IUPAC Technical Report). *Pure Appl. Chem.* **2022**, *94* (9), 1079–1084. DOI: 10.1515/pac-2021-0115.

(62) Odian, G. *Principles of Polymerization (Fourth Edition)*, 4th ed.; Wiley-Interscience, 2004. DOI: 10.1002/047147875X.

(63) Jong, E. de; Higson, A.; Walsh, P.; Wellisch, M. *Bio-based Chemicals*:*Value Added Products from Biorefineries*. http://www.ieabioenergy.com/wp-content/uploads/2013/10/Task-42-Biobased-Chemicals-value-added-products-from-biorefineries.pdf.

(64) BASF. *Bioethanol*:*New catalyst geometry poised to re-shape the ethanol-to-ethylene conversion process*. https://chemicals.basf.com/global/en/Catalysts/hydrogenation-specialty/products-we-offer/alumina/Ethanol-to-Ethylene-E2E.html.

(65) Zhang, M.; Yu, Y. Dehydration of Ethanol to Ethylene. *Ind. Eng. Chem. Res.* **2013**, *52* (28), 9505–9514. DOI: 10.1021/ie401157c.

(66) Lucky, C.; Wang, T.; Schreier, M. Electrochemical Ethylene Oxide Synthesis from Ethanol. *ACS Energy Lett.* **2022**, *7* (4), 1316–1321. DOI: 10.1021/acsenergylett.2c00265.

(67) Li, Y.; Ozden, A.; Leow, W. R.; Ou, P.; Huang, J. E.; Wang, Y.; Bertens, K.; Xu, Y.; Liu, Y.; Roy, C.; Jiang, H.; Sinton, D.; Li, C.; Sargent, E. H. Redox-mediated electrosynthesis of ethylene oxide from CO_2 and water. *Nat. Catal.* **2022**, *5* (3), 185–192. DOI: 10.1038/s41929-022-00749-8.

(68) Verkoyen, P.; Frey, H. Long-Chain Alkyl Epoxides and Glycidyl Ethers: An Underrated Class of Monomers. *Macromol. Rapid Commun.* **2020**, *41* (15). DOI: 10.1002/marc.202000225.

(69) Liu, F.; Frere, Y.; Francois, J. Association properties of poly(ethylene oxide) modified by pendant aliphatic groups. *Polymer* **2001**, *42* (7), 2969–2983. DOI: 10.1016/S0032-3861(00)00530-9.

(70) Holzmüller, P.; Gardiner, C.; Preis, J.; Frey, H. CO_2-Based Polycarbonates with Low Glass Transition Temperatures Sourced from Long-Chain Terpenes. *Macromolecules* **2024**, *57* (11), 5358–5367. DOI: 10.1021/acs.macromol.4c00349.

(71) Holzmüller, P.; Preis, J.; Frey, H. CO_2-based polycarbonates from biobased cyclic terpenes with end-of-life usage potential. *Polym. Chem.* **2024**, *15* (36), 3657–3666. DOI: 10.1039/D4PY00797B.

(72) Schüttner, S.; Gardiner, C.; Petrov, F. S.; Fotaras, N.; Preis, J.; Floudas, G.; Frey, H. Biobased Thermoplastic Elastomers Derived from Citronellyl Glycidyl Ether, CO_2, and Polylactide. *Macromolecules* **2023**, *56* (20), 8247–8259. DOI: 10.1021/acs.macromol.3c01329.

(73) Mouzin, G.; Cousse, H.; Rieu, J.-P.; Duflos, A. A Convenient One-Step Synthesis of Glycidyl Ethers. *Synthesis* **1983**, *1983* (02), 117–119. DOI: 10.1055/s-1983-30243.

(74) Schüttner, S.; Krappel, M.; Koziol, M.; Marquart, L.; Schneider, I.; Sottmann, T.; Frey, H. Anionic Ring-Opening Copolymerization of Farnesyl Glycidyl Ether: Fast Access to Terpenoid-Derived Amphiphilic Polyether Architectures. *Macromolecules* **2023.** DOI: 10.1021/acs.macromol.3c00999.

(75) Johann, T.; Houck, H. A.; Dinh, T.; Kemmer-Jonas, U.; Du Prez, F. E.; Frey, H. Multi-olefin containing polyethers and triazolinediones: a powerful alliance. *Polym. Chem.* **2019**, *10* (34), 4699–4708. DOI: 10.1039/C9PY00718K.

(76) Gu, X.-P.; Ikeda, I.; Okahara, M. Stereoselective Formation of Allyl Ethers by Reaction of Epoxides with Organic Chlorides under Liquid-Solid Phase-Transfer Catalysis. *Bull. Chem. Soc. Jpn.* **1987**, *60* (2), 667–672. DOI: 10.1246/bcsj.60.667.

(77) Brückner, R. *Reaktionsmechanismen*:*Organische Reaktionen, Stereochemie, moderne Synthesemethoden*, 3. Auflage, Nachdruck 2015; Lehrbuch; Springer Spektrum, 2004.

(78) Solvay. *Solvay Epicerol® Earns Roundtable on Sustainable Biomaterials Certification*. https://www.solvay.com/sites/g/files/srpend221/files/tridion/documents/17_RSB%20Certificate_Final.pdf (accessed 2022-09-09).

(79) Bell, B. M.; Briggs, J. R.; Campbell, R. M.; Chambers, S. M.; Gaarenstroom, P. D.; Hippler, J. G.; Hook, B. D.; Kearns, K.; Kenney, J. M.; Kruper, W. J.; Schreck, D. J.; Theriault, C. N.; Wolfe, C. P. Glycerin as a Renewable Feedstock for Epichlorohydrin Production. The GTE Process. *Clean* **2008**, *36* (8), 657–661. DOI: 10.1002/clen.200800067.

(80) Meng, Y.; Taddeo, F.; Aguilera, A. F.; Cai, X.; Russo, V.; Tolvanen, P.; Leveneur, S. The Lord of the Chemical Rings: Catalytic Synthesis of Important Industrial Epoxide Compounds. *Catalysts* **2021**, *11* (7), 765. DOI: 10.3390/catal11070765.

(81) Biermann, U.; Bornscheuer, U.; Meier, M. A. R.; Metzger, J. O.; Schäfer, H. J. Oils and fats as renewable raw materials in chemistry. *Angew. Chem. Int. Ed.* **2011**, *50* (17), 3854–3871. DOI: 10.1002/anie.201002767.

(82) Biermann, U.; Bornscheuer, U. T.; Feussner, I.; Meier, M. A. R.; Metzger, J. O. Fatty Acids and their Derivatives as Renewable Platform Molecules for the Chemical Industry. *Angew. Chem. Int. Ed.* **2021**, *60*, 20144–20165. DOI: 10.1002/anie.202100778.

(83) Noweck, K.; Grafahrend, W. Fatty Alcohols. In *Ullmann's Encyclopedia of Industrial Chemistry*; Wiley-VCH Verlag GmbH & Co. KGaA, 2000. DOI: 10.1002/14356007.a10_277.pub2.

(84) Baumann, H.; Bühler, M.; Fochem, H.; Hirsinger, F.; Zoebelein, H.; Falbe, J. Natural Fats and Oils—Renewable Raw Materials for the Chemical Industry. *Angew. Chem. Int. Ed. Engl.* **1988**, *27* (1), 41–62. DOI: 10.1002/anie.198800411.

(85) ISTA Mielke GmbH. *Oil World Annual 2020*, Hamburg, 2020.

(86) Tadros, T. F. *Encyclopedia of physical science and technology*, 3. ed.; Acad. Press, San Diego, 2002.

(87) Liu, X.; Sheng, J.; Curtiss, R. Fatty acid production in genetically modified cyanobacteria. *Proc. Natl. Acad. Sci. U.S.A* **2011**, *108* (17), 6899–6904. DOI: 10.1073/pnas.1103014108.

(88) Yan, J.; Yan, Y.; Madzak, C.; Han, B. Harnessing biodiesel-producing microbes: from genetic engineering of lipase to metabolic engineering of fatty acid biosynthetic pathway. *Crit. Rev. Biotechnol.* **2017**, *37* (1), 26–36. DOI: 10.3109/07388551.2015.1104531.

(89) Lu, X. A perspective: Photosynthetic production of fatty acid-based biofuels in genetically engineered cyanobacteria. *Biotechnol. Adv.* **2010**, *28* (6), 742–746. DOI: 10.1016/j.biotechadv.2010.05.021.

(90) Habermehl, G.; Hammann, P. E.; Krebs, H. C.; Ternes, W. *Naturstoffchemie*; Springer Berlin Heidelberg, 2008. DOI: 10.1007/978-3-540-73733-9.

(91) Hoyle, C. E.; Lowe, A. B.; Bowman, C. N. Thiol-click chemistry: a multifaceted toolbox for small molecule and polymer synthesis. *Chem. Soc. Rev.* **2010**, *39* (4), 1355–1387. DOI: 10.1039/b901979k.

(92) Lowe, A. B. Thiol–ene “click” reactions and recent applications in polymer and materials synthesis: a first update. *Polym. Chem.* **2014**, *5* (17), 4820–4870. DOI: 10.1039/C4PY00339J.

(93) Türünç, O.; Billiet, S.; Bruycker, K. de; Ouardad, S.; Winne, J.; Du Prez, F. E. From plant oils to plant foils: Straightforward functionalization and crosslinking of natural plant oils with triazolinediones. *Eur. Polym. J.* **2015**, *65*, 286–297. DOI: 10.1016/j.eurpolymj.2014.12.013.

(94) Tremblay-Parrado, K.-K.; García-Astrain, C.; Avérous, L. Click chemistry for the synthesis of biobased polymers and networks derived from vegetable oils. *Green Chem.* **2021**, *23* (12), 4296–4327. DOI: 10.1039/d1gc00445j.

(95) Lee, D. G.; Chen, T. Cleavage Reactions. In *Comprehensive Organic Synthesis*; Trost, B. M., Fleming, I., Eds.; Elsevier, 1991; pp 541–591. DOI: 10.1016/B978-0-08-052349-1.00202-X.

(96) García-Franco, A.; Godoy, P.; La Torre, J. de; Duque, E.; Ramos, J. L. United Nations sustainability development goals approached from the side of the biological production of fuels. *Microb. Biotechnol.* **2021**, *14* (5), 1871–1877. DOI: 10.1111/1751-7915.13912.

(97) Hill, J.; Nelson, E.; Tilman, D.; Polasky, S.; Tiffany, D. Environmental, economic, and energetic costs and benefits of biodiesel and ethanol biofuels. *Proc. Natl. Acad. Sci. U.S.A* **2006**, *103* (30), 11206–11210. DOI: 10.1073/pnas.0604600103.

(98) Thangaraj, B.; Solomon, P. R. Scope of biodiesel from oils of woody plants: a review. *Clean Energy* **2020**, *4* (2), 89–106. DOI: 10.1093/ce/zkaa006.

(99) Tuck, C. O.; Pérez, E.; Horváth, I. T.; Sheldon, R. A.; Poliakoff, M. Valorization of biomass: deriving more value from waste. *Science (New York, N.Y.)* **2012**, *337* (6095), 695–699. DOI: 10.1126/science.1218930.

(100) Nuhn, P. *Naturstoffchemie*:*Mikrobielle, pflanzliche und tierische Naturstoffe*, 4., neu bearb. Aufl.; Hirzel, 2006.

(101) Ludwiczuk, A.; Skalicka-Woźniak, K.; Georgiev, M. I. Terpenoids. In *Pharmacognosy*:*Fundamentals, Applications and Strategies*; Badal McCreath, S., Delgoda, R., Eds.; Elsevier Science, 2016; pp 233–266. DOI: 10.1016/B978-0-12-802104-0.00011-1.

(102) Nič, M.; Jirát, J.; Košata, B.; Jenkins, A.; McNaught, A. *IUPAC Compendium of Chemical Terminology*; IUPAC, 2009. DOI: 10.1351/goldbook.

(103) Tetali, S. D. Terpenes and isoprenoids: a wealth of compounds for global use. *Planta* **2019**, *249* (1), 1–8. DOI: 10.1007/s00425-018-3056-x.

(104) Carsanba, E.; Pintado, M.; Oliveira, C. Fermentation Strategies for Production of Pharmaceutical Terpenoids in Engineered Yeast. *Pharmaceuticals (Basel, Switzerland)* **2021**, *14* (4). DOI: 10.3390/ph14040295.

Chapter 2

Anionic Copolymerization of Epoxides and their Reactivity Ratios

2 Anionic Copolymerization of Epoxides and their Reactivity Ratios

Gregor M. Linden[1], [redacted]

[1]Department of Chemistry, Johannes Gutenberg University Mainz, Duesbergweg 10-14, 55128 Mainz, Germany.

[2]Graduate School Materials Science in Mainz, Staudingerweg 9, 55128 Mainz, Germany

G. M. L. and [redacted] equally contributed to this work.

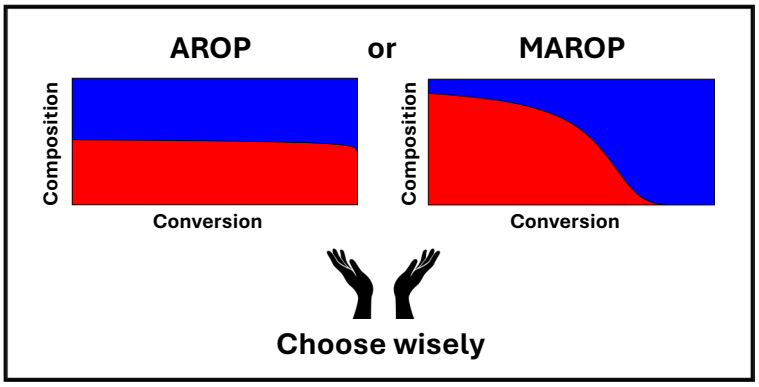

Abstract

Polyether copolymers hold significant interest in various applications, ranging from polyurethanes to lubricants. Their properties and applicability are highly dependent on their microstructure, which in batch copolymerizations is determined by the reactivity ratios of the comonomers. These ratios influence the copolymerization behavior and monomer sequence distribution, *i.e*. the monomer gradient along the polymer chains. This review summarizes experimental and theoretical approaches for determining reactivity ratios, based on key copolymerization models. NMR kinetic studies have provided insights into the copolymerization of binary systems. These involve functional epoxides through anionic ring-opening polymerization (AROP) and monomer-activated anionic ring-opening polymerization (MAROP), with a focus on the resulting microstructures. A broad range of epoxide monomers is covered including ethylene oxide, alkylene oxides, glycidyl ethers, glycidyl esters, and glycidyl amines, all contributing to the versatility of polyether copolymers.

Introduction

The recent decade has been marked by strongly increasing research regarding the control of monomer sequence and sequence statistics of copolymers and the resulting unique properties. Several reviews have provided an overview of the theory and potential applications of gradient polymers.[1–4] In this review article, we will focus on random, gradient, and block-like polyether copolymers relying on the anionic copolymerization of functional epoxide monomers in batch processes. Polyethers are of crucial importance for a vast number of commercial applications, ranging from surfactants, components of foam stabilizers, and lubricants to components of many medical and pharmaceutical products. Particular attention will be given to the determination of reactivity ratios using *in situ* techniques, as these parameters are crucial for understanding the resulting copolymer microstructure and consequently the properties of these materials. Following this, we will discuss the results of various kinetic studies on anionic epoxide copolymerizations, focusing on the microstructure of the multifunctional polymers produced. Ring-opening epoxide polymerization has seen a renaissance in recent years due to the emergence of novel borane catalysts. Copolymerizations with borane catalysts are not well explored and often focus on copolymerization with non-epoxide comonomers. For further information, we refer to the reviews of Naumann and Feng *et al*.[5,6] In this review, we will focus on epoxide copolymerization and leave out the emerging borane catalysis, as well as the established double metal cyanide (DMC) catalysis topic. This work has already been partly published in a dissertation.[7]

The Relevance of Microstructure

The reactivity ratios of the comonomers determine the microstructure of the copolymer. Staudinger observed the influence of monomer reactivity on composition drift as early as the 1930s.[8] Comonomer pairs exhibiting a gradient structure in spontaneous batch polymerization are often not disadvantageous, as this strongly depends on the desired properties of the copolymer. Different applications and examples will be discussed later. The reactivity ratios are derived from the reaction constants of the four possible propagation steps:[9]

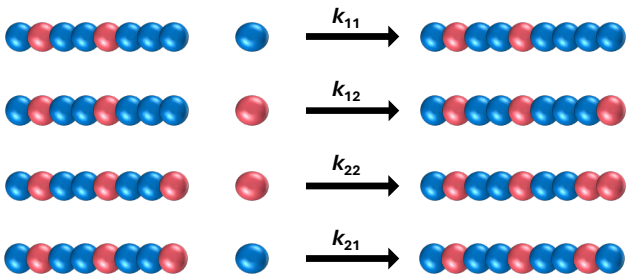

Figure 1: Schematic representation of the four propagation steps. The blue and red balls depict different monomer units (blue = monomer 1, red = monomer 2). The constants *k* represent the respective homo- and crosspropagation.

The reaction rates *R* for the four possible steps are therefore defined as:

$$R_{11} = k_{11}[\mathrm{M}_1^*][\mathrm{M}_1] \quad (1)$$

$$R_{12} = k_{12}[\mathrm{M}_1^*][\mathrm{M}_2] \quad (2)$$

$$R_{22} = k_{22}[\mathrm{M}_2^*][\mathrm{M}_2] \quad (3)$$

$$R_{21} = k_{21}[\mathrm{M}_2^*][\mathrm{M}_1] \quad (4)$$

With $[\mathrm{M_x}]$: concentration of the monomer x, $[\mathrm{M_x}^*]$: concentration of the M_x active chain end. By mathematical conversion,[9,10] one derives the following parameters, even without assuming a constant active chain end concentration (the so-called "steady-state" assumption):[11]

$$r_1 = \frac{k_{11}}{k_{12}} \quad (5)$$

$$r_2 = \frac{k_{22}}{k_{21}} \quad (6)$$

The reactivity ratios express the tendency of an active chain end to react with the same monomer as the active chain end or the other monomer. Detailed discussions can be found in several textbooks.[9,12–15] Methods to determine the reactivity ratios will be discussed in a later section.

Harrison *et al*. summarized the key synthetic approaches for preparing gradient copolymers using controlled radical techniques. All polymerization techniques can essentially be categorized into four classes: forced, stepwise, tandem catalysis, or spontaneous polymerization.[4] The latter involves

batch copolymerization with a comonomer pair having distinct reactivity ratios. In the absence of azeotropic points or when random copolymerization does not occur, the composition will change continuously, resulting in gradient copolymers, provided that high conversion is achieved. Knowing these parameters is imperative to manipulate the "natural" gradient occurring in batch polymerization due to the reactivity ratios. Allgaier *et al*. demonstrated that the gradient profile typically observed in the batch polymerization of ethylene oxide and butylene oxide can be flattened by the stepwise slow addition of both monomers.[16]

The terms "statistical", "random", "gradient" and "tapered" are sometimes used in the wrong manner. Statistical copolymerization means that the sequential distribution of monomer units of the resulting copolymer obeys known statistical laws, e.g. Markovian statistics.[17,18] This means, that random, gradient, tapered, and alternating copolymers are all statistical copolymers. However, the term "random" is inconsistently used in several publications and textbooks. IUPAC defines random copolymers in the following terms: "If the product of r_1 and r_2 is 1, then the probability of finding a given monomer unit at any given site in a macromolecule chain is independent of the nature of the adjacent units and the copolymer is called a random copolymer."[19] This is the case if $k_{11} = k_{21}$ and $k_{22} = k_{12}$, often denoted as "nonterminal", "ideal", or "chain-end independent" copolymerization. Though all terms are correct, the term "random" is recommended by the IUPAC. Random means the last added monomer does not influence the monomer addition probability of both monomers (Bernoulli or Markov zero-order statistics). Thereby, the monomer addition is "random" regarding the active chain end. However, the monomers can still exhibit different reactivities ($r_1 = r_2^{-1}$).[9,18–20] The term "ideal" cannot be referred to as a desired property, as this just comes from its agreement with the differential equations describing the boiling of a mixture of liquids which obey Raoult's law.[21,22] The properties of copolymers with the reactivity ratios $r_1 \cdot r_2 = 1$ can vary significantly depending on the specific reactivity ratios. For instance, in the hypothetical cases of $r_1 = 0.01$, $r_2 = 100$, and $r_1 = 1$, $r_2 = 1$, both yield a product of $r_1 \cdot r_2 = 1$, but the former behaves more like a block copolymer and will exhibit different properties compared to the latter. The relationship can be easily condensed in the following equations:

$$r_1 = r_2 = 1 \Rightarrow r_1 r_2 = 1 \quad (7)$$

$$r_1 r_2 = 1 \not\Rightarrow r_1 = r_2 = 1 \quad (8)$$

To the best of our knowledge, IUPAC currently provides no more appropriate terminology to demarcate the cases $r_1 \cdot r_2 = 1$ and $r_1 = r_2 = 1$ from each other. The definitions of the IUPAC are summarized in Figure 2 with added reactivity ratios for the case of a binary copolymerization.

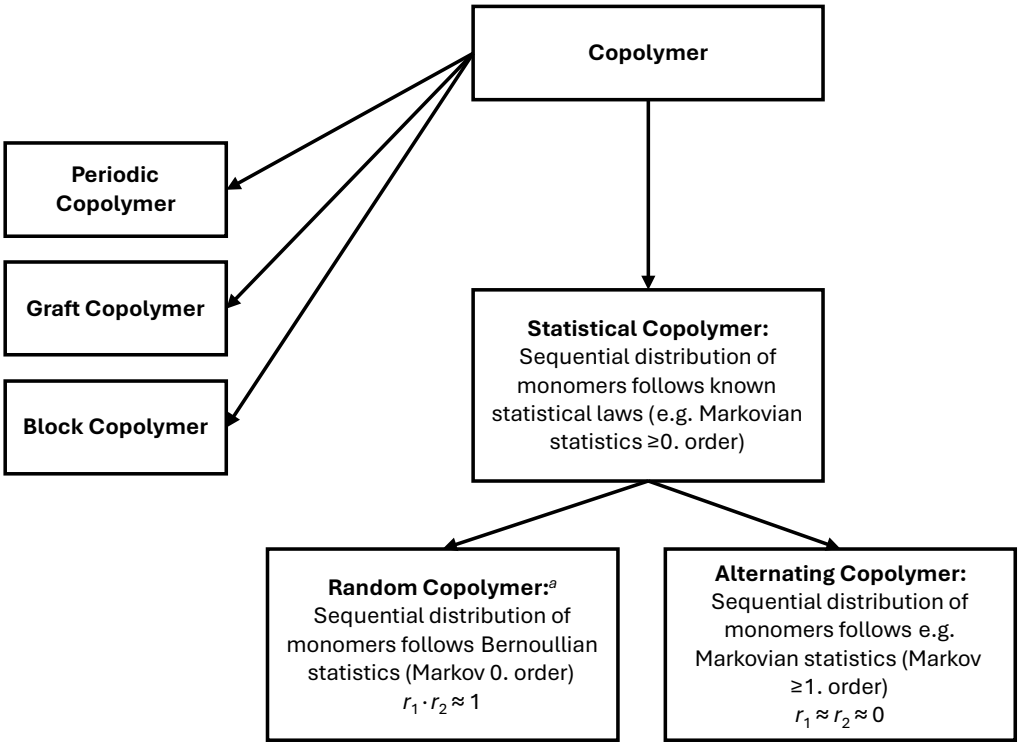

Figure 2: Definition of different types of copolymers according to IUPAC. Indices 1 and 2 follow no rules and can be assigned freely. Periodic copolymers are related to alternating copolymers, but not discussed here. [a]The term random is often interchanged with the term ideal, chain-end independent, or nonterminal, but all describe the relationship $r_1 \cdot r_2 \approx 1$.

However, that term is used in a different and often even vague manner by a vast variety of authors in textbooks and publications.[1,8,9,12,13,23–35] The term "random" is commonly understood as the special case $r_1 = r_2 = 1$. It denotes the random distribution of both monomer units throughout the copolymer chains. This interpretation appears more reasonable and is used throughout the review. To the case $r_1 \cdot r_2 = 1$ we will refer to as "ideal statistical copolymer". For brevity reasons, the term "ideal copolymer" is sufficient. The assignment of reactivity ratios towards the different types of copolymers is only reasonable for spontaneous batch copolymerizations. The kinetics of the comonomer addition cannot be suppressed, but by varying techniques, the forming copolymer can be modified during the copolymerization.[4] This means, that even if the reactivity ratios would indicate a statistical copolymer, a random copolymer can be obtained.[16] The IUPAC definitions are made from the position of spontaneous batch copolymerization but due to the emergence of controlled polymerization techniques, from our point of view, these definitions need to be redefined. We propose slight changes to the IUPAC definitions displayed in Figure 2 for spontaneous batch copolymerizations.

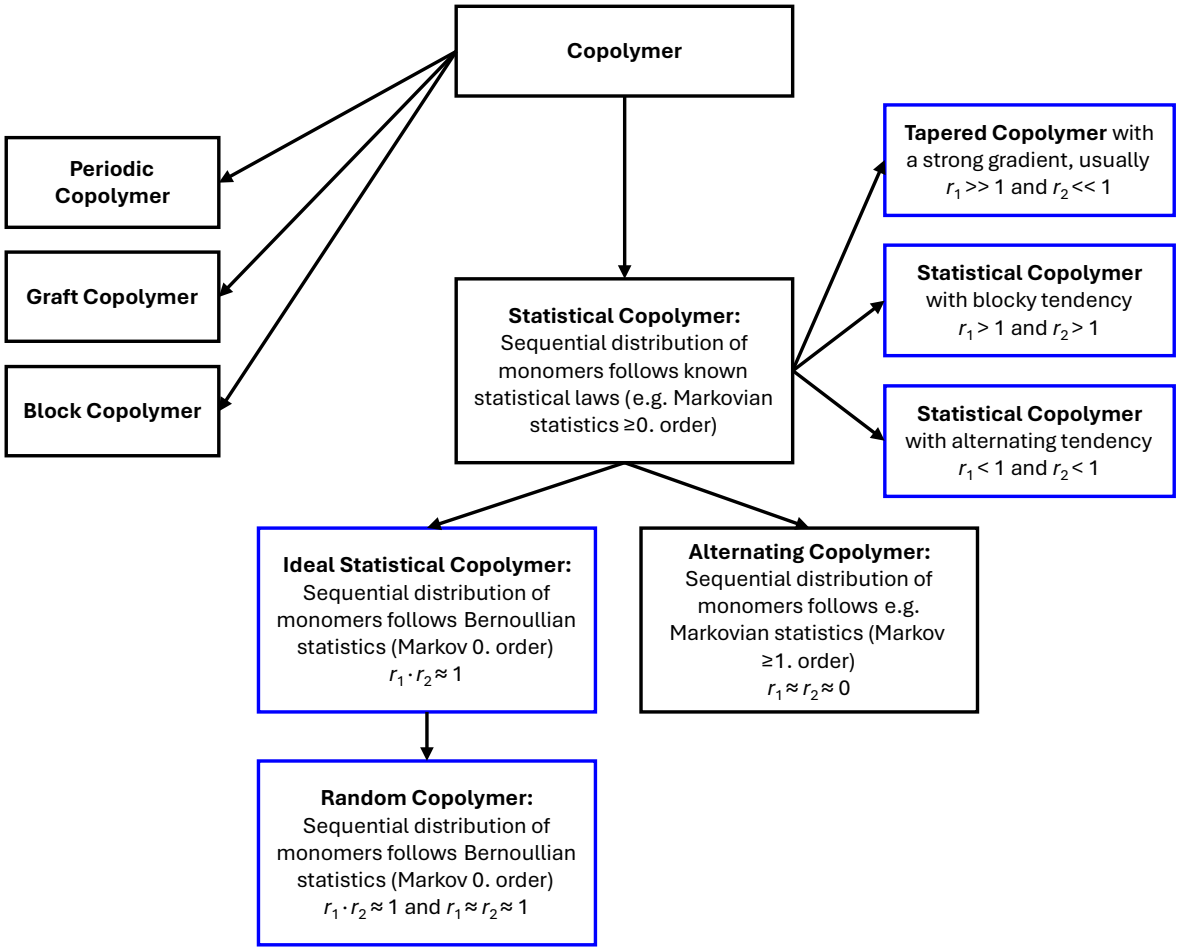

Figure 3: Definition of different types of copolymers according to our recommendation (blue borders) used in this review. Indices 1 and 2 follow no rules and can be assigned freely. Periodic copolymers are related to alternating copolymers, but not discussed here. The term ideal is also often denoted as chain-end independent, or nonterminal, but all describe the relationship $r_1 \cdot r_2 \approx 1$.

Gradient copolymers are available through living and various controlled copolymerization techniques, such as the controlled radical polymerization. Distinctive for this type of copolymers, is that their average chemical composition changes continuously along a certain section of the polymer chain.[36] Gradient copolymers are statistical copolymers with nonequal reactivity ratios, typically with $r_1 < 1$, $r_2 > 1$. Wurm *et al*. proposed defining a "soft gradient" by $r_1 \leq 2$, $r_2 \geq 0.5$.[37] However, it is worth noting that the hypothetical case, *e.g*. $r_1 = 2$, $r_2 = 5$ can also yield a copolymer with a soft gradient. In this case, the copolymer would show more consecutive monomer sequences, M_2 would be enriched at the beginning of the chain, and M_1 at the end. The same applies to the case when both reactivity ratios are below one. In Figure 3, these two special cases are denoted as statistical copolymers with either a blocky or alternating tendency, respectively. In contrast, the composition of block copolymers remains constant, until an abrupt transition occurs between the blocks, whereas random copolymers exhibit no change in composition along the

polymer chain at all.[1] Figure 4 schematically illustrates the composition of random, gradient, and block copolymers composed of two different monomers.

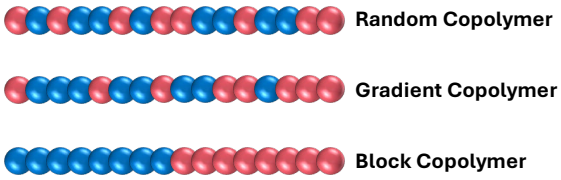

Figure 4: Schematic illustration of the monomer sequence in a random, gradient, and block copolymer consisting of two different monomers with equal composition (50 mol%). Adapted and reprinted with permission from Matyjaszewski *et al*.[1] Copyright © 2000 John Wiley & Sons, Ltd.

Impact of Reactivity Ratios on the Copolymer Microstructure

The so-called "copolymerization diagram" is a graphical representation of the differential copolymerization equation (21) in the interval of f_1 from 0 to 1. Its derivation is discussed in the section "Copolymerization Models". The copolymerization diagram shows graphically, which instantaneous copolymer composition results from a certain instantaneous comonomer feed. Furthermore, the composition drift always occurs along the curve in the copolymerization diagram. Exemplary copolymerization diagrams for ideal and non-ideal copolymerizations are shown in Figure 5.

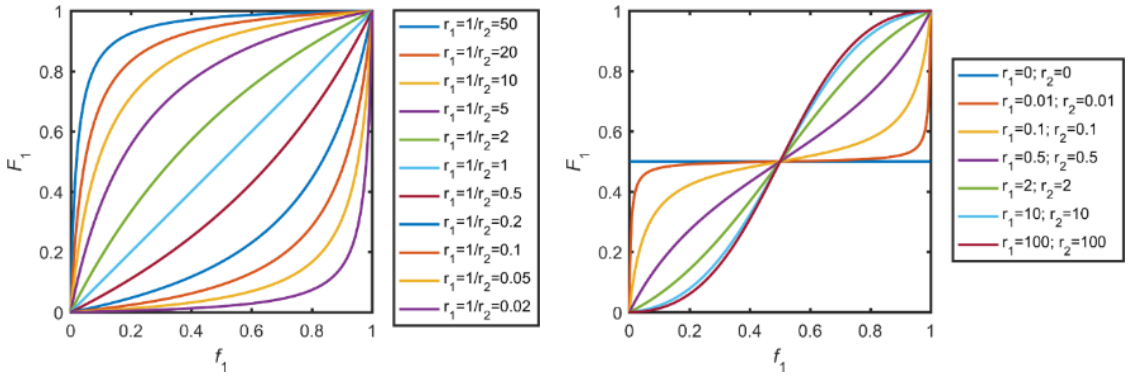

Figure 5: Copolymerization diagrams for different sets of reactivity ratios: ideal ($r_1 \cdot r_2 = 1$) copolymerization behavior (left) and non-ideal ($r_1 \cdot r_2 \neq 1$) behavior (right).

For non-ideal copolymerization, there are essentially two cases. If the product $r_1 \cdot r_2$ is below unity, the comonomer distribution in the polymer chain favors an alternating sequence. In the extreme case, where no homopropagation is possible for both comonomers, the reactivity ratios are equal to 0. In this case, the copolymerization diagram is a horizontal line with $F_1 = 0.5$. For every comonomer feed a copolymer with a strictly alternating monomer sequence is obtained which contains an equal amount of both comonomers. For large values of the $r_1 \cdot r_2$-product, the copolymers exhibit a tendency to form blocky structures. In the extreme case, only

homopolymerization of both comonomers occurs, and a polymer blend will form. However, this behavior is rarely observed, and most non-ideal systems show an alternating tendency. Non-ideal copolymerizations also show a so-called "azeotropic point" where $f_1 = F_1$. The term "azeotropic" again shows the similarity of the copolymerization equation with the vapor-liquid equilibria in ideal liquid mixtures.[9,22] At this point, the composition of the monomer feed and the forming copolymer is the same.[21]

In free radical copolymerization, for which the copolymerization models were originally developed, new chains are initiated and terminated throughout the copolymerization. Thus, the composition drift leads to an inhomogeneous copolymer mixture.[38] Chains started at an early stage of the copolymerization may strongly differ in composition from chains initiated in the final stages of the copolymerization. The reactivity ratios determine the degree of this composition drift and in some cases phase separation of the copolymers with different compositions occurring during chain propagation.[39]

The impact of reactivity ratios changed with the introduction of living and controlled polymerization methods.[40–46] In a living and controlled copolymerization, all chains are initiated only at the start of the reaction, commonly by a rapid initiation step (criterion for a controlled polymerization). As no termination or chain transfer occurs (criterion for a living polymerization), all polymer chains grow simultaneously. The change in instantaneous copolymer composition is reflected in the composition of a copolymer chain along the backbone.[46] Under conditions of living polymerization, the total conversion X is a linear function of the degree of polymerization (P_n), with the constant factor of the initiator concentration $[I]_0$ and total initial monomer concentration $[M]_0$.[42,47] In this case the total conversion X can be interchanged with the chain composition ($P_n/P_{n,final}$), as shown in equation (9).

$$P_n = \frac{[M]_0 - [M]}{[I]_0}; X = \frac{[M]_0 - [M]}{[M]_0} \Rightarrow X = \frac{[I]_0 P_n}{[M]_0} = \frac{P_n}{P_{n,final}} \quad (9)$$

For a given set of reactivity ratios r_1, r_2, and an initial monomer feed $f_{1,0}$, the average copolymer composition of copolymers synthesized by such controlled polymerization methods can be predicted with the Meyer-Lowry equation (25). The monomer feed f_1, which corresponds to the reasonable values of the conversion X in the interval from 0 to 1, must be determined. From these f_1 values, the instantaneous comonomer incorporation F_1 is determined using the equation (21). This gives the copolymer composition F_1 as a function of total monomer conversion X. Under living conditions equation (9) is valid, and the total conversion X can be interchanged with the normalized

chain length. The left column of Table 1 shows examples of copolymer microstructures for different reactivity ratios. These are ideal copolymerizations ($r_1 \cdot r_2 = 1$) with initial comonomer feed $f_{1,0} = 0.5$.

The visualization shown on the left side of Table 1 only represents the average copolymer composition, originally shown by Skeist,[48] and was refined by Meyer and Lowry.[49] F_1 corresponds to the probability of finding monomer 1 at position *X*. All copolymer chains have discrete values for the number and position of the comonomers and a smooth gradient results from the average over all chains. This should be kept in mind when discussing gradient copolymers.[4] For $P_n = 50$, representations of copolymer chains based on the same values for r_1, r_2, and $f_{1,0}$ under living conditions are simulated, as shown in the right column of Table 1.

Table 1: Simulated microstructures for ideal copolymerizations with an equimolar comonomer mixture: average copolymer composition along the chain (left) and individual copolymer chains with an average P_n = 50 (right).

r_1	r_2	Average copolymer composition	Individual chains
1	1	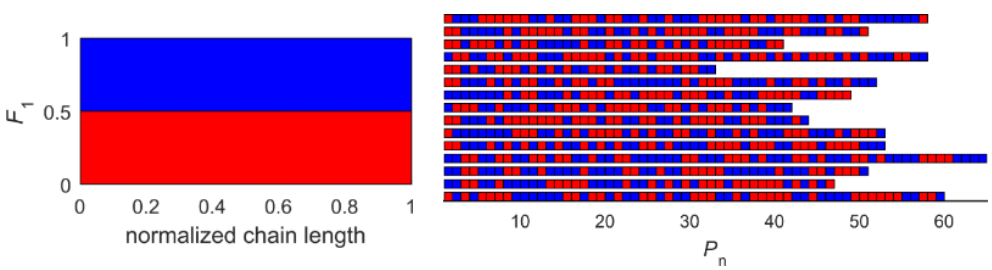	
2	0.5	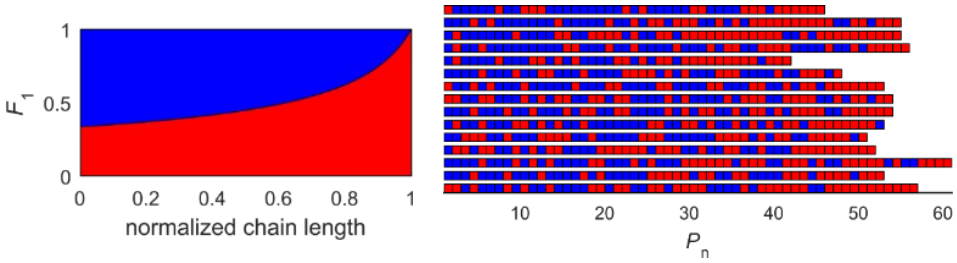	
5	0.2	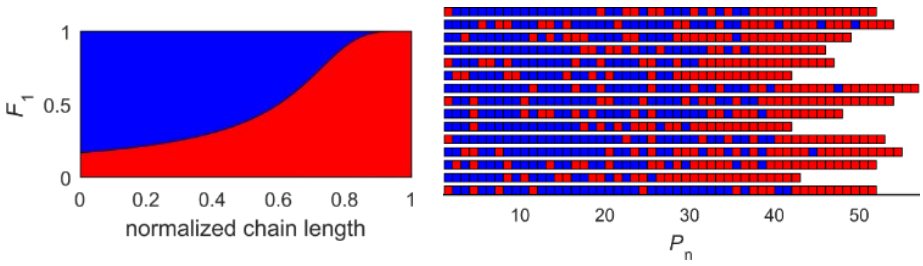	
20	0.05	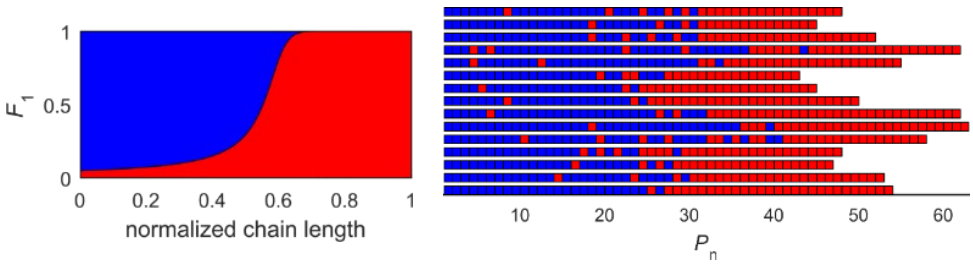	

The same visualization for two cases of non-ideal copolymerizations is shown in Table 2 at the azeotropic point. Both examples have a constant composition of F_1 = 0.5 along the copolymer chain. The first example is a copolymerization that favors an alternating sequence and the second tends to form blocky structures. These examples underline that the average copolymer composition does not give an exhaustive description of the copolymer microstructure for non-ideal copolymerizations.

Table 2: Simulated microstructures for non-ideal copolymerizations with an equimolar comonomer mixture at the azeotropic point: average copolymer composition along the chain (left) and individual copolymer chains with an average P_n = 50 (right).

r_1	r_2	Average copolymer composition	Individual chains
0.1	0.1	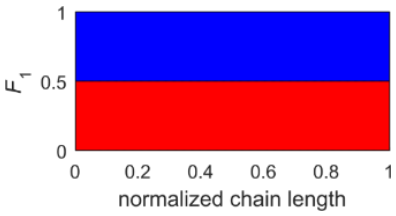	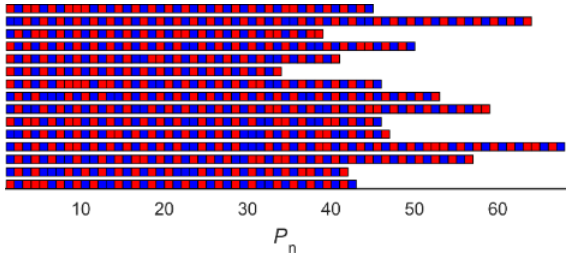
10	10	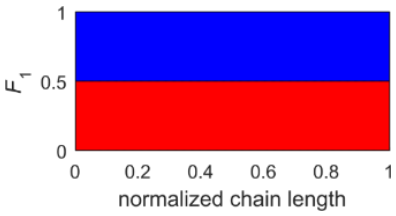	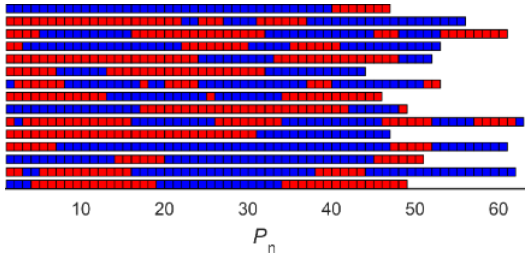

Sequence Length Distribution

The reactivity ratios have a direct impact on the probability of finding sequences with a distinctive length. The conditional probability p_{11} to add M_1 to an M_1 active chain end is defined as:[9]

$$p_{11} = \frac{R_{11}}{R_{11} + R_{12}} \tag{10}$$

By substituting R_{11} and R_{12} from equations (1)–(6), one obtains after rearrangement:

$$p_{11} = \frac{r_1}{r_1 + \left(\frac{[M_2]}{[M_1]}\right)} = \frac{r_1[M_1]}{r_1[M_1] + [M_2]} \tag{11}$$

The probability or mole fraction of forming a sequence of x consecutive monomer units $P(M_1)_x$ is then defined as:

$$P(M_1)_x = {p_{11}}^{x-1} \cdot p_{12} = \left(\frac{r_1[M_1]}{r_1[M_1] + [M_2]}\right)^{x-1} \cdot \frac{[M_2]}{r_1[M_1] + [M_2]} \tag{12}$$

The number-average sequence length $\bar{n}_1$ of M_1 is defined as:

$$\bar{n}_1 = \sum_{x=1}^{x=\infty} x \cdot P(M_1)_x \tag{13}$$

The equations (11–13) demonstrate the significance of the reactivity ratios towards the monomer sequence, which directly correlate towards the copolymer properties. Depending on the application, knowing the probability of forming certain sequence lengths is imperative.

Determination of Reactivity Ratios

Historically, it was only possible to analyze the copolymer composition after termination of the polymerization. Furthermore, the copolymer had to be separated from the residual monomer for characterization, which can cause significant errors. With the introduction of *in situ* techniques, the comonomer feed and copolymer composition can be determined at any point in the copolymerization experiments. In this manner, multiple data points for one copolymerization experiment can be obtained. For the observation of copolymerization experiments HPLC,[50] ^{1}H NMR,[51,52] ^{13}C NMR,[53] UV-vis spectroscopy,[54] Raman spectroscopy[55,56] and FTIR measurements[54,57] were employed. Duchateau *et al.* used MALDI-ToF-MS to extract the reactivity ratios from the resulting copolymer.[58] Today's most common method is *in situ* ^{1}H NMR spectroscopy, which has been applied to many different polymerization conditions.[51,59–62]

Despite the importance of gradient copolymers, to this date there are no reliable methods to directly characterize the gradient structure of a copolymer sample.[3] Nevertheless, with the introduction of *in situ* NMR kinetics in combination with suitable copolymerization models it is possible to predict the microstructure of copolymers.

Theoretical Approach: From Copolymerization Models to Gradient Copolymers

It should be noted that all copolymerization models were originally developed for describing radical copolymerization. However, these copolymerization models assume no nature of the active chain ends. Therefore, it is legitimate to apply them to other polymerization methods equally.[22] In the following, the different copolymerization models will be described. Then the application of these models for the description of experimental copolymerization data and the evaluation of reactivity ratios is presented.

Table 3: Overview of the most common copolymerization models and the corresponding methods to calculate reactivity ratios from experimental data.

	Non-terminal / ideal model	Terminal model
Introduced by	Wall[63] 1941	Mayo-Lewis[10] 1944 Alfrey-Goldfinger[64] 1944 Wall[21] 1944
Differential form	Wall[63] 1941	Mayo-Lewis[10] 1944 *linearized by* Fineman-Ross[65] 1950 Kelen-Tüdos[66] 1975
Integral form	Wall[22,63] 1941 Jaacks[67,68] 1972 Beckingham-Sanoja-Lynd[24] 2015	Mayo-Lewis[10] 1944
	Integration with Skeist-relation[48] 1946	
	Ideal integrated[69] 2019	Meyer-Lowry[49] 1965

Copolymerization Models

Non-Terminal Copolymerization Model

The non-terminal model is also referred to as Bernoullian model, zero-order Markov, or ideal model.[9,17] The term "ideal" cannot be referred to as a desired property, as this comes from its agreement with the differential equations describing the boiling of a mixture of liquids which obey Raoult's law.[21,22] This model was introduced by Wall in 1941, who was the first to neglect absolute rates and use relative rates to describe copolymerizations.[63] He proposed the following time-independent differential equation (14) for copolymerizations, assuming first-order polymerizations:

$$\frac{\mathrm{d}[\mathrm{M}_1]}{\mathrm{d}[\mathrm{M}_2]} = \varepsilon \frac{[\mathrm{M}_1]}{[\mathrm{M}_2]} \tag{14}$$

The quantity ε represents the fraction of the two first-order propagation constants. He also showed, that this equation can be integrated into the following two forms:[22,63]

$$\frac{[\mathrm{M}_1]}{[\mathrm{M}_{1,0}]} = \left(\frac{[\mathrm{M}_2]}{[\mathrm{M}_{2,0}]}\right)^{\varepsilon}; \text{or: } \log\left(\frac{[\mathrm{M}_1]}{[\mathrm{M}_{1,0}]}\right) = \varepsilon \cdot \log\left(\frac{[\mathrm{M}_2]}{[\mathrm{M}_{2,0}]}\right) \tag{15}$$

In the ideal or non-terminal model, the following equations apply:

$$r_1 \cdot r_2 = 1;\ r_1 = 1/r_2 \tag{16}$$

$$k_{11} = k_{21};\ k_{22} = k_{12} \tag{17}$$

The reaction of an M_1 chain end with M_1 is as fast as the reaction of an M_2 chain end with M_1, and vice versa. Thereby, the reaction rates are chain end independent and only controlled by the reactivity of the monomers, but not the identity of the chain end. Consumption of the respective monomers can display different rate constants. As one can see in equation (16), the copolymerization can be described by a sole reactivity ratio.

The radical homopolymerization of stilbene and maleic anhydride is not feasible. In 1930, the alternating copolymerization of maleic anhydride and stilbene was reportet.[70] This shows that the identity of the chain end can play a vital role in copolymerizations, due to the selectivity of the chain end towards the different comonomers. In such cases, the terminal copolymerization model must be employed.

Terminal Copolymerization Model

The terminal copolymerization model is sometimes referred to as first-order Markov model, as the spontaneous batch copolymerization of a comonomer pair obeying this model results in a comonomer distribution complying with first-order Markovian statistics.[9,17] Three years after the development of Wall's non-terminal model, three independent works regarding the terminal model were published in 1944. Basically, the same mathematical framework was obtained by Alfrey and Goldfinger[64] (submitted March, published June), Mayo and Lewis[10] (submitted May, published September), and Wall[21] (submitted July, published December). In contrast to Wall's first model, the terminal model differentiates between two different types of active chains, depending on the last monomer added, and can be expressed in the following time-independent differential equation:

$$\frac{\mathrm{d}[\mathrm{M}_1]}{\mathrm{d}[\mathrm{M}_2]} = \frac{k_{11}[\mathrm{M}_1^*][\mathrm{M}_1] + k_{21}[\mathrm{M}_2^*][\mathrm{M}_1]}{k_{12}[\mathrm{M}_1^*][\mathrm{M}_2] + k_{22}[\mathrm{M}_2^*][\mathrm{M}_2]} \tag{18}$$

The steady-state assumption ($k_{12}[M_1^*][M_2] = k_{21}[M_2^*][M_1]$) requires that the sum of active chains remains constant during copolymerization, which is true by definition for living polymerizations. The concentration of the active chains can be reduced, which results in the copolymerization equation of the terminal model in its typical differential form (Mayo-Lewis equation):

$$\frac{\mathrm{d}[\mathrm{M}_1]}{\mathrm{d}[\mathrm{M}_2]} = \frac{[\mathrm{M}_1]}{[\mathrm{M}_2]} \cdot \frac{r_1[\mathrm{M}_1] + [\mathrm{M}_2]}{r_2[\mathrm{M}_2] + [\mathrm{M}_1]} \tag{19}$$

The steady-state assumption is the "classic" way the copolymerization equation is derived and presented in many textbooks, however, it is not necessary.[9,11,71]

Today, equation (19) it is typically referred to as the “Mayo-Lewis equation”. A reason for this could be that Mayo and Lewis already gave instructions on how to use this equation to determine the reactivity ratios r_1 and r_2 from experimental copolymerization data.

The Mayo-Lewis equation describes the instantaneous composition d[M₁]/d[M₂] of copolymers formed in dependence of the ratio of the monomer feed concentration [M₁] and [M₂]. In many cases, the composition of the instantaneously formed copolymer is not equal to the monomer feed. This causes the monomer feed to change throughout the copolymerization, which in turn results in a change in copolymer composition, commonly referred to as “composition drift”.[8,9] To accurately describe copolymerization up to high conversion it is mandatory to integrate the equation (19). An integrated equation that allows for the description of copolymerizations for any conversion was first presented by Mayo and Lewis in 1944.[10]

This “integrated Mayo-Lewis equation” is rarely used, as it requires multiple experiments. More convenient is an expression that relates the change of monomer feed to the total conversion of both monomers. For this purpose, it is useful to express the ratios [M₁]/[M₂] and d[M₁]/d[M₂] in the form shown in equation (20). The values of the molar fraction of unreacted monomer f_1 and the molar fraction of formed copolymer F_1 are between 0 and 1.

$$f_1 = 1 - f_2 = \frac{[\mathrm{M}_1]}{[\mathrm{M}_1] + [\mathrm{M}_2]};\ F_1 = 1 - F_2 = \frac{\mathrm{d}[\mathrm{M}_1]}{\mathrm{d}[\mathrm{M}_1] + \mathrm{d}[\mathrm{M}_2]} \tag{20}$$

With the definitions of f_1 and F_1 from the equation (20), the Mayo-Lewis equation (19) takes the following mole fraction form:[72,73]

$$F_1 = \frac{r_1 f_1^2 + f_1 f_2}{r_1 f_1^2 + 2 f_1 f_2 + r_2 f_2^2} = \frac{r_1 f_1^2 + f_1(1 - f_1)}{r_1 f_1^2 + 2 f_1(1 - f_1) + r_2(1 - f_1)^2} \tag{21}$$

In 1946 Skeist derived a relationship between the total monomer conversion X

$$X = 1 - \frac{f_1 + f_2}{f_{1,0} + f_{2,0}} = 1 - \frac{M}{M_0} \tag{22}$$

and the molar comonomer fraction f_1.[48]

$$f_1 M - (M - \mathrm{d}M)(f_1 - \mathrm{d}f_1) = F_1 \mathrm{d}M \tag{23}$$

The term $\mathrm{d}M \cdot \mathrm{d}f_1$ can be neglected, as it is small. Integration yields:

$$\int_{M_0}^{M} \frac{\mathrm{d}M}{M} = \ln\left(\frac{M}{M_0}\right) = \int_{f_{1,0}}^{f_1} \frac{\mathrm{d}f_1}{F_1 - f_1} \tag{24}$$

Meyer and Lowry solved the Skeist relation analytically for the terminal model in 1965 with the restriction $r_1 \neq 1$; $r_2 \neq 1$. The conditions $r_1 = 1$; $r_2 \neq 1$ and vice versa are special cases that can be found in the original publication.[49]

$$X = 1 - \frac{M}{M_0} = 1 - \left[\frac{f_1}{f_{1,0}}\right]^{\alpha} \left[\frac{1-f_1}{1-f_{1,0}}\right]^{\beta} \left[\frac{f_{1,0}-\delta}{f_1-\delta}\right]^{\gamma}$$
$$\alpha = \frac{r_2}{1-r_2};\ \beta = \frac{r_1}{1-r_1};\ \gamma = \frac{1-r_1 r_2}{(1-r_1)(1-r_2)};\ \delta = \frac{1-r_2}{(2-r_1-r_2)} \quad (25)$$

In the case of ideal copolymerization ($r_1 \cdot r_2 = 1$; $r_1 = r_2^{-1}$) the formula converts to the one derived by Wall.[21]

The Meyer-Lowry equation (25) describes the total conversion X of the monomers as a function of the molar fraction of unreacted monomer f_1. This enables describing the composition drift up to high conversions when the initial feed composition $f_{1,0}$ and reactivity ratios r_1 and r_2 are known. The reactivity ratios can be determined by numerical approximation towards the data obtained by plotting M/M_0 versus f_1. Recently, an IUPAC project was completed that explains the use of data evaluation procedures for the terminal copolymerization model.[74]

Experimental Methods for the Determination of Reactivity Ratios

Essentially, there are two different methods for determining reactivity ratios from copolymerization experiments. The first option uses the differential copolymerization equations. These equations are only valid for small conversions since it can then be ensured that the monomer feed composition does not change significantly throughout the copolymerization experiment.[10] The second option uses integrated copolymerization equations, which are valid for any conversion and therefore can be applied to experiments with high conversions. Differential, nonintegrated equations should not be used anymore to determine reactivity ratios, as they require multiple experiments while being inaccurate.[75] However, they are still presented in detail in many textbooks. Due to their prominence, they are also discussed here.

Determination of Reactivity Ratios by the Differential Copolymerization Equation

Traditionally copolymerization experiments were conducted with known comonomer feeds and stopped at low conversion. The low conversion is necessary, since $d[M_1]/d[M_2]$ can be approximated by $\Delta[M_1]/\Delta[M_2]$. According to basic differential calculus, the slope of the tangent line of the function $[M_1]([M_2])$ at the point $[M_{2,0}]$ can be approximated by a secant for small values of $\Delta[M_1]$ and $\Delta[M_2]$. Therefore, only low monomer conversion leads to a valid description.

The comonomer feed $[M_1]/[M_2]$ corresponds to the known molar ratio of comonomers used in the copolymerization experiment, whereas $\Delta[M_1]/\Delta[M_2]$ refers to the copolymer composition, which can be determined after the experiment. In this manner, multiple copolymerization experiments with different comonomer feeds must be conducted and the resulting copolymer compositions must be determined. The Mayo-Lewis equation (19) will be expressed in the abbreviated form in the following.

$$x = \frac{[M_1]}{[M_2]}; y = \frac{d[M_1]}{d[M_2]} \approx \frac{\Delta[M_1]}{\Delta[M_2]} \Rightarrow y = x \cdot \frac{r_1 x + 1}{r_2 + x} \tag{26}$$

From the copolymerization experiments described above, value pairs for *x* and *y* are obtained. The first method to obtain reactivity ratios from this data was described by Mayo and Lewis in 1944.[10] By solving equation (26) for r_1, expression (27) is obtained (*m*: slope, *b*: coordinate section), which gives a linear relationship between r_1 and r_2.

$$r_1 = m \cdot r_2 + b; m = \frac{y}{x^2}; \text{ and } b = \frac{y-1}{x} \tag{27}$$

Each copolymerization experiment corresponds to a pair of values for *m* and *b* and can be expressed as a straight line. By finding the point of interception of these straight lines the reactivity ratios r_1 and r_2 are determined. Unfortunately, due to experimental errors, these straight lines rarely intersect at a single point, making the determination of the reactivity ratios ambiguous. An alternative approach was given by Fineman and Ross in 1950.[65] They rearranged equation (26) in the following form:

$$\frac{x(y-1)}{y} = r_1 \frac{x^2}{y} - r_2 \tag{28}$$

Equation (28) represents a linear equation with r_1 as the slope and $-r_2$ as the ordinate intercept. The values for $x(y-1)/y$ and x^2/y are calculated for every copolymerization experiment. A linear least-square fit of this data gives the reactivity ratios as slope and ordinate intercept. A disadvantage of this method is that the values $x(y-1)/y$ and x^2/y are unequally weighted. Therefore, the copolymerization experiments have different weights in the least square fit. This was improved by Kelen and Tüdos with the introduction of the parameter η, which ensures an even distribution of the data points.[66] The data is transformed and fitted by a linear least square fit to obtain the reactivity ratios.

An additional extension of this method is the so-called “extended Kelen-Tüdos” approach, which approximates the composition drift by Wall’s non-terminal model.[76,77] This extension expands the applicability of the Kelen-Tüdos method to higher conversions.

A drawback of these methods is that the linearization of the Mayo-Lewis equation (19) leads to a distortion in the error structure.[78,79] Today, with the help of computers it is possible to perform non-linear least squares to fit data directly to the differential copolymerization equations (19) or (21).[52,56,80] Another source of error is the approximation in the equation (26) when the condition of a low conversion is not met.

The differential equations by Mayo-Lewis, Fineman-Ross, or Kelen-Tüdos are often used to determine reactivity ratios from *in situ* data. The values of $[M_1]/[M_2]$ are directly obtained from the measurement. To obtain the instantaneous copolymerization composition, the copolymerization experiment is divided into small intervals, in which the condition of a low conversion applies. By applying equation (26) for each interval, values for $\Delta[M_1]/\Delta[M_2]$ can be calculated. Then, the methods described above can be applied to retrieve values for the reactivity ratios. This strategy has been especially utilized for ^{1}H NMR data.[51,60,81–85]

However, this procedure is only valid for copolymerization with a slight composition drift. It was demonstrated to be error-prone when linearizing the copolymerization data for more disparate reactivity ratios, causing a high composition drift even in small intervals.[62,86] Switching the indices of the reactivity ratios results in different values.[74] For data of the composition drift of a copolymerization experiment carried out to high conversion, it is more reasonable to evaluate reactivity ratios by utilizing the integrated form of the equation, as was impressively demonstrated by Beckingham, Lynd *et al*. in 2019.[75] In contrast to F_1, the values for f_1 are usually directly obtained from the data. In the determination of reactivity ratios with the integrated copolymerization equation, there is no need to evaluate F_1 indirectly from the measured data.

Determination of Reactivity Ratios by Integrated Copolymerization Equations

The data of the drift of the monomer feed f_1 ratio in the copolymerization mixture can be directly fitted to an integrated copolymerization equation to obtain reactivity ratios. For this purpose, the integrated Mayo-Lewis equation was used in the past.[51] More commonly used is the non-linear fit of the data of total conversion X and monomer feed f_1 to the Meyer-Lowry equation (25) to obtain reactivity ratios (exemplary fit Figure 6).[49,87–89]

Jaacks demonstrated that a large excess of one comonomer leads to a copolymerization that is only determined by one reactivity ratio. In this case, the copolymerization equation (19) can be approximated by the ideal copolymerization equation.[67,68] This equation, equal to the integrated Wall equation (15), is then used to fit the data of two copolymerization experiments, each with a large excess of one monomer. For both experiments, the logarithm of the monomer concentration

is fitted with the linear equation (15). The reactivity ratios r_1 and r_2 are equal to the slopes of this fit. In an ideal copolymerization without any influence of the terminal unit ($r_1 \cdot r_2 = 1$), it is possible to describe the copolymerization with equation (15) for any ratio of M_1/M_2 (exemplary fit see Figure 6).[89,90] Due to the equality of the derivations made by Jaacks and Wall, the large excess of one comonomer is not necessary for ideal copolymerizations.

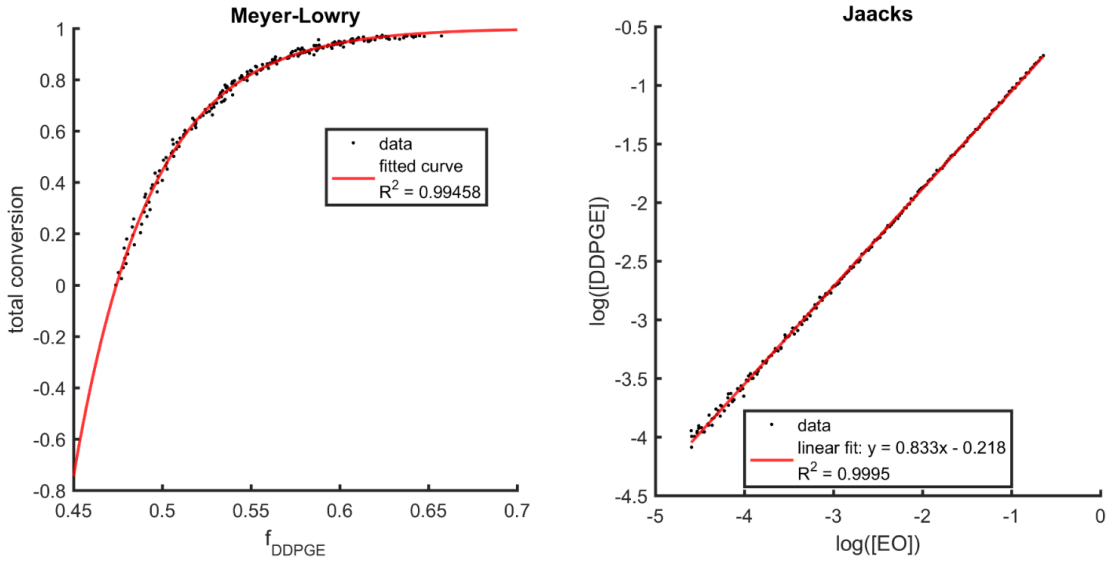

Figure 6: Example of the determination of reactivity ratios via the fit to the Meyer-Lowry equation (left) and via the Jaacks method (right). Reprinted with permission from reference[89]. Copyright © 2019 American Chemical Society.

In 2015 Lynd *et al.* showed that an equation based on the ideal Wall model can successfully describe a variety of epoxide copolymerizations.[24] Beckingham *et al.* demonstrated the superior accuracy of the integrated compared to the traditional linearized models on a set of copolymerization data with prescribed reactivity ratios in 2019.[75] Frey *et al.* derived an integrated expression based on the ideal Wall model similar to the Meyer-Lowry equation (25) for the terminal model in 2019. This ideal integrated equation can be fitted to the same *in situ* NMR data set used for the Meyer-Lowry equation and thereby the quality of the fit can be directly compared.[69]

Discussion of the Choice of the Copolymerization Model

The application of the terminal model for radical copolymerization is reasonable. Very frequently both reactivity ratios in radical copolymerizations are below one.[91] In these cases the product $r_1 \cdot r_2$ cannot equal one, which indicates an influence of the terminal units, necessitating the use of the terminal model. Various authors transferred this practice to other copolymerization methods like ionic copolymerization. Often, only the terminal model is considered to fit experimental data. However, following the principle of Ockham's razor, the simplest model that successfully describes

the experimental data should be used.[92] A direct consequence of using a model with too many degrees of freedom is overfitting.[93] Systematic errors in the measurement data will then cause incorrect predictions of the copolymerization behavior.[56] The translation of Ockham's razor principle to the field of copolymerization is that the non-terminal, ideal model should always be considered first. Only in cases where the data cannot be explained satisfactorily with the non-terminal model, the terminal model should be consulted. Apart from the well-known nonterminal, terminal, and penultimate model,[94] the complex participation model (CPM)[95], the complex dissociation model (CDM),[96] and the comp-pen model[97] can be found in the literature.[98] As they are not known to be applicable to epoxide copolymerization, they are not discussed here.

In the conventional anionic ring-opening polymerization (AROP), the intensely studied comonomer pair EO and PO is known to exhibit a product $r_1 \cdot r_2 = 0.9$, close to one, indicating the terminal units possess neglectable influence.[99] A newer study could show that the ideal, nonterminal model sufficiently describes the data.[100] Many other epoxide copolymerizations under AROP conditions were also shown to have $r_1 \cdot r_2$ values close to one.[16,59,89,101–108] Copolymerizations under conditions of the monomer-activated anionic ring-opening polymerization (MAROP), adding *i*Bu$_3$Al also showed ideal behavior for various epoxide comonomer combinations.[59,109–112] This seems to apply to aziridine comonomers under the conditions of the AROP as well, as demonstrated in recent works.[113,114] These findings suggest that Wall's model sufficiently describes the anionic ring-opening copolymerization, as was also stated in recent works.[69,75] The AROP and MAROP mechanisms are compared in Figure 7.

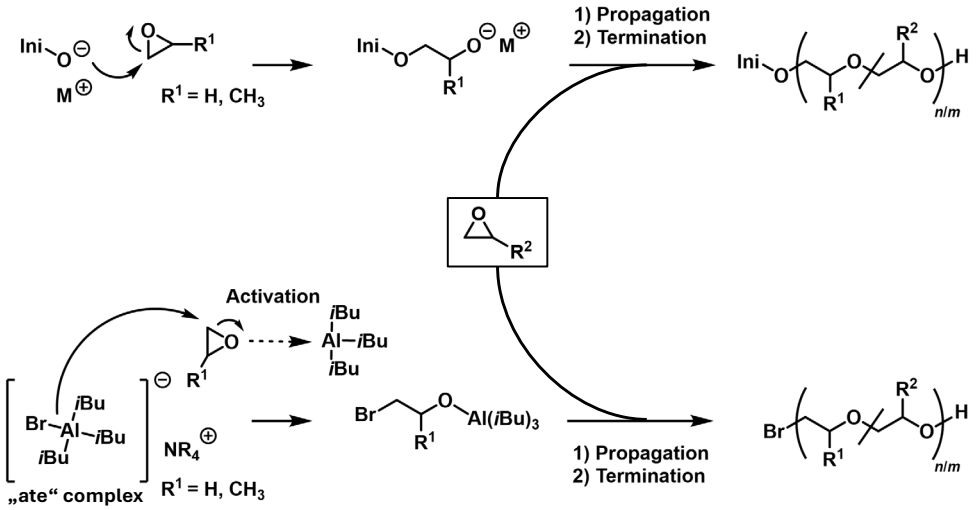

Figure 7: Exemplary mechanisms for the copolymerization of EO (R^1 = H) and PO (R^1 = CH_3) with functional epoxides *via* AROP (top) and MAROP (bottom), resulting in multifunctional polyether copolymers.

Multi-Functional Polyether Copolymers

Although poly(ethylene glycol) (PEG) is a well-established polymer, multifunctional PEGs have only been introduced in the last decades.[115–117] The living copolymerization of EO with epoxide derivatives allows for the distribution of functional groups along the polymer backbone, resulting in multifunctional PEGs.[118] This approach not only imparts new properties to these polyethers but also significantly expands their application range.[118,119] Frey *et al*. emphasized the importance of PEG, poly(propylene oxide) (PPO), and their multifunctional copolymers in a comprehensive review.[117]

The incorporation of glycidyl amines such as *N*,*N*-diethyl glycidyl amine (DEGA) introduces pH-responsive behavior into PEG, while the copolymerization of EO with ferrocenyl glycidyl ether (fcGE) leads to electroactive and thermo-responsive behavior.[120–123] Catechol moieties are highly suitable for complexing ions or biomimetic adhesion to a large variety of surfaces. By incorporation and acidic deprotection of the acetonide-protected catechyl glycidyl ether CAGE, these properties can be transferred to PEG.[101] In addition, these properties can be tailored by the variation of the comonomer content.

Bio-derived terpenyl glycidyl ethers can be used to introduce hydrophobicity to hydrophilic PEG, either as block or nearly random copolymers. This results in amphiphilic polymers derived from natural, renewable resources, offering an alternative to traditional fossil-based α-alkylene oxides like PO or butylene oxide (BO),[124] which besides exhibit a gradient.[16,99] Statistical copolymers of linear polyglycerol and poly(ethyl glycidyl ether) enable tailoring of the cloud point of these PEG-related polymers while preserving their biocompatibility.[125] Copolymerization of EO with ethoxyvinyl glycidyl ether (EVGE) results in nearly random copolymers that can be modified to include lithium trifluoromethanesulfonamide in the side chain, enabling lithium-ion conductivity for solid-state battery applications.[126] Triblock copolymers composed of hydrophobic random copolymers of EO and long-chain alkyl glycidyl ethers as outer blocks, with a hydrophilic PEO (also referred to as PEG, see Frey *et al*.[117] for details) inner block, can form pH-independent and biocompatible hydrogels.[127] Glycidol is a vital initiator monomer (“inimer”) for the synthesis of hyperbranched polyether structures and is usually combined with EO to control the molar mass and dispersity[128,129] Investigations of the copolymerization revealed a gradient microstructure, as the hydroxyl group of glycidol can presumably activate the epoxide functionality, which results in an enhanced reactivity compared to EO (Figure 8).[130]

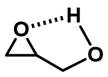

Figure 8: Presumed intramolecular activation of the epoxide functionality of glycidol (G). Reprinted and adapted with permission from Frey *et al.*[130] Copyright © 2016 American Chemical Society.

The AROP of EO with functional epoxide monomers allows for the tailoring of the properties of PEG and the modification of the polymer architecture. The subsequent addition of monomers leads to block copolymers, while the AROP of a monomer mixture results in statistical copolymers. The microstructure of the resulting copolymers is highly dependent on the reactivity of the respective epoxide comonomers. As a result, the copolymers can form either random or gradient copolymers with varying gradient strengths, ranging from weak to strong (tapered) gradients.[59,99,102,130]

One critical issue in the polymerization of substituted epoxides is that undesirable chain transfer reactions are frequently observed under conventional oxyanionic polymerization conditions.[117,131–133] The abstraction of a proton from the methyl- or methylene group at the epoxide moiety leads to the formation of an allyl alkoxide, which may act as an initiator itself, resulting in a limitation of the achievable molar mass and an increased dispersity.

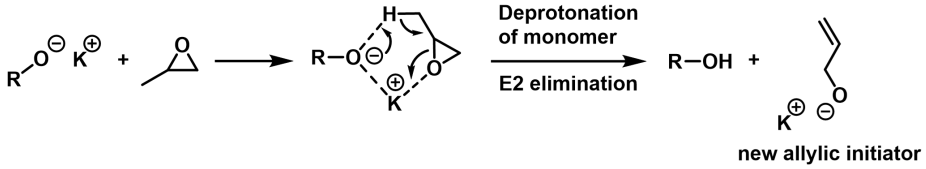

Figure 9: Transfer reaction from an active chain end to the PO monomer, yielding an allylic alkoxide initiator and a lower degree of deprotonation. Isomerization of the double bond to the vinyl species is omitted. Adapted and reprinted from Grobelny *et al.*[134] Wiley © 2016.

Elevated reaction temperatures and the use of strong bases further limit the range of tolerated functional groups. Therefore, the AROP is not suitable for the direct polymerization of glycidyl esters,[135,136] nitrile,[137–139] or the incorporation of protic functional groups such as hydroxy, catechol,[101,140] or alkyne units.[109] Instead, protecting group chemistry or the considerably milder MAROP must be applied.[117,133,141] Due to the different polymerization mechanisms, the reactivity ratios of the comonomer pair can be altered (compare Table 4 and Table 9). However, the MAROP also exhibits drawbacks as incompatibility towards highly coordinating functionalities like amines. Polymerization only results in low molar mass polymers.[142] Transfer reactions can occur as the above-discussed transfer to monomer due to proton abstraction, hydride- or *iso*-butyl-initiation.[117,133,143,144] This limits the end-group fidelity of the resulting polymers, and this late-stage initiation leads to inhomogeneous products in gradient copolymers.[25,145,146] Achieving a gradual shift in instantaneous composition requires initiating all chains simultaneously and ensuring their

activity persists until the polymerization is complete.[1] The removal of commonly used quaternary ammonium salts is laborious, due to their amphiphilic nature and typically results in lower polymer yields.[147] Additionally, polymers for biomedical applications require rigorous removal of the catalyst, as aluminum is neurotoxic.[148–150]

Reactivity Ratios of Functional Epoxides

Copolymerizations of functional epoxides are summarized in the following section, focusing on the copolymer microstructure. A special spotlight is on copolymers of EO and PO. Copolymerization kinetics from conventional AROP[117] and MAROP[133] are illuminated. An emphasis is placed on NMR kinetics studies (^{1}H NMR analysis of aliquots obtained by sampling, ^{13}C NMR triad analysis, *in situ* ^{1}H NMR kinetics) as an evaluation method.

Numerous works focused on the determination of the incorporation preferences of epoxide comonomers making conclusions regarding the copolymer microstructure without determination of the actual reactivity ratios e.g., *via* ^{13}C NMR triad sequence analysis (TSA)[99,151–155] or by extracting the monomer conversion over time from the *in situ* NMR experiments.[156] From end-group dyads (EGD) Lynd *et al.* extracted the relative monomer reactivity directly from the NMR and determined the reactivity ratios utilizing a simple kinetics model.[107] Typically mathematical evaluation of NMR data was performed according to a variety of methods like Yezuielev-Brohkina-Roskin (YBR),[157–159] Fineman-Ross (FR),[51,103,104,131] Kelen-Tüdos (KT),[52,104,112] Mayo-Lewis (integral form, MaL),[99] Meyer-Lowry (ML),[104,124,160–162] Jaacks (JA),[100,124,162,163] Beckingham-Sanoja-Lynd (BSL)[164] and Ideal Integrated (IdI).[69,162]

Functional epoxide derivatives can be broadly classified into four categories: glycidyl ethers (GEs), glycidyl amines (GAs), alkylene oxides (AOs), and others.[117] In the class of other functional monomers, a case-specific subdivision must be made. While glycidyl esters can be synthesized e.g. by the reaction of ECH with activated (deprotonated) carboxylic acids,[136,165] epihalohydrins can be obtained in analogy to AOs from the oxidation of allylic halides.[166,167] The asymmetric structure of monofunctional epoxides raises the additional question of regioselectivity. They are mainly incorporated regioselectively by head-to-tail connections because of steric reasons. The head-to-head content is in the range of 3–4%.[168–170] For racemic epoxides, an atactic polymer structure is obtained.[117,171]

Anionic Ring-Opening Polymerization (AROP)

The copolymerization kinetics of functional epoxides will be summarized and discussed, focusing first on the AROP of EO as the primary comonomer, followed by PO. AROP is the most widely used

method in both academia and industry for the copolymerization of functional epoxides due to its efficiency and versatility.[172] It dates back to the 1860s when the synthesis of PEG with a low molar mass was first described by Lourenco and Wurtz.[173–175] This foundational work was later expanded in the first polymer-focused research by Staudinger.[176,177] Flory predicted the controlled character of the AROP in 1940.[178] Many reviews summarized the AROP of functional epoxides, including reaction conditions, properties, and possible applications of the resulting polyether copolymers.[117,118,172,179–183]

The influence of different conditions during the AROP, *e.g.*, counterion or temperature, was investigated in several studies. Heatley *et al.* showed that the determined incorporation preferences in the copolymerization of EO and PO were not affected by the choice of sodium or potassium during the polymerization.[99] A similar conclusion could be obtained for the presence of crown ethers, but the reactivity ratio for EO was higher compared to bulk polymerization without crown ether.[16,184] Frey *et. al.* showed that the counterion has a small impact on the reactivity ratios of the copolymerization of EO and glycidol.[130] The impact of reaction temperature has been investigated in numerous studies, with several employing *in situ* NMR techniques. These studies have shown that the resulting polymer microstructure is independent of temperature,[99,156,184–187] but a recent work shows small changes by increasing the temperature.[100] Therefore, despite the different reaction conditions applied during the AROP the resulting preferences concerning the incorporation of epoxides are roughly comparable. However, as there are numerous reports of reactivity ratios, comparing different copolymerization systems should be treated cautiously. The combination of the parameters temperature, counterion, comonomer pair, solvent, additives, and the degree of deprotonation, have not been elucidated sufficiently to the best of our knowledge. The choice of the copolymerization model also plays a role, as discussed above. Heatley *et al.* summarized literature mentioning the reactivity ratios of the EO/PO comonomer pair in 1991. They ranged from $r_{EO} = 1.34$, $r_{PO} = 0.14$ to $r_{EO} = 6.5$, $r_{PO} = 1.49$. The reaction conditions sometimes were not clear and non-recommended calculation methods were used. The experiments of Heatley *et. al.* were analyzed using the Mayo-Lewis equation and they reported $r_{EO} = 2.8$, $r_{PO} = 0.25$. The reactivity ratios were reported to be independent of temperature, but the term “independent” could also mean just slight variations.[99] Even slight variations in the reactivity ratios still lead to changes in the monomer sequence distribution. Depending on the issue and potential application, this can have an impact. However, the variations are comparably insensitive to the system, the reactivity ratios do not invert like in the carbanionic copolymerization.[161] Therefore, we recommend future researchers investigate their specific system as closely as possible under the actual copolymerization conditions.

Copolymerization of Glycidyl Ethers with EO under AROP conditions

The copolymerization of EO with GEs via AROP is the most studied reaction for determining the reactivity ratios of functional epoxides.

The copolymerization of EEGE with other epoxides is a well-known strategy for the introduction of multiple hydroxyl groups at polyethers. The investigations of the copolymerization behavior showed random incorporation of EO and EEGE. Reactivity ratios were determined by Huang *et al*.[158] and Frey *et al*., resulting in $r_1 \approx r_2 \approx 1$.[59] The results are in good agreement with the random incorporation of both monomers found by Frey *et al*. via TSA.[188,189] IGG, a similar GE as EEGE, was also found to be randomly incorporated.[156,189] Table 4 summarizes the resulting reactivity ratios or incorporation preferences. The reactivity ratios from the comonomer pairs can differ. In general, TSA can confirm a random or more gradient structure, however, it is unprecise compared to *in situ* methods. Monomer conversion over time (MCT) can indicate a random or preferential incorporation, but is insufficient, especially since modern methods to calculate the reactivity ratios are available. As described above, integrated methods are superior to differential methods. Different reaction conditions can also explain the resulting deviations in reactivity ratios. The following trends in conventional anionic copolymerization can be observed: GEs with small or flexible residual groups exhibit a similar reactivity ratio as EO or are even faster. The comparison of DMPGE with DDPGE shows that branching near the glycidyl ether functionality leads to sterical hindering. This results in reduced incorporation compared to EO. Chelatisation of the counterion (e.g. potassium) explains the similar reactivity ratios between GEs and EO. Disturbance of this chelation by sterically demanding residual groups plausibly leads to a faster EO incorporation.[163]

Table 4: GE comonomers copolymerized with EO under AROP conditions with determined reactivity ratios or incorporation behavior and analysis methods.

Comonomer	r_{CO}	r_{EO}	Analysis	Ref.
GME 	1.02	0.98	JA	190
	1.43	0.70	JA	190
	1.60	0.63	JA	190
	1.55	0.64	JA	190
EEGE 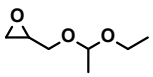	0.76	1.20	YBR	158
	0.94	1.05	BSL	59
	1.00	1.00	BSL	59
	random		TSA	188

		random		TSA	[189]
IGG	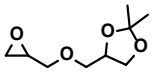	random		TSA	[156]
		random		TSA	[189]
AGE	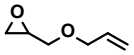	1.31	0.54	EGD	[107]
		random		TSA	[185]
		1.08	0.92	JA	[163]
		1.29	0.78	JA	[163]
		1.31	0.54	EGD	[163]
EGVGE EVGE	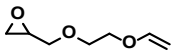	3.50	0.32	EGD	[107]
		1.23	0.81	JA	[163]
		2.05	0.48	JA	[163]
		random		TSA	[163]
		random		TSA	[151]
DMPGE	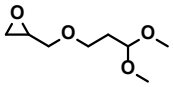	1.04	0.96	JA	[89]
DDPGE	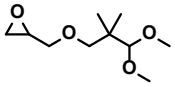	0.83	1.20	JA	[89]
DEGE	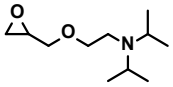	1.28	0.82	EGD	[106]
MTEGE	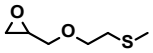	1.06	0.92	BSL	[102]
CAGE	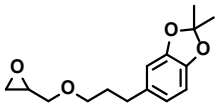	0.88	1.14	FR	[101]
fcGE	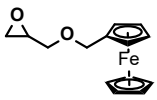	random		TSA	[122]
rcGE	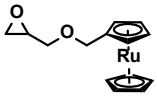	random		MCT	[191]
C_{12}-AlkGE	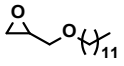	1.03	0.97	JA	[127]

OlGE	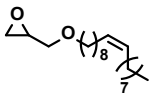	0.78	1.27	JA	[192]
IsoPreGE	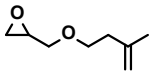	0.97	1.03	JA	[193]
PreGE	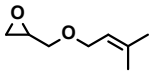	0.94	1.06	JA	[193]
NerGE	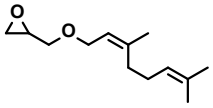	0.93	1.07	JA	[193]
GeraGE	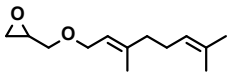	0.93	1.08	JA	[193]
DHPreGE	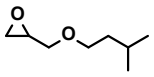	0.85	1.18	JA	[193]
THGeraGE	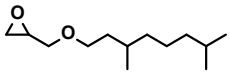	0.83	1.21	JA	[193]
HHFarGE	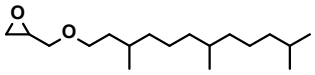	0.80	1.25	JA	[193]
FarGE	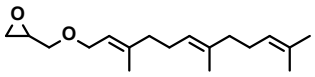	0.85	1.18	JA	[124]

YBR: Yezrielev-Brokhina-Roskin;[194] BSL: Beckingham-Sanoja-Lynd;[24] TSA: Triad sequence analysis; EGD: end-groud dyad analysis;[107] JA: Jaacks;[67,68] FR: Fineman-Ross;[65] MCT: monomer conversion over time.

Copolymerization of Glycidyl Ethers with EO under AROP conditions

PO is only slightly more sterically hindered than EO. In copolymerizations with EEGE or GME, the significantly lower preference for PO incorporation, compared to EO, is apparent. The key factor lies in the influence of the glycidyl ether motif, which alters the copolymerization behavior.

Table 5: GE comonomers copolymerized with PO under AROP conditions with determined reactivity ratios or incorporation behavior and characterization methods.

Comonomer		r_{CO}	r_{PO}	Analysis	Ref.
EEGE	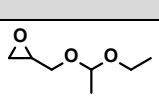	preferred		MCT	[186]
MGE = GME	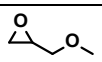	3.15	0.305	FR	[103]

FR: Fineman-Ross;[65] MCT: monomer conversion over time.

Copolymerization of Alkylene Oxides with EO under AROP conditions

As discussed above, the substitution of the alkylene oxides leads to less favored incorporation compared to EO. This becomes more evident if one compares PO and BO with EO, respectively. Glycidol (G), which can be referred to as the oxide of allylic alcohol, shows a favored incorporation, which is due to the activation of the epoxide moiety by the pendant hydroxy group. The following Table 6 summarizes the literature dealing with the copolymerization of EO with the comonomers PO, BO, and G.

Table 6: AO comonomers copolymerized with EO under AROP conditions with determined reactivity ratios or incorporation behavior and analysis methods.

Comonomer	r_{co}	r_{EO}	Analysis	Ref.
PO 	0.25	2.8	MaL	[99]
	0.30	3.1	TSA	[99]
	1.49	2.35	FR	[103]
	0.3	1.8	FR	[195]
	0.30	3.4	IdI	[162]
	0.29	3.2	ML	[162]
BO 	0.148	6.46	MCT*	[16]
	0.22	4.36	KT	[184]
	0.17	4.1	KT	[184]
G 	2.34	0.42	FR	[130]
	2.64	0.44	FR	[130]

*fitted by least-square method;[196] TSA: Triad sequence analysis; FR: Fineman-Ross;[65] MCT: monomer conversion over time; KT: Kelen-Tüdos;[66] IdI: Ideal Integrated;[69] MaL: Mayo-Lewis;[10] ML: Meyer-Lowry.[49]

Copolymerization of Glycidyl Amines with EO under AROP conditions

Glycidyl amines (GAs) represent the nitrogen analog of glycidyl ethers. Tertiary amines must be used to achieve linear copolymers. This leads to sterical hindrance near the epoxide moiety, compared to GEs with branched substituents (see above Table 4). Table 7 summarizes the available literature regarding the copolymerization of GAs with EO.

Table 7: GA comonomers copolymerized with EO under AROP conditions with determined reactivity ratios or incorporation behavior and characterization methods.

Comonomer		r_{co}	r_{EO}	Analysis	Ref.
DEGA	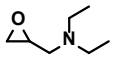		preferred	TSA, MCT	[121]
DButGA	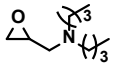	0.49	1.84	FR	[105]
DOctGA	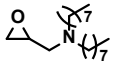	0.42	1.78	FR	[105]
DAGA	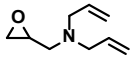		preferred	TSA, MCT	[197]
DBAG	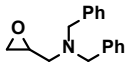		preferred	TSA, MCT	[187]

TSA: Triad sequence analysis; FR: Fineman-Ross;[65] MCT: monomer conversion over time.

Copolymerization of Functional Epoxides under AROP conditions

Table 8 lists the reactivity ratios of monomers copolymerized with other epoxide monomers than EO and PO. The following trends can be observed: 1) GEs react faster compared to AOs. 2) Sterical hindrance by branching of the substituents lowers the reactivity ratio.

Table 8: Comonomers copolymerized under AROP conditions with determined reactivity ratios or incorporation behavior and analysis methods.

Comonomer 1		Comonomer 2		r_1	r_2	Analysis	Ref.
DBGA	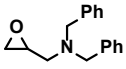	BMGA	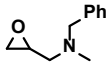	0.91	0.98	KT	[198]
DBAG		BGE	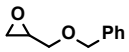	0.80	3.24	KT	[198]
BO		A	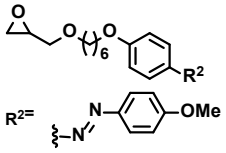	0.17	6.0	*a*	[108]
BO		C	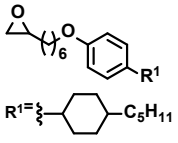	1.1	0.91	*a*	[108]
BO		E	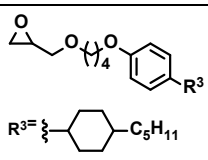	0.14	7.3	*a*	[108]

A	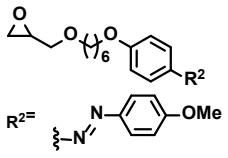	E	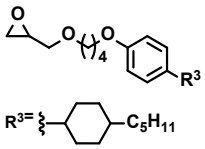	0.96	1.02	*a*	108
C	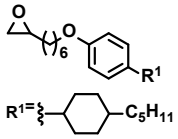	E	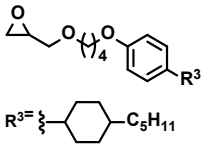	0.12	8.8	*a*	108
GME		EGE	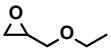	1.31	0.55	FR	199
				1.42	0.53	ML	199
				1.33	0.72	ML	199
EEGE	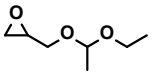	EGE	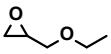	1.787	0.560	JA	125
EEGE	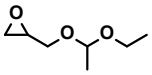	TGE ThpGE	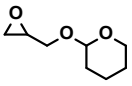	1.49	0.69	BSL	200
MTEGE	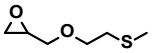	G		0.27	3.7	FR	201
SSG	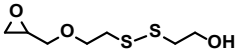	G		G faster		MCT	202
BBAG	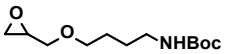	G		G faster		MCT	203
BO		G		0.19	6.1	FR	204
				0.19	6.08	FR	130
				0.11	7.94	FR	130
AGE	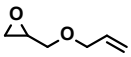	AHGE	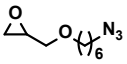	1.31	0.77	BSL	205
AGE	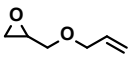	DOGE	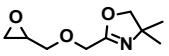	0.74	1.40	BSL	206
AGE	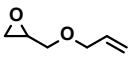	fcGE	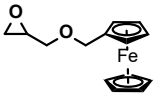	random		MCT	53
PO		EPB		1.0	1.0	FR	103
PO		DEGA	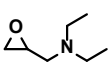	1.90	0.30	FR	103
				1.75	0.88	FR	104
				1.71	0.86	KT	104
				1.74	0.88	ML	104

PO		GMTE		0.54	4.45	FR	[103]
PO		SO		0.62	2.07	FR	[103]
PO		GME		0.31	3.15	FR	[103]
PO		TFPO		0.16	18.0	FR	[103]
PO		G		0.17	4.70	FR	[130]

[a]numerically solved; BSL: Beckingham-Sanoja-Lynd;[24] TSA: Triad sequence analysis; EGD: end-groud dyad analysis;[107] JA: Jaacks;[67,68] FR: Fineman-Ross;[65] MCT: monomer conversion over time; KT: Kelen-Tüdos;[66] ML: Meyer-Lowry.[49]

Monomer-activated Anionic Ring-Opening Polymerization (MAROP)

The copolymerization of functional epoxides with EO and PO via Lewis acid-activated polymerization is discussed, with an emphasis on the resulting copolymer microstructure.

The use of aluminum-based catalysis for the activation and polymerization of epoxides dates back to the 1960s, pioneered by Vandenberg.[207] Aida and Inoue developed a diethyl aluminum chloride-based 5,10,15,20-tetraphenyl porphyrin system, which was significantly improved by introducing sterically demanding Lewis acids.[208–212] Tsvetanov *et al*. developed a porphyrin-free catalytic system for the polymerization of EO using $NaAlBu_4$.[213] Another porphyrin-free system, developed by Braune and Okuda, employed neutral Lewis acid precursors and “ate” complexes for the polymerization of PO.[214]

In 2004, Deffieux and Carlotti published a seminal work on the polymerization of PO that marked a breakthrough in polymerization techniques, now commonly referred to as "monomer-activated anionic ring-opening polymerization" (MAROP).[215] MAROP has become an important alternative to conventional AROP.[133] The key element of MAROP is the initiator-catalyst system, typically composed of an organic salt such as tetraoctylammonium bromide ($NOct_4Br$) or methyl triphenylphosphonium bromide ($MePPh_3Br$), serving as an initiator, in combination with a Lewis acid such as triisobutylaluminum (TIBAL).[216–219]

The MAROP requires one equivalent of iBu$_3$Al based on the initiator to form the necessary “ate” complex. Additional iBu$_3$Al is required to activate the corresponding epoxide.[110,135,220] Monomers containing oxygen atoms capable of coordination, such as GEs, demand higher equivalents of iBu$_3$Al to achieve full monomer conversion.[147] Carlotti *et al*. investigated the influence of the catalyst-to-initiator ratio in the homopolymerization of ethoxyethyl glycidyl ether (EEGE) and found that

increasing the catalyst-to-initiator ratio led to shorter reaction times and higher monomer conversions.[110]

It is worth noting that the reactivity ratios determined for copolymerizations under MAROP conditions may depend on the catalyst-to-initiator ratio. However, to the best of our knowledge, no comprehensive study has been conducted on the influence of the amount of catalyst on the resulting polymer microstructure.

Copolymerization of Glycidyl Ethers with EO under MAROP conditions

The copolymerization of GEs under MAROP conditions typically results in gradient or tapered, block-like structures, with EO being preferentially incorporated. This preference is presumably due to the additional oxygen atom in glycidyl ethers, such as EEGE, which can coordinate with the catalyst, thereby reducing the activation of the epoxide moiety. As a result, GEs are considered less activated compared to EO, leading to distinct reactivity ratios, as summarized in Table 9.[59]

Table 9: GE comonomers copolymerized with EO under conditions of MAROP with respective reactivity ratios or incorporation behavior and characterization methods.

Comonomer		r_{co}	r_{EO}	Analysis	Ref.
GME			preferred	TSA	[147]
GPgE	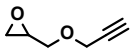	0.076	14.8	BSL	[109]
EEGE	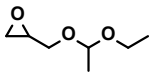	0.125	8.00	BSL	[59]
GTE	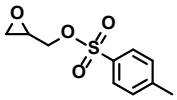	0.45	2.2	IdI, JA	[221]
		0.73	2.3	ML	[221]

BSL: Beckingham-Sanoja-Lynd;[24] TSA: Triad sequence analysis; JA: Jaacks;[67,68] ML: Meyer-Lowry;[49] IdI: Ideal Integrated.[69]

Copolymerization of Glycidyl Ethers with PO under MAROP Conditions

The copolymerization of EEGE with PO displays similar incorporation tendencies, although the gradient is less pronounced. This suggests that the additional methyl group in PO reduces its binding efficiency to the catalyst compared to the unsubstituted EO. Under conventional AROP conditions, the incorporation tendency of PO and EEGE is opposite to MAROP conditions. This inversion allows for the tailoring of different polymer microstructures by simply selecting the copolymerization method. Glycidyl tosyl ether (GTE) differs from typical glycidyl ethers in both electronic structure and steric demand. These differences result in almost random copolymerization with PO, as the opposing effects of the tosyl group balance each other, leading to reactivity ratios similar to those

of PO. Pasini, Coulembier *et al*. copolymerized AGE with PO utilizing an unusual [18]crown-6/potassium acetate catalyst. Although long reaction times were required, a quasi-alternating microstructure was reported.[222]

Table 10: GE comonomers copolymerized with PO under conditions of MAROP with determined reactivity ratios or incorporation behavior and analysis methods.

Comonomer		r_{CO}	r_{PO}	Analysis	Ref.
AGE	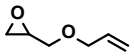	0.07	0.25	FR	[222]
EEGE	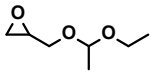	0.18	3.58	KT	[110]
GTE	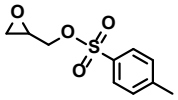	1.2	0.85	IdI, JA	[221]
		1.6	0.95	ML	[221]

JA: Jaacks;[67,68] ML: Meyer-Lowry;[49] IdI: Ideal Integrated;[69] FR: Fineman-Ross;[65] KT: Kelen-Tüdos.[66]

Copolymerization of Alkylene Oxides with EO under MAROP conditions

The copolymerization of EO with PO has been studied by different groups, with reactivity ratios determined through distinct analytical methods. Despite these varied approaches, a consistent trend emerges: EO, as the unsubstituted monomer, typically reacts faster than the methyl-substituted PO. This highlights the role of steric hindrance in reducing the monomer's coordination with the catalyst, impacting its reactivity. Epichlorohydrin (ECH) gives a tapered structure with EO, whereas copolymerization with the related epicyanohydrin (EPICH) results in a random or gradient incorporation. The copolymerization of EO with EPICH was investigated by TSA, a method that is more useful in confirming block structures, limiting the validity.[137] Methyl-4,5-epoxypentenoate (MEP) gives a random microstructure with EO, whereas *tert*-butyl-4-5-epoxypentenoate (^{t}BEP) exhibits a lower reactivity ratio than EO. The difference between the ester functionalities lies in the steric demand, possibly explaining their different incorporation behavior.

Table 11: AO comonomers copolymerized with EO under conditions of MAROP with determined reactivity ratios or incorporation behavior and analysis methods.

Comonomer		r_{co}	r_{EO}	Analysis	Ref.
PO		0.013	2.05	KT	[223]
		0.16	6.4	IdI	[69]
		0.13	5.8	ML	[69]
		0.5	0.3	KT	[209]
		0.13	7.9	IdI	[162]
		0.085	6.1	ML	[162]
		0.32	2.15	FR	[224]
ECH		0.10	9.2	FR	[225]
		0.03	6.55	FR	[224]
EPICH	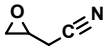	random/gradient		TSA	[137]
MEP	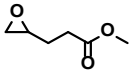	1.0	0.99	JA	[31]
^{t}BEP	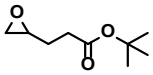	0.28	3.5	JA	[31]
		0.35	2.9	IdI	[31]

TSA: Triad sequence analysis; JA: Jaacks;[67,68] ML: Meyer-Lowry;[49] IdI: Ideal Integrated;[69]FR: Fineman- Ross;[65] KT: Kelen-Tüdos.[66]

Copolymerization of Functional Epoxides under MAROP Conditions

Table 12 lists several comonomer combinations copolymerized under MAROP conditions. The following trends can be seen: 1) the larger the substituent, the lower the reactivity ratio of the monomer (PO/BO). 2) Comonomers with similar structures show similar reactivity ratios (GME/EGE, GME/EEGE), leading to almost random incorporation. 3) Glycidyl esters have higher reactivity ratios than glycidyl ethers (GME/GMA, GC/EEGE). Deffieux *et al.*,[220] as well as Inoue *et al*.[209] investigated the copolymerization of PO and epichlorohydrin. The former used *i*Bu_3Al, the latter a tetraphenyl porphyrine-based aluminum catalyst. As one can see in the first two entries in Table 12, this results in completely different reactivity ratios. More data is needed to identify the reasons behind that difference.

Table 12: Comonomers copolymerized under MAROP conditions with determined reactivity ratios or incorporation behavior and analysis methods.

Comonomer 1	Comonomer 2	r_1	r_2	Analysis	Ref.
PO	ECH	1.21	0.16	KT	[220]
		5.1	6.3	KT	[209]
		2.75	0.11	FR	[224]
PO	BO	1.4	0.9	KT	[209]
PO	2,3-BO	1.8	≈0	KT	[209]
GME	EGE	0.95	0.92	FR	[112]
		0.98	0.95	KT	[112]
GME	EEGE	1.11	0.90	JA	[111]
		1.33	1.02	KT	[111]
GME	GMA	0.37	1.24	KT	[135]
EEGE	ECH	ECH preferred		MCT	[226]
AGE	ECH	1.4	6.6	KT	[227]
		1.42	0.49	FR	[224]
GC	EEGE	3.6	0.28	IdI	[136]
		3.9	0.25	JA	[136]
		2.7	0.16	ML	[136]

JA: Jaacks;[67,68] ML: Meyer-Lowry;[49] IdI: Ideal Integrated;[69]FR: Fineman-Ross;[65] KT: Kelen-Tüdos.[66]

Comparison of AROP and MAROP

Copolymerization can give different reactivity ratios, depending on whether conventional AROP or MAROP is utilized. A comparison of the generated polymers' microstructure of some binary systems will be given in the following. For a better visualization, the monomer distribution of the polyether copolymers was simulated, based on the reactivity ratios determined from the *in situ* NMR experiments for an equimolar comonomer mixture. As stated in the section "Impact of Reactivity Ratios on the Copolymer Microstructure", the graphical visualization only represents the average copolymer composition.

Copolymerization of EEGE with EO

Numerous works have investigated the copolymerization of EO with GEs. A comparison of the resulting copolymer microstructures for the EO/EEGE comonomer pair obtained *via* AROP and MAROP is shown in Figure 10.

	AROP	MAROP
	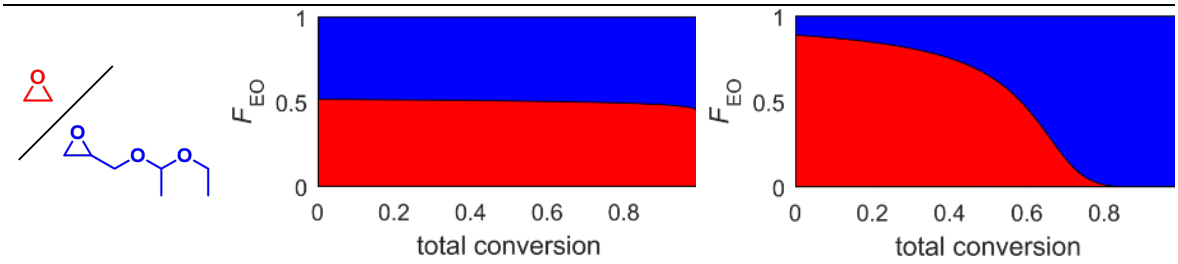	
Reactivity ratios	r_{EO} = 1.05 | r_{EEGE} = 0.94	r_{EO} = 8.00 | r_{EEGE} = 0.125
Reference	Frey *et al.*[59]	Frey *et al.*[59]

Figure 10: Simulated copolymer composition for an equimolar comonomer mixture, according to determined reactivity ratios for AROP (left) and MAROP (right) of EO/EEGE.

Depending on the applied copolymerization technique, the copolymerization of EO and EEGE results in either a random copolymer (AROP) or a copolymer with a strong gradient (MAROP).

Copolymerization of Alkylene Oxides

Heatley *et al.* demonstrated a gradient structure formed in the copolymerization of EO and PO *via* AROP. This gradient microstructure is more pronounced *via* MAROP, due to an increase in the reactivity of EO, which was investigated by Frey *et al.*[69]

	AROP	MAROP
	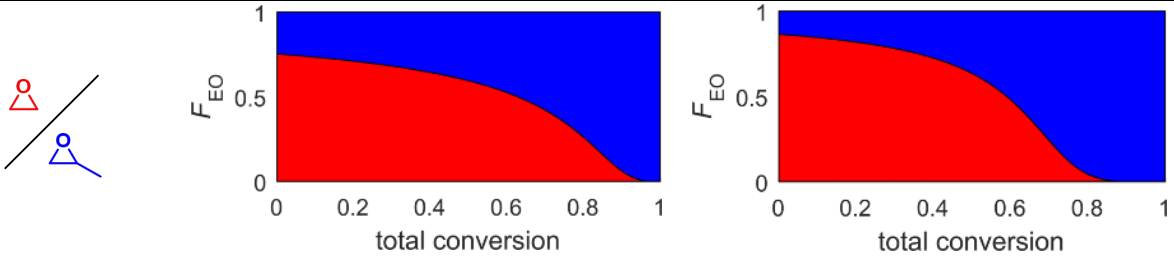	
Reactivity ratios	r_{EO} = 2.8 | r_{PO} = 0.25	r_{EO} = 6.4 | r_{PO} = 0.16
Reference	Heatley *et al.*[99]	Frey *et al.*[69]

Figure 11: Simulated copolymer composition for an equimolar comonomer mixture, according to determined reactivity ratios for AROP (left) and MAROP (right) of EO/PO.

Copolymerization of Glycidyl Ethers

The copolymerization of a binary system involving two GEs via AROP leads to a weak gradient structure, as demonstrated by Schmalz *et al.*[199] Under MAROP conditions, Weinhart *et al.*[112] observed equal monomer reactivity between GME and EGE. The polymerization method significantly influences the distribution of monomers along the polymer chain.

	AROP	MAROP
	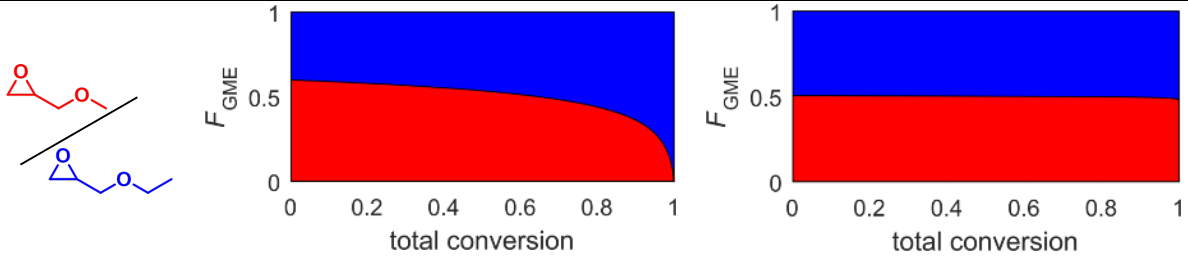	
Reactivity ratios	r_{GME} = 1.42 | r_{EGE} = 0.53	r_{GME} = 0.98 | r_{EGE} = 0.95
Reference	Schmalz *et al.*[199]	Weinhart *et al.*[112]

Figure 12: Simulated copolymer microstructure for an equimolar comonomer mixture, according to determined reactivity ratios for AROP (left) and MAROP (right) of GME/EGE.

The results cannot be generalized to every system, as more studies regarding the influence of the distinct reaction conditions for a broad range of monomers are needed.

Gradient Copolymers and How to Prepare Them

In order to achieve a continuous change in copolymer composition, all chains must be initiated fast and simultaneously. Further, no termination or chain transfer must occur until the end of the polymerization, *i.e.*, full monomer consumption. Since termination reactions lead to heterogeneity in the copolymer, living and controlled polymerization methods are essential for the synthesis of gradient copolymers.[3] In controlled radical polymerizations, the reversible termination of active chains, often described as “degenerative transfer,” plays a crucial role in maintaining control over the polymerization process.[1,43,44,228] The gradient can also be forced by continuously changing the feed rate of the monomers.[4]

In living and controlled anionic copolymerization, all chains grow continuously due to the simultaneous and rapid initiation, and ideally, no termination reactions occur.[40,42,229,230] Slow initiation leads to a broad dispersity, but according to calculations reported by Gold long ago, it should not exceed ≈ 1.38.[231]

Established techniques like the anionic[232] and cationic[30,233–237] polymerization as well as catalytic techniques like catalyst transfer polycondensation[238], catalyzed copolymerization of olefins[239] and epoxides[240] and ring-opening metathesis polymerization (ROMP)[241–244] are applied for the synthesis of gradient copolymers. The most common examples of gradient copolymers prepared by living anionic polymerization are copolymers of styrene, or styrene derivatives with butadiene or isoprene,[29,245–250] as well as polyether copolymers from EO and other epoxide monomers.[117,251] In the carbanionic copolymerization in apolar solvents like cyclohexane or benzene, small changes in the reaction conditions of the copolymerization of styrene and isoprene lead to completely different gradient structures. For instance, by adding tetrahydrofuran (THF) to cyclohexane, the gradient can be tailored and changes from r(Isoprene) = 10.03, r(Styrene) = 0.015 to r(Isoprene) = 0.012, r(Styrene) = 12.58. The strong gradient changes in this system are a result of the coordination of the lithium counterion.[161]

The particular properties of gradient copolymers differ from those of random and block copolymers.[2–4,252] A unique and probably the best-known feature of gradient copolymers is their broad glass transition temperature (T_g) range.[33,253–262] These broad glass transition temperatures result from incomplete microphase-segregation and are typically found between the T_gs of the respective homopolymers.[32,256,263] The T_gs of gradient copolymers show a stronger dependency regarding the polymer's thermal history compared to random or block copolymers.[1]

An investigation of the elasticity of gradient copolymers compared to the corresponding random copolymers revealed close Young's moduli, while the toughness of the gradient copolymers was increased.[255,264] Analysis of shear moduli revealed that diblock copolymers exhibit two segmental relaxation processes, while random copolymers show only one. In contrast, gradient copolymers display a single, but extremely broad, segmental relaxation, indicating a broad concentration distribution related to a continuous composition change in the microphase-separated state of the gradient copolymer.[1] They also exhibit a lower elastic modulus and greater elongation at break, while maintaining similar tensile strength. This behavior is attributed to the facilitation of stress concentration resulting from the gradual change in local modulus across different, and often smaller, nanodomain types.[3,265,266]

Gradient copolymers in selective solvents display behavior similar to their corresponding block copolymers, particularly in their tendency to form spherical micelles, provided the gradient in composition is sufficiently steep. Unlike block copolymers, which exhibit an abrupt change in composition along the polymer chain, gradient copolymers do not have a distinct point of composition change. As a result, micelles formed from gradient copolymers typically show less

pronounced segregation of monomer units and less defined core-shell structures.[267] The critical micelle concentration (CMC) of gradient copolymers can be higher or comparable to that of the corresponding block copolymers due to the lower probability of long hydrophobic segments.[268–270] The surface properties are strongly influenced by the monomer unit sequence (steepness of the gradient).[270–272] The monomer sequence plays a significant role in controlling the micellar size in water. Random copolymers produce more size-uniform micelles compared to gradient or block copolymers composed of random or gradient blocks.[273]

Block copolymers of EO and PO are highly relevant nonionic surfactants and have been extensively studied.[274,275] The hydrophilic PEO and hydrophobic PPO confer these copolymers with amphiphilic and biocompatible properties, making them useful in various applications, from everyday products like soaps to pharmaceutical and agricultural formulations.[117,275,276] Block and statistical copolymers are also used in lubricants, such as water-based fire-resistant hydraulic fluids, and metal-working applications like high-speed machining of stainless steel. When heated, these copolymers precipitate and coat the interface between the tool and metal, providing excellent lubrication. However, careful selection of the used polymers and formulation is required to prevent excessive foaming due to their amphiphilic nature.[277] In the field of lubrication, copolymers are often referred to as “random”, but we want to emphasize that they exhibit a pronounced gradient.[99] The cloud point of the block and statistical copolymers depends on the composition, molar mass,[274,278–281] and the gradient[100] (controlled by the reactivity ratios in the chosen polymerization method[69]). Determination of the reactivity ratios is crucial for controlling the cloud point, among other factors. Statistical copolymers of EO and BO are known to exhibit an ordinary gradient structure[184] (see Table 6), yet they behave similarly to block copolymers concerning their association properties. This allows the desired characteristics to be achieved in a single step, without a sequential monomer addition.[282] In contrast, the copolymerization of EO with GME results in a random microstructure, with no discernible pattern in the arrangement of monomer units. The copolymer maintains a uniform monomer distribution throughout the reaction, regardless of conversion. This structure closely mimics PEG and is discussed as a potential alternative in drug delivery applications, as its disordered structure prevents anti-PEG antibodies from recognizing and binding to it.[190]

Conclusion

In the past decade, *in situ* NMR techniques have become well-established for studying living or controlled statistical copolymerizations. Unlike free radical copolymerizations, which involve transfer and termination reactions, controlled copolymerizations allow for the direct correlation between reactivity ratios and the gradient of the resulting copolymer structure. *In situ* NMR allows

for investigating the microstructure of polyether copolymers based on common monomers such as ethylene oxide (EO) and propylene oxide (PO), as well as comonomers like alkylene oxides, glycidyl ethers, glycidyl amines, and glycidyl esters. By applying different qualitative and quantitative methods discussed in this review, the reactivity of functional epoxides can be precisely determined. A detailed understanding of copolymer microstructure is essential for evaluating structure-property relationships.

Functional polyethers hold potential for various applications, including surfactants, dispersants, and foam stabilizers. This review has provided a detailed analysis of binary systems comprising functional epoxides, highlighting their distinct reactivities based on the chosen polymerization method—whether AROP or MAROP. The selection of polymerization techniques allows for synthesizing custom copolymer architectures such as random, gradient, or tapered structures in a single step.

The microstructure of copolymers containing EO or PO is influenced by the choice of the binary systems. In AROP, glycidyl ethers generally yield random copolymers with EO, except for a few cases where a weak gradient is observed. The lower reactivity of PO compared to EO results in more gradient-like structures. Overall, alkylene oxides tend to be less reactive than EO and glycidyl ethers, typically resulting in gradient microstructures. Glycidyl amines are a unique class of functional epoxides, revealing a lower reactivity than glycidyl ethers and alkylene oxides. Therefore, glycidyl amines are more likely incorporated at the end of the polymer chain.

Copolymerizations of EO or PO with glycidyl ethers and alkylene oxides *via* MAROP typically result in gradient and tapered microstructures, with few exceptions. MAROP has been observed to enhance gradient structures in binary systems compared to AROP. The findings outlined in this review are crucial for understanding and fine-tuning the properties of multifunctional PEG and PPO, which hold great potential in bioconjugation, drug transport, and controlled release. In these applications, achieving a uniform distribution of functional groups along the polyether backbone is often a key objective. Additionally, the synthesis of strongly tapered polyethers through straightforward statistical copolymerization presents opportunities for various pharmaceutical and biomedical uses. Statistical copolymers with a strong gradient can exhibit similar properties to block copolymers but can be prepared in batches.

The reactivity ratios presented in this review should be approached with some caution. To the best of our knowledge, a comprehensive comparison of reaction parameters, (solvents, temperature, additives, comonomer pairs, catalysts and their equivalents, etc.) is not published. We have

compiled as many reactivity ratios from various copolymerization studies as possible. The data were analyzed with a diverse range of models under distinct conditions, which makes direct comparison impractical. We encourage researchers to refer to the system that most closely aligns with their own as a preliminary reference point.

Furthermore, we emphasize the importance of determining reactivity ratios specific to the researcher's own system. Modern techniques, such as *in situ* NMR, make this feasible. When evaluating reactivity ratios, it is highly recommended to use integrated models. One should begin with integrated nonterminal models (BSL, Jaacks, Ideal Integrated) to analyze the experimental data. If these models do not sufficiently explain the experimental data, only then should integrated terminal models (Meyer-Lowry) be considered.

Acknowledgments

The authors thank [redacted] for the thorough correction of the manuscript. [redacted] thank the Graduate School "Materials Science in Mainz (MAINZ)" for financial support.

References

(1) Matyjaszewski, K.; Ziegler, M. J.; Arehart, S. V.; Greszta, D.; Pakula, T. Gradient copolymers by atom transfer radical copolymerization. *J. Phys. Org. Chem.* **2000**, *13* (12), 775–786. DOI: 10.1002/1099-1395(200012)13:12<775:AID-POC314>3.0.CO;2-D.

(2) Beginn, U. Gradient copolymers. *Colloid. Polym. Sci.* **2008**, *286* (13), 1465–1474. DOI: 10.1007/s00396-008-1922-y.

(3) Zaremski, M. Y.; Kalugin, D. I.; Golubev, V. B. Gradient copolymers: Synthesis, structure, and properties. *Polym. Sci. Ser. A* **2009**, *51* (1), 103–122. DOI: 10.1134/S0965545X09010088.

(4) Zhang, J.; Farias-Mancilla, B.; Destarac, M.; Schubert, U. S.; Keddie, D. J.; Guerrero-Sanchez, C.; Harrisson, S. Asymmetric Copolymers: Synthesis, Properties, and Applications of Gradient and Other Partially Segregated Copolymers. *Macromol. Rapid Commun.* **2018**, *39* (19), e1800357. DOI: 10.1002/marc.201800357.

(5) Zhang, C.; Geng, X.; Zhang, X.; Gnanou, Y.; Feng, X. Alkyl borane-mediated metal-free ring-opening (co)polymerizations of oxygenated monomers. *Prog. Polym. Sci.* **2023**, *136*, 101644. DOI: 10.1016/j.progpolymsci.2022.101644.

(6) Naumann, S. Borane catalysis for epoxide (co)polymerization. *Polym. Chem.* **2023**, *14* (16), 1834–1862. DOI: 10.1039/D3PY00018D.

(7) Linker, O. Development of Epoxide Monomers for Ion-Complexation and Non-Covalent Interactions in Polyether Copolymers. Dissertation, Johannes Gutenberg-Universität, Mainz, 2019.

(8) Cowie, J. M. G.; Arrighi, V. *Polymers*:*Chemistry and physics of modern materials*, 3rd edn.; CRC Press Taylor & Francis group, 2007. DOI: 10.1201/9781420009873.

(9) Odian, G. *Principles of Polymerization*, 4th ed.; Wiley-Interscience, 2004. DOI: 10.1002/047147875X.

(10) Mayo, F. R.; Lewis, F. M. Copolymerization. I. A Basis for Comparing the Behavior of Monomers in Copolymerization; The Copolymerization of Styrene and Methyl Methacrylate. *J. Am. Chem. Soc.* **1944**, *66* (9), 1594–1601. DOI: 10.1021/ja01237a052.

(11) Goldfinger, G.; Kane, T. Derivation of the copolymerization equation without steady-state assumptions. *J. Polym. Sci.* **1948**, *3* (3), 462–463. DOI: 10.1002/pol.1948.120030322.

(12) Kucera, M. *Mechanism and kinetics of addition polymerizations*, 2., rev. ed.; Comprehensive chemical kinetics / ed. by R. G. Compton Section 10, Modern methods, theory, and data, Vol. 31; Elsevier, 1992.

(13) Matyjaszewski, K.; Gnanou, Y.; Leibler, L. *Macromolecular Engineering*:*Precise Synthesis, Materials Properties, Applications*; Wiley, 2007. DOI: 10.1002/9783527631421.

(14) Coates, G. W.; Sawamoto, M. Chain polymerization of vinyl monomers. In *Polymer Science*:*A comprehensive reference*; Matyjaszewski, K., Möller, M., Eds.; Elsevier, 2012.

(15) Tieke, B. *Makromolekulare Chemie*:*Eine Einführung*, 3. Aufl.; Wiley-VCH, 2014.

(16) Zhang, W.; Allgaier, J.; Zorn, R.; Willbold, S. Determination of the Compositional Profile for Tapered Copolymers of Ethylene Oxide and 1,2-Butylene Oxide by In-situ-NMR. *Macromolecules* **2013**, *46* (10), 3931–3938. DOI: 10.1021/ma400166n.

(17) Jenkins, A. D.; Kratochvíl, P.; Stepto, R. F. T.; Suter, U. W. Glossary of basic terms in polymer science (IUPAC Recommendations 1996). *Pure Appl. Chem.* **1996**, *68* (12), 2287–2311. DOI: 10.1351/pac199668122287.

(18) Jones, R. G.; Wilks, E. S.; Metanomski, W. V.; Kahovec, J.; Hess, M.; Stepto, R.; Kitayama, T. *Compendium of polymer terminology and nomenclature*:*IUPAC Recommendations 2008; issued by the polymer division*; RSC Publishing, 2009. DOI: 10.1039/9781847559425.

(19) Luscombe, C. K.; Moad, G.; Hiorns, R. C.; Jones, R. G.; Keddie, D. J.; Matson, J. B.; Merna, J.; Nakano, T.; Russell, G. T.; Topham, P. D. A brief guide to polymerization terminology (IUPAC Technical Report). *Pure Appl. Chem.* **2022**, *94* (9), 1079–1084. DOI: 10.1515/pac-2021-0115.

(20) Penczek, S.; Moad, G. Glossary of terms related to kinetics, thermodynamics, and mechanisms of polymerization (IUPAC Recommendations 2008). *Pure Appl. Chem.* **2008**, *80* (10), 2163–2193. DOI: 10.1351/pac200880102163.

(21) Wall, F. T. The Structure of Copolymers. II 1. *J. Am. Chem. Soc.* **1944**, *66* (12), 2050–2057. DOI: 10.1021/ja01240a014.

(22) Mayo, F. R.; Walling, C. Copolymerization. *Chem. Rev.* **1950**, *46* (2), 191–287. DOI: 10.1021/cr60144a001.

(23) Rudin, A.; Choi, P. *The elements of polymer science & engineering*, 3. ed.; Elsevier Academic Press, 2013.

(24) Beckingham, B. S.; Sanoja, G. E.; Lynd, N. A. Simple and Accurate Determination of Reactivity Ratios Using a Nonterminal Model of Chain Copolymerization. *Macromolecules* **2015**, *48* (19), 6922–6930. DOI: 10.1021/acs.macromol.5b01631.

(25) *Encyclopedia of polymeric nanomaterials*; Springer reference; Springer, 2015.

(26) Introduction to polymer science. In *Plastics in the Circular Economy*; Voet, V., Jager, J., Folkersma, R., Eds.; De Gruyter, 2024; pp 11–83. DOI: 10.1515/9783111201443-002.

(27) Carlotti, S.; Peruch, F. Cyclic Monomers: Epoxides, Lactide, Lactones, Lactams, Cyclic Silicon-Containing Monomers, Cyclic Carbonates, and Others. In *Anionic Polymerization*; Hadjichristidis, N., Hirao, A., Eds.; Springer Japan, 2015; pp 191–305. DOI: 10.1007/978-4-431-54186-8_5.

(28) Szwarc, M.; Beylen, M. *Ionic Polymerization and Living Polymers*; Springer Netherlands, 1993. DOI: 10.1007/978-94-011-1478-3.

(29) Beckingham, B. S.; Register, R. A. Synthesis and Phase Behavior of Block-Random Copolymers of Styrene and Hydrogenated Isoprene. *Macromolecules* **2011**, *44* (11), 4313–4319. DOI: 10.1021/ma200913k.

(30) Hoogenboom, R.; Fijten, M. W. M.; Wijnans, S.; van den Berg, A. M. J.; Thijs, H. M. L.; Schubert, U. S. High-throughput synthesis and screening of a library of random and gradient copoly(2-oxazoline)s. *J. Comb. Chem.* **2006**, *8* (2), 145–148. DOI: 10.1021/cc050087q.

(31) Linker, O.; Blankenburg, J.; Maciol, K.; Bros, M.; Frey, H. Ester Functional Epoxide Monomers for Random and Gradient Poly(ethylene glycol) Polyelectrolytes with Multiple Carboxylic Acid Moieties. *Macromolecules* **2020**, *53* (9), 3524–3534. DOI: 10.1021/acs.macromol.9b02320.

(32) Slimani, M. Z.; Moreno, A. J.; Rossi, G.; Colmenero, J. Dynamic Heterogeneity in Random and Gradient Copolymers: A Computational Investigation. *Macromolecules* **2013**, *46* (12), 5066–5079. DOI: 10.1021/ma400577d.

(33) Wong, C. L. H.; Kim, J.; Torkelson, J. M. Breadth of glass transition temperature in styrene/acrylic acid block, random, and gradient copolymers: Unusual sequence distribution effects. *J. Polym. Sci. B Polym. Phys.* **2007**, *45* (20), 2842–2849. DOI: 10.1002/polb.21296.

(34) Debrie, C.; Coudert, N.; Abdul, J.; Harrisson, S.; Colombani, O.; Rieger, J. Controlling the Composition Profile of Acrylic Acid Copolymers by Tuning the pH of Polymerization in Aqueous

Dispersed Media. *Macromolecules* **2023**, *56* (21), 8497–8506. DOI: 10.1021/acs.macromol.3c01507.

(35) Guerassimoff, L.; Ferrere, M.; van Herck, S.; Dehissi, S.; Nicolas, V.; Geest, B. G. de; Nicolas, J. Thermosensitive polymer prodrug nanoparticles prepared by an all-aqueous nanoprecipitation process and application to combination therapy. *J. Control. Release* **2024**, *369*, 376–393. DOI: 10.1016/j.jconrel.2024.03.049.

(36) Pakula, T.; Matyjaszewski, K. Copolymers with controlled distribution of comonomers along the chain, 1. Structure, thermodynamics and dynamic properties of gradient copolymers. Computer simulation. *Macromol. Theory Simul.* **1996**, *5* (5), 987–1006. DOI: 10.1002/mats.1996.040050514.

(37) Gleede, T.; Markwart, J. C.; Huber, N.; Rieger, E.; Wurm, F. R. Competitive Copolymerization: Access to Aziridine Copolymers with Adjustable Gradient Strengths. *Macromolecules* **2019**, *52* (24), 9703–9714. DOI: 10.1021/acs.macromol.9b01623.

(38) Simha, R.; Wall, L. A. Copolymerization. *J. Res. Natl. Bur. Stan.* **1948**, *41* (5), 521. DOI: 10.6028/jres.041.042.

(39) Molau, G. E. Heterogeneous polymer systems. III. Phase separation in styrene-acrylonitrile copolymers. *J. Polym. Sci. B Polym. Lett.* **1965**, *3* (12), 1007–1015. DOI: 10.1002/pol.1965.110031207.

(40) Szwarc, M. 'Living' Polymers. *Nature* **1956**, *178* (4543), 1168–1169. DOI: 10.1038/1781168a0.

(41) Sogah, D. Y.; Hertler, W. R.; Webster, O. W.; Cohen, G. M. Group transfer polymerization. Polymerization of acrylic monomers. *Macromolecules* **1987**, *20* (7), 1473–1488. DOI: 10.1021/ma00173a006.

(42) Webster, O. W. Living polymerization methods. *Science (New York, N.Y.)* **1991**, *251* (4996), 887–893. DOI: 10.1126/science.251.4996.887.

(43) Wang, J.-S.; Matyjaszewski, K. Controlled/"living" radical polymerization. Atom transfer radical polymerization in the presence of transition-metal complexes. *J. Am. Chem. Soc.* **1995**, *117* (20), 5614–5615. DOI: 10.1021/ja00125a035.

(44) Chiefari, J.; Chong, Y. K.; Ercole, F.; Krstina, J.; Jeffery, J.; Le, T. P. T.; Mayadunne, R. T. A.; Meijs, G. F.; Moad, C. L.; Moad, G.; Rizzardo, E.; Thang, S. H. Living Free-Radical Polymerization by

Reversible Addition−Fragmentation Chain Transfer: The RAFT Process. *Macromolecules* **1998**, *31* (16), 5559–5562. DOI: 10.1021/ma9804951.

(45) Nicolas, J.; Guillaneuf, Y.; Lefay, C.; Bertin, D.; Gigmes, D.; Charleux, B. Nitroxide-mediated polymerization. *Prog. Polym. Sci.* **2013**, *38* (1), 63–235. DOI: 10.1016/j.progpolymsci.2012.06.002.

(46) Matyjaszewski, K.; Möller, M., Eds. *Polymer Science*:*A comprehensive reference*; Elsevier, 2012.

(47) Waack, R.; Rembaum, A.; Coombes, J. D.; Szwarc, M. Molecular weights of "living" polymers. *J. Am. Chem. Soc.* **1957**, *79* (8), 2026–2027. DOI: 10.1021/ja01565a077.

(48) Skeist, I. Copolymerization: the composition distribution curve. *J. Am. Chem. Soc.* **1946**, *68* (9), 1781–1784. DOI: 10.1021/ja01213a031.

(49) Meyer, V. E.; Lowry, G. G. Integral and differential binary copolymerization equations. *J. Polym. Sci. A Gen. Pap.* **1965**, *3* (8), 2843–2851. DOI: 10.1002/pol.1965.100030811.

(50) Narita, H.; Hoshii, Y.; Machida, S. Determination of monomer reactivity ratios in copolymerizations with *N*-vinylpyrrolidone by means of high-speed liquid chromatography. *Angew. Makromol. Chem.* **1976**, *52* (1), 117–127. DOI: 10.1002/apmc.1976.050520111.

(51) Natansohn, A. Method for reactivity ratio determination in high-conversion copolymerisations by means of ^{1}H-n.m.r. spectroscopy. *Brit. Poly. J.* **1978**, *10* (3), 218–220. DOI: 10.1002/pi.4980100313.

(52) Gramm, S.; Komber, H.; Schmaljohann, D. Copolymerization kinetics of *N*-isopropylacrylamide and diethylene glycol monomethylether monomethacrylate determined by online NMR spectroscopy. *J. Polym. Sci. Part A: Polym. Chem.* **2005**, *43* (1), 142–148. DOI: 10.1002/pola.20514.

(53) Alkan, A.; Natalello, A.; Wagner, M.; Frey, H.; Wurm, F. R. Ferrocene-Containing Multifunctional Polyethers: Monomer Sequence Monitoring via Quantitative ^{13}C NMR Spectroscopy in Bulk. *Macromolecules* **2014**, *47* (7), 2242–2249. DOI: 10.1021/ma500323m.

(54) Quinebèche, S.; Navarro, C.; Gnanou, Y.; Fontanille, M. In situ mid-IR and UV–visible spectroscopies applied to the determination of kinetic parameters in the anionic copolymerization of styrene and isoprene. *Polymer* **2009**, *50* (6), 1351–1357. DOI: 10.1016/j.polymer.2009.01.041.

(55) Hunley, M. T.; Beers, K. L. Nonlinear Method for Determining Reactivity Ratios of Ring-Opening Copolymerizations. *Macromolecules* **2013**, *46* (4), 1393–1399. DOI: 10.1021/ma302015e.

(56) van den Brink, M.; Smulders, W.; van Herk, A. M.; German, A. L. Nonlinear regression by visualization of the sum of residual space applied to the integrated copolymerization equation with errors in all variables. II. Application to the system methyl methacrylate-α-methylene-γ-butyrolactone using on-line Raman spectroscopy. *J. Polym. Sci. Part A: Polym. Chem.* **1999**, *37* (20), 3804–3816. DOI: 10.1002/(SICI)1099-0518(19991015)37:20<3804:AID-POLA9>3.0.CO;2-B.

(57) Pasquale, A. J.; Long, T. E. Determination of monomer reactivity ratios using in situ FTIR spectroscopy for maleic anhydride/norbornene-free-radical copolymerization. *J. Appl. Polym. Sci.* **2004**, *92* (5), 3240–3246. DOI: 10.1002/app.20355.

(58) Huijser, S.; Mooiweer, G. D.; van der Hofstad, R.; Staal, B. B. P.; Feenstra, J.; van Herk, A. M.; Koning, C. E.; Duchateau, R. Reactivity Ratios of Comonomers from a Single MALDI-ToF-MS Measurement at One Feed Composition. *Macromolecules* **2012**, *45* (11), 4500–4510. DOI: 10.1021/ma300400d.

(59) Herzberger, J.; Leibig, D.; Liermann, J. C.; Frey, H. Conventional Oxyanionic versus Monomer-Activated Anionic Copolymerization of Ethylene Oxide with Glycidyl Ethers: Striking Differences in Reactivity Ratios. *ACS Macro Lett.* **2016**, *5* (11), 1206–1211. DOI: 10.1021/acsmacrolett.6b00701.

(60) Debnath, D.; Baughman, J. A.; Datta, S.; Weiss, R. A.; Pugh, C. Determination of the Radical Reactivity Ratios of 2-(*N*-Ethylperfluorooctanesulfonamido)ethyl Acrylate and Methacrylate in Copolymerizations with *N*,*N*-Dimethylacrylamide by *in Situ* ^{1}H NMR Analysis As Established for Styrene-Methyl Methacrylate Copolymerizations. *Macromolecules* **2018**, *51* (20), 7951–7963. DOI: 10.1021/acs.macromol.8b01526.

(61) Tsai, S. D.; Register, R. A. Endo/Exo Reactivity Ratios in Living Vinyl Addition Polymerization of Substituted Norbornenes. *Macromol. Chem. Phys.* **2018**, *219* (11). DOI: 10.1002/macp.201800059.

(62) Grune, E.; Johann, T.; Appold, M.; Wahlen, C.; Blankenburg, J.; Leibig, D.; Müller, A. H. E.; Gallei, M.; Frey, H. One-Step Block Copolymer Synthesis versus Sequential Monomer Addition: A Fundamental Study Reveals That One Methyl Group Makes a Difference. *Macromolecules* **2018**, *51* (9), 3527–3537. DOI: 10.1021/acs.macromol.8b00404.

(63) Wall, F. T. The Structure of Vinyl Copolymers. *J. Am. Chem. Soc.* **1941**, *63* (7), 1862–1866. DOI: 10.1021/ja01852a016.

(64) Alfrey, T.; Goldfinger, G. The Mechanism of Copolymerization. *J. Chem. Phys.* **1944**, *12* (6), 205–209. DOI: 10.1063/1.1723934.

(65) Fineman, M.; Ross, S. D. Linear method for determining monomer reactivity ratios in copolymerization. *J. Polym. Sci.* **1950**, *5* (2), 259–262. DOI: 10.1002/pol.1950.120050210.

(66) Kelen, T.; Tüdos, F. Analysis of the Linear Methods for Determining Copolymerization Reactivity Ratios. I. A New Improved Linear Graphic Method. *J. Macromol. Sci. - Chem.* **1975**, *9* (1), 1–27. DOI: 10.1080/00222337508068644.

(67) Jaacks, V. Eine neuartige Methode zur Bestimmung von Copolymerisationsparametern. *Angew. Chem.* **1967**, *79* (9), 419. DOI: 10.1002/ange.19670790927.

(68) Jaacks, V. A Novel Method of Determination of Reactivity Ratios in Binary and Ternary Copolymerizations. *Makromol. Chem.* **1972**, *161* (1), 161–172. DOI: 10.1002/macp.1972.021610110.

(69) Blankenburg, J.; Kersten, E.; Maciol, K.; Wagner, M.; Zarbakhsh, S.; Frey, H. The poly(propylene oxide-*co*-ethylene oxide) gradient is controlled by the polymerization method: determination of reactivity ratios by direct comparison of different copolymerization models. *Polym. Chem.* **2019**, *10* (22), 2863–2871. DOI: 10.1039/C9PY00500E.

(70) Wagner-Jauregg, T. Über addierende Hetero-polymerisation. *Ber. dtsch. Chem. Ges. A/B* **1930**, *63* (11), 3213–3224. DOI: 10.1002/cber.19300631140.

(71) Melville, H. W.; Noble, B.; Watson, W. F. Copolymerization. I. Kinetics and some experimental considerations of a general theory. *J. Polym. Sci.* **1947**, *2* (2), 229–245. DOI: 10.1002/pol.1947.120020210.

(72) Rudin, A. *The elements of polymer science and engineering*:*An introductory text for engineers and chemists*; Acad. Press, 1982.

(73) Fried, J. R. *Polymer science and technology*, 2. ed.; Prentice Hall PTR, 2003.

(74) Autzen, A. A. A.; Beuermann, S.; Drache, M.; Fellows, C. M.; Harrisson, S.; van Herk, A. M.; Hutchinson, R. A.; Kajiwara, A.; Keddie, D. J.; Klumperman, B.; Russell, G. T. IUPAC recommended experimental methods and data evaluation procedures for the determination of radical copolymerization reactivity ratios from composition data. *Polym. Chem.* **2024**, *15* (18), 1851–1861. DOI: 10.1039/D4PY00270A.

(75) Lynd, N. A.; Ferrier, R. C.; Beckingham, B. S. Recommendation for Accurate Experimental Determination of Reactivity Ratios in Chain Copolymerization. *Macromolecules* **2019**, *52* (6), 2277–2285. DOI: 10.1021/acs.macromol.8b01752.

(76) Tüdos, F.; Kelen, T.; Földes-berezsnich, T.; Turcsányi, B. Analysis of Linear Methods for Determining Copolymerization Reactivity Ratios. III. Linear Graphic Method for Evaluating Data Obtained at High Conversion Levels. *J. Macromol. Sci. - Chem.* **1976**, *10* (8), 1513–1540. DOI: 10.1080/00222337608060768.

(77) Kelen, T.; Tüdos, F.; Turcsányi, B.; Kennedy, J. P. Analysis of the linear methods for determining copolymerization reactivity ratios. IV. A comprehensive and critical reexamination of carbocationic copolymerization data. *J. Polym. Sci. Polym. Chem. Ed.* **1977**, *15* (12), 3047–3074. DOI: 10.1002/pol.1977.170151219.

(78) Behnken, D. W. Estimation of copolymer reactivity ratios: An example of nonlinear estimation. *J. Polym. Sci. A Gen. Pap.* **1964**, *2* (2), 645–668. DOI: 10.1002/pol.1964.100020207.

(79) Tidwell, P. W.; Mortimer, G. A. An improved method of calculating copolymerization reactivity ratios. *J. Polym. Sci. A Gen. Pap.* **1965**, *3* (1), 369–387. DOI: 10.1002/pol.1965.100030137.

(80) van Herk, A. M. Least-Squares Fitting by Visualization of the Sum of Squares Space. *J. Chem. Educ.* **1995**, *72* (2), 138. DOI: 10.1021/ed072p138.

(81) Mahdavian, A. R.; Abdollahi, M.; Mokhtabad, L.; Reza Bijanzadeh, H.; Ziaee, F. Kinetic study of radical polymerization. IV. Determination of reactivity ratio in copolymerization of styrene and itaconic acid by ^{1}H-NMR. *J. Appl. Polym. Sci.* **2006**, *101* (3), 2062–2069. DOI: 10.1002/app.23795.

(82) Abdollahi, M.; Sharifpour, M. A new simple procedure to calculate monomer reactivity ratios by using on-line ^{1}H NMR kinetic experiments: Copolymerization system with greater difference between the monomer reactivity ratios. *Polymer* **2007**, *48* (1), 25–30. DOI: 10.1016/j.polymer.2006.11.010.

(83) Barner-Kowollik, C.; Heuts, J. P. A.; Davis, T. P. Free-radical copolymerization of styrene and itaconic acid studied by ^{1}H NMR kinetic experiments. *J. Polym. Sci. Part A: Polym. Chem.* **2001**, *39* (5), 656–664. DOI: 10.1002/1099-0518(20010301)39:5<656:AID-POLA1037>3.0.CO;2-9.

(84) Barner, L.; Barner-Kowollik, C.; Davis, T. P. Free-radical copolymerization of styrene and *m*-isopropenyl-α,α'-dimethylbenzyl isocyanate studied by ^{1}H NMR kinetic experiments. *J. Polym. Sci. Part A: Polym. Chem.* **2002**, *40* (8), 1064–1074. DOI: 10.1002/pola.10195.

(85) Mahdavian, A.-R.; Abdollahi, M.; Bijanzadeh, H. R. Kinetic study of radical polymerization. III. Solution polymerization of acrylamide by ^{1}H-NMR. *J. Appl. Polym. Sci.* **2004**, *93* (5), 2007–2013. DOI: 10.1002/app.20649.

(86) Bataille, P.; Bourassa, H. Determination of the reactivity parameters for the copolymerization of butyl acrylate with vinyl acetate. *J. Polym. Sci. Part A: Polym. Chem.* **1989**, *27* (1), 357–365. DOI: 10.1002/pola.1989.080270130.

(87) O'Driscoll, K. F.; Kale, L. T.; Rubio, L. H. G.; Reilly, P. M. Applicability of the Mayo-Lewis equation to high conversion copolymerization of styrene and methylmethacrylate. *J. Polym. Sci. Polym. Chem. Ed.* **1984**, *22* (11), 2777–2788. DOI: 10.1002/pol.1984.170221104.

(88) Tiedemann, P. von; Blankenburg, J.; Maciol, K.; Johann, T.; Müller, A. H. E.; Frey, H. Copolymerization of Isoprene with *p*-Alkylstyrene Monomers: Disparate Reactivity Ratios and the Shape of the Gradient. *Macromolecules* **2019**, *52* (3), 796–806. DOI: 10.1021/acs.macromol.8b02280.

(89) Blankenburg, J.; Maciol, K.; Hahn, C.; Frey, H. Poly(ethylene glycol) with Multiple Aldehyde Functionalities Opens up a Rich and Versatile Post-Polymerization Chemistry. *Macromolecules* **2019**, *52* (4), 1785–1793. DOI: 10.1021/acs.macromol.8b02639.

(90) Jaacks, V. Anomalien bei der kationischen Copolymerisation von Trioxan. 32. Mitt. über Polyoxymethylene. *Makromol. Chem.* **1967**, *101* (1), 33–57. DOI: 10.1002/macp.1967.021010103.

(91) Heuts, J. P. A.; Gilbert, R. G.; Maxwell, I. A. Penultimate Unit Effect in Free-Radical Copolymerization. *Macromolecules* **1997**, *30* (4), 726–736. DOI: 10.1021/ma960704m.

(92) Hoffman, R.; Carpenter, B. K.; Minkin, V. I. Ockham's Razor and Chemistry. *HYLE* **1997**, *3*, 3–28.

(93) Hawkins, D. M. The problem of overfitting. *J. Chem. Inf. Comput. Sci.* **2004**, *44* (1), 1–12. DOI: 10.1021/ci0342472.

(94) Fordyce, R. G.; Ham, G. E. Copolymerization. VIII. Reactivity of Fumaronitrile in Vinyl Copolymerization. *J. Am. Chem. Soc.* **1951**, *73* (3), 1186–1189. DOI: 10.1021/ja01147a092.

(95) Seiner, J. A.; Litt, M. The Role of Monomer Charge-Transfer Complexes in Free Radical Copolymerization. I. Derivation of Terminal Complex Model Equations. *Macromolecules* **1971**, *4* (3), 308–311. DOI: 10.1021/ma60021a009.

(96) Hill, D. J. T.; O'Donnell, J. H.; O'Sullivan, P. W. Analysis of the complex-dissociation model for free-radical copolymerization. *Macromolecules* **1983**, *16* (8), 1295–1300. DOI: 10.1021/ma00242a008.

(97) Brown, P. G.; Fujimori, K. The comppen model: A combined complex-participation/penultimate effect model for free-radical copolymerization. *J. Polym. Sci. Part A: Polym. Chem.* **1994**, *32* (15), 2971–2978. DOI: 10.1002/pola.1994.080321520.

(98) Müller, A. H. E. Macromolecular architectures and soft nano-objects. In *Polymer Science*:*A comprehensive reference*; Matyjaszewski, K., Möller, M., Eds.; Elsevier, 2012.

(99) Heatley, F.; Yu, G.; Booth, C.; Blease, T. G. Determination of reactivity ratios for the anionic copolymerization of ethylene oxide and propylene oxide in bulk. *Eur. Polym. J.* **1991**, *27* (7), 573–579. DOI: 10.1016/0014-3057(91)90138-E.

(100) Hesse, M. S.; Linden, G. M.; Frey, H. Reaction Temperature and Solvent Determine Reactivity Ratios in the Copolymerization of Ethylene Oxide and Propylene Oxide. Manuscript in preparation.

(101) Niederer, K.; Schüll, C.; Leibig, D.; Johann, T.; Frey, H. Catechol Acetonide Glycidyl Ether (CAGE): A Functional Epoxide Monomer for Linear and Hyperbranched Multi-Catechol Functional Polyether Architectures. *Macromolecules* **2016**, *49* (5), 1655–1665. DOI: 10.1021/acs.macromol.5b02441.

(102) Herzberger, J.; Fischer, K.; Leibig, D.; Bros, M.; Thiermann, R.; Frey, H. Oxidation-Responsive and "Clickable" Poly(ethylene glycol) via Copolymerization of 2-(Methylthio)ethyl Glycidyl Ether. *J. Am. Chem. Soc.* **2016**, *138* (29), 9212–9223. DOI: 10.1021/jacs.6b04548.

(103) Ponomarenko, V. A.; Khomutov, A. M.; Il'chenko, S. I.; Ignatenko, A. V. The effect of substituents of the anionic polymerization of α-oxides. *Polym. Sci. U.S.S.R.* **1971**, *13* (7), 1735–1740. DOI: 10.1016/0032-3950(71)90364-9.

(104) Blankenburg, J.; Wagner, M.; Frey, H. Well-Defined Multi-Amino-Functional and Stimuli-Responsive Poly(propylene oxide) by Crown Ether Assisted Anionic Ring-Opening Polymerization. *Macromolecules* **2017**, *50* (22), 8885–8893. DOI: 10.1021/acs.macromol.7b01324.

(105) Herzberger, J.; Kurzbach, D.; Werre, M.; Fischer, K.; Hinderberger, D.; Frey, H. Stimuli-Responsive Tertiary Amine Functional PEGs Based on *N*,*N*-Dialkylglycidylamines. *Macromolecules* **2014**, *47* (22), 7679–7690. DOI: 10.1021/ma501367b.

(106) Lee, A.; Lundberg, P.; Klinger, D.; Lee, B. F.; Hawker, C. J.; Lynd, N. A. Physiologically relevant, pH-responsive PEG-based block and statistical copolymers with *N*,*N*-diisopropylamine units. *Polym. Chem.* **2013**, *4* (24), 5735–5742. DOI: 10.1039/C3PY00747B.

(107) Lee, B. F.; Wolffs, M.; Delaney, K. T.; Sprafke, J. K.; Leibfarth, F. A.; Hawker, C. J.; Lynd, N. A. Reactivity ratios, and mechanistic insight for anionic ring-opening copolymerization of epoxides. *Macromolecules* **2012**, *45* (9), 3722–3731. DOI: 10.1021/ma300634d.

(108) Wu, Z.; Liu, P.; Liu, Y.; Wei, W.; Zhang, X.; Wang, P.; Xu, Z.; Xiong, H. Regulating sequence distribution of polyethers via ab initio kinetics control in anionic copolymerization. *Polym. Chem.* **2017**, *8* (37), 5673–5678. DOI: 10.1039/C7PY01073G.

(109) Herzberger, J.; Leibig, D.; Langhanki, J.; Moers, C.; Opatz, T.; Frey, H. "Clickable PEG" via anionic copolymerization of ethylene oxide and glycidyl propargyl ether. *Polym. Chem.* **2017**, *8* (12), 1882–1887. DOI: 10.1039/C7PY00173H.

(110) Gervais, M.; Brocas, A.-L.; Cendejas, G.; Deffieux, A.; Carlotti, S. Synthesis of Linear High Molar Mass Glycidol-Based Polymers by Monomer-Activated Anionic Polymerization. *Macromolecules* **2010**, *43* (4), 1778–1784. DOI: 10.1021/ma902286a.

(111) Schubert, C.; Dreier, P.; Nguyen, T.; Maciol, K.; Blankenburg, J.; Friedrich, C.; Frey, H. Synthesis of linear polyglycerols with tailored degree of methylation by copolymerization and the effect on thermorheological behavior. *Polymer* **2017**, *121*, 328–339. DOI: 10.1016/j.polymer.2017.05.030.

(112) Heinen, S.; Rackow, S.; Schäfer, A.; Weinhart, M. A Perfect Match: Fast and Truly Random Copolymerization of Glycidyl Ether Monomers to Thermoresponsive Copolymers. *Macromolecules* **2017**, *50* (1), 44–53. DOI: 10.1021/acs.macromol.6b01904.

(113) Gleede, T.; Rieger, E.; Blankenburg, J.; Klein, K.; Wurm, F. R. Fast Access to Amphiphilic Multiblock Architectures by the Anionic Copolymerization of Aziridines and Ethylene Oxide. *J. Am. Chem. Soc.* **2018**, *140* (41), 13407–13412. DOI: 10.1021/jacs.8b08054.

(114) Rieger, E.; Blankenburg, J.; Grune, E.; Wagner, M.; Landfester, K.; Wurm, F. R. Controlling the Polymer Microstructure in Anionic Polymerization by Compartmentalization. *Angew. Chem. Int. Ed.* **2018**, *57* (9), 2483–2487. DOI: 10.1002/anie.201710417.

(115) Koyama, Y.; Umehara, M.; Mizuno, A.; Itaba, M.; Yasukouchi, T.; Natsume, K.; Suginaka, A. Synthesis of novel poly(ethylene glycol) derivatives having pendant amino groups and aggregating

behavior of its mixture with fatty acid in water. *Bioconjugate Chem.* **1996**, *7* (3), 298–301. DOI: 10.1021/bc9600123.

(116) Taton, D.; Le Borgne, A.; Sepulchre, M.; Spassky, N. Synthesis of chiral and racemic functional polymers from glycidol and thioglycidol. *Macromol. Chem. Phys.* **1994**, *195* (1), 139–148. DOI: 10.1002/macp.1994.021950111.

(117) Herzberger, J.; Niederer, K.; Pohlit, H.; Seiwert, J.; Worm, M.; Wurm, F. R.; Frey, H. Polymerization of Ethylene Oxide, Propylene Oxide, and Other Alkylene Oxides: Synthesis, Novel Polymer Architectures, and Bioconjugation. *Chem. Rev.* **2016**, *116* (4), 2170–2243. DOI: 10.1021/acs.chemrev.5b00441.

(118) Obermeier, B.; Wurm, F.; Mangold, C.; Frey, H. Multifunctional Poly(ethylene glycol)s. *Angew. Chem. Int. Ed.* **2011**, *50* (35), 7988–7997. DOI: 10.1002/anie.201100027.

(119) Mangold, C.; Wurm, F.; Frey, H. Functional PEG-based polymers with reactive groups via anionic ROP of tailor-made epoxides. *Polym. Chem.* **2012**, *3* (7), 1714. DOI: 10.1039/c2py00489e.

(120) Kurzbach, D.; Wilms, V. S.; Frey, H.; Hinderberger, D. Impact of Amino-Functionalization on the Response of Poly(ethylene glycol) (PEG) to External Stimuli. *ACS Macro Lett.* **2013**, *2* (2), 128–131. DOI: 10.1021/mz300596r.

(121) Reuss, V. S.; Werre, M.; Frey, H. Thermoresponsive copolymers of ethylene oxide and *N*,*N*-diethyl glycidyl amine: polyether polyelectrolytes and PEGylated gold nanoparticle formation. *Macromol. Rapid Commun.* **2012**, *33* (18), 1556–1561. DOI: 10.1002/marc.201200307.

(122) Tonhauser, C.; Alkan, A.; Schömer, M.; Dingels, C.; Ritz, S.; Mailänder, V.; Frey, H.; Wurm, F. R. Ferrocenyl Glycidyl Ether: A Versatile Ferrocene Monomer for Copolymerization with Ethylene Oxide to Water-Soluble, Thermoresponsive Copolymers. *Macromolecules* **2013**, *46* (3), 647–655. DOI: 10.1021/ma302241w.

(123) Alkan, A.; Klein, R.; Shylin, S. I.; Kemmer-Jonas, U.; Frey, H.; Wurm, F. R. Water-soluble and redox-responsive hyperbranched polyether copolymers based on ferrocenyl glycidyl ether. *Polym. Chem.* **2015**, *6* (40), 7112–7118. DOI: 10.1039/C5PY01162K.

(124) Schüttner, S.; Krappel, M.; Koziol, M.; Marquart, L.; Schneider, I.; Sottmann, T.; Frey, H. Anionic Ring-Opening Copolymerization of Farnesyl Glycidyl Ether: Fast Access to Terpenoid-Derived Amphiphilic Polyether Architectures. *Macromolecules* **2023.** DOI: 10.1021/acs.macromol.3c00999.

(125) Müller, V.; Matthes, R.; Wagner, M.; Bros, M.; Dreier, P.; Frey, H. Tailoring thermoresponsiveness of biocompatible polyethers: copolymers of linear glycerol and ethyl glycidyl ether. *Polym. Chem.* **2023**, *14* (21), 2599–2609. DOI: 10.1039/d3py00064h.

(126) Dreier, P.; Pipertzis, A.; Spyridakou, M.; Mathes, R.; Floudas, G.; Frey, H. Introduction of Trifluoromethanesulfonamide Groups in Poly(ethylene oxide): Ionic Conductivity of Single-Ion-Conducting Block Copolymer Electrolytes. *Macromolecules* **2022**, *55* (4), 1342–1353. DOI: 10.1021/acs.macromol.1c02507.

(127) Verkoyen, P.; Dreier, P.; Bros, M.; Hils, C.; Schmalz, H.; Seiffert, S.; Frey, H. "Dumb" pH-Independent and Biocompatible Hydrogels Formed by Copolymers of Long-Chain Alkyl Glycidyl Ethers and Ethylene Oxide. *Biomacromolecules* **2020**, *21* (8), 3152–3162. DOI: 10.1021/acs.biomac.0c00576.

(128) Schömer, M.; Schüll, C.; Frey, H. Hyperbranched aliphatic polyether polyols. *J. Polym. Sci. Part A: Polym. Chem.* **2013**, *51* (5), 995–1019. DOI: 10.1002/pola.26496.

(129) Sunder, A.; Hanselmann, R.; Frey, H.; Mülhaupt, R. Controlled Synthesis of Hyperbranched Polyglycerols by Ring-Opening Multibranching Polymerization. *Macromolecules* **1999**, *32* (13), 4240–4246. DOI: 10.1021/ma990090w.

(130) Leibig, D.; Seiwert, J.; Liermann, J. C.; Frey, H. Copolymerization Kinetics of Glycidol and Ethylene Oxide, Propylene Oxide, and 1,2-Butylene Oxide: From Hyperbranched to Multiarm Star Topology. *Macromolecules* **2016**, *49* (20), 7767–7776. DOI: 10.1021/acs.macromol.6b01477.

(131) Price, C. C.; Atarashi, Y.; Yamamoto, R. Polymerization and copolymerization of some epoxides by potassium *tert*-butoxide in DMSO. *J. Polym. Sci. A-1 Polym. Chem.* **1969**, *7* (2), 569–574. DOI: 10.1002/pol.1969.150070211.

(132) Hans, M.; Keul, H.; Moeller, M. Chain transfer reactions limit the molecular weight of polyglycidol prepared via alkali metal based initiating systems. *Polymer* **2009**, *50* (5), 1103–1108. DOI: 10.1016/j.polymer.2009.01.012.

(133) Brocas, A.-L.; Mantzaridis, C.; Tunc, D.; Carlotti, S. Polyether synthesis: From activated or metal-free anionic ring-opening polymerization of epoxides to functionalization. *Prog. Polym. Sci.* **2013**, *38* (6), 845–873. DOI: 10.1016/j.progpolymsci.2012.09.007.

(134) Grobelny, Z.; Swinarew, A.; Jurek-Suliga, J.; Skrzeczyna, K.; Gabor, J.; Łężniak, M. The Influence of Crown Ether and Alcohol on Unsaturation and Molar Mass of Poly(propylene oxide)s Prepared

by Use of Potassium *t*-Butoxide: Reinvestigation of Chain Transfer Reactions. *Int. J. Anal. Chem.* **2016**, *2016*, 3727062. DOI: 10.1155/2016/3727062.

(135) Labbé, A.; Brocas, A.-L.; Ibarboure, E.; Ishizone, T.; Hirao, A.; Deffieux, A.; Carlotti, S. Selective Ring-Opening Polymerization of Glycidyl Methacrylate: Toward the Synthesis of Cross-Linked (Co)polyethers with Thermoresponsive Properties. *Macromolecules* **2011**, *44* (16), 6356–6364. DOI: 10.1021/ma201075n.

(136) Maciol, K.; Schüttner, S.; Blankenburg, J.; Johann, T.; Frey, H. Glycidyl Cinnamate: Copolymerization with Glycidyl Ethers, In-Situ NMR Kinetics, and Photocrosslinking. *Macromol. Chem. Phys.* **2023**, *224* (3), 2200366. DOI: 10.1002/macp.202200366.

(137) Herzberger, J.; Frey, H. Epicyanohydrin: Polymerization by Monomer Activation Gives Access to Nitrile-, Amino-, and Carboxyl-Functional Poly(ethylene glycol). *Macromolecules* **2015**, *48* (22), 8144–8153. DOI: 10.1021/acs.macromol.5b02178.

(138) Cantor, S. E.; Brindell, G. D.; Brett, T. J. Synthesis and Polymerization Studies of Cyano Epoxides. *J. Macromol. Sci. - Chem.* **1973**, *7* (7), 1483–1508. DOI: 10.1080/10601327308060515.

(139) Wei, P. E.; Butler, P. E. Synthesis and polymerization studies of several chloro and cyano epoxides. *J. Polym. Sci. A-1 Polym. Chem.* **1968**, *6* (9), 2461–2475. DOI: 10.1002/pol.1968.150060904.

(140) Mattson, K. M.; Latimer, A. A.; McGrath, A. J.; Lynd, N. A.; Lundberg, P.; Hudson, Z. M.; Hawker, C. J. A facile synthesis of catechol-functionalized poly(ethylene oxide) block and random copolymers. *J. Polym. Sci. Part A: Polym. Chem.* **2015**, *53* (23), 2685–2692. DOI: 10.1002/pola.27749.

(141) Deffieux, A.; Carlotti, S.; Barrère, A. Anionic Ring-Opening Polymerization of Epoxides and Related Nucleophilic Polymerization Processes. In *Polymer Science*:*A comprehensive reference*; Matyjaszewski, K., Möller, M., Eds.; Elsevier, 2012; pp 117–140. DOI: 10.1016/B978-0-444-53349-4.00099-6.

(142) Huguet, J.; Vert, M.; Spassky, N.; Selegny, E. Polymerization of oxiranylalkylamines and thiiranylalkylamines derived from achiral and racemic secondary amines. *Makromol. Chem.* **1973**, *170* (1), 23–37. DOI: 10.1002/macp.1973.021700103.

(143) Sakakibara, K.; Nakano, K.; Nozaki, K. Regio-controlled ring-opening polymerization of perfluoroalkyl-substituted epoxides. *Chem. Commun.* **2006** (31), 3334–3336. DOI: 10.1039/b606693c.

(144) Allgaier, J.; Willbold, S.; Chang, T. Synthesis of Hydrophobic Poly(alkylene oxide)s and Amphiphilic Poly(alkylene oxide) Block Copolymers. *Macromolecules* **2007**, *40* (3), 518–525. DOI: 10.1021/ma062417g.

(145) He, J.; Wang, Y.; Lin, Q.; Chen, L.; Zhou, X. Synthesis and Characterization of Functional Gradient Copolymers of 2-Hydroxyethyl Methacrylate and *tert*-Butyl Acrylate by Atom Transfer Radical Polymerization. *J. Macromol. Sci., Part A: Pure Appl. Chem.* **2009**, *46* (4), 405–411. DOI: 10.1080/10601320902728702.

(146) Min, K.; Li, M.; Matyjaszewski, K. Preparation of gradient copolymers via ATRP using a simultaneous reverse and normal initiation process. I. Spontaneous gradient. *J. Polym. Sci. Part A: Polym. Chem.* **2005**, *43* (16), 3616–3622. DOI: 10.1002/pola.20809.

(147) Müller, S. S.; Moers, C.; Frey, H. A Challenging Comonomer Pair: Copolymerization of Ethylene Oxide and Glycidyl Methyl Ether to Thermoresponsive Polyethers. *Macromolecules* **2014**, *47* (16), 5492–5500. DOI: 10.1021/ma501280k.

(148) Kozlowski, H.; Kolkowska, P.; Watly, J.; Krzywoszynska, K.; Potocki, S. General aspects of metal toxicity. *Curr. Med. Chem.* **2014**, *21* (33), 3721–3740. DOI: 10.2174/09298673216661407160938 38.

(149) Linert, W. *Metal Ions in Neurological Systems*, 1st ed.; Springer Wien, 2012.

(150) Shaw, C. A.; Tomljenovic, L. Aluminum in the central nervous system (CNS): toxicity in humans and animals, vaccine adjuvants, and autoimmunity. *Immunol. Res.* **2013**, *56* (2-3), 304–316. DOI: 10.1007/s12026-013-8403-1.

(151) Mangold, C.; Dingels, C.; Obermeier, B.; Frey, H.; Wurm, F. PEG-based Multifunctional Polyethers with Highly Reactive Vinyl-Ether Side Chains for Click-Type Functionalization. *Macromolecules* **2011**, *44* (16), 6326–6334. DOI: 10.1021/ma200898n.

(152) Bailey, D. B.; Henrichs, P. M. Diad, triad, and pentad sequence-distribution analysis of acrylonitrile-vinylidene chloride model copolymers by ^{13}C-NMR. *J. Polym. Sci. Polym. Chem. Ed.* **1978**, *16* (12), 3185–3199. DOI: 10.1002/pol.1978.170161213.

(153) Deng, Y.; Ding, J.; Yu, G.; Mobbs, R. H.; Heatley, F.; Price, C.; Booth, C. Preparation and properties of *stat*-copoly-(oxyethylene-oxypropylene)-*block*-poly (oxyethylene): 1. Use of crown ether in the anionic copolymerization of propylene oxide and ethylene oxide. *Polymer* **1992**, *33* (9), 1959–1962. DOI: 10.1016/0032-3861(92)90500-V.

(154) Newmark, R. A. Sequence distribution in polyethylene/tetramethylene terephthalate copolyesters by ^{13}C-NMR. *J. Polym. Sci. Polym. Chem. Ed.* **1980**, *18* (2), 559–563. DOI: 10.1002/pol.1980.170180216.

(155) Oguni, N.; Lee, K.; Tani, H. Microstructure Analysis of Poly(propylene oxide) by ^{13}C Nuclear Magnetic Resonance Spectroscopy. *Macromolecules* **1972**, *5* (6), 819–820. DOI: 10.1021/ma60030a032.

(156) Mangold, C.; Wurm, F.; Obermeier, B.; Frey, H. "Functional Poly(ethylene glycol)": PEG-Based Random Copolymers with 1,2-Diol Side Chains and Terminal Amino Functionality. *Macromolecules* **2010**, *43* (20), 8511–8518. DOI: 10.1021/ma1015352.

(157) Zhang, L.; Du, W.; Wang, D.; Wang, F.; Fang, K.; Yu, J.; Sheng, B. Syntheses of polycarboxylate superplasticizers: Microwave induction versus conventional thermal induction. *Composites, Part B* **2021**, *207*, 108560. DOI: 10.1016/j.compositesb.2020.108560.

(158) Pang, X.; Jing, R.; Huang, J. Synthesis of amphiphilic macrocyclic graft copolymer consisting of a poly(ethylene oxide) ring and multi-poly(ε-caprolactone) lateral chains. *Polymer* **2008**, *49* (4), 893–900. DOI: 10.1016/j.polymer.2007.12.034.

(159) Garg, B. K.; Corredor, J.; Subramanian, R. V. Copolymerization of Tri-n-butyltin Acrylate and Tri-n-butyltin Methacrylate Monomers with Vinyl Monomers Containing Functional Groups. *J. Macromol. Sci. - Chem.* **1977**, *11* (9), 1567–1601. DOI: 10.1080/00222337708063077.

(160) Kazemi, N.; Duever, T. A.; Penlidis, A. Reactivity Ratio Estimation from Cumulative Copolymer Composition Data. *Macromol. React. Eng.* **2011**, *5* (9-10), 385–403. DOI: 10.1002/mren.201100009.

(161) Steube, M.; Johann, T.; Hübner, H.; Koch, M.; Dinh, T.; Gallei, M.; Floudas, G.; Frey, H.; Müller, A. H. E. Tetrahydrofuran: More than a "Randomizer" in the Living Anionic Copolymerization of Styrene and Isoprene: Kinetics, Microstructures, Morphologies, and Mechanical Properties. *Macromolecules* **2020**, *53* (13), 5512–5527. DOI: 10.1021/acs.macromol.0c01022.

(162) Kersten, E.; Linker, O.; Blankenburg, J.; Wagner, M.; Walther, P.; Naumann, S.; Frey, H. Revealing the Monomer Gradient of Polyether Copolymers Prepared Using *N*-Heterocyclic Olefins:

Metal-Free Anionic versus Zwitterionic Lewis Pair Polymerization. *Macromol. Chem. Phys.* **2023**, *224* (16). DOI: 10.1002/macp.202300097.

(163) Dreier, P.; Matthes, R.; Barent, R. D.; Schüttner, S.; Müller, A. H. E.; Frey, H. In Situ Kinetics Reveal the Influence of Solvents and Monomer Structure on the Anionic Ring-Opening Copolymerization of Epoxides. *Macromol. Chem. Phys.* **2022**, 2200209. DOI: 10.1002/macp.202200209.

(164) Zhu, C.; Burkey, A. A.; Adams, C. P.; Uruchurtu Patino, D.; Lynd, N. A. Concurrent Ring-Opening/Ring-Closing Polymerization of Glycidyl Acetate to Acid-Degradable Poly(ether-*co*-orthoester) Materials Using a Mono(*μ*-alkoxo)bis(alkylaluminum) Initiator. *Macromolecules* **2022**, *55* (7), 2797–2805. DOI: 10.1021/acs.macromol.2c00009.

(165) Rusu, E.; Comanita, E.; Airinei, A.; Rusu, G. Photosensitive monomers and polymers derived from glycidyl cinnamate. *Iran. Polym. J.* **1998**, *7*, 157–162.

(166) Pandey, R. K.; Kumar, R. Eco-friendly synthesis of epichlorohydrin catalyzed by titanium silicate (TS-1) molecular sieve and hydrogen peroxide. *Catal. Commun.* **2007**, *8* (3), 379–382. DOI: 10.1016/j.catcom.2006.07.007.

(167) Singh, G. S.; Mollet, K.; D'hooghe, M.; Kimpe, N. de. Epihalohydrins in organic synthesis. *Chem. Rev.* **2013**, *113* (3), 1441–1498. DOI: 10.1021/cr3003455.

(168) Gee, G.; Higginson, W. C. E.; Levesley, P.; Taylor, K. J. 266. Polymerisation of epoxides. Part I. Some kinetic aspects of the addition of alcohols to epoxides catalysed by sodium alkoxides. *J. Chem. Soc.* **1959** (0), 1338. DOI: 10.1039/JR9590001338.

(169) Yu, G.-E.; Masters, A. J.; Heatley, F.; Booth, C.; Blease, T. G. Anionic polymerisation of propylene oxide. Investigation of double-bond and head-to-head content by NMR spectroscopy. *Macromol. Chem. Phys.* **1994**, *195* (5), 1517–1538. DOI: 10.1002/macp.1994.021950506.

(170) Mark, H. F., Ed. *Encyclopedia of Polymer Science and Engineering*, 2. ed.; A Wiley Interscience publication; Wiley, 1985.

(171) Chisholm, M. H.; Navarro-Llobet, D. NMR Assignments of Regioregular Poly(propylene oxide) at the Triad and Tetrad Level. *Macromolecules* **2002**, *35* (6), 2389–2392. DOI: 10.1021/ma0119934.

(172) Klein, R.; Wurm, F. R. Aliphatic Polyethers: Classical Polymers for the 21st Century. *Macromol. Rapid Commun.* **2015**, *36* (12), 1147–1165. DOI: 10.1002/marc.201500013.

(173) Lourenço, A. V. Intermediäre Aether des Glykols. *J. Prakt. Chem.* **1860**, *79* (1), 212–213. DOI: 10.1002/prac.18600790130.

(174) Lourenço, A. V. Ueber die Polyäthylenalkohole. *J. Prakt. Chem.* **1862**, *85* (1), 389–392. DOI: 10.1002/prac.18620850149.

(175) Wurtz, A. Neue Untersuchungen über das Aethylenoxyd. *Justus Liebigs Ann. Chem.* **1860**, *116* (2), 249–252. DOI: 10.1002/jlac.18601160212.

(176) Staudinger, H.; Schweitzer, O. Über hochpolymere Verbindungen, 20. Mitteil.: Über die Polyäthylenoxyde. *Ber. dtsch. Chem. Ges. A/B* **1929**, *62* (8), 2395–2405. DOI: 10.1002/cber.19290620879.

(177) Staudinger, H.; Lohmann, H. Über hochpolymere Verbindungen. 81. Mitteilung. Über eukolloides Polyäthylenoxyd. *Justus Liebigs Ann. Chem.* **1933**, *505* (1), 41–51. DOI: 10.1002/jlac.19335050104.

(178) Flory, P. J. Molecular Size Distribution in Ethylene Oxide Polymers. *J. Am. Chem. Soc.* **1940**, *62* (6), 1561–1565. DOI: 10.1021/ja01863a066.

(179) Dingels, C.; Schömer, M.; Frey, H. Die vielen Gesichter des Poly(ethylenglykol)s. *Chem. Unserer Zeit* **2011**, *45* (5), 338–349. DOI: 10.1002/ciuz.201100551.

(180) Müller, S. S.; Dingels, C.; Hofmann, A. M.; Frey, H. Polyether-Based Lipids Synthesized with an Epoxide Construction Kit: Multivalent Architectures for Functional Liposomes, *1135*, 11–25. DOI: 10.1021/bk-2013-1135.ch002.

(181) Penczek, S.; Cypryk, M.; Duda, A.; Kubisa, P.; Slomkowski, S. Living ring-opening polymerizations of heterocyclic monomers. *Prog. Polym. Sci.* **2007**, *32* (2), 247–282. DOI: 10.1016/j.progpolymsci.2007.01.002.

(182) Solov'yanov, A. A.; Kazanskii, K. S. The kinetics and mechanism of anionic polymerization of ethylene oxide in ether solvents. *Polym. Sci. U.S.S.R.* **1972**, *14* (5), 1186–1195. DOI: 10.1016/0032-3950(72)90162-1.

(183) Thomas, A.; Müller, S. S.; Frey, H. Beyond poly(ethylene glycol): linear polyglycerol as a multifunctional polyether for biomedical and pharmaceutical applications. *Biomacromolecules* **2014**, *15* (6), 1935–1954. DOI: 10.1021/bm5002608.

(184) Dickson, S.; Yu, G.; Heatley, F.; Booth, C. Reactivity ratios for the anionic copolymerization of ethylene oxide and butylene oxide in bulk. *Eur. Polym. J.* **1993**, *29* (2-3), 281–286. DOI: 10.1016/0014-3057(93)90094-V.

(185) Obermeier, B.; Frey, H. Poly(ethylene glycol-*co*-allyl glycidyl ether)s: a PEG-based modular synthetic platform for multiple bioconjugation. *Bioconjugate Chem.* **2011**, *22* (3), 436–444. DOI: 10.1021/bc1004747.

(186) Schömer, M.; Frey, H. Water-Soluble "Poly(propylene oxide)" by Random Copolymerization of Propylene Oxide with a Protected Glycidol Monomer. *Macromolecules* **2012**, *45* (7), 3039–3046. DOI: 10.1021/ma300249c.

(187) Obermeier, B.; Wurm, F.; Frey, H. Amino Functional Poly(ethylene glycol) Copolymers via Protected Amino Glycidol. *Macromolecules* **2010**, *43* (5), 2244–2251. DOI: 10.1021/ma902245d.

(188) Mangold, C.; Wurm, F.; Obermeier, B.; Frey, H. Hetero-Multifunctional Poly(ethylene glycol) Copolymers with Multiple Hydroxyl Groups and a Single Terminal Functionality. *Macromol. Rapid Commun.* **2010**, *31* (3), 258–264. DOI: 10.1002/marc.200900472.

(189) Hofmann, A. M.; Wurm, F.; Frey, H. Rapid Access to Polyfunctional Lipids with Complex Architecture via Oxyanionic Ring-Opening Polymerization. *Macromolecules* **2011**, *44* (12), 4648–4657. DOI: 10.1021/ma200367c.

(190) Dreier, P.; Matthes, R.; Fuß, F.; Schmidt, J.; Schulz, D.; Linden, G. M.; Barent, R. D.; Schüttner, S.; Bros, M.; Frey, H. Isomerization of poly(ethylene glycol): A strategy for the evasion of immune recognition. *submitted*.

(191) Alkan, A.; Gleede, T.; Wurm, F. R. Ruthenocenyl Glycidyl Ether: A Ruthenium-Containing Epoxide for Anionic Polymerization. *Organometallics* **2017**, *36* (16), 3023–3028. DOI: 10.1021/acs.organomet.7b00278.

(192) Linden, G. M.; Schüttner, S.; Fribiczer, N.; Seiffert, S.; Frey, H. Polymers of Biobased Oleyl Glycidyl Ether: Insights into Copolymerization with Ethylene Oxide, Postmodification, Thermal Properties, and Micellization Behavior. *submitted*.

(193) Schüttner, S.; Linden, G. M.; Hoffmann, E. C.; Holzmüller, P.; Frey, H. Glycidyl Ethers from Acyclic Terpenes: A Versatile Toolbox for Multifunctional Poly(Ethylene Glycol)s with Modification Opportunities. *Polym. Chem.* **2024.** DOI: 10.1039/D4PY01201A.

(194) Yezrielev, A. I.; Brokhina, E. L.; Roskin, Y. An analytical method for calculating reactivity ratios. *Polym. Sci. U.S.S.R.* **1969**, *11* (8), 1894–1907. DOI: 10.1016/0032-3950(69)90478-X.

(195) P. Flodin; E. Gottberg-Klingskog; K. Holmberg. Determination of Monomer Reactivity Ratios in the Copolymerization of Ethylene Oxide and Propylene Oxide. *Tenside, Surfactants, Deterg.* **105** (1), 9–11. DOI: 10.1515/tsd-1994-310105.

(196) Rubin, D. B. The Bayesian Bootstrap. *Ann. Stat.* **1981**, *9* (1), 130–134.

(197) Reuss, V. S.; Obermeier, B.; Dingels, C.; Frey, H. *N*,*N*-Diallylglycidylamine: A Key Monomer for Amino-Functional Poly(ethylene glycol) Architectures. *Macromolecules* **2012**, *45* (11), 4581–4589. DOI: 10.1021/ma300292m.

(198) Isono, T.; Asai, S.; Satoh, Y.; Takaoka, T.; Tajima, K.; Kakuchi, T.; Satoh, T. Controlled/Living Ring-Opening Polymerization of Glycidylamine Derivatives Using *t*-Bu-P_4 /Alcohol Initiating System Leading to Polyethers with Pendant Primary, Secondary, and Tertiary Amino Groups. *Macromolecules* **2015**, *48* (10), 3217–3229. DOI: 10.1021/acs.macromol.5b00556.

(199) Reinicke, S.; Schmelz, J.; Lapp, A.; Karg, M.; Hellweg, T.; Schmalz, H. Smart hydrogels based on double responsive triblock terpolymers. *Soft Matter* **2009.** DOI: 10.1039/b900539k.

(200) Song, J.; Hwang, E.; Lee, Y.; Palanikumar, L.; Choi, S.-H.; Ryu, J.-H.; Kim, B.-S. Tailorable degradation of pH-responsive all polyether micelles via copolymerisation with varying acetal groups. *Polym. Chem.* **2019**, *10* (5), 582–592. DOI: 10.1039/C8PY01577E.

(201) Seiwert, J.; Herzberger, J.; Leibig, D.; Frey, H. Thioether-Bearing Hyperbranched Polyether Polyols with Methionine-Like Side-Chains: A Versatile Platform for Orthogonal Functionalization. *Macromol. Rapid Commun.* **2017**, *38* (1). DOI: 10.1002/marc.201600457.

(202) Son, S.; Shin, E.; Kim, B.-S. Redox-Degradable Biocompatible Hyperbranched Polyglycerols: Synthesis, Copolymerization Kinetics, Degradation, and Biocompatibility. *Macromolecules* **2015**, *48* (3), 600–609. DOI: 10.1021/ma502242v.

(203) Song, S.; Lee, J.; Kweon, S.; Song, J.; Kim, K.; Kim, B.-S. Hyperbranched Copolymers Based on Glycidol and Amino Glycidyl Ether: Highly Biocompatible Polyamines Sheathed in Polyglycerols. *Biomacromolecules* **2016**, *17* (11), 3632–3639. DOI: 10.1021/acs.biomac.6b01136.

(204) Seiwert, J.; Leibig, D.; Kemmer-Jonas, U.; Bauer, M.; Perevyazko, I.; Preis, J.; Frey, H. Hyperbranched Polyols via Copolymerization of 1,2-Butylene Oxide and Glycidol: Comparison of

Batch Synthesis and Slow Monomer Addition. *Macromolecules* **2016**, *49* (1), 38–47. DOI: 10.1021/acs.macromol.5b02402.

(205) Lee, J.; Han, S.; Kim, M.; Kim, B.-S. Anionic Polymerization of Azidoalkyl Glycidyl Ethers and Post-Polymerization Modification. *Macromolecules* **2020**, *53* (1), 355–366. DOI: 10.1021/acs.macromol.9b02236.

(206) Park, J.; Yu, Y.; Lee, J. W.; Kim, B.-S. Anionic Ring-Opening Polymerization of a Functional Epoxide Monomer with an Oxazoline Protecting Group for the Synthesis of Polyethers with Carboxylic Acid Pendants. *Macromolecules* **2022**, *55* (13), 5448–5458. DOI: 10.1021/acs.macromol.2c00761.

(207) Vandenberg, E. J. Organometallic catalysts for polymerizing monosubstituted epoxides. *J. Polym. Sci.* **1960**, *47* (149), 486–489. DOI: 10.1002/pol.1960.1204714947.

(208) Inoue, S.; Aida, T. Control of Ring-Opening Polymerization with Metalloporphyrin Catalysts. In *Anionic Polymerization*:*Kinetics, Mechanisms, and Synthesis*; McGrath, J. E., Ed.; ACS symposium series; American Chemical Society, 1981; pp 137–146. DOI: 10.1021/bk-1985-0286.ch010.

(209) Aida, T.; Wada, K.; Inoue, S. Copolymerization of epoxides by aluminum porphyrin. Reactivity of (porphinato)aluminum alkoxide as growing species. *Macromolecules* **1987**, *20* (2), 237–241. DOI: 10.1021/ma00168a001.

(210) Aida, T.; Mizuta, R.; Yoshida, Y.; Inoue, S. Polymerization of epoxides catalysed by metalloporphine. *Makromol. Chem.* **1981**, *182* (4), 1073–1079. DOI: 10.1002/macp.1981.021820408.

(211) Aida, T.; Inoue, S. Living polymerization of epoxides with metalloporphyrin and synthesis of block copolymers with controlled chain lengths. *Macromolecules* **1981**, *14* (5), 1162–1166. DOI: 10.1021/ma50006a004.

(212) Sugimoto, H.; Kawamura, C.; Kuroki, M.; Aida, T.; Inoue, S. Lewis Acid-Assisted Anionic Ring-Opening Polymerization of Epoxide by the Aluminum Complexes of Porphyrin, Phthalocyanine, Tetraazaannulene, and Schiff Base as Initiators. *Macromolecules* **1994**, *27* (8), 2013–2018. DOI: 10.1021/ma00086a006.

(213) Petrova, E. B.; Panayotov, I. M. Polymerization of 1,2-Epoxides Initiated by Tetraalkyl Aluminates. I. Polymerization of Ethylene Oxide in the Presence of Sodium Tetrabutyl Aluminate. *J. Macromol. Sci. - Chem.* **1985**, *22* (9), 1309–1324. DOI: 10.1080/00222338508063335.

(214) Braune, W.; Okuda, J. An efficient method for controlled propylene oxide polymerization: the significance of bimetallic activation in aluminum Lewis acids. *Angew. Chem. Int. Ed.* **2003**, *42* (1), 64–68. DOI: 10.1002/anie.200390054.

(215) Billouard, C.; Carlotti, S.; Desbois, P.; Deffieux, A. "Controlled" High-Speed Anionic Polymerization of Propylene Oxide Initiated by Alkali Metal Alkoxide/Trialkylaluminum Systems. *Macromolecules* **2004**, *37* (11), 4038–4043. DOI: 10.1021/ma035768t.

(216) Brocas, A.-L.; Gervais, M.; Carlotti, S.; Pispas, S. Amphiphilic diblock copolymers based on ethylene oxide and epoxides bearing aliphatic side chains. *Polym. Chem.* **2012**, *3* (8), 2148. DOI: 10.1039/c2py20189e.

(217) Carlotti, S.; Desbois, P.; Billouard, C.; Deffieux, A. Reactivity control in anionic polymerization of ethylenic and heterocyclic monomers through formation of 'ate' complexes. *Polym. Int.* **2006**, *55* (10), 1126–1131. DOI: 10.1002/pi.1981.

(218) Labbé, A.; Carlotti, S.; Billouard, C.; Desbois, P.; Deffieux, A. Controlled High-Speed Anionic Polymerization of Propylene Oxide Initiated by Onium Salts in the Presence of Triisobutylaluminum. *Macromolecules* **2007**, *40* (22), 7842–7847. DOI: 10.1021/ma070288d.

(219) Roos, K.; Carlotti, S. Grignard-based anionic ring-opening polymerization of propylene oxide activated by triisobutylaluminum. *Eur. Polym. J.* **2015**, *70*, 240–246. DOI: 10.1016/j.eurpolymj.2015.07.016.

(220) Carlotti, S.; Labbé, A.; Rejsek, V.; Doutaz, S.; Gervais, M.; Deffieux, A. Living/Controlled Anionic Polymerization and Copolymerization of Epichlorohydrin with Tetraoctylammonium Bromide-Triisobutylaluminum Initiating Systems. *Macromolecules* **2008**, *41* (19), 7058–7062. DOI: 10.1021/ma801422c.

(221) Jung, P.; Ziegler, A. D.; Blankenburg, J.; Frey, H. Glycidyl Tosylate: Polymerization of a "Non-Polymerizable" Monomer permits Universal Post-Functionalization of Polyethers. *Angew. Chem. Int. Ed.* **2019**, *58* (37), 12883–12886. DOI: 10.1002/anie.201904203.

(222) Fornaciari, C.; Lemaur, V.; Pasini, D.; Coulembier, O. Quasi-alternating copolymerization of oxiranes driven by a benign acetate-based catalyst. *Commun. Chem.* **2023**, *6* (1), 235. DOI: 10.1038/s42004-023-01031-z.

(223) Rejsek, V.; Sauvanier, D.; Billouard, C.; Desbois, P.; Deffieux, A.; Carlotti, S. Controlled Anionic Homo- and Copolymerization of Ethylene Oxide and Propylene Oxide by Monomer Activation. *Macromolecules* **2007**, *40* (18), 6510–6514. DOI: 10.1021/ma070450c.

(224) Xie, H.-Q.; Guo, J.-S.; Yu, G.-Q.; Zu, J. Ring-opening polymerization of epichlorohydrin and its copolymerization with other alkylene oxides by quaternary catalyst system. *J. Appl. Polym. Sci.* **2001**, *80* (13), 2446–2454. DOI: 10.1002/app.1351.

(225) Danner, A.-K.; Leibig, D.; Vogt, L.-M.; Frey, H. Monomer-activated Copolymerization of Ethylene Oxide and Epichlorohydrin: In Situ Kinetics Evidences Tapered Block Copolymer Formation. *Chin. J. Polym. Sci.* **2019**, *37* (9), 912–918. DOI: 10.1007/s10118-019-2296-y.

(226) Meyer, J.; Keul, H.; Möller, M. Poly(glycidyl amine) and Copolymers with Glycidol and Glycidyl Amine Repeating Units: Synthesis and Characterization. *Macromolecules* **2011**, *44* (11), 4082–4091. DOI: 10.1021/ma200757v.

(227) Brocas, A.-L.; Cendejas, G.; Caillol, S.; Deffieux, A.; Carlotti, S. Controlled synthesis of polyepichlorohydrin with pendant cyclic carbonate functions for isocyanate-free polyurethane networks. *J. Polym. Sci. Part A: Polym. Chem.* **2011**, *49* (12), 2677–2684. DOI: 10.1002/pola.24699.

(228) Zaremski, M. Y.; Xin, C.; Orlova, A. P.; Golubev, V. B.; Kurochkin, S. A.; Grachev, V. P. Effect of the nature of a solvent on pseudoliving free-radical polymerization of styrene mediated by TEMPO. *Polym. Sci. Ser. B* **2010**, *52* (9-10), 528–541. DOI: 10.1134/S1560090410090034.

(229) Quirk, R. P.; Lee, B. Experimental Criteria for Living Polymerizations. *Polym. Int.* **1992**, *27* (4), 359–367. DOI: 10.1002/pi.4990270412.

(230) Leibig, D.; Morsbach, J.; Grune, E.; Herzberger, J.; Müller, A. H.; Frey, H. Die lebende anionische Polymerisation. *Chem. Unserer Zeit* **2017**, *51* (4), 254–263. DOI: 10.1002/ciuz.201700774.

(231) Gold, L. Statistics of Polymer Molecular Size Distribution for an Invariant Number of Propagating Chains. *J. Chem. Phys.* **1958**, *28* (1), 91–99. DOI: 10.1063/1.1744088.

(232) Clough, A.; Sigle, J. L.; Tapash, A.; Gill, L.; Patil, N. V.; Zhou, J.; White, J. L. Component-Specific Heterogeneity and Differential Phase Partitioning in Gradient Copolymers Revealed by Solids NMR. *Macromolecules* **2014**, *47* (8), 2625–2631. DOI: 10.1021/ma500213k.

(233) Hoogenboom, R.; Lambermont-Thijs, H. M. L.; Jochems, M. J. H. C.; Hoeppener, S.; Guerlain, C.; Fustin, C.-A.; Gohy, J.-F.; Schubert, U. S. A schizophrenic gradient copolymer: switching and reversing poly(2-oxazoline) micelles based on UCST and subtle solvent changes. *Soft Matter* **2009**, *5* (19), 3590. DOI: 10.1039/B912491H.

(234) Hoogenboom, R.; Thijs, H. M. L.; Fijten, M. W. M.; van Lankvelt, B. M.; Schubert, U. S. One-pot synthesis of 2-phenyl-2-oxazoline-containing quasi-diblock copoly(2-oxazoline)s under microwave irradiation. *J. Polym. Sci. Part A: Polym. Chem.* **2007**, *45* (3), 416–422. DOI: 10.1002/pola.21711.

(235) Milonaki, Y.; Kaditi, E.; Pispas, S.; Demetzos, C. Amphiphilic gradient copolymers of 2-methyl- and 2-phenyl-2-oxazoline: self-organization in aqueous media and drug encapsulation. *J. Polym. Sci. Part A: Polym. Chem.* **2012**, *50* (6), 1226–1237. DOI: 10.1002/pola.25888.

(236) Uchman, M.; Hajduová, J.; Vlassi, E.; Pispas, S.; Appavou, M.-S.; Štěpánek, M. Self- and co-assembly of amphiphilic gradient polyelectrolyte in aqueous solution: Interaction with oppositely charged ionic surfactant. *Eur. Polym. J.* **2015**, *73*, 212–221. DOI: 10.1016/j.eurpolymj.2015.10.015.

(237) Vlassi, E.; Pispas, S. Solution Behavior of Hydrolyzed Gradient Methyl/Phenyl Oxazoline Copolymers and Complexation with DNA. *Macromol. Chem. Phys.* **2015**, *216* (8), 873–883. DOI: 10.1002/macp.201400552.

(238) Hardeman, T.; Koeckelberghs, G. The Synthesis of Poly(thiophene-*co*-fluorene) Gradient Copolymers. *Macromolecules* **2015**, *48* (19), 6987–6993. DOI: 10.1021/acs.macromol.5b01384.

(239) Xiang, P.; Ye, Z. Alternating, gradient, block, and block-gradient copolymers of ethylene and norbornene by Pd-Diimine-Catalyzed “living” copolymerization. *J. Polym. Sci. Part A: Polym. Chem.* **2013**, *51* (3), 672–686. DOI: 10.1002/pola.26419.

(240) Liu, Y.; Ren, W.-M.; He, K.-K.; Lu, X.-B. Crystalline-gradient polycarbonates prepared from enantioselective terpolymerization of meso-epoxides with CO_2. *Nat. Commun.* **2014**, *5*, 5687. DOI: 10.1038/ncomms6687.

(241) Chang, A. B.; Lin, T.-P.; Thompson, N. B.; Luo, S.-X.; Liberman-Martin, A. L.; Chen, H.-Y.; Lee, B.; Grubbs, R. H. Design, Synthesis, and Self-Assembly of Polymers with Tailored Graft Distributions. *J. Am. Chem. Soc.* **2017**, *139* (48), 17683–17693. DOI: 10.1021/jacs.7b10525.

(242) Dettmer, C. M.; Gray, M. K.; Torkelson, J. M.; Nguyen, S. T. Synthesis and Functionalization of ROMP-Based Gradient Copolymers of 5-Substituted Norbornenes. *Macromolecules* **2004**, *37* (15), 5504–5512. DOI: 10.1021/ma036002w.

(243) Kim, K. O.; Choi, T.-L. Synthesis of Dendronized Polymers via Macromonomer Approach by Living ROMP and Their Characterization: From Rod-Like Homopolymers to Block and Gradient Copolymers. *Macromolecules* **2013**, *46* (15), 5905–5914. DOI: 10.1021/ma401132u.

(244) Lin, T.-P.; Chang, A. B.; Chen, H.-Y.; Liberman-Martin, A. L.; Bates, C. M.; Voegtle, M. J.; Bauer, C. A.; Grubbs, R. H. Control of Grafting Density and Distribution in Graft Polymers by Living Ring-Opening Metathesis Copolymerization. *J. Am. Chem. Soc.* **2017**, *139* (10), 3896–3903. DOI: 10.1021/jacs.7b00791.

(245) Cunningham, R. E. Preparation and stress-strain properties of ABA block copolymers of *α*-methylstyrene and butadiene. *J. Appl. Polym. Sci.* **1978**, *22* (10), 2907–2913. DOI: 10.1002/app.1978.070221017.

(246) Ishizu, K.; Sunahara, K.; Asai, S. Synthesis and solution properties of gradient-modulus star copolymers. *Polymer* **1998**, *39* (4), 953–957. DOI: 10.1016/S0032-3861(97)00838-0.

(247) Natalello, A.; Alkan, A.; Tiedemann, P. von; Wurm, F. R.; Frey, H. Functional Group Distribution and Gradient Structure Resulting from the Living Anionic Copolymerization of Styrene and *para*-But-3-enyl Styrene. *ACS Macro Lett.* **2014**, *3* (6), 560–564. DOI: 10.1021/mz500255h.

(248) Natalello, A.; Werre, M.; Alkan, A.; Frey, H. Monomer Sequence Distribution Monitoring in Living Carbanionic Copolymerization by Real-Time ^{1}H NMR Spectroscopy. *Macromolecules* **2013**, *46* (21), 8467–8471. DOI: 10.1021/ma401847y.

(249) Sardelis, K.; Michels, H. J.; Allen, G. Toughened polystyrene containing block, graded block and randomized copolymers of butadiene-styrene. *Polymer* **1987**, *28* (2), 244–250. DOI: 10.1016/0032-3861(87)90412-5.

(250) Sardelis, K.; Michels, H. J.; Allen, G.; S, F. R. Graded block and randomized copolymers of butadiene-styrene. *Polymer* **1984**, *25* (7), 1011–1019. DOI: 10.1016/0032-3861(84)90089-2.

(251) Yu, G.; Mistry, D.; Ludhera, S.; Heatley, F.; Attwood, D.; Booth, C. Association and surface properties of tapered statistical copolymers of ethylene oxide and butylene oxide in water. *Faraday Trans.* **1997**, *93* (18), 3383–3390. DOI: 10.1039/A703545D.

(252) Lefebvre, M. D.; Dettmer, C. M.; McSwain, R. L.; Xu, C.; Davila, J. R.; Composto, R. J.; Nguyen, S. T.; Shull, K. R. Effect of Sequence Distribution on Copolymer Interfacial Activity. *Macromolecules* **2005**, *38* (25), 10494–10502. DOI: 10.1021/ma0509762.

(253) Gray, M. K.; Zhou, H.; Nguyen, S. T.; Torkelson, J. M. Synthesis and Glass Transition Behavior of High Molecular Weight Styrene/4-Acetoxystyene and Styrene/4-Hydroxystyrene Gradient Copolymers Made via Nitroxide-Mediated Controlled Radical Polymerization. *Macromolecules* **2004**, *37* (15), 5586–5595. DOI: 10.1021/ma0496652.

(254) Karaky, K.; Péré, E.; Pouchan, C.; Desbrières, J.; Dérail, C.; Billon, L. Effect of the synthetic methodology on molecular architecture: from statistical to gradient copolymers. *Soft Matter* **2006**, *2* (9), 770–778. DOI: 10.1039/B607797H.

(255) Shinoda, H.; Matyjaszewski, K.; Okrasa, L.; Mierzwa, M.; Pakula, T. Structural Control of Poly(methyl methacrylate)-*g*-poly(dimethylsiloxane) Copolymers Using Controlled Radical Polymerization: Effect of the Molecular Structure on Morphology and Mechanical Properties. *Macromolecules* **2003**, *36* (13), 4772–4778. DOI: 10.1021/ma034064g.

(256) Lefebvre, M. D.; La Olvera de Cruz, M.; Shull, K. R. Phase Segregation in Gradient Copolymer Melts. *Macromolecules* **2004**, *37* (3), 1118–1123. DOI: 10.1021/ma035141a.

(257) Guo, Y.; Zhang, J.; Xie, P.; Gao, X.; Luo, Y. Tailor-made compositional gradient copolymer by a many-shot RAFT emulsion polymerization method. *Polym. Chem.* **2014**, *5* (10), 3363–3371. DOI: 10.1039/C4PY00003J.

(258) Buzin, A. I.; Pyda, M.; Costanzo, P.; Matyjaszewski, K.; Wunderlich, B. Calorimetric study of block-copolymers of poly(*n*-butyl acrylate) and gradient poly(*n*-butyl acrylate-*co*-methyl methacrylate). *Polymer* **2002**, *43* (20), 5563–5569. DOI: 10.1016/S0032-3861(02)00358-0.

(259) Jakubowski, W.; Juhari, A.; Best, A.; Koynov, K.; Pakula, T.; Matyjaszewski, K. Comparison of thermomechanical properties of statistical, gradient and block copolymers of isobornyl acrylate and *n*-butyl acrylate with various acrylate homopolymers. *Polymer* **2008**, *49* (6), 1567–1578. DOI: 10.1016/j.polymer.2008.01.047.

(260) Zhang, G.; Zhang, Q.; Wang, Q.; Zhan, X.; Chen, F. Synthesis and properties of gradient copolymers of butyl methacrylate and fluorinated acrylate via RAFT miniemulsion copolymerizations. *J. Appl. Polym. Sci.* **2016**, *133* (5). DOI: 10.1002/app.42936.

(261) Zhang, J.; Li, J.; Huang, L.; Liu, Z. Gradient copolymers of styrene-methyl acrylate and styrene-acrylic acid by organostibine-mediated controlled/living radical polymerization and their glass transition behaviors. *Polym. Chem.* **2013**, *4* (17), 4639. DOI: 10.1039/C3PY00484H.

(262) Zhou, Y.-N.; Li, J.-J.; Luo, Z.-H. Synthesis of gradient copolymers with simultaneously tailor-made chain composition distribution and glass transition temperature by semibatch ATRP: From modeling to application. *J. Polym. Sci. Part A: Polym. Chem.* **2012**, *50* (15), 3052–3066. DOI: 10.1002/pola.26091.

(263) Mok, M. M.; Kim, J.; Wong, C. L. H.; Marrou, S. R.; Woo, D. J.; Dettmer, C. M.; Nguyen, S. T.; Ellison, C. J.; Shull, K. R.; Torkelson, J. M. Glass Transition Breadths and Composition Profiles of Weakly, Moderately, and Strongly Segregating Gradient Copolymers: Experimental Results and Calculations from Self-Consistent Mean-Field Theory. *Macromolecules* **2009**, *42* (20), 7863–7876. DOI: 10.1021/ma9009802.

(264) Cui, J.; Ma, Z.; Pan, L.; An, C.-H.; Liu, J.; Zhou, Y.-F.; Li, Y.-S. Self-healable gradient copolymers. *Mater. Chem. Front.* **2019**, *3* (3), 464–471. DOI: 10.1039/C8QM00592C.

(265) Guo, Y.; Gao, X.; Luo, Y. Mechanical properties of gradient copolymers of styrene and *n*-butyl acrylate. *J. Polym. Sci. B Polym. Phys.* **2015**, *53* (12), 860–868. DOI: 10.1002/polb.23709.

(266) Matyjaszewski, K.; Shipp, D. A.; McMurtry, G. P.; Gaynor, S. G.; Pakula, T. Simple and effective one-pot synthesis of (meth)acrylic block copolymers through atom transfer radical polymerization. *J. Polym. Sci. Part A: Polym. Chem.* **2000**, *38* (11), 2023–2031. DOI: 10.1002/(SICI)1099-0518(20000601)38:11<2023:AID-POLA110>3.0.CO;2-L.

(267) Kravchenko, V. S.; Abetz, V.; Potemkin, I. I. Self-assembly of gradient copolymers in a selective solvent. New structures and comparison with diblock and statistical copolymers. *Polymer* **2021**, *235*, 124288. DOI: 10.1016/j.polymer.2021.124288.

(268) Liu, X.; Wang, M.; Harrisson, S.; Debuigne, A.; Marty, J.-D.; Destarac, M. Enhanced Stabilization of Water/scCO$_2$ Interface by Block-Like Spontaneous Gradient Copolymers. *ACS Sustainable Chem. Eng.* **2017**, *5* (11), 9645–9650. DOI: 10.1021/acssuschemeng.7b02779.

(269) Bonné, T. B.; Lüdtke, K.; Jordan, R.; Papadakis, C. M. Effect of Polymer Architecture of Amphiphilic Poly(2-oxazoline) Copolymers on the Aggregation and Aggregate Structure. *Macromol. Chem. Phys.* **2007**, *208* (13), 1402–1408. DOI: 10.1002/macp.200700140.

(270) Shull, K. R. Interfacial Activity of Gradient Copolymers. *Macromolecules* **2002**, *35* (22), 8631–8639. DOI: 10.1021/ma020698w.

(271) Karaky, K.; Billon, L.; Pouchan, C.; Desbrières, J. Amphiphilic Gradient Copolymers Shape Composition Influence on the Surface/Bulk Properties. *Macromolecules* **2007**, *40* (3), 458–464. DOI: 10.1021/ma062456s.

(272) Sandoval, R. W.; Williams, D. E.; Kim, J.; Roth, C. B.; Torkelson, J. M. Critical micelle concentrations of block and gradient copolymers in homopolymer: Effects of sequence distribution, composition, and molecular weight. *J. Polym. Sci. B Polym. Phys.* **2008**, *46* (24), 2672–2682. DOI: 10.1002/polb.21592.

(273) Hattori, G.; Hirai, Y.; Sawamoto, M.; Terashima, T. Self-assembly of PEG/dodecyl-graft amphiphilic copolymers in water: consequences of the monomer sequence and chain flexibility on uniform micelles. *Polym. Chem.* **2017**, *8* (46), 7248–7259. DOI: 10.1039/C7PY01719G.

(274) Fusco, S.; Borzacchiello, A.; Netti, P. A. Perspectives on: PEO-PPO-PEO Triblock Copolymers and their Biomedical Applications. *J. Bioact. Compat. Polym.* **2006**, *21* (2), 149–164. DOI: 10.1177/0883911506063207.

(275) Chiappetta, D. A.; Sosnik, A. Poly(ethylene oxide)-poly(propylene oxide) block copolymer micelles as drug delivery agents: improved hydrosolubility, stability and bioavailability of drugs. *Eur. J. Pharm. Biopharm.* **2007**, *66* (3), 303–317. DOI: 10.1016/j.ejpb.2007.03.022.

(276) Edens, M. W.; Whitmarsh, R. H. Applications of Block Copolymer Surfactants. In *Developments in Block Copolymer Science and Technology*; Hamley, I. W., Ed.; Wiley, 2004; pp 325–340. DOI: 10.1002/0470093943.ch10.

(277) Rudnick, L. R., Ed. *Synthetics, Mineral oils, and Bio-Based Lubricants*:*Chemistry and Technology*, 3rd edn.; Chemical industries, Vol. 135; CRC PRESS, 2020. DOI: 10.1201/9781315158150.

(278) Louai, A.; Sarazin, D.; Pollet, G.; François, J.; Moreaux, F. Properties of ethylene oxide-propylene oxide statistical copolymers in aqueous solution. *Polymer* **1991**, *32* (4), 703–712. DOI: 10.1016/0032-3861(91)90484-Z.

(279) Bailey, F. E.; Callard, R. W. Some properties of poly(ethylene oxide)[1] in aqueous solution. *J. Appl. Polym. Sci.* **1959**, *1* (1), 56–62. DOI: 10.1002/app.1959.070010110.

(280) Persson, J.; Kaul, A.; Tjerneld, F. Polymer recycling in aqueous two-phase extractions using thermoseparating ethylene oxide-propylene oxide copolymers. *J. Chromatogr. B Biomed. Sci. Appl.* **2000**, *743* (1-2), 115–126. DOI: 10.1016/s0378-4347(00)00213-9.

(281) Johansson, H. O.; Karlstroem, G.; Tjerneld, F. Experimental and theoretical study of phase separation in aqueous solutions of clouding polymers and carboxylic acids. *Macromolecules* **1993**, *26* (17), 4478–4483. DOI: 10.1021/ma00069a012.

(282) Yang, Y.-W.; Brine, G.; Yu, G.; Heatley, F.; Attwood, D.; Booth, C.; Malmsten, M. Association and phase behaviour of statistical and block copolymers of ethylene oxide and butylene oxide in water. *Polymer* **1997**, *38* (7), 1659–1668. DOI: 10.1016/S0032-3861(96)00672-6.

Chapter 3

Influence of Solvent and Degree of Deprotonation on Reactivity Ratios and Reaction Rates in Ethylene Oxide/Glycidyl Methyl Ether Copolymerization

3 Influence of Solvent and Degree of Deprotonation on Reactivity Ratios and Reaction Rates in Ethylene Oxide/Glycidyl Methyl Ether Copolymerization

Gregor M. Linden[1], [redacted]

[1]Department of Chemistry, Johannes Gutenberg University Mainz, Duesbergweg 10-14, 55128 Mainz, Germany.

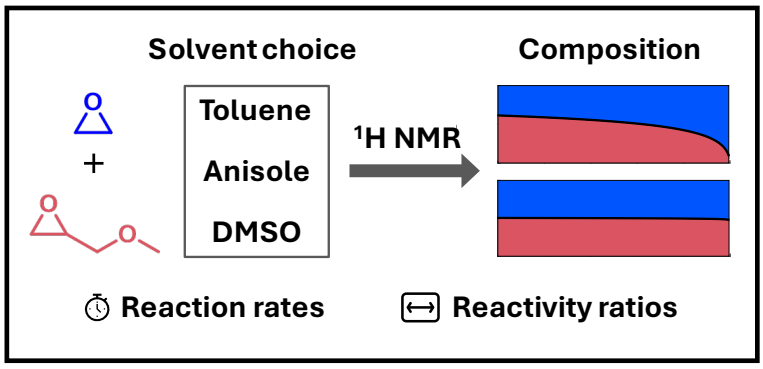

Abstract

Copolymerization of ethylene oxide (EO) and glycidyl methyl ether (GME) results in perfect structural isomers of poly(ethylene glycol) (PEG). These copolymers are being explored for their potential to evade immune recognition. This study investigates the influence of the solvents DMSO, toluene, and anisole on the copolymerization of these monomers. Reactivity ratios and apparent rates of copolymerization and homopolymerization were determined using online ^{1}H NMR kinetics. A striking observation was made for bifunctional initiators. In this case, a pronounced induction period was observed in the monomer conversion plots. The copolymerization of EO and GME in DMSO leads to an almost ideally random microstructure, while a slight gradient is observed in toluene and anisole, correlating with the permittivity. The degree of deprotonation was found to have a minor impact on the polymerization process. Among the solvents, DMSO was identified as the most effective for producing random copolymers, which can disrupt anti-PEG antibody binding and prevent crystallinity. The solvent choice significantly affects both the copolymerization rate and microstructure, with toluene demonstrating an unexpectedly high polymerization rate. This study underscores the importance of solvent selection in tailoring polymer properties, with significant implications for biomedical and materials science applications.

Introduction

The copolymerization of ethylene oxide (EO) and racemic glycidyl methyl ether (GME) represents a significant advancement in the design of polymers with tailored microstructures and properties. Poly(ethylene oxide) (PEO) crystallizes readily due to its regular structure. PEO and poly(ethylene glycol) (PEG) denote the same polymer, however, for detailed information regarding the denotation we refer to a review from Frey *et al*.[1] PEO transitions from a viscous liquid to a waxy state once its molar mass exceeds 1000 g/mol and becomes semicrystalline. PEO is obtained as a powder at molar masses above 6000 g/mol.[2] While this crystallinity can be advantageous in some applications,[1] it poses significant limitations in solid-state batteries[3,4] and membrane technology, where amorphous regions are essential for molecular interactions.[5,6] The challenge of reducing the crystallinity of PEO without compromising its hydrophilicity has led to exploring copolymerization strategies, with GME emerging as a promising comonomer. GME can be conceptualized as an isomeric dimer of EO. The anionic ring-opening (co)polymerization (AROP) with EO in solvents like dimethyl sulfoxide (DMSO) leads to the formation of copolymers with ideally random microstructures.[7] Unlike the more commonly used propylene oxide (PO), which forms a pronounced gradient microstructure with EO[8–10] and significantly lowers the polymer's cloud point,[11–15] GME maintains a high degree of hydrophilicity akin to EO, while effectively disabling crystallization when incorporated at levels

exceeding 25 mol%.[7] This ability to suppress crystallinity without drastically affecting the cloud point renders GME an attractive comonomer alternative to PO in applications requiring amorphous, hydrophilic, and biocompatible PEOs. Despite the potential of GME in modifying the properties of PEO, some general aspects of its copolymerization with EO remain underexplored. The solvent choice in the copolymerization was found to change the reactivity ratios of the EO/allyl glycidyl ether and EO/ethoxy vinyl glycidyl ether comonomer pairs.[16,17] Polymerizations in DMSO are known to occur at a high rate,[18,19] but the high boiling point (189 °C) makes the full removal tedious. Anisole features a lower boiling point of 154 °C and is regarded as a green solvent.[20,21] Additionally, the permittivity ε of anisole is higher than that of toluene (ε = 4.3724 and 2.408)[22,23] Moreover, the degree of deprotonation during polymerization needs to be investigated, as it could subtly influence the resulting polymer architecture.

In addition to structural considerations, the interaction of these copolymers at the interface as a PEG-alternative is of growing interest. PEGylation, the conjugation of PEG (PEO) to *e.g.* proteins or nanoparticles, has been observed to cause enhanced occurrence of anti-PEG antibodies (APAs). These target specific motifs of consecutive EO units in the chains[24] and pose an issue of increasing significance in biomedical applications involving PEGylated materials.[25,26] The randomness of the microstructure introduced by GME has been shown to reduce the occurrence of these motifs, potentially antibody binding. *In vitro* studies have shown the success of this strategy, making this material a promising alternative.[7] However, balancing the amount of GME is crucial, as incorporation exceeding 70 mol% lowers the microstructural variation, and complicates the synthesis of higher molar mass copolymers. The latter is caused by the abstraction of a proton from the α-position of the epoxide monomer, leading to an allylic alkoxide species, which itself can initiate a new polymer chain.[27]

This study aims to provide a comprehensive understanding of the copolymerization of EO and GME across different solvents (DMSO, anisole, and toluene), also investigating the effects of the degree of deprotonation and the microstructural implications for polymer crystallinity and interaction at the biological interface. By understanding these parameters, one can tailor and control the properties of EO-*co*-GME copolymers, paving the way for their application in advanced materials and biomedical technologies.

Experimental Section

Information regarding the reagents, detailed polymer synthesis, and the characterization techniques employed, is available in the Supporting Information (SI).

Results and Discussion

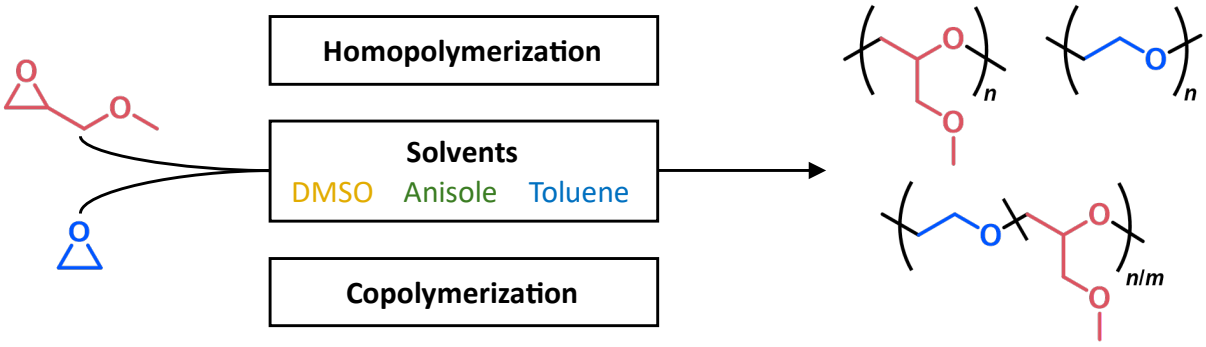

Scheme 1: Overview of online ^{1}H NMR kinetic studies of the homo- and copolymerization of EO and GME.

We investigated the homo- and copolymerization of EO and GME in the solvents DMSO, anisole, and toluene by online ^{1}H NMR kinetic studies. EO and GME were copolymerized in the respective solvents in an NMR tube with a sealable Teflon stopcock while recording ^{1}H NMR spectra. Partially deprotonated potassium alkoxides were used as initiators. All experimental details can be found in the SI together with SEC data (number-averaged molar mass M_n and dispersity $Đ$) of the synthesized polymers. We examined the reaction rates of homo- and copolymerization, and reactivity ratios were determined in a detailed manner, providing insights into the behavior of the monomers under various conditions. EO and GME were also homopolymerized using the monofunctional initiator 2-(benzyloxy)ethanol (BnO). The reaction rates were compared to those observed in the copolymerization of the two monomers, and the reactivity ratios were determined from the copolymerization. We examined reaction rates and reactivity ratios in detail, providing insights into the behavior of the monomers under various conditions.

Homopolymerization of EO and GME

EO and GME Homopolymerization Using a Monofunctional Initiator

The monofunctional initiator BnO was employed for the homopolymerization of EO and GME in the two apolar solvents, anisole and toluene at two different degrees of deprotonation (DOD, further explanation is available in the SI (equation S1), namely 50% and 90% (Table 1, entries 1–8). To compare the reaction rates in different solvents, we analyzed the slope of the linear regime from the pseudo-first-order plots of the copolymerization (Figures S1–S8). The apparent rate constant for each monomer (k_{app} (M)) was determined from the respective monomer signals. The following well-known equation yields the pseudo-first-order plot, and the slope affords k_{app}. It indicates how quickly the reaction progresses. This value was used as a proxy for comparison (derivation is provided in the SI, equations S2–S10).

$$\ln\left(\frac{[\mathrm{M}]_0}{[\mathrm{M}]_t}\right) = k_{\mathrm{app}} * t \qquad (1)$$

This allows for comparison of the solvents concerning reaction rates at a fixed initiator concentration. An induction period, caused by the crown-ether effect[28–30] from the initial addition of approximately 5–6 monomer units, has been observed for most of the conducted polymerizations. GME homopolymerization in anisole showed a poor signal-to-noise ratio, and the induction period could not be observed. In general, the induction period indicates the solvation of the potassium ion by the growing polyether chain (Figure 1), leading to better charge separation between the alkoxide chain end and the potassium counterion.[28–31]

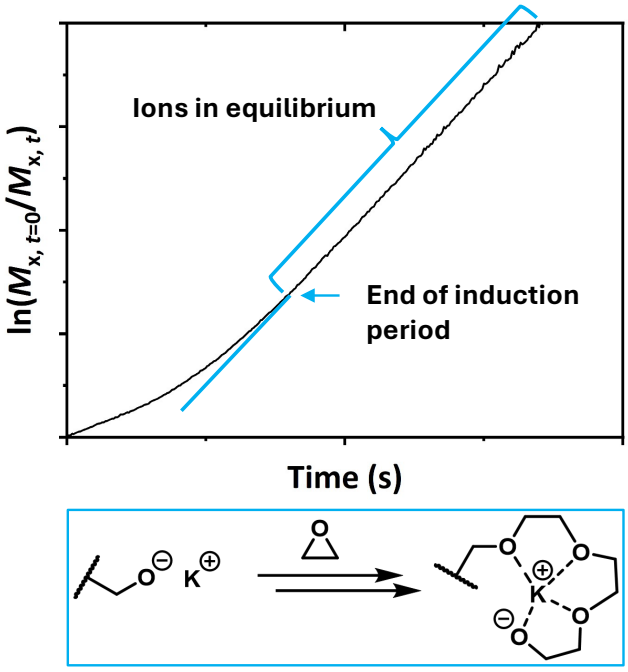

Figure 1: Exemplary pseudo-first-order plot with a visible induction period, also known as "crown ether effect" or "Weibull-Törnquist effect".[32] The turquoise elongation shows the graph without the induction period. Lower Scheme: Solvation of the counterion (potassium) by the growing polyether chain. Reprinted and adapted from *Reference Module in Chemistry* 2016, Penczek, S.; Pretula, J.B., *Ring-Opening Polymerization*, Page 23, Copyright 2016, with permission from Elsevier.[30]

In anisole, the EO reaction rate increased by a factor of ≈21 when the DOD was increased from 50% to 90% (entries 1 and 2). Conversely, in the less polar toluene (entries 3 and 4), the reaction rate decreased by 5%, likely due to the increased formation of dormant aggregate species in this apolar solvent. At 50% DOD, the difference between the two solvents is negligible (entries 1 and 3). Contrastingly, at 90% DOD, the reaction rate in the slightly more polar solvent anisole becomes much higher (entries 2 and 4). In literature, the propagation rate in THF at 20 °C is reported to be $4.8 \cdot 10^{-2}$ L·mol^{-1}·s^{-1} (Table IV in reference[33]), while at 70 °C it has been determined as 0.94 L·mol^{-1}·s^{-1} (Table 2 in reference[34]). The reaction rate of GME in anisole and toluene is lower compared to the

respective EO reaction rates under the same conditions. In anisole, the GME reaction rate doubled, when the DOD was increased from 50% to 90% (entries 5 and 6), similar to the EO reaction rate, but to a lower extent. In toluene, the reaction rate increases by ≈20% (entries 7 and 8), from which we conclude less dormant aggregate formation compared to the same conditions with EO. Alkoxides at a higher degree of substitution are more dissociated,[35] which directly corresponds to less aggregation as one might expect upon increasing the DOD. In summary, utilizing a higher DOD can increase the reaction rate, but the aggregation phenomenon can counter the higher concentration of active chain ends.

EO was further copolymerized in DMSO (entry 9) as a solvent of high polarity (entries 2 and 4). Due to the high dielectric constant and polymerization temperature, a fast reaction occurred, necessitating a reduction in initiator concentration compared to the polymerizations of entries 1–8. Without this change in conditions, the reaction was complete before starting the measurements. Despite the initiator concentration being reduced by a factor of 13.6, the reaction rate was still comparable to that in anisole. Polymerizations in polar solvents like DMSO and hexamethylphosphoric acid triamide (HMPTA) are well-known for their high reaction rates.[18,19,28,36] The high temperature leads to an initial rate acceleration, causing a subsequent temperature increase. The high dispersity ($Đ$ = 1.21) may indicate an inhomogeneous temperature distribution within the NMR tube at the start, with polymerization occurring faster in "hotspots" compared to colder areas (Figure S9).

Table 1: Apparent rate constants of EO and GME in the respective homopolymerization with the monofunctional initiator BnO. Fit was applied for the linear regime in the pseudo-first-order plots.

Entry (M)	Solvent	T / °C	DOD[a]	[I][b] / 10^{-2} mol/L	k_{app} (M) / s^{-1}	R^2
1 (EO)	Anisole	55	50%	9.66	(7.34 ± 0.01) ·10^{-5}	0.99946
2 (EO)	Anisole	55	90%	9.66	(1.54 ± 0.01) ·10^{-3}	0.99977
3 (EO)	Toluene	55	50%	9.66	(7.14 ± 0.01) ·10^{-5}	0.99972
4 (EO)	Toluene	55	90%	9.66	(6.80 ± 0.01) ·10^{-5}	0.99983
5 (GME)	Anisole	55	50%	9.66	(5.00 ± 0.02) ·10^{-5}	0.98708
6 (GME)	Anisole	55	90%	9.66	(1.02 ± 0.01) ·10^{-4}	0.99421
7 (GME)	Toluene	55	50%	9.66	(4.16 ± 0.01) ·10^{-5}	0.99993
8 (GME)	Toluene	55	90%	9.66	(5.04 ± 0.01) ·10^{-5}	0.99995
9 (EO)	DMSO	55	90%	0.71[c]	(9.10 ± 0.01) ·10^{-4}	0.99969

[a]Degree of deprotonation, [b]theoretical chain end concentration, [c]the initiator concentration had to be drastically reduced because, at higher concentrations, the polymerization was completed before recording started.

EO Homopolymerization Using a Bifunctional Initiator

Bifunctional initiators are valuable for block copolymer synthesis and for the preparation of telechelic polymers.[37] EO homopolymerization is known to be first-order with respect to the monomer.[18,19,38,39] In preliminary copolymerization experiments, we observed an unexpected and pronounced induction period in DMSO when a bifunctional initiator was used, which was not present with a monofunctional initiator (compare Figure S12 and Figure S17). To determine whether this induction period was specific for copolymerizations, we homopolymerized EO with the bifunctional initiator 3-ethoxy-1,2-propanediol (EPD, DOD: 25% and 50%) in DMSO. In both cases, a pronounced induction period was observable (Figure 2). The induction period ended when approximately 41–46 EO units were consumed, while the dispersity remained low (<1.07, Figures S44–S45). Once the chain reached a certain threshold of added EO units, the polymerization proceeded at a constant rate. In pronounced contrast, the polymerization initiated with monofunctional BnO displayed a fully linear trend in the pseudo-first-order plot (Figure S12) This leads us to conclude that the bifunctional initiator with a short distance between the active centers indeed causes the induction period shown in Figure 2. The black line shows that the induction periods last until ≈20 000 s, afterwards a constant slope is observed. The apparent reaction rate k_{app} from the linear regime increased by only 15% with the increase in the DOD from 25% to 50% (Table S1), although the hypothetical amount of active chain ends is doubled.

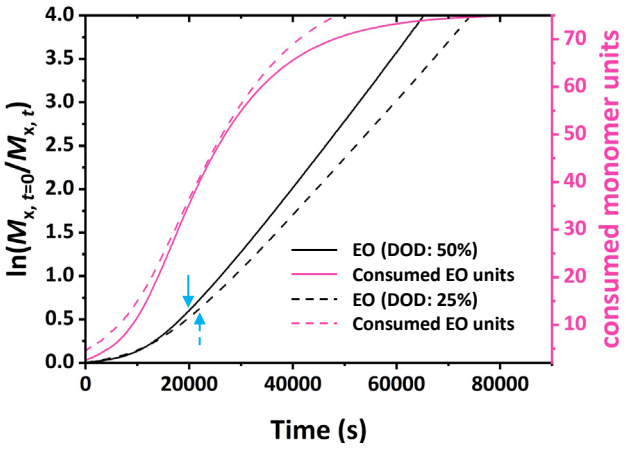

Figure 2: Pseudo-first-order plot of the homopolymerization of EO in DMSO with EPD as initiator at different degrees of deprotonation (DOD). The turquoise arrows indicate the end of the induction period and the beginning of the linear regime of the pseudo-first-order plot.

We attribute this to the small distance between the active sites, which results in a lower disaggregation constant (from aggregates to ion pairs) and a lower dissociation constant (from contact ion pairs to free ions) at the start. A DOD of 90% was not achievable, as bifunctional initiators are known to aggregate strongly and become insoluble upon full deprotonation, even in

a polar solvent like DMSO.[40] We scarcely found previous reports that examined the role of bifunctional initiators in the AROP of epoxides. The polymerization of EO in THF using living PEO showed no induction period. In contrast, naphthalenide initiators, which can be either mono- or bifunctional, showed an induction period for EO in THF.[34] Tymczyński *et al*. used glycoxides with [18]crown-6 for the polymerization of a glycidyl ether in DMSO, which did not exhibit an induction phase. However, SEC showed high dispersities between 1.40 and 2.74, which may raise some questions about the reliability of the results and suggest other issues.[41] Stolarzewicz equally polymerized different glycidyl ethers with KOH as an initiator in anisole and reported a short induction period at the beginning of the reaction.[42] Polymerization of methyl methacrylate using a bifunctional initiator in THF also showed an induction period. The results suggest that in the first stage of the polymerization the two ends of the molecule aggregate intramolecularly, forming a transient cyclic structure. Intermolecular aggregation was not observed due to the low concentration of living chain ends. The aggregated end groups are less reactive than disaggregated ones and the equilibrium between cyclic and linear polymers depends on the chain length.[43–45] Polymerization using a monofunctional initiator shows no such induction, which agrees with the hypothesis of a cyclic structure.[46] An induction period was also observed for the polymerization of styrene using a bifunctional initiator, with intramolecular formed negative triple ions. Bifunctional growing polymers can propagate slower than those with only one active group.[43,47,48]

We want to note that it is plausible that residual water (hydroxide), which can function as an initiator, is not necessarily found at low elution volumes in SEC. After the nucleophilic attack of an epoxide monomer, it will form a (substituted) bifunctional ethylene glycol initiator (Scheme S1), requiring more time to add significant amounts of monomer. Monofunctional initiators, on the other hand, can grow without this induction period in DMSO. If the monomer is consumed before the bifunctional chains reach their equilibrium reaction rate, this might result in only short bifunctional polymer chains. However, a more detailed investigation regarding the reaction rate and multifunctional initiators is postponed to future studies.

Reaction Rates in the EO/GME Copolymerization.

To compare the reaction rates of the copolymerization in the investigated solvents, the slope of the pseudo-first-order plots of the copolymerization (Figures S12–S15) derived from the EO signal was used to obtain the apparent rate constant of EO ($k_{app,copo}$ (EO)), which served as a proxy. This enables us to compare the solvents concerning the respective reaction rate at the fixed initiator concentration. Surprisingly, the reaction rates under the chosen copolymerization conditions have

not been reported, despite their significant role in technical applications. This know-how enables targeted polymer synthesis with respect to reaction time.

Copolymerization in DMSO showed linear behavior without an induction period in the pseudo-first-order plots (Figure S12). In anisole, a slight induction period was present at the beginning of the copolymerization at both DODs (Figure S13, zoom in Figure S14). In toluene (Figure 3), the induction period is merely visible at a DOD of 50% (zoom in Figure S16).

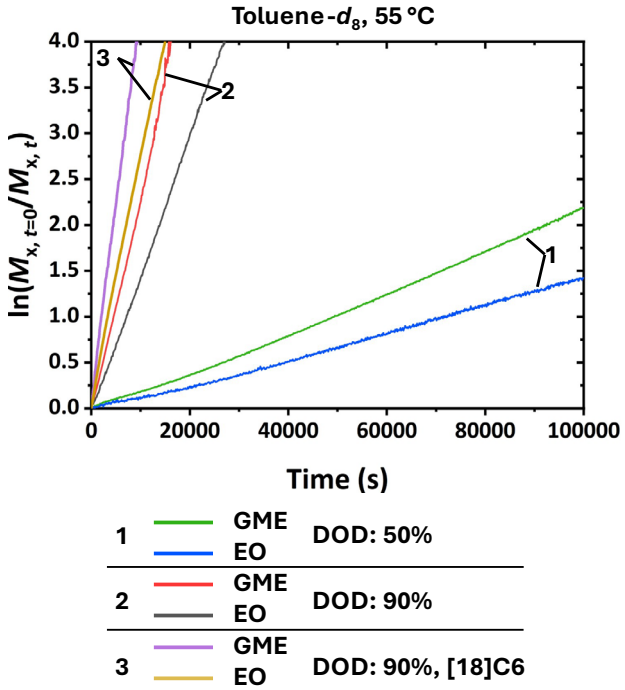

Figure 3: Pseudo-first-order plot of the copolymerization of EO with GME. 1) DOD: 50%, green: GME, blue: EO. 2) DOD: 90%, red: GME, black: EO. 3) DOD: 90%, with addition of [18]crown-6. Purple: GME, yellow: EO.

At the very beginning in the green and blue graph (Figure 3, zoom in Figure S16), the reaction rate increased, probably due to the dissolution of aggregates, leading to more reactive species in the system. This is probably accompanied by a slight temperature increase, which also accelerates the reaction. The slope then increases slowly after this first initial period, similar to the anisole conditions (Figures S13 and S14). An induction period at a DOD of 90% without crown ether addition was hardly observable (black and red line in Figure 3), probably due to the high reaction rate. A few monomer units had already been added to the initiator before the recording in the NMR device started. The same might have happened under DMSO conditions. As anticipated, we did not observe an induction period in toluene with crown ether addition (purple and yellow line in Figure 3), because potassium ions are already chelated. This will be described in more detail in another upcoming paper on the copolymerization of EO with propylene oxide.[49] If a bifunctional initiator is

used instead of the monofunctional initiator BnO, a pronounced induction period is observed in DMSO (DOD: 50%, Figure S17). This induction period slows down the overall reaction, due to the relative inactivity at the start of copolymerization. After the induction period, the reaction rate was comparable to the conditions utilizing a monofunctional initiator (see Figures S12 and S17).

The reaction rates of EO in copolymerization cannot be directly inferred from those of homopolymerization. This is because, in addition to homopropagation, there is also the crossover reaction when EO is added to a GME chain end, contributing as a second process to the depletion of EO in the mixture. Determination of the propagation constant k_p ($[k_p] = L \cdot mol^{-1} \cdot s^{-1}$) is impossible, as the aggregation number is unknown. Furthermore, the reported reaction rates should only be compared under similar conditions, as the complex equilibria between different types of ions play an important role in the propagation. The apparent reaction rate of GME in copolymerization is omitted in Figure 4. The reaction rate only slightly differs when the DOD is changed from 50% to 90% in DMSO. Polymerization in anisole was twice as fast as in toluene at 50%, but when increased to 90%, the polymerization rate in toluene increased further by a factor of ≈1.8. Adding [18]crown-6 further increased the reaction rate by a factor of ≈1.9 compared to the run without the additive. In this case, the ion pairs are converted into crown ether-separated ion pairs, but not into free ions.[30] As previously reported, if cryptands are used instead of crown ethers, the reactivity further increases by a factor of 70.[33,50,51] This phenomenon was explained by the oxygen anion being partially inserted into the cavity of the complexing agent.[29,52] Remarkably, the copolymerization in toluene with crown ether addition at a DOD of 90%, exceeded 99% conversion after ≈4 hours. The rate constants of homopolymerization differ significantly from those of copolymerization (compare Table 1 and Table S2). The significant increase in the homopolymerization reaction rate of EO in anisole upon an increase of the DOD is much less pronounced in copolymerization. Conversely, while the homopolymerization reaction rate of EO in toluene slightly decreases with an increase in DOD, it increases by a factor of 10 in copolymerization.

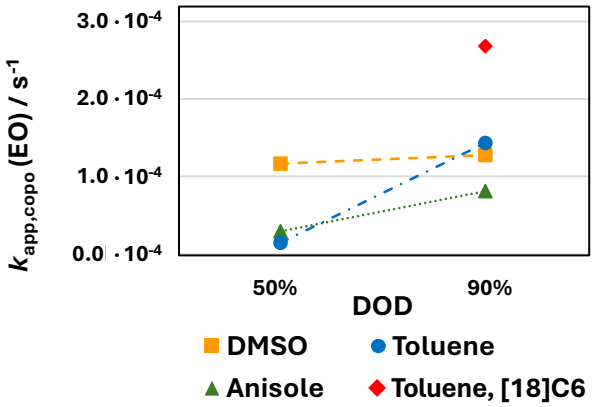

Figure 4: Apparent reaction rates of EO in the copolymerization with GME. The values for experiments in DMSO were adjusted to fit the initiator concentrations of the anisole and toluene experiments. DOD: degree of deprotonation. The values can be found in the SI (Table S2).

Reactivity Ratios of EO/GME by *In Situ* ^{1}H NMR Copolymerization Kinetics

Determination of the reactivity ratios (r) can be performed by various methods, such as i) differential (Kelen-Tüdos[53], Fineman-Ross[54], Mayo-Lewis[55]) and ii) integral methods (Jaacks[56,57], BSL[58], Meyer-Lowry[59], Ideal Integrated[60], DNI[61]), to name the best-known. Differential methods suffer from inaccuracy and require high experimental effort. In a conclusive publication, Beckingham *et al*. described that they are no longer recommended for use.[62] Chain-end independent or so-called "Ideal" models ($r_1 \cdot r_2 = 1$, such as BSL, Jaacks, Ideal Integrated), should be applied first. Chain-end dependent, also called terminal or non-ideal models ($r_1 \cdot r_2 \neq 1$, such as Meyer-Lowry, DNI) should only be used if the ideal models do not adequately describe the data.[58,60] This principle of preferring the simplest explanation of the data is known as "Ockham's Razor", coined by Sir William Hamilton.[63] Given the negligible differences between the Jaacks and BSL methods, we chose to present the results using the Jaacks method. The Jaacks equation is derived from the Wall equation[64] by integration and change of the basis of the logarithm.[65] It is straightforward to comprehend and can be easily recalculated. The Jaacks equation is defined by the following equation:[57]

$$\log\left(\frac{[\mathrm{M}_1]_t}{[\mathrm{M}_1]_0}\right) = r_1 \cdot \log\left(\frac{[\mathrm{M}_2]_t}{[\mathrm{M}_2]_0}\right) \quad (2)$$

By plotting $\log([M_1]_t/[M_1]_0)$ versus $\log([M_2]_t/[M_2]_0)$, r_1 can be derived from the slope. With the relation $r_1 \cdot r_2 = 1$, so $r_2 = r_1^{-1}$, both reactivity ratios can be calculated.

Reactivity ratios of the EO/GME comonomer pair were investigated in DMSO, anisole, and toluene at two different degrees of deprotonation, using the monofunctional initiator BnO. The summarized results are given in Table S3. The results were obtained using the *NIREVAL* software.[66] Figure 5

shows the reactivity ratios in dependence of the DOD. In DMSO, the reactivity ratios do not change significantly. Furthermore, the results indicate a fully random copolymer, as both reactivity ratios are almost one. In anisole and toluene, the reactivity ratios diverge significantly. This divergence becomes slightly more pronounced when the degree of deprotonation is increased.

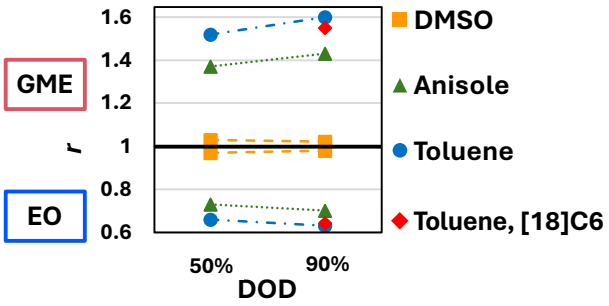

Figure 5: Reactivity ratios of the P(EO-*co*-GME) copolymers. DMSO experiments were conducted at 25 °C, anisole and toluene experiments at 55 °C. DOD: degree of deprotonation, [18]C6: [18]crown-6.

The difference in reactivity ratios directly affects the polymer composition. While the resulting difference may seem small, Figure 6 demonstrates that polymerization in toluene results in a slight gradient microstructure. At the start of the polymerization, more GME is incorporated, while towards the end, the chains become enriched with EO. In contrast, polymerization in DMSO produces a fully random microstructure.

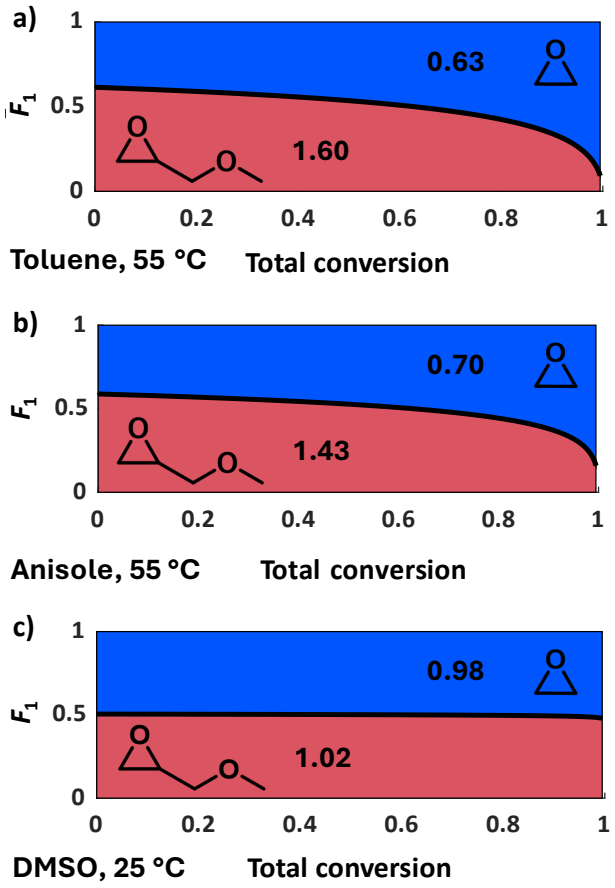

Figure 6: Simulated copolymer composition at the denoted polymerization conditions with an equimolar monomer feed. The degree of deprotonation was 90% in all cases.

In an earlier article, we proposed that this is due to the chelating properties of GE's second oxygen atom, leading to the activation of the epoxide functionality,[16] confirming the density functional theory (DFT) results of Hawker and Lynd.[17] This sets GEs apart from alkene oxides such as propylene oxide (r_{PO} = 0.30, r_{EO} = 3.1, bulk)[10], which exhibits a more pronounced gradient microstructure compared to GEs creating a random microstructure when copolymerized with EO.[67–69] To determine if the reactivity ratios from the DMSO experiment can be applied to the toluene experiment, [18]crown-6 was added to reduce the chelation of GME with the potassium counterion. The reaction condition with a DOD of 90% in toluene was chosen, as the highest difference in reactivity ratios was observed here. Unexpectedly, the reactivity ratios converged just slightly (Figure 5, red squares). This unexpected observation suggests that the mechanism of copolymerization and the role of DMSO are not fully understood. The exact reactivity ratios from Figure 5 can be found in Table S3 and the resulting SEC curves in Figures S36–S38. As expected, the use of EPD as a bifunctional initiator yielded the same reactivity ratios BnO (Table S3, entry 8). The copolymer composition was simulated for all experiments and is available in the SI (Figures S26–S32). The change in reactivity ratios caused by DOD should be considered when using bi- or multifunctional

initiators. For a high DOD, multifunctional initiators aggregate strongly and impair the control over initiation and propagation.[70] Therefore, a low DOD in the range of 20–30% is typically preferred to maintain better control.[71,72] To sum up, the choice of solvent and DOD has a non-negligible effect on the reactivity ratios and the resulting microstructure.

Conclusion

A detailed examination of the copolymerization of EO and GME has been provided, focusing on the influence of solvent and DOD on reaction rates and microstructure. Our findings show that while GME is consumed faster during copolymerization, it polymerizes slower than EO in homopolymerization. This is explained by the secondary alkoxides of the GME chain ends, while EO causes primary alkoxide chain ends. The reaction rates in apolar solvents like toluene and anisole, although lower overall, demonstrate that such solvents remain viable alternatives to DMSO, particularly when specific circumstances make DMSO unsuitable, *e.g*. its difficult removal from the polymers formed due to its high boiling point. Regarding efficient production processes, the faster copolymerization in toluene compared to anisole further supports the importance of solvent choice. Our results further reveal that increasing the DOD from 50% to 90% with a monofunctional initiator significantly accelerates both homo- and copolymerization rates for toluene and anisole while the impact for DMSO is minimal. This suggests that while DOD is a critical factor under certain conditions, it may be less significant in highly polar solvents like DMSO, which shifts the equilibrium from contact ion pairs to faster propagating species. Copolymerization in DMSO leads to fully random copolymers, while slight gradient structures are observed in toluene and anisole. Adding [18]crown-6 to disrupt the potassium counterion chelation by GME did not significantly alter the reactivity ratios in toluene, indicating that solvent-specific effects play a major role in defining the polymer microstructure. The microstructure plays a crucial role in the copolymer's physical properties. A more random microstructure reduces the likelihood of consecutive motifs, which is critical for applications at the biological interface. Consequently, understanding reactivity ratios and their correlation with polymerization conditions is essential for designing materials with specific properties. Although the impact of solvent and DOD on reactivity ratios in AROP is subtler, compared to carbanionic polymerization,[65] solvent choice and degree of deprotonation remain key in fine-tuning copolymer microstructures.

Acknowledgments

The authors thank [redacted] for the thorough manuscript correction and [redacted] for experimental support. [redacted] are thanked for their support in measuring kinetics. [redacted] is acknowledged for helpful and in-depth discussions.

References

(1) Herzberger, J.; Niederer, K.; Pohlit, H.; Seiwert, J.; Worm, M.; Wurm, F. R.; Frey, H. Polymerization of Ethylene Oxide, Propylene Oxide, and Other Alkylene Oxides: Synthesis, Novel Polymer Architectures, and Bioconjugation. *Chem. Rev.* **2016**, *116* (4), 2170–2243. DOI: 10.1021/acs.chemrev.5b00441.

(2) Sedlák, M. Recent Advances in Chemistry and Applications of Substituted Poly(ethylene glycol)s. *Collect. Czech. Chem. Commun.* **2005**, *70* (3), 269–291. DOI: 10.1135/cccc20050269.

(3) Croce, F.; Appetecchi, G. B.; Persi, L.; Scrosati, B. Nanocomposite polymer electrolytes for lithium batteries. *Nature* **1998**, *394* (6692), 456–458. DOI: 10.1038/28818.

(4) Quartarone, E.; Mustarelli, P. Electrolytes for solid-state lithium rechargeable batteries: recent advances and perspectives. *Chem. Soc. Rev.* **2011**, *40* (5), 2525–2540. DOI: 10.1039/c0cs00081g.

(5) Lin, H.; Freeman, B. D. Materials selection guidelines for membranes that remove CO_2 from gas mixtures. *J. Mol. Struct.* **2005**, *739* (1-3), 57–74. DOI: 10.1016/j.molstruc.2004.07.045.

(6) Juber, F. A. H.; Jawad, Z. A.; Chin, B. L. F.; Yeap, S. P.; Chew, T. L. The prospect of synthesis of PES/PEG blend membranes using blend NMP/DMF for CO2/N2 separation. *J. Polym. Res.* **2021**, *28* (5). DOI: 10.1007/s10965-021-02500-6.

(7) Dreier, P.; Matthes, R.; Fuß, F.; Schmidt, J.; Schulz, D.; Linden, G. M.; Barent, R. D.; Schüttner, S.; Bros, M.; Frey, H. Isomerization of poly(ethylene glycol): A strategy for the evasion of immune recognition. *submitted*.

(8) Deng, Y.; Ding, J.; Yu, G.; Mobbs, R. H.; Heatley, F.; Price, C.; Booth, C. Preparation and properties of *stat*-copoly-(oxyethylene-oxypropylene)-*block*-poly (oxyethylene): 1. Use of crown ether in the anionic copolymerization of propylene oxide and ethylene oxide. *Polymer* **1992**, *33* (9), 1959–1962. DOI: 10.1016/0032-3861(92)90500-V.

(9) Rastogi, A. K.; St. Pierre, L. E. Copolymerization of ethylene oxide and propylene oxide by anhydrous potassium hydroxide. *J. Appl. Polym. Sci.* **1970**, *14* (5), 1179–1182. DOI: 10.1002/app.1970.070140505.

(10) Heatley, F.; Yu, G.; Booth, C.; Blease, T. G. Determination of reactivity ratios for the anionic copolymerization of ethylene oxide and propylene oxide in bulk. *Eur. Polym. J.* **1991**, *27* (7), 573–579. DOI: 10.1016/0014-3057(91)90138-E.

(11) Weber, C.; Hoogenboom, R.; Schubert, U. S. Temperature responsive bio-compatible polymers based on poly(ethylene oxide) and poly(2-oxazoline)s. *Prog. Polym. Sci.* **2012**, *37* (5), 686–714. DOI: 10.1016/j.progpolymsci.2011.10.002.

(12) Bailey, F. E.; Callard, R. W. Some properties of poly(ethylene oxide)[1] in aqueous solution. *J. Appl. Polym. Sci.* **1959**, *1* (1), 56–62. DOI: 10.1002/app.1959.070010110.

(13) Persson, J.; Kaul, A.; Tjerneld, F. Polymer recycling in aqueous two-phase extractions using thermoseparating ethylene oxide-propylene oxide copolymers. *J. Chromatogr. B Biomed. Sci. Appl.* **2000**, *743* (1-2), 115–126. DOI: 10.1016/s0378-4347(00)00213-9.

(14) Louai, A.; Sarazin, D.; Pollet, G.; François, J.; Moreaux, F. Properties of ethylene oxide-propylene oxide statistical copolymers in aqueous solution. *Polymer* **1991**, *32* (4), 703–712. DOI: 10.1016/0032-3861(91)90484-Z.

(15) Louai, A.; Sarazin, D.; Pollet, G.; François, J.; Moreaux, F. Effect of additives on solution properties of ethylene oxide-propylene oxide statistical copolymers. *Polymer* **1991**, *32* (4), 713–720. DOI: 10.1016/0032-3861(91)90485-2.

(16) Dreier, P.; Matthes, R.; Barent, R. D.; Schüttner, S.; Müller, A. H. E.; Frey, H. In Situ Kinetics Reveal the Influence of Solvents and Monomer Structure on the Anionic Ring-Opening Copolymerization of Epoxides. *Macromol. Chem. Phys.* **2022**, 2200209. DOI: 10.1002/macp.202200209.

(17) Lee, B. F.; Wolffs, M.; Delaney, K. T.; Sprafke, J. K.; Leibfarth, F. A.; Hawker, C. J.; Lynd, N. A. Reactivity ratios, and mechanistic insight for anionic ring-opening copolymerization of epoxides. *Macromolecules* **2012**, *45* (9), 3722–3731. DOI: 10.1021/ma300634d.

(18) Solov'yanov, A. A.; Kazanskii, K. S. Polymerization of ethylene oxide in dimethyl sulphoxide (DMS). *Polym. Sci. U.S.S.R.* **1972**, *14* (5), 1196–1206. DOI: 10.1016/0032-3950(72)90163-3.

(19) Kucera, M. *Mechanism and kinetics of addition polymerizations*, 2., rev. ed.; Comprehensive chemical kinetics / ed. by R. G. Compton Section 10, Modern methods, theory, and data, Vol. 31; Elsevier, 1992.

(20) Babij, N. R.; McCusker, E. O.; Whiteker, G. T.; Canturk, B.; Choy, N.; Creemer, L. C.; Amicis, C. V. de; Hewlett, N. M.; Johnson, P. L.; Knobelsdorf, J. A.; Li, F.; Lorsbach, B. A.; Nugent, B. M.; Ryan, S. J.; Smith, M. R.; Yang, Q. NMR Chemical Shifts of Trace Impurities: Industrially Preferred Solvents Used in Process and Green Chemistry. *Org. Process Res. Dev.* **2016**, *20* (3), 661–667. DOI: 10.1021/acs.oprd.5b00417.

(21) Gottlieb, H. E.; Graczyk-Millbrandt, G.; Inglis, G. G. A.; Nudelman, A.; Perez, D.; Qian, Y.; Shuster, L. E.; Sneddon, H. F.; Upton, R. J. Development of GSK's NMR guides – a tool to encourage the use of more sustainable solvents. *Green Chem.* **2016**, *18* (13), 3867–3878. DOI: 10.1039/C6GC00446F.

(22) Wohlfarth, C. Dielectric constant of toluene. In *Supplement to IV/6*; Martienssen, W., Lechner, M. D., Eds.; Landolt-Börnstein - Group IV Physical Chemistry; Springer Berlin Heidelberg, 2008; pp 392–394. DOI: 10.1007/978-3-540-75506-7_228.

(23) Parthipan, G.; Thenappan, T. Dielectric and thermodynamic behavior of binary mixture of anisole with morpholine and aniline at different temperatures. *J. Mol. Liq.* **2008**, *138* (1-3), 20–25. DOI: 10.1016/j.molliq.2007.06.010.

(24) Huckaby, J. T.; Jacobs, T. M.; Li, Z.; Perna, R. J.; Wang, A.; Nicely, N. I.; Lai, S. K. Structure of an anti-PEG antibody reveals an open ring that captures highly flexible PEG polymers. *Commun. Chem.* **2020**, *3* (1), 10272. DOI: 10.1038/s42004-020-00369-y.

(25) Zhang, P.; Sun, F.; Liu, S.; Jiang, S. Anti-PEG antibodies in the clinic: Current issues and beyond PEGylation. *J. Control. Release* **2016**, *244* (Pt B), 184–193. DOI: 10.1016/j.jconrel.2016.06.040.

(26) Verhoef, J. J. F.; Carpenter, J. F.; Anchordoquy, T. J.; Schellekens, H. Potential induction of anti-PEG antibodies and complement activation toward PEGylated therapeutics. *Drug Discov. Today* **2014**, *19* (12), 1945–1952. DOI: 10.1016/j.drudis.2014.08.015.

(27) Hans, M.; Keul, H.; Moeller, M. Chain transfer reactions limit the molecular weight of polyglycidol prepared via alkali metal based initiating systems. *Polymer* **2009**, *50* (5), 1103–1108. DOI: 10.1016/j.polymer.2009.01.012.

(28) Berlinova, I. V.; Panayotov, I. M.; Tsvetanov, C. Influence of the polyether chain on the dissociation of “living” polymers obtained in the anionic polymerization of ethylene oxide. *Eur. Polym. J.* **1977**, *13* (10), 757–760. DOI: 10.1016/0014-3057(77)90018-0.

(29) Boileau, S. Anionic Ring-opening Polymerization: Epoxides and Episulfides. In *Comprehensive polymer science and supplements*:*Reference work*; Allen, G., Bevington, J. C., Eds.; Pergamon, 1996; pp 467–487. DOI: 10.1016/B978-0-08-096701-1.00094-X.

(30) Penczek, S.; Pretula, J. B. Ring-Opening Polymerization. In *Reference Module in Chemistry, Molecular Sciences and Chemical Engineering*; Elsevier, 2016. DOI: 10.1016/B978-0-12-409547-2.11351-4.

(31) Deffieux, A.; Carlotti, S.; Barrère, A. Anionic Ring-Opening Polymerization of Epoxides and Related Nucleophilic Polymerization Processes. In *Polymer Science*:*A comprehensive reference*; Matyjaszewski, K., Möller, M., Eds.; Elsevier, 2012; pp 117–140. DOI: 10.1016/B978-0-444-53349-4.00099-6.

(32) Hermann, P. D.; Cents, T.; Klemm, E.; Ziegenbalg, D. Determination of the Kinetics of the Ethoxylation of Octanol in Homogeneous Phase. *Ind. Eng. Chem. Res.* **2017**, *56* (21), 6176–6185. DOI: 10.1021/acs.iecr.7b00948.

(33) McGrath, J. E., Ed. *Ring-opening polymerization*:*Kinetics, mechanisms, and synthesis*; ACS symposium series, Vol. 286; American Chemical Society, 1985.

(34) Kazanskii, K. S.; Solovyanov, A. A.; Entelis, S. G. Polymerization of ethylene oxide by alkali metal-naphthalene complexes in tetrahydrofuran. *Eur. Polym. J.* **1971**, *7* (10), 1421–1433. DOI: 10.1016/0014-3057(71)90036-X.

(35) Exner, J. H.; Steiner, E. C. Solvation and ion pairing of alkali-metal alkoxides in dimethyl sulfoxide. Conductometric studies. *J. Am. Chem. Soc.* **1974**, *96* (6), 1782–1787. DOI: 10.1021/ja00813a022.

(36) Figueruelo, J. E.; Worsfold, D. J. The anionic polymerization of ethylene oxide in hexamethyl phosphoramide. *Eur. Polym. J.* **1968**, *4* (4), 439–444. DOI: 10.1016/0014-3057(68)90062-1.

(37) Matyjaszewski, K.; Gnanou, Y.; Leibler, L. *Macromolecular Engineering*:*Precise Synthesis, Materials Properties, Applications*; Wiley, 2007. DOI: 10.1002/9783527631421.

(38) Matyjaszewski, K.; Möller, M., Eds. *Polymer Science*:*A comprehensive reference*; Elsevier, 2012.

(39) Bawn, C.; Ledwith, A.; McFarlane, N. Anionic polymerization of ethylene oxide in dimethyl sulphoxide. *Polymer* **1969**, *10*, 653–659. DOI: 10.1016/0032-3861(69)90085-8.

(40) Sunder, A.; Türk, H.; Haag, R.; Frey, H. Copolymers of Glycidol and Glycidyl Ethers: Design of Branched Polyether Polyols by Combination of Latent Cyclic AB_2 and ABR Monomers. *Macromolecules* **2000**, *33* (21), 7682–7692. DOI: 10.1021/ma992166u.

(41) Jedliński, Z.; Stolarzewicz, A.; Szewczyk, P.; Tymczyński, R. Polymerization of chlorophenyl glycidyl ethers. VI. *Polym. Bull.* **1980**, *2* (8), 555–563. DOI: 10.1007/BF00255259.

(42) Jedliński, Z.; Stolarzewicz, A. Polymerization of chlorinated phenyl glycidyl ethers—I. *Eur. Polym. J.* **1969**, *5* (4), 515–519. DOI: 10.1016/0014-3057(69)90080-9.

(43) Szwarc, M.; Beylen, M. *Ionic Polymerization and Living Polymers*; Springer Netherlands, 1993. DOI: 10.1007/978-94-011-1478-3.

(44) Warzelhan, V.; Höcker, H.; Schulz, G. V. The Anionic Polymerization of Methyl Methacrylate with a Bifunctional Initiator. *Makromol. Chem.* **1980**, *181* (1), 149–163. DOI: 10.1002/macp.1980.021810114.

(45) Warzelhan, V.; Schulz, G. V. On a new active species in the anionic polymerisation of methyl methacrylate in tetrahydrofuran using a bifunctional initiator with sodium as gegenion. *Makromol. Chem.* **1976**, *177* (7), 2185–2190. DOI: 10.1002/macp.1976.021770721.

(46) Warzelhan, V.; Höcker, H.; Schulz, G. V. Kinetic studies of the anionic polymerization of methyl methacrylate in tetrahydrofuran with Na^+ as counter ion, using monofunctional initiators. *Makromol. Chem.* **1978**, *179* (9), 2221–2240. DOI: 10.1002/macp.1978.021790911.

(47) Bhattacharyya, D. N.; Smid, J.; Szwarc, M. A Novel Approach to Studies of Triple-Ion Formation. *J. Am. Chem. Soc.* **1964**, *86* (22), 5024–5025. DOI: 10.1021/ja01076a072.

(48) Bhattacharyya, D. N.; Lee, C. L.; Smid, J.; Szwarc, M. The absolute rate constants of anionic propagation by free ions and ion-pairs of living polystyrene. *Polymer* **1964**, *5*, 54–56. DOI: 10.1016/0032-3861(64)90118-1.

(49) Hesse, M. S.; Linden, G. M.; Frey, H. Reaction Temperature and Solvent Determine Reactivity Ratios in the Copolymerization of Ethylene Oxide and Propylene Oxide. Manuscript in preparation.

(50) Deffieux, A.; Boileau, S. Anionic polymerization of ethylene oxide with cryptates as counterions: 1. *Polymer* **1977**, *18* (10), 1047–1050. DOI: 10.1016/0032-3861(77)90011-8.

(51) Deffieux, A.; Graf, E.; Boileau, S. Anionic polymerization of ethylene oxide with cryptates as counterions: 2. *Polymer* **1981**, *22* (4), 549–552. DOI: 10.1016/0032-3861(81)90178-6.

(52) Boileau, S. Use of Cryptates in Anionic Polymerization of Heterocyclic Compounds. In *Anionic Polymerization*:*Kinetics, Mechanisms, and Synthesis*; McGrath, J. E., Ed.; ACS symposium series; American Chemical Society, 1981; pp 283–305. DOI: 10.1021/bk-1981-0166.ch019.

(53) Kelen, T.; Tüdos, F. Analysis of the Linear Methods for Determining Copolymerization Reactivity Ratios. I. A New Improved Linear Graphic Method. *J. Macromol. Sci. - Chem.* **1975**, *9* (1), 1–27. DOI: 10.1080/00222337508068644.

(54) Fineman, M.; Ross, S. D. Linear method for determining monomer reactivity ratios in copolymerization. *J. Polym. Sci.* **1950**, *5* (2), 259–262. DOI: 10.1002/pol.1950.120050210.

(55) Mayo, F. R.; Lewis, F. M. Copolymerization. I. A Basis for Comparing the Behavior of Monomers in Copolymerization; The Copolymerization of Styrene and Methyl Methacrylate. *J. Am. Chem. Soc.* **1944**, *66* (9), 1594–1601. DOI: 10.1021/ja01237a052.

(56) Jaacks, V. Eine neuartige Methode zur Bestimmung von Copolymerisationsparametern. *Angew. Chem.* **1967**, *79* (9), 419. DOI: 10.1002/ange.19670790927.

(57) Jaacks, V. A Novel Method of Determination of Reactivity Ratios in Binary and Ternary Copolymerizations. *Makromol. Chem.* **1972**, *161* (1), 161–172. DOI: 10.1002/macp.1972.021610110.

(58) Beckingham, B. S.; Sanoja, G. E.; Lynd, N. A. Simple and Accurate Determination of Reactivity Ratios Using a Nonterminal Model of Chain Copolymerization. *Macromolecules* **2015**, *48* (19), 6922–6930. DOI: 10.1021/acs.macromol.5b01631.

(59) Meyer, V. E.; Lowry, G. G. Integral and differential binary copolymerization equations. *J. Polym. Sci. A Gen. Pap.* **1965**, *3* (8), 2843–2851. DOI: 10.1002/pol.1965.100030811.

(60) Blankenburg, J.; Kersten, E.; Maciol, K.; Wagner, M.; Zarbakhsh, S.; Frey, H. The poly(propylene oxide-*co*-ethylene oxide) gradient is controlled by the polymerization method: determination of reactivity ratios by direct comparison of different copolymerization models. *Polym. Chem.* **2019**, *10* (22), 2863–2871. DOI: 10.1039/C9PY00500E.

(61) Kazemi, N.; Duever, T. A.; Penlidis, A. Reactivity Ratio Estimation from Cumulative Copolymer Composition Data. *Macromol. React. Eng.* **2011**, *5* (9-10), 385–403. DOI: 10.1002/mren.201100009.

(62) Lynd, N. A.; Ferrier, R. C.; Beckingham, B. S. Recommendation for Accurate Experimental Determination of Reactivity Ratios in Chain Copolymerization. *Macromolecules* **2019**, *52* (6), 2277–2285. DOI: 10.1021/acs.macromol.8b01752.

(63) Hoffman, R.; Carpenter, B. K.; Minkin, V. I. Ockham's Razor and Chemistry. *HYLE* **1997**, *3*, 3–28.

(64) Wall, F. T. The Structure of Vinyl Copolymers. *J. Am. Chem. Soc.* **1941**, *63* (7), 1862–1866. DOI: 10.1021/ja01852a016.

(65) Steube, M.; Johann, T.; Barent, R. D.; Müller, A. H.; Frey, H. Rational design of tapered multiblock copolymers for thermoplastic elastomers. *Prog. Polym. Sci.* **2022**, *124*, 101488. DOI: 10.1016/j.progpolymsci.2021.101488.

(66) Steube, M.; Johann, T.; Plank, M.; Tjaberings, S.; Gröschel, A. H.; Gallei, M.; Frey, H.; Müller, A. H. E. Kinetics of Anionic Living Copolymerization of Isoprene and Styrene Using in Situ NIR Spectroscopy: Temperature Effects on Monomer Sequence and Morphology. *Macromolecules* **2019**, *52* (23), 9299–9310. DOI: 10.1021/acs.macromol.9b01790.

(67) Herzberger, J.; Leibig, D.; Liermann, J. C.; Frey, H. Conventional Oxyanionic versus Monomer-Activated Anionic Copolymerization of Ethylene Oxide with Glycidyl Ethers: Striking Differences in Reactivity Ratios. *ACS Macro Lett.* **2016**, *5* (11), 1206–1211. DOI: 10.1021/acsmacrolett.6b00701.

(68) Blankenburg, J.; Maciol, K.; Hahn, C.; Frey, H. Poly(ethylene glycol) with Multiple Aldehyde Functionalities Opens up a Rich and Versatile Post-Polymerization Chemistry. *Macromolecules* **2019**, *52* (4), 1785–1793. DOI: 10.1021/acs.macromol.8b02639.

(69) Verkoyen, P.; Dreier, P.; Bros, M.; Hils, C.; Schmalz, H.; Seiffert, S.; Frey, H. "Dumb" pH-Independent and Biocompatible Hydrogels Formed by Copolymers of Long-Chain Alkyl Glycidyl Ethers and Ethylene Oxide. *Biomacromolecules* **2020**, *21* (8), 3152–3162. DOI: 10.1021/acs.biomac.0c00576.

(70) Penczek, S.; Cypryk, M.; Duda, A.; Kubisa, P.; Slomkowski, S. Living ring-opening polymerizations of heterocyclic monomers. *Prog. Polym. Sci.* **2007**, *32* (2), 247–282. DOI: 10.1016/j.progpolymsci.2007.01.002.

(71) Feng, X.-S.; Taton, D.; Chaikof, E. L.; Gnanou, Y. Toward an easy access to dendrimer-like poly(ethylene oxide)s. *J. Am. Chem. Soc.* **2005**, *127* (31), 10956–10966. DOI: 10.1021/ja0509432.

(72) Knischka, R.; Lutz, P. J.; Sunder, A.; Mülhaupt, R.; Frey, H. Functional Poly(ethylene oxide) Multiarm Star Polymers: Core-First Synthesis Using Hyperbranched Polyglycerol Initiators. *Macromolecules* **2000**, *33* (2), 315–320. DOI: 10.1021/ma991192p.

Supporting Information

Experimental Section

Reagents

Ethylene oxide (EO) was procured from *Air Liquide*. Deuterated solvents were purchased from *Deutero GmbH* (Germany). GME was prepared according to the reference[1]. Benzene (Rotipuran®, ≥99.5%, p.a.) was procured from *Carl Roth GmbH + Co. KG* and [18]crown-6 (99%) from *chemPUR Feinchemikalien und Forschungsbedarf GmbH* (Germany).

Instrumentation

Nuclear Magnetic Resonance (NMR) Spectroscopy

Polymerization kinetics were conducted on a *Bruker Avance III HD* (400 MHz) with a 5 mm nitrogen-cooled BBO-cryoprobe-head (BB+H+F) with *z*-gradient, automated tune and match (ATM) and autosampler SampleXPress 60. All spectra were acquired at 25 °C, if not stated otherwise. Spectra were referenced to the residual protons of the used solvents. Data were processed with *MestReNova 14.3.3-33362*. When kinetics in anisole (non-deuterated) were measured, the lock was turned off. Shim was performed with TopShim (gradient shim) using the protons of the anisole methoxy group.

Size Exclusion Chromatography (SEC)

Polymerization samples were analyzed after solvent removal by applying a gentle N_2-stream on the samples. An *Agilent 1100 series* SEC system, equipped with UV-detector (254 nm) and RI-detector. A HEMA 300/100/40 Å column cascade was used, with *N*,*N*-dimethylformamide (DMF) as eluent, containing 1 g/L LiBr. The column oven was set to 50 °C, measurements were performed with a flow rate of 1 ml/min. Toluene was added to the samples as an internal standard. Calibration was performed using poly(ethylene oxide) standards from *Polymer Standard Service* (PSS). Data were recorded and processed using the software *PSS WinGPC Unichrom*.

Polymerization Procedures

Investigation of copolymerization kinetics by *in situ* ^{1}H NMR analysis of GME and EO

The following procedure was applied for copolymerization as well as the homopolymerization. Due to their parallelism, only this procedure is described. This exemplary procedure describes the copolymerization of EO with GME in anisole at 55 °C with 90% degree of deprotonation. Measurements in DMSO and toluene were performed using the respective deuterated solvents.

Reactivity ratios and reaction rates were determined from online ^{1}H NMR measurements.

Preparation of the initiator salt solution: In a flame-dried Schlenk flask equipped with a rubber septum and a stirring bar, 2-(benzyloxy)ethanol (44.7 mg, 0.294 mmol, 1 eq.) and KO^tBu (29.7 mg, 0.264 mmol, 0.9 eq.) were dissolved in benzene (8 mL, dried over MS 4 Å). If [18]crown-6 was present in the polymerization, it would have been added in a dry benzene solution (2 eq. per potassium) now. The mixture was heated under static vacuum for 1 h at 60 °C. Then the solvents were removed *in vacuo* overnight at 60 °C, yielding the dry, partially deprotonated initiator salt. Subsequently, anisole (2.22 mL, dried over CaH_2) was added. The mixture was heated for 1 h at 60 °C and allowed to cool to room temperature.

Preparation of the polymerization mixture: ethylene oxide was cryo-transferred into an oven-dried *Norell S-500-VT-7* sealable NMR tube with a Teflon stopcock using an acetone/liquid N_2 bath and static vacuum. Under Ar-counterflow, GME (0.05 mL, 0.587 mmol, 10 eq., dried twice over CaH_2) and one-fifth of the initiator salt solution was added. The mixture was degassed by applying three freeze-pump-thaw cycles using the acetone/liquid N_2 bath. Then, the NMR tube was transferred to the preheated NMR device.

Sample spinning was turned off, one spectrum was recorded to acquire the receiver gain. One spectrum was recorded every two minutes. The respective shifts of the monomers were used to track the consumption. To analyze the normalized monomer consumption, the software *NIREVAL* was used.[2] After the kinetics study, the solvents were removed by applying a nitrogen stream to the solution. Subsequently, the polymer was analyzed by SEC.

Caveat: We rarely experienced a break of the NMR tube if subjected to liquid nitrogen. We strongly recommend only using an acetone/liquid N_2 bath. Ethylene oxide is a highly flammable and toxic gas; it should only be handled by trained researchers!

Degree of deprotonation (DOD)

The DOD denotes how much base equivalent was added per hydroxyl group of the initiator alcohol to prepare the initiator salt. In our case, KO^{t}Bu was used for deprotonation, and the resulting *tert*-butyl alcohol was removed in a vacuum. For more information, see Polymerization Procedures.

$$\mathrm{DOD} = \frac{\text{base eq.}}{\text{hydroxyl group}} \cdot 100\% \tag{S1}$$

Derivation of the pseudo-first-order plot

$$-\frac{\mathrm{d[M]}}{\mathrm{d}t} = k_\mathrm{p} * [\mathrm{I}] * [\mathrm{M}] \tag{S2}$$

$$k_\mathrm{app} = k_\mathrm{p} * [\mathrm{I}] \tag{S3}$$

$$-\frac{\mathrm{d[M]}}{\mathrm{d}t} = k_\mathrm{app}[\mathrm{M}] \tag{S4}$$

$$-\mathrm{d[M]}\frac{1}{[\mathrm{M}]} = k_\mathrm{app}\,\mathrm{d}t \tag{S5}$$

$$-\int_{[\mathrm{M}]_0}^{[\mathrm{M}]_t} \frac{1}{[\mathrm{M}]}\mathrm{d[M]} = k_\mathrm{app}\int_0^t \mathrm{d}t \tag{S6}$$

$$\int \frac{1}{x} = \ln(x) \tag{S7}$$

$$-(\ln([\mathrm{M}]_t) - \ln([\mathrm{M}]_0)) = k_\mathrm{app} * t \tag{S8}$$

$$-\ln\left(\frac{[\mathrm{M}]_t}{[\mathrm{M}]_0}\right) = k_\mathrm{app} * t \tag{S9}$$

$$\ln\left(\frac{[\mathrm{M}]_0}{[\mathrm{M}]_t}\right) = k_\mathrm{app} * t \tag{S10}$$

The Initiator concentration [I] consists of deprotonated and protonated initiator species and assuming all initiator reacts, this equals the concentration of the growing polymer chain ends. The apparent rate constant k_app cannot be converted to k_p by the relation $k_\mathrm{p} = \frac{k_\mathrm{app}}{[\mathrm{I}]}$, if the degree of association (or aggregation) is unknown.[3,4] If $\ln\left(\frac{[\mathrm{M}]_0}{[\mathrm{M}]_t}\right)$ is plotted versus t, the slope yields k_app.

Data of homopolymerization kinetics

Monofunctional initiators for EO and GME homopolymerization

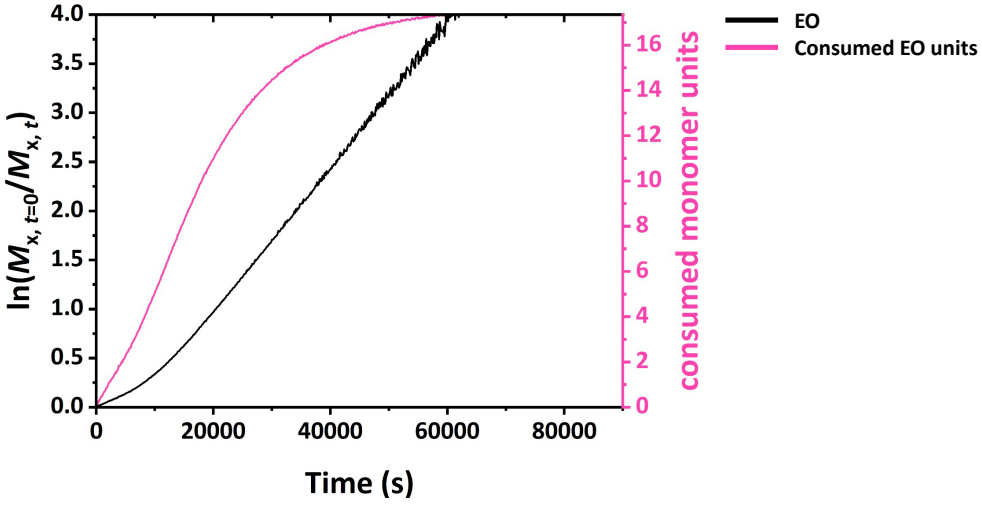

Figure S1: Pseudo-first-order plot of the homopolymerization of EO from Table 1, entry 1. The pink graph shows the consumed EO units throughout the homopolymerization.

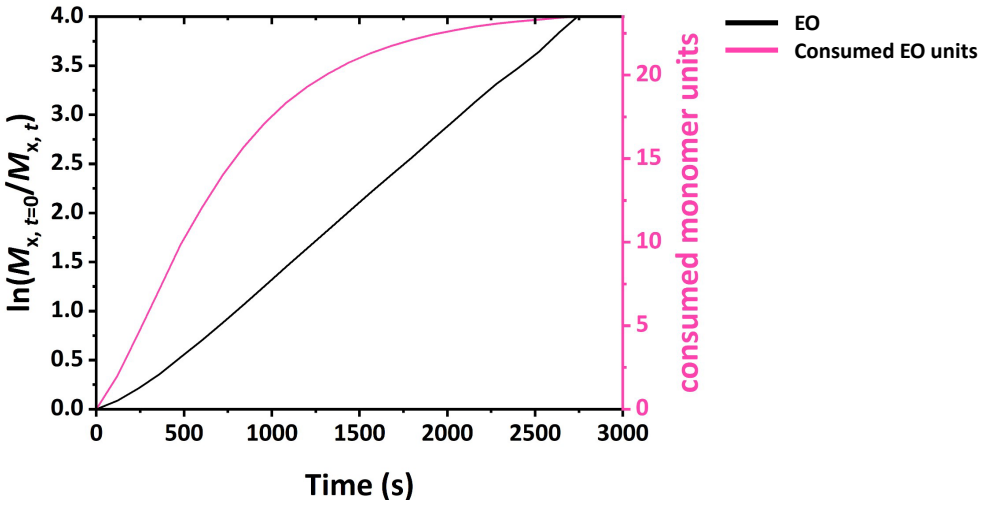

Figure S2: Pseudo-first-order plot of the homopolymerization of EO from Table 1, entry 2. The pink graph shows the consumed EO units throughout the homopolymerization. Some EO units were already added to the chain ends before the recording but could not be calculated due to the overlap of the anisole methoxy group with the polyether backbone.

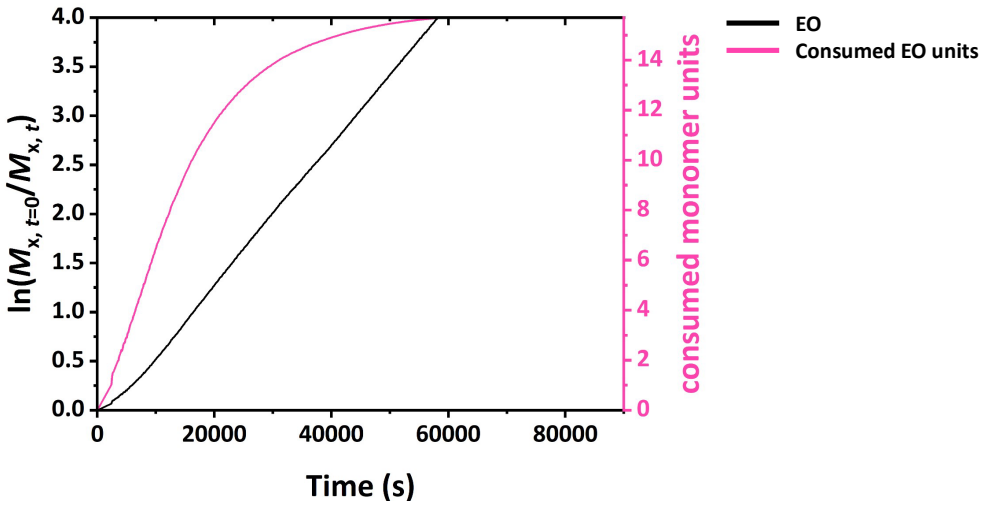

Figure S3: Pseudo-first-order plot of the homopolymerization of EO from Table 1, entry 3. The pink graph shows the consumed EO units throughout the homopolymerization.

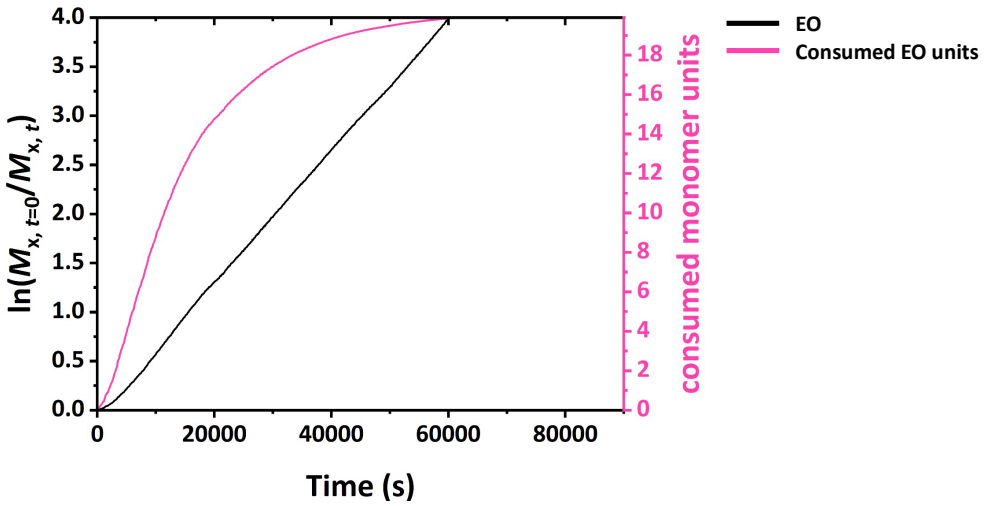

Figure S4: Pseudo-first-order plot of the homopolymerization of EO from Table 1, entry 4. The pink graph shows the consumed EO units throughout the homopolymerization.

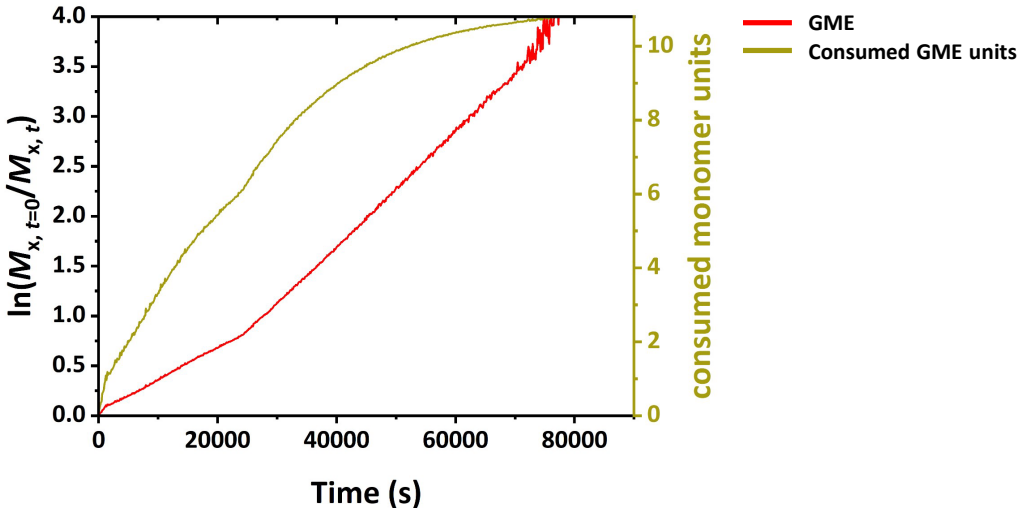

Figure S5: Pseudo-first-order plot of the homopolymerization of GME from Table 1, entry 5. The yellow graph shows the consumed GME units throughout the homopolymerization. The kink in the red graph is presumably due to a non-zero baseline. The fit was applied throughout the whole period.

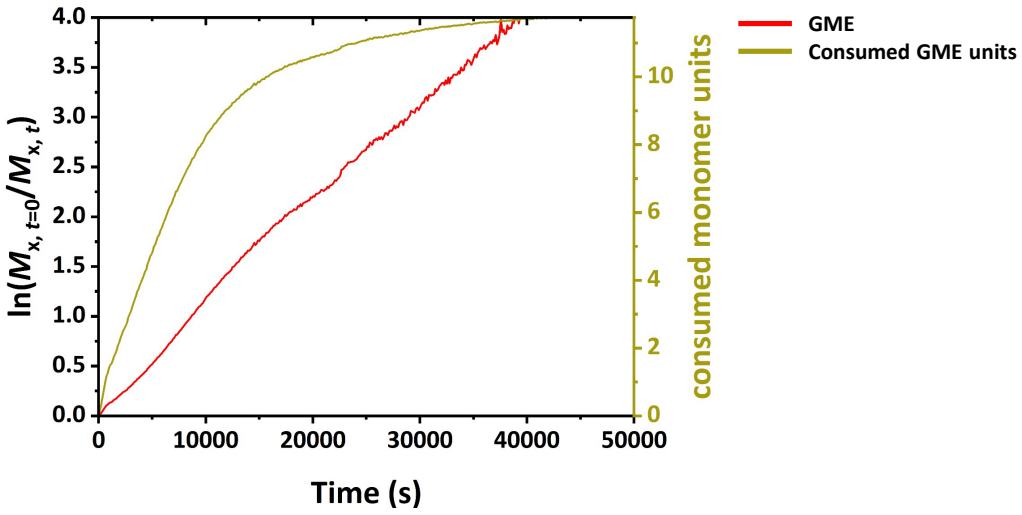

Figure S6: Pseudo-first-order plot of the homopolymerization of GME from Table 1, entry 7. The yellow graph shows the consumed GME units throughout the homopolymerization. The fit was applied throughout the whole period.

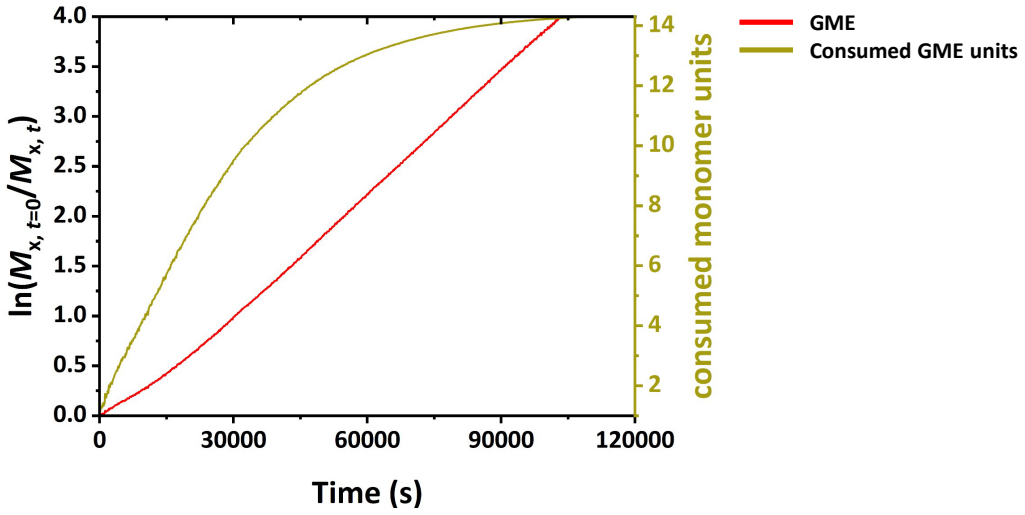

Figure S7: Pseudo-first-order plot of the homopolymerization of GME from Figure 4, entry 7. The yellow graph shows the consumed GME units throughout the homopolymerization.

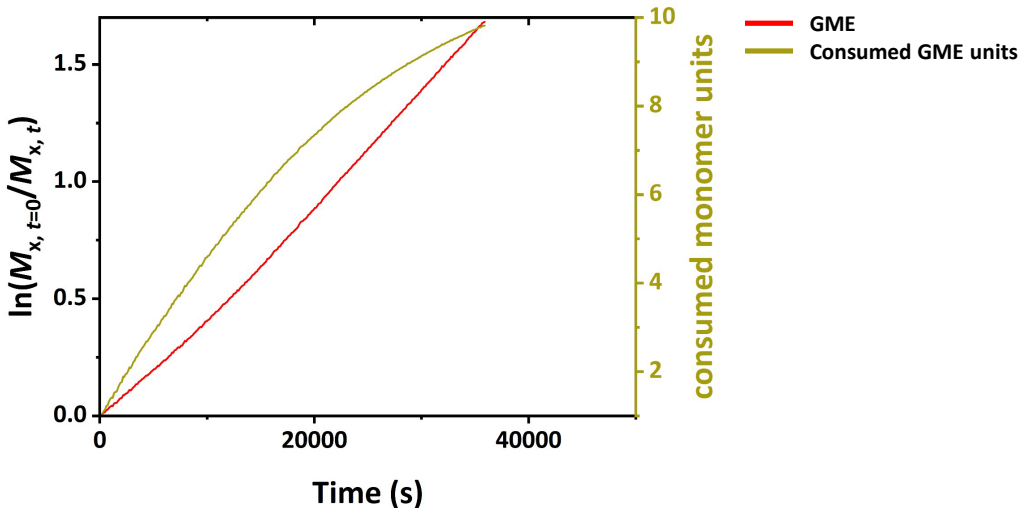

Figure S8: Pseudo-first-order plot of the homopolymerization of GME from Figure 4, entry 8. The yellow graph shows the consumed GME units throughout the homopolymerization.

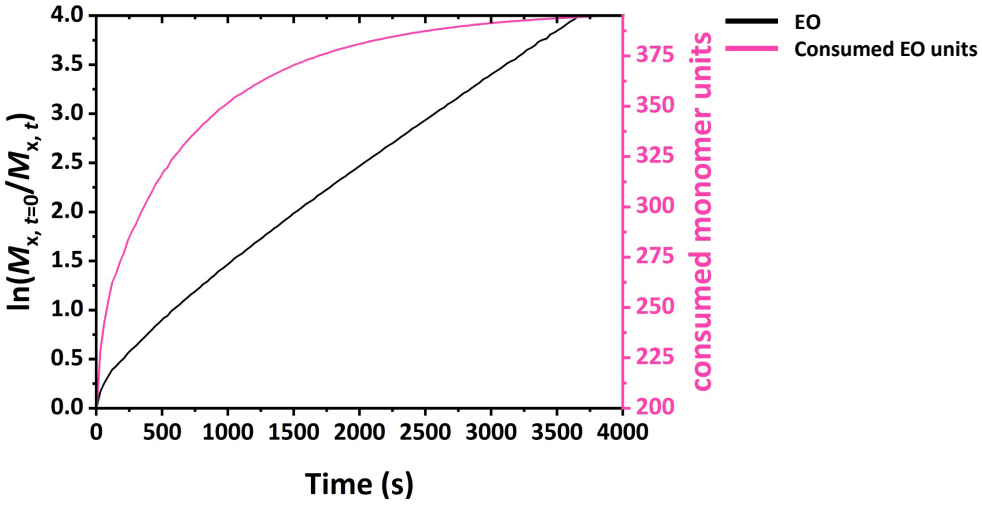

Figure S9: Pseudo-first-order plot of the homopolymerization of EO from Table 1, entry 9. The pink graph shows the consumed EO units throughout the homopolymerization. Around 200 EO units were already added to the chain ends before the recording. The decrease in reaction rate at the beginning is not due to chain transfer but is caused by temperature equilibration after initiation, which leads to a rise in temperature.

Bifunctional initiators for EO homopolymerization

Table S1: Apparent rate constants of EO in the homopolymerization with the bifunctional initiator EPD. Fit was applied for the linear regime in the pseudo-first-order plots.

Entry	Solvent	T / °C	DOD[a]	[I][b] / 10^{-2} mol/L	Initiator	k_{app} (EO) / s^{-1}	R^2
1	DMSO	25	25%	$9.66 \cdot 10^{-2}$	EPD	$6.78 \cdot 10^{-5}$	0.99956
2	DMSO	25	50%	$9.66 \cdot 10^{-2}$	EPD	$7.81 \cdot 10^{-5}$	0.99985

[a]Degree of deprotonation, [b]theoretical chain end concentration.

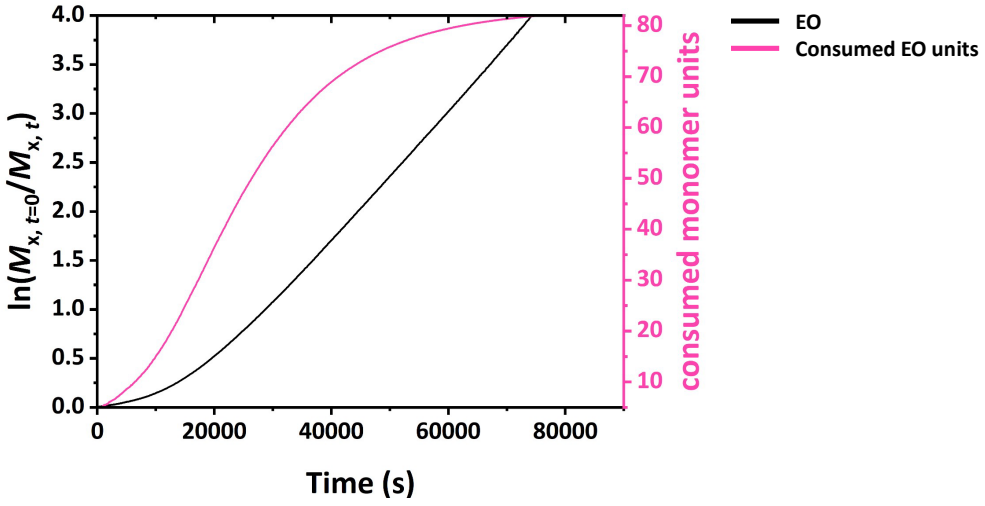

Figure S10: Pseudo-first-order plot of the homopolymerization of EO from Table S1, entry 1. The pink graph shows the consumed EO units throughout the homopolymerization. Some EO units were already added to the chain ends before the recording.

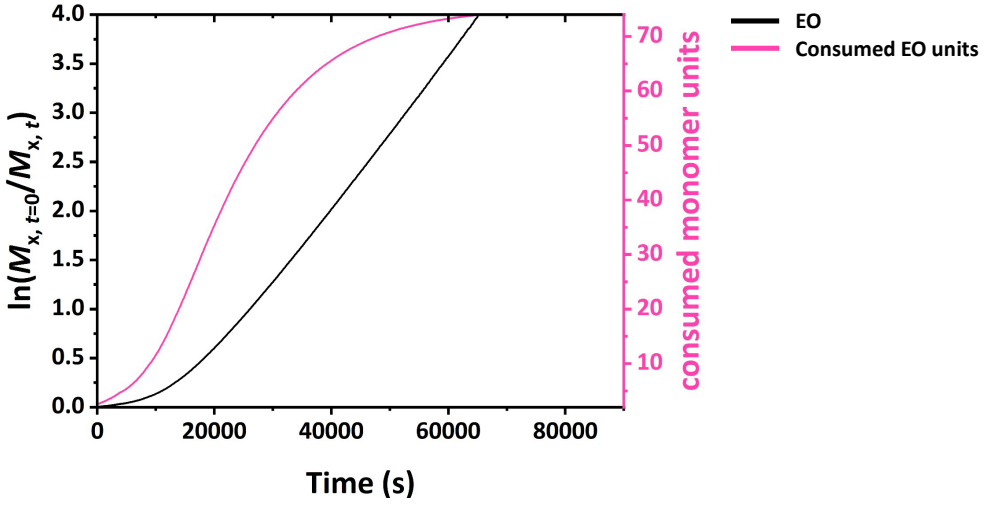

Figure S11: Pseudo-first-order plot of the homopolymerization of EO from Table S1, entry 2. The pink graph shows the consumed EO units throughout the homopolymerization. Some EO units were already added to the chain ends before the recording.

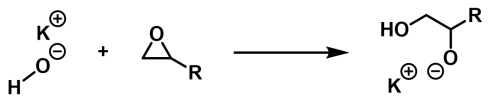

Scheme S1: Water (or hydroxide) initiation of an epoxide, forming a glycol initiator.

Data of copolymerization kinetics

Table S2: Apparent rate constants of EO in the copolymerization with GME and 2-(benzyloxy)ethanol as initiator. Fit was applied for the linear regime in the pseudo-first-order plots.

Entry	Solvent	T / °C	DOD[a]	[I][b] / 10^{-2} mol/L	$k_{app,copo}$ (EO) / s^{-1}	R^2
1	DMSO	25	50%	3.80	1.17E-04[d]±0.01	0.99997
2	DMSO	25	90%	3.80	1.28E-04[d]±0.01	0.99995
3	Anisole	55	50%	9.66	2.99E-05±0.01	0.99807
4	Anisole	55	90%	9.66	8.10E-05±0.01	0.99969
5	Toluene	55	50%	9.66	1.46E-05±0.01	0.99720
6	Toluene	55	90%	9.66	1.43E-04±0.01	0.99923
7	Toluene	55	90%	9.66[c]	2.68E-04±0.01	0.99950
8	DMSO	25	50%	3.60[d]	4.78E-05±0.01	0.99998

[a]Degree of deprotonation, [b]theoretical chain end concentration, [c]addition of 2 eq. of [18]crown-6 per potassium, [d]multiplied by a factor of (9.66/3.80) to be comparable to the [I] of the anisole and toluene experiments. [d]EPD was used as initiator.

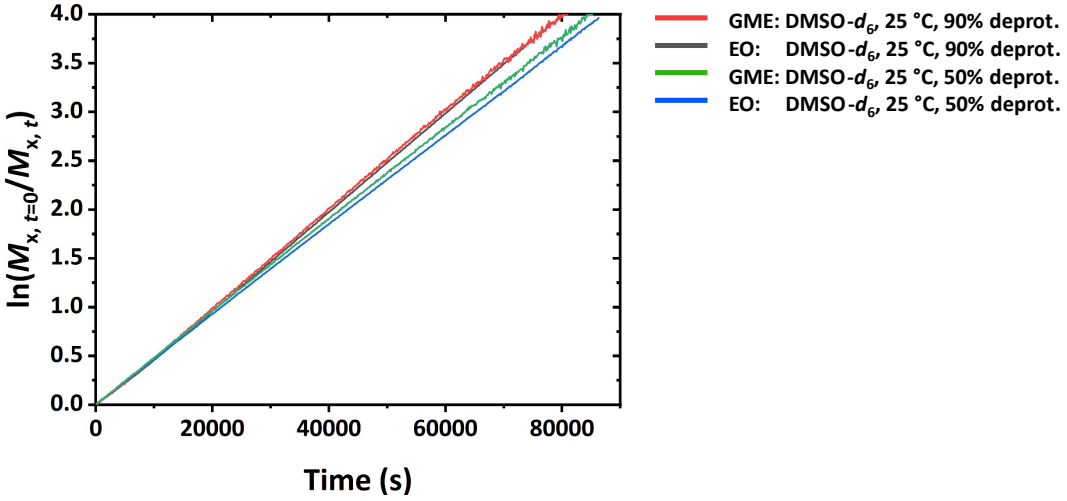

Figure S12: Pseudo-first-order plot of the copolymerization of EO with GME from Table S2. Green and blue: entry 1. Red and black: entry 2.

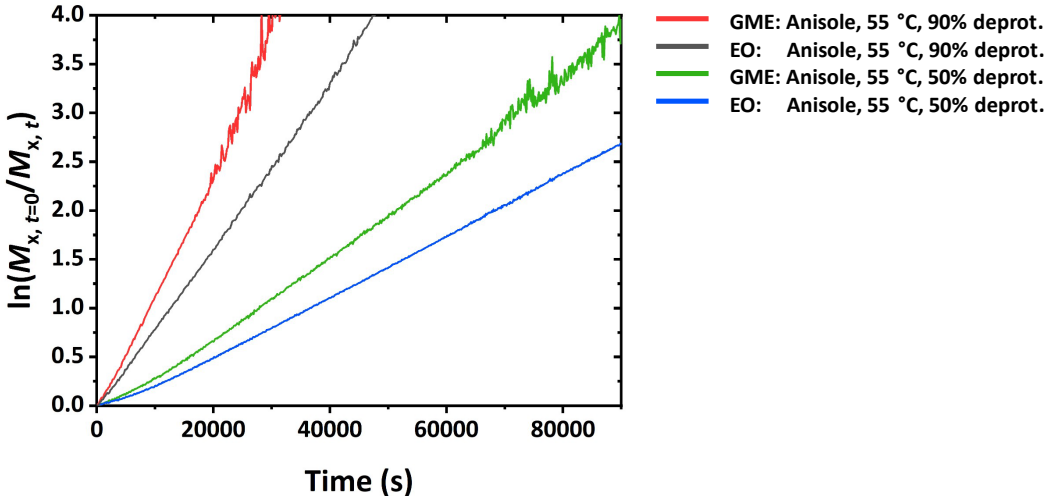

Figure S13: Pseudo-first-order plot of the copolymerization of EO with GME from Table S2. Green and blue: entry 3. Red and black: entry 4.

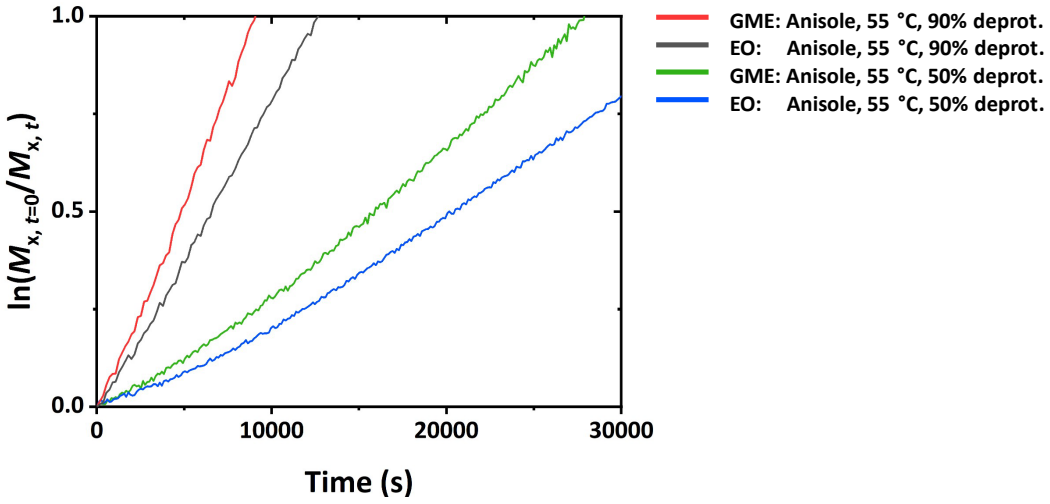

Figure S14: Enlargement of the pseudo-first-order plot of the copolymerization of EO with GME from Table S2. Green and blue: entry 3. Red and black: entry 4. The graphs follow nonlinear behavior at the beginning of the copolymerization, indicating an induction period.

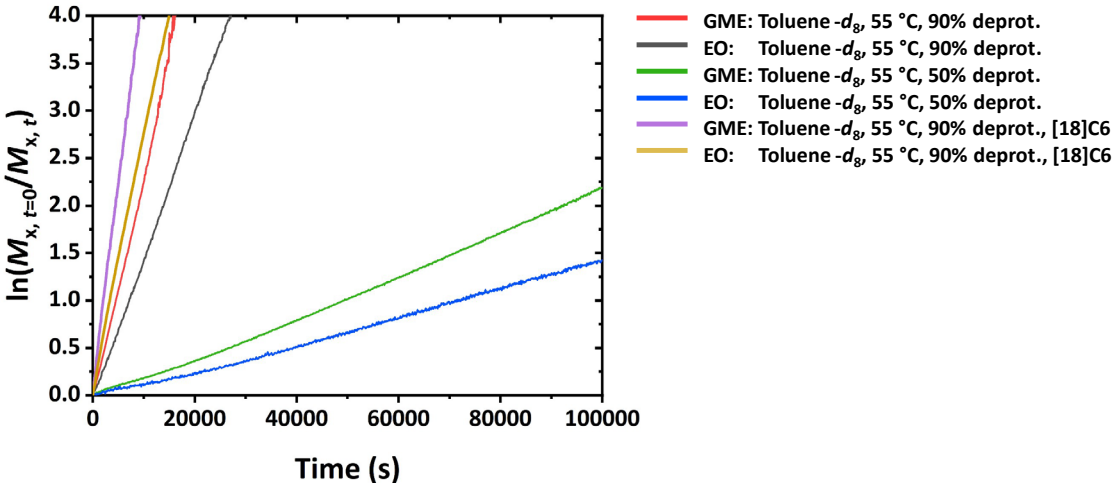

Figure S15: Pseudo-first-order plot of the copolymerization of EO with GME from Table S2. Green and blue: entry 5. Red and black: entry 6. Purple and yellow: entry 7.

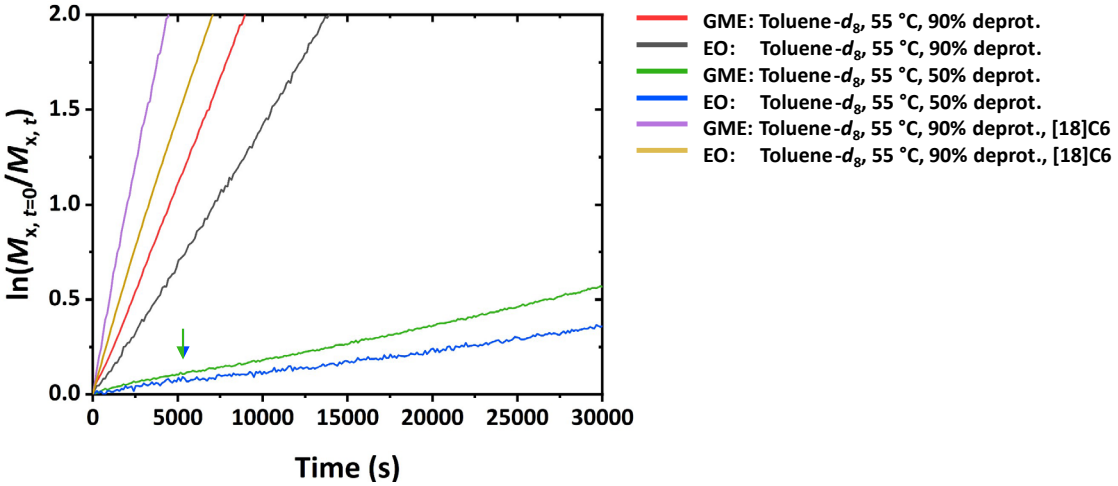

Figure S16: Enlargement of the pseudo-first-order plot of the copolymerization of EO with GME from Table S2. Green and blue: entry 5. Red and black: entry 6. Purple and yellow: entry 7. Green-blue arrow marks the end of the time range with an increased reaction rate due to the dissolution of aggregates and/or overheating.

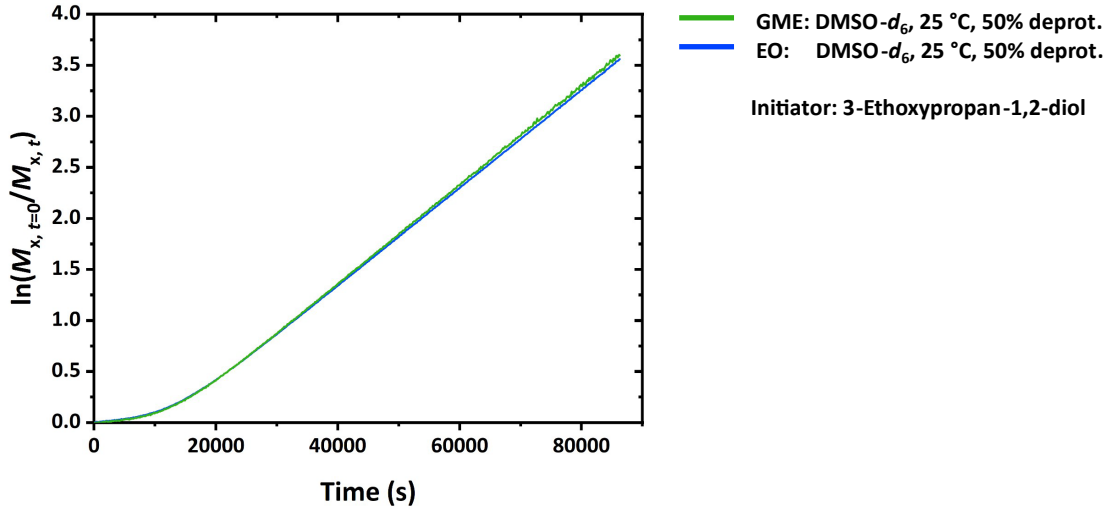

Figure S17: Pseudo-first-order plot of the copolymerization of EO with GME from Table S2, entry 8. Active chain end concentration: $3.60 \cdot 10^{-2}$ mol/L.

Table S3: Copolymerization kinetics of GME and EO with potassium 2-(benzyloxy)ethoxide as initiator.

Entry	Solvent	T / °C	DOD[a]	[I][b] / 10^{-2} mol/L	r_{GME}	r_{EO}	R^2	$Đ$[d]
1	DMSO	25	50%	3.80	1.03±0.01	0.97±0.01	0.99998	1.06
2	DMSO	25	90%	3.80	1.02±0.01	0.98±0.01	0.99989	1.07
3	Anisole	55	50%	9.66	1.37±0.01	0.73±0.01	0.99976	1.09
4	Anisole	55	90%	9.66	1.43±0.01	0.70±0.01	0.99951	1.08
5	Toluene	55	50%	9.66	1.52±0.01	0.66±0.01	0.99879	1.10
6	Toluene	55	90%	9.66	1.60±0.01	0.63±0.01	0.99927	1.10
7	Toluene	55	90%	9.66[c]	1.55±0.01	0.64±0.01	0.99935	1.10
8	DMSO	25	50%	3.60[e]	1.01±0.01	0.99±0.01	0.99996	1.10

[a]Degree of deprotonation, [b]theoretical chain end concentration, [c]addition of 2 eq. of [18]crown-6, [d]determined by SEC (eluent: DMF, PEG calibration, RI detector), [e] active chain ends of 3-ethoxy-1,2-propanediol.

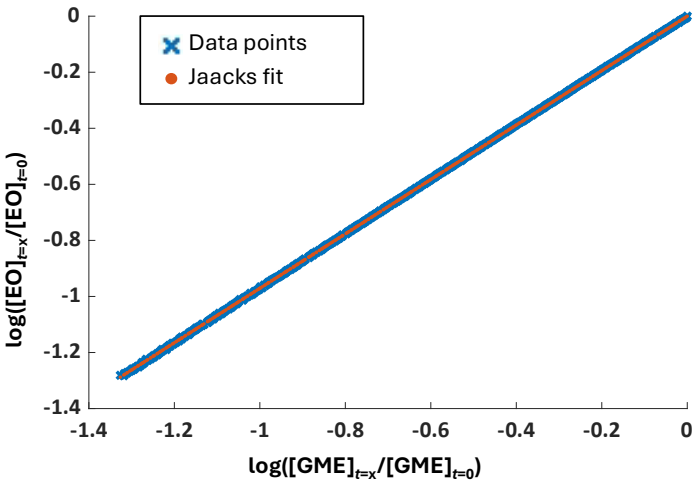

Figure S18: Jaacks fit of the copolymerization of EO and GME from Table S3, entry 1.

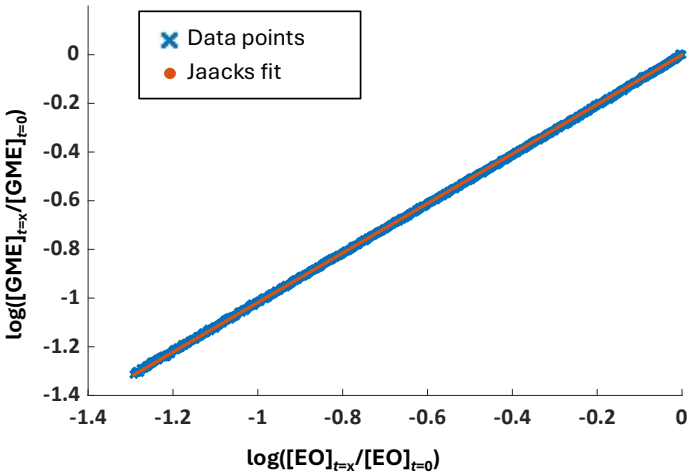

Figure S19: Jaacks fit of the copolymerization of EO and GME from Table S3, entry 2.

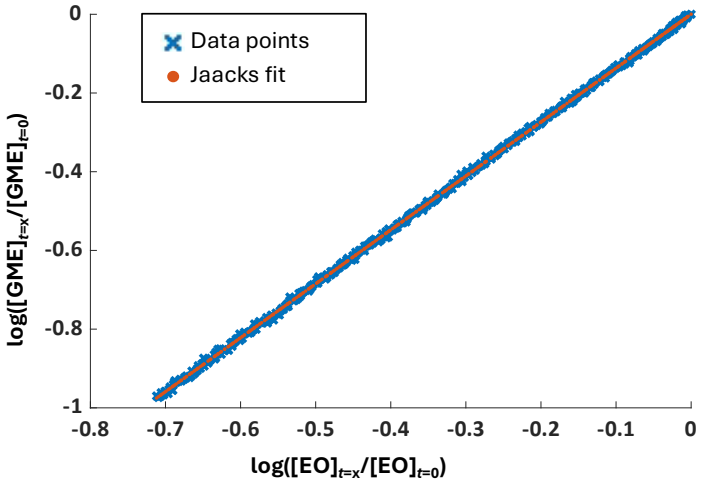

Figure S20: Jaacks fit of the copolymerization of EO and GME from Table S3, entry 3. Fit was applied over the whole copolymerization until a conversion of 85%, due to a declining signal-to-noise ratio.

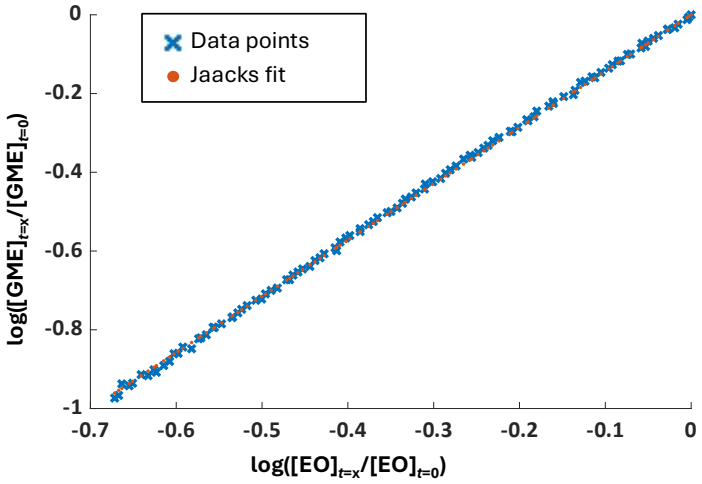

Figure S21: Jaacks fit of the copolymerization of EO and GME from Table S3, entry 4. Fit was applied over the whole copolymerization until a conversion of 84%, due to a declining signal-to-noise ratio.

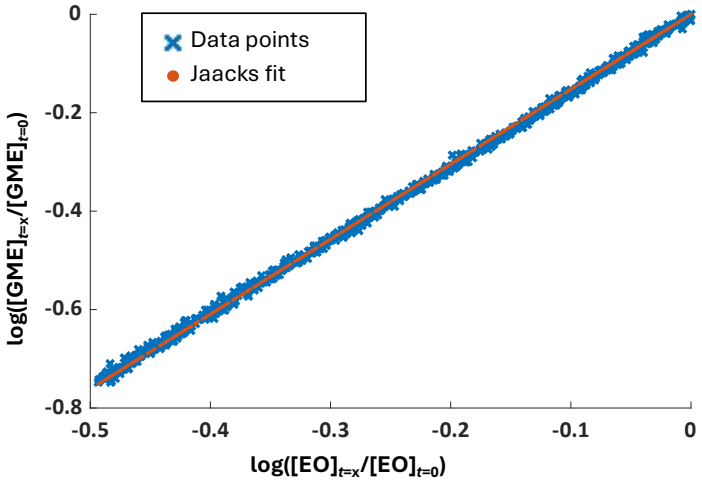

Figure S22: Jaacks fit of the copolymerization of EO and GME from Table S3, entry 5. Fit was applied over the whole copolymerization until a conversion of 75%, due to a declining signal-to-noise ratio.

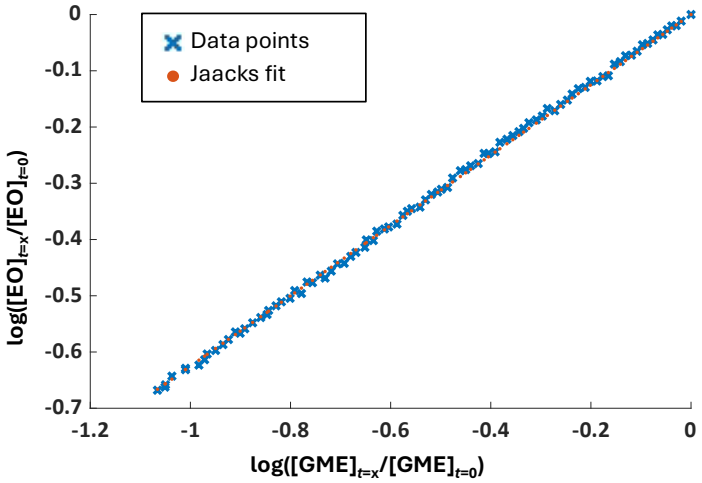

Figure S23: Jaacks fit of the copolymerization of EO and GME from Table S3, entry 6. Fit was applied over the whole copolymerization until a conversion of 85%, due to a declining signal-to-noise ratio.

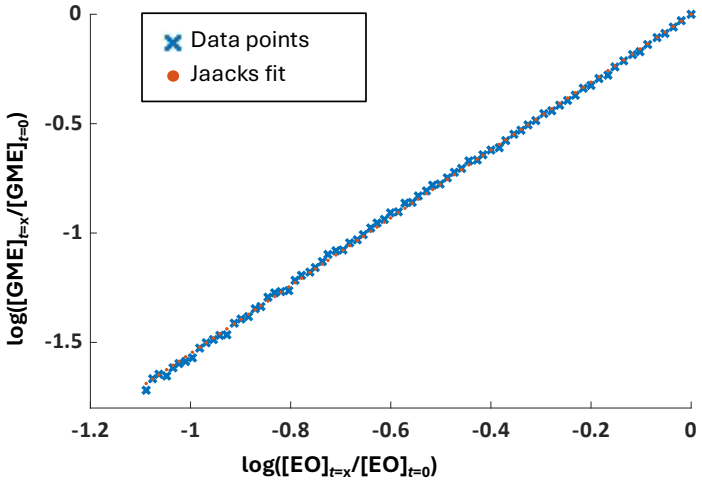

Figure S24: Jaacks fit of the copolymerization of EO and GME from Table S3, entry 7.

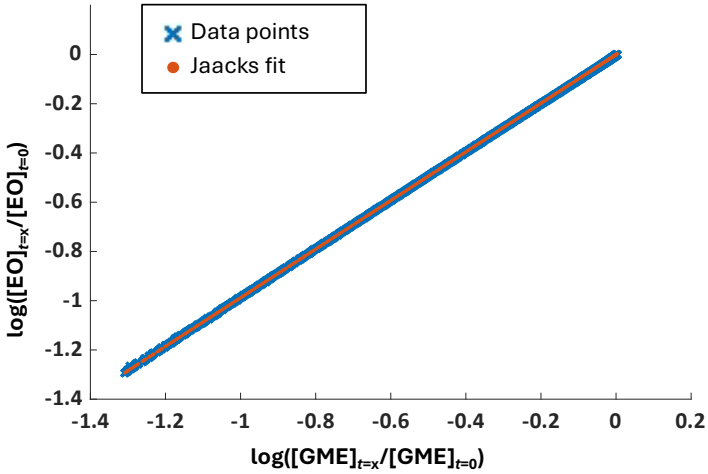

Figure S25: Jaacks fit of the copolymerization of EO and GME from Table S3, entry 8. Fit was applied over the whole copolymerization.

Copolymer compositions

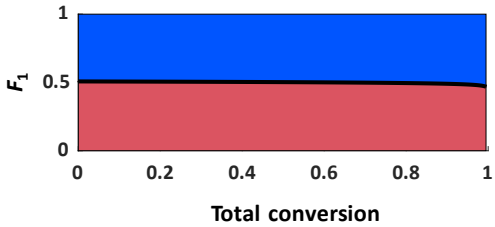

Figure S26: Composition plot of the *in situ* ^{1}H NMR copolymerization kinetic study of EO (blue) with GME (red) with an equimolar monomer ratio (Solvent: DMSO-d_6, 25 °C, DOD: 50%) with r(GME)=1.03, r(EO)=0.97.

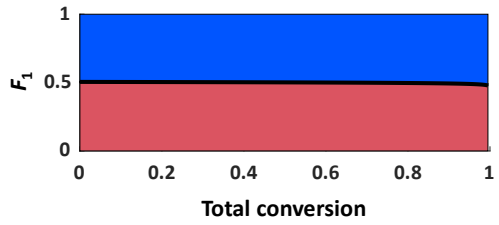

Figure S27: Composition plot of the *in situ* ^{1}H NMR copolymerization kinetic study of EO (blue) with GME (red) with an equimolar monomer ratio (Solvent: DMSO-d_6, 25 °C, DOD: 90%) with *r*(GME)=1.02, *r*(EO)=0.98.

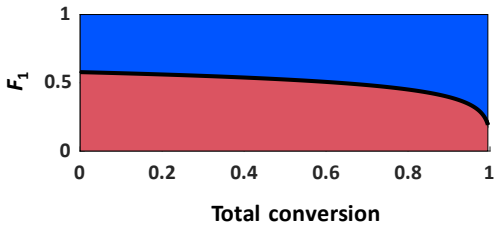

Figure S28: Composition plot of the *in situ* ^{1}H NMR copolymerization kinetic study of EO (blue) with GME (red) with an equimolar monomer ratio (Solvent: anisole, 55 °C, DOD: 50%) with *r*(GME)=1.37, *r*(EO)=0.73.

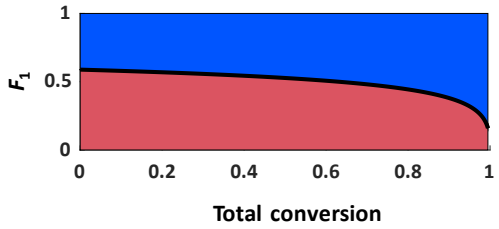

Figure S29: Composition plot of the *in situ* ^{1}H NMR copolymerization kinetic study of EO (blue) with GME (red) with an equimolar monomer ratio (Solvent: anisole, 55 °C, DOD: 90%) with *r*(GME)=1.43, *r*(EO)=0.70.

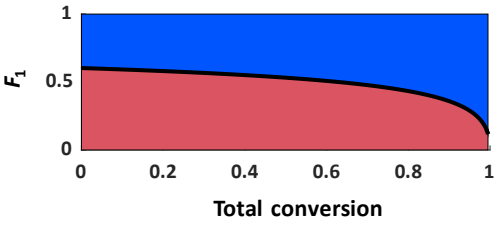

Figure S30: Composition plot of the *in situ* ^{1}H NMR copolymerization kinetic study of EO (blue) with GME (red) with an equimolar monomer ratio (Solvent: toluene-d_8, 55 °C, DOD: 50%) with *r*(GME)=1.52, *r*(EO)=0.66.

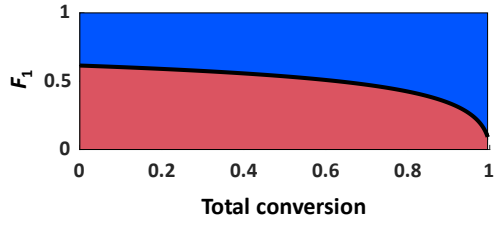

Figure S31: Composition plot of the *in situ* ^{1}H NMR copolymerization kinetic study of EO (blue) with GME (red) with an equimolar monomer ratio (Solvent: toluene-d_8, 55 °C, DOD: 90%) with *r*(GME)=1.60, *r*(EO)=0.63.

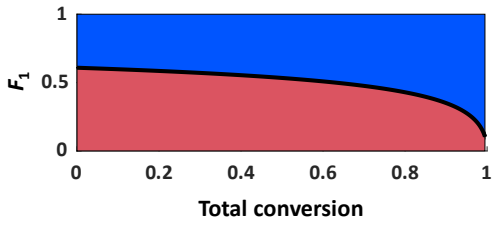

Figure S32: Composition plot of the *in situ* ^{1}H NMR copolymerization kinetic study of EO (blue) with GME (red) with an equimolar monomer ratio (Solvent: toluene-d_8, 55 °C, DOD: 90%) with *r*(GME)=1.55, *r*(EO)=0.64.

NMR spectra of statistical P(EO-*co*-GME) copolymers

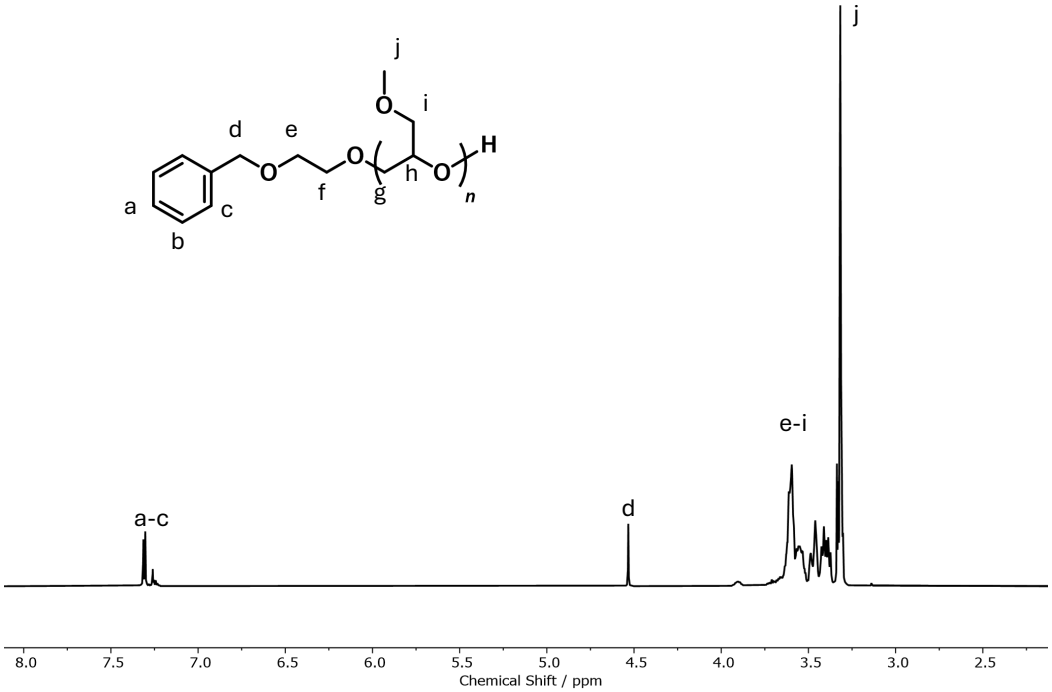

Figure S33: Exemplary ^{1}H NMR spectrum of PGME. $CDCl_3$, 400 MHz.

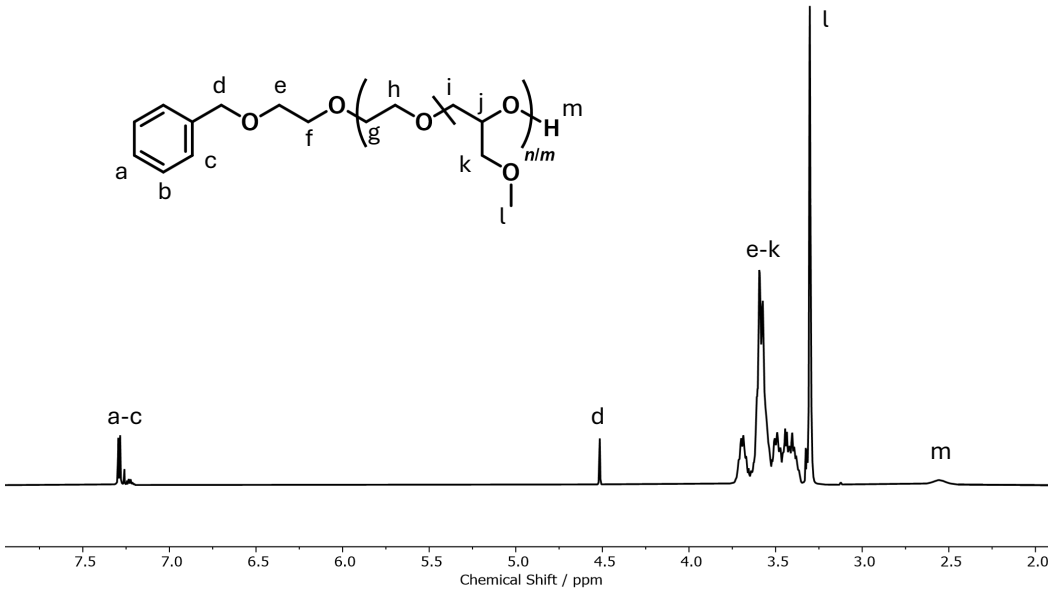

Figure S34: Exemplary ^{1}H NMR spectrum of P(EO-*co*-GME). $CDCl_3$, 400 MHz.

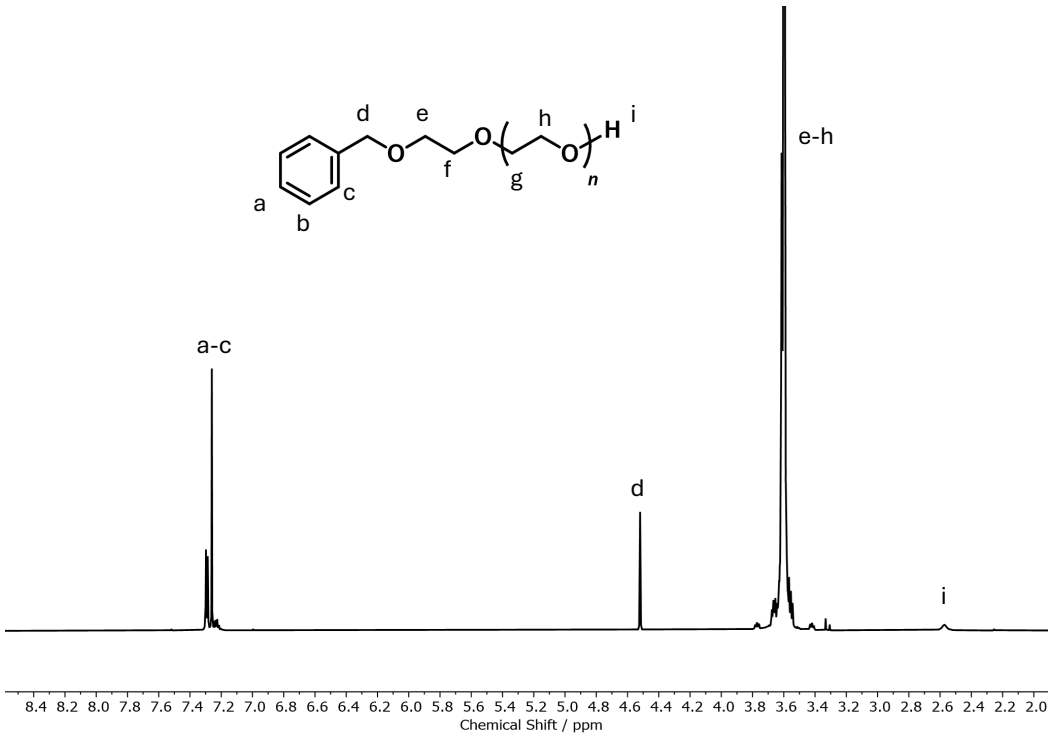

Figure S35: Exemplary ^{1}H NMR spectrum of PEO. $CDCl_3$, 400 MHz.

Size exclusion chromatography

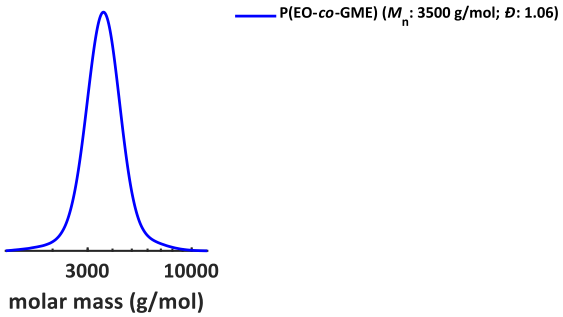

Figure S36: SEC of the polymer obtained after ^{1}H NMR kinetics (eluent: DMF with 1 g/L LiBr, RI detector, calibration: PEG). Initiator 2-(benzyloxy)ethanol, solvent DMSO-d_6, degree of deprotonation 50%, temperature 25 °C.

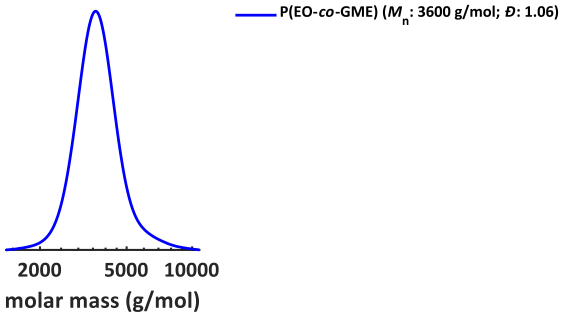

Figure S37: SEC of the polymer obtained after ^{1}H NMR kinetics (eluent: DMF with 1 g/L LiBr, RI detector, calibration: PEG). Initiator 2-(benzyloxy)ethanol, solvent DMSO-d_6, degree of deprotonation 90%, temperature 25 °C.

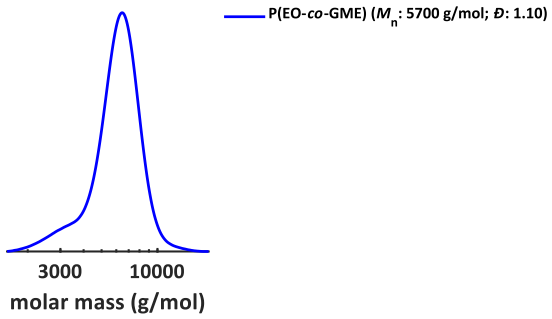

Figure S38: SEC of the polymer obtained after ^{1}H NMR kinetics (eluent: DMF with 1 g/L LiBr, RI detector, calibration: PEG). Initiator 3-ethoxypropane-1,2-diol, solvent DMSO-d_6, degree of deprotonation 50%, temperature 25 °C.

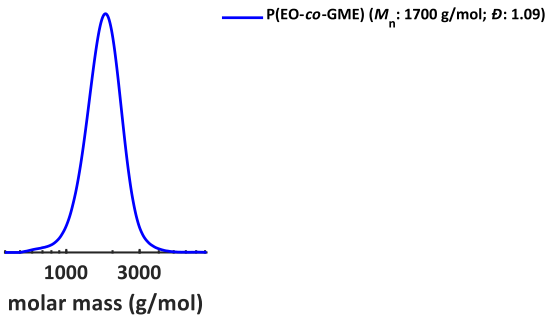

Figure S39: SEC of the polymer obtained after ^{1}H NMR kinetics (eluent: DMF with 1 g/L LiBr, RI detector, calibration: PEG). Initiator 2-(benzyloxy)ethanol, solvent anisole, degree of deprotonation 50%, temperature 55 °C.

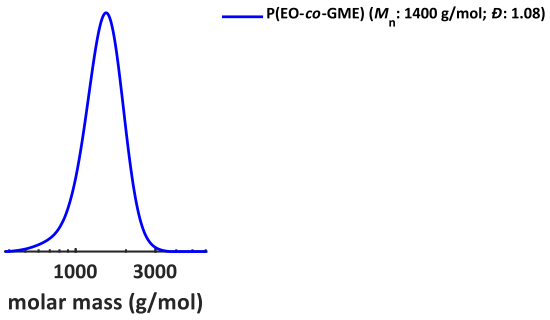

Figure S40: SEC of the polymer obtained after ^{1}H NMR kinetics (eluent: DMF with 1 g/L LiBr, RI detector, calibration: PEG). Initiator 2-(benzyloxy)ethanol, solvent anisole, degree of deprotonation 90%, temperature 55 °C.

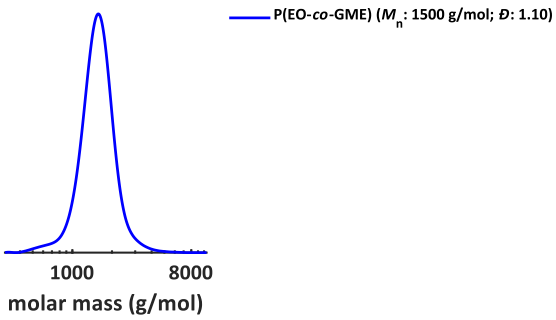

Figure S41: SEC of the polymer obtained after ^{1}H NMR kinetics (eluent: DMF with 1 g/L LiBr, RI detector, calibration: PEG). Initiator 2-(benzyloxy)ethanol, solvent toluene-d_8, degree of deprotonation 50%, temperature 55 °C.

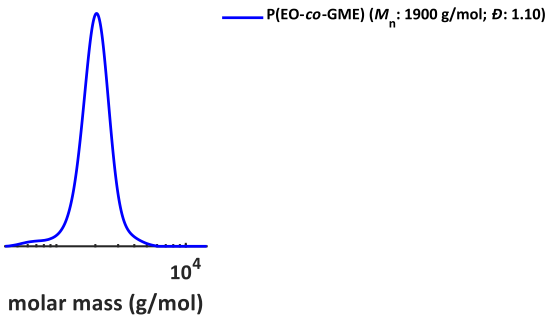

Figure S42: SEC of the polymer obtained after ^{1}H NMR kinetics (eluent: DMF with 1 g/L LiBr, RI detector, calibration: PEG). Initiator 2-(benzyloxy)ethanol, solvent toluene-d_8, degree of deprotonation 90%, temperature 55 °C.

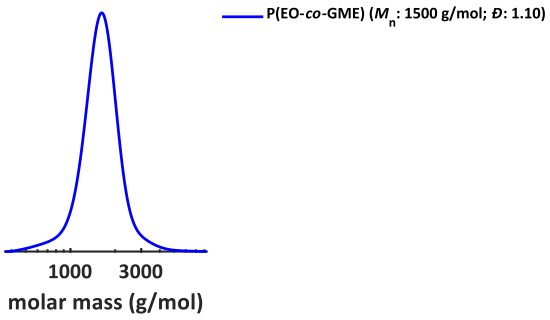

Figure S43: SEC of the polymer obtained after ^{1}H NMR kinetics (eluent: DMF with 1 g/L LiBr, RI detector, calibration: PEG). Initiator 2-(benzyloxy)ethanol, solvent toluene-d_8, degree of deprotonation 90%, temperature 55 °C, addition of 2 eq. of [18]crown-6 per potassium equivalent.

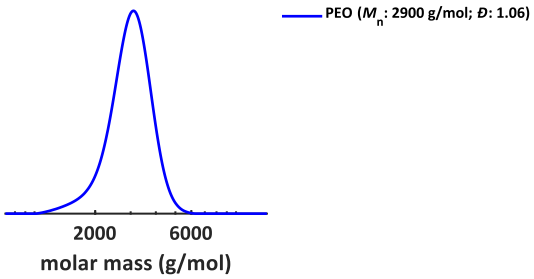

Figure S44: SEC of the polymer obtained after ^{1}H NMR kinetics (eluent: DMF with 1 g/L LiBr, RI detector, calibration: PEG). Initiator 3-ethoxypropane-1,2-diol, solvent DMSO-d_6, degree of deprotonation 25%, temperature 25 °C.

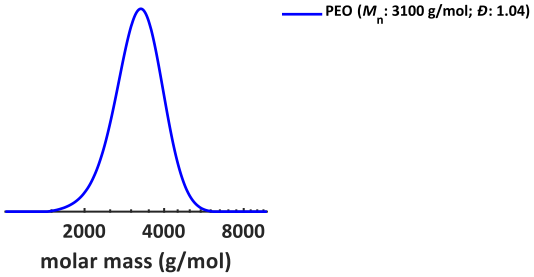

Figure S45: SEC of the polymer obtained after ^{1}H NMR kinetics (eluent: DMF with 1 g/L LiBr, RI detector, calibration: PEG). Initiator 3-ethoxypropane-1,2-diol, solvent DMSO-d_6, degree of deprotonation 50%, temperature 25 °C.

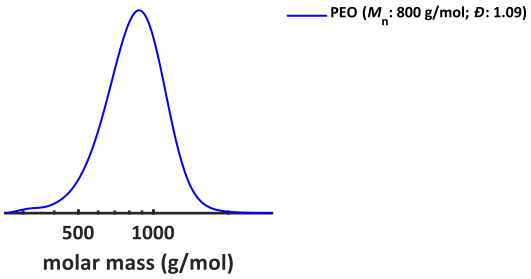

Figure S46: SEC of the polymer obtained after ^{1}H NMR kinetics (eluent: DMF with 1 g/L LiBr, RI detector, calibration: PEG). Initiator 2-(benzyloxy)ethanol, solvent toluene-d_8, degree of deprotonation 50%, temperature 55 °C.

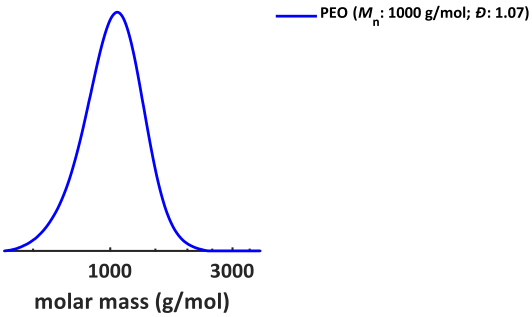

Figure S47: SEC of the polymer obtained after ^{1}H NMR kinetics (eluent: DMF with 1 g/L LiBr, RI detector, calibration: PEG). Initiator 2-(benzyloxy)ethanol, solvent toluene-d_8, degree of deprotonation 90%, temperature 55 °C.

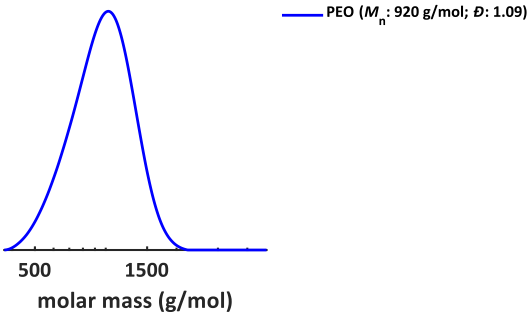

Figure S48: SEC of the polymer obtained after ^{1}H NMR kinetics (eluent: DMF with 1 g/L LiBr, RI detector, calibration: PEG). Initiator 2-(benzyloxy)ethanol, solvent anisole, degree of deprotonation 50%, temperature 55 °C.

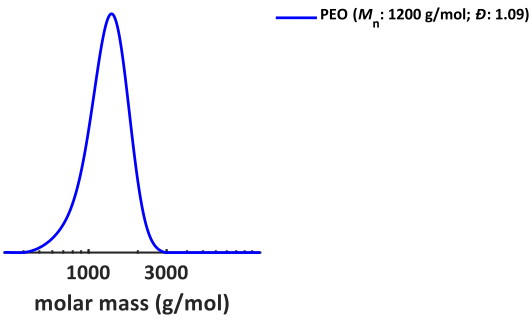

Figure S49: SEC of the polymer obtained after ^{1}H NMR kinetics (eluent: DMF with 1 g/L LiBr, RI detector, calibration: PEG). Initiator 2-(benzyloxy)ethanol, solvent anisole, degree of deprotonation 90%, temperature 55 °C.

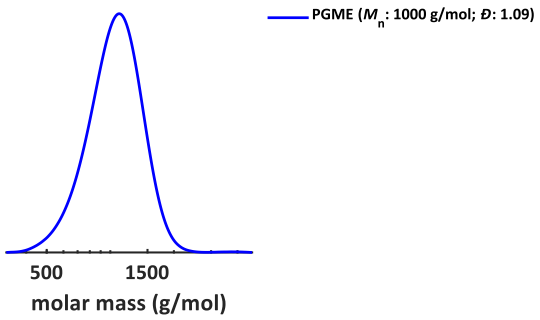

Figure S50: SEC of the polymer obtained after ^{1}H NMR kinetics (eluent: DMF with 1 g/L LiBr, RI detector, calibration: PEG). Initiator 2-(benzyloxy)ethanol, solvent anisole, degree of deprotonation 50%, temperature 55 °C.

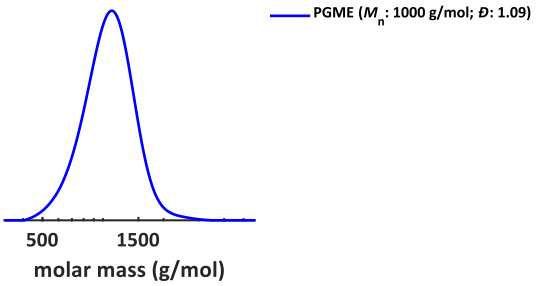

Figure S51: SEC of the polymer obtained after ^{1}H NMR kinetics (eluent: DMF with 1 g/L LiBr, RI detector, calibration: PEG). Initiator 2-(benzyloxy)ethanol, solvent toluene-d_8, degree of deprotonation 50%, temperature 55 °C.

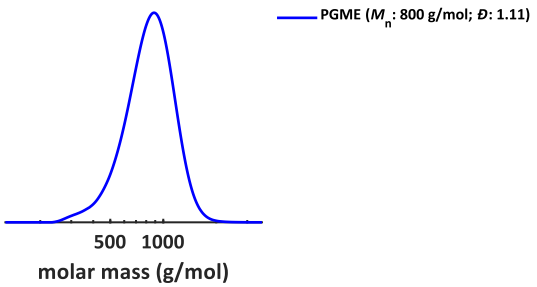

Figure S52: SEC of the polymer obtained after ^{1}H NMR kinetics (eluent: DMF with 1 g/L LiBr, RI detector, calibration: PEG). Initiator 2-(benzyloxy)ethanol, solvent toluene-d_8, degree of deprotonation 90%, temperature 55 °C.

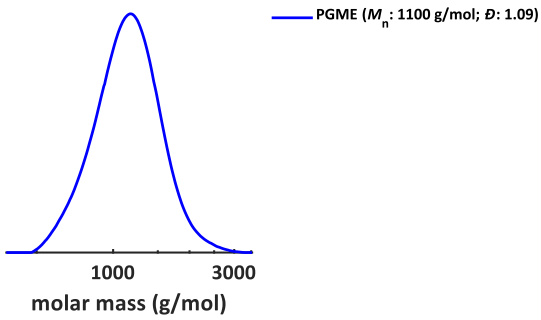

Figure S53: SEC of the polymer obtained after ^{1}H NMR kinetics (eluent: DMF with 1 g/L LiBr, RI detector, calibration: PEG). Initiator 2-(benzyloxy)ethanol, solvent anisole, degree of deprotonation 90%, temperature 55 °C.

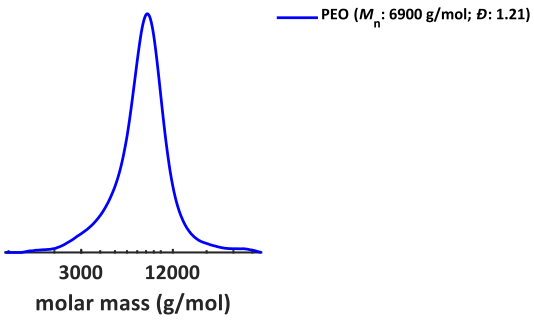

Figure S54: SEC of the polymer obtained after ^{1}H NMR kinetics (eluent: DMF with 1 g/L LiBr, RI detector, calibration: PEG). Initiator 2-(benzyloxy)ethanol, solvent DMSO-d_6, degree of deprotonation 90%, temperature 55 °C.

References

(1) Frey, H.; Mohr, R.; Dreier, P. POLY(ETHYLENE GLYCOL) HAVING C1 TO C3-ALKYLOXYMETHYL SIDE CHAINS, BIOCONJUGATES THEREOF, PROCESS FOR ITS PREPARATION AND ITS USE. EP4089133A1.

(2) Steube, M.; Johann, T.; Plank, M.; Tjaberings, S.; Gröschel, A. H.; Gallei, M.; Frey, H.; Müller, A. H. E. Kinetics of Anionic Living Copolymerization of Isoprene and Styrene Using in Situ NIR Spectroscopy: Temperature Effects on Monomer Sequence and Morphology. *Macromolecules* **2019**, *52* (23), 9299–9310. DOI: 10.1021/acs.macromol.9b01790.

(3) Solov'yanov, A. A.; Kazanskii, K. S. The kinetics and mechanism of anionic polymerization of ethylene oxide in ether solvents. *Polym. Sci. U.S.S.R.* **1972**, *14* (5), 1186–1195. DOI: 10.1016/0032-3950(72)90162-1.

(4) Duda, A.; Penczek, S. Determination of the Absolute Propagation Rate Constants in Polymerization with Reversible Aggregation of Active Centers. *Macromolecules* **1994**, *27* (18), 4867–4870. DOI: 10.1021/ma00096a002.

Chapter 4

Reaction Temperature and Solvent Determine Reactivity Ratios in the Copolymerization of Ethylene Oxide and Propylene Oxide

4 Reaction Temperature and Solvent Determine Reactivity Ratios in the Copolymerization of Ethylene Oxide and Propylene Oxide

[redacted], Gregor M. Linden[1], [redacted]

[1]Department of Chemistry, Johannes Gutenberg University Mainz, Duesbergweg 10-14, 55128 Mainz, Germany.

[redacted] and G.M.L. contributed to this work equally.

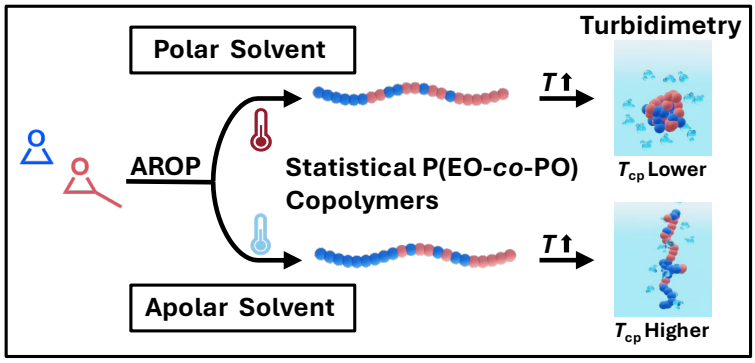

Abstract

Statistical copolymers of ethylene oxide (EO) and propylene oxide (PO) are widely used in industry and academia. Despite their decade-long use, the influence of the polymerization conditions on reactivity ratios is underexplored, and surprisingly solution and bulk properties of the resulting polyether copolymers have not been reported in a systematic manner. In this study, we examined the copolymerization of EO and PO in a variety of solvents (dimethyl sulfoxide, toluene, anisole) and at different temperatures, correlating reaction conditions with the thermal and solubility properties of the resulting P(EO-*co*-PO) copolymers. The copolymerization was monitored online by *in situ* ^{1}H NMR spectroscopy to determine the reactivity ratios for the full conversion range. The results show a temperature-dependent trend in reactivity ratios (*r*) for different solvents. In toluene, the reactivity ratios converge with increasing temperature, changing from r_{PO} = 0.26 and r_{EO} = 3.78 at 40 °C to r_{PO} = 0.31 and r_{EO} = 3.21 at 60 °C. A similar pattern is observed in anisole, with the reactivity ratios shifting from r_{PO} = 0.28 and r_{EO} = 3.52 at 40 °C to r_{PO} = 0.30 and r_{EO} = 3.32 at 60 °C, respectively. In contrast, the reactivity ratios in DMSO are generally more similar, with r_{PO} = 0.32 and r_{EO} = 3.10 at 40 °C.

Thermal characterization revealed similar melting points of approximately 10 °C and enthalpies of around 40 J·g^{-1}. Cloud point measurements of the copolymers showed decreased aqueous solubility as the differences in reactivity ratios decreased. These findings demonstrate that the statistical EO/PO copolymerization reaction conditions significantly influence copolymer physical properties, highlighting the need to consider such factors in applications.

Introduction

Statistical copolymers of the type poly(ethylene oxide-*co*-propylene oxide) (P(EO-*co*-PO)) are a crucially important class of materials.[1] They are commonly produced by copolymerizing ethylene oxide (EO) with propylene oxide (PO), enabling tailoring the properties of poly(ethylene oxide) (PEO), as aiming at reducing or fully avoiding crystallization. On the other hand, introducing a certain amount of EO in PPO structures can be used to increase the polarity of polyols.[2–5] The resulting polyether copolymers are widely used for the large-scale industrial production of polar polyether polyols in polyurethane (PU) manufacturing,[6,7] while also being tailored for various applications such as surfactants for drug delivery, tissue engineering, and biomolecule delivery.[8–11] In PU foam fabrication, P(EO-*co*-PO) copolymers with moderate hydrophilicity act as intrinsic surfactants, enhancing compatibility with water used as a blowing agent. This results in the formation of a highly uniform cellular structure. P(EO-*co*-PO) copolymers with a high EO content

enable the production of flexible and soft polyurethane foams without the need for auxiliary blowing agents, such as dichloromethane. However, incorporating more than 25% PO is essential to prevent the EO-rich segments from forming crystalline domains.[12] P(EO-*co*-PO) copolymers exhibit a lower critical solution temperature (LCST), which allows them to be dissolved in aqueous solutions at lower temperatures, while undergoing phase separation at higher temperatures, particularly at the cloud point temperature (T_{cp}).[13] At temperatures above T_{cp}, the copolymer chains aggregate due to inter- and intramolecular interactions. This transition is thermodynamically driven by unfavorable entropy of mixing, leading to numerous applications that require precise control over release mechanisms and selective separations in aqueous environments.[8,10] The adaptation of the thermoresponsive behavior of P(EO-*co*-PO) copolymers is closely linked to their microstructure, which determines the lower critical solution temperature (LCST).[8] The distribution of EO and PO units within the copolymer chains significantly influences both thermal properties and the interaction with water.[14] Early fundamental studies, such as that of Bailey and Callard in 1959, have shown that the statistical copolymerization of EO and PO allows for tuneable LCSTs that can be adjusted depending on the ratio of these two monomers.[2,15] Further studies by Tjerneld *et al*. could determine the temperature versus copolymer concentration phase diagram of P(EO_{45}-*co*-PO_{34}) based on the Flory-Huggins theory of polymer solubility.[11,13] More recent studies, such as those by Persson *et al*., investigated the phase behavior of copolymers with different PO contents and provided information on how changes in composition affect the cloud point temperature.[11] In addition, Louai *et al*. studied the influence of salt addition on the solution properties of EO/PO copolymers.[16] Overall, this research illustrates the crucial role of microstructural control in optimizing the thermoresponsive features of P(EO-*co*-PO) copolymers for a wide range of practical applications.[2]

Various studies have investigated the kinetics of EO/PO copolymerization, focusing on the resulting copolymer microstructure. This is represented by the reactivity ratios ($r_{PO} = k_{PO,PO}/k_{PO,EO}$; $r_{EO} = k_{EO,EO}/k_{EO,PO}$) with the rate constants k for homo- and crosspropagation, respectively. In the widely employed anionic ring-opening copolymerization (AROP), EO reacts faster than PO, which contains a methyl group attached to the epoxide moiety. In 1991, Heatley *et al*. reviewed the available literature on the reactivity ratios for the EO/PO comonomer pair, which varied widely from $r_{EO} = 1.34$, $r_{PO} = 0.14$ to $r_{EO} = 6.5$, $r_{PO} = 1.49$. In some cases, details of the reaction conditions were not reported.[17–22] Furthermore, the calculation methods used are considered outdated and not recommended anymore.[23] Heatley *et al*. investigated the copolymerization in bulk and analyzed the results using the Mayo-Lewis equation,[24] obtaining reactivity ratios of $r_{EO} = 2.8$ and $r_{PO} = 0.25$. Although the reactivity ratios were stated as independent of temperature, this could imply only

slight variations.[17] Three years later, in 1994, Holmberg *et al*. reported reactivity ratios of r_{EO} = 1.8 and r_{PO} = 0.3 for copolymerization in *N*,*N*-dimethyl formamide (DMF) at 90 °C,[25] using the Fineman-Ross method for data analysis.[26] Santacesaria *et al*. investigated the bulk copolymerization between 100 °C and 130 °C in 1996, reporting reactivity ratios of r_{EO} = 4.8–2.5 and r_{PO} = 0.22–0.17, depending on the temperature.[27] Applying the related monomer-activated anionic ring-opening polymerization (MAROP) further increases this reactivity difference (r_{PO} = 0.16, r_{EO} = 6.4).[5] In contrast, copolymerizations employing the industrially established double metal cyanide (DMC) catalysis[28] reverse these reactivity ratios, with PO becoming the more reactive monomer (r_{PO} = 2.4, r_{EO} = 0.42).[5]

To the best of our knowledge, no conclusive study presents the influence of solvents and temperatures on the reactivity ratios of the EO/PO comonomer pair in AROP. In industrial synthesis, EO/PO copolymers are commonly prepared in bulk or by using the DMC catalyst.[12] No conclusive study has investigated the influence of solvent or temperature on the reactivity ratios for this comonomer pair. The reactivity ratios of EO and allyl glycidyl ether (AGE) vary with the choice of solvent. Copolymerization in dimethyl sulfoxide (DMSO) yields ratios of r_{EO} = 0.92 and r_{AGE} = 1.08, while THF gives r_{EO} = 0.78 and r_{AGE} = 1.29. For EO and ethoxy vinyl glycidyl ether (EVGE), the difference in reactivity ratios is even more pronounced, leading to a soft gradient structure.[29] A similar trend is observed for the copolymerization of EO with glycidyl methyl ether (GME). In DMSO, the copolymerization yields random copolymers ($r_{EO} \approx r_{GME} \approx 1$),[30] whereas slight gradient structures are procured in the more apolar solvents toluene and anisole.[31,32]

AROP is typically carried out in polar, aprotic solvents like tetrahydrofuran (THF), DMSO, or hexamethylphosphoric triamide (HMPTA).[12] Polymerizations in DMSO proceed at a high rate,[33,34] albeit its high boiling point (189 °C) makes complete solvent removal challenging. Toluene is less polar and has been used occasionally, despite the low polymerization rate of epoxides in this solvent.[35,36] Anisole, with a lower boiling point of 154 °C, is considered a green solvent alternative.[37,38]

A critical issue in the AROP of substituted epoxides is the frequent occurrence of undesirable chain transfer reactions. Proton abstraction from the methyl or methylene group of the epoxide moiety generates an allyl alkoxide, which can act as an initiator. This process limits the achievable molar mass and increases the dispersity of the resulting polymer.[28,39–41] A low temperature, a moderate degree of deprotonation, a low monomer-to-initiator ratio, and using a suitable solvent can decrease it.[12] Allgaier *et al*. suppressed the transfer reaction by adding [18]crown-6 in toluene while maintaining a reasonable polymerization rate.[42]

This study aims to elucidate the copolymerization kinetics of EO and PO under varied reaction conditions, using the solvents DMSO, anisole, and toluene at different temperatures. Copolymers with comparable molar masses and comonomer composition were synthesized to assess (i) the nature of the gradient formed and (ii) the extent of chain transfer under the chosen reaction conditions. Since there is a lack of systematic data on the physical properties of EO/PO copolymers in literature, the aqueous solubility and thermal properties in solution and in bulk of the series of copolymers prepared have been analyzed in a detailed manner.

Experimental Section

Detailed information regarding the reagents, polymer synthesis, and the characterization techniques employed, is available in the Supporting Information (SI).

Results and Discussion

The influence of the copolymerization conditions on the microstructure of the resulting P(EO-*co*-PO) copolymers was investigated. Therefore, multiple copolymerizations were conducted in sealable NMR tubes, performing *in situ* ^{1}H NMR kinetics. Copolymers were synthesized under corresponding copolymerization conditions in anionic flasks in an additional series to investigate how variations of the microstructure impact the physical properties of the copolymers. The frequently employed initiator alcohol 2-(benzyloxy)ethanol was partially deprotonated and used for the ^{1}H NMR kinetics measurements as it provided an integrable benzyl group in the ^{1}H NMR and exhibited good solubility in the solvents.[43–45] Partially deprotonated triethylene glycol monomethyl ether was employed for the synthesis of the P(EO-*co*-PO) copolymers to reduce the impact of the initiator on the physical properties, as it comprises three EO repeating units (Scheme 1).

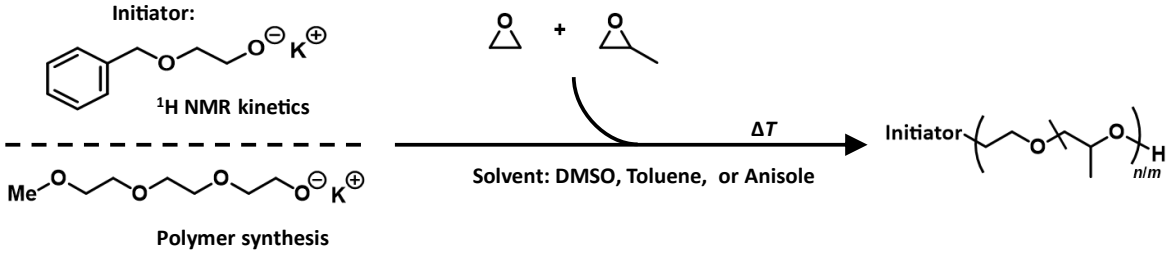

Scheme 1: Polymerization of EO/PO copolymers. ^{1}H NMR kinetics were conducted using 2-(benzyloxy)ethanolate as initiator, while monomethyl triethylene glycolate was employed for copolymer synthesis. The termination step is omitted for clarity reasons.

To investigate the kinetics of copolymerization *in situ*, the polymerizations were conducted within an NMR tube. The initiator salt, potassium 2-(benzyloxy)ethanolate, was synthesized by heating KO^{t}Bu with 2-(benzyloxy)ethanol overnight under azeotropic distillation in vacuo using a Schlenk

flask. The resulting salt was then dissolved in different solvents employed for polymerization (DMSO-d_6, toluene-d_8, anisole) and transferred to the NMR tube. Dried and freshly distilled PO was also transferred into the NMR tube under an argon counterflow. EO was condensed into the tube under vacuum at -78 °C, achieving a comonomer ratio of 40/4 eq. (EO/PO) with respect to the initiator. Subsequently, the NMR tube was sealed and transferred to the NMR spectrometer, where it was heated to the desired polymerization temperatures (25 °C, 40 °C, 50 °C, 60 °C). The entire polymerization process was monitored by acquiring ^{1}H NMR spectra usually every 2 minutes throughout the reaction. To isolate the effects of solvent and temperature on the polymerization process, all other parameters were maintained constant. The degree of deprotonation (base equivalents per hydroxyl group of the initiator) was set to 0.45 for all reactions to ensure a homogenous solution. All copolymers obtained from the kinetics measurements were subjected to SEC characterization and showed monomodal molar mass distributions with a dispersity $Đ$ of <1.1. The respective SECs can be found in the SI (Figure S67–Figure S78).

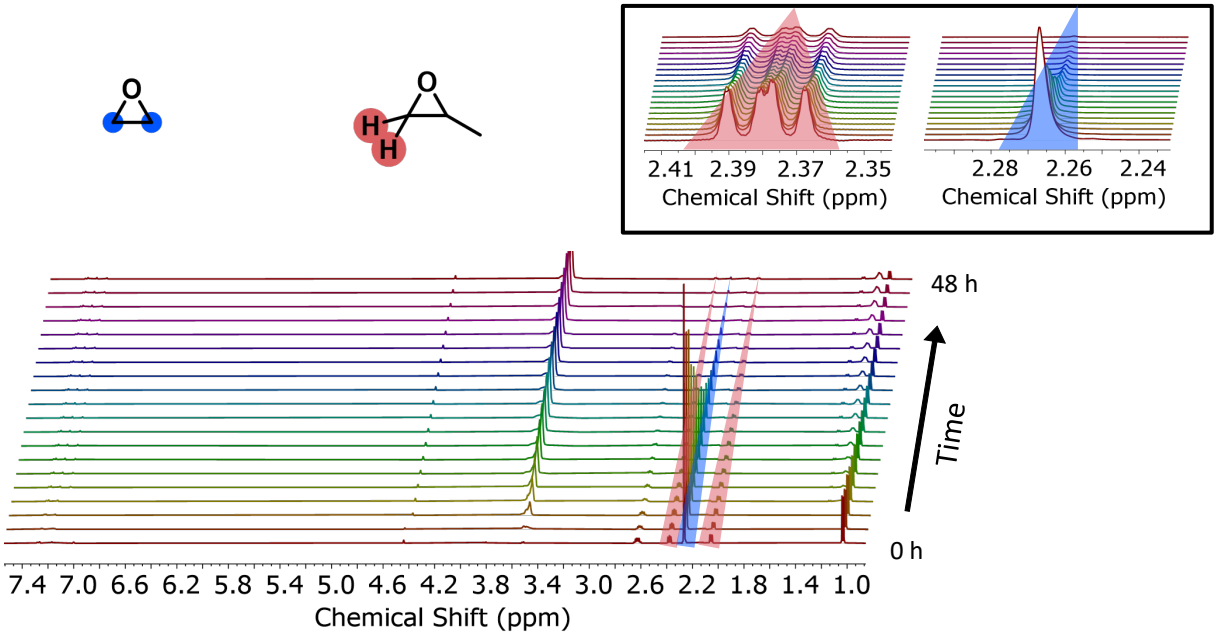

Figure 1: Stacked ^{1}H NMR spectra of the copolymerization of EO and PO. Zoom-in shows the decrease of the PO (red) and EO monomer signals (blue). Polymerization temperature 60 °C, solvent: toluene-d_8, 400 MHz. Since spectra were acquired every 2 minutes, only every 75th spectrum is displayed.

Experimental details can be found in the SI. An example of the stacked spectra is shown in Figure 1, demonstrating the time-dependent decrease of the signals of both monomers. The resulting time-conversion plots and individual versus total monomer conversion can be found in the SI (Figure S1–Figure S59).

Comparison of the Reaction Rates

To compare the solvents in terms of reaction rate, pseudo-first-order plots of the online ^{1}H NMR kinetics measurements were created (see Figure S60–Figure S66). The apparent rate constant of EO ($k_{app,\ copo}$ (EO)) was determined from the decrease of the monomer signals with time. The following equation 1 leads to the pseudo-first-order plot and the slope yields k_{app}. It indicates how quickly the reaction progresses. This value was used as a proxy for comparing the reaction conditions.

$$\ln\left(\frac{[\mathrm{M}]_0}{[\mathrm{M}]_t}\right) = k_{\mathrm{app}} * t \qquad (1)$$

Both monomers exhibited linear conversion behavior in DMSO, whereas an induction period was observed for anisole and toluene at all temperatures. A similar behavior was observed in THF for the polymerization of EO in the presence of Li and a phosphazene base by Müller *et al.*[46] This induction period is attributed to the so-called "crown ether effect";[47–49] after the addition of the first 5–6 monomer units, the slope becomes linear. The potassium ions are more effectively solvated by the growing polyether chain, enhancing charge separation between the ions and the active alkoxide chain end.

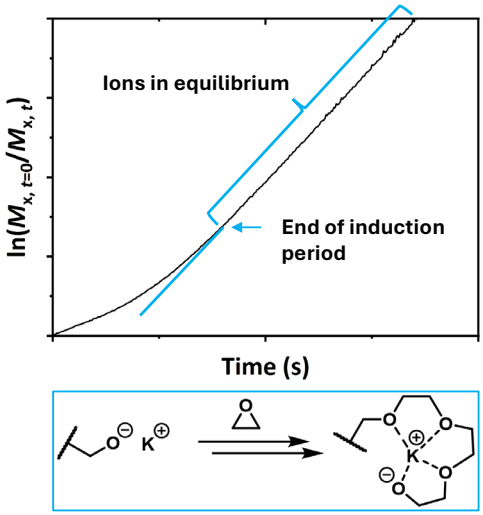

Figure 2: Exemplary pseudo-first-order plot with a visible induction period. The turquoise elongation shows the graph without the induction period. Lower Scheme: Solvation of the counterion (potassium) by the growing polyether chain, referred to as the Weibull-Törnquist effect.[50–52] Reprinted and adapted from *Reference Module in Chemistry* 2016, Penczek, S.; Pretula, J.B., *Ring-Opening Polymerization*, Page 23, Copyright 2016, with permission from Elsevier.[49]

The experiments involving crown ether addition in anisole and toluene displayed linear behavior from the beginning, like that observed in DMSO. However, these reactions showed a much smaller slope and consequently a lower reaction rate. Figure 3 highlights the induction period in toluene-d_8,

clearly showing the starting phase. Alkoxides are known to aggregate even in polar solvents like THF, and their propagation follows fractional-order kinetics depending on the active chain end concentration. Kazanskii *et al*. observed that potassium and cesium alkoxides formed trimers, while sodium alkoxides formed tetramers.[53,54] At the beginning of the reaction, the growing polyether chain complexes with the counterion, shifting the equilibrium from contact ion pairs to solvent-separated ion pairs. This leads to an increase in the propagation constant. An increased degree of ion pair dissociation towards free ions is possible.[55] Therefore, the observed induction period in solvents that are less polar than THF, such as anisole and toluene, is expected. The induction period is not strongly pronounced, as we used a degree of deprotonation of 45%. The aggregation of the potassium alkoxides was already decreased, due to the fast proton transfer between alcohols and alkoxides.[28,56,57] This finding is confirmed by the linear behavior of the polymerization with the addition of [18]crown-6 (Figure 3, turquois graph). The crown ether complexes the potassium cation, preventing alkoxide aggregation and significantly accelerating the reaction. This enhancement goes beyond the typical "crown ether effect". We would like to emphasize that all the reactions were first order with respect to monomer after the induction period, as can be seen in Figure S61, Figure S62, and Figure S65.

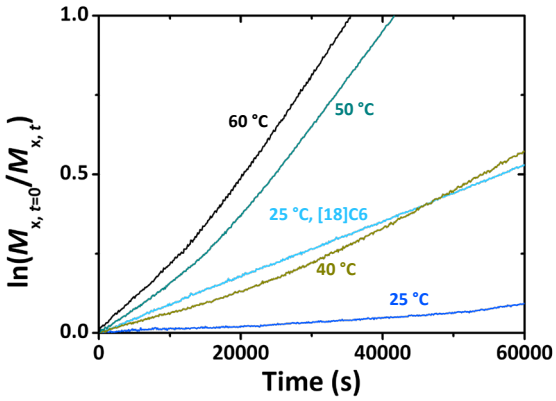

Figure 3: Enlargement of the pseudo-first-order plot of the copolymerization of EO with PO in Toluene-d_8 at different conditions obtained by ^{1}H NMR kinetics. The enlarged starting period shows the induction of the EO signal. The graphs for PO are omitted for clarity reasons.

The linear regime in the pseudo-first-order plots was analyzed using a linear fit to compare the reaction rates at different conditions. We would also like to emphasize that $k_{app,\,copo}$(EO) is not equal to the propagation constant of EO in homopolymerization, but works as a proxy to compare the different conditions. The results are visualized in Figure 4, while the values can be found in Table S1.

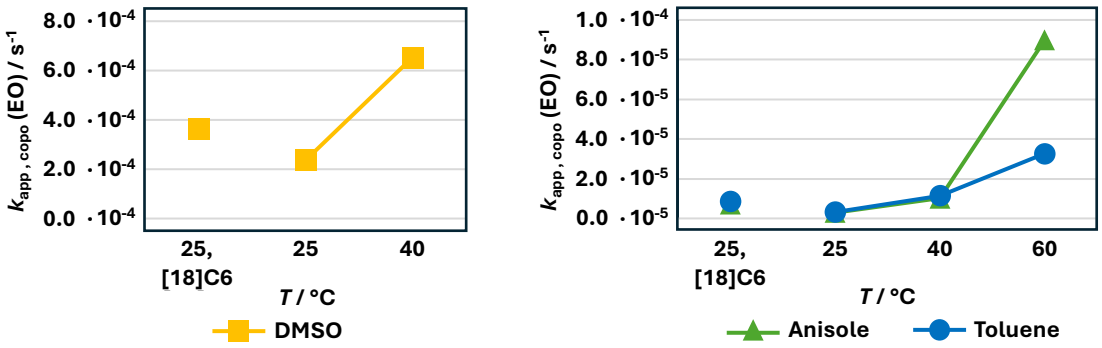

Figure 4: Comparison of the apparent propagation rate constant of EO in the copolymerization with PO. Left: DMSO-d_6. Right: Comparison of toluene-d_8 and anisole. Please note that this does not equal the propagation rate constant k_p of a homopolymerization.

In DMSO, [18]crown-6 at 25 °C leads to an increase in the reaction rate, despite the high polarity of the solvent (dielectric constant ε = 47.13).[58] However, the increase occurs only by a factor of ≈1.5. In contrast, raising the temperature to 40 °C results in a 2.8-fold increase. The reaction rate in toluene (ε = 2.408),[59] and anisole (ε = 4.3724)[60] is similarly influenced by adding crown ether at 25 °C. The change in reaction rate with increasing temperature remains consistent until the temperature reaches 60 °C, at which point the reaction rate in anisole becomes faster by a factor of 2.8 compared to toluene at 60 °C.

Influence of the Polymerization Conditions on Chain Transfer

A major challenge in the AROP of substituted epoxides is the occurrence of undesirable chain transfer reactions. Proton abstraction from the α-methyl or methylene group of the epoxide moiety leads to the formation of an allyl alkoxide that can act as a new initiator (Scheme 2).[28,39–41] Chain transfer of alkoxides to monomer impacts the polymerization outcomes by limiting the achievable molar mass, increasing dispersity, and incorporating undesired allylic end groups. Understanding the extent of chain transfer is important with respect to the physical properties and microstructural control of EO/PO copolymers explored in this study.[28] Chain transfer reduces the degree of deprotonation, slowing down the reaction, and producing undesired allylic chain ends.[18,61–63] As demonstrated in previous studies, several factors are known to increase the abundance of proton abstraction from the PO monomer. These factors include a high degree of deprotonation,[64] a small size of the counterion ($Li^+ > Na^+ > K^+ > Cs^+$),[28,65] and high target molar masses. Conversely, the addition of crown ether has been shown to reduce the formation of allyl species.[66,67] It has also been shown that the solvent has an impact on this transfer reaction.[68,69]

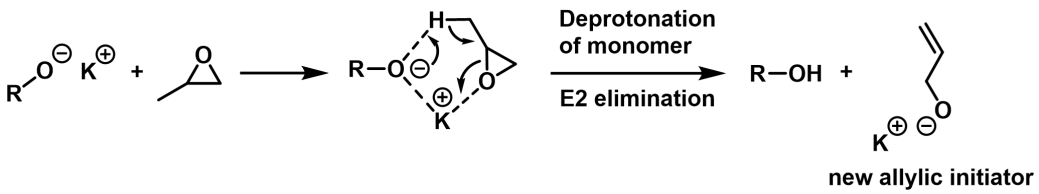

Scheme 2: Transfer reaction of an active chain end to the monomer PO, resulting in a new allylic initiator and a lower degree of deprotonation. Subsequent isomerization of the double bond to the vinyl species is omitted. Adapted and reprinted from Grobelny *et al.*,[64] Wiley © 2016.

Therefore, we also examined the transfer reactions occurring during the copolymerization in our selected solvents (DMSO, anisole, and toluene) and the extent of proton abstraction. The ratio of proton abstraction was quantified by assessing the ratio of the integral of allylic protons to the integral of protons from the initiator, 2-(benzyloxy)ethanol (exemplarily shown in Figure S80). The results are summarized in Table 1.

Table 1: Fraction χ of allylic species from active chain end transfer to PO at different reaction conditions in an EO/PO mixture of 40/4 eq.

Solvent	*T* / °C	χ (Allylic Species) / %
DMSO-d_6	25[a]	7
DMSO-d_6	25	7
DMSO-d_6	40	6
Anisole	25[a]	0
Anisole	25	0
Anisole	40	1
Anisole	60	3
Toluene-d_8	25[a]	0
Toluene-d_8	25	0
Toluene-d_8	40	2
Toluene-d_8	50	2
Toluene-d_8	60	2

[a]2 eq. [18]crown-6 per potassium.

Our study shows that the polar solvent DMSO-d_6 leads to a higher extent of proton abstraction from the PO monomer, consistent with previous findings.[70,71] Boileau stated that DMSO is known to be excellent for proton abstraction reactions and exhibits low propagation-to-transfer constant ratios.[48] At 25 °C and 40 °C, DMSO-d_6 exhibits a stable presence of allylic species (6–7%). This trend underscores the impact of solvent polarity, as polar environments increase the deprotonation

potential and transfer reaction abundance.[68] In contrast, the results for the apolar solvents anisole and toluene-d_8 demonstrate a significantly lower abundance of allylic species. Notably, at 25 °C, no allylic chain ends were detected in anisole or toluene-d_8, strongly indicating that apolar environments suppress proton abstraction. It should be noted that this result applies only to the specific conditions chosen for this study (T = 25 °C, EO/PO/I = 40/4/1, [M] = 7 mol/L, [I] = 0.16 mol/L, degree of deprotonation = 45%) and can therefore only be meaningfully compared with polymerizations conducted under identical conditions. However, even at 60 °C, the occurrence of allyl groups remains relatively low in toluene-d_8 (2%) and anisole (3%). These findings highlight that solvent polarity plays a critical role in the chain transfer reactions and the formation of allylic chain ends. The apolar solvents anisole and toluene show a significant reduction compared to the polar DMSO. Nevertheless, it should be noted that this positive effect is accompanied by a significant reduction in polymerization rate. Consequently, depending on the primary focus of the synthesis, apolar solvents may not always be the preferred choice.

Moreover, the data reveal that the addition of crown ether in DMSO-d_6 did not produce the expected reduction in allylic species. Across the experiments conducted at 25 °C and 40 °C, the observed levels of allylic chain ends remained consistent at 6–7%, indicating that the mitigating effect of crown ether was not as pronounced in DMSO as anticipated. This result suggests that while crown ether is effective at reducing allyl end group formation in apolar solvents by complexing with the counterions and reducing deprotonation, its efficacy in polar solvents like DMSO may be limited.[66] The data imply that the strong solvation and high polarity of DMSO may overshadow the counterion complexation effect of crown ether, resulting in similar levels of proton abstraction and allylic chain formation, regardless of the addition of crown ether.

Reactivity Ratios of EO/PO by *In Situ* ^{1}H NMR Copolymerization Kinetics

The highly established homopolymers PEO and PPO exhibit completely different properties. Poly(ethylene oxide) (PEO) is crystalline and highly hydrophilic, while poly(propylene oxide) (PPO) structures are amorphous and hydrophobic. Copolymerization of these two monomers affords materials that combine both sets of characteristics, with the specific balance influenced by both the monomer composition and the polymerization method as shown in previous works.[5,14] This highlights the critical role of copolymer microstructure in determining the physical properties of the resulting copolymer. Thus, gaining a deeper understanding of how fundamental parameters, such as polymerization temperature and solvent, impact the microstructure is highly relevant. To this end, online kinetics measurements have been conducted to investigate these effects.

Several methods are available to calculate the reactivity ratios from the monomer conversion.[5,26,72–74] Among those, Beckingham *et al*. recommended using integrated models over differential models, as they propose greater accuracy.[23] Furthermore, nonterminal or chain end independent models should be preferred over terminal models if they describe the data with sufficient precision.[5,73] This principle of relying on the simplest explanation of the data is termed "Ockham´s Razor".[75] We compared the data from the online kinetics measurements by applying a terminal model of Meyer and Lowry[74] and a nonterminal or ideal model from Jaacks,[76,77] both of which are integrated methods. Since the integrated nonterminal BSL model[73] delivered the very same results as the Jaacks model, we decided to omit these results. Equation 2 includes the respective monomer concentration at time t ($[M_x]_t$) and the initial concentration ($[M_x]_0$). The Jaacks fit is plotted as follows.

$$\log\left(\frac{[M_1]_t}{[M_1]_0}\right) = r_1 \cdot \log\left(\frac{[M_2]_t}{[M_2]_0}\right) \quad (2)$$

The slope is used to derive r_1. Given the relations $r_1 \cdot r_2 = 1$ (because of the nonterminal nature of the model) and $r_2 = 1/r_1$ both reactivity ratios can be obtained. The Meyer-Lowry fit is shown in the SI (Equation S2), together with both plotted graphs and the simulated composition plots (Figure S1–Figure S59). The results of the kinetics experiments are summarized in Table 2. The Jaacks model affords conclusive reactivity ratios throughout all experiments, with coefficients of determination $R^2 > 0.99$ in all cases except for toluene at 25 °C, due to the relatively noisy signal, as shown in Figure S36. The Meyer-Lowry model also gives reasonable results, showing good agreement with the Jaacks model in DMSO. However, for anisole and toluene, the reactivity ratios diverge significantly and show higher errors. In the case of copolymerization in toluene at 25 °C, the fit resulted in no reasonable solution, indicating the weakness of the terminal model towards noise, which leads to overfitting.[5,78] Since the Jaacks model provided consistent results for all solvents, we focus on this model to explain the data.

Table 2: Summarized results of the reactivity ratios obtained under different conditions.

Solvent	*T* / °C	Jaacks			Meyer-Lowry		
		r_{PO}	r_{EO}	R^2	r_{PO}	r_{EO}	NormRes
DMSO-d_6	25[a]	0.32 ± 0.01	3.15 ± 0.01	0.999	0.31 ± 0.01	2.97 ± 0.06	0.006
DMSO-d_6	25	0.31 ± 0.01	3.25 ± 0.01	0.999	0.30 ± 0.01	3.11 ± 0.03	0.004
DMSO-d_6	40	0.32 ± 0.01	3.10 ± 0.01	0.999	0.33 ± 0.01	3.21 ± 0.09	0.001
Anisole	25[a]	0.31 ± 0.01	3.26 ± 0.01	0.991	0.83 ± 0.37	5.25 ± 1.43	0.021
Anisole	25	0.28 ± 0.01	3.54 ± 0.13	0.995	0.22 ± 0.16	2.87 ± 1.72	0.006
Anisole	40	0.28 ± 0.01	3.52 ± 0.01	0.998	0.39 ± 0.01	4.38 ± 0.08	0.037
Anisole	60	0.30 ± 0.01	3.32 ± 0.01	0.991	0.32 ± 0.01	3.92 ± 0.14	0.137
Toluene-d_8	25[a]	0.33 ± 0.01	3.05 ± 0.01	0.990	0.85 ± 0.10	5.87 ± 0.50	0.062
Toluene-d_8	25	0.29 ± 0.01	3.49 ± 0.02	0.958	-[b]	-[b]	-[b]
Toluene-d_8	40	0.26 ± 0.01	3.78 ± 0.01	0.999	0.33 ± 0.01	4.59 ± 0.02	0.028
Toluene-d_8	50	0.28 ± 0.01	3.62 ± 0.01	0.998	0.33 ± 0.01	4.54 ± 0.01	0.015
Toluene-d_8	60	0.31 ± 0.01	3.21 ± 0.01	0.999	0.34 ± 0.01	3.64 ± 0.02	0.029

[a]2 eq. [18]crown-6 per potassium. [b]Fit did not result in a reasonable solution.

The kinetics could not be conducted for DMSO at 60 °C due to chain transfer to monomer. The reactivity ratios indicate a gradient structure between the two monomers in all cases. The expected composition of an equimolar copolymer is given in Figure 5 as an example. All other composition plots can be found in the SI.

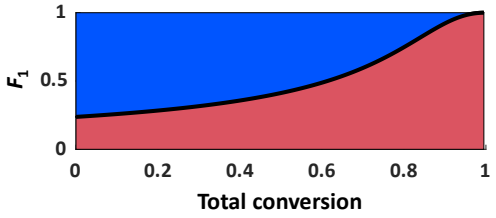

Figure 5: Composition plot of the *in situ* ^{1}H NMR copolymerization kinetic study of EO (blue) and PO (red) with a hypothetical equimolar monomer ratio (Solvent: toluene-d_8, 60 °C) showing r_{PO} = 0.31, r_{EO} = 3.21.

Effect of [18]Crown-6 on the Reactivity Ratios

Crown ethers are known to accelerate the AROP of epoxides, since they complex the respective counterion, enhancing the reactivity of the alkoxide chain end. For long-chain epoxide monomers, the addition of crown ether often represents a key step to enable polymerization.[79] Since potassium was used as a counterion in the AROP, [18]crown-6 was added to the EO/PO copolymerization. The effect of crown ether addition on the copolymerization and specifically the reactivity ratios was

investigated at 25 °C. The crown ether caused the reactivity ratios to converge slightly in all cases. Deviations from the values without crown ether are more pronounced for r_{EO}, due to its larger numerical value, making changes in its reactivity ratio more visible. The change observed for the polar solvent DMSO is rather small between the experiment with and without crown ether addition (3%). In anisole, a much less polar solvent than DMSO, the r_{EO} decreases by 8% with the addition of crown ether, equaling r_{EO} in DMSO without crown ether. In toluene, the effect is similar, but slightly larger, with a 13% decrease. The addition of crown ether accelerates the reaction rate but has only a minor impact on the reactivity ratios in apolar solvents, with an even smaller effect observed in DMSO.

Effect of the Temperature on the Reactivity Ratios

The increase in temperature to 40 °C in DMSO results in a more pronounced decrease (r_{EO} = 3.10) compared to the addition of crown ether at 25 °C (r_{EO} = 3.15). This suggests that the elevated temperature increases the reactivity of the chain end, reducing the disparity between the reactivity of the two monomers. This conclusion is supported by the higher reaction rate, as discussed before. In anisole, the r_{EO} is similar at 25 °C and 40 °C but decreases at 60 °C, suggesting it passes through a maximum. A similar pattern is observed in toluene, where r_{EO} peaks at 40 °C and decreases even more significantly than in anisole at 60 °C. The intermediate step in toluene at 50 °C underlines this gradual decrease as this bridges the r_{EO} between 40 °C and 60 °C. A similar trend was observed for the bulk copolymerization of EO and PO between 70 °C and 120 °C. The reactivity ratios shifted from r_{EO} = 3.0, r_{PO} = 0.17 to r_{EO} = 1.6, r_{PO} = 0.36.[12,18]

Synthesis of P(EO-*co*-PO) Copolymers for Physical Property Characterization

Despite the widespread use of EO/PO copolymers, we have not been able to find a compilation of the physical properties of the copolyethers, neither in aqueous solution nor in bulk. To explore the potential impact of varying solvents and reaction temperatures on the physical properties, a series of P(EO-*co*-PO) copolymers was synthesized under meticulously controlled conditions. All copolymers were prepared to have a comparable molar mass (≈ 5000 g/mol) and EO/PO monomer ratio of 78/33. The molar mass and comonomer ratio were selected to produce semicrystalline materials with distinct melting endotherms and measurable cloud point temperatures. All polymerization parameters, apart from the solvent and reaction temperature, were held constant. The chosen solvents and temperature conditions matched those used in the kinetic studies. However, unlike the kinetics experiments, the initiator applied here was triethylene glycol monomethyl ether rather than 2-(benzyloxy)ethanol. Due to its structural similarity to the polymer backbone, triethylene glycol monomethyl ether was selected to minimize the influence of the

initiator on the copolymers' physical properties. Furthermore, polymerizations at room temperature had to be carried out with the addition of crown ether, as the reaction rates in anisole and toluene were so slow at this temperature that achieving molar masses sufficient for the characterization of crystallinity and thermoresponsive properties would not be feasible within a practical timeframe.

The initiator salt synthesis was conducted in accordance with the protocol for the kinetic measurements, involving heating of triethylene glycol monomethyl ether with KO^{t}Bu, followed by overnight solvent removal. However, unlike the kinetic experiments, both EO and PO monomers were introduced under static vacuum while the reaction mixture was maintained at -78 °C in an ethanol/liquid nitrogen bath. Additionally, these polymerizations were performed in a reaction flask rather than an NMR tube, with a degree of deprotonation of 90% to reduce the reaction time. Upon completion, the polymerizations were terminated. The reaction times were 72 hours for copolymerizations in toluene above 40 °C and DMSO. From preliminary experiments we knew, that copolymerizations in apolar solvents at lower temperatures required ca. 12 days to complete. This included an extra reaction time of 2–4 days to ensure completion due to safety precautions. The resulting polymers were purified by dialysis against *Milli-Q*® water, followed by characterization using NMR spectroscopy, size exclusion chromatography (SEC), and MALDI-ToF mass spectrometry. The synthesized copolymers are summarized in Table 3. The obtained ^{1}H NMR spectra (Figure S81–Figure S86), SEC traces (Figure S87) and mass spectra (Figure S88–Figure S93) are summarized in the SI.

The molar mass of the copolymers could not be determined by ^{1}H NMR spectroscopy due to the overlap of the initiator's methyl group signal with signals from the copolyether backbone. SEC measurements underestimated the molar mass compared to values obtained from MALDI-ToF MS analysis. This discrepancy arises because SEC, a relative method calibrated with PEG standards, does not account for the reduced hydrodynamic volume caused by the incorporation of the PO comonomer, leading to lower calculated molar masses. In contrast, MALDI-ToF MS analysis provided molar masses that were consistent with the target values of approximately 5000 g/mol. The comonomer ratio was calculated from the ratio of the copolymer backbone signal and the signal of the methyl group stemming from the PO units (Equation S1).

Melting Temperature and Enthalpy by DSC Measurements

The thermal properties were examined through differential scanning calorimetry (DSC) measurements. The corresponding DSC curves are shown in the SI (Figure S96–Figure S97). Clusters

of EO units along the copolymer backbone, which can assemble into PEO segments, are expected to enhance not only the solubility of the copolymers in water but also their crystallinity. This increased crystallinity should, in turn, result in higher melting temperatures and greater melting enthalpy.

Table 3: Characterization data for the series of statistical P(EO-*co*-PO) copolymers and the corresponding thermal properties.

Entry	mol%$_{EO}$[a] / %	Solvent	T / °C	Δr[b]	M_n[c] / g·mol^{-1}	M_n[d] / g·mol^{-1}	$Đ$[d]	T_g[e] / °C	T_m[f] / °C	ΔH[g] / J·g^{-1}
1	72	Toluene[h]	25	2.72	4600	4200	1.11	-69	5	38
2	75	Toluene	40	3.52	4500	4200	1.09	-69	13	42
3	73	Toluene	50	3.34	4900	4300	1.07	-69	10	40
4	72	Toluene	60	2.90	4900	4400	1.06	-70	7	39
5	72	Anisole	40	3.24	4900	4200	1.05	-70	8	39
6	72	DMSO	40	2.78	4700	4200	1.05	-70	6	38

[a]Determined by ^{1}H-NMR spectroscopy. [b]$\Delta r = r_{EO}$-r_{PO}. [c]Determined via MALDI-ToF MS measurement ($CHCl_3$, DCTB matrix). [d]Determined via SEC measurements (DMF, RI signal, PEG calibration). [e]Glass transition temperature. [f]Melting temperature. [g]Melting enthalpy. [h]2 eq. [18]crown-6 per potassium.

The copolymers exhibited similar thermal properties, with glass transition temperatures (T_g) around -70 °C, regardless of the copolymerization conditions. The endothermic melting peaks were broad, with maxima near 10 °C, approximately 55 °C lower than that of a corresponding PEG homopolymer.[28] This behavior is typical of many gradient copolymers, as the crystalline PEG sequences in the P(EO-*co*-PO) copolymers are disrupted by the incorporation of PO comonomer units along the copolymer chains.[80–82] The different copolymerization conditions listed in Table 3 are associated with a compositional gradient, as reflected by the difference in reactivity ratios ($\Delta r = r_{EO} - r_{PO}$). However, the melting points (T_m) and melting enthalpies (ΔH) remain nearly identical, indicating that the observed variations in reactivity ratios show very small influence on the physical bulk properties of the copolymers. It is important to emphasize that the differences in reactivity ratios are small, and these results align with expectations. Notably, all copolymers exhibited a PEG melting point despite containing 30 mol% PO comonomer. This is attributed to the gradient microstructure, which arises from differences in reactivity ratios. In contrast, related glycidyl ethers (GEs) exhibit random or near-random incorporation with EO in AROP ($r_{EO} \approx r_{GE} \approx 1$),[29,43,83–86] leading to the random distribution of comonomer units along the polyether backbone. As a result, the typically crystalline PEG domains are prevalently disrupted, reducing

crystallinity as the comonomer content increases. EO copolymers with glycidyl ether comonomer contents of approximately 10–20 mol% become fully amorphous.[44,83] This highlights the influence of reactivity ratios on the thermal properties of copolymers, although the differences observed in this study were too small to produce pronounced effects.

Cloud Point Temperatures by Turbidimetry Measurements

The thermoresponsive properties of the synthesized polymers were evaluated by turbidimetry to determine the influence of the variation of the polymerization conditions on their physical characteristics. The cloud point temperature T_{cp} of a polymer solution marks the temperature at which the polymer transitions from a soluble state to an aggregated, insoluble state, resulting in a cloudy appearance of the solution.[87] Commonly, turbidimetry is employed to determine T_{cp}. This technique records changes in light transmittance as the temperature increases. When the solution reaches T_{cp}, concentrated polymer droplets form, scattering light and causing a sudden decrease in transmittance. This effect can be conveniently measured with a standard UV-vis spectrometer equipped with temperature control. T_{cp} can be finely tuned by adjusting the hydrophilic-hydrophobic balance of the copolymer chains.[3] This tuning can be achieved via chemical modifications such as copolymerization[88] or end-group alterations,[89] as well as through physical factors like ionic strength,[16,90] making T_{cp} highly adaptable to meet specific application requirements. T_{cp} values are closely related to the polymer's microstructure, therefore, variations in the arrangement of monomer units or end groups may alter intermolecular interactions, thereby impacting the temperature at which phase separation occurs.[8]

Copolymers of EO and PO are known for their thermoresponsive behavior, they precipitate from aqueous solutions upon heating.[91] According to Bailey and Callard, copolymers with a PO content of 33 mol% exhibited a T_{cp} of ≈ 47–60 °C, depending on the copolymer concentration in the aqueous solution.[15] Extrapolation of their data suggests that a corresponding copolymer with 50 mol% PO would not be soluble in water.[91] However, the molar mass and synthesis conditions of the commercial copolymer were not reported.[15] Similarly, Louai observed comparable results but investigated a three-arm star copolymer.[80] Tjerneld *et al*. measured the T_{cp}s of three commercial EO/PO copolymers with varying PO content. The copolymer with the highest PO content, P(EO_{15}-*co*-PO_{47}) (24/76 mol% EO/PO), exhibited a T_{cp} of 30 °C.[92] However, as T_{cp} values are influenced by molar mass and polymer concentration in water, direct comparisons should be interpreted cautiously.[13,15]

The cloud point temperatures of all synthesized P(EO-*co*-PO) copolymers were investigated. The temperature-dependent transmittance of the polymer solution in *Milli-Q*® water with a

concentration of 5 mg·ml^{-1} was determined. The T_{cp} is defined as the temperature at which the normalized transmittance decreases to 50%. Figure S94 and Figure S95 illustrate the transmittance vs. temperature profiles for the temperature and solvent variation series, respectively. The synthesized copolymers are summarized in Table 4 along with their cloud point temperatures T_{cp}.

Table 4: Characterization data for the series of statistical P(EO-*co*-PO) copolymers and the corresponding cloud point temperature T_{cp} in aqueous solution.

Entry	mol%$_{EO}$[a] / %	Solvent	T / °C	Δr[b]	M_n[c] / g·mol^{-1}	M_n[d] / g·mol^{-1}	$Đ$[d]	T_{cp}[e] / °C
1	72	Toluene[f]	25	2.72	4600	4200	1.11	76
2	75	Toluene	40	3.52	4500	4200	1.09	86
3	73	Toluene	50	3.34	4900	4300	1.07	80
4	72	Toluene	60	2.90	4900	4400	1.06	78
5	72	Anisole	40	3.24	4900	4200	1.05	79
6	72	DMSO	40	2.78	4700	4200	1.05	78

[a]Determined by ^{1}H-NMR spectroscopy. [b]$\Delta r = r_{EO}$-r_{PO}. [c]Determined via MALDI-ToF MS measurement ($CHCl_3$, DCTB matrix). [d]Determined via SEC measurements (DMF, RI signal, PEG calibration). [e]Cloud point temperature determined in aqueous solution via turbidimetry for c = 5 mg·ml^{-1}. [f]2 eq. [18]crown-6 per potassium.

Influence of Polymerization Temperature on T_{cp}

A comparison of the copolymers synthesized in toluene at different temperatures shows that decreasing polymerization temperatures from 60 °C to 40 °C led to an increase in the cloud point temperature from 78 °C to 86 °C (see Table 4, entries 1–4, and Figure 6).

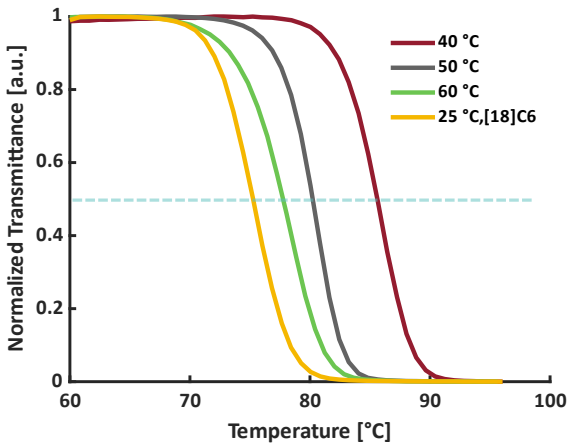

Figure 6: Results of the turbidimetry measurements in aqueous solution (c = 5 mg·ml^{-1}) of the polymers obtained from toluene at 25 °C with [18]crown-6, 40 °C, 50 °C, and 60 °C. The blue line represents 50% normalized transmittance, which is used to determine the cloud point temperatures.

Obviously, the polymerization temperature has a significant influence on the thermoresponsive behavior of P(EO-*co*-PO) copolymers. This is likely due to the microstructure of the copolymers. As determined via online kinetics, the polymerization temperature affects the reactivity ratios of the copolymerization, impacting the monomer gradient.

The nature of this compositional gradient is reflected by the difference in the reactivity ratios ($\Delta r = r_{EO} - r_{PO}$). The observed increase in T_{cp} in our data indicates enhanced solubility in water, demonstrating that the copolymers with a steeper gradient synthesized in this study dissolve more readily than those with a gradual composition gradient.

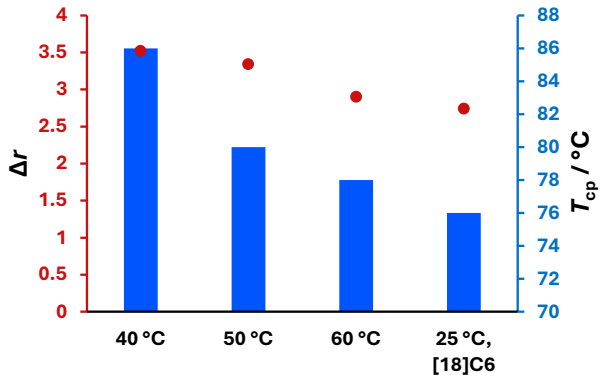

Figure 7: Cloud point temperature (T_{cp}, blue bars) and reactivity ratio difference (Δr, red line) of P(EO-*co*-PO) copolymers synthesized at various polymerization temperatures in toluene. The far-right column represents a polymerization conducted at room temperature in toluene with the addition of crown ether, while the remaining polymerizations were performed in pure toluene without crown ether.

This is explained by the clustering of EO units in some chain segments, which allows the formation of highly water-soluble PEO segments. Consequently, polymers synthesized at lower temperatures likely possess a sharper gradient, resulting in more distinct EO-rich segments and thereby higher aqueous solubility compared to those synthesized at elevated temperatures. The results of the online kinetics measurements correlate with this observation. The reactivity ratios for polymerizations conducted at 40 °C in toluene exhibit a greater disparity (r_{PO} = 0.26, r_{EO} = 3.78, Δr = 3.52, entry 2 in Table 4) than those for polymerizations at 60 °C (r_{PO} = 0.31, r_{EO} = 3.21, Δr = 2.90, entry 4 in Table 4), which aligns with a steeper compositional gradient in the first case. The reactivity ratio difference for the copolymer synthesized at 25 °C with crown ether (r_{PO} = 0.33, r_{EO} = 3.05, Δr = 2.72, Table 4, entry 1) is the smallest compared to those synthesized in toluene at 40–60 °C, which also results in reduced aqueous solubility.

The reactivity ratios do not exhibit as pronounced a difference as typically observed in carbanionic polymerizations.[93] However, the variations in gradient, as anticipated, significantly influence the physical properties, particularly the aqueous solubility of the copolymers.

Influence of Solvent on T_{cp}

An examination of the cloud point temperatures for polymers synthesized in different solvents at 40 °C strongly suggests that solvent choice plays a significant role in influencing copolymer properties (Figure S95). The T_{cp} values increase by 8 °C from the copolymer synthesized in the polar solvent DMSO (78 °C, Table 4, entry 6) to the one synthesized in the apolar solvent toluene (86 °C, Table 4, entry 2), indicating that solvent polarity also influences the solubility behavior of the copolymers (Figure 8). This trend is further supported by the reactivity ratios: in DMSO (r_{PO} = 0.32, r_{EO} = 3.10, Δr = 2.78), the reactivity ratios exhibit a smaller difference than those observed in toluene (r_{PO} = 0.26, r_{EO} = 3.78, Δr = 3.52), which corresponds to a more gradual compositional gradient in DMSO and a more segmented structure in toluene. The T_{cp} of the copolymer synthesized in anisole (79 °C, Table 4, entry 5) is similar to that of the copolymer synthesized in DMSO, despite the moderate difference in the reactivity ratios. This suggests the existence of a threshold below which differences in reactivity ratios have a minor effect. However, further investigation is referred to another study.

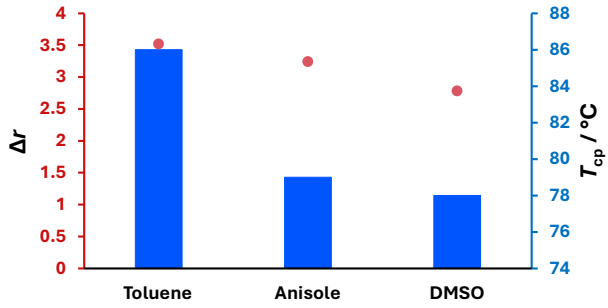

Figure 8: Cloud point temperature (T_{cp}, blue bars) and reactivity ratio difference (Δr, red line) of P(EO-*co*-PO) copolymers synthesized at 40 °C in different solvents (toluene, anisole, DMSO).

Conclusion

This study aimed to elucidate the effects of solvent choice, temperature, and crown ether addition on the copolymerization of ethylene oxide (EO) and propylene oxide (PO), as well as the resulting physical properties of P(EO-*co*-PO) copolymers with a comonomer ratio of 70/30 mol% (EO/PO) and a molar mass of ≈ 5000 g/mol. The potential changes in the physical properties due to different copolymerization conditions were expected to be clearly visible. We investigated the copolymerization by online ^{1}H NMR kinetics measurements in DMSO, anisole, and toluene at temperatures ranging from 25 °C to 60 °C, as well as in the presence of [18]crown-6 at 25 °C. The reaction rates were highest in DMSO, while anisole and toluene exhibited comparable rates under most polymerization conditions. Notably, at 60 °C, the reaction rate in anisole was 2.8 times higher than in toluene. For copolymerizations conducted in anisole and toluene, an induction period was

observed, attributed to the Weibull-Törnquist or “crown ether” effect, which was eliminated upon adding [18]crown-6. NMR spectroscopy indicated that the transfer reaction of active chains to PO monomer was significantly higher in DMSO than in toluene and anisole. This lower abundance of copolymer chains initiated by allylic species is advantageous, however, it is accompanied by the drawback of a reduced reaction rate, especially at low temperatures. This leads to reaction times of up to twelve days in toluene and anisole.

Reactivity ratios in bulk copolymerization of EO and PO were reported as r_{EO} = 2.8 and r_{PO} = 0.25.[17] Our online kinetics measurements in DMSO, toluene and anisole revealed higher reactivity ratios in the range of r_{EO} = 3.05–3.78 and r_{PO} = 0.33–0.26, depending on the copolymerization conditions. In DMSO, we observed copolymerization to produce less pronounced gradient structures compared to anisole and toluene at 25 °C and 40 °C. As temperature increases, the reactivity ratio differences decrease in all solvents. In toluene, reactivity ratio differences initially increase from 25 °C to 40 °C before converging at higher temperatures. The addition of [18]crown-6 slightly reduces the difference in reactivity ratios across all solvents at 25 °C. Thermal analysis of the copolymers revealed a broad melting peak with a maximum of around 10 °C. Differences in the reactivity ratios had no significant effect on the thermal properties. The P(EO-*co*-PO) copolymers exhibited a lower melting peak compared to a corresponding PEG homopolymer (65 °C).[28] The melting peak is visible despite the PO comonomer content of 30%. The gradient comonomer structure leads to EO-rich segments which are capable of crystallization. Copolymers were synthesized in toluene at various temperatures (40 °C, 50 °C, 60 °C, and 25 °C with [18]crown-6), and aqueous solubility was assessed via cloud point measurements. A decreased difference in reactivity ratios correlated with a slightly lower cloud point, which can be explained by fewer EO-rich segments in the softer gradient structure responsible for solubility. A similar trend in cloud point reduction was observed in copolymers prepared at 40 °C across the solvents.

The results demonstrate that selected reaction conditions significantly impact the physical properties of the copolymer, primarily due to variations in the gradient, as expressed by the reactivity ratios. While the influence of reaction conditions on reactivity ratios may not be predominant, they represent an effective tool for tuning material properties. The parameters studied here – solvent, temperature, and, in part, crown ether addition – constitute some of the possible variables. Future research could explore the effects of various solvents and solvent mixtures, as well as different degrees of deprotonation. These findings underscore the critical role of reaction conditions in shaping the physical properties of P(EO-*co*-PO) copolymers.

Acknowledgments

The authors thank [redacted] for MALDI-ToF MS measurements. [redacted] is thanked for designing copolymer structures for the graphical abstract. The authors thank the NMR facility at Johannes Gutenberg University for extended measurement periods.

References

(1) Abderrahim Louai, Dominique Sarazin, Gilbert Pollet Jeanne Francois. Properties of ethylene oxide-propylene oxide statistical copolymers in aqueous solution. *Polymer* **1991** (32), 703–712.

(2) Weber, C.; Hoogenboom, R.; Schubert, U. S. Temperature responsive bio-compatible polymers based on poly(ethylene oxide) and poly(2-oxazoline)s. *Prog. Polym. Sci.* **2012**, *37* (5), 686–714. DOI: 10.1016/j.progpolymsci.2011.10.002.

(3) Aubrecht, K. B.; Grubbs, R. B. Synthesis and characterization of thermoresponsive amphiphilic block copolymers incorporating a poly(ethylene oxide-*stat*-propylene oxide) block. *J. Polym. Sci. A Polym. Chem.* **2005**, *43* (21), 5156–5167. DOI: 10.1002/pola.21007.

(4) Klein, R.; Wurm, F. R. Aliphatic Polyethers: Classical Polymers for the 21st Century. *Macromol. Rapid Commun.* **2015**, *36* (12), 1147–1165. DOI: 10.1002/marc.201500013.

(5) Blankenburg, J.; Kersten, E.; Maciol, K.; Wagner, M.; Zarbakhsh, S.; Frey, H. The poly(propylene oxide-*co*-ethylene oxide) gradient is controlled by the polymerization method: determination of reactivity ratios by direct comparison of different copolymerization models. *Polym. Chem.* **2019**, *10* (22), 2863–2871. DOI: 10.1039/C9PY00500E.

(6) Desroches, M.; Escouvois, M.; Auvergne, R.; Caillol, S.; Boutevin, B. From Vegetable Oils to Polyurethanes: Synthetic Routes to Polyols and Main Industrial Products. *Polymer Reviews* **2012**, *52* (1), 38–79. DOI: 10.1080/15583724.2011.640443.

(7) Gagnon, S. D. Polyethers, Propylene Oxide Polymers. In *Kirk-Othmer Encyclopedia of Chemical Technology*; Ley, C., Ed. DOI: 10.1002/0471238961.1618151607010714.a01.

(8) Müller, V.; Matthes, R.; Wagner, M.; Bros, M.; Dreier, P.; Frey, H. Tailoring thermoresponsiveness of biocompatible polyethers: copolymers of linear glycerol and ethyl glycidyl ether. *Polym. Chem.* **2023**, *14* (21), 2599–2609. DOI: 10.1039/d3py00064h.

(9) Durand-Gasselin, C.; Capelot, M.; Sanson, N.; Lequeux, N. Tunable and reversible aggregation of poly(ethylene oxide-*st*-propylene oxide) grafted gold nanoparticles. *Langmuir* **2010**, *26* (14), 12321–12329. DOI: 10.1021/la1015669.

(10) Tuncaboylu, D. C.; Wischke, C. Opportunities and Challenges of Switchable Materials for Pharmaceutical Use. *Pharmaceutics* **2022**, *14* (11). DOI: 10.3390/pharmaceutics14112331.

(11) Persson, J.; Johansson, H.-O.; Tjerneld, F. Biomolecule Separation Using Temperature-Induced Phase Separation with Recycling of Phase-Forming Polymers. *Ind. Eng. Chem. Res.* **2000**, *39* (8), 2788–2796. DOI: 10.1021/ie9804125.

(12) Ionescu, M. *Chemistry and Technology of Polyols for Polyurethanes*; Rapra Technology Ltd, 2005.

(13) Johansson, H.-O.; Karlström, G.; Tjerneld, F. Experimental and Theoretical Study of Phase Separation in Aqueous Solutions of Clouding Colymers and Carboxylic Acids. *Macromolecules* **1993**, *26* (17), 4478–4483. DOI: 10.1021/ma00069a012.

(14) Zhao, J.; Zhang, G.; Pispas, S. Thermoresponsive Brush Copolymers with Poly(propylene oxide-*ran*-ethylene oxide) Side Chains via Metal-Free Anionic Polymerization "Grafting From" Technique. *J. Polym. Sci. A Polym. Chem.* **2010**, *48* (11), 2320–2328. DOI: 10.1002/pola.23997.

(15) Bailey, F. E.; Callard, R. W. Some Properties of Poly(ethylene oxide)[1] in Aqueous Solution. *J. Appl. Polym. Sci.* **1959**, *1* (1), 56–62. DOI: 10.1002/app.1959.070010110.

(16) Louai, A.; Sarazin, D.; Pollet, G.; François, J.; Moreaux, F. Effect of additives on solution properties of ethylene oxide-propylene oxide statistical copolymers. *Polymer* **1991**, *32* (4), 713–720. DOI: 10.1016/0032-3861(91)90485-2.

(17) Heatley, F.; Yu, G.-E.; Booth, C.; Blease, T. G. Determination of reactivity ratios for the anionic copolymerization of ethylene oxide and propylene oxide in bulk. *Eur. Polym. J.* **1991**, *27* (7), 573–579. DOI: 10.1016/0014-3057(91)90138-E.

(18) Becker, H.; Wagner, G.; Stolarzewicz, A. Zur Übertragungsreaktion bei der anionischen Polymerisation von Oxiranen. II. Zur Kettenübertragung bei der Copolymerisation von Propylen- und Ethylenoxid. *Acta Polym.* **1981**, *32* (12), 764–766. DOI: 10.1002/actp.1981.010321207.

(19) Stolarzewicz, A.; Becker, H.; Wagner, G. Zum Einfluß von Elektronendonatoren auf die anionische Copolymerisation von Oxiranen. *Acta Polym.* **1980**, *31* (12), 743–745. DOI: 10.1002/actp.1980.010311205.

(20) Rastogi, A. K.; St. Pierre, L. E. Copolymerization of ethylene oxide and propylene oxide by anhydrous potassium hydroxide. *J. Appl. Polym. Sci.* **1970**, *14* (5), 1179–1182. DOI: 10.1002/app.1970.070140505.

(21) Ponomarenko, V. A.; Khomutov, A. M.; Il'chenko, S. I.; Ignatenko, A. V. The effect of substituents of the anionic polymerization of α-oxides. *Polym. Sci. U.S.S.R.* **1971**, *13* (7), 1735–1740. DOI: 10.1016/0032-3950(71)90364-9.

(22) Gladkovskii, G. A.; Ryzhenkova, Y. Anionic copolymerization reactions of ethylene oxide and propylene oxide. *Polym. Sci. U.S.S.R.* **1971**, *13* (3), 723–730. DOI: 10.1016/0032-3950(71)90038-4.

(23) Lynd, N. A.; Ferrier, R. C.; Beckingham, B. S. Recommendation for Accurate Experimental Determination of Reactivity Ratios in Chain Copolymerization. *Macromolecules* **2019**, *52* (6), 2277–2285. DOI: 10.1021/acs.macromol.8b01752.

(24) Mayo, F. R.; Lewis, F. M. Copolymerization. I. A Basis for Comparing the Behavior of Monomers in Copolymerization; The Copolymerization of Styrene and Methyl Methacrylate. *J. Am. Chem. Soc.* **1944**, *66* (9), 1594–1601. DOI: 10.1021/ja01237a052.

(25) Adal, M.; Flodin, P.; Gottberg-Klingskog, E.; Holmberg, K. Determination of Monomer Reactivity Ratios in the Copolymerization of Ethylene Oxide and Propylene Oxide. *Tenside, Surfactants, Deterg.* **1994**, *31* (1), 9–11. DOI: 10.1515/tsd-1994-310105.

(26) Fineman, M.; Ross, S. D. Linear method for determining monomer reactivity ratios in copolymerization. *J. Polym. Sci.* **1950**, *5* (2), 259–262. DOI: 10.1002/pol.1950.120050210.

(27) Di Serio, M.; Vairo, G.; Iengo, P.; Felippone, F.; Santacesaria, E. Kinetics of Ethoxylation and Propoxylation of 1- and 2-Octanol Catalyzed by KOH. *Ind. Eng. Chem. Res.* **1996**, *35* (11), 3848–3853. DOI: 10.1021/ie960200c.

(28) Herzberger, J.; Niederer, K.; Pohlit, H.; Seiwert, J.; Worm, M.; Wurm, F. R.; Frey, H. Polymerization of Ethylene Oxide, Propylene Oxide, and Other Alkylene Oxides: Synthesis, Novel Polymer Architectures, and Bioconjugation. *Chem. Rev.* **2016**, *116* (4), 2170–2243. DOI: 10.1021/acs.chemrev.5b00441.

(29) Dreier, P.; Matthes, R.; Barent, R. D.; Schüttner, S.; Müller, A. H. E.; Frey, H. In Situ Kinetics Reveal the Influence of Solvents and Monomer Structure on the Anionic Ring-Opening Copolymerization of Epoxides. *Macromol. Chem. Phys.* **2022**, 2200209. DOI: 10.1002/macp.202200209.

(30) Frey, H.; Mohr, R.; Dreier, P. POLY(ETHYLENE GLYCOL) HAVING C1 TO C3-ALKYLOXYMETHYL SIDE CHAINS, BIOCONJUGATES THEREOF, PROCESS FOR ITS PREPARATION AND ITS USE. EP4089133A1.

(31) Linden, G. M.; Mathes, B.; Fuß, F.; Dreier, P.; Frey, H. Influence of Solvent and Degree of Deprotonation on Reactivity Ratios and Reaction Rates in Ethylene Oxide/Glycidyl Methyl Ether Copolymerization. To be submitted.

(32) Dreier, P.; Matthes, R.; Fuß, F.; Schmidt, J.; Schulz, D.; Linden, G. M.; Barent, R. D.; Schüttner, S.; Bros, M.; Frey, H. Isomerization of poly(ethylene glycol): A strategy for the evasion of immune recognition. *submitted*.

(33) Solov'yanov, A. A.; Kazanskii, K. S. Polymerization of ethylene oxide in dimethyl sulphoxide (DMS). *Polym. Sci. U.S.S.R.* **1972**, *14* (5), 1196–1206. DOI: 10.1016/0032-3950(72)90163-3.

(34) Kucera, M. *Mechanism and kinetics of addition polymerizations*, 2., rev. ed.; Comprehensive chemical kinetics / ed. by R. G. Compton Section 10, Modern methods, theory, and data, Vol. 31; Elsevier, 1992.

(35) Rangelov, S. Synthesis and polymerization of novel oxirane bearing an aliphatic double chain moiety. *Polymer* **2001**, *42* (10), 4483–4491. DOI: 10.1016/S0032-3861(00)00826-0.

(36) Misaka, H.; Tamura, E.; Makiguchi, K.; Kamoshida, K.; Sakai, R.; Satoh, T.; Kakuchi, T. Synthesis of end-functionalized polyethers by phosphazene base-catalyzed ring-opening polymerization of 1,2-butylene oxide and glycidyl ether. *J. Polym. Sci. A Polym. Chem.* **2012**, *50* (10), 1941–1952. DOI: 10.1002/pola.25969.

(37) Babij, N. R.; McCusker, E. O.; Whiteker, G. T.; Canturk, B.; Choy, N.; Creemer, L. C.; Amicis, C. V. de; Hewlett, N. M.; Johnson, P. L.; Knobelsdorf, J. A.; Li, F.; Lorsbach, B. A.; Nugent, B. M.; Ryan, S. J.; Smith, M. R.; Yang, Q. NMR Chemical Shifts of Trace Impurities: Industrially Preferred Solvents Used in Process and Green Chemistry. *Org. Process Res. Dev.* **2016**, *20* (3), 661–667. DOI: 10.1021/acs.oprd.5b00417.

(38) Gottlieb, H. E.; Graczyk-Millbrandt, G.; Inglis, G. G. A.; Nudelman, A.; Perez, D.; Qian, Y.; Shuster, L. E.; Sneddon, H. F.; Upton, R. J. Development of GSK's NMR guides – a tool to encourage the use of more sustainable solvents. *Green Chem.* **2016**, *18* (13), 3867–3878. DOI: 10.1039/C6GC00446F.

(39) Price, C. C.; Atarashi, Y.; Yamamoto, R. Polymerization and copolymerization of some epoxides by potassium *tert*-butoxide in DMSO. *J. Polym. Sci. A-1 Polym. Chem.* **1969**, *7* (2), 569–574. DOI: 10.1002/pol.1969.150070211.

(40) Hans, M.; Keul, H.; Moeller, M. Chain transfer reactions limit the molecular weight of polyglycidol prepared via alkali metal based initiating systems. *Polymer* **2009**, *50* (5), 1103–1108. DOI: 10.1016/j.polymer.2009.01.012.

(41) Brocas, A.-L.; Mantzaridis, C.; Tunc, D.; Carlotti, S. Polyether synthesis: From activated or metal-free anionic ring-opening polymerization of epoxides to functionalization. *Prog. Polym. Sci.* **2013**, *38* (6), 845–873. DOI: 10.1016/j.progpolymsci.2012.09.007.

(42) Allgaier, J.; Hövelmann, C. H.; Wei, Z.; Staropoli, M.; Pyckhout-Hintzen, W.; Lühmann, N.; Willbold, S. Synthesis and rheological behavior of poly(1,2-butylene oxide) based supramolecular architectures. *RSC Adv.* **2016**, *6* (8), 6093–6106. DOI: 10.1039/C5RA24547H.

(43) Schüttner, S.; Linden, G. M.; Hoffmann, E. C.; Holzmüller, P.; Frey, H. Glycidyl Ethers from Acyclic Terpenes: A Versatile Toolbox for Multifunctional Poly(Ethylene Glycol)s with Modification Opportunities. *Polym. Chem.* **2024.** DOI: 10.1039/D4PY01201A.

(44) Schüttner, S.; Krappel, M.; Koziol, M.; Marquart, L.; Schneider, I.; Sottmann, T.; Frey, H. Anionic Ring-Opening Copolymerization of Farnesyl Glycidyl Ether: Fast Access to Terpenoid-Derived Amphiphilic Polyether Architectures. *Macromolecules* **2023.** DOI: 10.1021/acs.macromol.3c00999.

(45) Verkoyen, P.; Dreier, P.; Bros, M.; Hils, C.; Schmalz, H.; Seiffert, S.; Frey, H. "Dumb" pH-Independent and Biocompatible Hydrogels Formed by Copolymers of Long-Chain Alkyl Glycidyl Ethers and Ethylene Oxide. *Biomacromolecules* **2020**, *21* (8), 3152–3162. DOI: 10.1021/acs.biomac.0c00576.

(46) Schmalz, H.; Lanzendörfer, M. G.; Abetz, V.; Müller, A. H. E. Anionic Polymerization of Ethylene Oxide in the Presence of the Phosphazene Base Bu^tP_4 – Kinetic Investigations Using In-Situ FT-NIR Spectroscopy and MALDI-ToF MS. *Macromol. Chem. Phys.* **2003**, *204* (8), 1056–1071. DOI: 10.1002/macp.200390077.

(47) Berlinova, I. V.; Panayotov, I. M.; Tsvetanov, C. Influence of the polyether chain on the dissociation of “living” polymers obtained in the anionic polymerization of ethylene oxide. *Eur. Polym. J.* **1977**, *13* (10), 757–760. DOI: 10.1016/0014-3057(77)90018-0.

(48) Boileau, S. Anionic Ring-opening Polymerization: Epoxides and Episulfides. In *Comprehensive Polymer Science and Supplements*:*The Synthesis, Characterization, Reactions & Applications of Polymers*; Allen, G., Bevington, J. C., Eds.; Pergamon, 1996; pp 467–487. DOI: 10.1016/B978-0-08-096701-1.00094-X.

(49) Penczek, S.; Pretula, J. B. Ring-Opening Polymerization. In *Reference Module in Chemistry, Molecular Sciences and Chemical Engineering*; Elsevier, 2016. DOI: 10.1016/B978-0-12-409547-2.11351-4.

(50) VI. Internationaler Kongreß für grenzflächenaktive Stoffe, Zürich 11.—15. 9. 1972 (II). *Tenside, Surfactants, Deterg.* **1973**, *10* (2), 83–85. DOI: 10.1515/tsd-1973-100207.

(51) Hermann, P. D.; Cents, T.; Klemm, E.; Ziegenbalg, D. Determination of the Kinetics of the Ethoxylation of Octanol in Homogeneous Phase. *Ind. Eng. Chem. Res.* **2017**, *56* (21), 6176–6185. DOI: 10.1021/acs.iecr.7b00948.

(52) Sallay, P.; Morgós, J.; Farkas, L.; Rusznák, I.; Veress, G.; Bartha, B. On the complex forming effect of the product in ethoxylation in the presence of sodium hydroxide. *Tenside, Surfactants, Deterg.* **1980**, *17* (6), 298–300. DOI: 10.1515/tsd-1980-170611.

(53) Kazanskii, K. S.; Solovyanov, A. A.; Entelis, S. G. Polymerization of ethylene oxide by alkali metal-naphthalene complexes in tetrahydrofuran. *Eur. Polym. J.* **1971**, *7* (10), 1421–1433. DOI: 10.1016/0014-3057(71)90036-X.

(54) Solov’yanov, A. A.; Kazanskii, K. S. The kinetics and mechanism of anionic polymerization of ethylene oxide in ether solvents. *Polym. Sci. U.S.S.R.* **1972**, *14* (5), 1186–1195. DOI: 10.1016/0032-3950(72)90162-1.

(55) Penczek, S.; Cypryk, M.; Duda, A.; Kubisa, P.; Slomkowski, S. Living ring-opening polymerizations of heterocyclic monomers. *Prog. Polym. Sci.* **2007**, *32* (2), 247–282. DOI: 10.1016/j.progpolymsci.2007.01.002.

(56) Deffieux, A.; Carlotti, S.; Barrère, A. Anionic Ring-Opening Polymerization of Epoxides and Related Nucleophilic Polymerization Processes. In *Polymer Science*:*A comprehensive reference*;

Matyjaszewski, K., Möller, M., Eds.; Elsevier, 2012; pp 117–140. DOI: 10.1016/B978-0-444-53349-4.00099-6.

(57) Szwarc, M. *Living polymers and mechanisms of anionic polymerization*; Advances in polymer science, Vol. 49; Springer, 1983.

(58) Wohlfarth, C. Dielectric constant of dimethylsulfoxide. In *Supplement to IV/6*; Martienssen, W., Lechner, M. D., Eds.; Landolt-Börnstein - Group IV Physical Chemistry; Springer Berlin Heidelberg, 2008; pp 140–143. DOI: 10.1007/978-3-540-75506-7_58.

(59) Wohlfarth, C. Dielectric constant of toluene. In *Supplement to IV/6*; Martienssen, W., Lechner, M. D., Eds.; Landolt-Börnstein - Group IV Physical Chemistry; Springer Berlin Heidelberg, 2008; pp 392–394. DOI: 10.1007/978-3-540-75506-7_228.

(60) Martienssen, W.; Lechner, M. D., Eds. *Supplement to IV/6*; Landolt-Börnstein - Group IV Physical Chemistry; Springer Berlin Heidelberg, 2008. DOI: 10.1007/978-3-540-75506-7.

(61) Steiner, E. C.; Pelletier, R. R.; Trucks, R. O. A study of the polymerization of propylene oxide catalyzed by anhydrous potassium hydroxide. *J. Am. Chem. Soc.* **1964**, *86* (21), 4678–4686. DOI: 10.1021/ja01075a031.

(62) Yu, G.-E.; Masters, A. J.; Heatley, F.; Booth, C.; Blease, T. G. Anionic polymerisation of propylene oxide. Investigation of double-bond and head-to-head content by NMR spectroscopy. *Macromol. Chem. Phys.* **1994**, *195* (5), 1517–1538. DOI: 10.1002/macp.1994.021950506.

(63) Wojtech, V. B. Zur Darstellung hochmolekularer Polyäthylenoxyde. *Makromol. Chem.* **1963**, *66* (1), 180–195. DOI: 10.1002/macp.1963.020660118.

(64) Grobelny, Z.; Swinarew, A.; Jurek-Suliga, J.; Skrzeczyna, K.; Gabor, J.; Łężniak, M. The Influence of Crown Ether and Alcohol on Unsaturation and Molar Mass of Poly(propylene oxide)s Prepared by Use of Potassium *t*-Butoxide: Reinvestigation of Chain Transfer Reactions. *Int. J. Anal. Chem.* **2016**, *2016*, 3727062. DOI: 10.1155/2016/3727062.

(65) Kirk, R. E.; Othmer, D. F., Eds. *Encyclopedia of chemical technology*, 5th ed.; Wiley, 2004. DOI: 10.1002/0471238961.

(66) Allgaier, J.; Willbold, S.; Chang, T. Synthesis of Hydrophobic Poly(alkylene oxide)s and Amphiphilic Poly(alkylene oxide) Block Copolymers. *Macromolecules* **2007**, *40* (3), 518–525. DOI: 10.1021/ma062417g.

(67) Ding, J.; Price, C.; Booth, C. Use of crown ether in the anionic polymerization of propylene oxide—1. Rate of polymerization. *Eur. Polym. J.* **1991**, *27* (9), 891–894. DOI: 10.1016/0014-3057(91)90028-M.

(68) Blanchard, L. P.; Hornof, V.; Moinard, J.; Tahiani, F. Anionic polymerization of propylene oxide. *J. Polym. Sci. A-1 Polym. Chem.* **1972**, *10* (10), 3089–3102. DOI: 10.1002/pol.1972.170101025.

(69) Stolarzewicz, A.; Becker, H.; Wagner, G. Zur Übertragungsreaktion bei der anionischen Polymerisation von Oxiranen. I. Zum Einfluß des Initiatorsystems auf die Kettenübertragung. *Acta Polym.* **1981**, *32* (8), 483–486. DOI: 10.1002/actp.1981.010320811.

(70) Banks, P.; Peters, R. H. Polymerization and crosslinking of epoxides: Base-catalyzed polymerization of phenyl glycidyl ether. *J. Polym. Sci. A-1 Polym. Chem.* **1970**, *8* (9), 2595–2610. DOI: 10.1002/pol.1970.150080925.

(71) Price, C. C.; Akkapeddi, M. K. Kinetics of base-catalyzed polymerization of epoxides in dimethyl sulfoxide and hexamethylphosphoric triamide. *J. Am. Chem. Soc.* **1972**, *94* (11), 3972–3975. DOI: 10.1021/ja00766a053.

(72) Kelen, T.; Tüdos, F. Analysis of the Linear Methods for Determining Copolymerization Reactivity Ratios. I. A New Improved Linear Graphic Method. *J. Macromol. Sci., Chem.* **1975**, *9* (1), 1–27. DOI: 10.1080/00222337508068644.

(73) Beckingham, B. S.; Sanoja, G. E.; Lynd, N. A. Simple and Accurate Determination of Reactivity Ratios Using a Nonterminal Model of Chain Copolymerization. *Macromolecules* **2015**, *48* (19), 6922–6930. DOI: 10.1021/acs.macromol.5b01631.

(74) Meyer, V. E.; Lowry, G. G. Integral and differential binary copolymerization equations. *J. Polym. Sci. A Gen. Pap.* **1965**, *3* (8), 2843–2851. DOI: 10.1002/pol.1965.100030811.

(75) Hoffman, R.; Carpenter, B. K.; Minkin, V. I. Ockham's Razor and Chemistry. *HYLE* **1997**, *3*, 3–28.

(76) Jaacks, V. Eine neuartige Methode zur Bestimmung von Copolymerisationsparametern. *Angew. Chem.* **1967**, *79* (9), 419. DOI: 10.1002/ange.19670790927.

(77) Jaacks, V. A Novel Method of Determination of Reactivity Ratios in Binary and Ternary Copolymerizations. *Makromol. Chem.* **1972**, *161* (1), 161–172. DOI: 10.1002/macp.1972.021610110.

(78) Hawkins, D. M. The problem of overfitting. *J. Chem. Inf. Model.* **2004**, *44* (1), 1–12. DOI: 10.1021/ci0342472.

(79) Verkoyen, P.; Frey, H. Long-Chain Alkyl Epoxides and Glycidyl Ethers: An Underrated Class of Monomers. *Macromol. Rapid Commun.* **2020**, *41* (15). DOI: 10.1002/marc.202000225.

(80) Louai, A.; Sarazin, D.; Pollet, G.; François, J.; Moreaux, F. Properties of ethylene oxide-propylene oxide statistical copolymers in aqueous solution. *Polymer* **1991**, *32* (4), 703–712. DOI: 10.1016/0032-3861(91)90484-Z.

(81) Beginn, U. Gradient copolymers. *Colloid. Polym. Sci.* **2008**, *286* (13), 1465–1474. DOI: 10.1007/s00396-008-1922-y.

(82) Hardeman, T.; Koeckelberghs, G. The Synthesis of Poly(thiophene-*co*-fluorene) Gradient Copolymers. *Macromolecules* **2015**, *48* (19), 6987–6993. DOI: 10.1021/acs.macromol.5b01384.

(83) Blankenburg, J.; Maciol, K.; Hahn, C.; Frey, H. Poly(ethylene glycol) with Multiple Aldehyde Functionalities Opens up a Rich and Versatile Post-Polymerization Chemistry. *Macromolecules* **2019**, *52* (4), 1785–1793. DOI: 10.1021/acs.macromol.8b02639.

(84) Lee, B. F.; Wolffs, M.; Delaney, K. T.; Sprafke, J. K.; Leibfarth, F. A.; Hawker, C. J.; Lynd, N. A. Reactivity ratios, and mechanistic insight for anionic ring-opening copolymerization of epoxides. *Macromolecules* **2012**, *45* (9), 3722–3731. DOI: 10.1021/ma300634d.

(85) Lee, A.; Lundberg, P.; Klinger, D.; Lee, B. F.; Hawker, C. J.; Lynd, N. A. Physiologically relevant, pH-responsive PEG-based block and statistical copolymers with *N*,*N*-diisopropylamine units. *Polym. Chem.* **2013**, *4* (24), 5735–5742. DOI: 10.1039/C3PY00747B.

(86) Koyama, Y.; Umehara, M.; Mizuno, A.; Itaba, M.; Yasukouchi, T.; Natsume, K.; Suginaka, A. Synthesis of novel poly(ethylene glycol) derivatives having pendant amino groups and aggregating behavior of its mixture with fatty acid in water. *Bioconjugate Chem.* **1996**, *7* (3), 298–301. DOI: 10.1021/bc9600123.

(87) Zhang, Q.; Weber, C.; Schubert, U. S.; Hoogenboom, R. Thermoresponsive polymers with lower critical solution temperature: from fundamental aspects and measuring techniques to recommended turbidimetry conditions. *Mater. Horiz.* **2017**, *4* (2), 109–116. DOI: 10.1039/C7MH00016B.

(88) Zhang, Q.; Schattling, P.; Theato, P.; Hoogenboom, R. Tuning the upper critical solution temperature behavior of poly(methyl methacrylate) in aqueous ethanol by modification of an activated ester comonomer. *Polym. Chem.* **2012**, *3* (6), 1418. DOI: 10.1039/c2py20073b.

(89) Jochum, F. D.; zur Borg, L.; Roth, P. J.; Theato, P. Thermo- and Light-Responsive Polymers Containing Photoswitchable Azobenzene End Groups. *Macromolecules* **2009**, *42* (20), 7854–7862. DOI: 10.1021/ma901295f.

(90) Zhang, Y.; Furyk, S.; Bergbreiter, D. E.; Cremer, P. S. Specific ion effects on the water solubility of macromolecules: PNIPAM and the Hofmeister series. *J. Am. Chem. Soc.* **2005**, *127* (41), 14505–14510. DOI: 10.1021/ja0546424.

(91) Harris, J. M. *Poly(Ethylene Glycol) Chemistry*; Springer US, 1992.

(92) Persson, J.; Kaul, A.; Tjerneld, F. Polymer recycling in aqueous two-phase extractions using thermoseparating ethylene oxide-propylene oxide copolymers. *J. Chromatogr. B Biomed. Sci. Appl.* **2000**, *743* (1-2), 115–126. DOI: 10.1016/s0378-4347(00)00213-9.

(93) Fuchs, D. A. H.; Hübner, H.; Kraus, T.; Niebuur, B.-J.; Gallei, M.; Frey, H.; Müller, A. H. E. The effect of THF and the chelating modifier DTHFP on the copolymerisation of β-myrcene and styrene: kinetics, microstructures, morphologies, and mechanical properties. *Polym. Chem.* **2021**, *12* (32), 4632–4642. DOI: 10.1039/D1PY00791B.

Supporting Information

Experimental Section

Reagents

Ethylene oxide (EO) was procured from *Air Liquide*. Deuterated solvents were purchased from *Deutero GmbH* (Germany). Potassium *tert*-Butanolate (KO^tBu), propylene oxide (PO), 2-(Benzyloxy)ethanol (>98%, GC), and triethylene glycol monomethyl ether were purchased from *TCI GmbH (Germany)* while DMSO and toluene (99% purity over molecular sieve) as well as anisole and [18]crown-6 ([18]C6) were purchased from *Acros/Fisher scientific*.

Instrumentation

Nuclear Magnetic Resonance (NMR) Spectroscopy

All ^{1}H NMR spectroscopic measurements were performed with a *Bruker Avance II 400* at a frequency of 400 MHz while the kinetic measurements were performed with a *Bruker Avance III HD 400* at a frequency of 400 MHz. The chemical shifts are all reported as ppm in relation to the proton signals of the deuteride solvents. Analysis of all spectra was performed with *MestReNova 14.3.3* from *Mestrelab Research*. When kinetics in anisole (non-deuterated) were measured, the lock was turned off. Shim was performed with *TopShim* (gradient shim) using the protons of the anisole methoxy group.

Size Exclusion Chromatography (SEC)

SEC characterization was performed using an *Agilent 1100 series* system, equipped with an UV-detector (254 nm) and RI-detector. *N*,*N*-dimethylformamide (DMF) was utilized as eluent, with 1 g/L LiBr. The applied HEMA 300/100/40 Å column cascade was heated by a column oven, set to 50 °C. The measurements were performed with a flow rate of 1 ml/min. One drop of internal standard (toluene) was added to the samples. Poly(ethylene oxide) standards from *Polymer Standard Service* (*PSS*) were used for calibration. Data were recorded and processed using the software *PSS WinGPC Unichrom*.

Matrix-assisted Laser Desorption Ionization Time-of-Flight (MALDI-ToF) Mass Spectrometry

MALDI-ToF MS measurements were carried out at a *Bruker autoflex maX MALDI-TOF/TOF* using a smartbeam-II solid state laser with a wavelength of 337 nm. The potassium salt of triflouroacetic acid (KTFA, ≥99%, HPLC-grade, *Sigma Aldrich*) and *trans*-2-[3-(4-*tert*-Butylphenyl)-2-methyl-2-propenylidene]malononitrile (DCTB, >98%, *TCI GmbH (Germany)*) were utilized as ionization salt and matrix, respectively. For sample preparation the polymers were dissolved in chloroform at 10

mg/mL. 20 µL of this solution were combined with 20 µL of a 10 mg/mL solution of the matrix in chloroform. 5 µL of a 0.1 M solution of the salt in methanol were added and 1 µL of the resulting mixture was spotted onto a *MTP 384* ground steel target plate. The solvents were allowed to evaporate completely before the measurement.

Differential Scanning Calorimetry (DSC)

The differential scanning calorimetry measurements were carried out with a *DSC250* device from *TA Instruments*. For this purpose, 10–15 mg of the polymers were weighed in *Tzero* aluminum pans. Before the actual measurement, the sample was first heated to 90 °C and recrystallized at a cooling rate of 3 °C/min to obtain an ordered structure of the polymer. The measurements were then carried out over a temperature range of -90 °C to 70 °C at a heating rate of 10 °C/min. The data obtained was analyzed using the second heating curve by *Trios* software from *TA Instruments*.

Turbidimetry

A *Jasco V-730* spectrometer was used for turbidimetry measurements. The polymers were dissolved in *Milli-Q*® water (5 mg/mL) and 0.7 mL of this solution were transferred to a glass cuvette. The transmission of this solution was then determined over a temperature range of 60 °C to 100 °C using a heating rate of 1 °C/min at a wavelength of λ = 600 nm. The data was obtained using *JASCO spectra manager* version 2.

Polymerization Procedures

Synthesis of statistical P(EO-*co*-PO) copolymers

The following section provides a representative synthesis procedure for the Poly(EO-*co*-PO) copolymers. For the synthesis of statistical P(EO-*co*-PO) copolymers, 1 eq. of triethylene glycol monomethyl ether (0.14 mg, 0.14 mL, 0.9 mmol) was dissolved in a mixture of 2 mL of benzene and 1 mL of THF. This solution was added to an anionic flask in Ar counterflow. Afterwards, 0.9 eq. of KO^{t}Bu (0.89 mg, 0.8 mmol) dissolved in 2 mL of THF and 2 drops of *Milli-Q*® water were added as well. This mixture was frozen using a liquid nitrogen bath and static vacuum conditions were established. Thereafter, the mixture was heated to 60 °C and stirred for 1 hour. The potassium salt of the initiator triethylene glycol monomethyl ether was formed under removal of the solvents and *tert*-butanol in vacuo overnight. In the crown ether containing polymerizations, 1.8 eq. of [18]crown-6 (420 mg, 1.6 mmol) dissolved in benzene were added together with KO^{t}Bu before heating and drying azeotropically.

The initiator salt was dissolved in the respective amount of solvent (DMSO, anisole, toluene) to obtain an initiator concentration of 0.18 M. PO (1753 mg, 2.10 mL, 30.2 mmol), dried over CaH_2 and freshly distilled, was added to the flask under static vacuum conditions and cooling with liquid nitrogen bath. EO (3102 mg, 3.20 mL, 70.4 mmol) was condensed under static vacuum conditions as well by employing an ethanol/liquid nitrogen bath at -78 °C. The polymerization mixture was slowly heated to the respective polymerization temperature (25 °C, 40 °C, 50 °C, 60 °C).

After full monomer conversion, as determined by ^{1}H NMR spectroscopy, the polymerization was terminated by adding 4 eq. of acetic acid per initiator dissolved in 10 mL diethyl ether and 2 mL toluene. Precipitated salt was filtered using *Celite*® and a por 4 frit and the crude polymer was isolated by removal of the solvents under vacuum at 40 °C. In a final purification step, remaining impurities were removed by dialysis against *Milli-Q*® water using a dialysis membrane (*Spectrum Labs*) with a molecular weight cut-off of 1 kDa. The purified polymer was dried by lyophilization.

The proportions of the respective monomers in the copolymer were determined using ^{1}H NMR spectroscopy. The ratio of the integrals of the copolymer backbone (3.65–3.30 ppm) and the methyl group of propylene oxide (1.12–1.02 ppm) were used for this purpose following the method of Booth *et al*.[1] The integral of the methyl group was set to 3 protons.

$$\chi_{\mathrm{EO}} = \frac{I_{\mathrm{Backbone}} - 3}{I_{\mathrm{Backbone}} + 1} \quad \text{(S1)}$$

It should be mentioned here that the signals of the initiator shift into the backbone signal of the polymer. However, since the initiator is composed of EO units, its contribution was included in the EO content of the polymer.

Investigation of copolymerization kinetics by *in situ* ^{1}H NMR analysis of PO and EO

For copolymerization of PO and EO during an online kinetics experiment, a *Norell S-500-VT-7* sealable NMR tube with a Teflon stopcock was employed. The initiator salt potassium 2-(benzyloxy)ethanolate was prepared in a fivefold batch in a Schlenk flask equipped with a magnetic stirrer in the following manner.

1 eq. of 2-(benzyloxy)ethanol (15 mg, 14 mL, 0.09 mmol) was dissolved in a mixture of 2 mL benzene and 1 mL THF. This solution was added to a Schlenk flask in Ar counterflow. Afterwards, 0.45 eq. of KO^{t}Bu (5 mg, 0.04 mmol) dissolved in 2 mL of THF and 2 drops of *Milli-Q*® water were added as well. This mixture was frozen using a liquid nitrogen bath and static vacuum conditions were established. Thereafter, the mixture was heated to 60 °C and stirred for 1 hour. The partially deprotonated initiator salt potassium 2-(benzyloxy)ethanolate was formed under the removal of the solvents in vacuo overnight.

In the crown ether containing kinetics, 2 eq. of [18]crown-6 were added together with KO^{t}Bu before heating and drying azeotropically.

The initiator salt was dissolved in the respective amount of solvent (2 mL) (DMSO-d_6, anisole, toluene-d_8). Anisole was not deuterated. EO (40 eq., 173 mg, 0.17 ml, 3.9 mmol) was condensed under static vacuum conditions into the NMR tube by employing an acetone/liquid nitrogen bath at -78 °C. PO (4 eq., 23 mg, 0.03 mL, 0.39 mmol), dried over CaH_2 and freshly distilled, and one-fifth of the initiator stock solution with a concentration of 0.16 mol/L was added under Ar counterflow while still cooling. The mixture was subjected to three freeze-pump-thaw cycles to remove residual Ar before being inserted into the preheated NMR spectrometer at the respective temperature. No sample spinning was applied, in the case of deuterated solvents one spectrum was recorded to determine the receiver gain. In the case of anisole, one spectrum was recorded to shim, and a second spectrum was recorded to determine the receiver gain. Online kinetics were conducted with measuring times between 10 and 92 hours with one scan every one to three minutes. After the kinetics, the copolymers underwent SEC analysis. It is important to note that the kinetic studies

conducted using toluene-d_8 as the solvent at 25 °C were monitored offline. In this approach, the polymerization was fully carried out in the kinetic tube under analogous conditions. However, instead of continuous online monitoring throughout the entire polymerization process, the polymerization tube was periodically transferred to the NMR spectrometer for analysis every 24 to 48 hours. This offline monitoring method was chosen because the extended duration of the polymerization made continuous *in situ* tracking impractical.

The respective chemical shift of the PO and EO Epoxide signal was tracked to calculate the individual monomer consumption. PO has three epoxide signals that can be utilized for this purpose. Whenever possible, we used the signal at around 2.38 ppm of the methylene group. When this signal merged with another signal, for example from EO, we utilized the methine proton. The software *NIREVAL*, created by Frey *et al.*,[2] was utilized to analyze the normalized monomer consumption. The equation for the Jaacks fit can be found in the main manuscript. The equation for the Meyer-Lowry equation with the restriction $r_1 \neq 1$, $r_2 \neq 1$ is as follows:[3]

$$\frac{M}{M_0} = \left(\frac{f_1}{f_{1,0}}\right)^{\frac{r_2}{1-r_2}} \cdot \left(\frac{1-f_1}{1-f_{1,0}}\right)^{\frac{r_1}{1-r_1}} \cdot \left(\frac{f_{1,0} - \frac{1-r_2}{2-r_1-r_2}}{f_1 - \frac{1-r_2}{2-r_1-r_2}}\right)^{\frac{1-r_1 r_2}{(1-r_1)\cdot(1-r_2)}} \tag{S2}$$

With f_1 as the fraction of monomer 1 from the whole unreacted monomers:

$$f_1 = \frac{[\mathrm{M}_1]}{[\mathrm{M}_1] + [\mathrm{M}_2]} \tag{S3}$$

Caveat: EO is a highly flammable and toxic gas, we recommend handling it only by trained researchers. We experienced breakage of the sealable NMR tubes from time to time when it was subjected to liquid nitrogen. We strongly recommend using an acetone/liquid nitrogen cooling bath of -78 °C.

Data of copolymerization kinetics

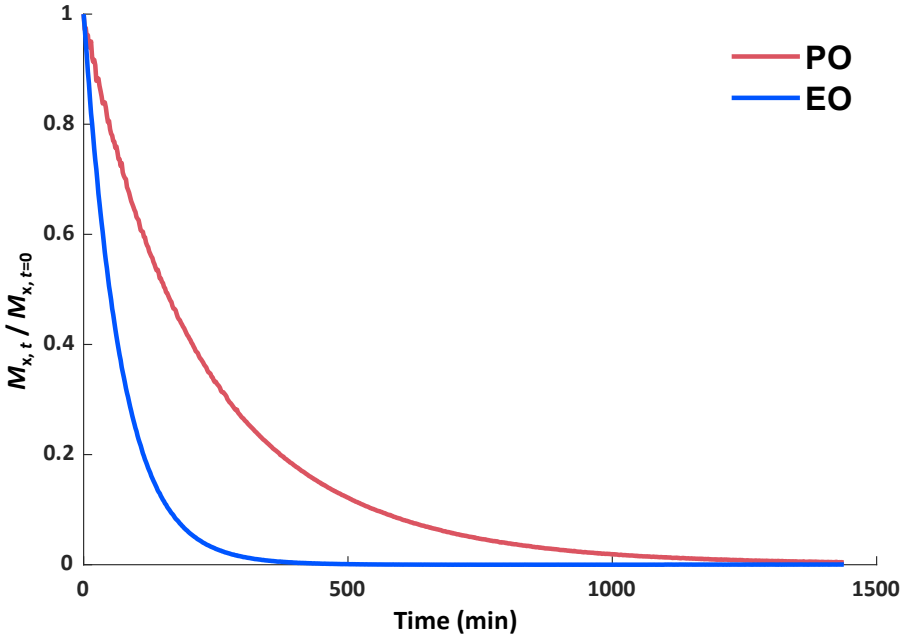

Figure S1: Time-conversion plot of the *in situ* ^{1}H NMR copolymerization kinetic study of EO with PO. (Solvent: DMSO-d_6, 25 °C).

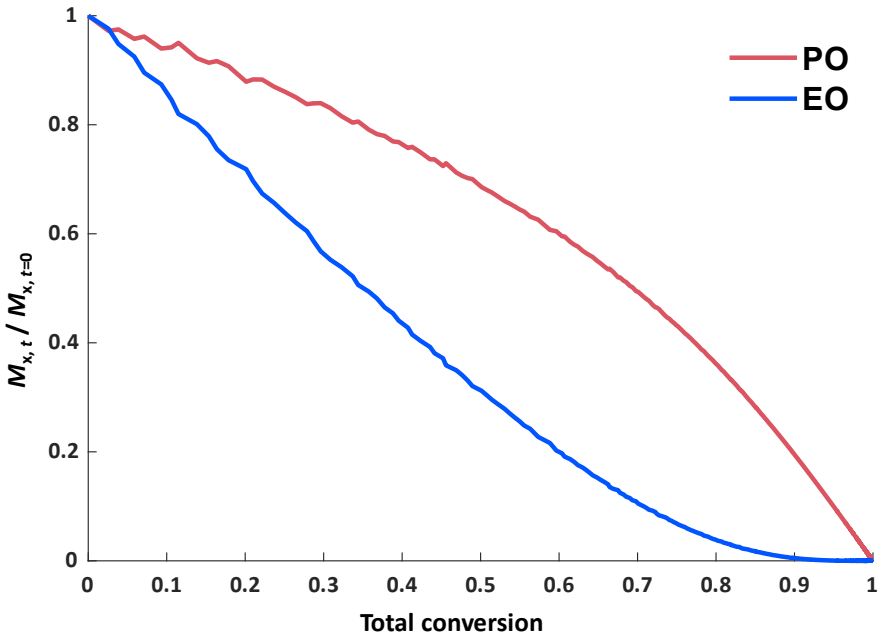

Figure S2: Individual versus total conversion of the *in situ* ^{1}H NMR copolymerization kinetic study of EO with PO. (Solvent: DMSO-d_6, 25 °C).

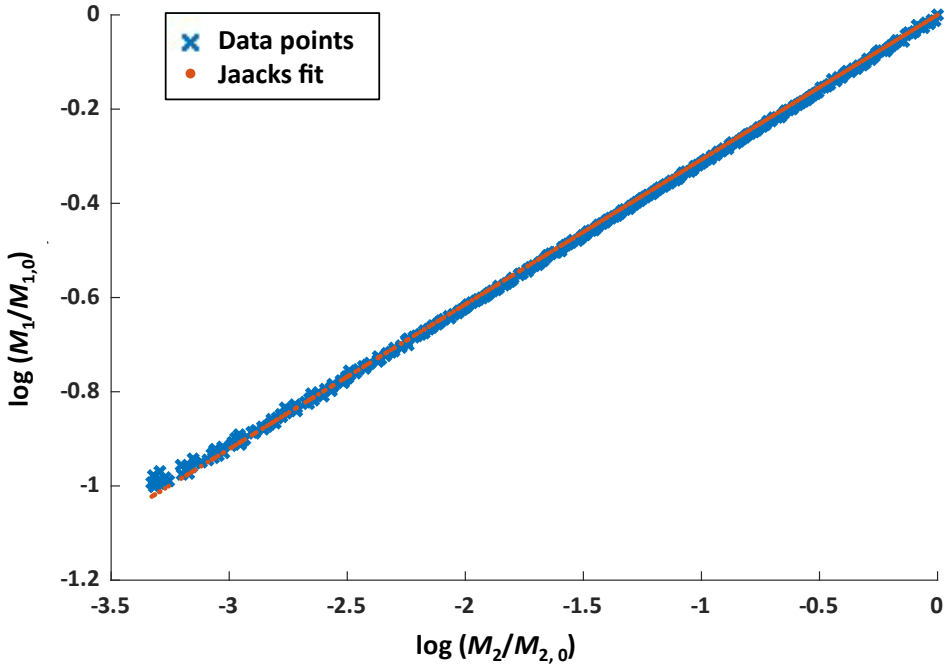

Figure S3: Jaacks fit of the *in situ* ^{1}H NMR copolymerization kinetic study of EO with PO. (Solvent: DMSO-d_6, 25 °C).

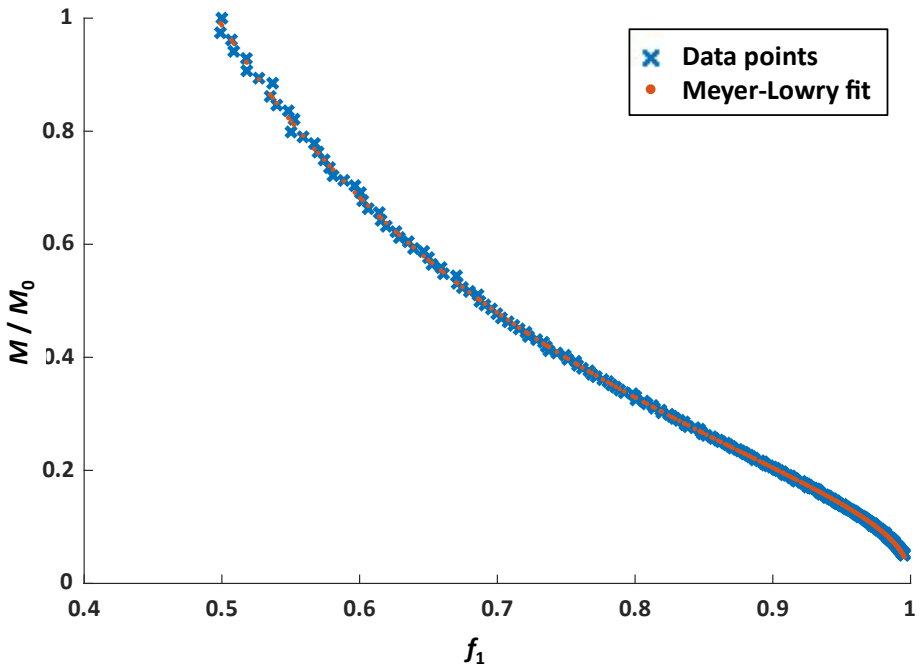

Figure S4: Meyer-Lowry fit of the *in situ* ^{1}H NMR copolymerization kinetic study of EO with PO. (Solvent: DMSO-d_6, 25 °C).

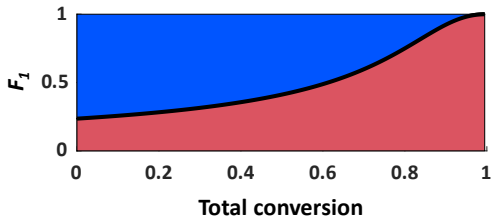

Figure S5: Composition plot of the *in situ* ^{1}H NMR copolymerization kinetic study of EO (blue) with PO (red) with a hypothetical equimolar monomer ratio (Solvent: DMSO-d_6, 25 °C) with r(PO)=0.31, r(EO)=3.25.

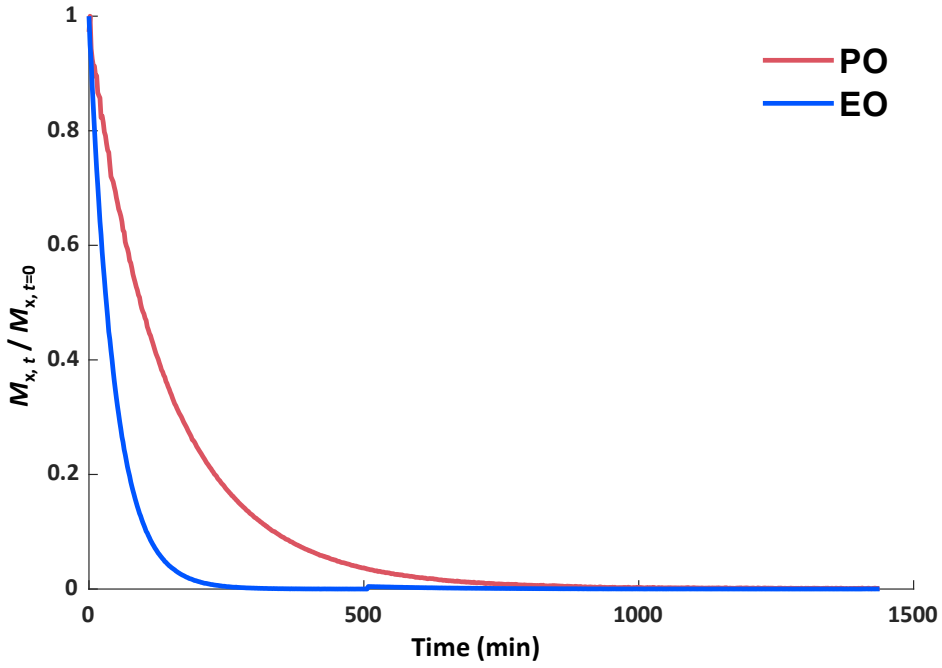

Figure S6: Time-conversion plot of the *in situ* ^{1}H NMR copolymerization kinetic study of EO with PO. (Solvent: DMSO-d_6, 25 °C, addition of [18]crown-6).

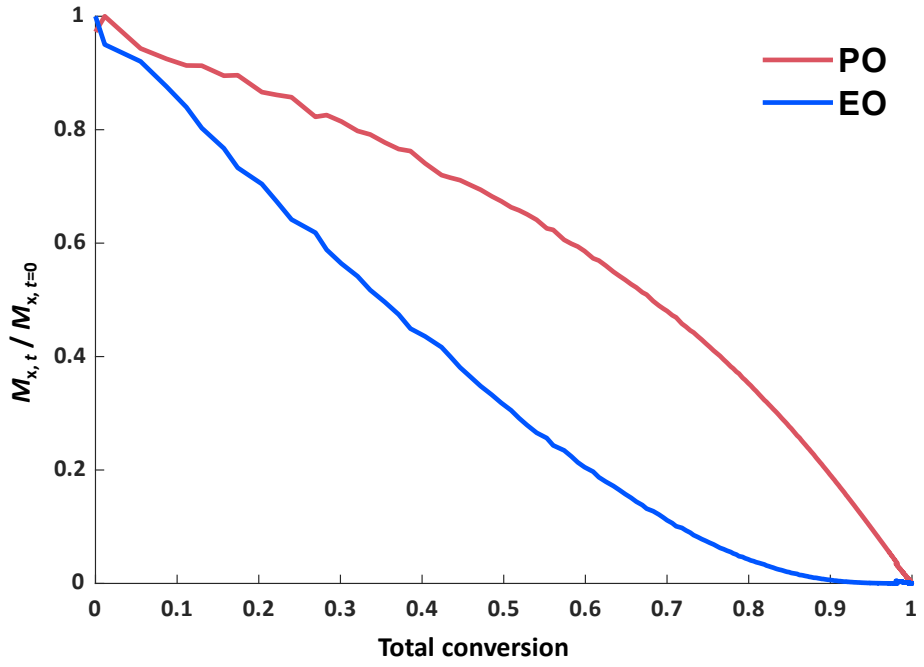

Figure S7: Individual versus total conversion of the *in situ* ^{1}H NMR copolymerization kinetic study of EO with PO. (Solvent: DMSO-d_6, 25 °C, addition of [18]crown-6).

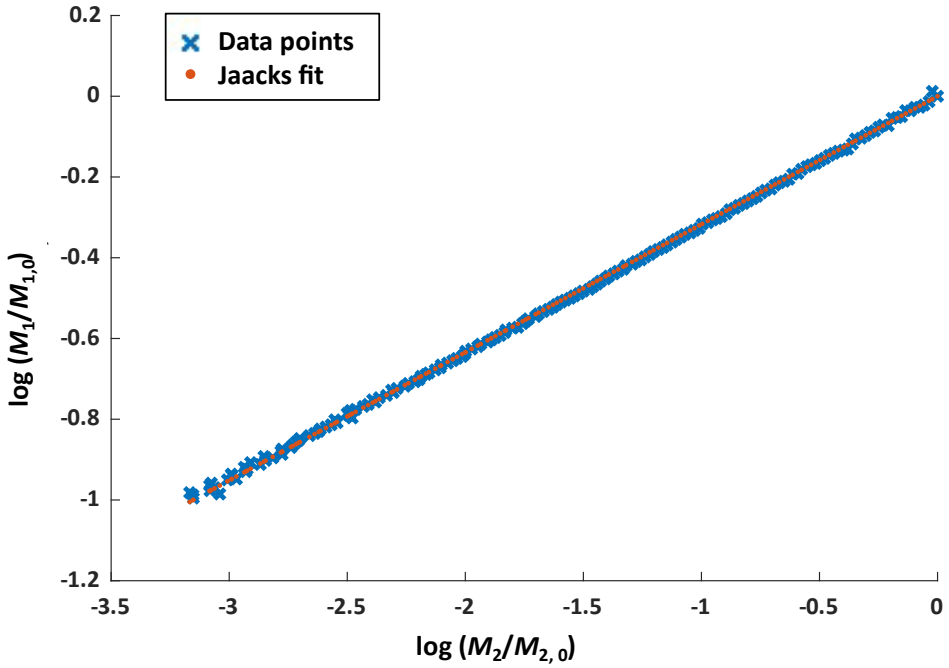

Figure S8: Jaacks fit of the *in situ* ^{1}H NMR copolymerization kinetic study of EO with PO. (Solvent: DMSO-d_6, 25 °C, addition of [18]crown-6).

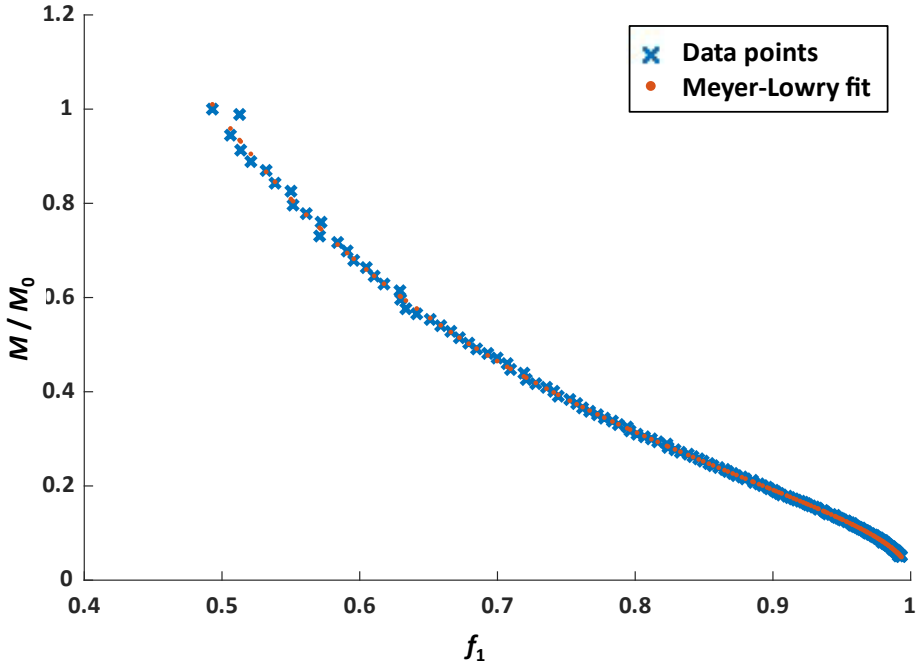

Figure S9: Meyer-Lowry fit of the *in situ* ^{1}H NMR copolymerization kinetic study of EO with PO. (Solvent: DMSO-d_6, 25 °C, addition of [18]crown-6).

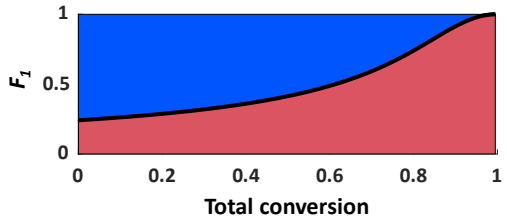

Figure S10: Composition plot of the *in situ* ^{1}H NMR copolymerization kinetic study of EO (blue) with PO (red) with a hypothetical equimolar monomer ratio (Solvent: DMSO-d_6, 25 °C, addition of [18]crown-6) with *r*(PO)=0.32, *r*(EO)=3.15.

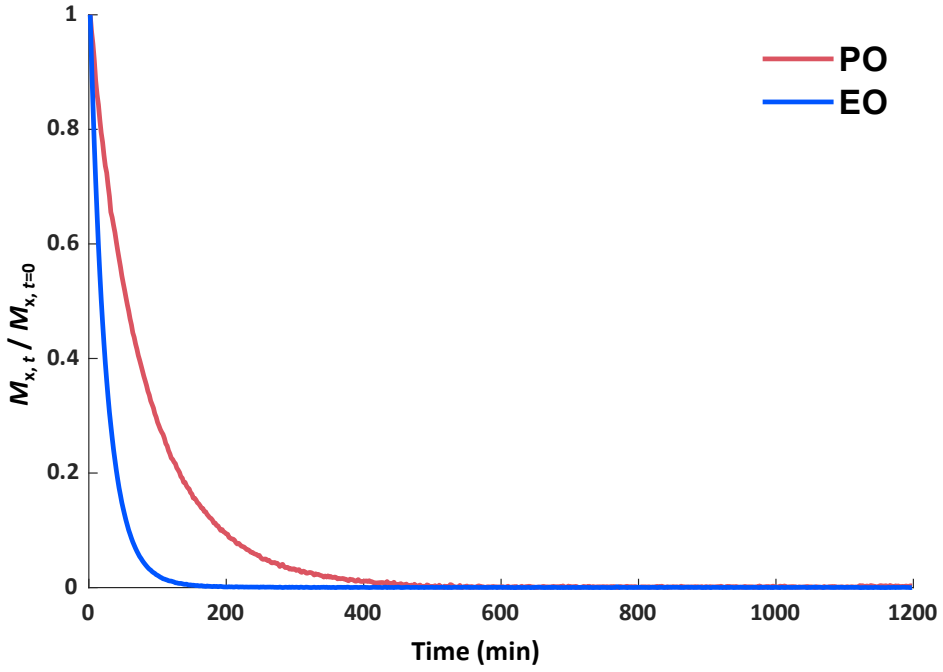

Figure S11: Time-conversion plot of the *in situ* ^{1}H NMR copolymerization kinetic study of EO with PO. (Solvent: DMSO-d_6, 40 °C).

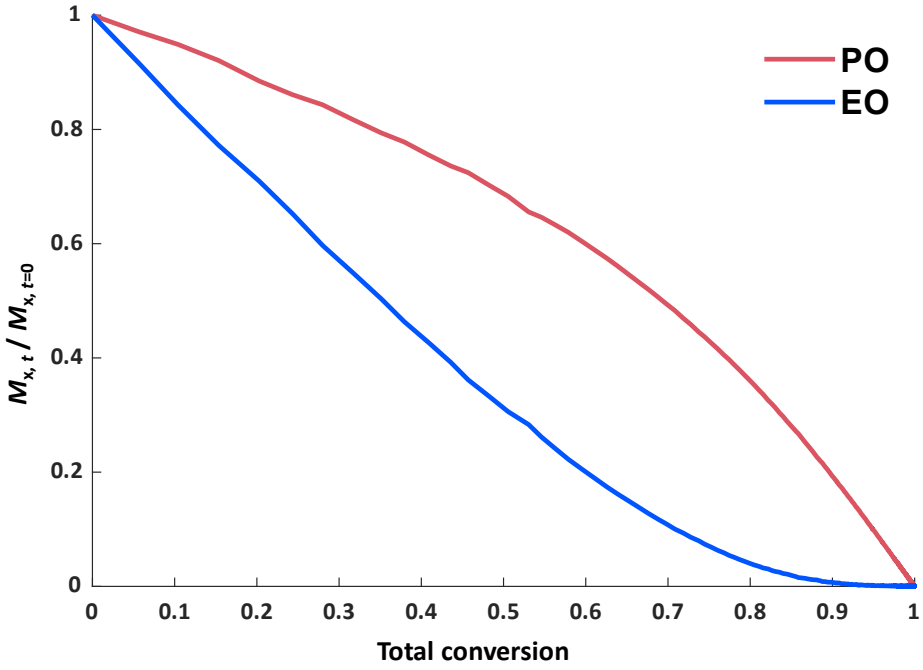

Figure S12: Individual versus total conversion of the *in situ* ^{1}H NMR copolymerization kinetic study of EO with PO. (Solvent: DMSO-d_6, 40 °C).

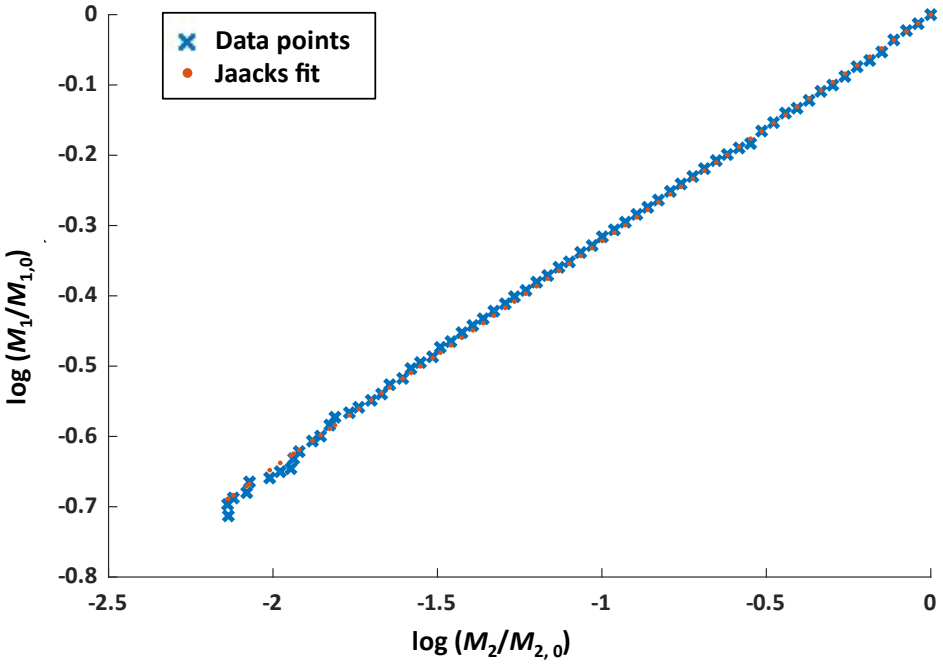

Figure S13: Jaacks fit of the *in situ* ^{1}H NMR copolymerization kinetic study of EO with PO. (Solvent: DMSO-d_6, 40 °C).

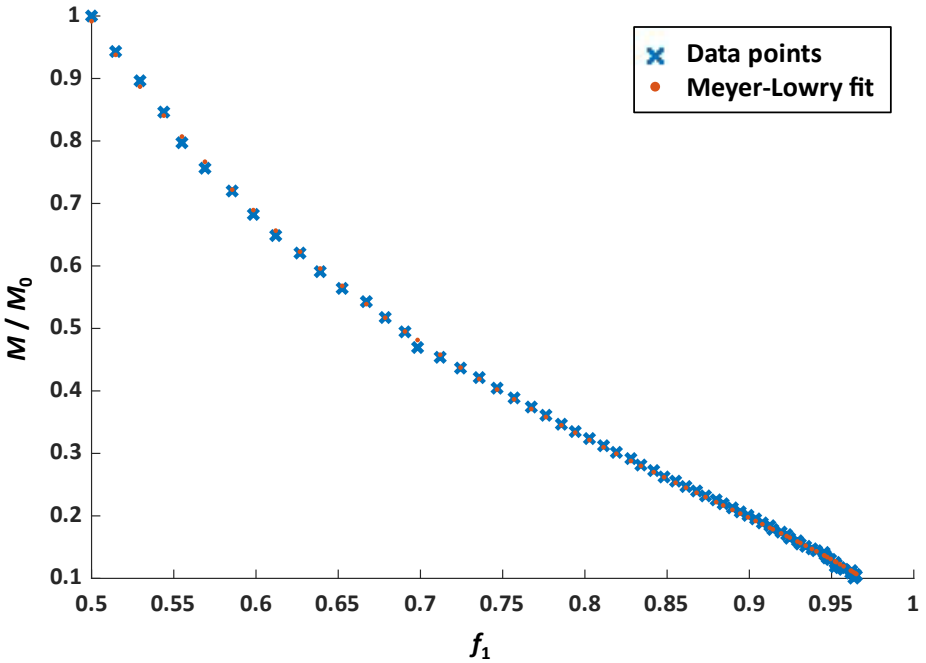

Figure S14: Meyer-Lowry fit of the *in situ* ^{1}H NMR copolymerization kinetic study of EO with PO. (Solvent: DMSO-d_6, 40 °C).

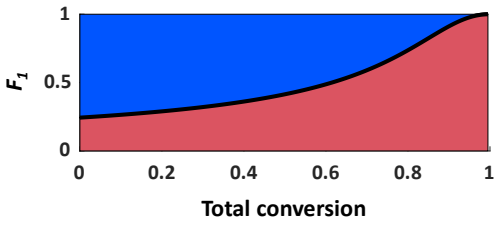

Figure S15: Composition plot of the *in situ* ^{1}H NMR copolymerization kinetic study of EO (blue) with PO (red) with a hypothetical equimolar monomer ratio (Solvent: DMSO-d_6, 40 °C) with r(PO)=0.32, r(EO)=3.10.

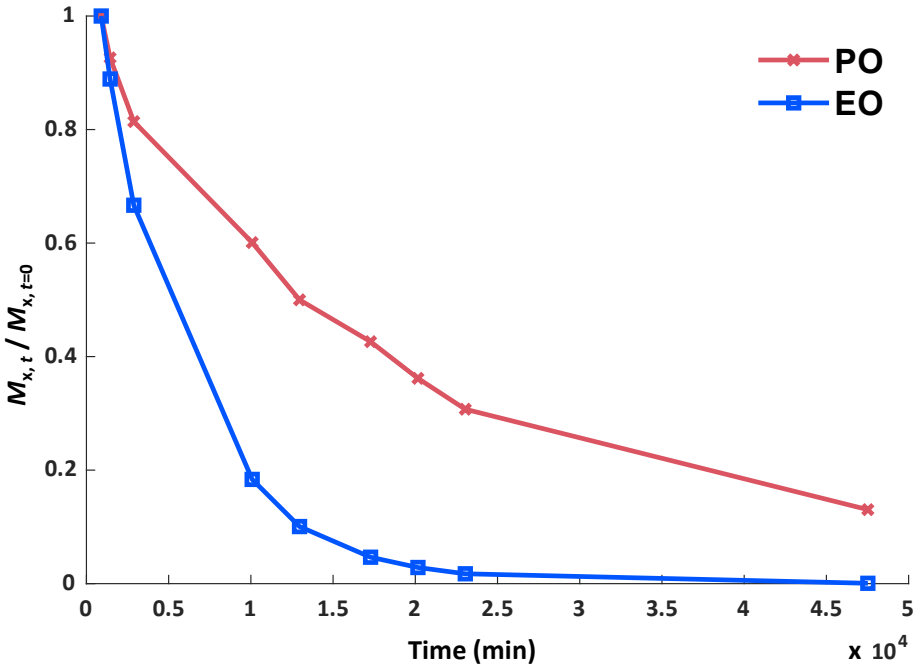

Figure S16: Time-conversion plot of the *in situ* ^{1}H NMR copolymerization kinetic study of EO with PO. (Solvent: Anisole, 25 °C). Data were acquired during an offline ^{1}H NMR kinetic experiment.

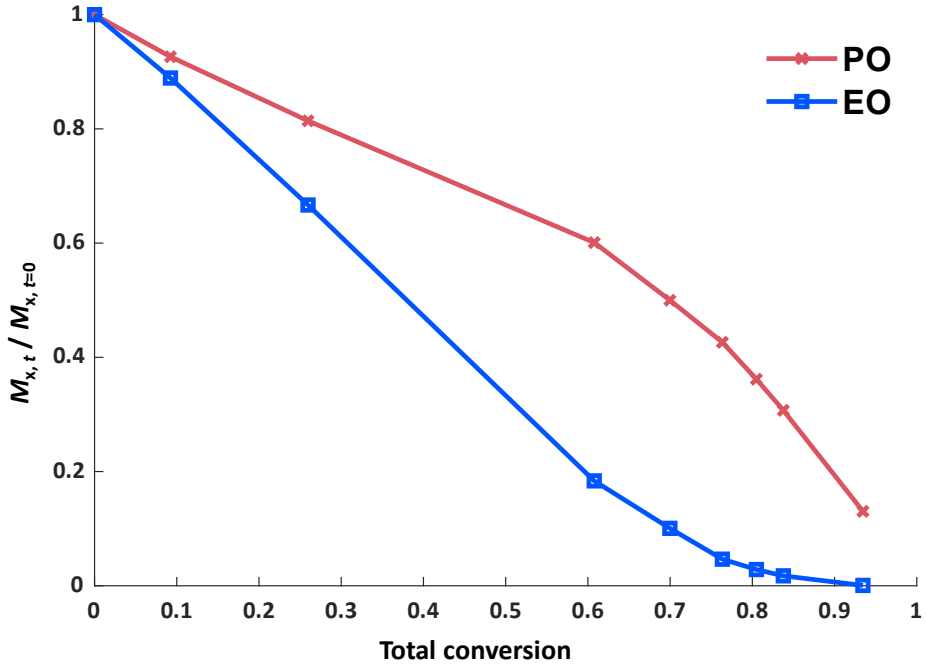

Figure S17: Individual versus total conversion of the *in situ* ^{1}H NMR copolymerization kinetic study of EO with PO. (Solvent: Anisole, 25 °C). Data were acquired during an offline ^{1}H NMR kinetic experiment.

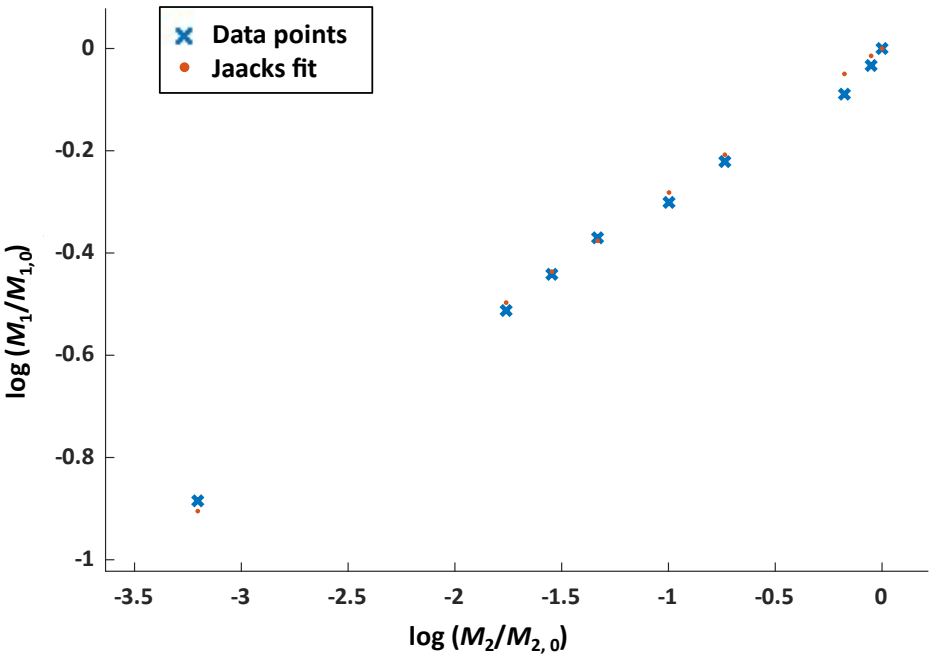

Figure S18: Jaacks fit of the *in situ* ^{1}H NMR copolymerization kinetic study of EO with PO. (Solvent: Anisole, 25 °C). Data were acquired during an offline ^{1}H NMR kinetic experiment.

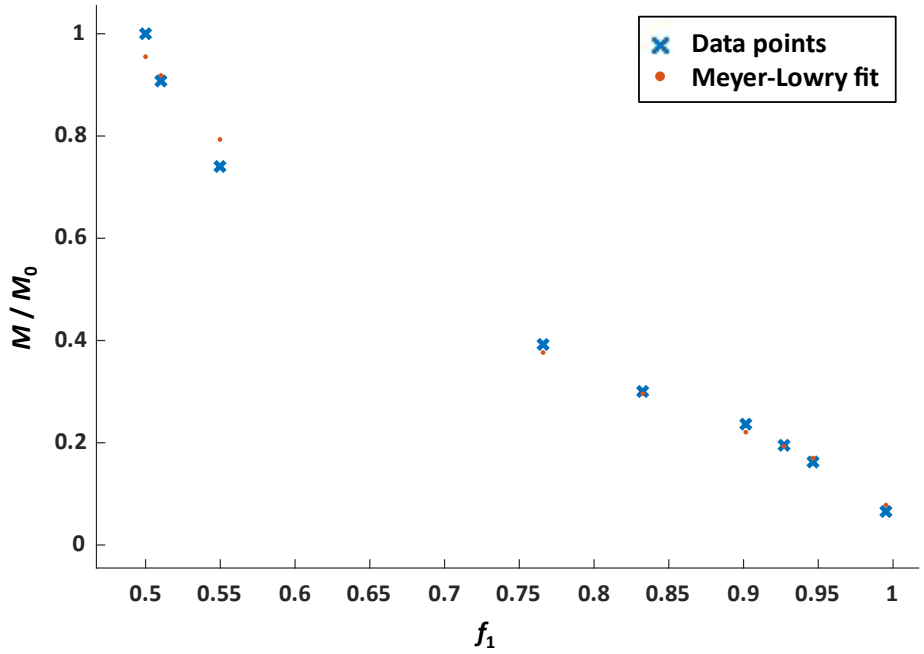

Figure S19: Meyer-Lowry fit of the *in situ* ^{1}H NMR copolymerization kinetic study of EO with PO. (Solvent: Anisole, 25 °C). Data were acquired during an offline ^{1}H NMR kinetic experiment.

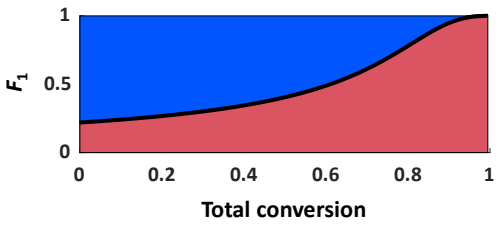

Figure S20: Composition plot of the *in situ* ^{1}H NMR copolymerization kinetic study of EO (blue) with PO (red) with a hypothetical equimolar monomer ratio (Solvent: Anisole, 25 °C) with *r*(PO)=0.28, *r*(EO)=3.54.

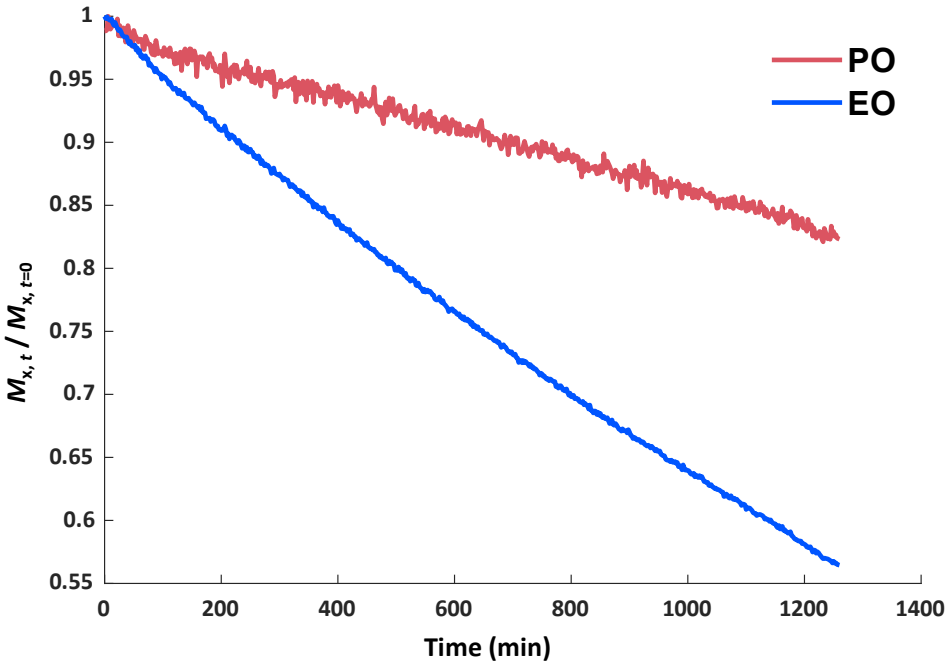

Figure S21: Time-conversion plot of the *in situ* ^{1}H NMR copolymerization kinetic study of EO with PO. (Solvent: Anisole, 25 °C, addition of [18]crown-6).

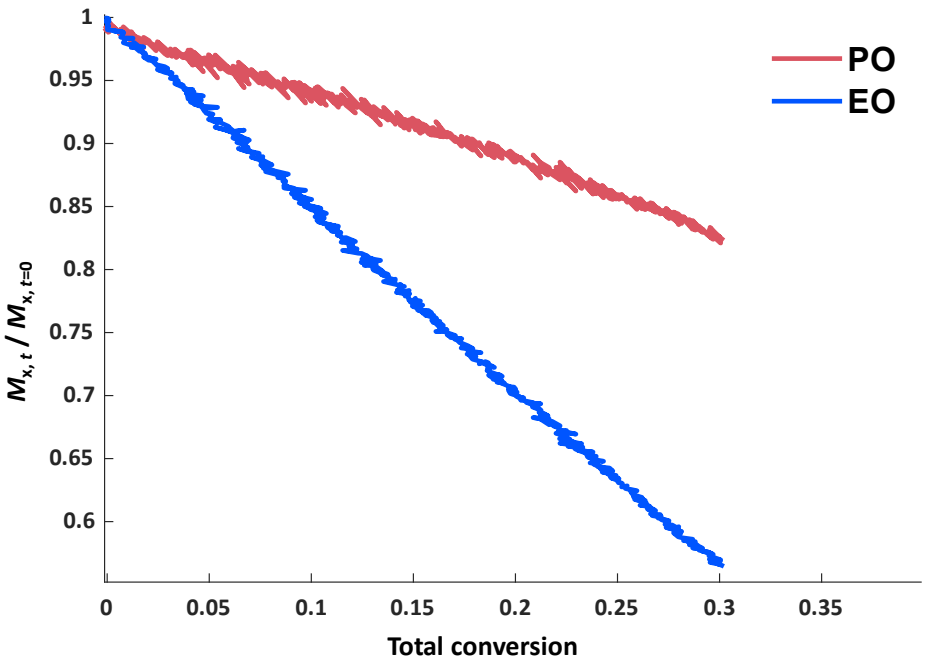

Figure S22: Individual versus total conversion of the *in situ* ^{1}H NMR copolymerization kinetic study of EO with PO. (Solvent: Anisole, 25 °C, addition of [18]crown-6).

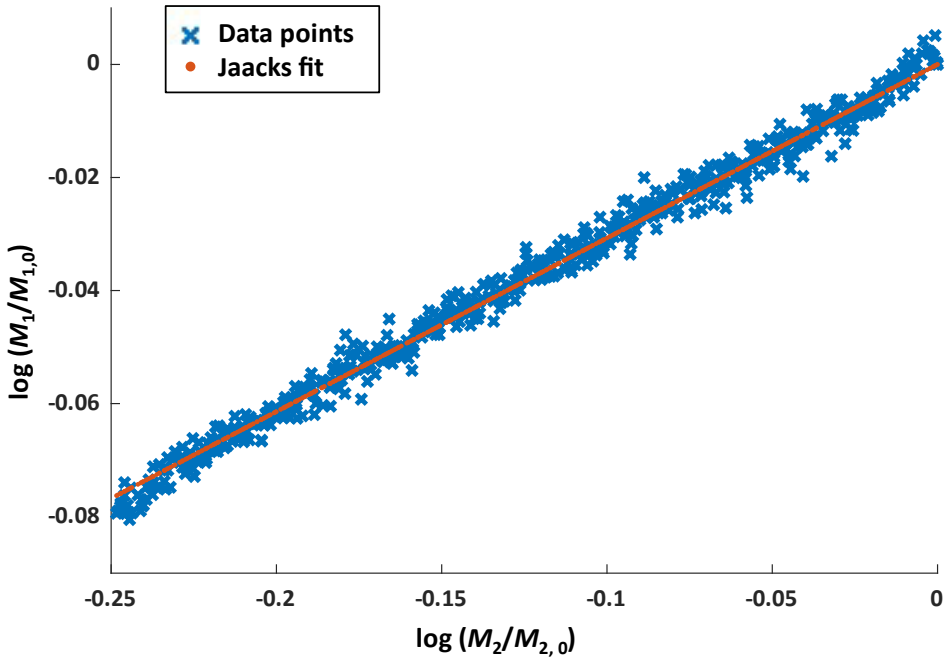

Figure S23: Jaacks fit of the *in situ* ^{1}H NMR copolymerization kinetic study of EO with PO. (Solvent: Anisole, 25 °C, addition of [18]crown-6).

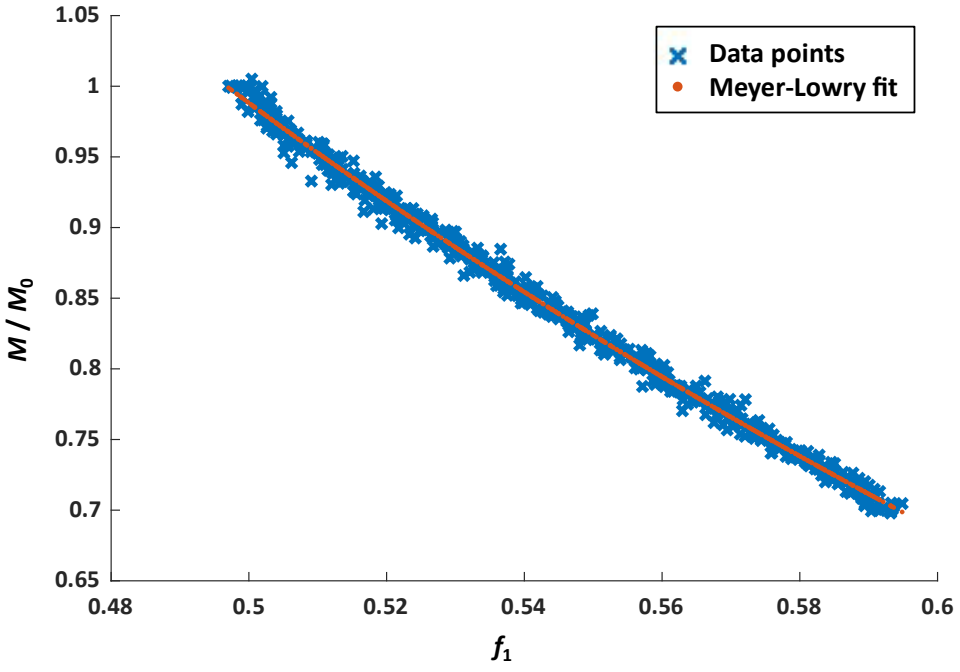

Figure S24: Meyer-Lowry fit of the *in situ* ^{1}H NMR copolymerization kinetic study of EO with PO. (Solvent: Anisole, 25 °C, addition of [18]crown-6).

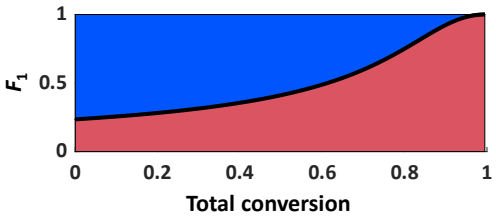

Figure S25: Composition plot of the *in situ* ^{1}H NMR copolymerization kinetic study of EO (blue) with PO (red) with a hypothetical equimolar monomer ratio (Solvent: Anisole, 25 °C, addition of [18]crown-6) with *r*(PO)=0.31, *r*(EO)=3.26.

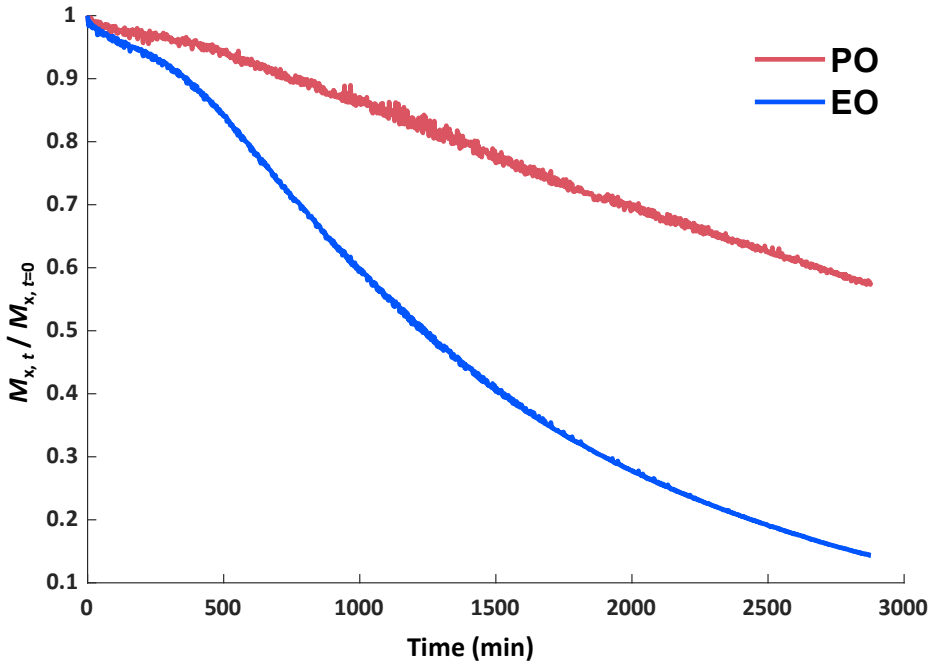

Figure S26: Time-conversion plot of the *in situ* ^{1}H NMR copolymerization kinetic study of EO with PO. (Solvent: Anisole, 40 °C).

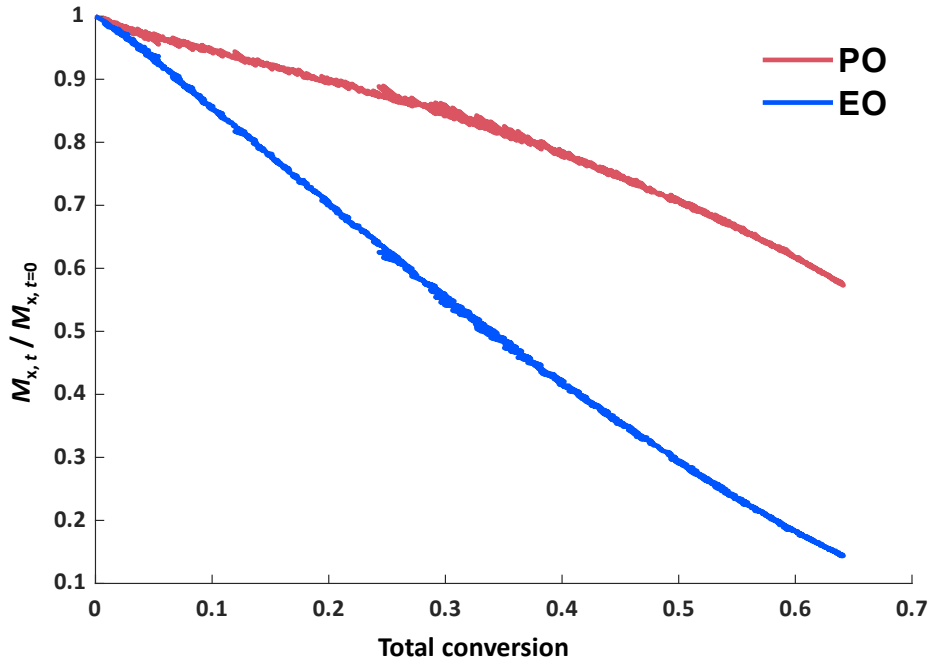

Figure S27: Individual versus total conversion of the *in situ* ^{1}H NMR copolymerization kinetic study of EO with PO. (Solvent: Anisole, 40 °C).

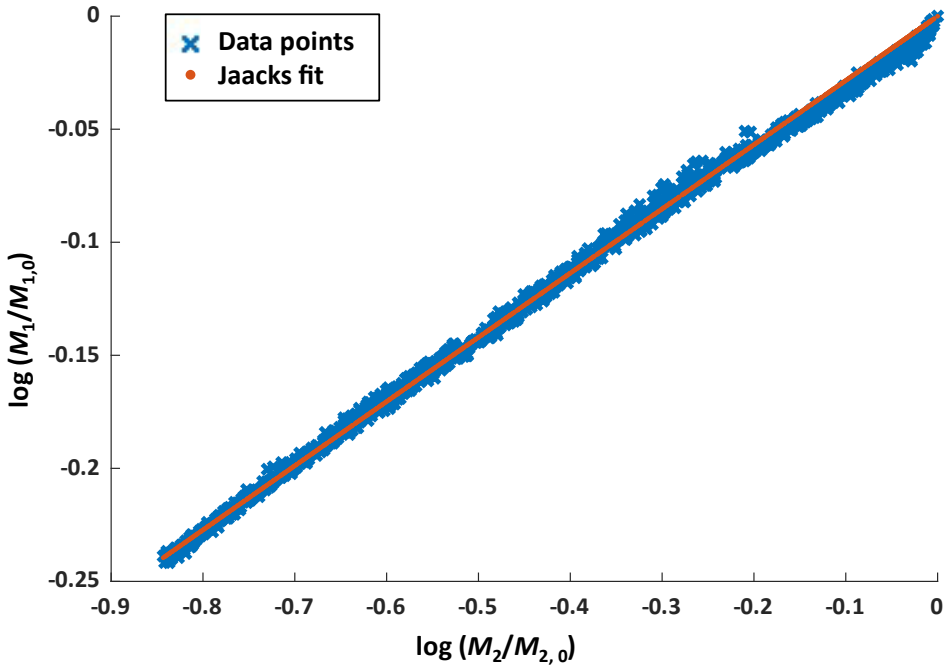

Figure S28: Jaacks fit of the *in situ* ^{1}H NMR copolymerization kinetic study of EO with PO. (Solvent: Anisole, 40 °C).

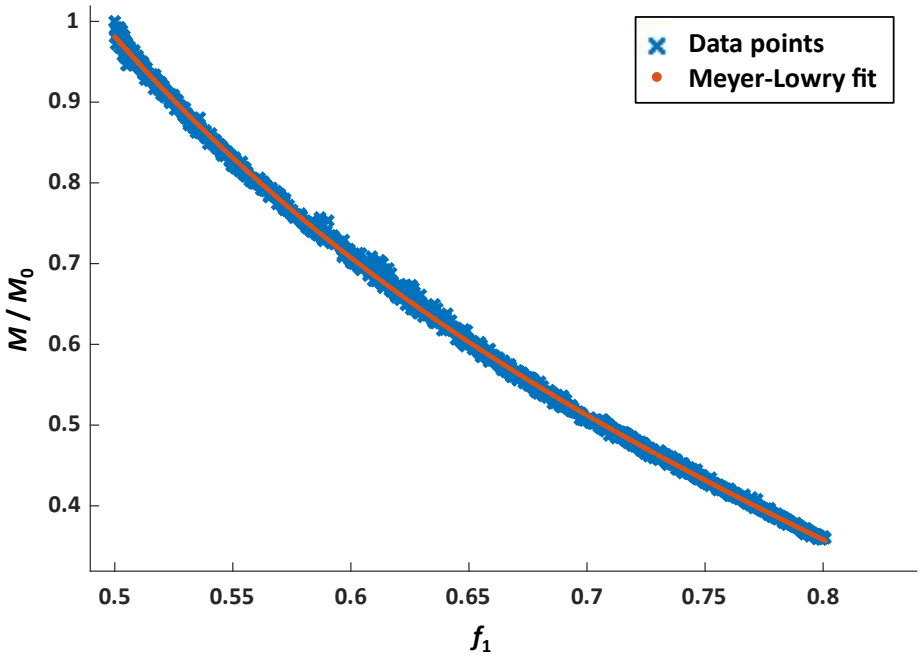

Figure S29: Meyer-Lowry fit of the *in situ* ^{1}H NMR copolymerization kinetic study of EO with PO. (Solvent: Anisole, 40 °C).

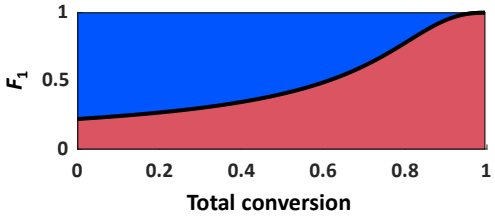

Figure S30: Composition plot of the *in situ* ^{1}H NMR copolymerization kinetic study of EO (blue) with PO (red) with a hypothetical equimolar monomer ratio (Solvent: Anisole, 40 °C) with *r*(PO)=0.28, *r*(EO)=3.52.

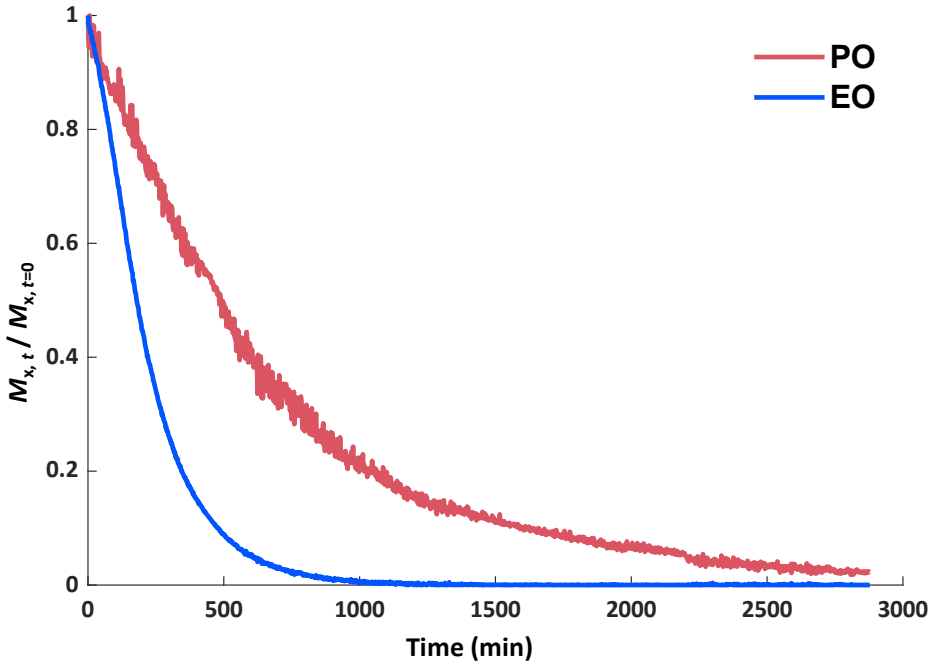

Figure S31: Time-conversion plot of the *in situ* ^{1}H NMR copolymerization kinetic study of EO with PO. (Solvent: Anisole, 60 °C).

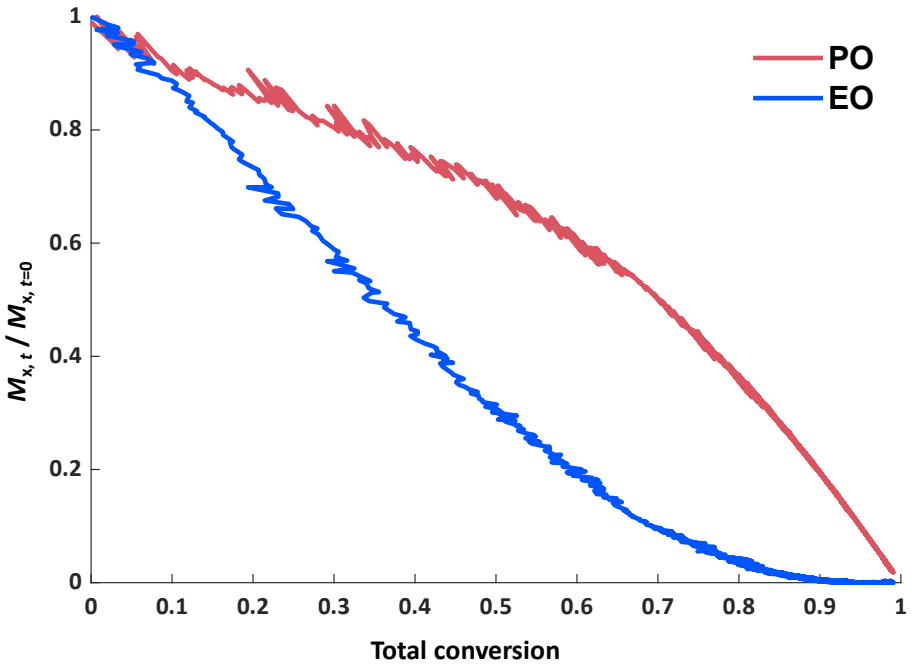

Figure S32: Individual versus total conversion of the *in situ* ^{1}H NMR copolymerization kinetic study of EO with PO. (Solvent: Anisole, 60 °C).

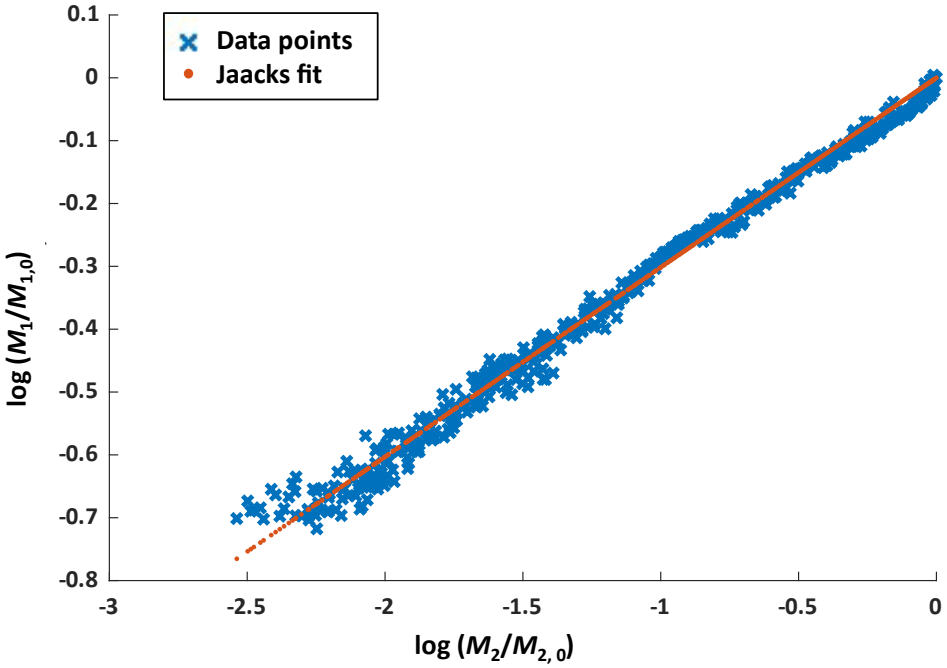

Figure S33: Jaacks fit of the *in situ* ^{1}H NMR copolymerization kinetic study of EO with PO. (Solvent: Anisole, 60 °C).

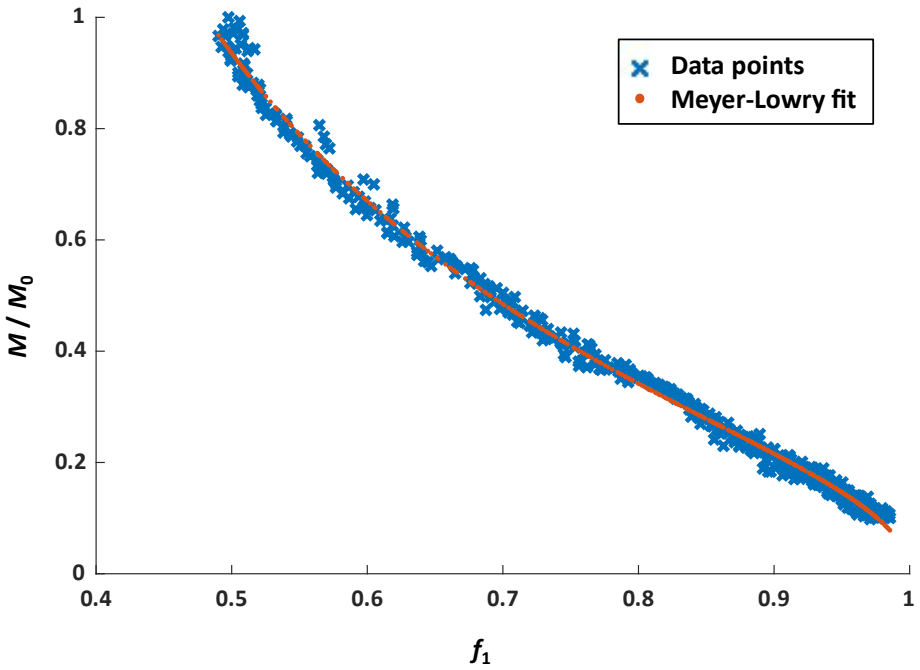

Figure S34: Meyer-Lowry fit of the *in situ* ^{1}H NMR copolymerization kinetic study of EO with PO. (Solvent: Anisole, 60 °C).

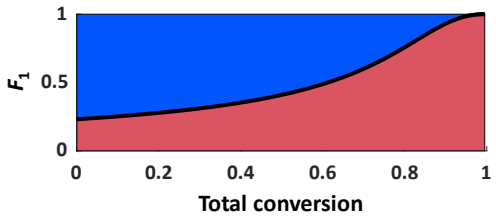

Figure S35: Composition plot of the *in situ* ^{1}H NMR copolymerization kinetic study of EO (blue) with PO (red) with a hypothetical equimolar monomer ratio (Solvent: Anisole, 60 °C) with *r*(PO)=0.30, *r*(EO)=3.32.

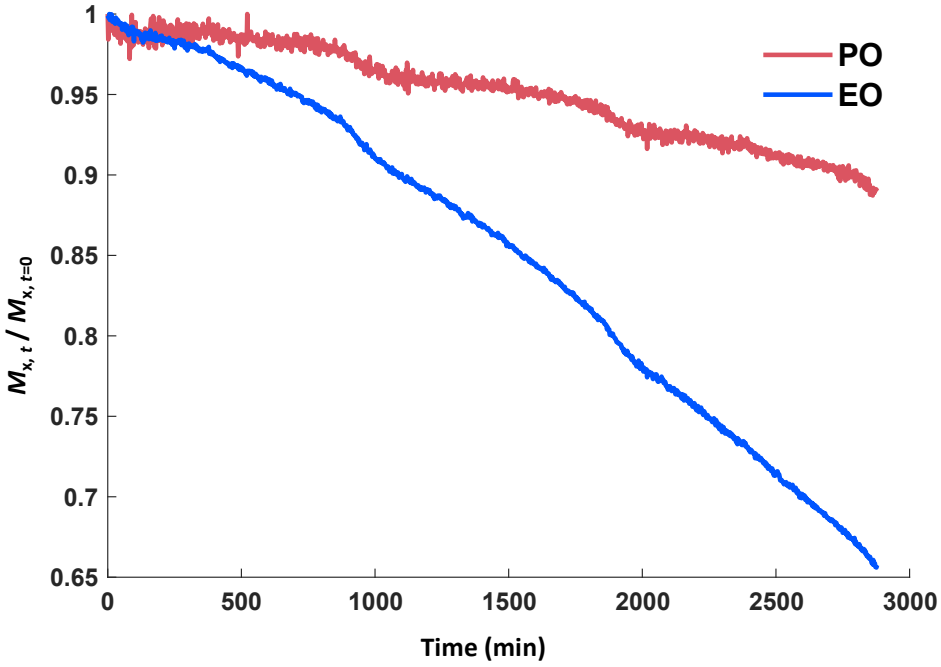

Figure S36: Time-conversion plot of the *in situ* ^{1}H NMR copolymerization kinetic study of EO with PO. (Solvent: Toluene-d_8, 25 °C).

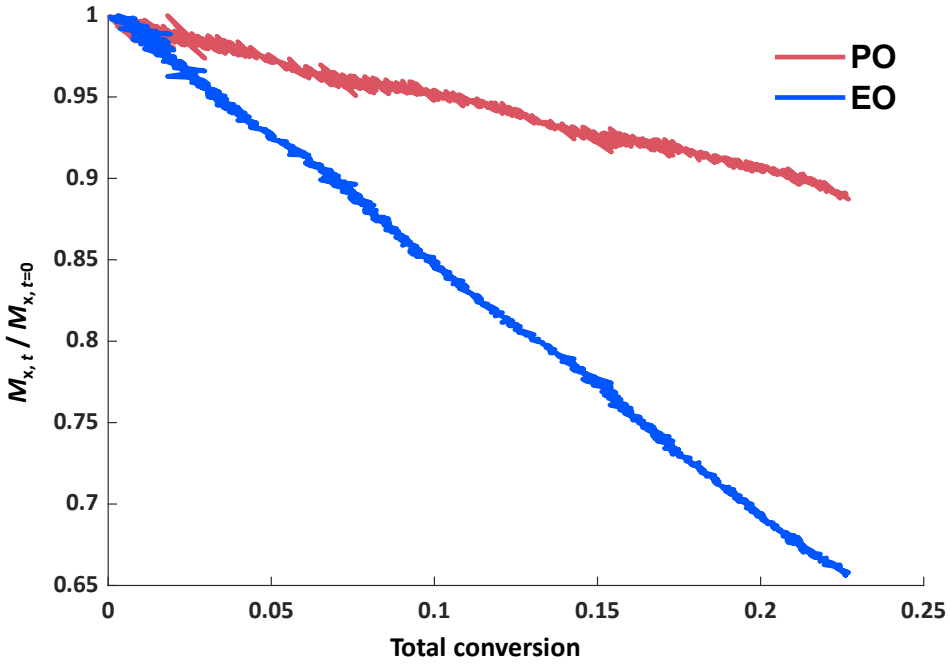

Figure S37: Individual versus total conversion of the *in situ* ^{1}H NMR copolymerization kinetic study of EO with PO. (Solvent: Toluene-d_8, 25 °C).

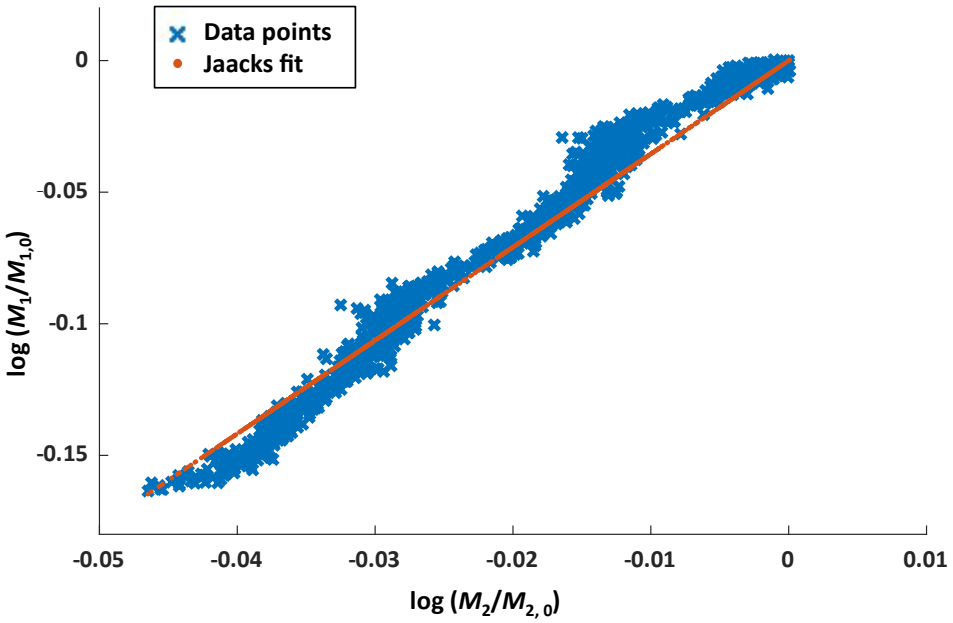

Figure S38: Jaacks fit of the *in situ* ^{1}H NMR copolymerization kinetic study of EO with PO. (Solvent: Toluene-d_8, 25 °C).

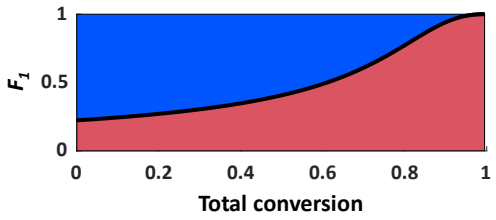

Figure S39: Composition plot of the *in situ* ^{1}H NMR copolymerization kinetic study of EO (blue) with PO (red) with a hypothetical equimolar monomer ratio (Solvent: Toluene-d_8, 25 °C) with *r*(PO)=0.29, *r*(EO)=3.49.

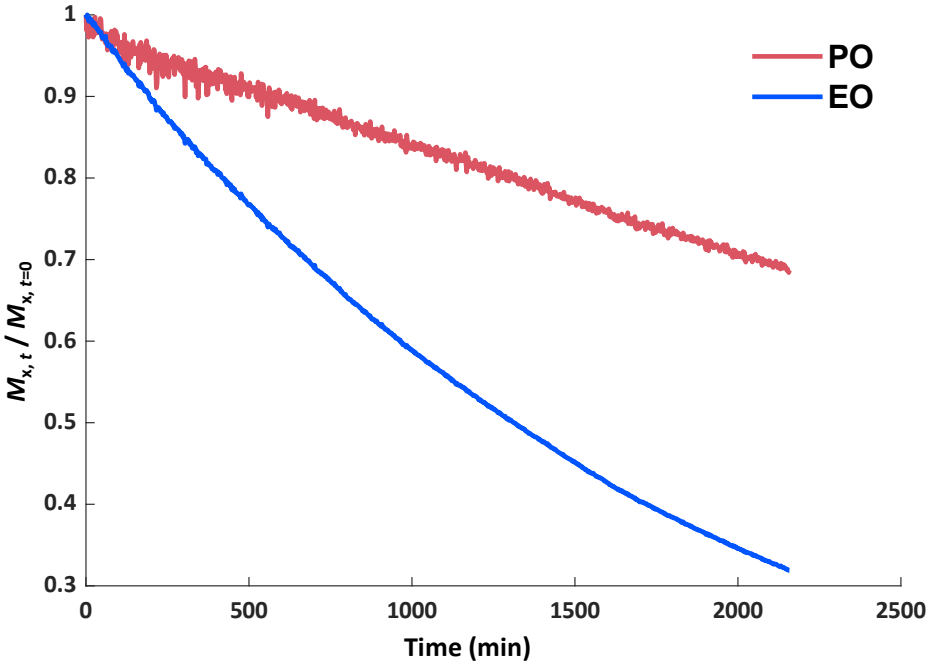

Figure S40: Time-conversion plot of the *in situ* ^{1}H NMR copolymerization kinetic study of EO with PO. (Solvent: Toluene-d_8, 25 °C, addition of [18]crown-6).

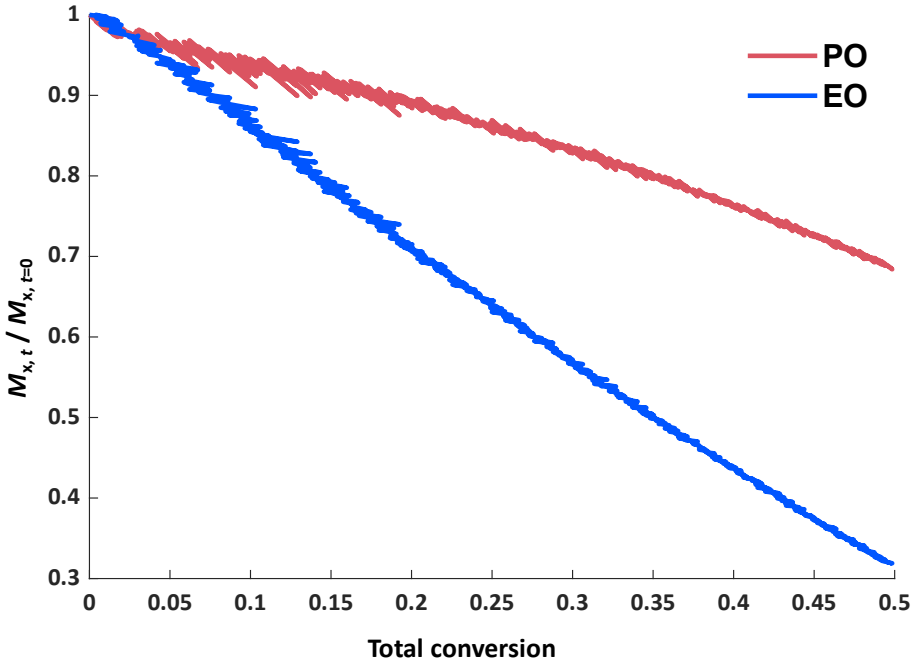

Figure S41: Individual versus total conversion of the *in situ* ^{1}H NMR copolymerization kinetic study of EO with PO. (Solvent: Toluene-d_8, 25 °C, addition of [18]crown-6).

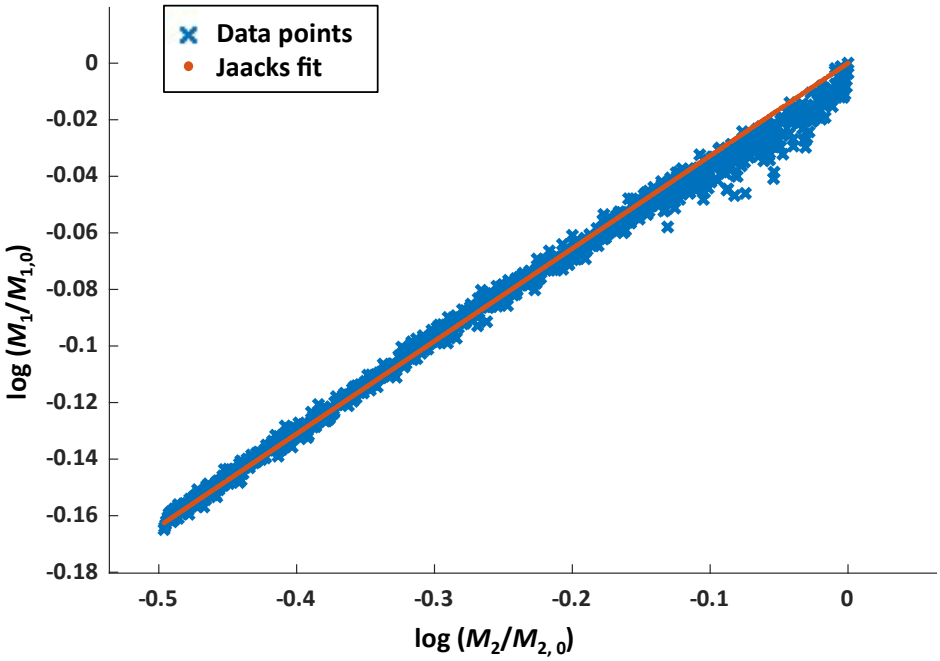

Figure S42: Jaacks fit of the *in situ* ^{1}H NMR copolymerization kinetic study of EO with PO. (Solvent: Toluene-d_8, 25 °C, addition of [18]crown-6).

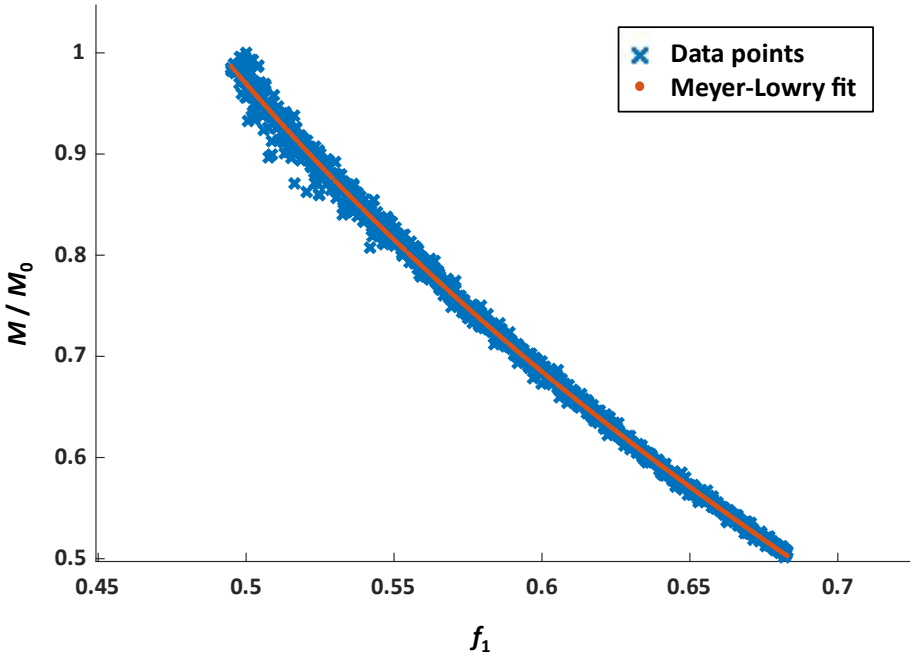

Figure S43: Meyer-Lowry fit of the *in situ* ^{1}H NMR copolymerization kinetic study of EO with PO. (Solvent: Toluene-d_8, 25 °C, addition of [18]crown-6).

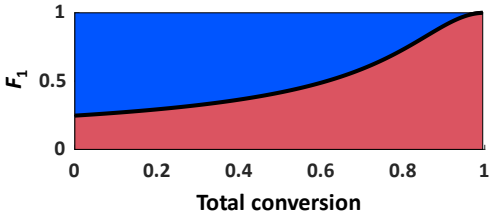

Figure S44: Composition plot of the *in situ* ^{1}H NMR copolymerization kinetic study of EO (blue) with PO (red) with a hypothetical equimolar monomer ratio (Solvent: Toluene-d_8, 25 °C, addition of [18]crown-6) with r(PO)=0.33, r(EO)=3.05.

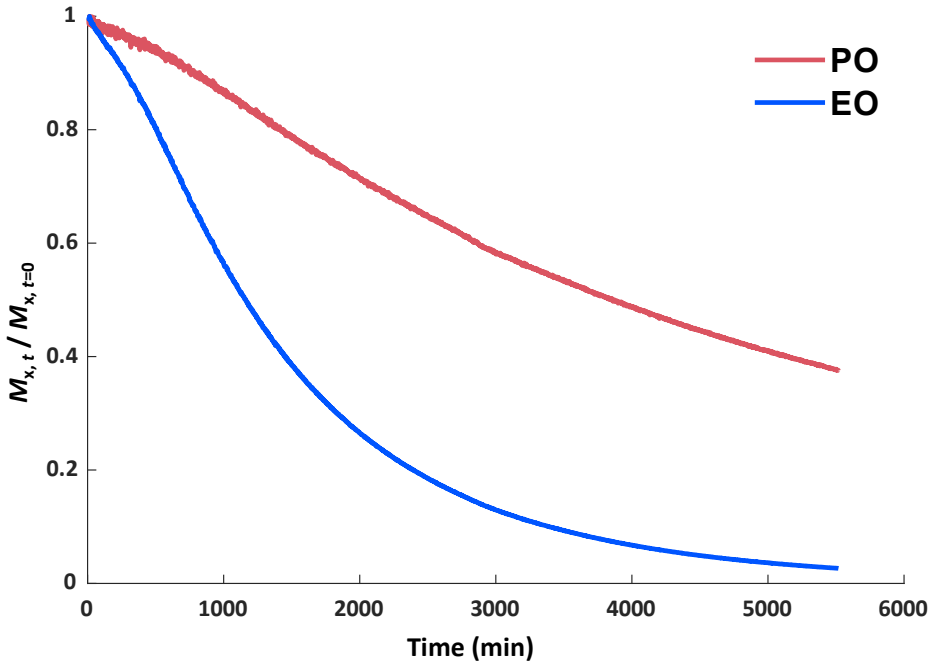

Figure S45: Time-conversion plot of the *in situ* ^{1}H NMR copolymerization kinetic study of EO with PO. (Solvent: Toluene-d_8, 40 °C).

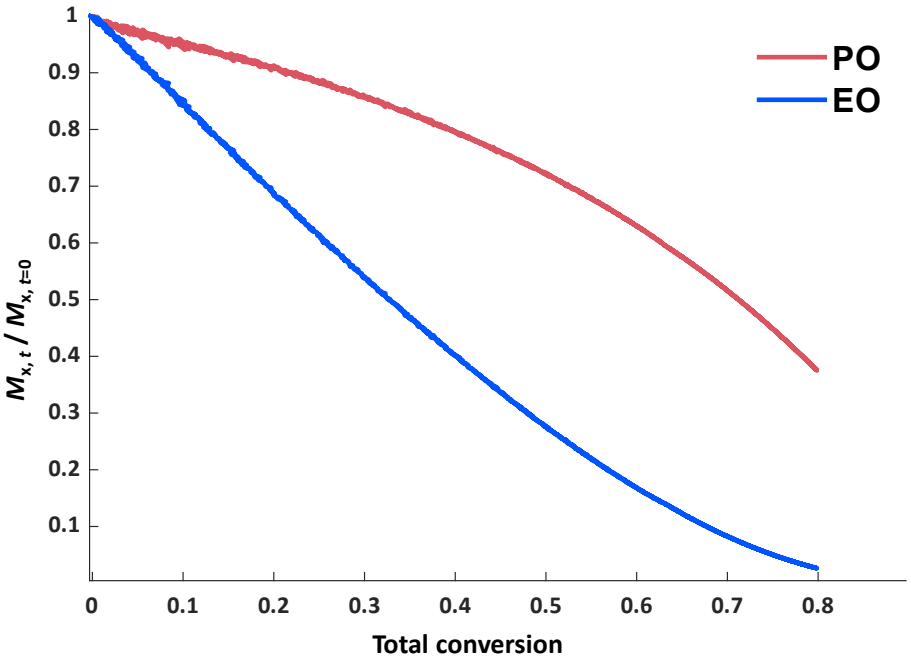

Figure S46: Individual versus total conversion of the *in situ* ^{1}H NMR copolymerization kinetic study of EO with PO. (Solvent: Toluene-d_8, 40 °C).

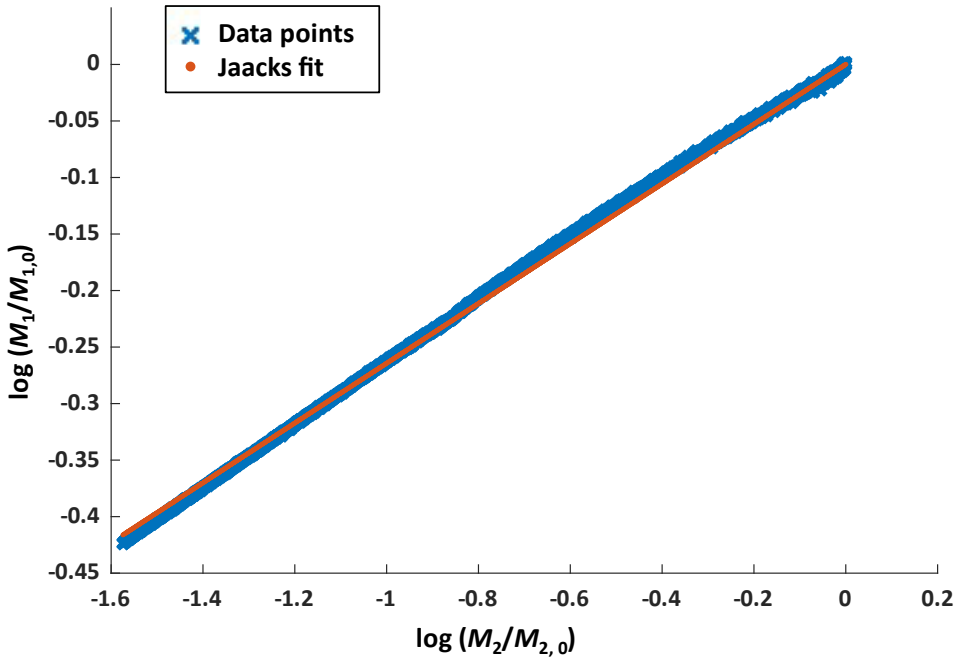

Figure S47: Jaacks fit of the *in situ* ^{1}H NMR copolymerization kinetic study of EO with PO. (Solvent: Toluene-d_8, 40 °C).

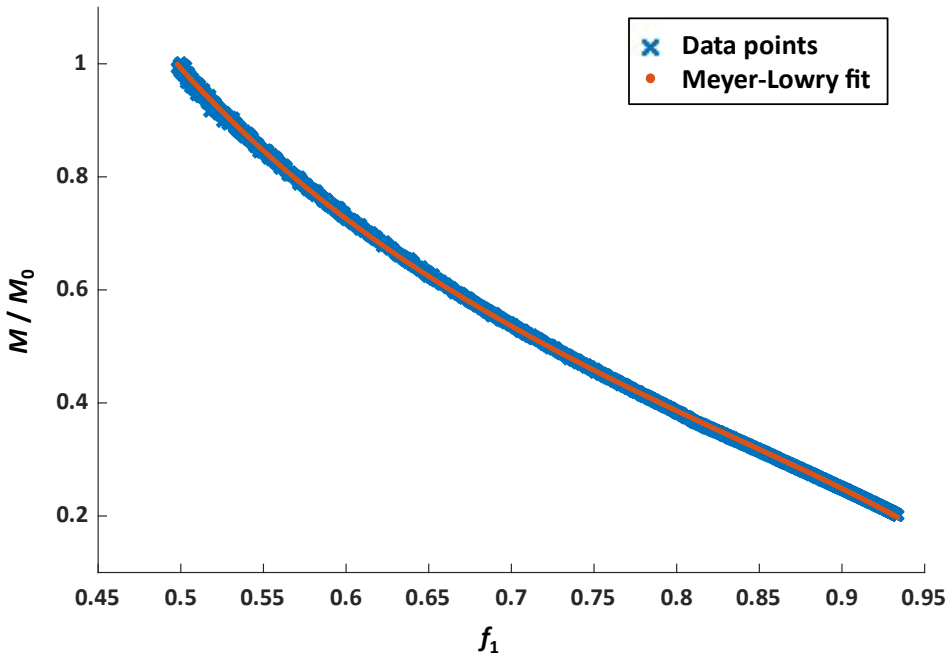

Figure S48: Meyer-Lowry fit of the *in situ* ^{1}H NMR copolymerization kinetic study of EO with PO. (Solvent: Toluene-d_8, 40 °C).

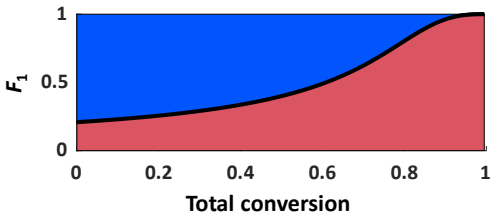

Figure S49: Composition plot of the *in situ* ^{1}H NMR copolymerization kinetic study of EO (blue) with PO (red) with a hypothetical equimolar monomer ratio (Solvent: Toluene-d_8, 40 °C) with r(PO)=0.26, r(EO)=3.78.

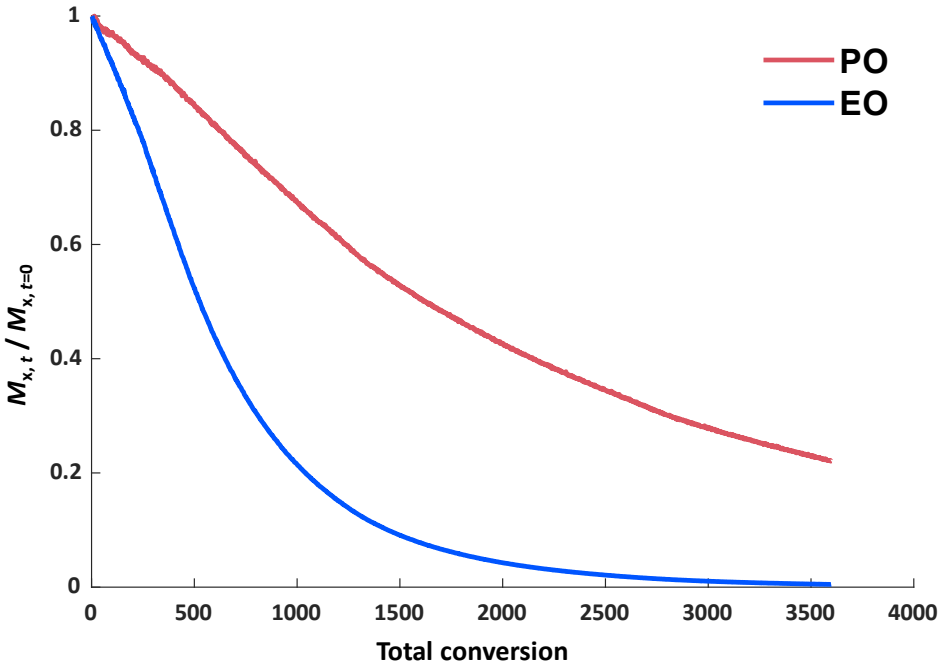

Figure S50: Time-conversion plot of the *in situ* ^{1}H NMR copolymerization kinetic study of EO with PO. (Solvent: Toluene-d_8, 50 °C).

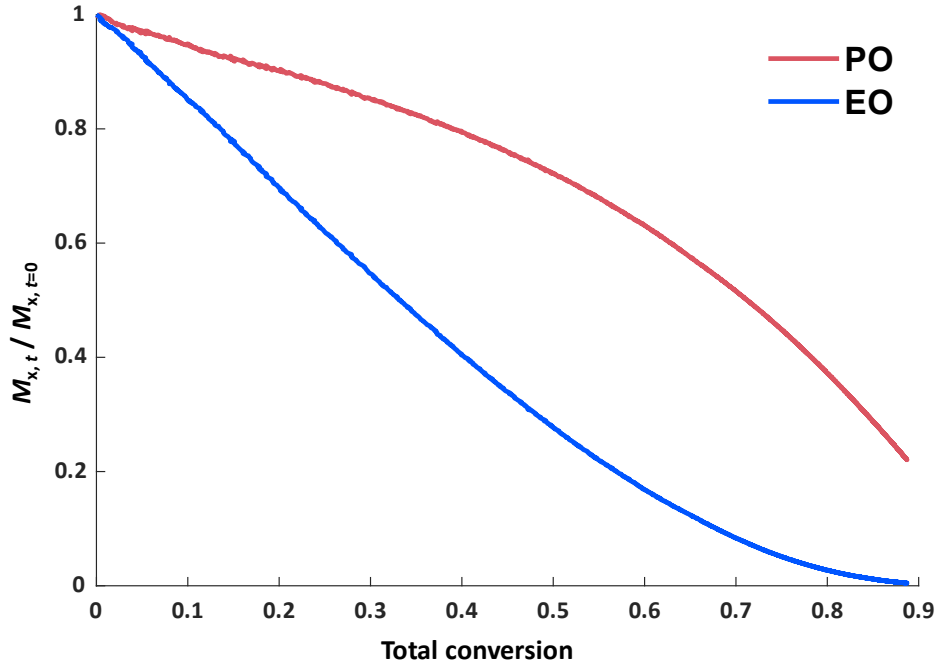

Figure S51: Individual versus total conversion of the *in situ* ^{1}H NMR copolymerization kinetic study of EO with PO. (Solvent: Toluene-d_8, 50 °C).

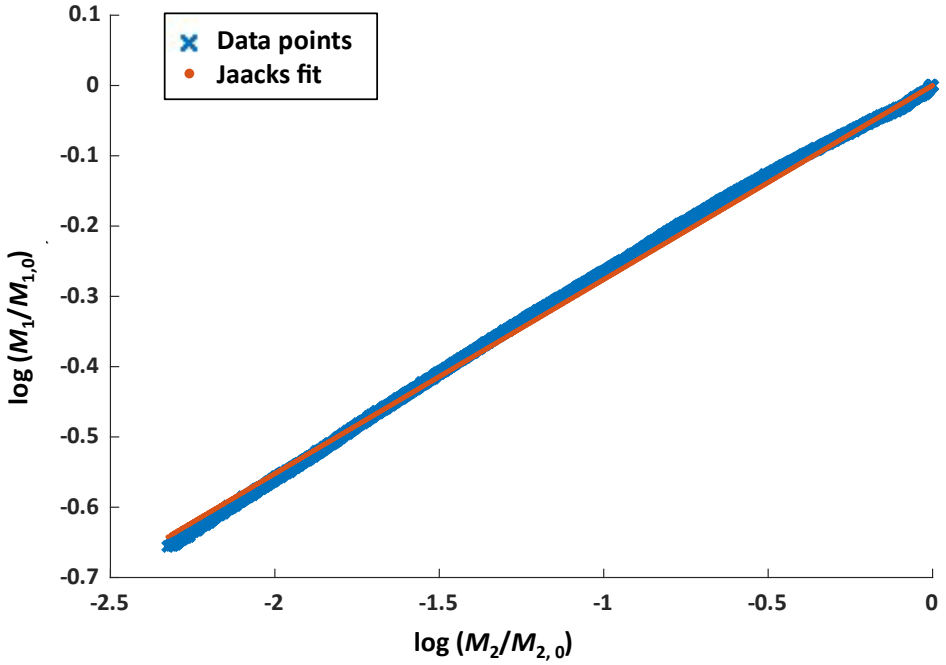

Figure S52: Jaacks fit of the *in situ* ^{1}H NMR copolymerization kinetic study of EO with PO. (Solvent: Toluene-d_8, 50 °C).

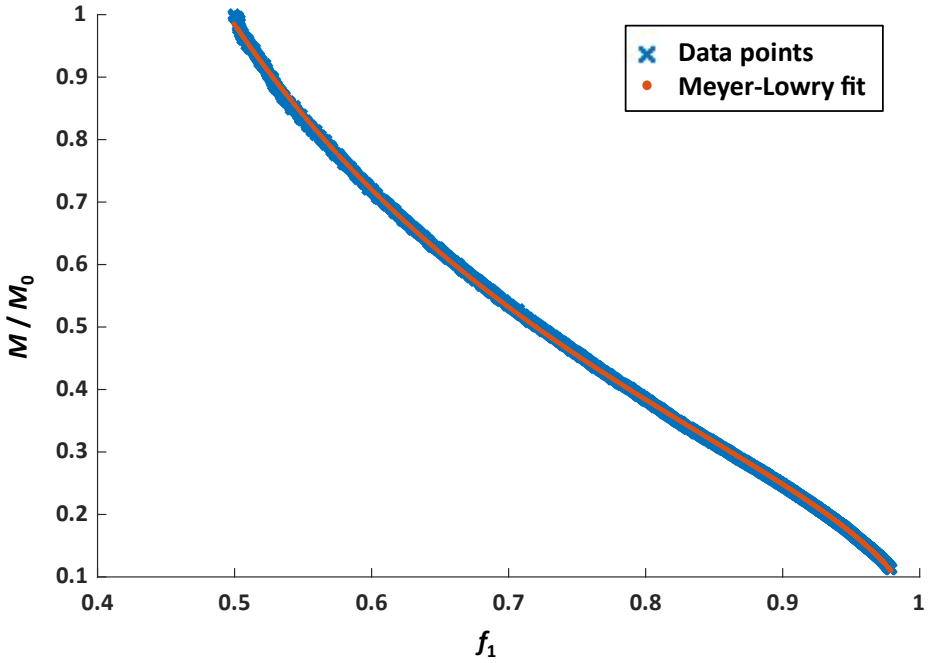

Figure S53: Meyer-Lowry fit of the *in situ* ^{1}H NMR copolymerization kinetic study of EO with PO. (Solvent: Toluene-d_8, 50 °C).

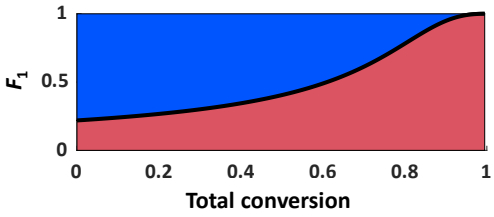

Figure S54: Composition plot of the *in situ* ^{1}H NMR copolymerization kinetic study of EO (blue) with PO (red) with a hypothetical equimolar monomer ratio (Solvent: Toluene-d_8, 50 °C) with *r*(PO)=0.28, *r*(EO)=3.62.

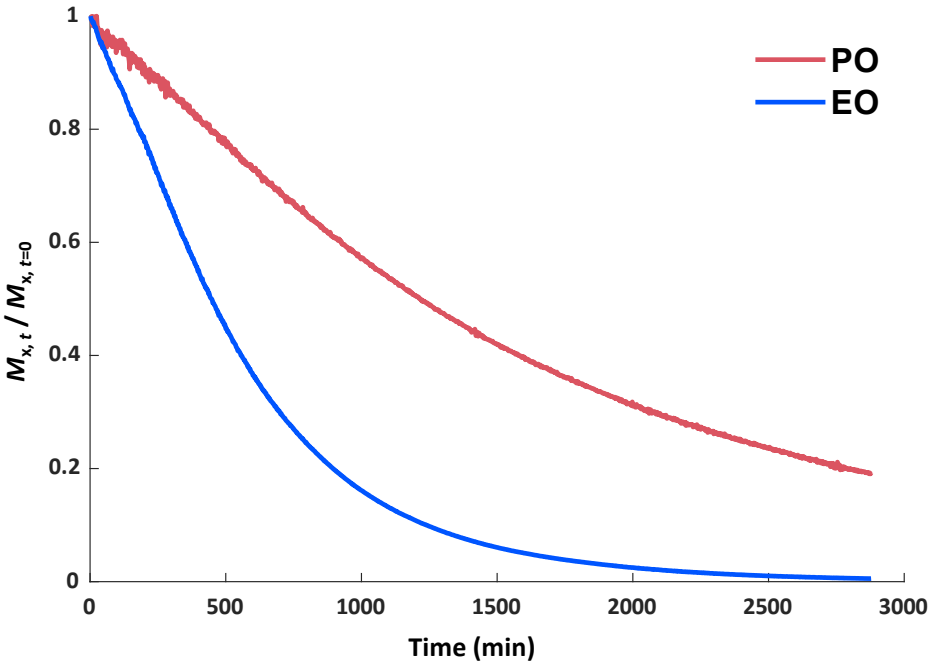

Figure S55: Time-conversion plot of the *in situ* ^{1}H NMR copolymerization kinetic study of EO with PO. (Solvent: Toluene-d_8, 60 °C).

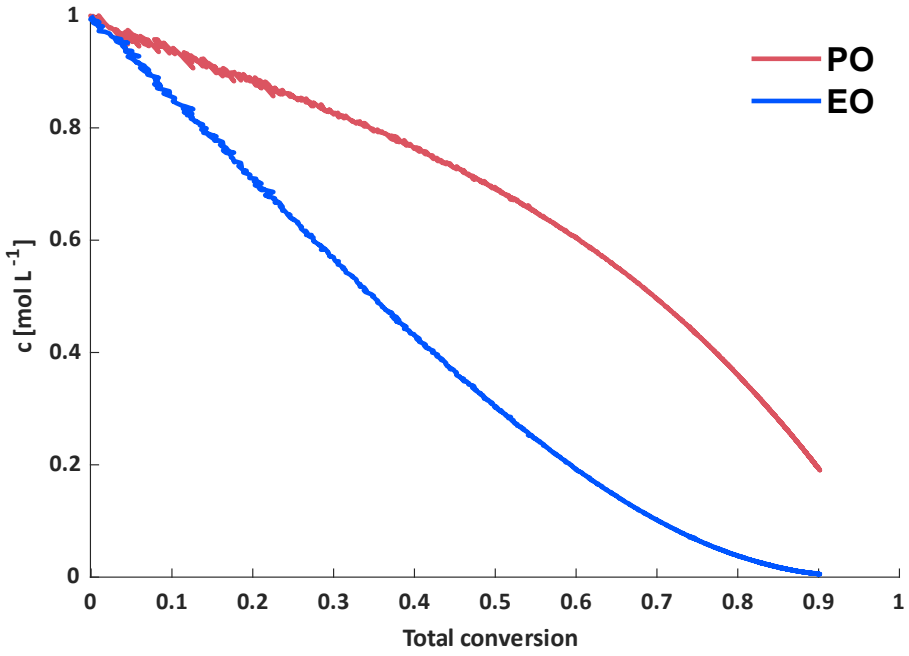

Figure S56: Individual versus total conversion of the *in situ* ^{1}H NMR copolymerization kinetic study of EO with PO. (Solvent: Toluene-d_8, 60 °C).

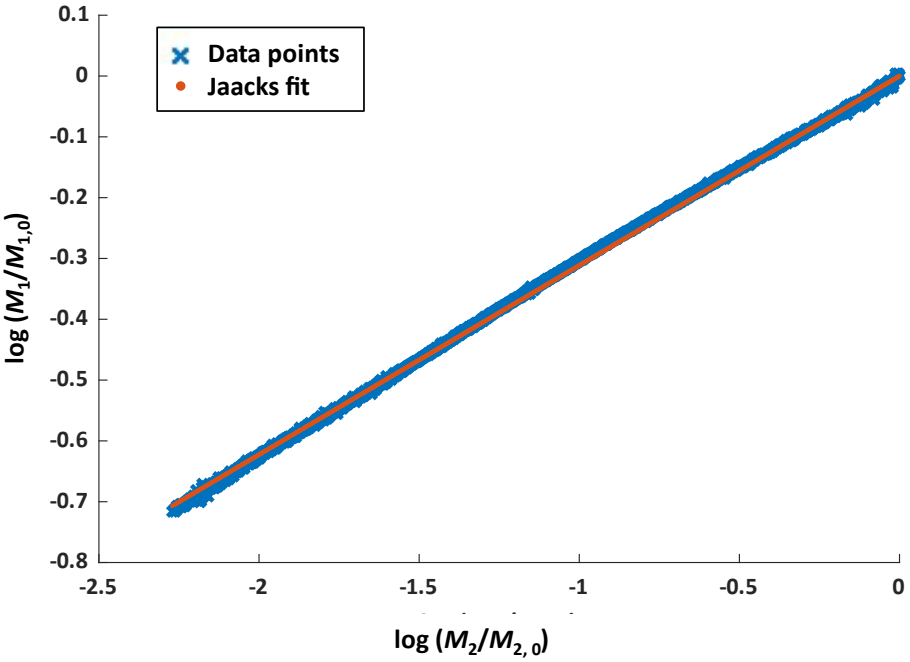

Figure S57: Jaacks fit of the *in situ* ^{1}H NMR copolymerization kinetic study of EO with PO. (Solvent: Toluene-d_8, 60 °C).

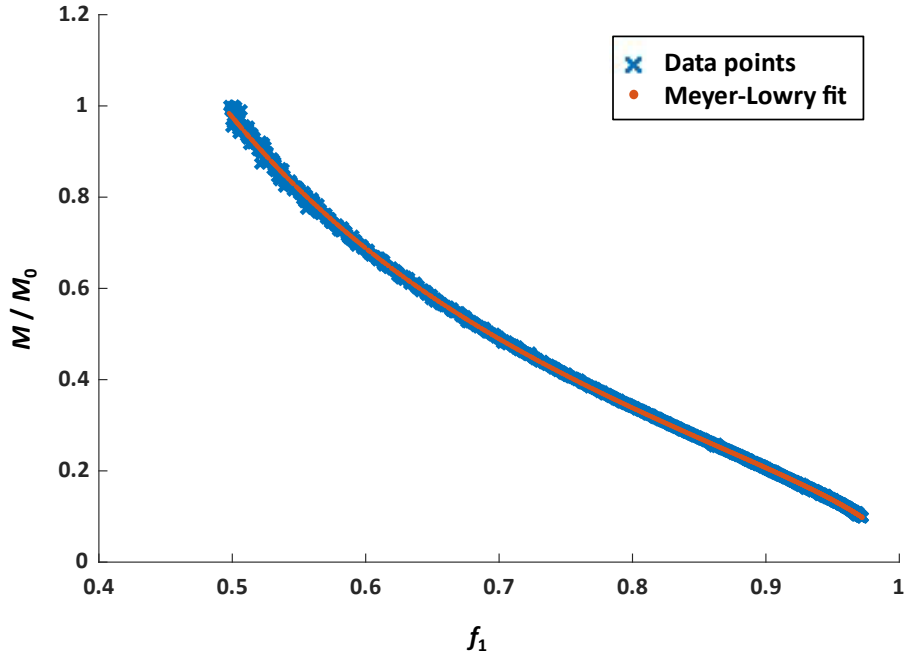

Figure S58: Meyer-Lowry fit of the *in situ* ^{1}H NMR copolymerization kinetic study of EO with PO. (Solvent: Toluene-d_8, 60 °C).

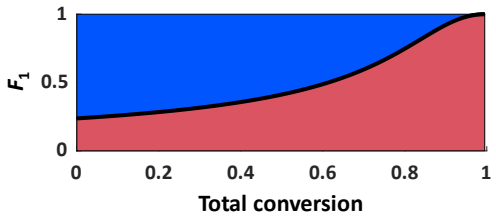

Figure S59: Composition plot of the *in situ* ^{1}H NMR copolymerization kinetic study of EO (blue) with PO (red) with a hypothetical equimolar monomer ratio (Solvent: Toluene-d_8, 60 °C) with r(PO)=0.31, r(EO)=3.21.

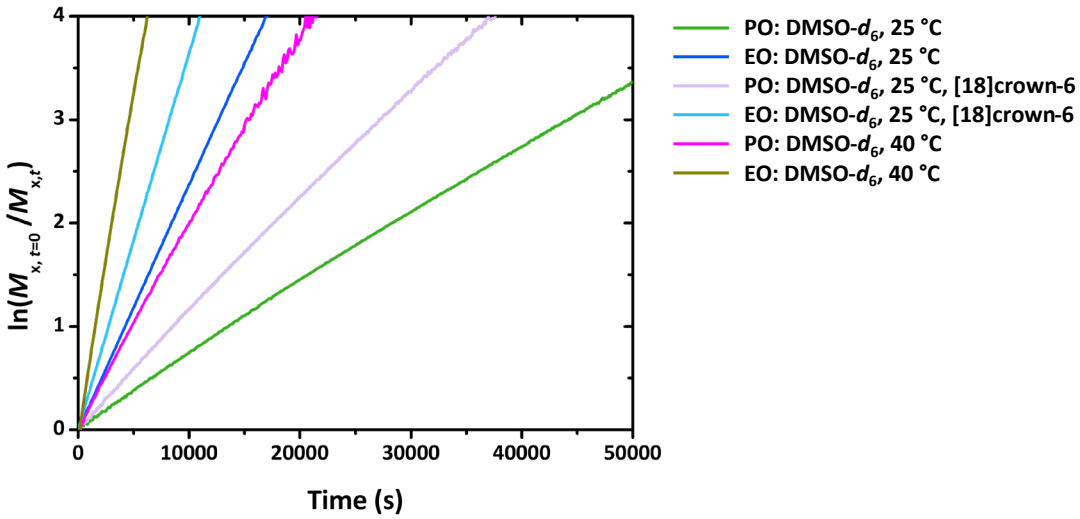

Figure S60: Pseudo-first-order plot of the copolymerization of EO with PO in DMSO at different conditions obtained by ^{1}H NMR kinetics.

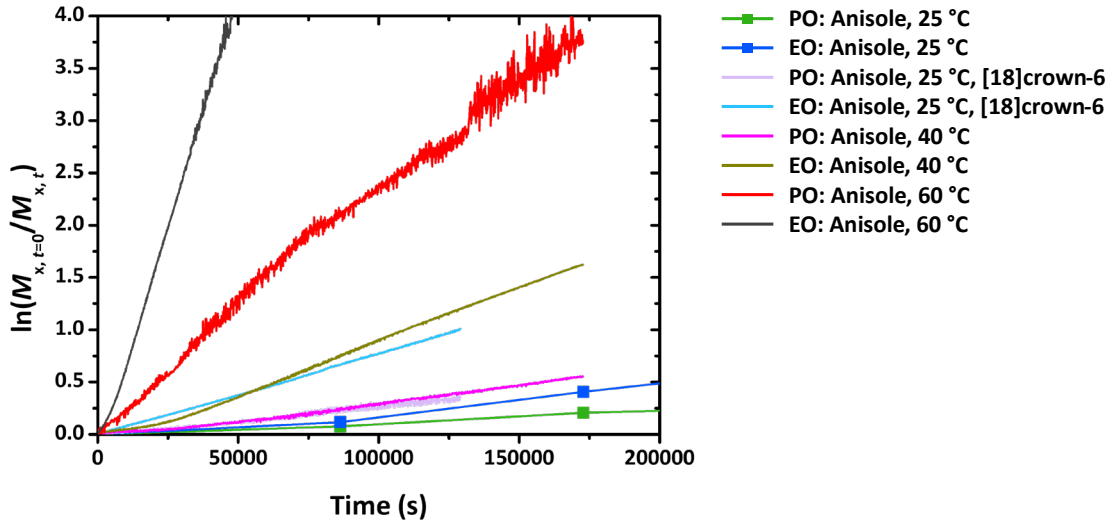

Figure S61: Pseudo-first-order plot of the copolymerization of EO with PO in Anisole at different conditions obtained by ^{1}H NMR kinetics. Anisole measurements at 25 °C without [18]crown-6 were acquired offline, data points are marked by squares.

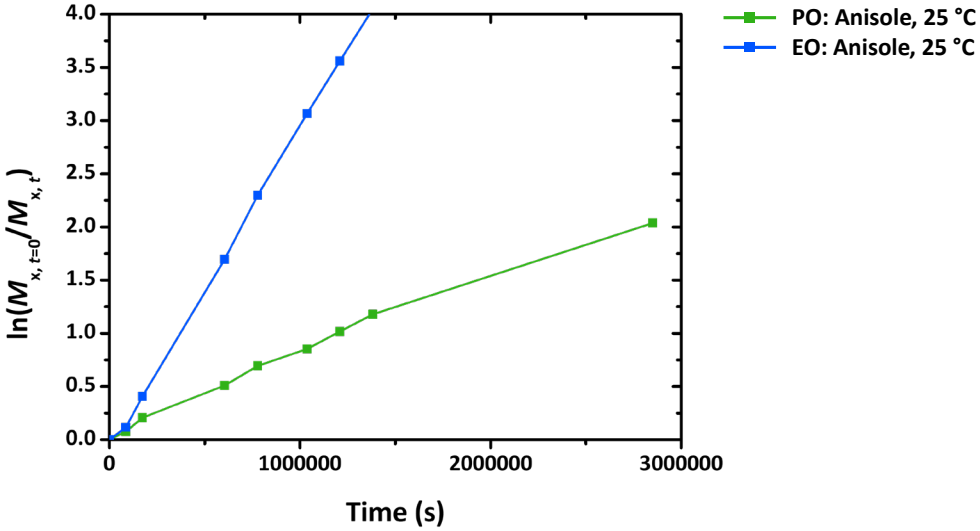

Figure S62: Pseudo-first-order plot of the copolymerization of EO with PO in Anisole at 25 °C obtained by offline NMR kinetics. Data points are marked by squares.

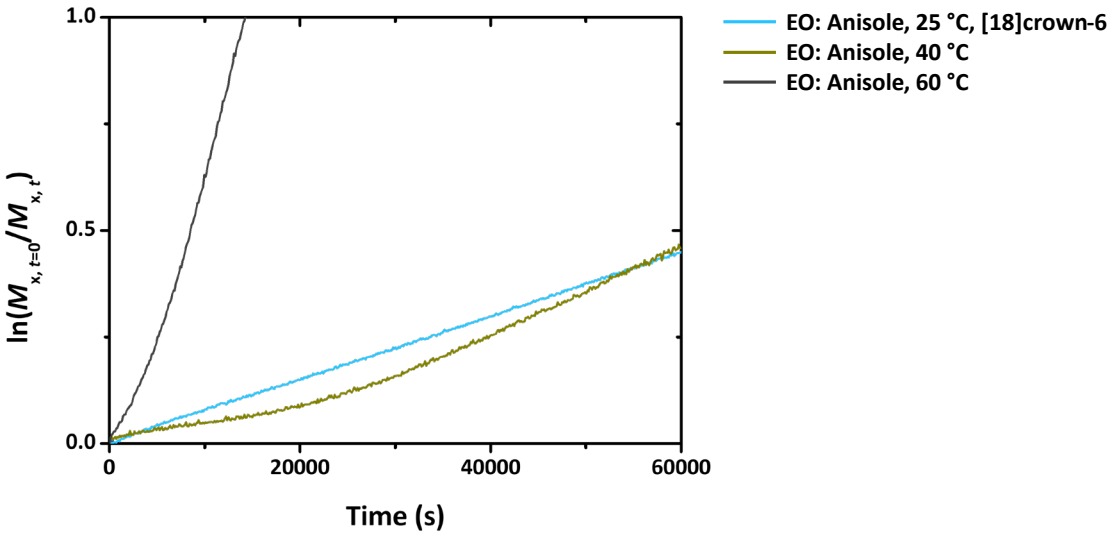

Figure S63: Enlargement of the pseudo-first-order plot of the copolymerization of EO with PO in Anisole at different conditions obtained by ^{1}H NMR kinetics. The enlarged start period shows the induction of the EO signal. The PO graphs are omitted for clarity reasons. The polymerization condition of Anisole at 25 °C without [18]crown-6 was omitted for scale reasons and is displayed in the following graph.

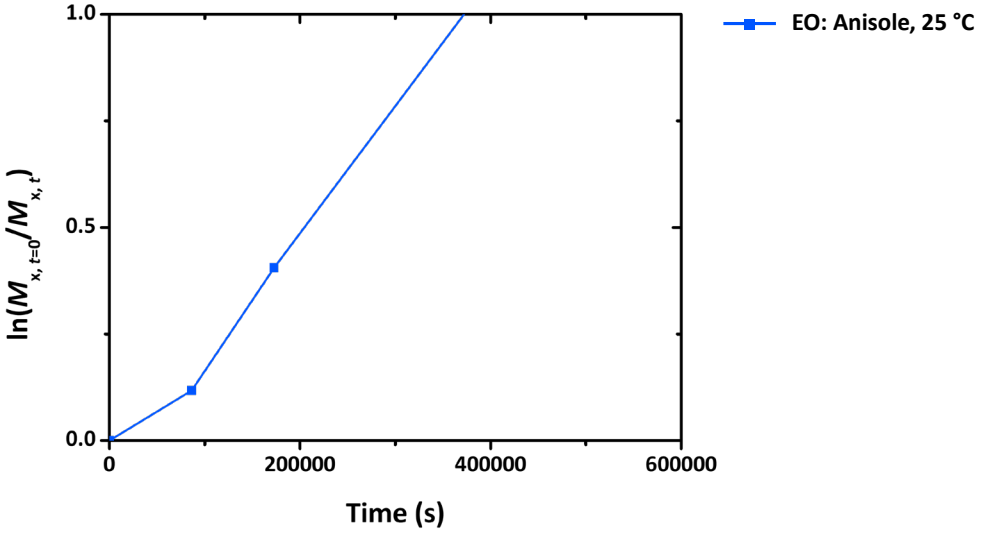

Figure S64: Enlargement of the pseudo-first-order plot of the copolymerization of EO with PO in Anisole at 25 °C obtained by offline kinetics. The enlarged start period shows the induction of the EO signal. The PO graph is omitted for clarity reasons.

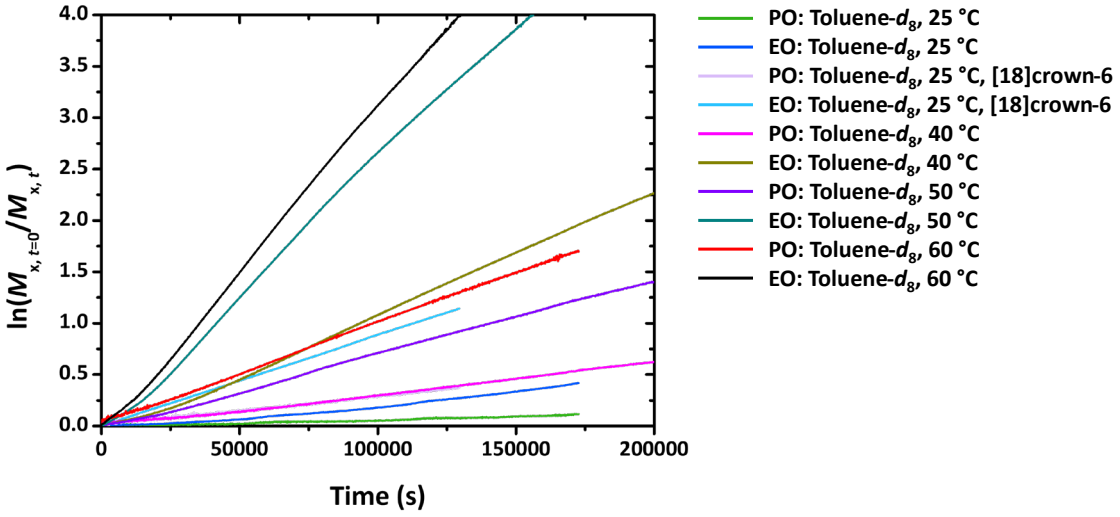

Figure S65: Pseudo-first-order plot of the copolymerization of EO with PO in Toluene-d_8 at different conditions obtained by ^{1}H NMR kinetics.

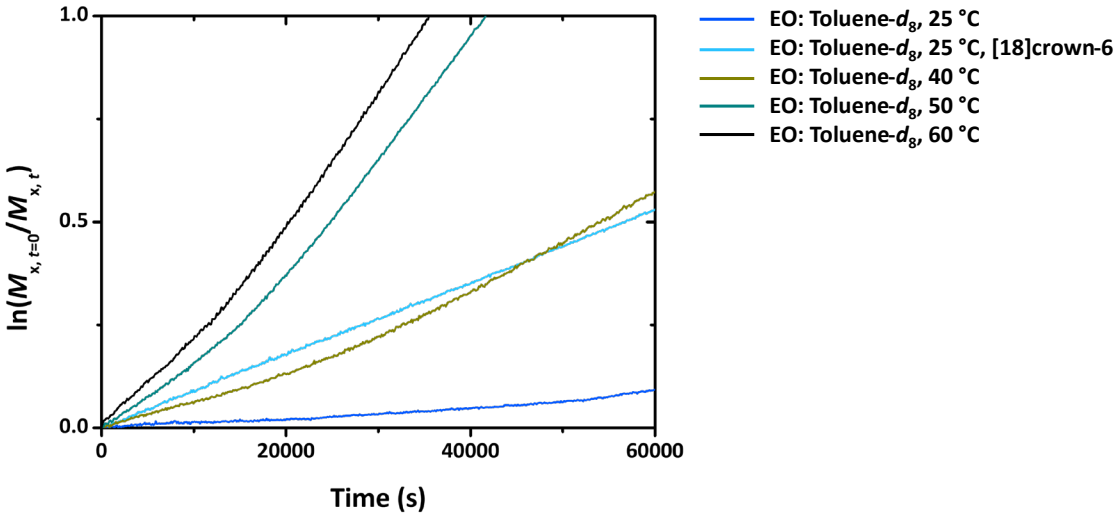

Figure S66: Enlargement of the pseudo-first-order plot of the copolymerization of EO with PO in Toluene-d_8 at different conditions obtained by ^{1}H NMR kinetics. The enlarged start period shows the induction of the EO signal. The PO graphs are omitted for clarity reasons.

Table S1: Apparent propagation constant of EO in the copolymerization ($k_{app,\ copo}$) from the ^{1}H NMR kinetics.

Solvent	T / °C	$k_{app,\ copo}$ (EO) / (10^{-4} s^{-1})
DMSO-d_6	25[a]	3.63 ± 0.01
DMSO-d_6	25	2.37 ± 0.01
DMSO-d_6	40	6.53 ± 0.03
Anisole	25[a]	0.0741 ± 0.0001
Anisole	25	0.0305 ± 0.0003
Anisole	40	0.103 ± 0.001
Anisole	60	0.899 ± 0.002
Toluene-d_8	25[a]	0.0885 ± 0.0001
Toluene-d_8	25	0.0334 ± 0.0001
Toluene-d_8	40	0.116 ± 0.001
Toluene-d_8	50	0.260 ± 0.001
Toluene-d_8	60	0.327 ± 0.001

[a]2 eq. [18]crown-6 per potassium.

Size exclusion chromatography

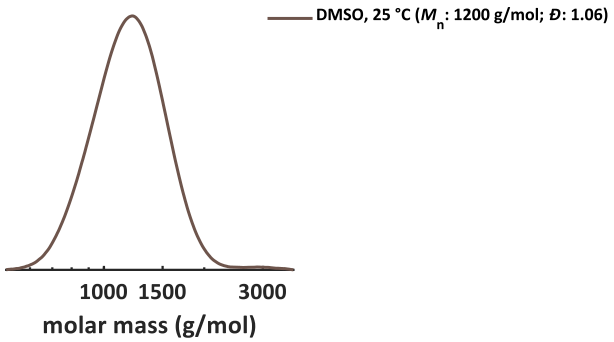

Figure S67: SEC of the copolymer obtained after ^{1}H NMR kinetics (eluent: DMF with 1 g/L LiBr, RI detector, calibration: PEG). Reaction conditions are in the graph's description.

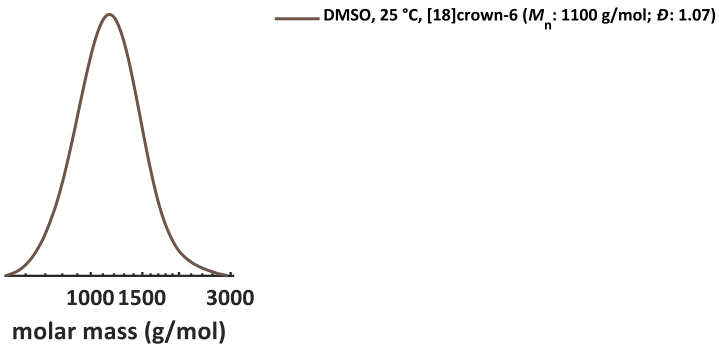

Figure S68: SEC of the copolymer obtained after ^{1}H NMR kinetics (eluent: DMF with 1 g/L LiBr, RI detector, calibration: PEG). Reaction conditions are in the graph's description.

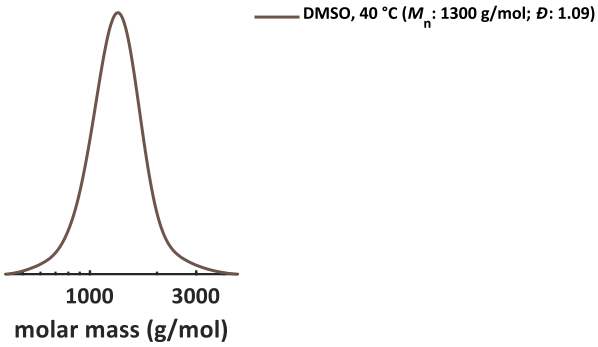

Figure S69: SEC of the copolymer obtained after ^{1}H NMR kinetics (eluent: DMF with 1 g/L LiBr, RI detector, calibration: PEG). Reaction conditions are in the graph's description.

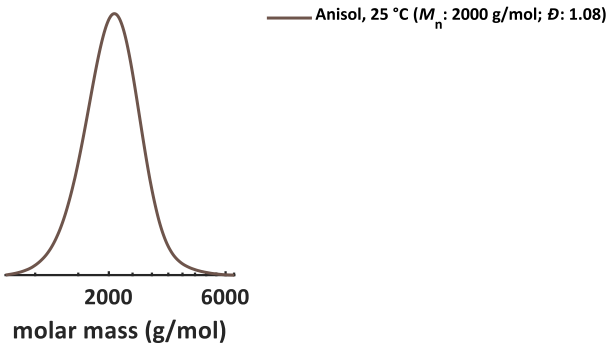

Figure S70: SEC of the copolymer obtained after ^{1}H NMR kinetics (eluent: DMF with 1 g/L LiBr, RI detector, calibration: PEG). Reaction conditions are in the graph's description.

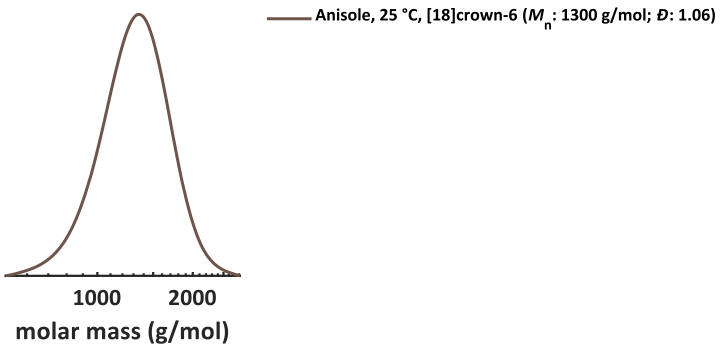

Figure S71: SEC of the copolymer obtained after ^{1}H NMR kinetics (eluent: DMF with 1 g/L LiBr, RI detector, calibration: PEG). Reaction conditions are in the graph's description.

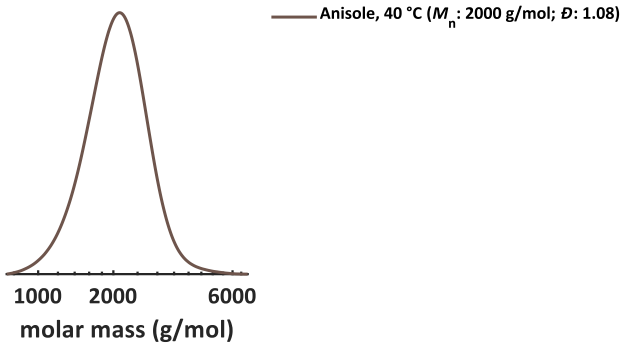

Figure S72: SEC of the copolymer obtained after ^{1}H NMR kinetics (eluent: DMF with 1 g/L LiBr, RI detector, calibration: PEG). Reaction conditions are in the graph's description.

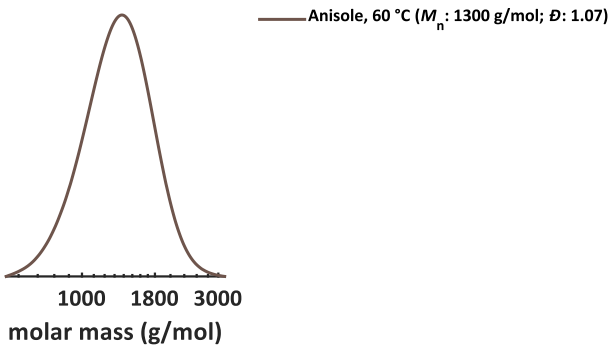

Figure S73: SEC of the copolymer obtained after ^{1}H NMR kinetics (eluent: DMF with 1 g/L LiBr, RI detector, calibration: PEG). Reaction conditions are in the graph's description.

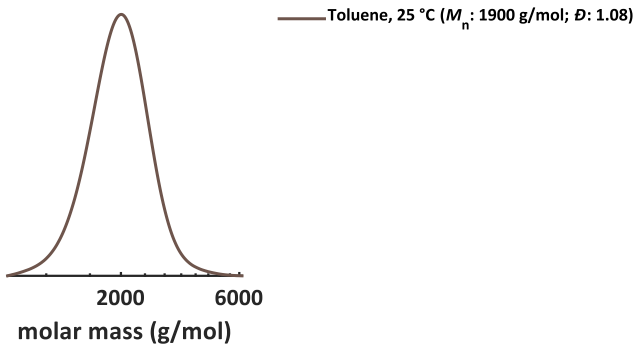

Figure S74: SEC of the copolymer obtained after ^{1}H NMR kinetics (eluent: DMF with 1 g/L LiBr, RI detector, calibration: PEG). Reaction conditions are in the graph's description.

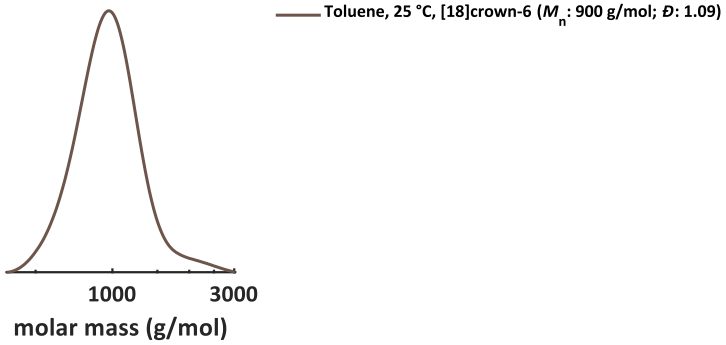

Figure S75: SEC of the copolymer obtained after ^{1}H NMR kinetics (eluent: DMF with 1 g/L LiBr, RI detector, calibration: PEG). Reaction conditions are in the graph's description.

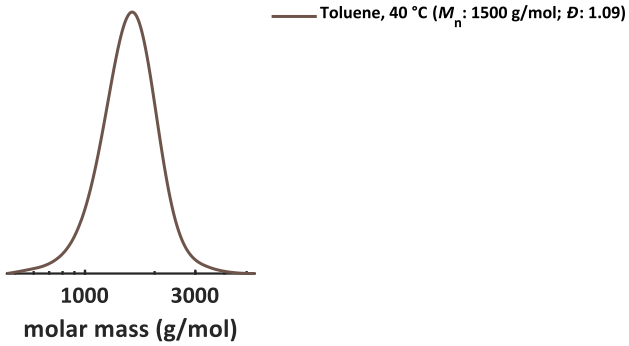

Figure S76: SEC of the copolymer obtained after ^{1}H NMR kinetics (eluent: DMF with 1 g/L LiBr, RI detector, calibration: PEG). Reaction conditions are in the graph's description.

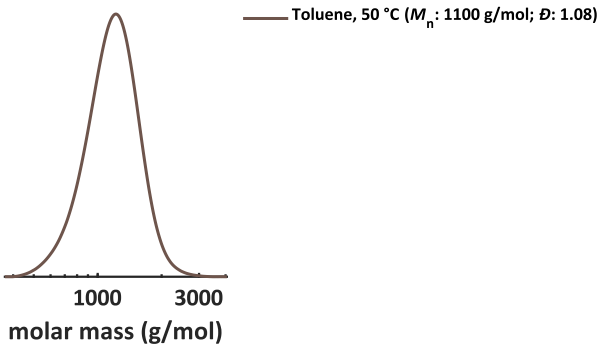

Figure S77: SEC of the copolymer obtained after ^{1}H NMR kinetics (eluent: DMF with 1 g/L LiBr, RI detector, calibration: PEG). Reaction conditions are in the graph's description.

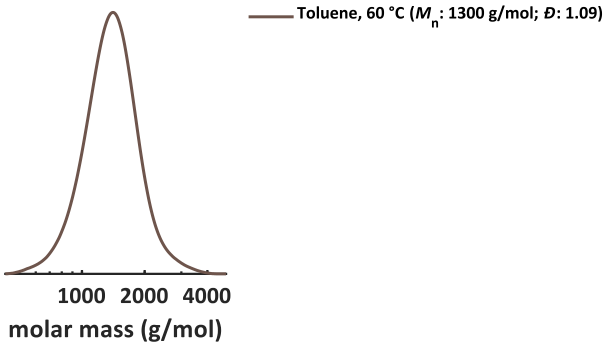

Figure S78: SEC of the copolymer obtained after ^{1}H NMR kinetics (eluent: DMF with 1 g/L LiBr, RI detector, calibration: PEG). Reaction conditions are in the graph's description.

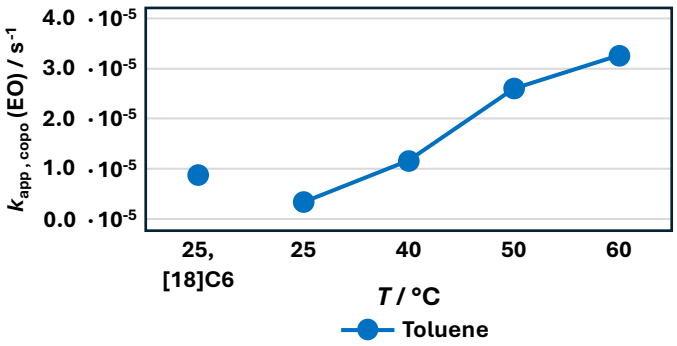

Figure S79: Propagation constant of EO in the copolymerization with PO. Please note that this does not equal a propagation constant k_p of a homopolymerization.

^{1}H NMR Spectroscopy

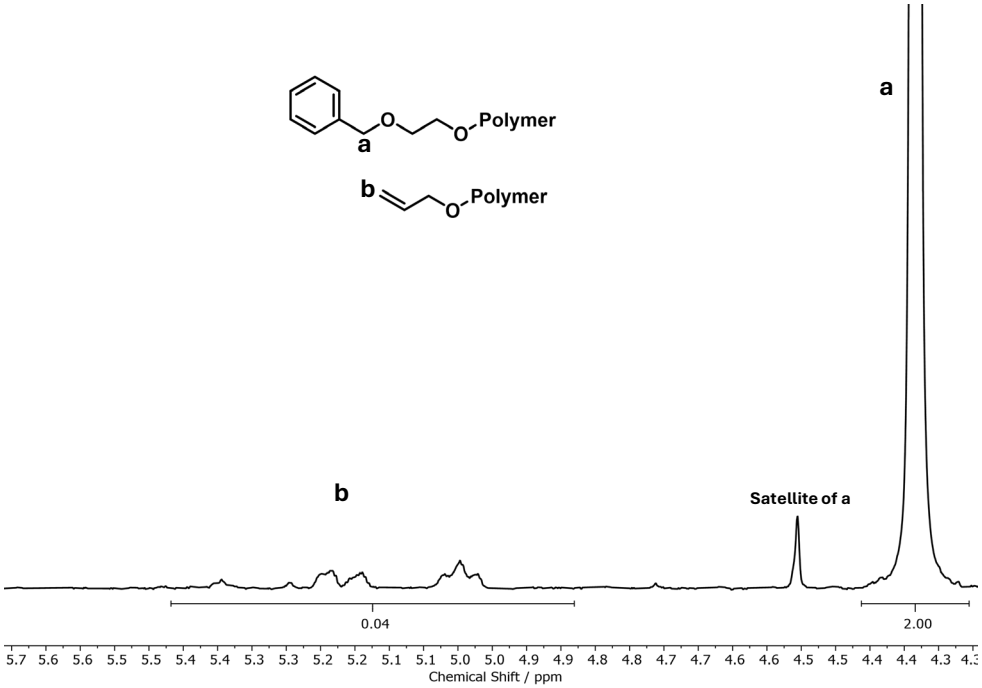

Figure S80: Section of the ^{1}H NMR Spectrum (400 MHz, Toluene-d_8) of the P(EO-*co*-PO) copolymer obtained in toluene-d_8 at 40 °C used for the calculation of the ratio of proton abstraction in relation to desired initiation.

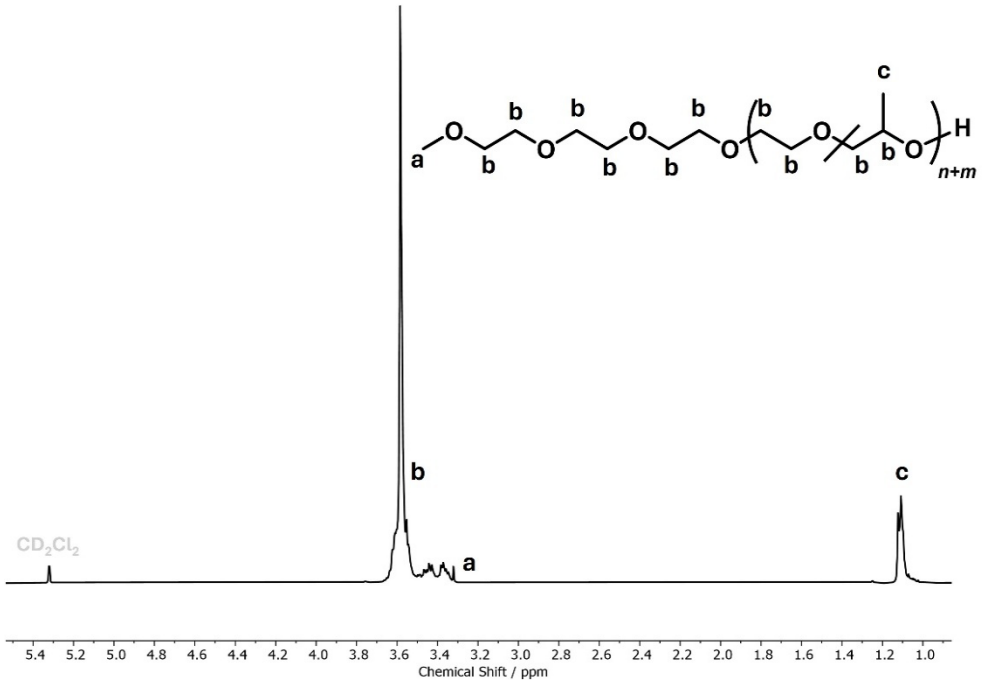

Figure S81: ^{1}H NMR Spectrum (400 MHz, CD_2Cl_2) of the P(EO-*co*-PO) copolymer obtained in toluene at 40 °C.

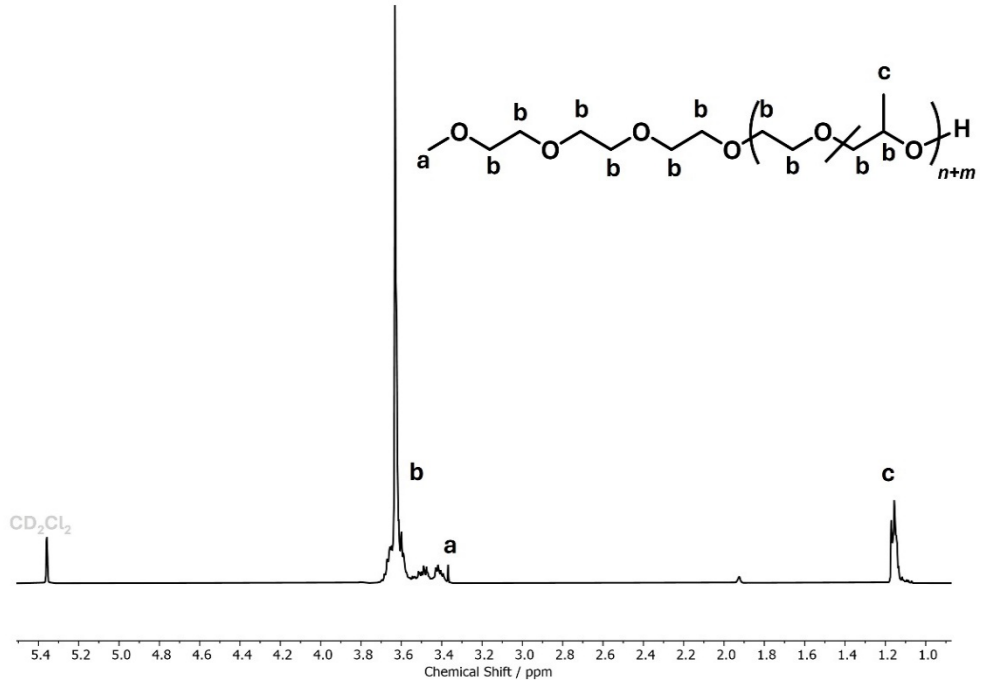

Figure S82: ^{1}H NMR Spectrum (400 MHz, CD_2Cl_2) of the P(EO-*co*-PO) copolymer obtained in toluene at 50 °C.

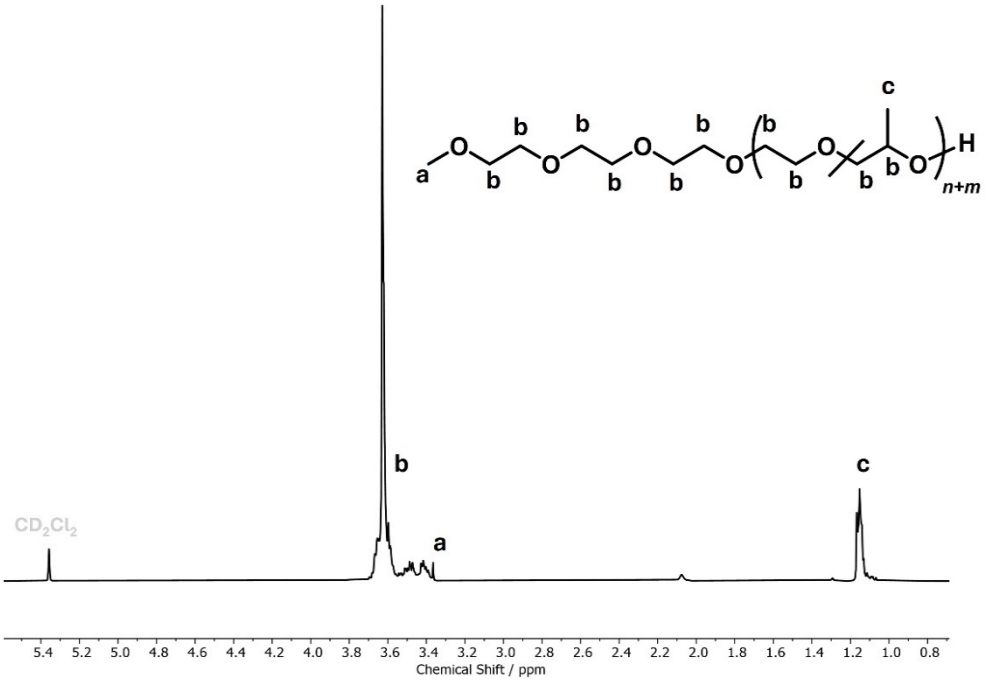

Figure S83: ^{1}H NMR Spectrum (400 MHz, CD_2Cl_2) of the P(EO-*co*-PO) copolymer obtained in toluene at 60 °C.

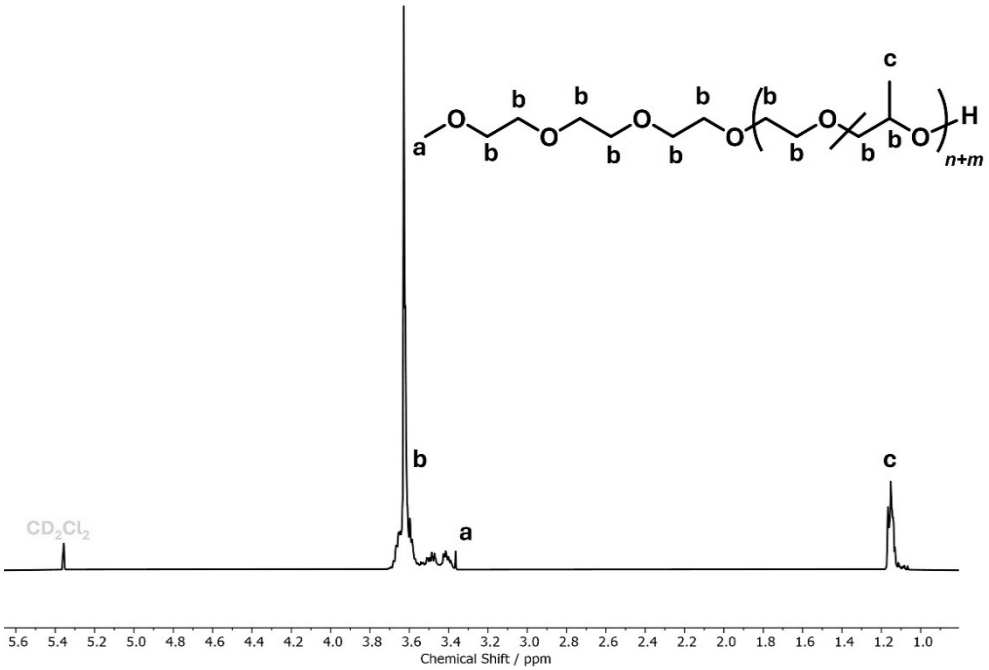

Figure S84: ^{1}H NMR Spectrum (400 MHz, CD_2Cl_2) of the P(EO-*co*-PO) copolymer obtained in toluene at 25 °C with addition of [18]C6.

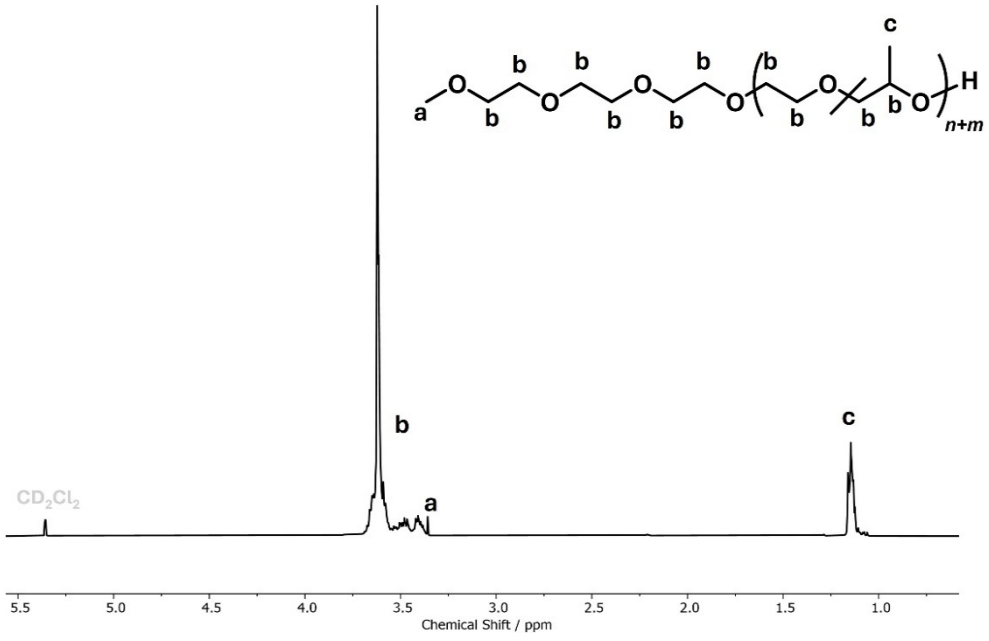

Figure S85: ^{1}H NMR Spectrum (400 MHz, CD_2Cl_2) of the P(EO-*co*-PO) copolymer obtained in anisole at 40 °C.

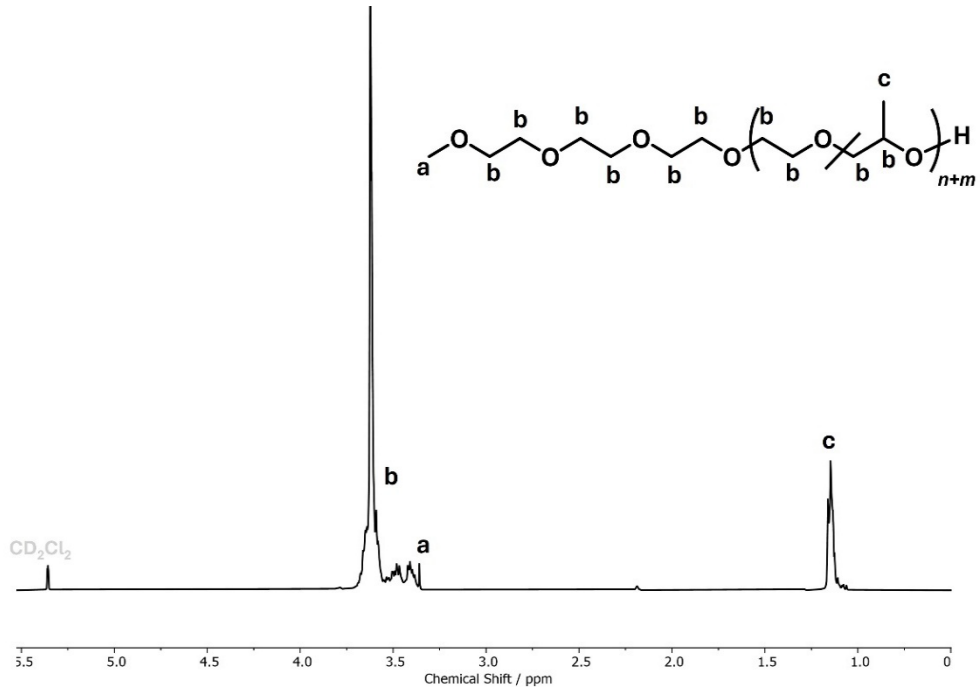

Figure S86: ^{1}H NMR Spectrum (400 MHz, CD_2Cl_2) of the P(EO-*co*-PO) copolymer obtained in DMSO at 40 °C.

Size exclusion chromatography

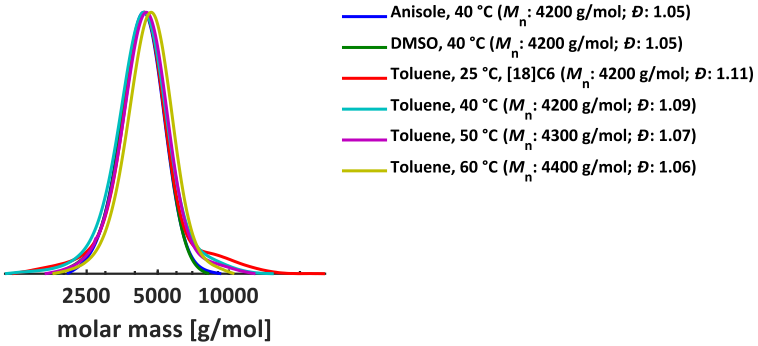

Figure S87: SECs of all polymers synthesized for turbidimetry and DSC measurements.

MALDI-ToF MS Spectrometry

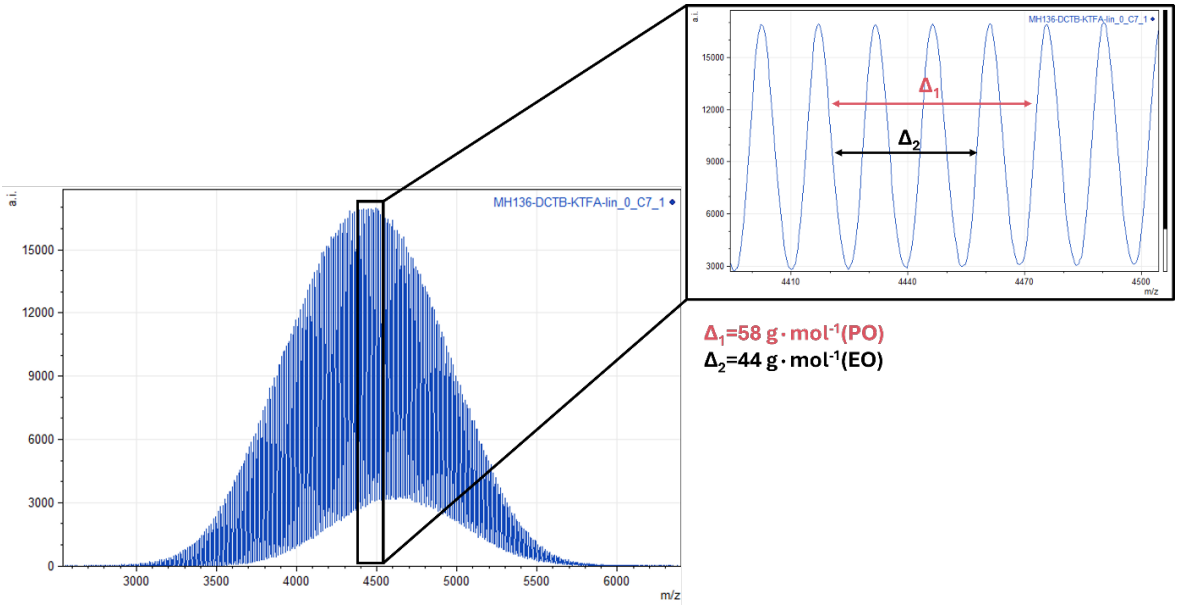

Figure S88: MALDI-ToF spectrum of the P(EO-*co*-PO) copolymer obtained in toluene at 40 °C.

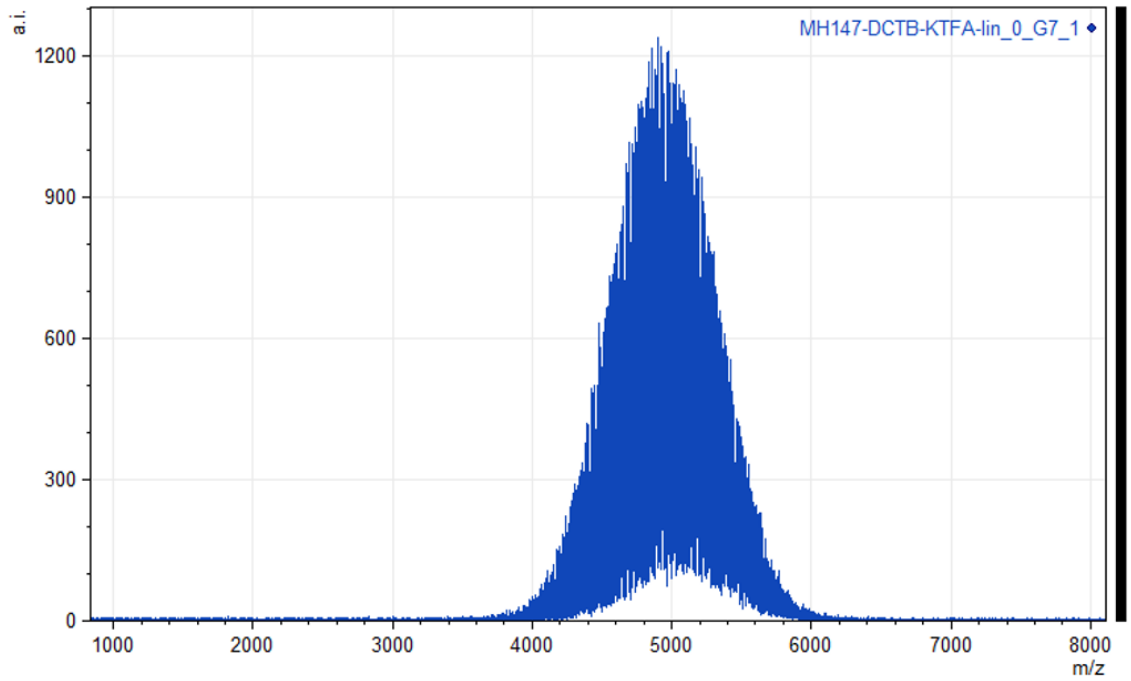

Figure S89: MALDI-ToF spectrum of the P(EO-*co*-PO) copolymer obtained in toluene at 50 °C.

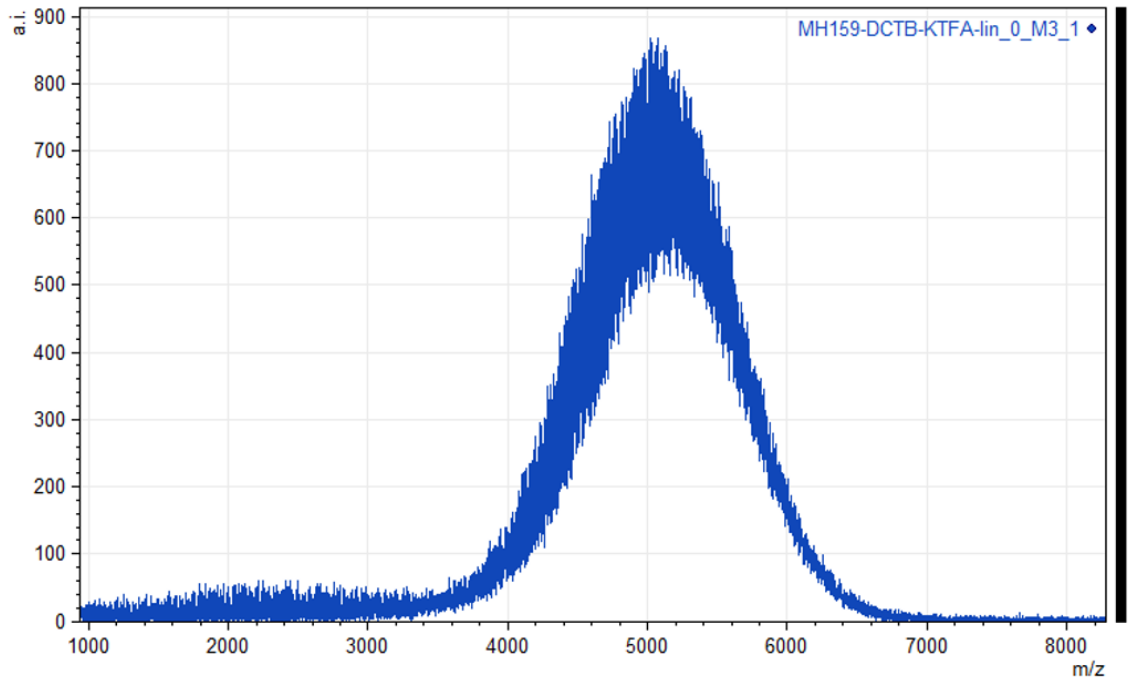

Figure S90: MALDI-ToF spectrum of the P(EO-*co*-PO) copolymer obtained in toluene at 60 °C.

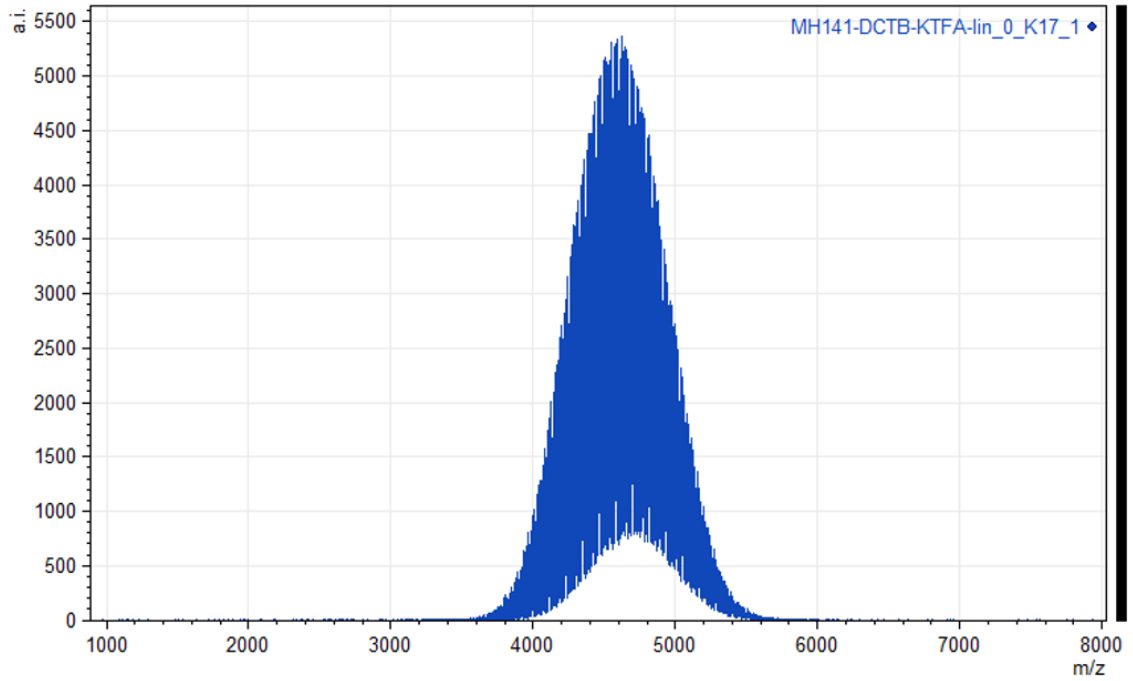

Figure S91: MALDI-ToF spectrum of the P(EO-*co*-PO) copolymer obtained in toluene at 25 °C with [18]C6.

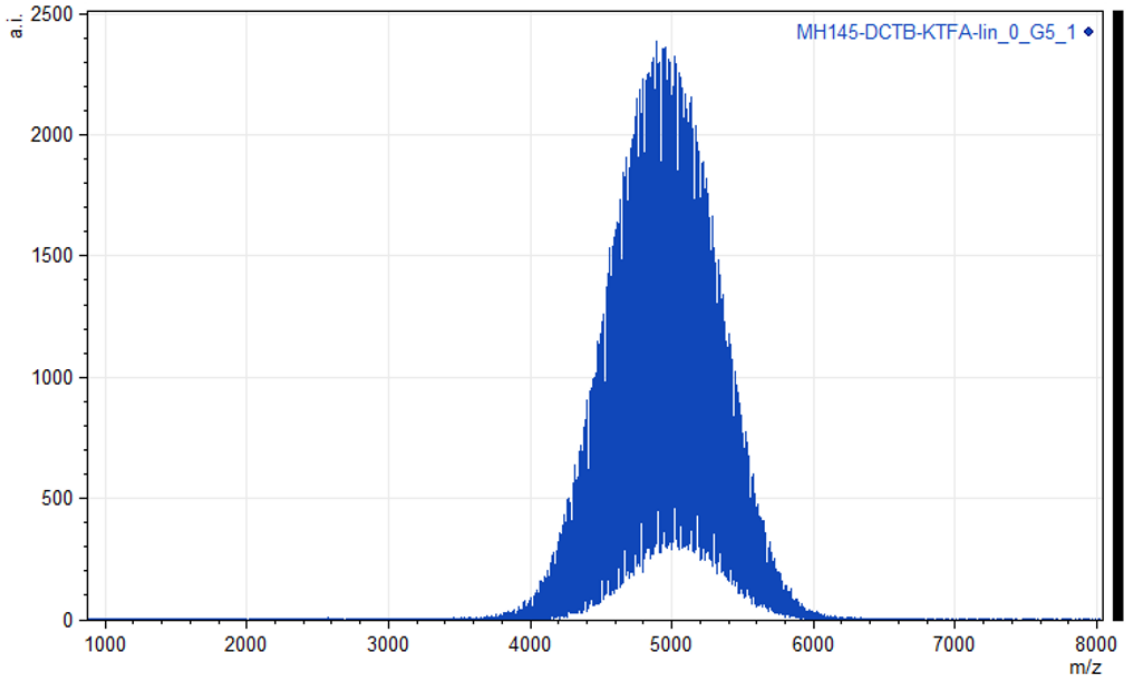

Figure S92: MALDI-ToF spectrum of the P(EO-*co*-PO) copolymer obtained in anisole at 40 °C.

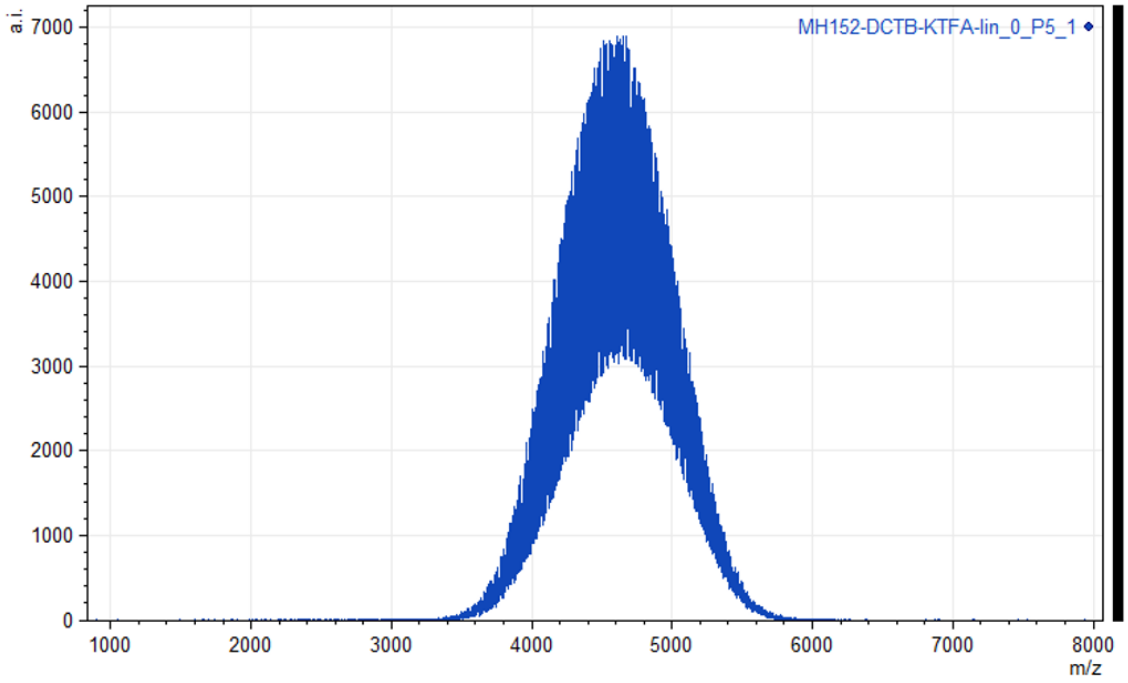

Figure S93: MALDI-ToF spectrum of the P(EO-*co*-PO) copolymer obtained in DMSO at 40 °C.

Turbidimetry measurements

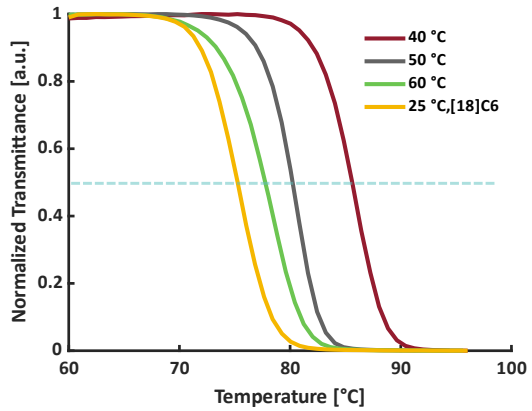

Figure S94: Results of the turbidimetry measurements of the polymers obtained from toluene at 25 °C with [18]C6, 40 °C, 50 °C, and 60 °C.

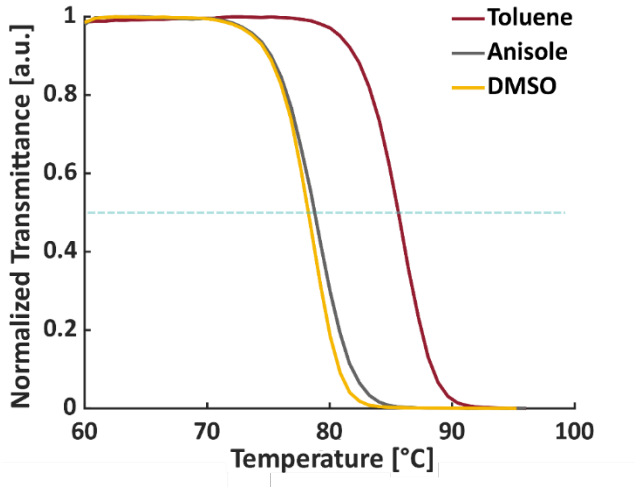

Figure S95: Results of the turbidimetry measurements of the polymers obtained at 40 °C in toluene, anisole, and DMSO.

DSC measurements

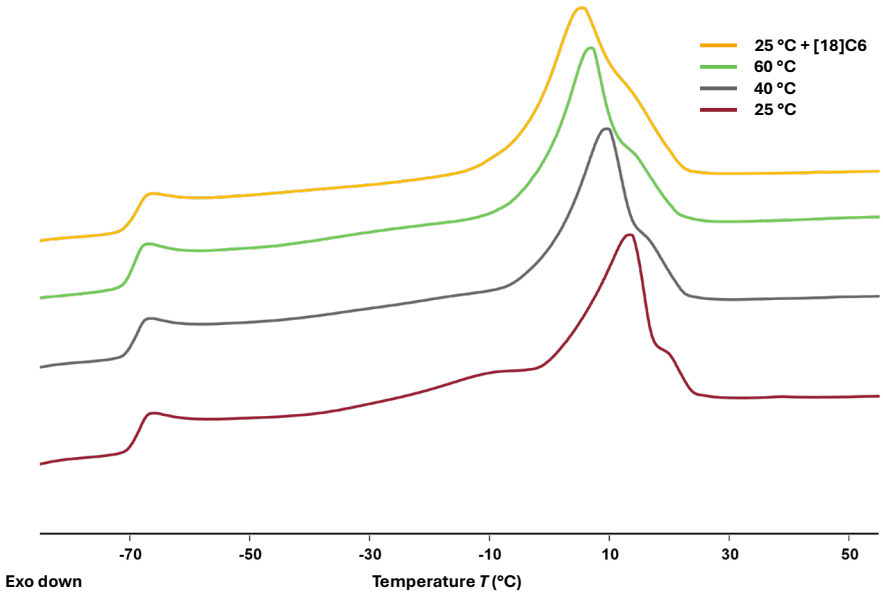

Figure S96: Results of the DSC measurements of the polymers obtained from toluene at 25 °C with [18]C6, 40 °C, 50 °C, and 60 °C.

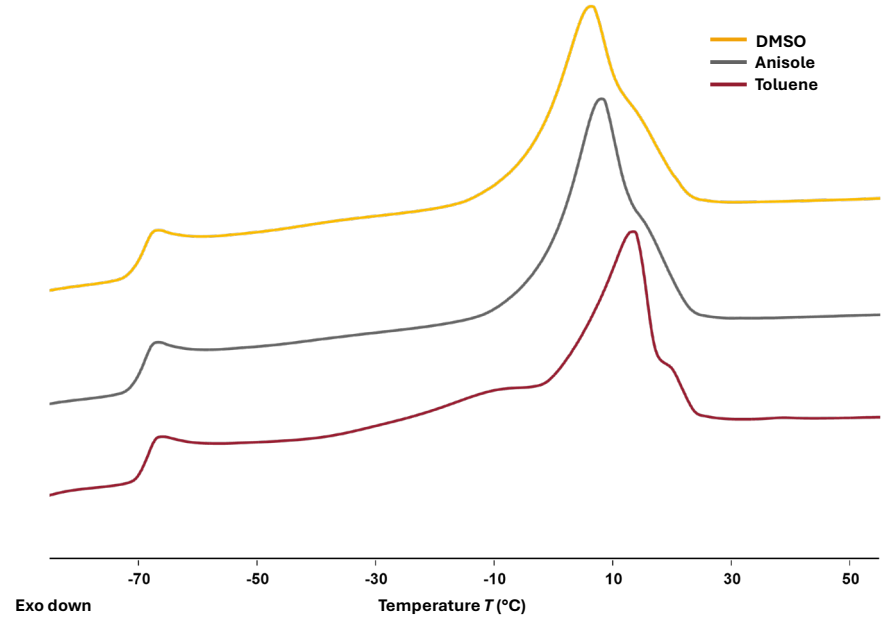

Figure S97: Results of the DSC measurements of the polymers obtained at 40 °C in toluene, anisole, and DMSO.

Table S2: Summary of obtained reactivity ratios, turbidimetry measurement results and DSC messurement results for the analyzed polymerization parameters.

Solvent	T [°C]	r_1 (PO)	r_2 (EO)	Δr[b]	T_{cp} [°C][c]	T_m [°C][d]	ΔH [J/g][e]
Toluene[a]	25	0.31	3.05	2.74	76	5	38
Toluene	40	0.26	3.78	3.52	86	13	42
Toluene	50	0.28	3.62	3.34	80	10	40
Toluene	60	0.31	3.21	2.90	78	7	39
Anisole	40	0.28	3.52	3.24	79	8	39
DMSO	40	0.32	3.10	2.78	78	6	37

[a]2 eq. [18]crown-6 per potassium. [b]$\Delta r = r_2 - r_1$. [c]Cloud point temperature determined via turbidimetry for c = 5 mg·ml^{-1}. [d]Melting temperature. [e]Melting enthalpy.

References

(1) Yu, G.-E.; Heatley, F.; Booth, C.; Blease, T. G. Anionic copolymerisation of ethylene oxide and propylene oxide. Investigation of double-bond content by NMR spectroscopy. *Eur. Polym. J.* **1995**, *31* (6), 589–593. DOI: 10.1016/0014-3057(94)00210-X.

(2) Steube, M.; Johann, T.; Plank, M.; Tjaberings, S.; Gröschel, A. H.; Gallei, M.; Frey, H.; Müller, A. H. E. Kinetics of Anionic Living Copolymerization of Isoprene and Styrene Using in Situ NIR Spectroscopy: Temperature Effects on Monomer Sequence and Morphology. *Macromolecules* **2019**, *52* (23), 9299–9310. DOI: 10.1021/acs.macromol.9b01790.

(3) Meyer, V. E.; Lowry, G. G. Integral and differential binary copolymerization equations. *J. Polym. Sci. A Gen. Pap.* **1965**, *3* (8), 2843–2851. DOI: 10.1002/pol.1965.100030811.

Chapter 5

Glycidyl Ethers from Acyclic Terpenes: A Versatile Toolbox for Multifunctional Poly(Ethylene Glycol)s with Modification Opportunities

5 Glycidyl Ethers from Acyclic Terpenes: A Versatile Toolbox for Multifunctional Poly(Ethylene Glycol)s with Modification Opportunities

[redacted], Gregor M. Linden[1], [redacted]

[1]Department of Chemistry, Johannes Gutenberg University Mainz, Duesbergweg 10-14, 55128 Mainz, Germany.

[redacted] and G.M.L. contributed to this work equally.

Published in: *Polym. Chem.* **2024**. DOI: 10.1039/D4PY01201A

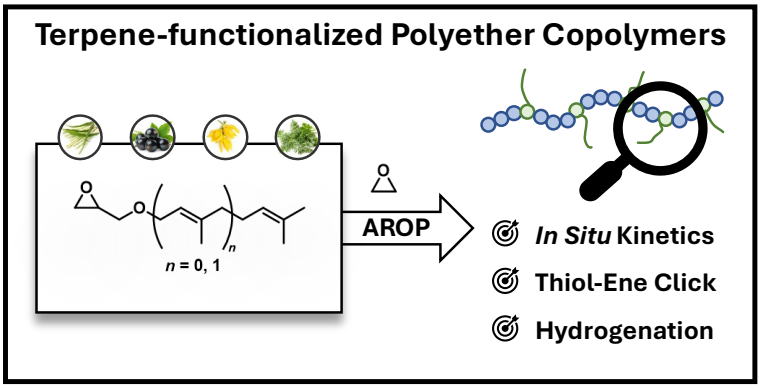

Abstract

Multifunctional poly(ethylene glycol) copolymers (*mf*PEGs) are accessible via the anionic copolymerization of functional epoxides with ethylene oxide (EO). Glycidyl ethers are conveniently synthesized from bio-renewable alcohols and epichlorohydrin (ECH). Herein, we present the synthesis of a series of acyclic terpenyl glycidyl ethers (TGEs) and their subsequent copolymerization with ethylene oxide (EO) via anionic ring-opening polymerization (AROP). The resulting library of copolymers with varying side chain length and comonomer composition comprises molar masses in the range of 4 800 to 8 300 g·mol^{-1} and narrow molar mass distributions ($Đ$ = 1.06 – 1.13). For the copolymerization of the TGEs with EO, detailed ^{1}H NMR *in situ* kinetic studies revealed a change from ideally random to slight gradient copolyether microstructures, with increasing chain length and hydrophobicity of the respective TGE. The living nature of AROP provides control of molar masses, and optimized reaction conditions, such as low reaction temperatures and a weakly bound cesium counterion, suppress the well-known proton abstraction of monosubstituted epoxides. Since the incorporation of the terpenyl side chains impedes crystallization, thermal properties can be tailored by the monomer feed ratio. Subsequently, hydrogenation and thiol-ene click reactions at the side chain double bonds were carried out as post-polymerization modifications. The application of potassium azodicarboxylate (PADA) in the diimide reduction of the polymers was demonstrated to possess immense potential for the full hydrogenation of the novel copolymers, offering facile purification options. Overall, the copolymerization of EO and TGEs gives access to bio-based, tailormade polyethers with options for post-functionalization.

Introduction

Poly(ethylene glycol) (PEG) marks a high-value polyether owing to its excellent biocompatibility and extraordinary solubility in aqueous media. Known as the gold standard for pharmaceutical and biomedical purposes, the application range of PEG also includes cosmetics, surface-active materials and polymer electrolytes.[1–4] To overcome the limited backbone functionality, the copolymerization of ethylene oxide (EO) with functional epoxide building blocks allows for the synthesis of multifunctional PEG (*mf*-PEG) featuring tailormade material properties.[1,5] Particularly glycidyl ethers (GE) represent an underrated monomer class, which is available from a plethora of alcohols and epichlorohydrin (ECH).[6,7] Alternatively, the reaction of an alcohol with allyl bromide, followed by the epoxidation using *meta*-chloroperoxybenzoic acid affords the respective GE.[8] However, despite aiming the use of renewable resources for polymer synthesis, bio-derived epoxides in general and specifically glycidyl ethers have scarcely been exploited for more sustainable

polyethers.[9] Simultaneously, several efforts have been reported that aim at more sustainable sources of conventional polyether building blocks, *e*. *g*. farnesyl glycidyl ether from farnesol.[10] Intriguingly, Sargent and coworkers have recently improved the electrochemical production of ethylene oxide (EO) from CO_2 and water.[11] Alternatively, "green ethylene" can be transformed into EO utilizing the conventional silver-catalyzed epoxidation.[12] Furthermore, "green ECH" is readily available from glycerol, a byproduct in the bio-fuel production from biomass.[13,14]

The use of natural product-based building blocks in glycidyl ether synthesis is a key objective. Fatty acids extracted as value-added chemicals from plant oils have been a long-standing raw material for the chemical industry and polymer synthesis.[15,16] Relevant parameters, which affect the chemical and physical properties, are the length and the degree of unsaturation of the fatty acid chain as well as the stereochemistry of the double bond.[17] Relying on fatty acids, the respective alcohols for glycidyl ether synthesis are accessible via reductive transformation into an alcohol and subsequent phase transfer catalysis.[16] Verkoyen *et al*. published an extensive overview of readily available long-chain alkyl epoxides and glycidyl ethers, characterized by their hydrophobicity, including some examples of fatty acid analogs.[7,18]

As another class of relevant, biomass-derived building blocks, terpenoids and terpenes have been established as attractive monomer precursors.[9,15,19–21] Following the "isoprene rule", acyclic terpenoids vary in their chain length based on their number of linear, head-to-tail condensed $(C_5H_8)_n$ units. Thus, the number of repeat isoprene units allows for the classification into hemi- (C_5), mono- (C_{10}) and sesquiterpenoids (C_{15}).[22,23] Linear, acyclic terpenoids are abundant in ethereal oils of fruits and plants and their application ranges from pharmaceutical products to flavors, fragrances, and pheromones.[24,25] Producing GEs from a range of acyclic terpenoids gives rise to a diverse platform of bio-renewable epoxide monomers (Scheme 1, left). The proposed terpenyl glycidyl ethers (TGEs) are characterized by their unsaturated, hydrophobic side chains. In general, their branched nature impedes crystallization, in stark contrast to their linear fatty acid analogs.[8] To date, only a handful of publications on polyethers and polycarbonates have capitalized on these terpene-derived epoxide building blocks, being suitable for anionic and catalytic polymerization techniques.[10,26–29] On one hand, the hydrophobic character of farnesyl glycidyl ether in combination with PEG enables the facile synthesis of amphiphilic polyethers.[10] On the other hand, the terpenyl side chain flexibility leads to a low glass transition temperature (T_g), thus permitting the generation of flexible, low-T_g polycarbonates.[28,29] Moreover, replacing the commonly applied propylene oxide as a hydrophobic building block takes effect on the copolymer microstructure. It is worth emphasizing that the

copolymerization of EO with PO entails a strong gradient microstructure, whereas GE and EO are expected to produce a random copolymer.[30–32]

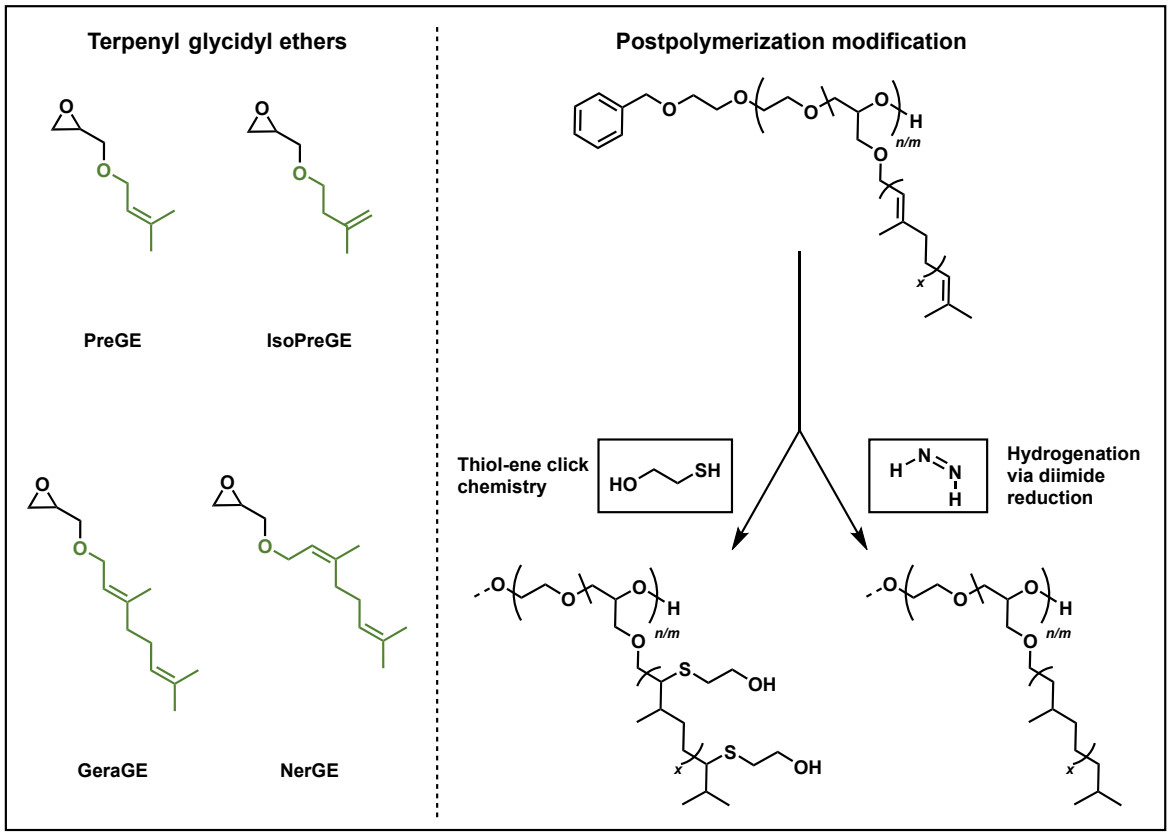

Scheme 1: Scope of prepared bio-renewable TGEs for copolyether synthesis (left). The TGE copolymers are amenable to post-polymerization modification *e.g.* by hydrogenation and thiol-ene click (right).

In addition, the unsaturated side chains of such acyclic TGEs serve as chemoselective handles due to the chemically differing double bonds and, in turn, enable tailor-made materials via post-functionalization.[15,19,25,33] For TGEs, cross-metathesis has been demonstrated by Morris and coworkers, who pioneered TGEs for polyether synthesis utilizing prenyl glycidyl ether (PreGE) and isoprenyl glycidyl ether (IsoPreGE).[26] In this context, PreGE and IsoPreGE can be considered as a bio-renewable analog of the commonly applied allyl glycidyl ether (AGE).[1,26] Moreover, successful click-TAD chemistry on a citronellyl glycidyl ether side chain led to terpene-derived polyether-based organo- and hydrogels.[27] Yet, the plentiful modification opportunities have not been investigated extensively. For instance, the thiol-ene click reaction of polymers offers flexible means to create custom materials, as documented in Lowe's comprehensive review.[34,35] In addition, hydrogenation is a widely adopted approach that enhances the thermal and oxidative stability of polyisoprene by using gaseous hydrogen and metal catalysts at high temperatures in a reactor.[36] Another small-scale modification method is hydrogenation using diimide, which can be generated from various sources and does not require high-pressure equipment.[37,38]

In this work, we present the use of different bio-based TGEs for the synthesis of *mf*-PEGs. Applying hemi- and monoterpenoids in the synthesis of TGEs (Scheme 1), we expanded the available bio-derived TGE library for polyether design and synthesis based on PreGE, IsoPreGE, geranyl glycidyl ether (GeraGE), and neryl glycidyl ether (NerGE). Statistical polyether copolymers P(EG_n-*co*-TGE_m) were prepared via living AROP of EO and the TGEs of varying acyclic chain length. The resulting polyethers exhibit the targeted molar masses and low dispersity $Đ$ (≤ 1.13), while the thermal properties can be fine-tuned by the applied TGE content. ^{1}H NMR *in situ* kinetics was employed to study the impact of the glycidyl ether side chains on the copolymerization behavior of the respective EO/TGE comonomer pairs and potential gradient formation. Furthermore, the structural variety regarding side chain length and double bond configuration was explored with respect to post-polymerization functionalization (Scheme 1). Aiming at introducing hydroxyl-functionalities, photochemical thiol-ene click chemistry was performed. Further, the double bond was hydrogenated using potassium azodicarboxylate (PADA) diimide reduction, which involves the *in situ* generation of the diimide via acidic decomposition of PADA. Subsequently, we address some of the limitations associated with the use of *para*-toluenesulfonyl hydrazide.

Experimental Section

Details on reagents used, instrumentation, methodical procedures and synthesis procedures are given in the Supporting Information (SI) Section 1 – 4.

Results and Discussion

Monomer Synthesis

The presented TGEs have all been prepared in a phase transfer catalysis, starting from epichlorohydrin and the respective terpenoid.[10,29] The products were isolated in high purity after distillation work up, which was performed subject to the monomer boiling temperature T_b.

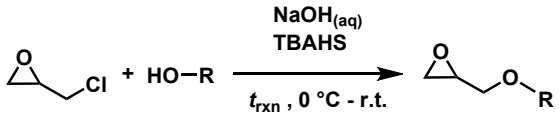

Scheme 2: General monomer synthesis via phase transfer catalysis. TBAHS: tetra-*n*-butylammonium hydrogen sulfate.

During the phase transfer catalysis, elimination and substitution reactions lead to the formation of undesired byproducts, specifically 3-chloro-allyl glycidyl ether and diglycidyl ether.[10,29] While the resulting byproducts can be easily separated from the long-chain TGEs (C_{10} and C_{15}) due to a significant difference in T_bs, the C_5-analogs, namely PreGE, IsoPreGE, and dihydroprenyl glycidyl ether (DHPreGE), required an altered synthetic protocol.[10,29] To suppress byproduct formation, the

synthesis approach utilizing the C_5-alcohols was performed under prolonged cooling and for shorter reaction times, ultimately resulting in lower overall yields (51 – 64%) compared to the C_{10} and C_{15}-analogs GeraGE and NerGE (78 – 83%). We designed a synthesis protocol that circumvented the purification step via column chromatography and improved the C_5-monomer yields compared to literature.[26] Detailed NMR characterization for all TGEs (Figures S1 – S14) as well as an explicit synthetic protocol are provided in the SI.

Statistical Copolymerization of EO and TGEs

Living statistical copolymerizations of bio-renewable TGEs with EO were performed in a THF-DMSO solvent mixture (V_{THF}:V_{DMSO} = 5:1) at 40 °C, using conventional AROP conditions, employing cesium 2-(benzyloxy)ethoxide as an initiator salt (Scheme 3).

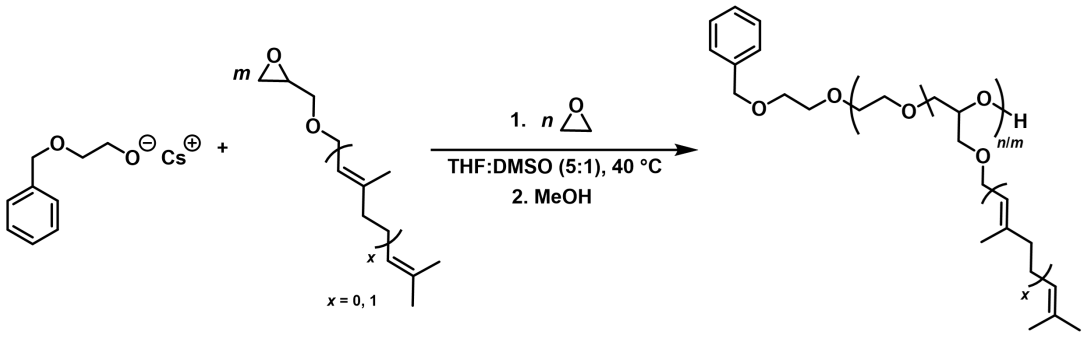

Scheme 3: Synthetic strategy for the copolymerization of EO with TGEs of varying terpenyl chain length, resulting in terpenyl-functionalized PEGs.

In order to maintain the remarkable properties of PEG while extending its functionality, we designed a series of copolymers for each TGE by varying the comonomer content between 3.0 and 9.6 mol%. The rationale for this intended low amount of TGE comonomer encompasses significant property changes using small TGE amounts while increasing functionality and maintaining the aqueous solubility of the copolymers. Table 1 summarizes the copolymerization results as well as the thermal characterization data of the statistical P(EG_n-*co*-TGE_m) copolymers. Number averaged molar masses (M_n) were calculated via ^{1}H NMR end group analysis by referencing to the methylene group of the 2-(benzyloxy) ethanol initiator (Figures S19, S21, S23, and S25), in the range of 4 800 to 8 300 g·mol^{-1}.

Typical ^{1}H NMR spectra show the anticipated signals of the polyether backbone and the terpenyl side chain, which can be clearly distinguished. Notably, we observed side chain isomerization for all polymers, which is a known phenomenon for allyl glycidyl ether, when applying the general basic conditions of AROP.[39–41] We will briefly readdress the isomerization in the kinetic investigation section. Size exclusion chromatography (SEC) indicates well-defined copolymers with monomodal

distributions and low dispersity $Đ$ (1.06 – 1.11) (Figures S15 – S18). Deviations of the M_n determined by SEC from ^{1}H NMR characterization are ascribed to the structural and polarity difference of the P(EG$_n$-*co*-TGE$_m$) copolymers compared to the PEG calibration standards for SEC.

Table 1: Overview of polymer characterization of P(EG$_n$-*co*-TGE$_m$) statistical copolymers

Entry	Sample	$X_{TGE,exp}$[a] / (mol%)	$M_{n,NMR}$[a] / g·mol^{-1}	$M_{n,SEC}$[b] / g·mol^{-1}	$Đ$[b]	T_g[c] / °C	T_m[c] / °C	ΔH_m[c] / J·g^{-1}
1	P(EG$_{121}$-*co*-PreGE$_5$)	4.0	6190	4800	1.08	-59	39	79
2	P(EG$_{113}$-*co*-PreGE$_5$)	4.2	5840	4600	1.06	-60	31	74
3	P(EG$_{107}$-*co*-PreGE$_{10}$)	8.5	6290	4700	1.09	-63	21	47
4	P(EG$_{102}$-*co*-PreGE$_{10}$)	8.9	6070	4900	1.07	-62	18	43
5	P(EG$_{96}$-*co*-IsoPreGE$_3$)	3.0	4810	4700	1.07	-61	40	76
6	P(EG$_{117}$-*co*-IsoPreGE$_7$)	5.6	6300	5200	1.07	-64	29	56
7	P(EG$_{100}$-*co*-IsoPreGE$_{10}$)	9.1	5980	4400	1.10	-66	18	44
8	P(EG$_{126}$-*co*-IsoPreGE$_{12}$)	8.7	7410	4800	1.11	-65	15	44
9	P(EG$_{123}$-*co*-GeraGE$_4$)	3.1	6250	4700	1.07	-61	40	77
10	P(EG$_{117}$-*co*-GeraGE$_6$)	4.9	6540	4800	1.08	-65	26	37
11	P(EG$_{110}$-*co*-GeraGE$_8$)	6.8	6680	4200	1.07	-66	23	40
12	P(EG$_{120}$-*co*-GeraGE$_{12}$)	9.1	7960	5400	1.10	-63	14	35
13	P(EG$_{109}$-*co*-NerGE$_4$)	3.5	5640	4400	1.07	-63	38	70
14	P(EG$_{125}$-*co*-NerGE$_8$)	6.0	7180	5100	1.07	-65	32	51
15	P(EG$_{115}$-*co*-NerGE$_{10}$)	8.0	7160	5600	1.07	-67	21	48
16	P(EG$_{123}$-*co*-NerGE$_{13}$)	9.6	7980	5500	1.08	-	-	-

[a]Number averaged molar mass and experimental monomer content determined via ^{1}H NMR spectroscopy. [b]Determined via SEC measurements (RI detector, eluent: DMF, calibration: PEG). [c]Determined from second heating cycle at a heating rate of 10 °C·min^{-1}.

In situ ^{1}H NMR Copolymerization Kinetics of TGEs with EO

Glycidyl ethers can be applied in the copolymerization with EO, introducing functionality along the polyether backbone.[5] For a detailed understanding of the material's properties, it is pivotal to elucidate the copolymer microstructure.[31] Capitalizing on *in situ* ^{1}H NMR kinetic investigations in combination with suitable copolymerization models, it is possible to translate monomer conversion into the respective reactivity ratios of a given comonomer pair.[31,42,43] Motivated by the different

structure of the terpenyl side chains, we systematically performed *in situ* ^{1}H NMR copolymerization kinetics in a vacuum-sealed NMR tube to compare the copolymerization behavior for all TGE/EO comonomer pairs. It is important to note that we also investigated the fully hydrogenated analogs of the C_5, C_{10} and C_{15} side chains to evaluate the influence of hydrophobicity on the copolymerization behavior, also aiming at further understanding the role of the allylic double bond. Based on the living AROP copolymerization without chain transfer and termination, we accurately followed monomer conversion, specifically for EO at 2.59 ppm (blue) and PreGE at 3.05 ppm (green, Figure 1 and Figure S39, left). As previously reported, the ideal non-terminal model is known to be valid for the copolymerization of EO and glycidyl ethers. The copolymerizations follow ideal copolymerization behavior, which is expressed by the simple relation: $r_1 = r_2^{-1}$.[31,44,45] Plotting the individual monomer conversion versus total conversion (Figure S39, right), we applied the ideal Jaacks fit (Figure S27) to obtain reactivity ratios of $r_{PreGE} = 0.94$ and $r_{EO} = 1.06$, revealing an almost ideally random copolymerization for PreGE and EO.[46]

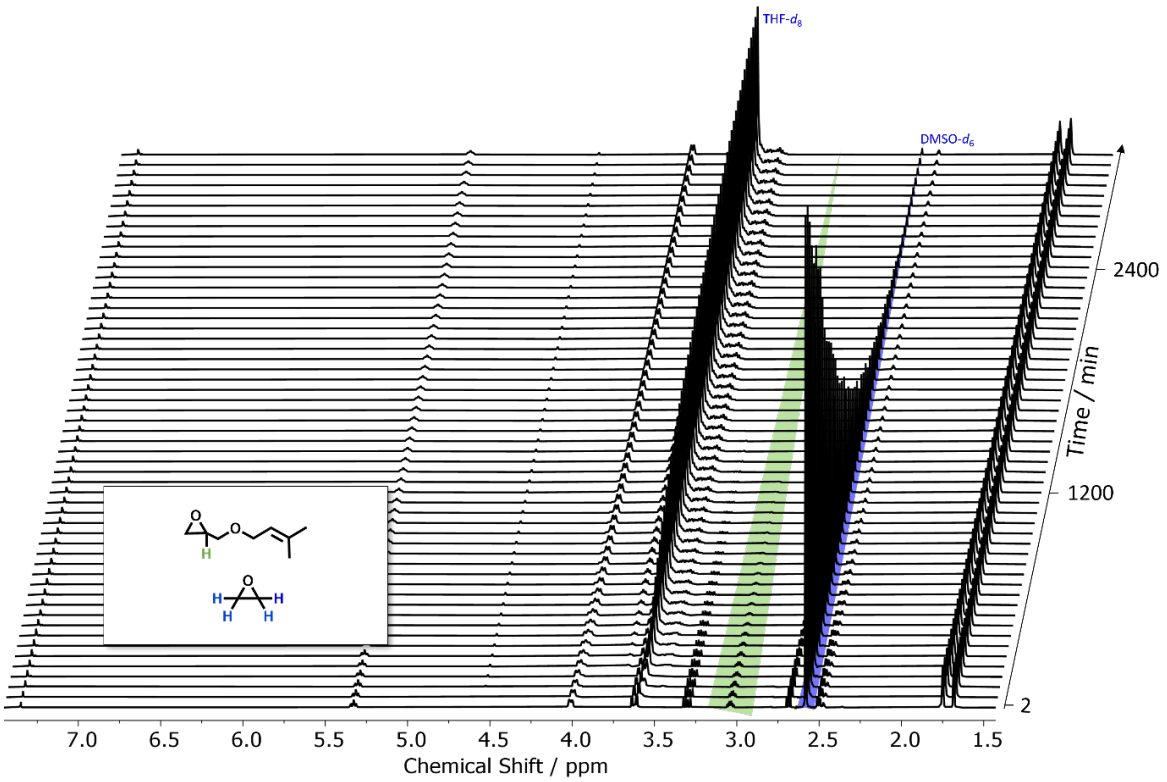

Figure 1: Selection of ^{1}H NMR spectra (400 MHz, THF-d_8 : DMSO-d_6= 5:1) of the *in situ* copolymerization kinetics of PreGE with EO at 40 °C. Relevant proton signals are highlighted in green (PreGE) at 3.05 ppm and blue (EO) at 2.59 ppm. As spectra were collected every 2 min over a period of 51.5 h, only every 30th spectrum is displayed.

Table 2 summarizes the reactivity ratios determined for the statistical copolymerization of EO with the TGEs employed in this work. Detailed *in situ* kinetic data, characterization as well as the respective SEC traces ($Đ \leq 1.13$) are compiled in the SI, Figures S27 – 33 and S39 – 58. In general,

the copolymerization behavior is governed by steric and electronic properties of the epoxide monomers.[31] The side chain impact on reactivity ratios is manifest as a collective of three parameters: (i) length, (ii) hydrophobicity, and (iii) flexibility. At first glance, an increase in chain length and hydrophobicity leads to a more pronounced incorporation of EO at the start of the copolymerization. This is consistent with previously reported results for farnesyl glycidyl ether.[10] PreGE and IsoPreGE manifest no significantly different copolymerization behavior, although the isoprenyl main chain is more flexible. Both copolymerizations show almost ideally random behavior. On the other hand, the reactivity ratio of EO is higher for all other comonomer pairs, resulting in a (soft) monomer gradient in the copolymer chain. The difference in *cis*- and *trans*-stereoconfiguration of NerGE and GeraGE, respectively, appear to be a negligible factor during the copolymerization. In contrast, an increase of side chain hydrophobicity by full hydrogenation appears to be the most influential parameter for the copolymer microstructure, affording a stronger gradient. Altogether, the observed trends are in good agreement with previously reported results, as GEs generally copolymerize in an ideally random manner with EO.[31,32] Due to the additional oxygen in the GE side chain, Lynd and coworkers postulated a "crown ether-effect" at the active polymer chain end, enhancing the GE reactivity.[32] Following our findings, we hypothesize that the steric demand of the branched terpene structures impedes counterion complexation and, in turn, leads to an inversion of the comonomer reactivity.[10] Furthermore, a slight deviation in reactivity ratios could also be due to solvent and counterion effects.[31,47]

Table 2: Reactivity ratios for the AROP of various TGEs with EO in a mixture of THF-d_8 and DMSO-d_6 (5:1) at 40 °C, evaluated by the non-terminal model and the ideal Jaacks fit.

Monomer	Pendant group	r_{EO}[a]	r_{TGE}[a]	R^2
Isoprenyl glycidyl ether	C_5H_9O	1.03 ± 0.01	0.97 ± 0.01	0.99
Prenyl glycidyl ether	C_5H_9O	1.06 ± 0.01	0.94 ± 0.01	0.99
Geranyl glycidyl ether	$C_{10}H_{17}O$	1.08 ± 0.01	0.93 ± 0.01	0.99
Neryl glycidyl ether	$C_{10}H_{17}O$	1.07 ± 0.01	0.93 ± 0.01	0.99
Farnesyl glycidyl ether[b]	$C_{15}H_{25}O$	1.18 ± 0.01	0.85 ± 0.01	0.99
Dihydroprenyl glycidyl ether	$C_5H_{11}O$	1.18 ± 0.01	0.85 ± 0.01	0.99
Tetrahydrogeranyl glycidyl ether	$C_{10}H_{21}O$	1.21 ± 0.01	0.83 ± 0.01	0.99
Hexahydrofarnesyl glycidyl ether	$C_{15}H_{31}O$	1.25 ± 0.01	0.80 ± 0.01	0.99

[a]Errors for reactivity ratios have been rounded up to the last significant digit. [b]Reactivity ratios of the FarGE/EO comonomer pair have been previously published for identical polymerization conditions.[10]

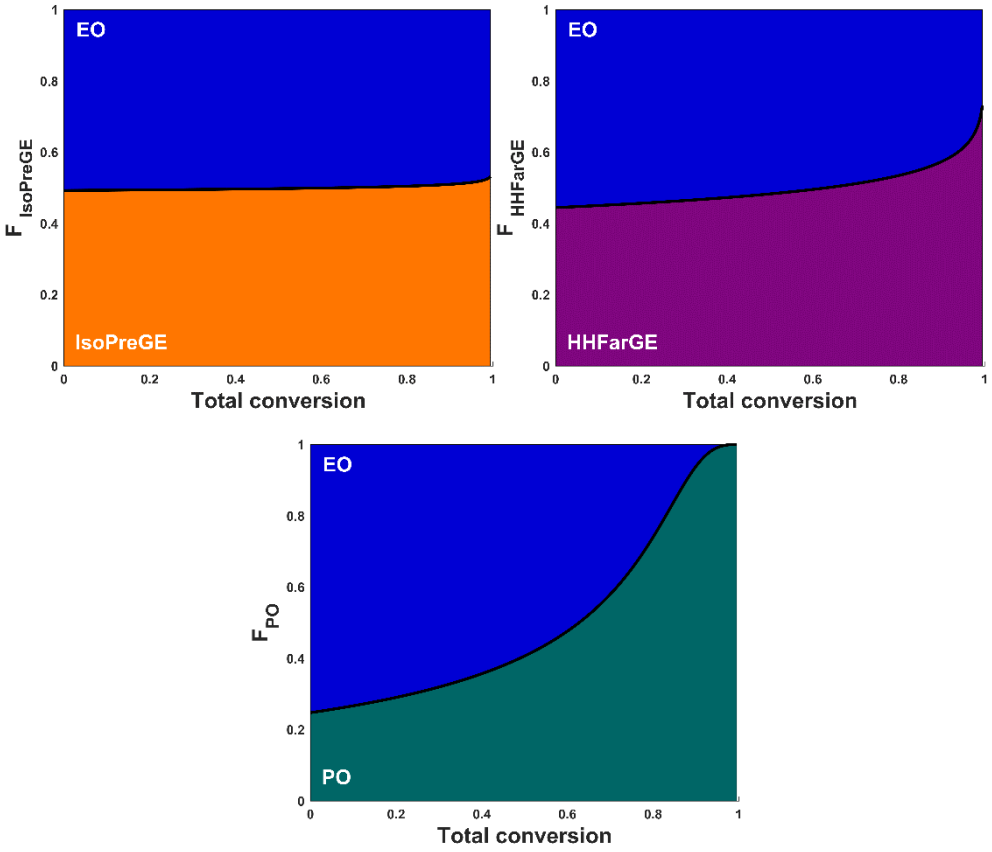

Figure 2: Molar-based composition diagrams of a P(EG$_n$-*co*-IsoPreGE$_m$) (top, left); a P(EG$_n$-*co*-HHFarGE$_m$) (top, right) and a P(EG$_n$-*co*-PO$_m$) copolymer (bottom), respectively, modelled at an equimolar monomer ratio, with F_X = molar fraction of TGE or PO. Calculations for TGEs are based on the reactivity ratios derived from a linear Jaacks fit[46] (top, right), whereas reactivity ratios for the EO/PO comonomer pair are derived from literature (r_{EO} = 2.80; r_{PO} = 0.25).[30]

In our kinetics study, IsoPreGE, and hexahydrofarnesyl glycidyl ether (HHFarGE) show the strongest discrepancy in their copolymerization behavior. To visually demonstrate the difference between the ideally random and gradient structures, we simulated the molar-based composition diagram of a statistical copolymer for EO with IsoPreGE and HHFarGE at an equimolar monomer ratio, respectively. Figure 2 demonstrates the effect of the reactivity ratio difference on the polymer microstructure. While the isoprenyl side chains are randomly distributed along the polyether chain, the copolymerization with HHFarGE produces a noticeable, but weak gradient copolyether, which determines the nature of the terminal units. HHFarGE units are slightly less incorporated at the onset of the growing polymer chain, whereas the gradient shows a noticeable increase towards the chain terminus. Based on a previous kinetic study by Heatley *et al*. and for comparison purposes we additionally depict the molar composition diagram for the highly relevant EO/PO comonomer pair (Figure 2, bottom).[30] While statistical P(EG$_n$-*co*-PO$_m$) copolymers feature a significantly stronger gradient composition profile, a nearly random microstructure can be realized by simply substituting PO by a TGE.

Having revealed the subtle reactivity differences of the available TGEs, we directed our attention to unraveling the unexpected appearance of novel signals during the *in situ* kinetics of the unsaturated C_5-TGEs. Figure 3 depicts a zoom-in of the time-resolved overlay of ^{1}H NMR spectra between 4.6 and 6.6 ppm, documenting the unexpected appearance of new signals during the copolymerization. Chain transfer to the monomer is a well-known drawback of the alkali metal mediated AROP of substituted epoxides, leading to the formation of new allylic species with signals in a similar down-field region, as evidenced by ^{1}H NMR spectroscopy.[48] More importantly, chain transfer would lead to an inaccurate PreGE consumption in our study, falsifying the determined reactivity ratios. Owing to the similarity of the signals' shifts, we sought to obtain a deeper understanding of our observations regarding (i) signal assignment and (ii) validity of the determined reactivity ratios. Interestingly, our findings indicate the occurrence of base-catalyzed γ-elimination of the prenyl protective group (Scheme S2) and formation of isoprene during the copolymerization (≤ 0.5% of overall monomer, Figure S34) rather than chain transfer.[49–51] A cryotransfer of all volatile compounds following our kinetic study corroborated our hypothesis, as we identified isoprene via GC and NMR analysis (Figures S35 – S37). Concurrently, a hydroxyl functionality is released, which can act as an additional initiating species due to the degenerative proton transfer in the AROP.[1] Yet, as the elimination occurs in trace amounts of less than 1%, a hyperbranched structure is not expected. The aforementioned observations and conclusions are conferrable to the copolymerization of EO and IsoPreGE as a structural isomer of PreGE (Figure S41).

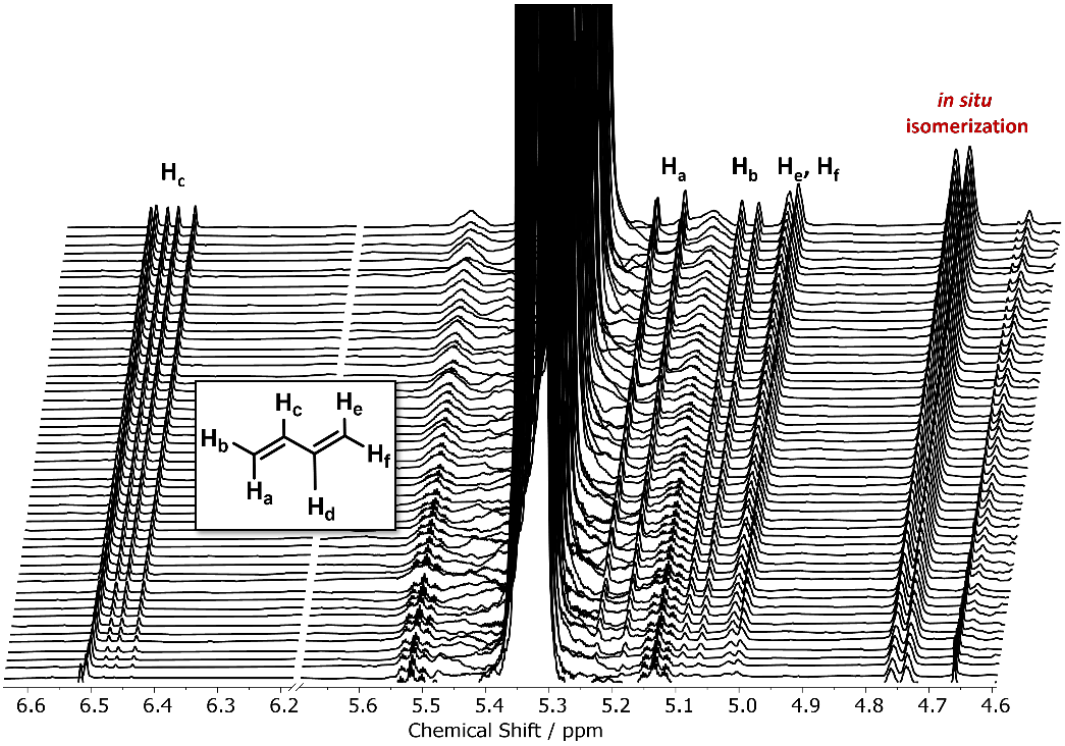

Figure 3: Zoom-in region of stacked ^{1}H NMR spectra (400 MHz, THF-d_8 : DMSO-d_6= 5:1) of the copolymerization kinetic investigation of PreGE and EO, validating the elimination of isoprene in small quantities. The doublet forming between 4.71 and 4.77 ppm shows the concurrent prenyl-to-isoprenyl isomerization under basic AROP conditions.

We observed that decreasing the base concentration in the NMR tube leads to a decrease in the overall isoprene formation by base-catalyzed elimination. This is in line with the results of the significantly more dilute copolymerization conditions in a flask, for which no isoprene formation has been observed. Additionally, we used dihydroprenyl glycidyl ether (DHPreGE) as a saturated model compound in an *in situ* kinetic measurement (Figures S50 – S52), for which, as anticipated, no new signals are witnessed (Figure S50). Intriguingly, the elimination reaction was only observed for the unsaturated C_5-TGEs, which is presumably favored by a six-membered transition state (Scheme S2). Conclusively, the chosen copolymerization conditions suppress chain transfer reactions whilst trace elimination does not impact the accurate determination of the reactivity ratios. An additional finding is the partial base-catalyzed prenyl-to-isoprenyl isomerization of the side chain under basic conditions (and vice versa for IsoPreGE), as evidenced in Figure 3 and Figure S38.[52] In contrast, the copolymerization EO with neryl and geranyl glycidyl ether (NerGE, GeraGE), respectively, shows little to no isomerization. The different degree of isomerization is further supported by ^{13}C NMR characterization of P(EG$_n$-*co*-PreGE$_m$) and P(EG$_n$-*co*-IsoPreGE$_m$) copolymers, which show more pronounced carbon shifts of the isomerized side chain (compare Figures S20 and S22 vs. Figures S24 and S26). Similar *in situ* isomerization has already been reported for the AROP of EO with AGE, which undergoes a transformation from allyl- to *cis*-prop-1-enyl

ether.[39,40] Due to the degree of substitution, PreGE isomerization is sterically promoted towards the isoprenyl structure. Overall, the different copolymerization behavior renders TGE highly promising building blocks to fine-tune the microstructure of *mf*-PEGs under the established AROP conditions.

Thermal Properties of Statistical P(EG-*co*-TGE) Copolymers

Differential scanning calorimetry (DSC) of the copolymers not only reveals the thermal properties (Figures S79 – S82), but also provides indirect support for the copolymer microstructure. PEG is a semicrystalline polyether with a melting temperature (T_m) of 65 °C. Generally, all synthesized co-polymers exhibit a T_m that depends on the comonomer content. Accordingly, a gradual TGE increase results in an incremental decrease of T_m and the respective melting enthalpy. In contrast to block-like structures, statistical copolymers with side chain functionalization show significant reduction of the PEG crystallization.[5,10] The branched terpenyl side chains lead to regularly distributed steric disturbances along the PEG chain, prohibiting packing in highly ordered crystalline domains. For instance, incorporation of approximately 3 mol% TGE already reduces the T_m by ~ 25 °C. Melting points in the range of 30 °C to 40 °C, *i.e.*, in a physiological temperature range are promising for a variety of pharmaceutical applications. Furthermore, branching does also not allow for side chain crystallization for the longer terpenyl side chains (C_{10}), as indicated by the absence of a second T_m.[8] As expected for statistical copolymers with a random or soft gradient microstructure, only a single glass transition temperature T_g in the range of -59 °C to -67 °C is observed.[53] The prenyl side chain leads to a slightly higher T_g than isoprenyl, which is tentatively ascribed to decreased chain flexibility. The results show that the difference in side chain length or side chain double bond configuration of the incorporated C_5 and C_{10} TGE chain does not represent a key parameter in tailoring the thermal properties. Overall, the thermal properties of the copolymers observed for a low content of the TGE comonomers are a consequence of the almost ideally random microstructure.

Post-Polymerization Modification

The unsaturated side chains of the P(EG-*co*-TGE) copolymers are characterized by chemically different double bonds. Therefore, we investigated the different copolymer structures, focusing on their post-polymerization potential capitalizing on thiol-ene click and hydrogenation.

Thiol-Ene Click Reaction

Thiol-ene click photo reactions were carried out overnight in DCM using 2,2-dimethoxy-2-phenylacetophenone (DMPA) as a radical photoinitiator and 2-mercaptoethanol as a functional thiol to demonstrate the general applicability. As trisubstituted, internal double bonds represent a

particular challenge with respect to modification, P(EG_{120}-*co*-$GeraGE_{12}$) was used as the model copolymer (Scheme 4). The ratios of double bonds/DMPA/thiol were varied to obtain fully functionalized copolymers with monomodal molar mass distributions. After the photoreaction, residual 2-mercaptoethanol was removed via aqueous extraction, followed by further purification via dialysis.

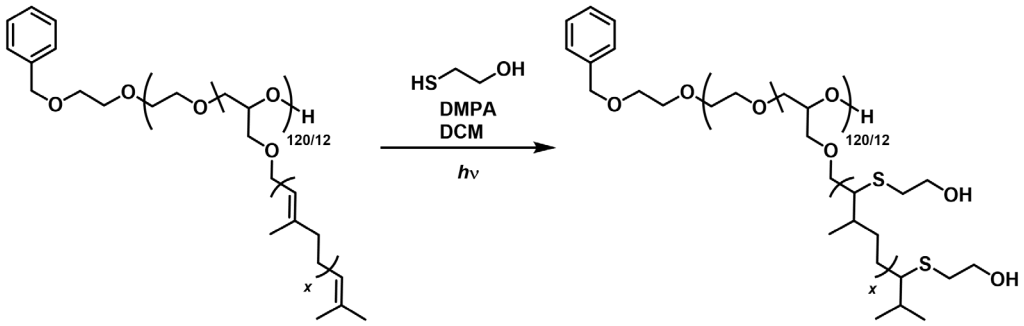

Scheme 4: Thiol-ene modification of P(EG_{120}-*co*-$GeraGE_{12}$) employing 2-mercaptoethanol as a functional thiol. The copolymers in entries 4, 8, and 16 were modified in the same manner. For experimental details see Table S1.

Generally, the reactivity of double bonds towards hydrothiolation decreases from terminal towards internal and subsequently multiple substituted double bonds.[54–56] As the formation of the carbon-sulfur bond is reversible and depends on the olefin and thiol structures, it is anticipated that the reverse reaction will be more pronounced for olefins with trisubstituted internal double bonds than less substituted olefins. Terpene-based small molecules with terminal double bonds can be modified with small amounts of excess equivalents of thiol.[25] However, the respective modification conditions commonly used for small molecules induce cross-linking of double bond-containing polymers, leading to a multimodal molar mass distribution. This is evidenced in the high M_n of the polymer as determined by SEC (Figure 4, gray curve). A strategy to overcome crosslinking is the use of large excess thiol equivalents (Figure 4, compare red, cyan and purple curve) while keeping the required amount of the photoinitiator DMPA at a minimum (Figure 4, red and green curve). When 200 equivalents of thiol per double bond are applied, a monomodal molar mass distribution is achieved. Comparing the functionalized copolymers to the starting P(EG_{120}-*co*-$GeraGE_{12}$) copolymer, a shift of the SEC elugram toward higher molar masses indicates the successful functionalization (dotted blue and purple curve).

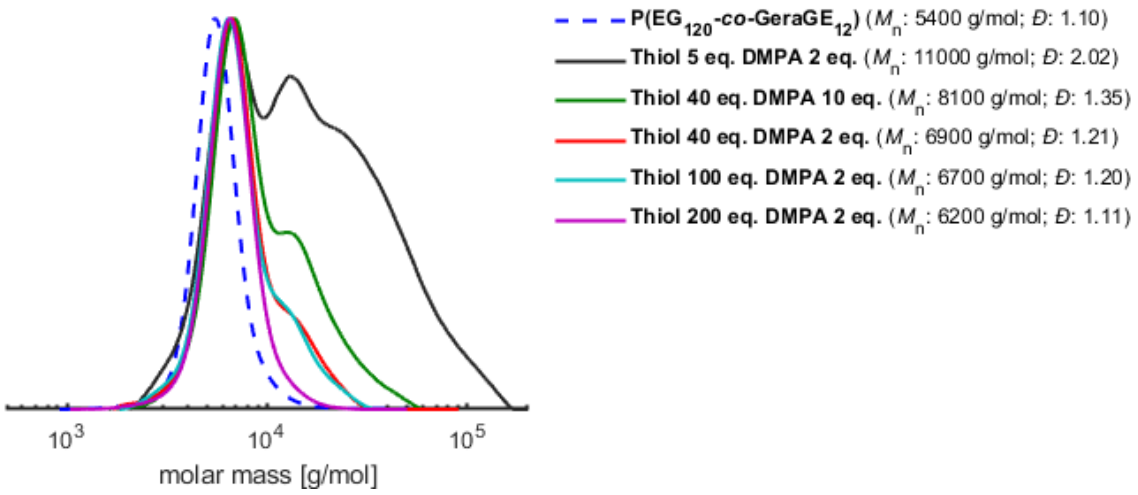

Figure 4: SEC traces of P(EG_{120}-*co*-$GeraGE_{12}$) modified with different equivalents of the thiol 2-mercaptoethanol and DMPA with respect to one double bond (Eluent DMF, RI detector, PEG calibration). Purple line represents the SEC curve of the successful modification without crosslinking.

Furthermore, ^{1}H NMR analysis revealed complete conversion of both double bonds in all experiments (Figures S63 – 66). The incisive protons at 2.75 and 2.36 ppm refer to the methine protons from the anti-Markovnikov product of the two double bonds (Figure S65). The infrared spectrum illustrates a broad band at approximately 3400 cm^{-1} due to the added hydroxyl functionalities. The absence of the R-S-H band at 2500 cm^{-1} indicates complete removal of 2-mercaptoethanol by dialysis (Figure S69). MALDI-ToF analysis provides further proof for complete modification, as the peak intervals solely correspond to the EO unit and the double functionalized GeraGE unit with 366 $g \cdot mol^{-1}$ (Figure S73). It is noteworthy that unreacted 2-mercaptoethanol was recovered by fractional distillation in yields of 80% (see SI for details), reducing the overall thiol equivalents required for functionalization. Equally, we modified P(EG_{102}-*co*-$PreGE_{10}$), requiring 600 eq. of thiol per double bond to suppress cross-linking (Figure S59). Surprisingly, SEC characterization still indicated a shoulder towards higher molar masses, even when 300 equivalents of thiol were used. P(EG_{123}-*co*-$NerGE_{13}$) required similar reaction conditions, despite its similarity to GeraGE. A different reactivity towards hydrothiolation of those species was not expected, however, adjusting the modification conditions enabled us to obtain monomodal distributions for both copolymer types (Figure S62).

Hydrogenation via diimide reduction

Typically, the production of diimide involves the thermal decomposition of *para*-toluenesulfonyl hydrazide (*p*TSH). Despite its effectiveness, the use of this reagent is accompanied by several limitations. These include the requirement for reflux in solvents with a high boiling point such as *ortho*-xylene, inefficient byproduct removal, and the occurrence of undesirable reactions towards

polyisoprene, such as chain degradation, cyclization, and nucleophilic attack of *para*-tolylsulfinate anion.[57,58] Chain degradation can be reduced by the addition of a tertiary amine and, conclusively, the *p*TSH route represents a reasonable alternative to catalyzed hydrogenation. While the diimide reduction using *p*TSH is a well-known hydrogenation method, the use of potassium azodicarboxylate (PADA) as an *in situ* hydrogenation agent has been scarcely investigated to date.[59] Thus, we investigated the post-polymerization hydrogenation of terpenoid structures employing PADA with respect to (i) hydrogenation temperature, (ii) applied PADA equivalents and (iii) the solvent volume required. Detailed experimental procedures and further results (Table S2) are provided in the SI. PADA was utilized to generate the diimide, which upon decomposition produced potassium acetate as a byproduct. The general procedure involved dissolving the dry polymer in dry pyridine, followed by the addition of PADA. A slurry was created, into which dry glacial acetic acid was added dropwise to induce decomposition. It is important to note that the decomposition of PADA is strongly influenced by the concentration of acid.[60]

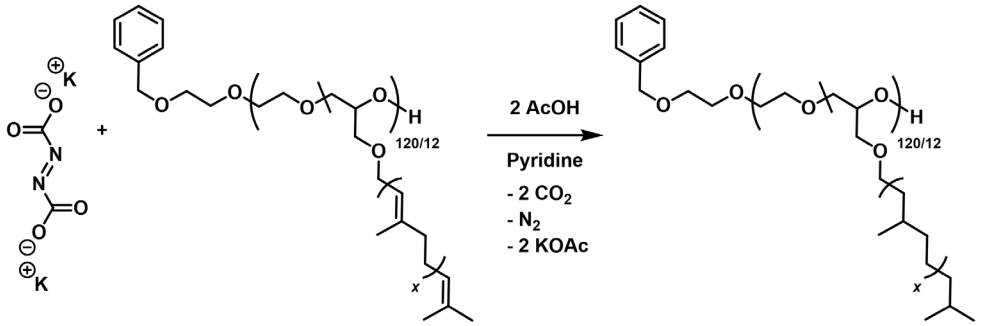

Scheme 5: Hydrogenation of P(EG_{120}-*co*-$GeraGE_{12}$) employing potassium azodicarboxylate (PADA). Intermediate steps towards diimide are omitted but can be found in the introduction.

The acyclic TGE side chains incorporate two types of double bonds: an in-chain double bond in allyl-position to the oxygen in either *cis*- or *trans*-configuration as well as a double bond of varying degree of substitution. In this study, we deliberately selected GeraGE carrying both types of double bonds to highlight the proof-of-principle and robustness of our approach. First experiments showed that decreasing the temperature from RT to 0 °C only affects the degree of hydrogenation in concentrated solutions, yet the efficiency was reduced to a maximum of 53% (Table S2, entry 1 – 4). Next, we increased the volume of the solvent to 3 ml, which increased the degree of hydrogenation from 25% to 53% according to ^{1}H NMR characterization (Table S2, entry 4 and 8). As the slower decomposition of PADA directly correlates with the slower dosage and reduced concentration of acetic acid in the reaction mixture, improved hydrogenation and reduction of side reactions are observed. A similar effect was observed upon increasing the PADA equivalents from 2.5 to a maximum of 15 per double bond (Table S2, entries 4 and 8). Figure 5 illustrates the double

bond resonances before and after hydrogenation, respectively, showing a decrease in double bond signals and an increase in the region of aliphatic resonances (Full analysis in Figures S75 – S77 of the SI).

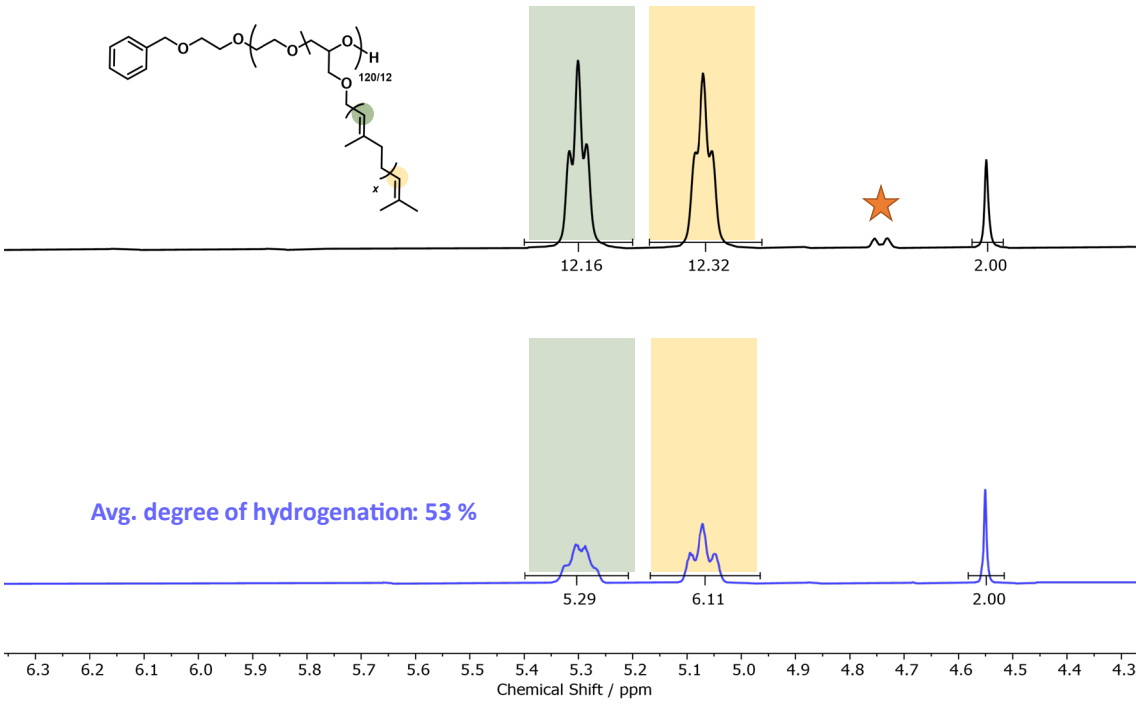

Figure 5: Stacked ^{1}H NMR spectra of P(EG$_{120}$-*co*-GeraGE$_{12}$) before (top) and after (bottom) hydrogenation employing PADA. The double bond with a deficiency of electrons (colored green, resonating at 5.30 ppm) undergoes hydrogenation with a slight preference. The orange star denotes the terminal double bond of the isomerized product and is not considered in the calculations.

This described method of producing diimide using PADA is suitable for post-polymerization hydrogenation, even with partial hydrogenation. We would like to emphasize that the structures presented are difficult to hydrogenate, both due to the trisubstituted double bonds and the attachment to a polymer chain. The reactivity of a double bond is lowered significantly by alkyl substitution.[61] For instance, the relative hydrogenation rate constant of 2-methyl-1-pentene, which represents a terminal disubstituted substrate, is 7.3 times higher than that of 2-methyl-2-butene, which is comparable to a terpene unit.[37,62] Additionally, upon an increase of acetic acid equivalents (> 2 equivalents), we observed a broadening of the molar mass distribution via SEC (Figure S78). Similar observations have been reported for the hydrogenation of polyisoprene-based polymers using *para*-toluenesulfonyl hydrazide, caused by the formation of *para*-toluene-sulfonic acid as a byproduct.[57] Ultimately, the diimide reduction of P(EG-*co*-TGE) copolymers requires further optimization, but PADA already shows good hydrogenation efficiencies of less substituted double

bonds in polymers in model experiments. Nevertheless, it is a particularly interesting method for the hydrogenation of amphiphilic structures, as facile purification is enabled due to the volatile coupling product, *i.e.*, carbon dioxide.

Conclusion

TGEs represent a bio-derived class of epoxide monomers, which yet have been hardly employed. The easy-to-synthesize nature and structural variety of terpenes lead to a versatile monomer platform for polyethers, polycarbonates, and polyester synthesis. We have demonstrated the successful copolymerization of EO with TGEs (PreGE, IsoPreGE, GeraGE, NerGE), introducing branched terpenyl side chains along the polyether backbone. Four systematic series of well-defined statistical copolymers with a TGE content up to 10 mol% have been prepared, maintaining aqueous solubility and crystallizability of PEG, while introducing backbone functionality. A molar mass range between 4 800 and 8 300 $g \cdot mol^{-1}$ was explored. Generally, the molar mass distribution showed low dispersities $Đ$ in the range of 1.05 – 1.13. As expected, the statistical distribution of the branched terpenyl side groups gradually reduced PEG crystallization with increasing TGE content. Thus, thermal properties can be tailored by varying the comonomer ratio. Melting points in the range of 14 to 40 °C were obtained. Only marginal differences in glass transition temperatures were observed, despite the differing side chain length.

In situ ^{1}H NMR kinetic investigations revealed a TGE reactivity trend and unraveled the copolymer microstructure. TGE reactivity only slightly decreases with increasing side chain length, flexibility, and hydrophobicity. Ideally random behavior was found for the EO/IsoPreGE comonomer pair, whereas HHFarGE features the strongest, but mild gradient in the copolyether series.

The unsaturated double bonds of the terpenyl side chains allow for post-polymerization modification.[33] Both modification reactions, thiol-ene click and hydrogenation, addressed the unsaturated double bonds (di- and trisubstituted) of the terpenyl side chains. A representative thiol-ene click reaction was performed using 2-mercaptoethanol on all four types of synthesized copolyethers, comprised of ~ 10 mol% of TGE units. We achieved full functionalization for all copolymers, however, the thiol equivalents had to be varied between 200 and 600, depending on the respective TGE side chain to prevent crosslinking. Recycling of the thiol equivalents was possible by up to 80%. Furthermore, the diimide reduction using PADA for side chain hydrogenation has been studied for the first time. Despite the difficulty of the hydrogenation of trisubstituted double bonds, we were able to achieve a hydrogenation of 53%, while the gaseous release of CO_2 as the coupling product did not require further purification.

In contrast to commonly reported *para*-toluenesulfonyl hydrazide for hydrogenation purposes, PADA may have been overlooked as a hydrogenation agent in previous research. However, if side chain double bonds are not desired, the utilization of fully hydrogenated TGEs may prove advantageous, given the low hydrogenation efficiency. While the subtle differences in the reactivity ratios of hydrogenated TGEs compared to their non-hydrogenated counterparts result in a slight gradient microstructure, the resulting copolyethers are likely to exhibit enhanced heat and oxidation resistance while minimizing crosslinking side reactions.

Altogether, we consider the extended TGE library as a versatile platform, allowing for the controlled synthesis of P(EG_n-*co*-TGE_m) copolymers as promising PEG derivatives of a partially bio-based nature. The structural variety and potential for postfunctionalization is promising for a diverse scope of applications, ranging from surfactants to polymeric drug carriers and microgels.[1,5,63,64]

Acknowledgments

The authors thank the NMR facility at Johannes Gutenberg University for extended measurement periods.

References

(1) Herzberger, J.; Niederer, K.; Pohlit, H.; Seiwert, J.; Worm, M.; Wurm, F. R.; Frey, H. Polymerization of Ethylene Oxide, Propylene Oxide, and Other Alkylene Oxides: Synthesis, Novel Polymer Architectures, and Bioconjugation. *Chem. Rev.* **2016**, *116* (4), 2170–2243. DOI: 10.1021/acs.chemrev.5b00441.

(2) Knop, K.; Hoogenboom, R.; Fischer, D.; Schubert, U. S. Poly(ethylene glycol) in drug delivery: pros and cons as well as potential alternatives. *Angew. Chem. Int. Ed.* **2010**, *49* (36), 6288–6308. DOI: 10.1002/anie.200902672.

(3) Fusco, S.; Borzacchiello, A.; Netti, P. A. Perspectives on: PEO-PPO-PEO Triblock Copolymers and their Biomedical Applications. *J. Bioact. Compat. Polym.* **2006**, *21* (2), 149–164. DOI: 10.1177/0883911506063207.

(4) Barteau, K. P.; Wolffs, M.; Lynd, N. A.; Fredrickson, G. H.; Kramer, E. J.; Hawker, C. J. Allyl Glycidyl Ether-Based Polymer Electrolytes for Room Temperature Lithium Batteries. *Macromolecules* **2013**, *46* (22), 8988–8994. DOI: 10.1021/ma401267w.

(5) Obermeier, B.; Wurm, F.; Mangold, C.; Frey, H. Multifunctional Poly(ethylene glycol)s. *Angew. Chem. Int. Ed.* **2011**, *50* (35), 7988–7997. DOI: 10.1002/anie.201100027.

(6) Mouzin, G.; Cousse, H.; Rieu, J.-P.; Duflos, A. A Convenient One-Step Synthesis of Glycidyl Ethers. *Synthesis* **1983** (02), 117–119. DOI: 10.1055/s-1983-30243.

(7) Verkoyen, P.; Frey, H. Long-Chain Alkyl Epoxides and Glycidyl Ethers: An Underrated Class of Monomers. *Macromol. Rapid Commun.* **2020**, *41* (15), e2000225. DOI: 10.1002/marc.202000225.

(8) Verkoyen, P.; Johann, T.; Blankenburg, J.; Czysch, C.; Frey, H. Polymerization of long chain alkyl glycidyl ethers: a platform for micellar gels with tailor-made melting points. *Polym. Chem.* **2018**, *9* (44), 5327–5338. DOI: 10.1039/C8PY01312H.

(9) Della Monica, F.; Kleij, A. W. From terpenes to sustainable and functional polymers. *Polym. Chem.* **2020**, *11* (32), 5109–5127. DOI: 10.1039/d0py00817f.

(10) Schüttner, S.; Krappel, M.; Koziol, M.; Marquart, L.; Schneider, I.; Sottmann, T.; Frey, H. Anionic Ring-Opening Copolymerization of Farnesyl Glycidyl Ether: Fast Access to Terpenoid-Derived Amphiphilic Polyether Architectures. *Macromolecules* **2023**, *56* (17), 6928–6940. DOI: 10.1021/acs.macromol.3c00999.

(11) Li, Y.; Ozden, A.; Leow, W. R.; Ou, P.; Huang, J. E.; Wang, Y.; Bertens, K.; Xu, Y.; Liu, Y.; Roy, C.; Jiang, H.; Sinton, D.; Li, C.; Sargent, E. H. Redox-mediated electrosynthesis of ethylene oxide from CO2 and water. *Nat. Catal.* **2022**, *5* (3), 185–192. DOI: 10.1038/s41929-022-00749-8.

(12) Pu, T.; Tian, H.; Ford, M. E.; Rangarajan, S.; Wachs, I. E. Overview of Selective Oxidation of Ethylene to Ethylene Oxide by Ag Catalysts. *ACS Catal.* **2019**, *9* (12), 10727–10750. DOI: 10.1021/acscatal.9b03443.

(13) Shukla, G.; Ferrier, R. C. The versatile, functional polyether, polyepichlorohydrin: History, synthesis, and applications. *J. Polym. Sci.* **2021**, *14* (17), 243. DOI: 10.1002/pol.20210514.

(14) Bell, B. M.; Briggs, J. R.; Campbell, R. M.; Chambers, S. M.; Gaarenstroom, P. D.; Hippler, J. G.; Hook, B. D.; Kearns, K.; Kenney, J. M.; Kruper, W. J.; Schreck, D. J.; Theriault, C. N.; Wolfe, C. P. Glycerin as a Renewable Feedstock for Epichlorohydrin Production. The GTE Process. *Clean Soil Air Water* **2008**, *36* (8), 657–661. DOI: 10.1002/clen.200800067.

(15) Zhu, Y.; Romain, C.; Williams, C. K. Sustainable polymers from renewable resources. *Nature* **2016**, *540* (7633), 354–362. DOI: 10.1038/nature21001.

(16) Biermann, U.; Bornscheuer, U. T.; Feussner, I.; Meier, M. A. R.; Metzger, J. O. Fatty Acids and their Derivatives as Renewable Platform Molecules for the Chemical Industry. *Angew. Chem. Int. Ed.* **2021**, *60* (37), 20144–20165. DOI: 10.1002/anie.202100778.

(17) Meier, M. A. R.; Metzger, J. O.; Schubert, U. S. Plant oil renewable resources as green alternatives in polymer science. *Chem. Soc. Rev.* **2007**, *36* (11), 1788–1802. DOI: 10.1039/b703294c.

(18) Konieczynska, M. D.; Lin, X.; Zhang, H.; Grinstaff, M. W. Synthesis of Aliphatic Poly(ether 1,2-glycerol carbonate)s via Copolymerization of CO2 with Glycidyl Ethers Using a Cobalt Salen Catalyst and Study of a Thermally Stable Solid Polymer Electrolyte. *ACS Macro Lett.* **2015**, *4* (5), 533–537. DOI: 10.1021/acsmacrolett.5b00193.

(19) Wahlen, C.; Frey, H. Anionic Polymerization of Terpene Monomers: New Options for Bio-Based Thermoplastic Elastomers. *Macromolecules* **2021**, *54* (16), 7323–7336. DOI: 10.1021/acs.macromol.1c00770.

(20) Kleij, A. W. Across the Board: Arjan Kleij. *ChemSusChem* **2018**, *11* (17), 2842–2844. DOI: 10.1002/cssc.201801648.

(21) Stadler, B. M.; Wulf, C.; Werner, T.; Tin, S.; Vries, J. G. de. Catalytic Approaches to Monomers for Polymers Based on Renewables. *ACS Catal.* **2019**, *9* (9), 8012–8067. DOI: 10.1021/acscatal.9b01665.

(22) Ruzicka, L. The isoprene rule and the biogenesis of terpenic compounds. *Experientia* **1953**, *9* (10), 357–367. DOI: 10.1007/BF02167631.

(23) Hillier, S. G.; Lathe, R. Terpenes, hormones and life: isoprene rule revisited. *J. Endocrinol.* **2019**, *242* (2), R9-R22. DOI: 10.1530/JOE-19-0084.

(24) Breitmeier, E. *Terpenes: Flavors, Fragrances, Pharmaca, Pheromones*; Wiley-VCH, 2006.

(25) Firdaus, M.; Montero de Espinosa, L.; Meier, M. A. R. Terpene-Based Renewable Monomers and Polymers via Thiol–Ene Additions. *Macromolecules* **2011**, *44* (18), 7253–7262. DOI: 10.1021/ma201544e.

(26) Morrison, S. D.; Liskamp, R. M. J.; Prunet, J. Tailoring Polyethers for Post-polymerization Functionalization by Cross Metathesis. *Org. Lett.* **2018**, *20* (8), 2253–2256. DOI: 10.1021/acs.orglett.8b00595.

(27) Johann, T.; Houck, H. A.; Dinh, T.; Kemmer-Jonas, U.; Du Prez, F. E.; Frey, H. Multi-olefin containing polyethers and triazolinediones: a powerful alliance. *Polym. Chem.* **2019**, *10* (34), 4699–4708. DOI: 10.1039/C9PY00718K.

(28) Schüttner, S.; Gardiner, C.; Petrov, F. S.; Fotaras, N.; Preis, J.; Floudas, G.; Frey, H. Biobased Thermoplastic Elastomers Derived from Citronellyl Glycidyl Ether, CO 2 , and Polylactide. *Macromolecules* **2023**, *56* (20), 8247–8259. DOI: 10.1021/acs.macromol.3c01329.

(29) Holzmüller, P.; Gardiner, C.; Preis, J.; Frey, H. CO_2 -Based Polycarbonates with Low Glass Transition Temperatures Sourced from Long-Chain Terpenes. *Macromolecules* **2024**, *57* (11), 5358–5367. DOI: 10.1021/acs.macromol.4c00349.

(30) Heatley, F.; Yu, G.; Booth, C.; Blease, T. G. Determination of reactivity ratios for the anionic copolymerization of ethylene oxide and propylene oxide in bulk. *Eur. Polym. J.* **1991**, *27* (7), 573–579. DOI: 10.1016/0014-3057(91)90138-E.

(31) Herzberger, J.; Leibig, D.; Liermann, J. C.; Frey, H. Conventional Oxyanionic versus Monomer-Activated Anionic Copolymerization of Ethylene Oxide with Glycidyl Ethers: Striking Differences in Reactivity Ratios. *ACS Macro Lett.* **2016**, *5* (11), 1206–1211. DOI: 10.1021/acsmacrolett.6b00701.

(32) Lee, B. F.; Wolffs, M.; Delaney, K. T.; Sprafke, J. K.; Leibfarth, F. A.; Hawker, C. J.; Lynd, N. A. Reactivity ratios, and mechanistic insight for anionic ring-opening copolymerization of epoxides. *Macromolecules* **2012**, *45* (9), 3722–3731. DOI: 10.1021/ma300634d.

(33) Gauthier, M. A.; Gibson, M. I.; Klok, H.-A. Synthesis of functional polymers by post-polymerization modification. *Angew. Chem. Int. Ed.* **2009**, *48* (1), 48–58. DOI: 10.1002/anie.200801951.

(34) Iha, R. K.; Wooley, K. L.; Nyström, A. M.; Burke, D. J.; Kade, M. J.; Hawker, C. J. Applications of orthogonal “click” chemistries in the synthesis of functional soft materials. *Chem. Rev.* **2009**, *109* (11), 5620–5686. DOI: 10.1021/cr900138t.

(35) Lowe, A. B. Thiol–ene “click” reactions and recent applications in polymer and materials synthesis: a first update. *Polym. Chem.* **2014**, *5* (17), 4820–4870. DOI: 10.1039/C4PY00339J.

(36) McManus, N. T.; Rempel, G. L. Chemical Modification of Polymers: Catalytic Hydrogenation and Related Reactions. *J. Macromol. Sci., Polym. Rev.* **1995**, *35* (2), 239–285. DOI: 10.1080/15321799508009638.

(37) Charette, A.; Bode, J.; Rovis, T.; Shenvi, R., Eds. *Encyclopedia of reagents for organic synthesis*; Wiley, 1995.

(38) Pasto, D. J.; Taylor, R. T. Reduction with Diimide. In *Organic reactions*; Wiley Online Library, 2004; pp 91–155. DOI: 10.1002/0471264180.or040.02.

(39) Lee, B. F.; Kade, M. J.; Chute, J. A.; Gupta, N.; Campos, L. M.; Fredrickson, G. H.; Kramer, E. J.; Lynd, N. A.; Hawker, C. J. Poly(allyl glycidyl ether)-A versatile and functional polyether platform. *J. Polym. Sci., Part A: Polym. Chem.* **2011**, *49* (20), 4498–4504. DOI: 10.1002/pola.24891.

(40) Obermeier, B.; Frey, H. Poly(ethylene glycol-co-allyl glycidyl ether)s: a PEG-based modular synthetic platform for multiple bioconjugation. *Bioconjug. Chem.* **2011**, *22* (3), 436–444. DOI: 10.1021/bc1004747.

(41) Worm, M.; Leibig, D.; Dingels, C.; Frey, H. Cleavable Polyethylene Glycol: 3,4-Epoxy-1-butene as a Comonomer to Establish Degradability at Physiologically Relevant pH. *ACS Macro Lett.* **2016**, *5* (12), 1357–1363. DOI: 10.1021/acsmacrolett.6b00735.

(42) Natalello, A.; Werre, M.; Alkan, A.; Frey, H. Monomer Sequence Distribution Monitoring in Living Carbanionic Copolymerization by Real-Time 1 H NMR Spectroscopy. *Macromolecules* **2013**, *46* (21), 8467–8471. DOI: 10.1021/ma401847y.

(43) Blankenburg, J.; Kersten, E.; Maciol, K.; Wagner, M.; Zarbakhsh, S.; Frey, H. The poly(propylene oxide-*co*-ethylene oxide) gradient is controlled by the polymerization method: determination of reactivity ratios by direct comparison of different copolymerization models. *Polym. Chem.* **2019**, *10* (22), 2863–2871. DOI: 10.1039/C9PY00500E.

(44) Wall, F. T. The Structure of Vinyl Copolymers. *J. Am. Chem. Soc.* **1941**, *63* (7), 1862–1866. DOI: 10.1021/ja01852a016.

(45) Beckingham, B. S.; Sanoja, G. E.; Lynd, N. A. Simple and Accurate Determination of Reactivity Ratios Using a Nonterminal Model of Chain Copolymerization. *Macromolecules* **2015**, *48* (19), 6922–6930. DOI: 10.1021/acs.macromol.5b01631.

(46) Jaacks, V. A novel method of determination of reactivity ratios in binary and ternary copolymerizations. *Makromol. Chem.* **1972**, *161* (1), 161–172. DOI: 10.1002/macp.1972.021610110.

(47) Dreier, P.; Matthes, R.; Barent, R. D.; Schüttner, S.; Müller, A. H. E.; Frey, H. In Situ Kinetics Reveal the Influence of Solvents and Monomer Structure on the Anionic Ring-Opening Copolymerization of Epoxides. *Macromol. Chem. Phys.* **2023**, *224* (1), 2200209. DOI: 10.1002/macp.202200209.

(48) Hans, M.; Keul, H.; Moeller, M. Chain transfer reactions limit the molecular weight of polyglycidol prepared via alkali metal based initiating systems. *Polymer* **2009**, *50* (5), 1103–1108. DOI: 10.1016/j.polymer.2009.01.012.

(49) Guibé, F. Allylic protecting groups and their use in a complex environment part I: Allylic protection of alcohols. *Tetrahedron* **1997**, *53* (40), 13509–13556. DOI: 10.1016/S0040-4020(97)00524-3.

(50) Vatèle, J.-M. The prenyl group: a versatile hydroxy protecting group, removable chemoselectively under mild conditions. *Tetrahedron* **2002**, *58* (28), 5689–5698. DOI: 10.1016/S0040-4020(02)00539-2.

(51) Wuts, P. G. M. *Greene's protective groups in organic synthesis*, 4. ed.; Wiley-Interscience, 2007.

(52) Prosser, T. J. The Rearrangement of Allyl Ethers to Propenyl Ethers. *J. Am. Chem. Soc.* **1961**, *83* (7), 1701–1704. DOI: 10.1021/ja01468a035.

(53) Fox, T. G. Influence of diluent of copolymer composition on the glass temperature of a polymer system. *Bull. Am. Phys. Soc.* **1956**, *1*, 123–125.

(54) Hoyle, C. E.; Lee, T. Y.; Roper, T. Thiol-enes: Chemistry of the past with promise for the future. *J. Polym. Sci., Part A: Polym. Chem.* **2004**, *42* (21), 5301–5338. DOI: 10.1002/pola.20366.

(55) Lowe, A. B. Thiol-ene "click" reactions and recent applications in polymer and materials synthesis. *Polym. Chem.* **2010**, *1* (1), 17–36. DOI: 10.1039/B9PY00216B.

(56) Matic, A.; Schlaad, H. Thiol-ene photofunctionalization of 1,4-polymyrcene. *Polym. Int.* **2018**, *67* (5), 500–505. DOI: 10.1002/pi.5534.

(57) Hahn, S. F. An improved method for the diimide hydrogenation of butadiene and isoprene containing polymers. *J. Polym. Sci., Part A: Polym. Chem.* **1992**, *30* (3), 397–408. DOI: 10.1002/pola.1992.080300307.

(58) Ballini, R.; Marcantoni, E.; Petrini, M. A new general synthesis of sulfones from alkyl or aryl halides and p-toluenesulfonhydrazide. *Tetrahedron* **1989**, *45* (21), 6791–6798. DOI: 10.1016/S0040-4020(01)89148-1.

(59) Schunicht, C.; Biffis, A.; Wulff, G. Microgel-supported Oxazaborolidines: Novel Catalysts for Enantioselective Reductions. *Tetrahedron* **2000**, *56* (12), 1693–1699. DOI: 10.1016/S0040-4020(00)00072-7.

(60) Groves, J. T.; Ma, K. W. Carbon cluster compounds. Generation and reorganization of the homobullvalenyl cation, an 11-fold degenerate species. *J. Am. Chem. Soc.* **1977**, *99* (12), 4076–4082. DOI: 10.1021/ja00454a028.

(61) Back, R. A. The preparation, properties and reactions of diimide. *Res. Chem. Intermed.* **1984**, *5* (3), 293–323. DOI: 10.1007/BF03155648.

(62) Garbisch, E. W.; Schildcrout, S. M.; Patterson, D. B.; Sprecher, C. M. Strain Effects. II. Diimide Reductions of Olefins. *J. Am. Chem. Soc.* **1965**, *87* (13), 2932–2944. DOI: 10.1021/ja01091a025.

(63) Liu, Y.; Hou, W.; Sun, H.; Cui, C.; Zhang, L.; Jiang, Y.; Wu, Y.; Wang, Y.; Li, J.; Sumerlin, B. S.; Liu, Q.; Tan, W. Thiol-ene click chemistry: a biocompatible way for orthogonal bioconjugation of colloidal nanoparticles. *Chem. Sci.* **2017**, *8* (9), 6182–6187. DOI: 10.1039/C7SC01447C.

(64) Fraser, A. K.; Ki, C. S.; Lin, C.-C. PEG-Based Microgels Formed by Visible-Light-Mediated Thiol-Ene Photo-Click Reactions. *Macromol. Chem. Phys.* **2014**, *215* (6), 507–515. DOI: 10.1002/macp.201300731.

Supporting Information

Experimental Section

Reagents

All chemicals and solvents were acquired from commercial suppliers (*Sigma-Aldrich, Fluka, Alfa Aesar, Acros, TCI*) and used without prior purification, unless otherwise stated. Deuterated solvents were purchased from *Deutero GmbH*. Ethylene oxide (EO) was obtained by *Air Liquide*. All terpenoids were purchased from *Sigma-Aldrich*. The long-chain terpenyl glycidyl ethers (TGEs), farnesyl glycidyl ether (FarGE) and hexahydrofarnesyl glycidyl ether (HHFarGE), were dried azeotropically with benzene overnight under reduced pressure. All other TGEs were dried by cryo-transfer after stirring over calcium hydride (CaH_2) for 2 h prior to polymerizaton. Tetrahydrofuran (THF) was dried over diphenylhexyllithium (adduct of sec-butyllithium and 1,1-diphenylethylene), degassed by three freeze-pump-thaw cycles and stored under vacuum until distilled into the polymerization flask. Anhydrous dimethyl sulfoxide (DMSO) stored over molecular sieves was used for the statistical copolymerizations. Prior to all *in situ* ^{1}H NMR kinetics, deuterated THF (THF-d_8) was cryo-transferred after stirring over CaH_2 overnight. For each kinetic, a new bottle of deuterated DMSO (DMSO-d_6) was utilized to ensure the absence of water residues.

Instrumentation

Nuclear Magnetic Resonance (NMR) Spectroscopy

Standard NMR spectra were recorded at 23 °C either on a *Bruker Avance II HD 400* spectrometer or on a *Bruker Advance III HD 300* spectrometer, referenced internally to residual protium signals of the deuterated solvent (^{1}H NMR spectra) and the deuterated solvent itself (^{13}C NMR spectra).

2D NMR analysis and *in situ* ^{1}H NMR copolymerization kinetics were investigated on a Bruker Avance III HD 400 spectrometer operated at 400 MHz (5 mm BBFO-SmartProbe (Z-gradient), an ATM and a SampleXPress 60 auto sampler). Diffusion-Ordered Spectroscopy (DOSY) spectra were collected using a *Bruker Avance III HD 400* spectrometer at 23 °C. Spectra were processed using *MestReNova* software 14.2.0. NMR spectroscopy data is reported as follows: chemical shift, multiplicity and integration. Spectra annotation uses lowercase letters for proton signals and capital letters for carbon signals.

Fourier-Transformations-Infrared Spectroscopy (FT-IR Spectroscopy)

FT-IR spectroscopy was performed on a *Nicolet* iS10 FT-IR spectrometer (*Thermo Scientific*, Waltham, MA, USA) equipped with a diamond ATR unit. Spectra were recorded in a frequency range of 650–3500 cm^{-1}.

Size Exclusion Chromatography (SEC)

SEC analysis was performed with an *Agilent* 1100 series SEC system with a HEMA 300/100/40 Å column cascade, equipped with UV (254 nm) and RI detectors. Measurements were conducted with a flow rate of 1 $mL \cdot min^{-1}$ with DMF as eluent (with 1 $g \cdot mL^{-1}$ lithium bromide) at 50 °C. Toluene was used as a reference for the baseline. The SEC calibration was carried out with poly(ethylene glycol) standards provided from *Polymer Standard Service* (PSS). *PSS WinGPC UniChrom* software was used for all data recording and processing.

Matrix-assisted Laser Desorption Ionization Time-of-Flight (MALDI-ToF) Mass Spectrometry

MALDI-ToF was conducted on a *Bruker autoflex maX MALDI-ToF-MS/MS* with multi target plate in linear mode. *Trans*-2-[3-(4-*tert*-Butylphenyl)-2-methyl-2-propenylidene]malononitrile was used as a matrix (DCTB) and potassium trifluoroacetate (KTFA) as a salt additive.

Differential Scanning Calorimetry (DSC)

DSC measurements of the polymer samples were carried out on a *DSC 250*, *TA Instrument*, applying indium and *n*-octane as calibration standard. After drying all samples azeotropically, each sample was sealed in an aluminum pan and measured against an empty pan as reference under a nitrogen atmosphere. The DSC samples were cooled from 40 °C to -90 °C and then heated to 100 °C, followed by an additional cooling and heating cycle in the temperature range of -90 °C and 100 °C. Heating and cooling cylces were set to a rate of 10 °C/min. All melting temperatures (T_ms) and glass transition temperatures (T_gs) values were evaluated from the second heating cycle to ensure the removal of the thermal history.

Gas Chromatography (GC)

GC measurements were conducted using a Shimadzu GC-2010 (*Shimadzu*, Japan) with a *VWR Avantor™ Hichrom HI-5 MS* column (*VWR International GmbH*, Germany). Dimensions of the column: Length 30 m, inner diameter 0.25 mm, coating thickness 0.25 µm. Carrier gas hydrogen. Injector temperature 250 °C, start temperature 27 °C for 3 min. Heating rate 1 °C/min to 32 °C, heating rate 40 °C/min to 300 °C, hold for 4 min. Detector temperature 330 °C. Total time 18.7 min.

Monomer Synthesis

The phase transfer catalysis by Mouzin et al. was modified subject to the terpenyl side chain targeted.[1,2] The presented synthesis for TGEs of hemiterpenoids has been altered to previously reported synthetic approaches.

Synthesis of TGEs from hemiterpenoids

The following synthesis protocol was used for the short-chain TGEs, namely prenyl glycidyl ether (PreGE), isoprenyl glycidyl ether (IsoPreGE) and dihydro glycidyl ether (DHPreGE).

An aqueous sodium hydroxide solution (33 % (*w*/*w*) solution, $V_{solution}$ = 150.5 mL; NaOH: 50.14 g, 1.25 mol, 12.7 equiv.), tetrabutylammonium hydrogen sulfate (TBAHS, 1.89 g, 0.006 mol, 0.04 equiv.) and epichlorohydrin (ECH, 57.9 mL, 68.32 g, 0.738 mol, 5.30 equiv.) were added to a three-necked flask, equipped with a dropping funnel and mechanical stirrer. The mixture was cooled to 0 °C using an ice bath and the prenol (3-methyl-2-buten-1-ol, 13.6 mL, 12.00 g, 0.139 mol, 1 equiv.) was added dropwise over 90 min whilst vigorously stirring the suspension. Note that it is imperative to keep the reaction temperature below 5 °C to avoid the augmented formation of side products. Stirring continued at 0 °C for 3.5 h, followed by another 90 min at r.t.. The reaction was quenched with ice and the crude product was extracted with diethyl ether (DEE). The combined organic phases were washed with brine until a neutral pH value was obtained and dried using magnesium sulfate ($MgSO_4$). DEE was removed under reduced pressure and a first distillation at 25 mbar enabled the removal of undesired side products. Fractionated distillation at high vacuum (p= 6·10^{-3} mbar, $T_{b,PreGE}$ = 30 - 33 °C) afforded PreGE as a colorless liquid in yields of 64 %.

Prenyl glycidyl ether

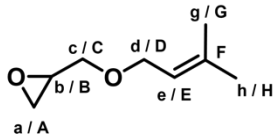

Yield: 64 %

Purification by distillation: p = 6·10^{-3} mbar, $T_{b,PreGE}$ = 30 - 33 °C

^{1}H NMR (400 MHz, chloroform-d_1): δ (ppm) = 5.26 (tdq, J = 7.1, 2.8, 1.4 Hz, 1H, H_e), 4.01 – 3.86 (m, 2H, H_d), 3.59 (dd, J = 11.4, 3.2 Hz, 1H, H_c), 3.29 (dd, J = 11.4, 5.8 Hz, 1H, H_c), 3.05 (ddt, J = 5.9, 4.2,

2.9 Hz, 1H, H_b), 2.69 (dd, *J* = 5.1, 4.1 Hz, 1H, H_a), 2.51 (dd, *J* = 5.1, 2.7 Hz, 1H, H_a), 1.66 (s, 3H, H_g), 1.59 (s, 3H, H_h).

^{13}C NMR (100 MHz, chloroform-d_1): δ (ppm) = 137.16 (C_F), 120.72 (C_E), 70.55 (C_C), 67.57 (C_D), 50.71 (C_B), 44.20 (C_A), 25.63 (C_G), 17.86 (C_H).

Isoprenyl glycidyl ether

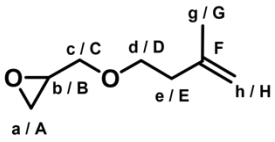

Yield: 59 %

Purification by distillation: $p = 11 \cdot 10^{-3}$ mbar, $T_{b,IsoPreGE} = 32 - 35$ °C

^{1}H NMR (300 MHz, chloroform-d_1): δ (ppm) = 4.81 – 4.67 (d, 2H, H_h), 3.72 (dd, *J* = 11.6, 3.0 Hz, 1H, H_d), 3.59 (qt, *J* = 9.4, 6.9 Hz, 2H, H_c), 3.37 (dd, *J* = 11.6, 5.8 Hz, 1H, H_d), 3.12 (ddt, *J* = 5.8, 4.1, 2.9 Hz, 1H, H_b), 2.77 (dd, *J* = 5.1, 4.1 Hz, 1H, H_a), 2.58 (dd, *J* = 5.0, 2.7 Hz, 1H, H_a), 2.35 – 2.23 (m, 2H, H_e), 1.73 (s, 3H, H_g).

^{13}C NMR (75 MHz, chloroform-d_1): δ (ppm) = 142.72 (C_F), 111.65 (C_H), 71.56 (C_C), 69.98 (C_D), 50.94 (C_B), 44.33 (C_A), 37.82 (C_E), 22.74 (C_G).

Dihydroprenyl glycidyl ether

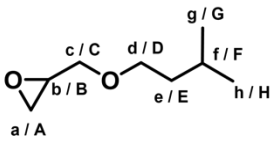

Yield: 51 %

Purification by distillation: $p = 3.5 \cdot 10^{-2}$ mbar, $T_{b,DHPreGE} = 27 – 28$ °C

^{1}H NMR (300 MHz, chloroform-d_1): δ (ppm) = 3.68 (dd, *J* = 11.5, 3.1 Hz, 1H, H_c), 3.58 – 3.40 (m, 2H, H_d), 3.35 (dd, *J* = 11.5, 5.8 Hz, 1H, H_c), 3.11 (ddt, *J* = 5.8, 4.2, 2.9 Hz, 1H, H_b), 2.76 (dd, *J* = 5.1, 4.1 Hz,

1H, H_a), 2.58 (dd, *J* = 5.1, 2.7 Hz, 1H, H_a), 1.81 – 1.57 (m, 1H, H_f), 1.46 (q, *J* = 6.7 Hz, 2H, H_e), 0.88 (d, *J* = 6.6 Hz, 6H, H_g, H_h).

^{13}C NMR (75 MHz, chloroform-d_1): δ (ppm) = 71.56 (C_C), 70.10 (C_D), 50.98 (C_B), 44.38 (C_A), 38.56 (C_E), 25.10 (C_F), 22.71 (C_G, C_H).

Synthesis of TGEs from mono- and sesquiterpenoids

The procedure refers to the synthesis of geranyl glycidyl ether (GeraGE), neryl glycidyl ether (NerGE), tetrahydrogeranyl glycidyl ether (THGeraGE) and hexahydrofarnesyl glycidyl ether (HHFarGE).[2,3]

A three-necked flask, equipped with a mechanical stirrer and dropping funnel, was charged with an aqueous sodium hydroxide solution (50 % (*w*/*w*) solution, $V_{solution}$ = 96.26 mL; NaOH: 48.13 g, 1.20 mol, 12.7 equiv.), tetrabutylammonium hydrogen sulfate (TBAHS, 1.29 g, 0.004 mol, 0.04 equiv.) and epichlorohydrin (ECH, 39.38 mL, 46.47 g, 0.738 mol, 5.30 equiv.). The reaction mixture was cooled to 0 °C with an ice bath, followed by the dropwise addition of tetrahydrogeraniol (3,7-dimethyloctan-1-ol, 15.0 mL, 17.05 g, 0.095 mol, 1 equiv.) within 30 min under vigorous stirring. Stirring was continued at r.t. until complete consumption of the terpenoid (20 – 24 h). After quenching the reaction with ice, the crude product was extracted with DEE and the combined organic phases were washed with brine until neutrality, then dried over $MgSO_4$. DEE was removed using rotary evaporation and subsequent Kugelrohr distillation served as a first purification step. A high vacuum distillation (p = 5 – 12 ·10^{-3} mbar) enables the removal of potential side products (3-Chloroallyl glycidyl ether (3-Chloro-AGE), diglycidyl ether). Finally, Kugelrohr distillation (p = 12·10^{-3} mbar, $T_{Kugelrohr,THGeraGE}$ = 130 – 135 °C) isolated purified THGeraGE as a colorless liquid in yields of 81%.

As previously established for long-chain TGEs, we pretreated the TGEs with methyl iodide (MeI) and sodium hydride (NaH), deactivating any residual protic impurities while extensively drying the monomer.[2] Therefore, a flame-dried Schlenk flask, charged with NaH (0.22 equiv.), was cooled to 0 °C, followed by the addition of the TGE (1.00 equiv.). MeI (0.10 equiv.) was syringed into the flask after 2 h and the reaction mixture was allowed to warm up to r.t.. After 22 h, the mixture was diluted with hexane and filtered multiple times to remove accrued sodium iodide. The TGEs were isolated in quantitative yields after Kugelrohr distillation.

Geranyl glycidyl ether

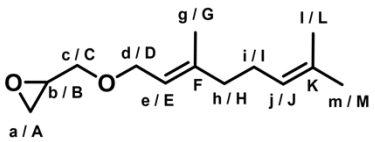

Yield: 83%

Purification by Kugelrohr distillation: $p = 7 \cdot 10^{-3}$ mbar, $T_{\text{Kugelrohr, GeraGE}} = 130 – 135$ °C

^{1}H NMR (400 MHz, chloroform-d_1): δ (ppm) = 5.32 (ddq, J = 6.8, 5.4, 1.3 Hz, 1H, H_e), 5.06 (ddp, J = 6.9, 5.7, 1.5 Hz, 1H, H_j), 4.10 – 3.95 (m, 2H, H_d), 3.65 (dd, J = 11.4, 3.2 Hz, 1H, H_c), 3.36 (dd, J = 11.4, 5.8 Hz, 1H, H_c), 3.12 (ddt, J = 5.9, 4.2, 3.0 Hz, 1H, H_b), 2.76 (dd, J = 5.1, 4.1 Hz, 1H, H_a), 2.57 (dd, J = 5.1, 2.7 Hz, 1H, H_a), 2.13 – 1.96 (m, 4H, H_i, H_h), 1.64 (dt, J = 2.3, 1.2 Hz, 6H, H_g, H_l), 1.57 (d, J = 1.4 Hz, 3H, H_m).

^{13}C NMR (100 MHz, chloroform-d_1): δ (ppm) = 140.64 (C_F), 131.66 (C_K), 123.98 (C_J), 120.53 (C_E), 70.63 (C_C), 67.77 (C_D), 50.89 (C_B), 44.45 (C_A), 39.62 (C_H), 26.37 (C_I), 25.71 (C_M), 17.70 (C_L), 16.49 (C_G).

Neryl glycidyl ether

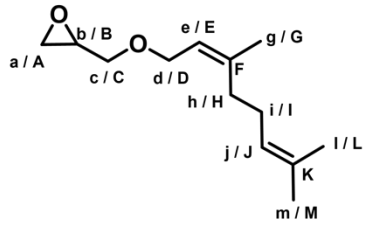

Yield: 81%

Purification by Kugelrohr distillation: $p = 7 \cdot 10^{-3}$ mbar, $T_{\text{Kugelrohr, NerGE}} = 135 – 145$ °C

^{1}H NMR (400 MHz, chloroform-d_1): δ (ppm) = 5.35 (tq, J = 6.9, 1.5 Hz, 1H, H_e), 5.08 (ttd, J = 5.9, 3.0, 1.5 Hz, 1H, H_j), 4.09 – 3.94 (m, 2H, H_d), 3.66 (dd, J = 11.3, 3.3 Hz, 1H, H_c), 3.38 (dd, J = 11.3, 5.8 Hz, 1H, H_c), 3.14 (ddt, J = 5.9, 4.1, 3.0 Hz, 1H, H_b), 2.78 (dd, J = 5.0, 4.1 Hz, 1H, H_a), 2.59 (dd, J = 5.0, 2.7 Hz, 1H, H_a),

2.12 – 1.99 (m, 4H, H_h, H_i), 1.74 (s, 3H, H_g), 1.68 (s, 3H, H_m), 1.59 (s, 3H, H_l).

^{13}C NMR (100 MHz, chloroform-d_1): δ (ppm) = 140.97 (C_F), 132.08 (C_K), 123.90 (C_J), 121.59 (C_E), 70.79 (C_C), 67.60 (C_D), 50.97 (C_B), 44.56 (C_A), 32.35 (C_H), 26.79 (C_I), 25.80 (C_M), 23.59 (C_G), 17.74 (C_L).

Tetrahydrogeranyl glycidyl ether

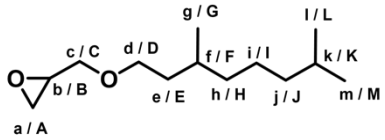

Yield: 81 %

Purification by Kugelrohr distillation: p = 12·10^{-3} mbar, $T_{Kugelrohr,THGeraGE}$ = 130 – 135 °C

^{1}H NMR (300 MHz, chloroform-d_1): δ (ppm) = 3.71 (dt, J = 11.5, 2.9 Hz, 1H, H_c), 3.63 – 3.42 (m, 2H, H_d), 3.38 (ddd, J = 11.5, 5.8, 3.0 Hz, 1H, H_c), 3.15 (ddt, J = 5.8, 4.1, 2.9 Hz, 1H, H_b), 2.80 (dd, J = 5.1, 4.1 Hz, 1H, H_a), 2.61 (dd, J = 5.1, 2.7 Hz, 1H, H_a), 1.73 – 1.01 (m, 8H, H_e, H_f, H_h, H_i, H_j, H_k), 0.88 (dd, J = 6.6, 5.2 Hz, 9H, H_g, H_l, H_m).

^{13}C NMR (75 MHz, chloroform-d_1): δ (ppm) = 71.59 (C_C), 70.07 (C_D), 51.00 (C_B), 44.41 (C_A), 39.36 (C_J), 37.46 (C_H), 36.79 (C_E), 29.91 (C_F), 28.06 (C_K), 24.76 (C_I), 22.80 (C_M, C_L), 19.76 (C_G).

Hexahydrofarnesyl glycidyl ether

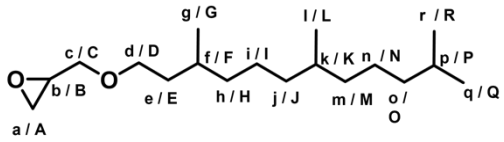

Yield: 78 %

Purification by Kugelrohr distillation: p = 5·10^{-3} mbar, $T_{Kugelrohr,HHFarGE}$ = 160 °C

^{1}H NMR (400 MHz, chloroform-d_1): δ (ppm) = 3.70 (dt, J = 11.5, 3.4 Hz, 1H, H_c), 3.60 – 3.43 (m, 2H, H_d), 3.38 (ddd, J = 11.5, 5.8, 4.2 Hz, 1H, H_c), 3.14 (ddt, J = 5.8, 4.1, 2.9 Hz, 1H, H_b), 2.79 (dd, J = 5.1, 4.1 Hz, 1H, H_a), 2.60 (ddd, J = 5.1, 2.8, 0.9 Hz, 1H, H_a), 1.70 – 0.96 (m, H_e, H_f, H_h, H_i, H_j, H_k, H_m, H_n, H_o), 0.96 – 0.78 (m, H_g, H_l H_r, H_q).

^{13}C NMR (100 MHz, chloroform-d_1): δ (ppm) = 71.63 (C_C), 70.17, 70.14 (C_D), 51.05 (C_B), 44.50, 44.49 (C_A), 39.50 (C_O), 37.63, 37.59 (C_M), 37.51 (C_H), 37.47, 37.40 (C_J), 36.88, 36.80, (C_E), 32.91 (C_K), 30.00, 29.99, 29.97 (C_F), 28.12 (C_P), 24.96, 24.93 (C_N), 24.49 (C_I), 22.86, 22.77 (C_Q, C_R), 19.88, 19.84, 19.81, 19.78 (C_G, C_L).

Polymerization Procedures

Synthesis procedure for statistical copolymerization of TGEs with EO

The statistical copolymerization of TGEs and EO was conducted in an equal manner for all epoxide monomers applied. In the following, the general polymerization procedure is exemplified for P(EG_{120}-*co*-$GeraGE_{12}$) (Table 1, entry 12). In a flame-dried anionic polymerization flask, cesium hydroxide monohydrate (95.4 mg, 0.57 mmol, 0.9 equiv.) and 2-(benzyloxy)ethanol (91.0 mg, 0.59 mmol, 1.0 equiv., BzEtOH), were suspended in benzene (10 mL) under an argon atmosphere. After stirring the mixture for 1 h at 60 °C, the removal of benzene under reduced pressure afforded the partially deprotonated initiator salt. Subsequently, the dried initiator was dissolved in anhydrous DMSO (0.80 mL) and tetrahydrofuran (THF, 4.2 mL) (V_{DMSO}/V_{THF}=1:5) and stirred for 20 min at r.t.. THF was added via cryo-transfer to remove protic stabilizers. The reaction mixture was cooled to -82 °C using an ethanol/liquid nitrogen bath and previously dried GeraGE (1.63 mL, 1.43 g, 6.82 mmol, 11.4 equiv.) was syringed into the flask. Quantification of EO (2.82 mL, 2.70 g, 61.3 mmol, 102.6 equiv.) was realized via distillation into a graduated ampule under vacuum, followed by a cryo-transfer into the cooled polymerization flask. The polymerization was undertaken at 40 °C for 24 h and terminated with an excess of methanol (MeOH). All solvents were evaporated under reduced pressure and dialysis (MWCO = 1000 g·mol^{-1}) against a Milli-Q® water/MeOH mixture (V_{MeOH}/V_{water}=5/1) removed salt impurities and DMSO traces. Lyophilization afforded a brown viscous copolymer in yields of 77 %. Table 1 summarizes the copolymer characterization data.

In situ ^{1}H NMR kinetic study of a statistical copolymerization of TGEs with EO

In situ ^{1}H NMR kinetic investigations for the copolymerization of a variety of TGEs with EO were performed in a sealable *Norell* S-500-VT-7 NMR tube subject to a procedure by Herzberger et al.[4] In general, the polymerization set up in an NMR tube is restricted by its volume. To reproduce the optimized polymerization conditions (40 °C, THF-d_8/DMSO-d_6 = 5/1 (V_{THF}/V_{DMSO})) for the TGE copolymerizations, batch calculations and theoretical comonomer ratios vary with each monomer in dependance of its chain length. This results from the varying molecular weights and densities of the applied TGEs. Note that EO is a highly toxic, flammable gas, which requires careful handling. As small amounts of EO are required for the *in situ* kinetic measurements, comonomer ratios are further impacted by small variations of the measured EO volumes.

The pre-dried initiator salt, cesium 2-(benzyloxy)ethanolate (degree of deprotonation: 95 %), was prepared in a 10-fold excess and dissolved in anhydrous DMSO-d_6 under stirring for 30 min (initiator stock solution). Its preparation was carried out in accordance with the statistical copolymerization protocol described in the previous section. After evacuating the oven-dried NMR tube, using a Teflon stopcock using Schlenk-line vacuum, EO was cryo-transferred into the NMR tube under static vacuum at -45 °C with an acetone/nitrogen bath. Subsequently, an aliquot of the initiator stock solution and THF-d_8 were syringed into the tube under argon atmosphere while cooling was maintained. After a final evacuation cycle, the reaction mixture was allowed to warm to room temperature and shaken vigorously to homogenize the solution. Then, the NMR tube was placed in the preheated NMR spectrometer (40 °C) and a control spectrum was recorded once a stable temperature in the probe head was reached (~10 min, ΔT = 0.1 K). The sample rotation was turned off and ^{1}H NMR spectra with 1 scan per spectrum were recorded in 2 min intervals. After the kinetic study, the copolymer was characterized via SEC analysis.

Monitoring the integrals of the epoxide functionality of EO and the respective TGE renders the calculation of the monomer consumption with preceding copolymerization possible. Therefore, the normalized monomer consumption was analyzed using the *NIREVAL* software from Johann *et al*.[5] For the evaluation of the reactivity ratios of the comonomer pair the Jaacks method was applied for a 90 % TGE conversion to ensure a significant signal-to-noise ratio.[6]

Procedures for Post-polymerization Functionalizations

Thiol-Ene Click

The following procedure was applied to all double bond containing monomers. As an example, the modification of P(EG_{120}-*co*-$GeraGE_{12}$) is described. The polymer (50 mg, 6.76 µmol) and 2,2-dimethoxy-2-phenylacetophenone (DMPA, 83.1 mg, 0.324 mmol, 48 eq., 0.01 eq. to the thiol) were added to a Schlenkflask equipped with a magnetic stirrer and rubber septum. 8 ml of DCM was added, followed by 2-mercaptoethanol (2.53 g, 32.4 mmol, 4800 eq., 200 eq. per double bond). After mixing, three freeze-pump-thaw cycles were applied. Subsequently, an argon-filled balloon was attached to the Schlenkflask through the septum. The stirred mixture was irradiated overnight using a UV lamp (254 nm) at a distance of 5 cm. After the reaction the mixture was extracted against water (20 ml) thrice. Additionally, the polymer was purified by dialysis against MeOH (*Orange*

Scientific, Molecular weight cut-off 1000 g/mol, 1 L, solvent changed thrice). The solvents were evaporated obtaining the modified polymer in typical yields of 80 %.

Since every copolymer needed slightly different ratios of DMPA and 2-mercaptoethanol the set-ups are displayed in the following table. The authors would like to emphasize that the quantities mentioned are not necessarily the lowest possible. The experimental procedure was optimized for P(EG_{120}-*co*-$GeraGE_{12}$) first. The amounts were adjusted to the polymers. DMPA was modified and/or 2-mercaptoethanol was increased to suppress crosslinking.

Table S1: Precursor polymers and the respective equivalents of Thiol and DMPA in the thiol-ene click postpolymerization modification.

Entry	Polymer	Thiol/Double bond	DMPA eq./Thiol
1	P(EG_{102}-*co*-$PreGE_{10}$)	600	0.010
2	P(EG_{126}-*co*-$IsoPreGE_{12}$)	200	0.010
3	P(EG_{120}-*co*-$GeraGE_{12}$)	200	0.010
4	P(EG_{123}-*co*-$NerGE_{13}$)	600	0.015

Recovery of unreacted 2-mercaptoethanol

After the reaction, the volatile compounds, mainly DCM and 2-mercaptoethanol, were cryotransferred into a schlenkflask equipped with a magnetic stirrer. The volatile compounds were fractionally distilled, 2-mercaptoethanol was received in a yield of 80 %.

Synthesis of potassium azodicarboxylate (PADA)

PADA was synthesized according to Groves and Ma.[7] 30 mL of a 40 *w*.-% aqueous potassium hydroxide solution was added to a 50 mL round-bottom flask equipped with a magnetic stirrer. The flask was immersed into a water bath at 6 °C. Azodicarboxylate (4.84 g, 41.7 mmol) was added portion wise over 2 h. The precipitate was filtered off using a glass frit and washed 20 times with ice cold methanol. The product was dried in a desiccator over 1.5 d employing vacuum, giving an intense yellow powder. The yield was 7.18 g, 37.0 mmol, 89 %.

Hydrogenation

Hydrogenation of polymers with potassium azodicarboxylate (PADA) is rarely employed.[8] The described procedure was developed during the optimization experiments and represents the best result. We oriented on the procedures described from Groves and Ma[7] as well as Snyder and Hamersma.[9]

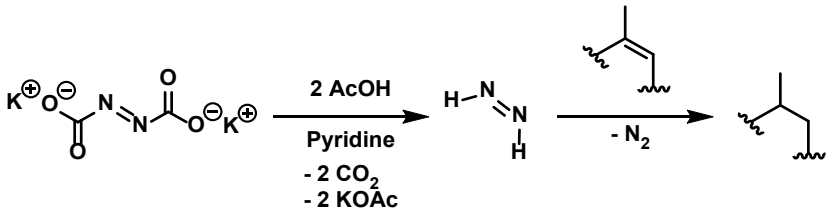

Scheme S1: Acidic decomposition of potassium azodicarboxylate (PADA) to generate diimide and subsequent polymer hydrogenation. Gaseous carbon dioxide and nitrogen as well as readily water-soluble potassium acetate are produced as coupling products.

The hydrogenation was applied to P(EG_{120}-*co*-$GeraGE_{12}$). 50 mg (6.76 µmol) were transferred in a flame dried Schlenk flask equipped with a rubber septum and a magnetic stirrer using Toluene. The solvent was removed *in vacuo* yielding the dried polymer due to azeotropic distillation. PADA (423 mg, 360 eq., 15 eq. per double bond) and 3 ml of dry pyridine (stored over mole sieve, *Fisher Scientific*) were added. To the stirred slurry glacial acetic acid (distilled from P_4O_{10} and stored over Argon, 0.28 ml, 720 eq., 2 eq. per PADA) was slowly added dropwise with a syringe. After complete addition of the glacial acetic acid the mixture was allowed to react overnight. The now colorless suspension was suspended in $CHCl_3$, solids were filtered off and the organic phase was washed with water twice (20 ml). The solvents were evaporated yielding the polymer in a yield of 85 %.

Table S2: Reaction conditions of the hydrogenation of P(EG_{120}-*co*-$GeraGE_{12}$) employing potassium azodicarboxylate (PADA).

				Remaining signal of the DB		
Entry	***T* / °C**	**Eq. PADA/DB**	**V(Py) / mL**	**5.30 ppm**	**5.08 ppm**	**avg. efficiency**
1	0	2.5	0.4	58 %	64 %	39 %
2	25	2.5	0.4	92 %	89 %	10 %
3	0	15	0.4	44 %	49 %	53 %
4	25	15	0.4	73 %	78 %	25 %
5	0	2.5	3	71 %	74 %	28 %
6	25	2.5	3	74 %	80 %	23 %
7	0	15	3	48 %	55 %	48 %
8	25	15	3	43 %	49 %	53 %

NMR Spectra of TGEs

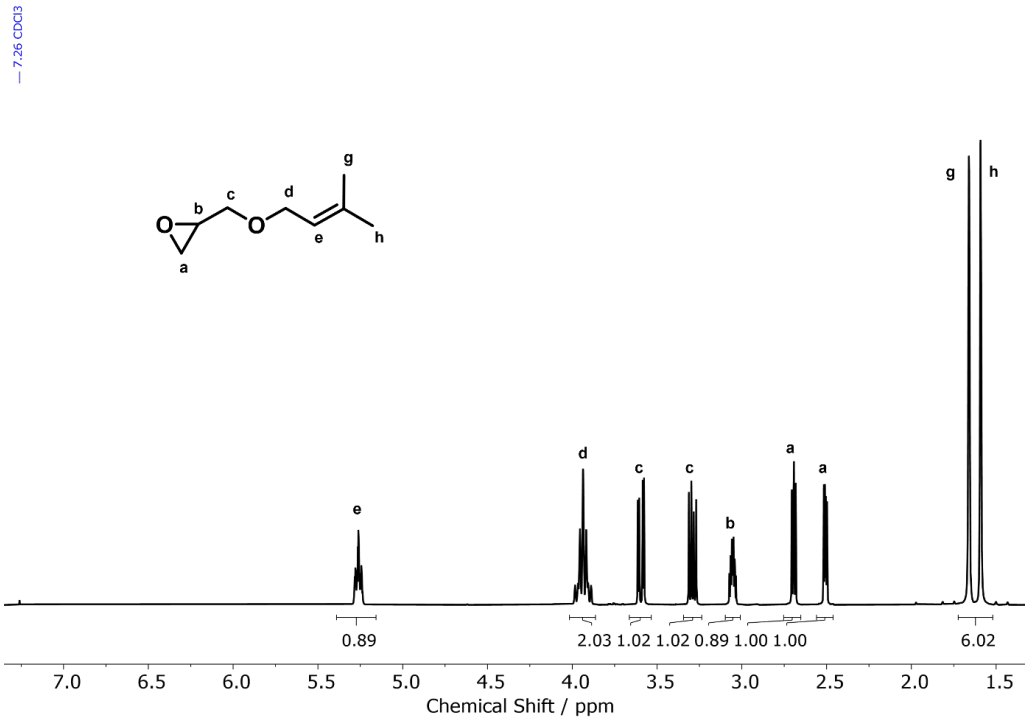

Figure S1: ^{1}H NMR spectrum (300 MHz, $CDCl_3$) of PreGE.

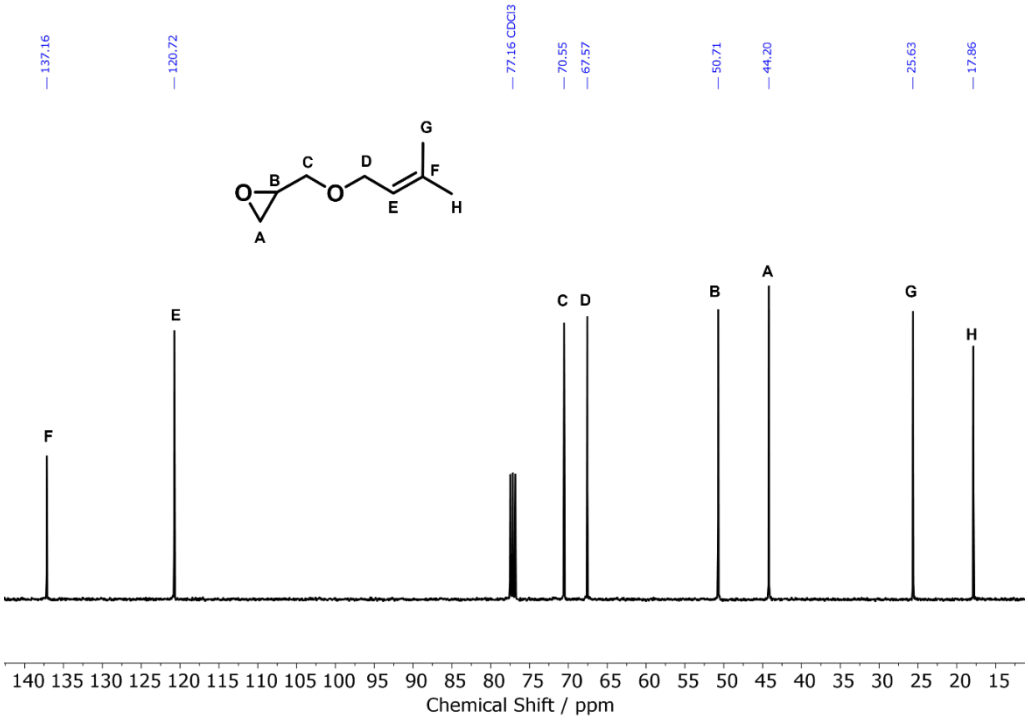

Figure S2: ^{13}C NMR spectrum (75 MHz, $CDCl_3$) of PreGE.

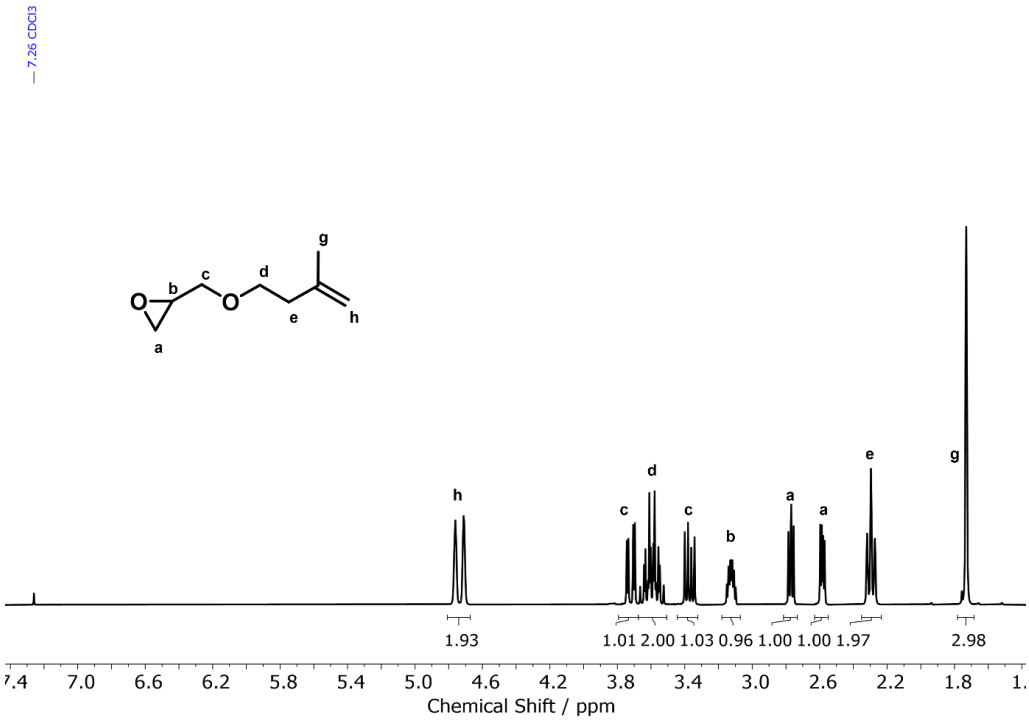

Figure S3: ^{1}H NMR spectrum (300 MHz, $CDCl_3$) of IsoPreGE.

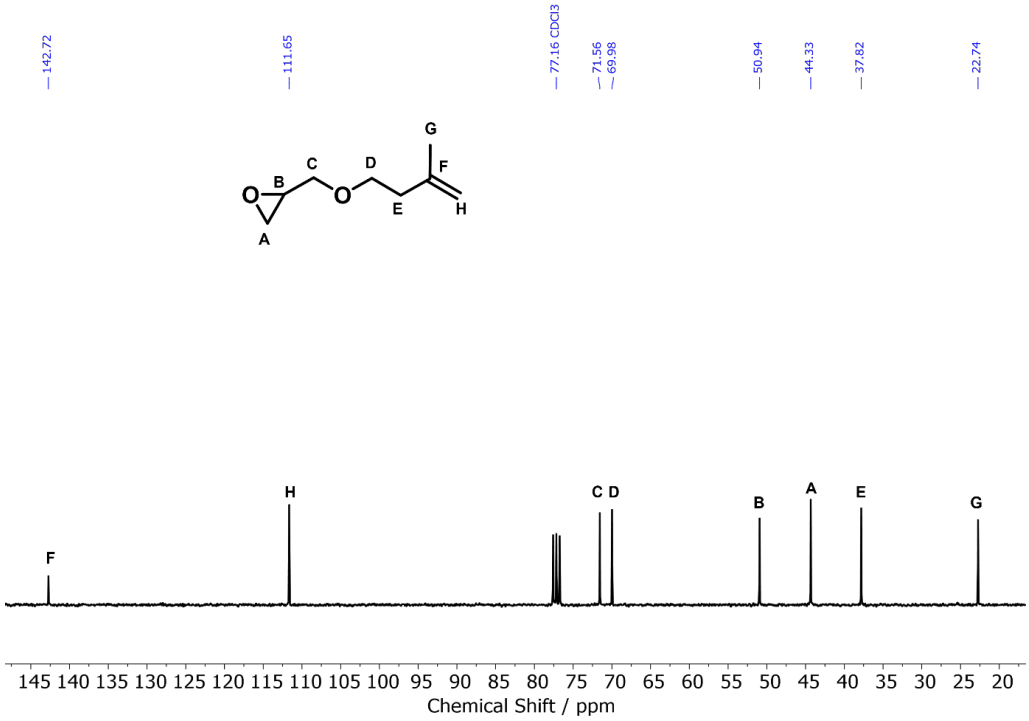

Figure S4: ^{13}C NMR spectrum (75 MHz, $CDCl_3$) of IsoPreGE.

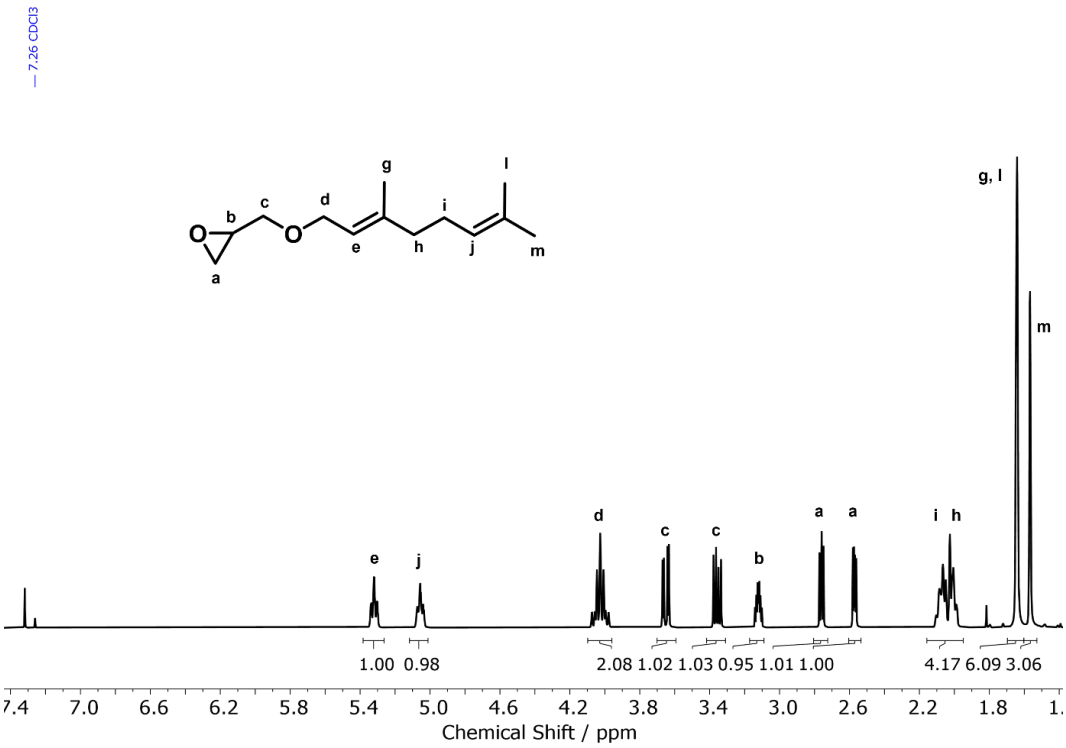

Figure S5: ^{1}H NMR spectrum (400 MHz, $CDCl_3$) of GeraGE.

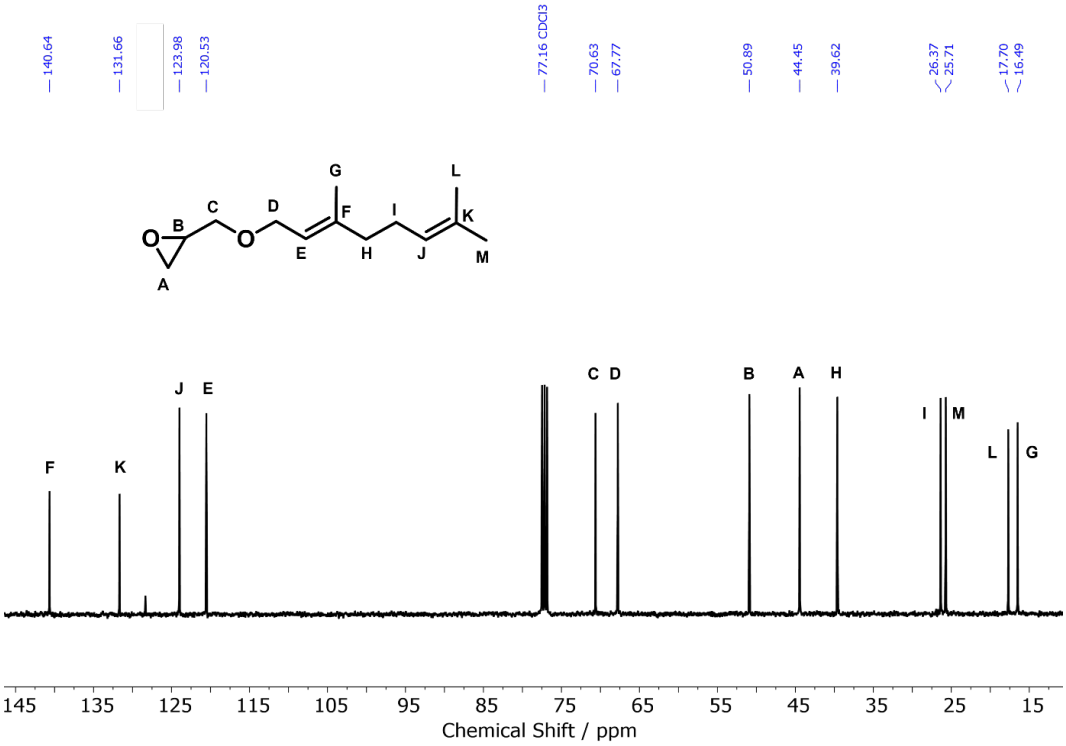

Figure S6: ^{13}C NMR spectrum (100 MHz, $CDCl_3$) of GeraGE.

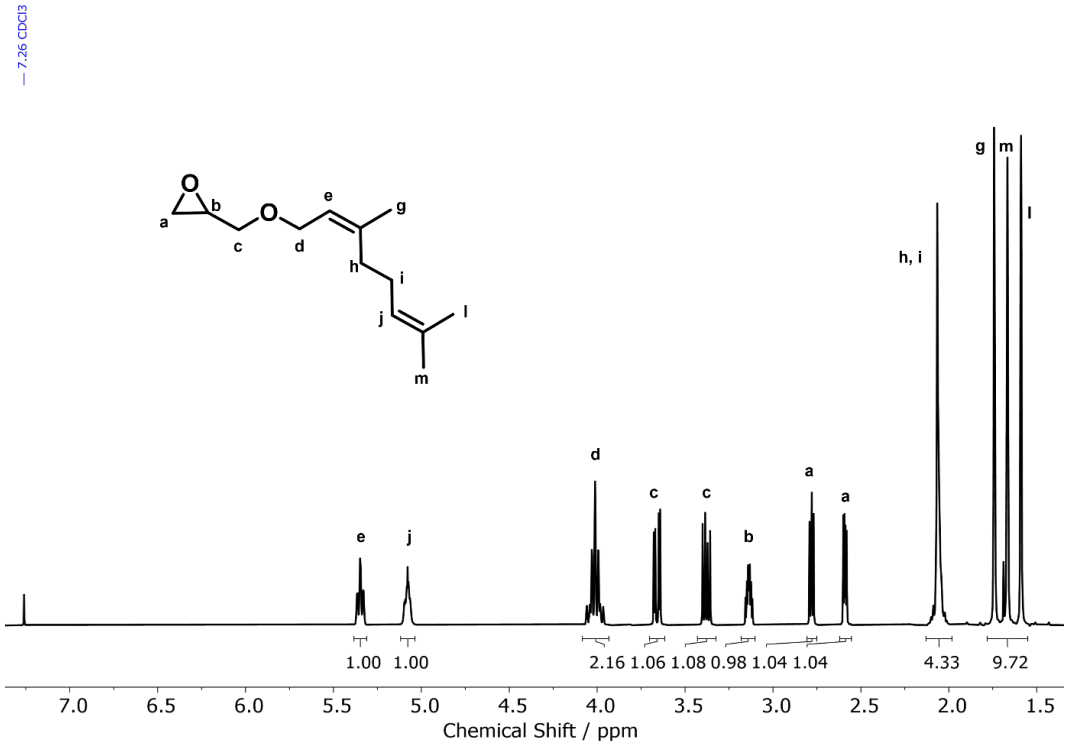

Figure S7: ^{1}H NMR spectrum (400 MHz, $CDCl_3$) of NerGE.

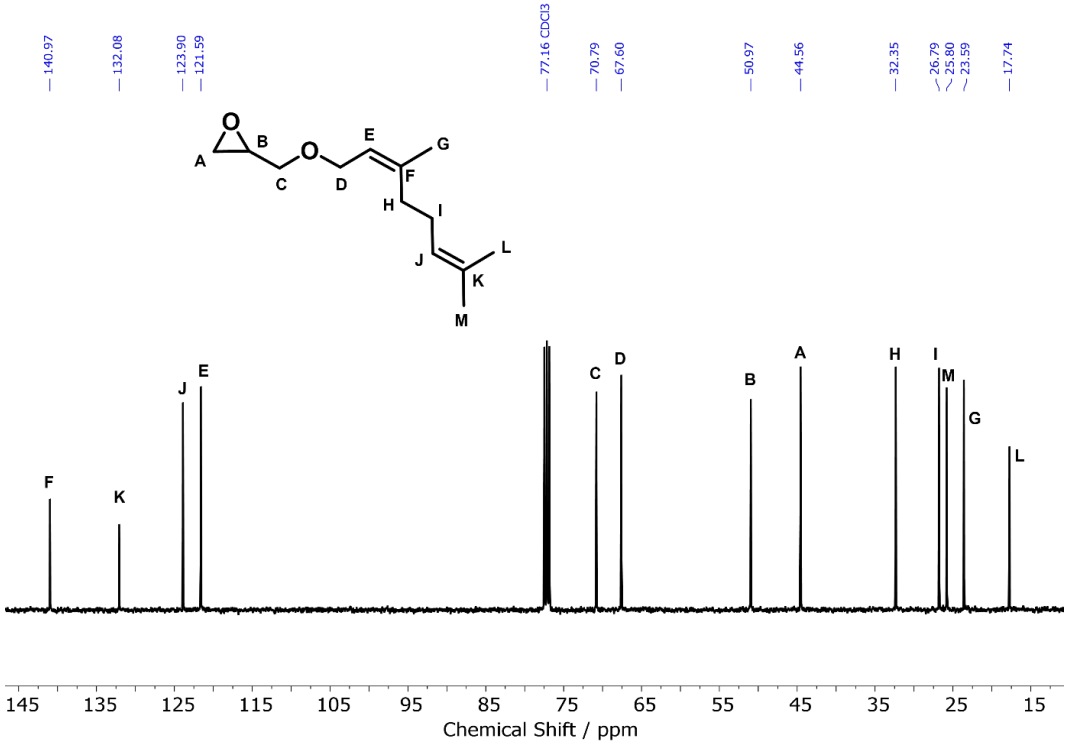

Figure S8: ^{13}C NMR spectrum (100 MHz, $CDCl_3$) of NerGE.

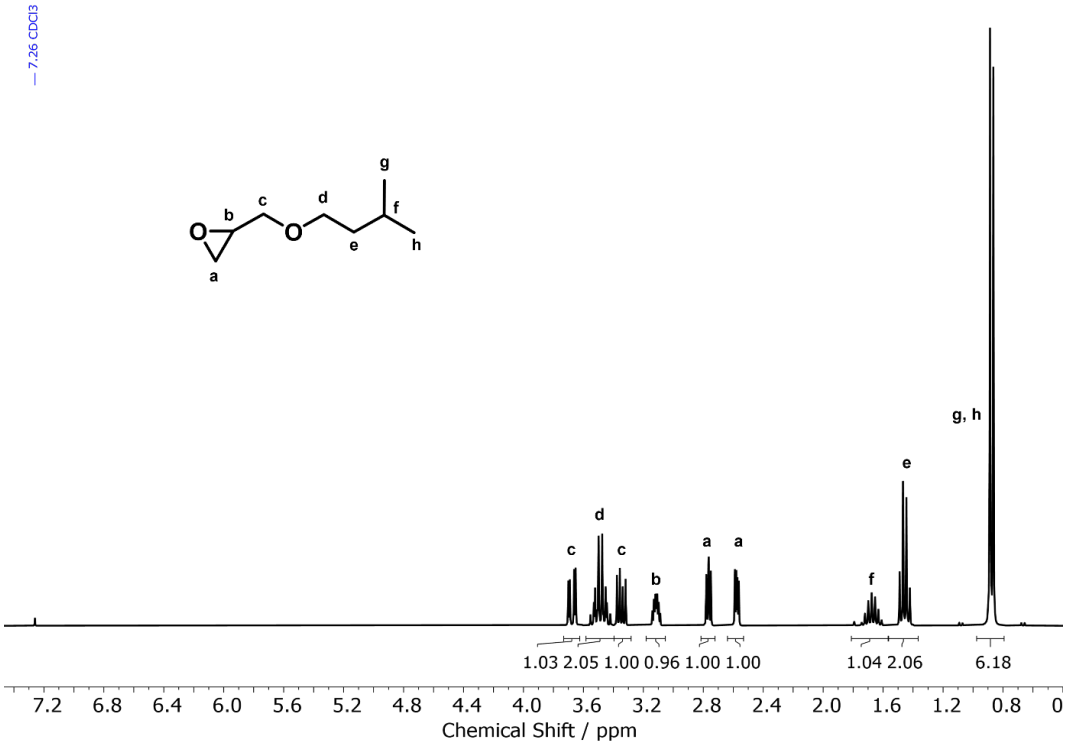

Figure S9: ^{1}H NMR spectrum (300 MHz, $CDCl_3$) of DHPreGE.

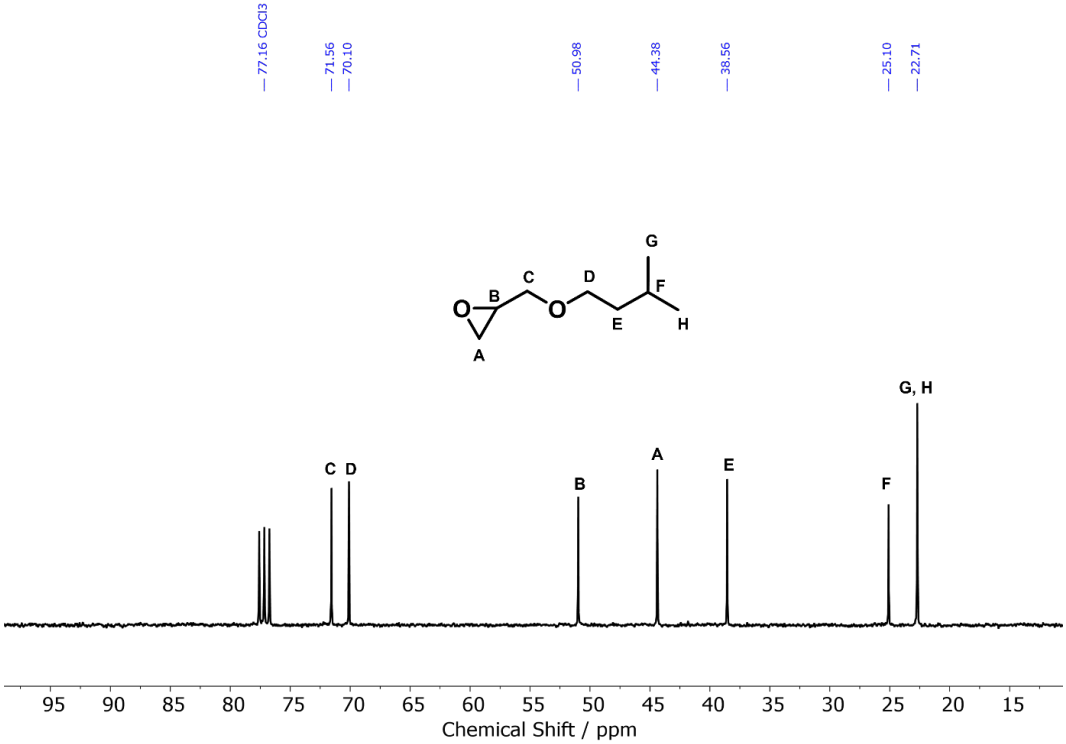

Figure S10: ^{13}C NMR spectrum (75 MHz, $CDCl_3$) of DHPreGE.

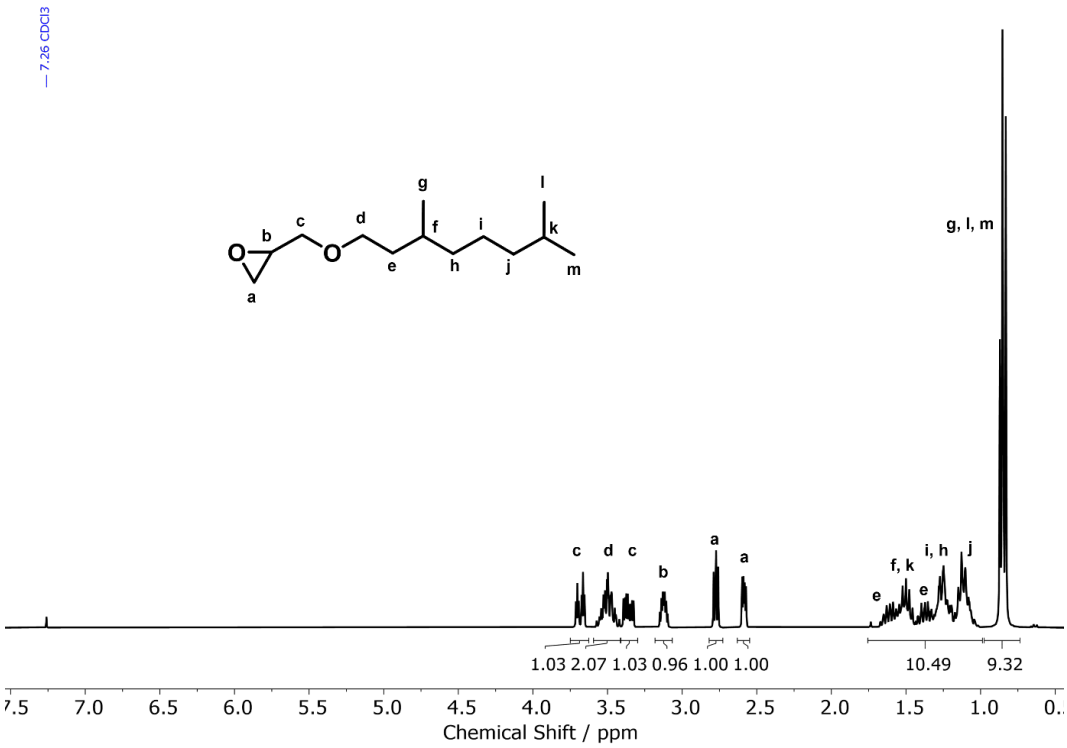

Figure S11: ^{1}H NMR spectrum (300 MHz, $CDCl_3$) of THGeraGE.

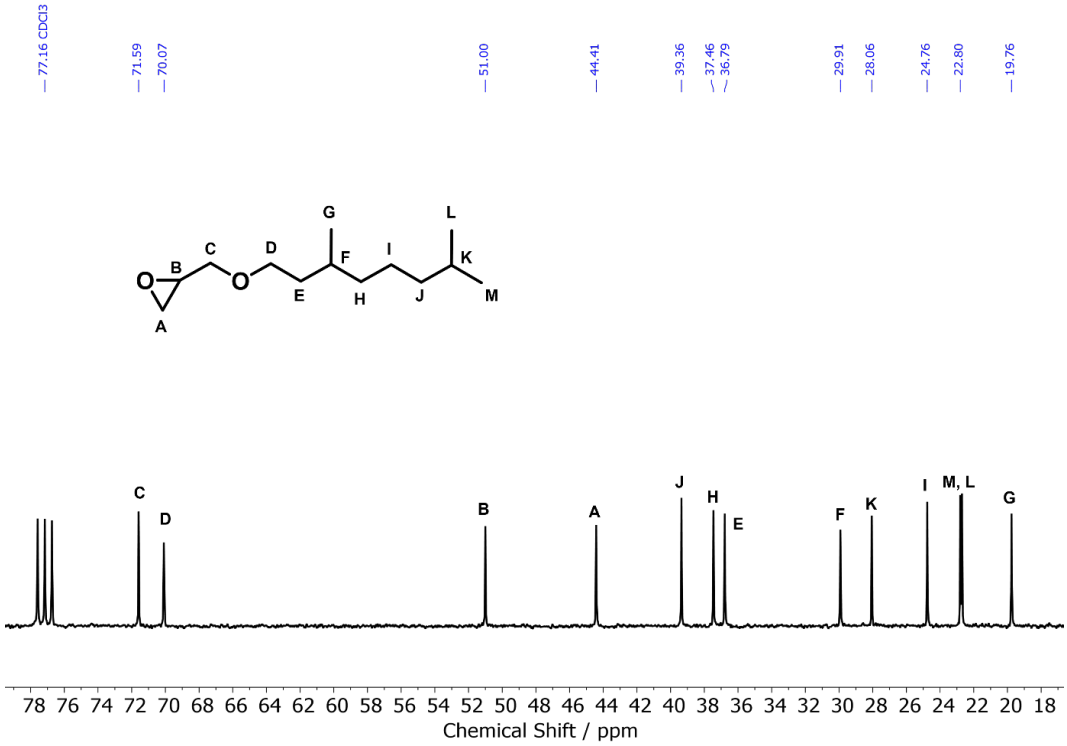

Figure S12: ^{13}C NMR spectrum (75 MHz, $CDCl_3$) of THGeraGE.

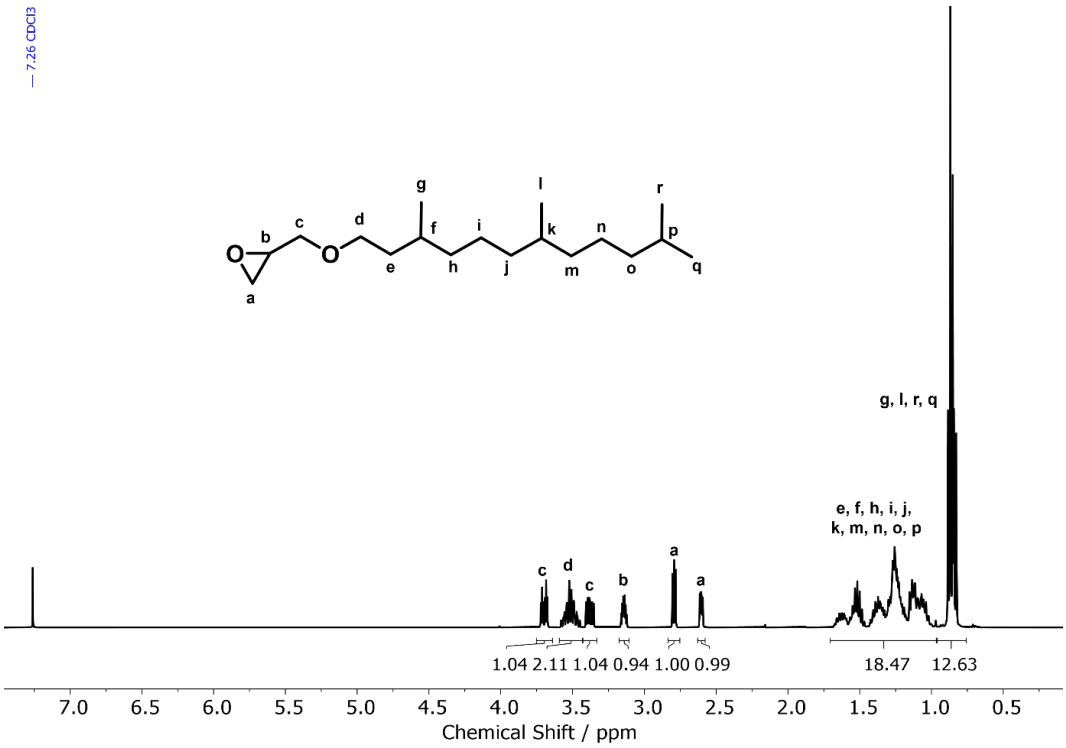

Figure S13: ^{1}H NMR spectrum (400 MHz, $CDCl_3$) of HHFarGE.

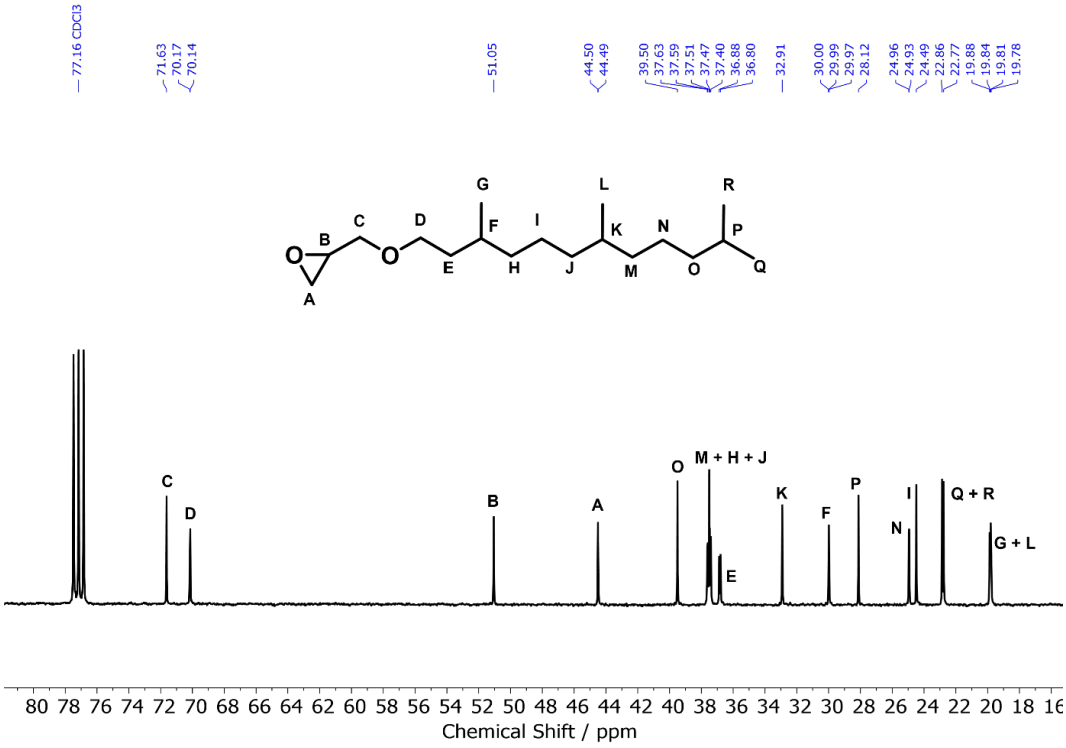

Figure S14: ^{13}C NMR spectrum (100 MHz, $CDCl_3$) of HHFarGE.

Characterization of Statistical Copolymers of TGEs and EO

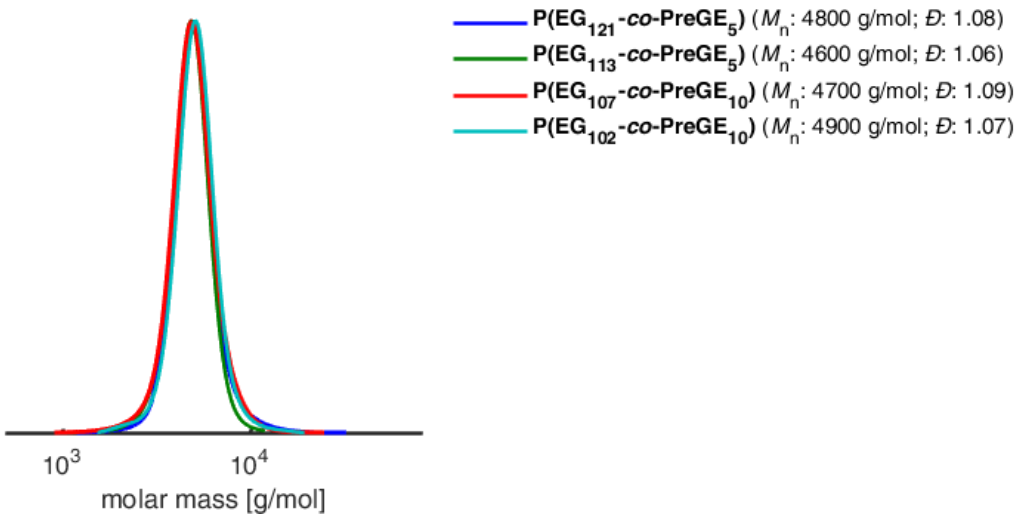

Figure S15: SEC traces of P(EG$_n$-*co*-PreGE$_m$) (RI detector, eluent: DMF, PEG calibration).

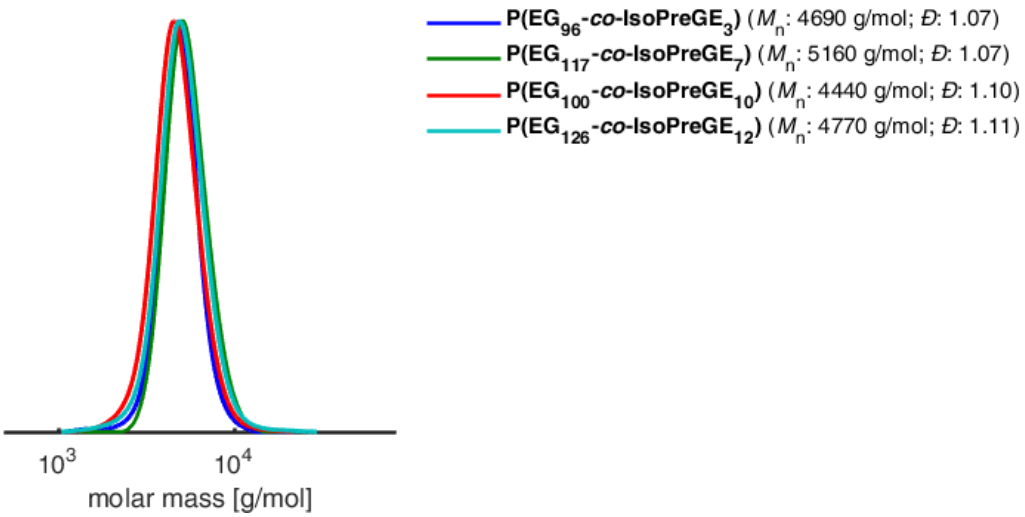

Figure S16: SEC traces of P(EG$_n$-*co*-IsoPreGE$_m$) (RI detector, eluent: DMF, PEG calibration).

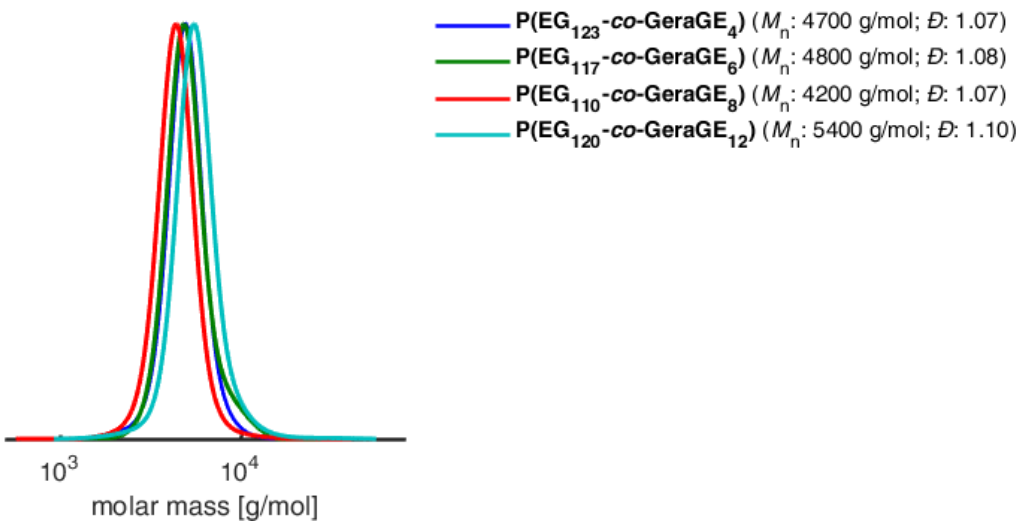

Figure S17: SEC traces of P(EG$_n$-*co*-GeraGE$_m$) (RI detector, eluent: DMF, PEG calibration).

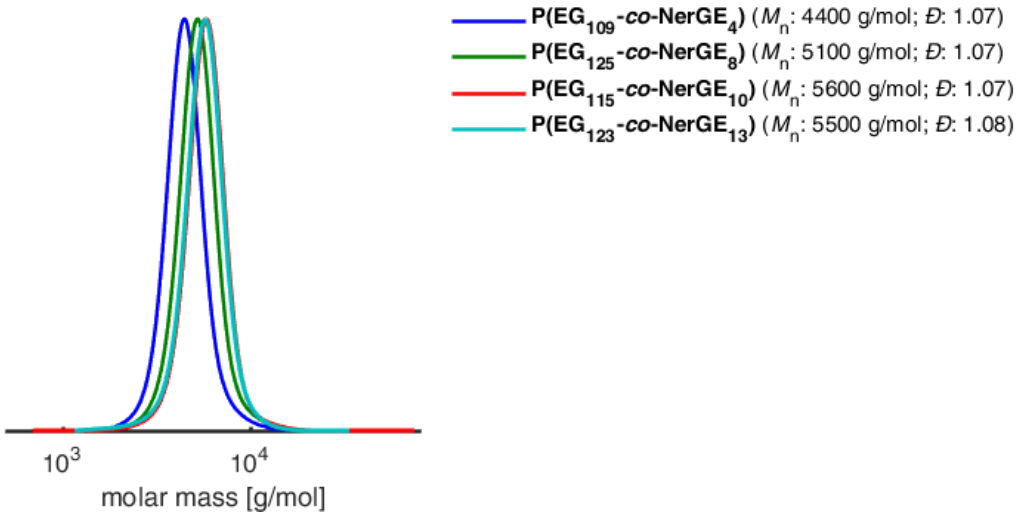

Figure S18: SEC traces of P(EG$_n$-*co*-NerGE$_m$) (RI detector, eluent: DMF, PEG calibration).

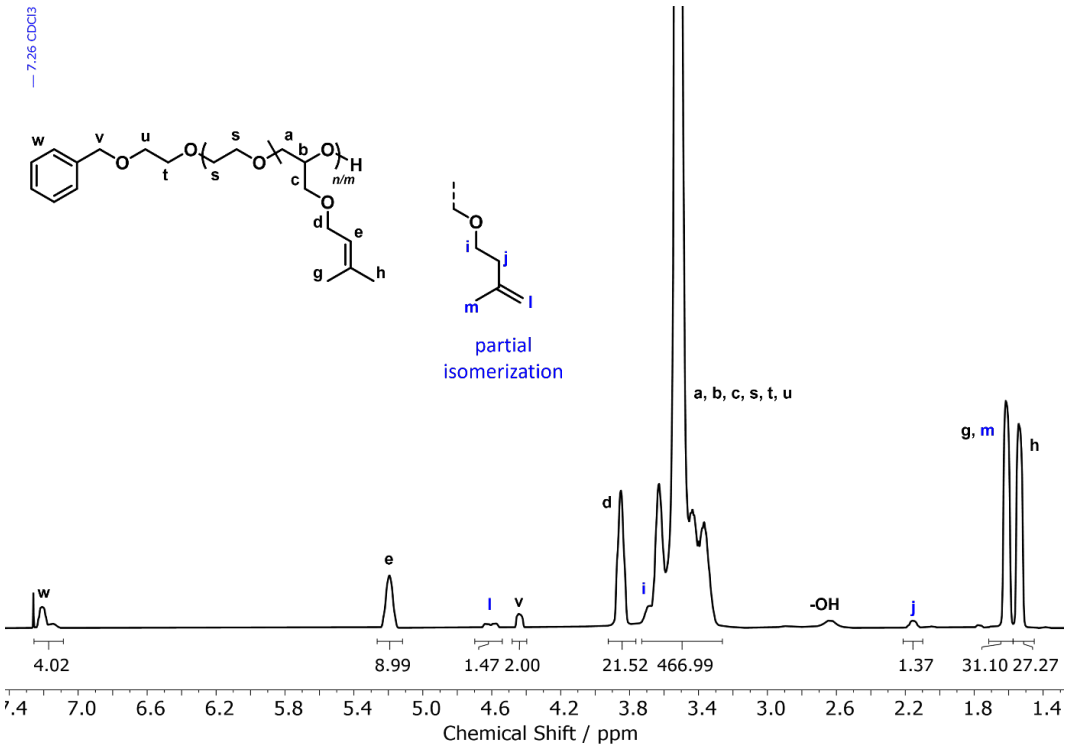

Figure S19: ^{1}H NMR spectrum (400 MHz, $CDCl_3$) of P(EG_{102}-*co*-PreGE_{10}).

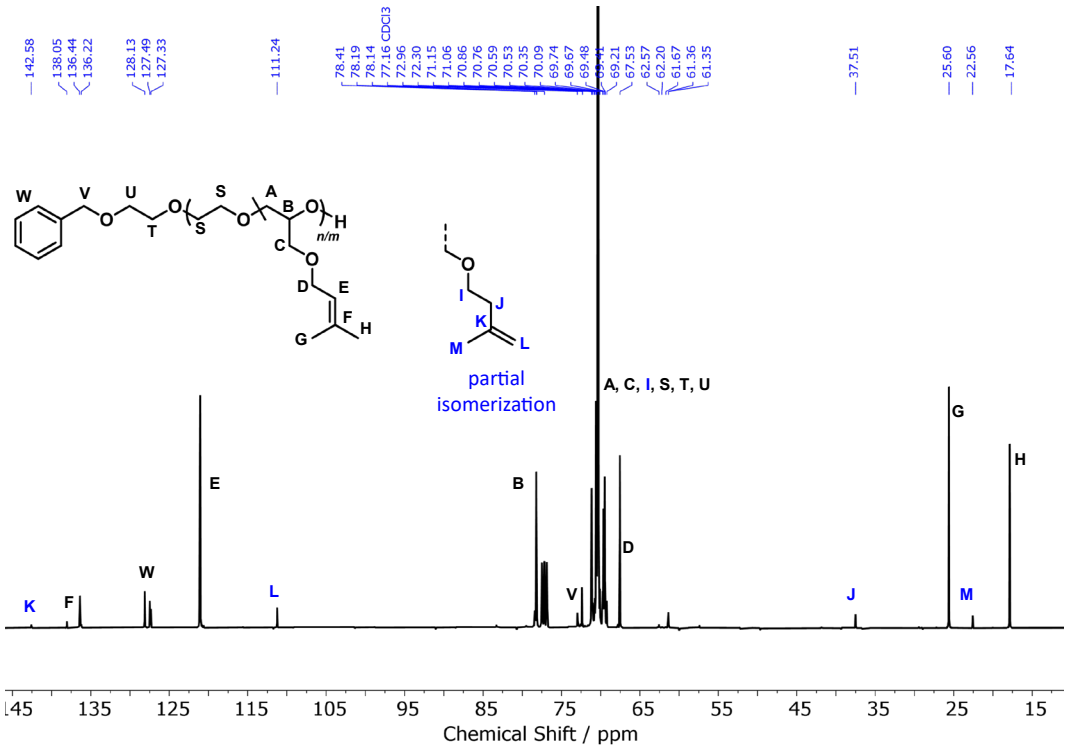

Figure S20: ^{13}C NMR spectrum (100 MHz, $CDCl_3$) of P(EG_{102}-*co*-PreGE_{10}).

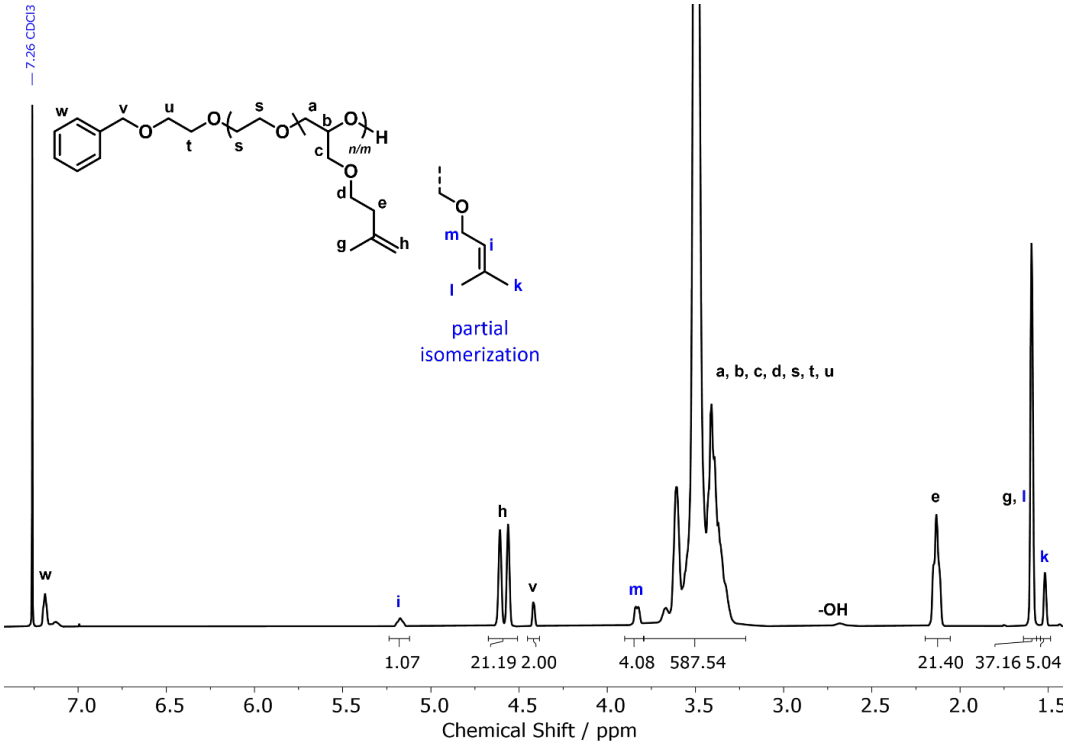

Figure S21: ^{1}H NMR spectrum (400 MHz, $CDCl_3$) of P(EG_{126}-*co*-IsoPreGE$_{12}$).

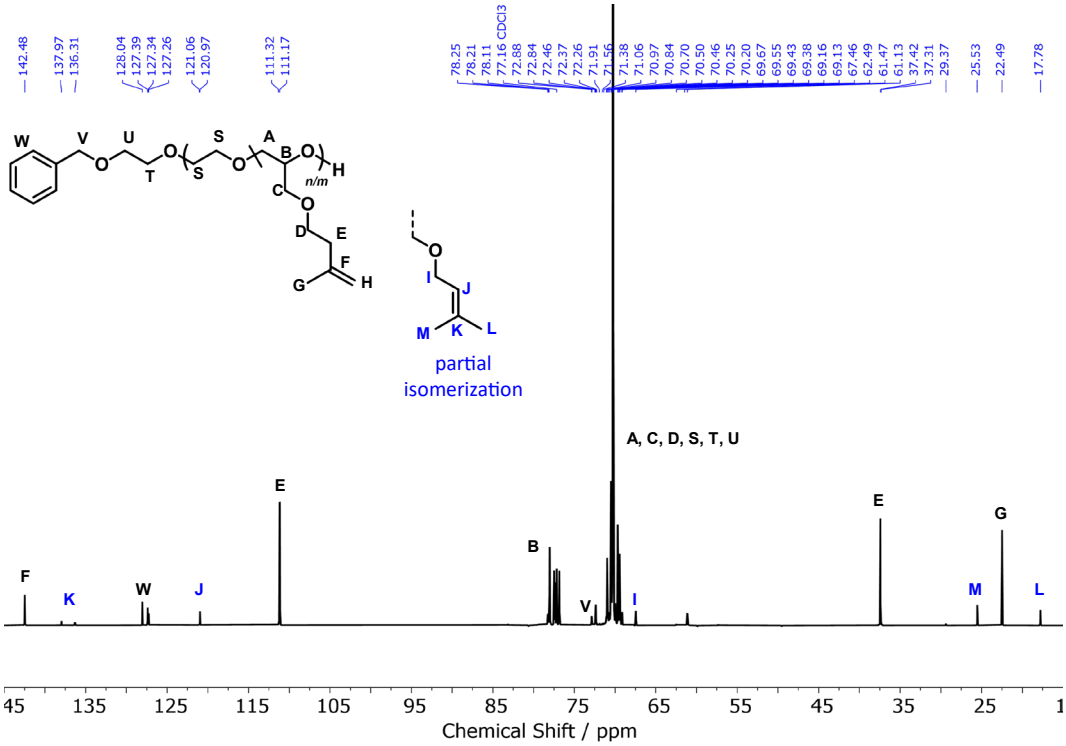

Figure S22: ^{13}C NMR spectrum (100 MHz, $CDCl_3$) of P(EG_{126}-*co*-IsoPreGE$_{12}$).

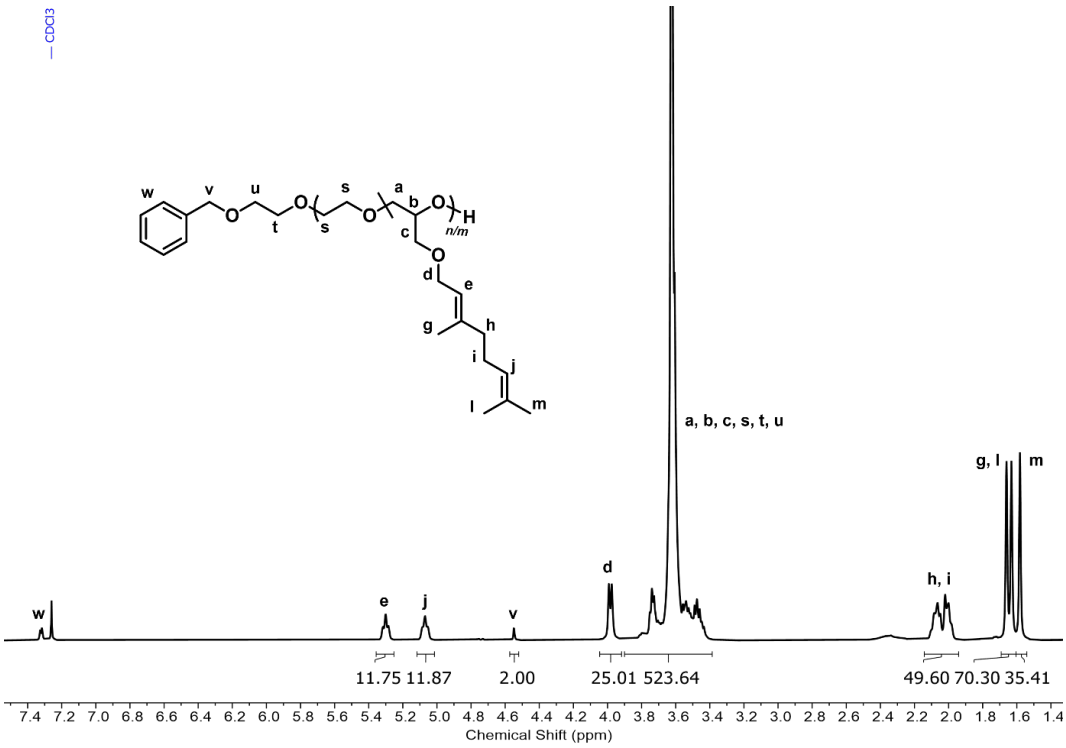

Figure S23: ^{1}H NMR spectrum (400 MHz, $CDCl_3$) of P(EG_{120}-*co*-GeraGE_{12}).

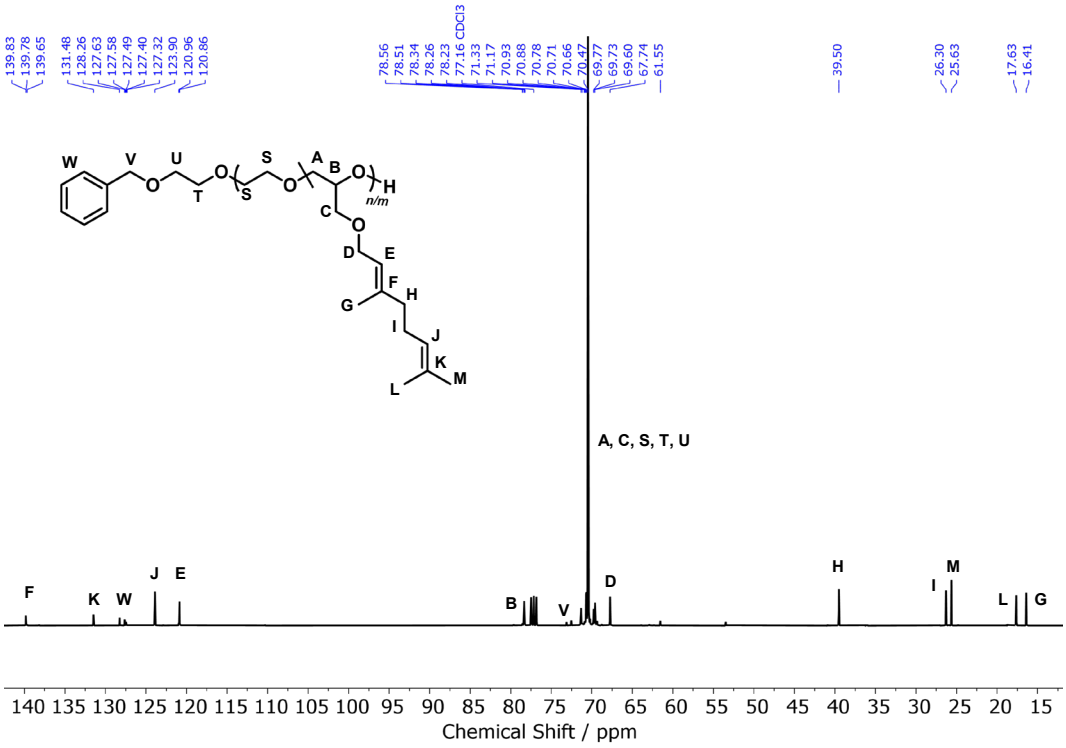

Figure S24: ^{13}C NMR spectrum (100 MHz, $CDCl_3$) of P(EG_{120}-*co*-GeraGE_{12}).

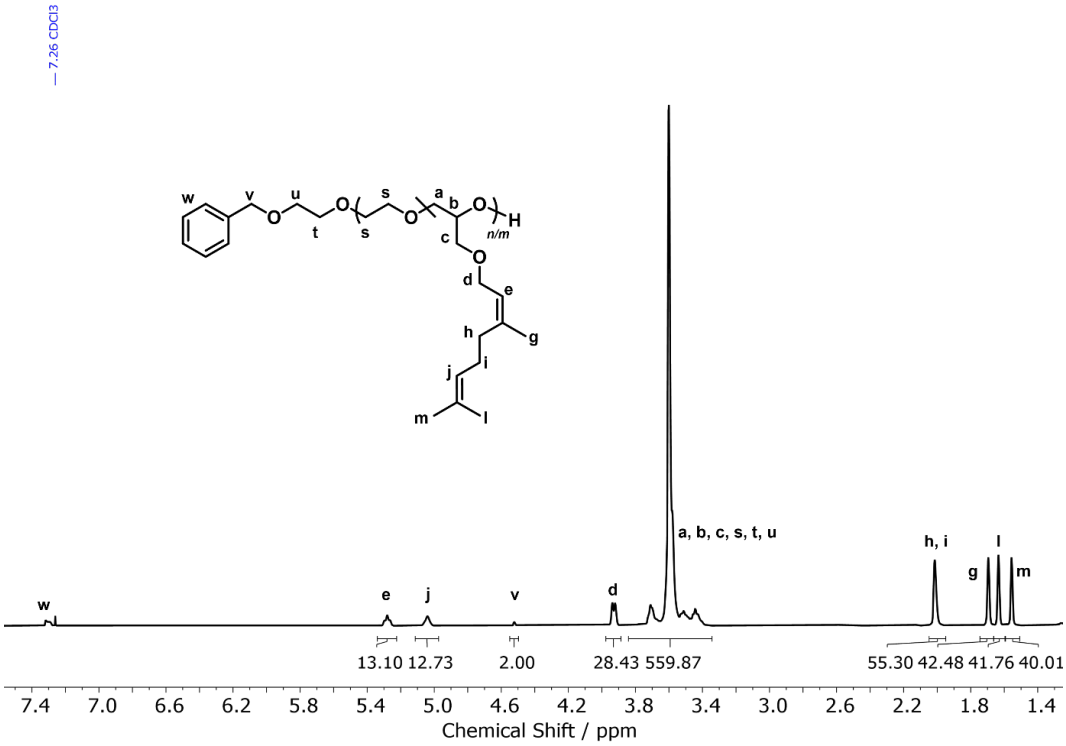

Figure S25: ^{1}H NMR spectrum (400 MHz, $CDCl_3$) of P(EG_{123}-*co*-$NerGE_{13}$).

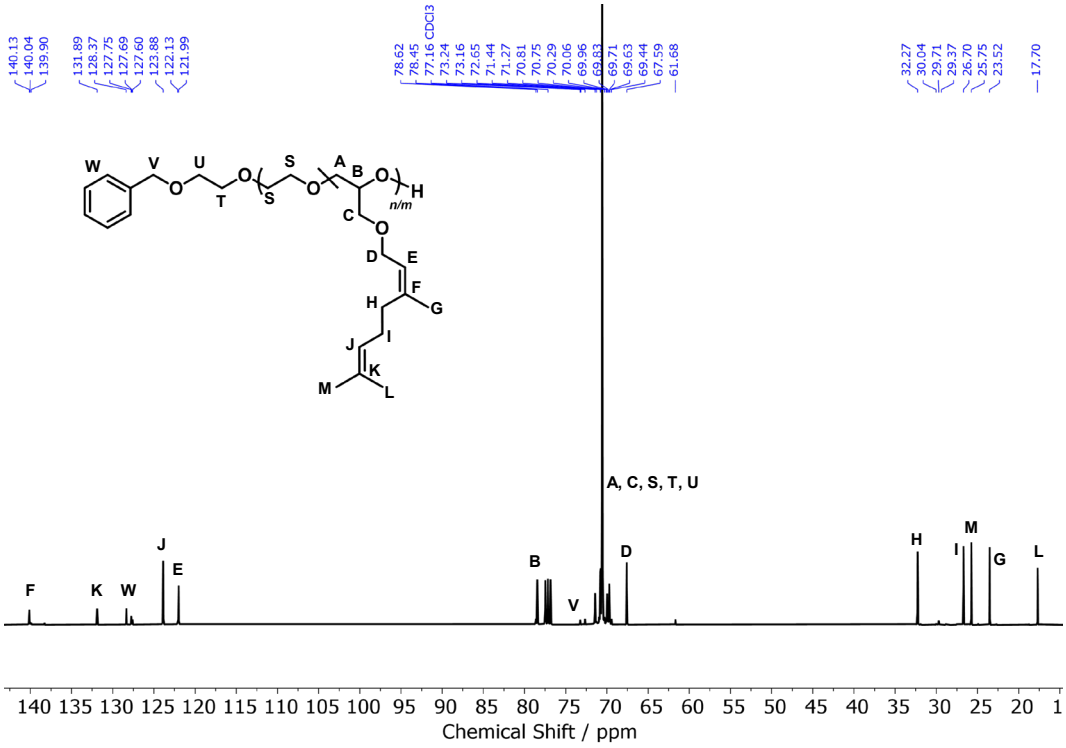

Figure S26: ^{13}C NMR spectrum (100 MHz, $CDCl_3$) of P(EG_{123}-*co*-$NerGE_{13}$).

In situ ^{1}H NMR Copolymerization Kinetics of TGEs with EO

Non-terminal, ideal copolymerization model and Jaacks fit

The evaluation of the reactivity ratios is based on the non-terminal, ideal copolymerization model, which was introduced by Wall in 1941.[10] Assuming first order polymerizations, the following polymerization rates apply for a binary copolymerization system:

$$\frac{d[\mathrm{M}_1]}{dt} = -k_1[\mathrm{M}_1][\mathrm{P}] \tag{1}$$

$$\frac{d[\mathrm{M}_2]}{dt} = -k_2[\mathrm{M}_2][\mathrm{P}] \tag{2}$$

[P] refers to the active chain end. Eliminating *t* from the equations by dividing rate (1) by rate (2), followed by rearrangement, the time-independent differential equation (4) is obtained:

$$\frac{d[\mathrm{M}_1]}{d[\mathrm{M}_2]} = \frac{k_1}{k_2}\frac{[\mathrm{M}_1]}{[\mathrm{M}_2]} \tag{3}$$

$$\frac{d[\mathrm{M}_1]}{[\mathrm{M}_1]} = r_1\frac{d[\mathrm{M}_2]}{[\mathrm{M}_2]} \quad \text{with } r_1 = \frac{k_1}{k_2} \tag{4}$$

Wall was the first to use relative rates to describe copolymerizations and the resulting reactivity ratios r_1 and r_2 represent the compositional drift due to different comonomer reactivities.[11] The model assumes a copolymerization behavior that is not dependent on the identity of the growing chain end, but solely on the comonomer reactivities.

The integration of the rearranged Wall's equation (4) leads to the Jaacks equation (5)[6]:

$$\log\frac{[\mathrm{M}_{1,t=x}]}{[\mathrm{M}_{1,t=0}]} = r_1\log\frac{[\mathrm{M}_{2,t=x}]}{[\mathrm{M}_{2,t=0}]} \tag{5}$$

The Jaacks equation allows for the determination of the reactivity ratios at any comonomer ratio when ideal copolymerization conditions are applicable *($r_1 \cdot r_2$ = 1)*.[6]

In line with the Ockhams razor, the non-terminal model represents the most basic model for the determination of the reactivity ratios and poses the model of choice to avoid overfitting.[12,13] Experimental data suggest its suitability for the copolymerization of EO and monosubstituted epoxides, which tend to obey ideal copolymerization behavior.[11]

Jaacks fit for the copolymerization of TGEs with EO

The signal scattering noticeably increases at high copolymerization conversions while the signal-to-noise ratio decreases. Hence, all reactivity ratios were calculated for a TGE monomer conversion of approximately 90 %. The results are summarized in Table 2.

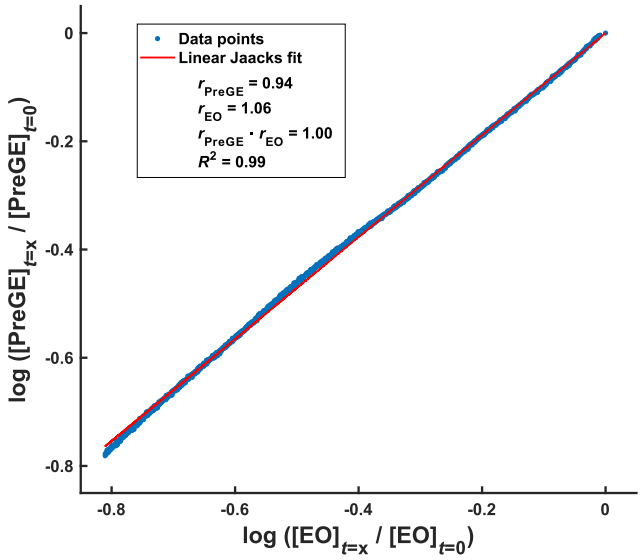

Figure S27: Jaacks fit of the *in situ* ^{1}H NMR copolymerization kinetics of PreGE with EO in a mixture of THF-d_8 and DMSO-d_6 (5:1) at 40 °C.

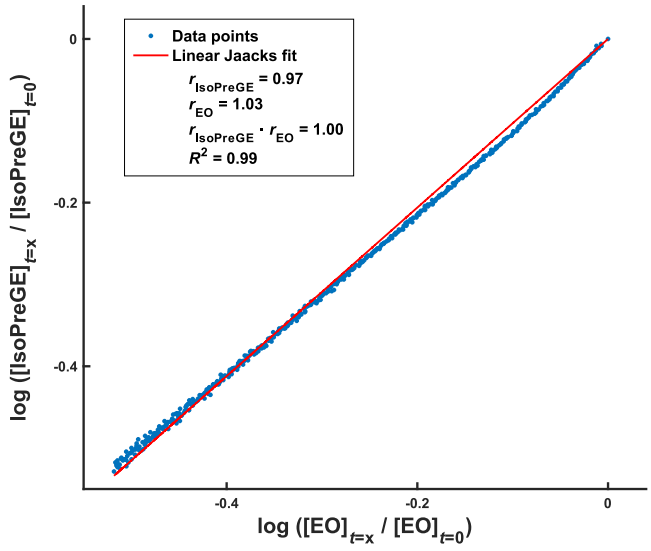

Figure S28: Jaacks fit of the *in situ* ^{1}H NMR copolymerization kinetics of IsoPreGE with EO in a mixture of THF-d_8 and DMSO-d_6 (5:1) at 40 °C.

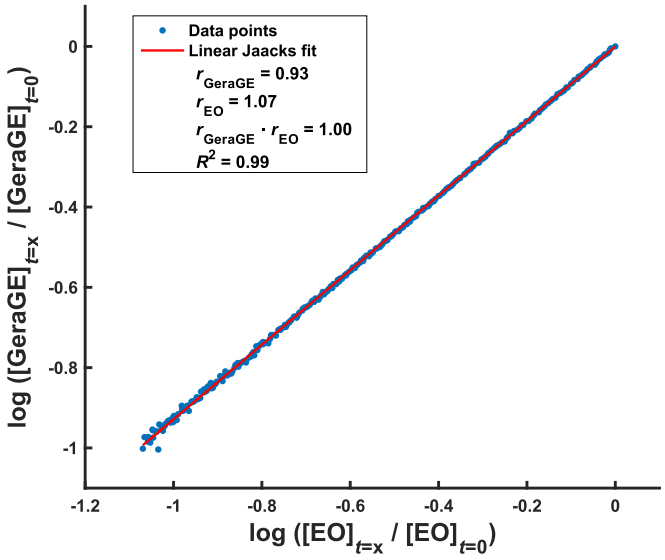

Figure S29: Jaacks fit of the *in situ* ^{1}H NMR copolymerization kinetics of GeraGE with EO in a mixture of THF-d_8 and DMSO-d_6 (5:1) at 40 °C.

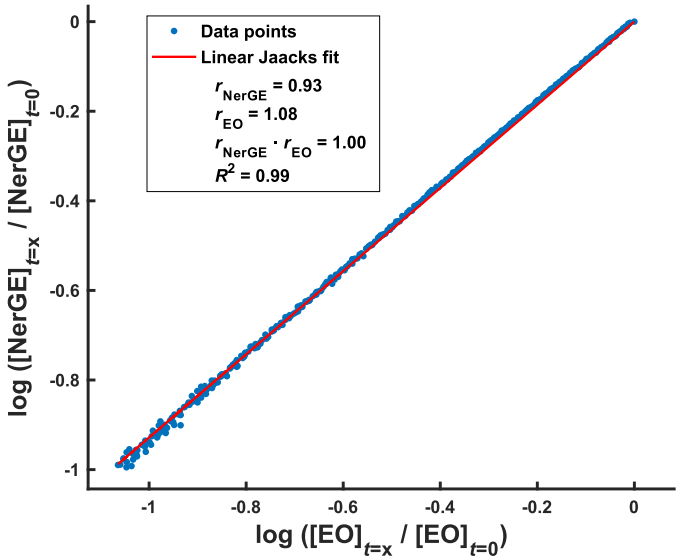

Figure S30: Jaacks fit of the *in situ* ^{1}H NMR copolymerization kinetics of NerGE with EO in a mixture of THF-d_8 and DMSO-d_6 (5:1) at 40 °C.

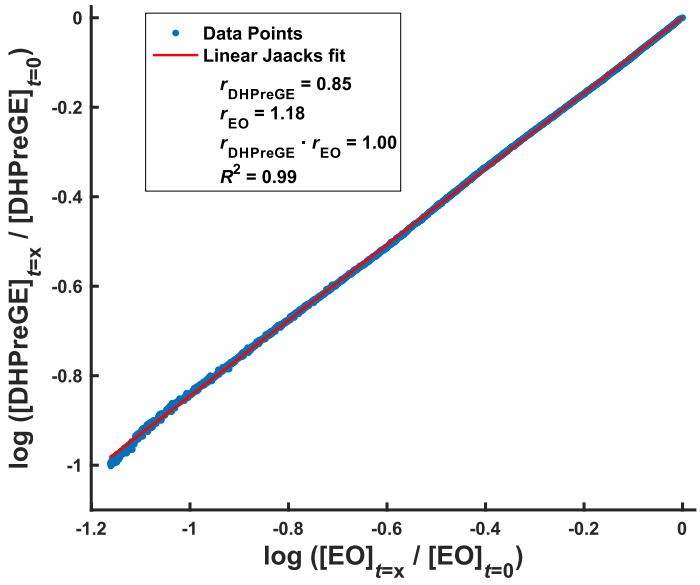

Figure S31: Jaacks fit of the *in situ* ^{1}H NMR copolymerization kinetics of DHPreGE with EO in a mixture of THF-d_8 and DMSO-d_6 (5:1) at 40 °C.

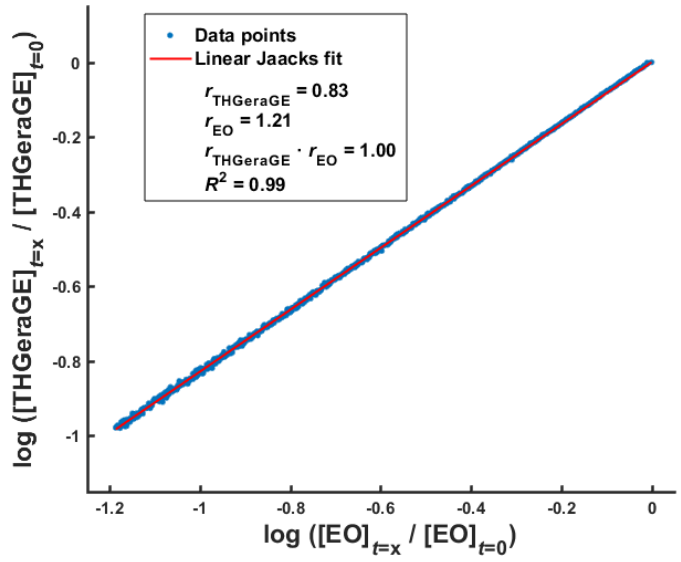

Figure S32: Jaacks fit of the *in situ* ^{1}H NMR copolymerization kinetics of THGeraGE with EO in a mixture of THF-d_8 and DMSO-d_6 (5:1) at 40 °C.

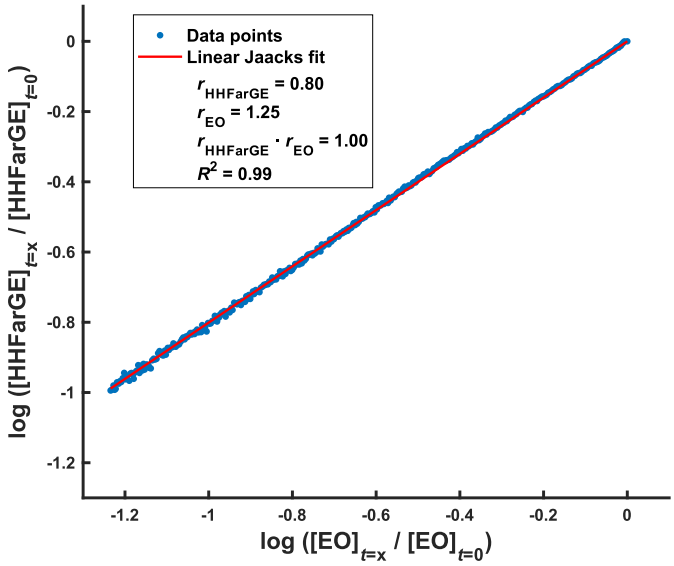

Figure S33: Jaacks fit of the *in situ* ^{1}H NMR copolymerization kinetics of HHFarGE with EO in a mixture of THF-d_8 and DMSO-d_6 (5:1) at 40 °C.

Investigation of side reaction during *in situ* copolymerization kinetics of PreGE with EO

Note that we unexpectedly observed the appearance of new signals between 4.9 – 6.6 ppm during the *in situ* copolymerization kinetics (Figure 3 + Figure S34). Chain transfer to the monomer due to proton abstraction of the α-methylene proton is a literature-known side reaction of the AROP, prevailing proton signals in a similar down-field region.[14] To reliably determine the reactivity ratios, we sought to further investigate this phenomenon as proton abstraction would falsely simulate an increased PreGE consumption. On account of previous reports applying the prenyl functionality as an OH protective group, we hypothesized that a base-catalyzed elimination by the alkoxide chain end leads to the formation of isoprene.[15,16] Scheme S2 suggests a six-membered transition state prior to elimination, which tentatively explains the elimination predominantly occuring for the short TGEs.

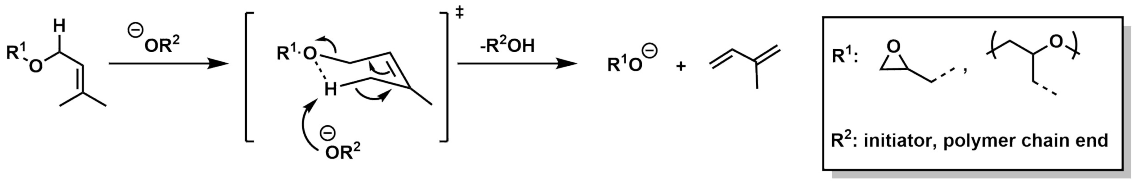

Scheme S2: Proposed base-catalyzed elimination of isoprene during the copolymerization of PreGE with EO.

In a second *in situ* kinetic experiment, all volatile components were cryo-transferred (THF-d_8, DMSO-d_6, isoprene) into a Young NMR tube. Subsequent NMR and GC analyses corroborate the hypothesis of isoprene forming during the copolymerization (Figure S35 – Figure S37). In summary,

monomer consumption is solely caused by monomer incorporation into the polymer chain, legitimizing the determined reactivity ratios and the related copolymer microstructure. Figure S38 additionally reveals the partial base-catalyzed prenyl-to-isoprenyl isomerization of the side chain under basic conditions (and vice versa for IsoPreGE).[17,18]

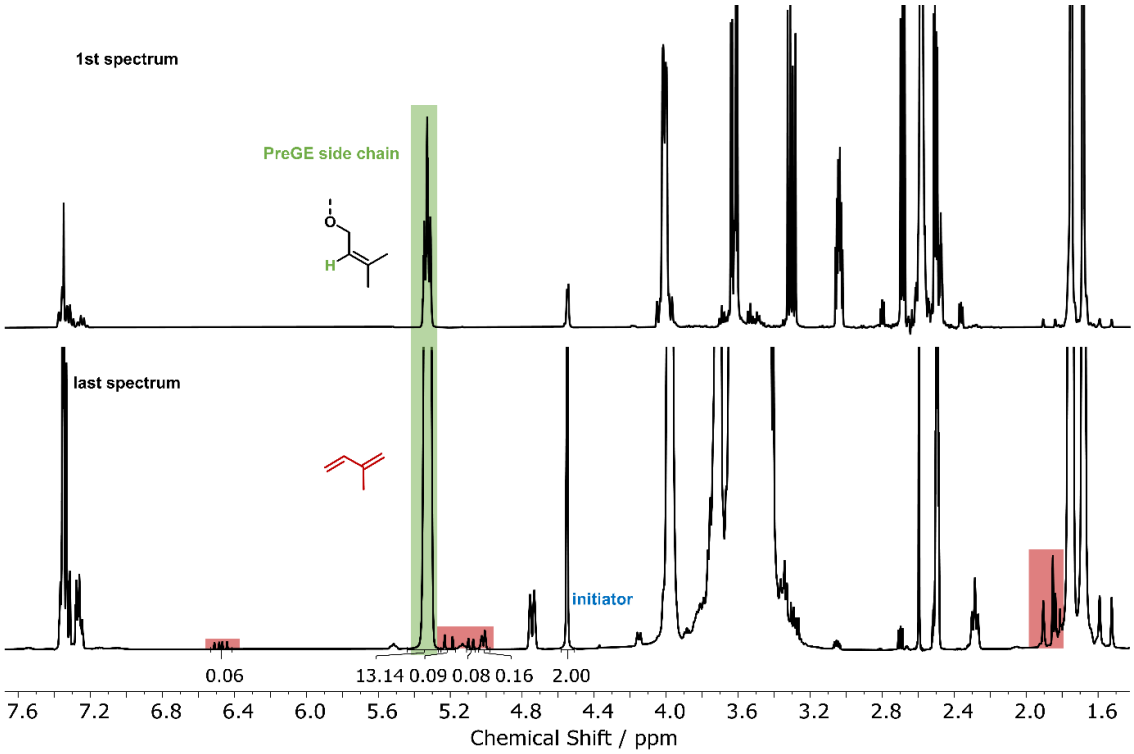

Figure S34: Overlay of the first and last ^{1}H NMR spectrum (400 MHz, THF-d_8) of the *in situ* kinetics, proving the elimination of isoprene in small quantities during copolymerization. The monomer amount undergoing elimination is below 0.5%.

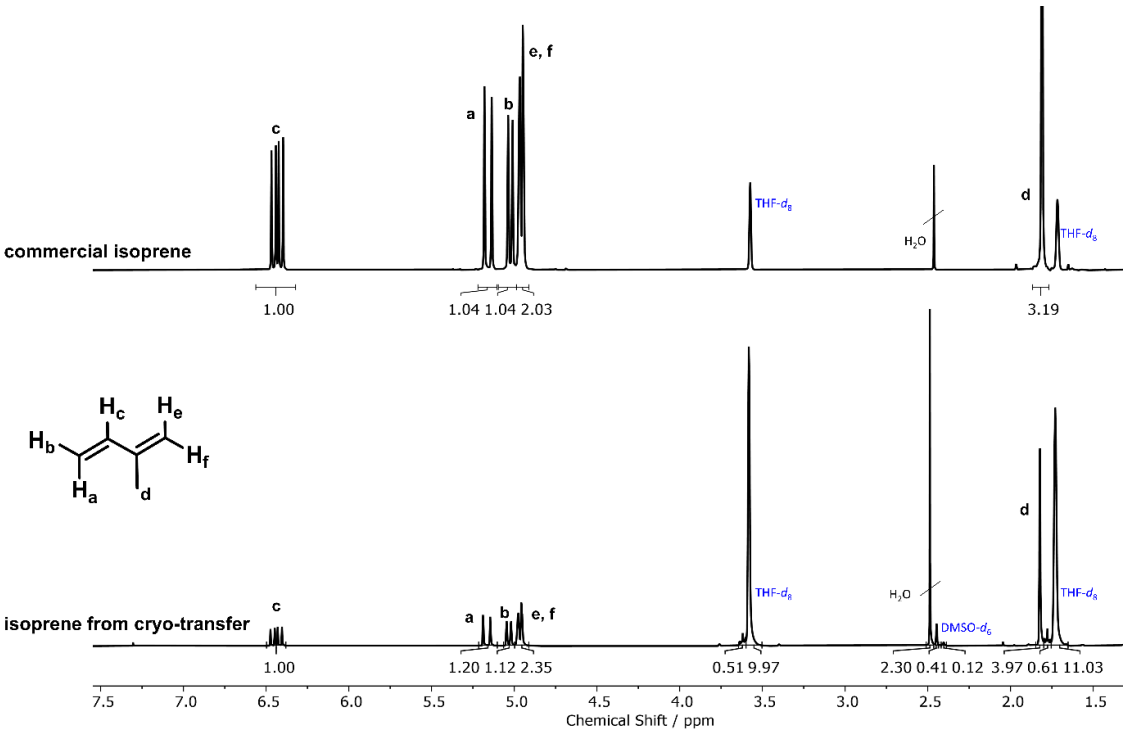

Figure S35: Overlay of ^{1}H NMR spectra (400 MHz, THF-d_8) of the commercial isoprene and cryo-transferred isoprene.

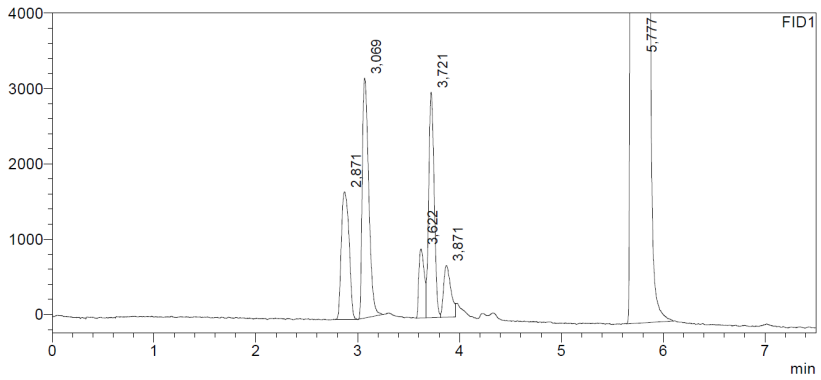

Figure S36: GC analysis of isoprene eliminated during the copolymerization with a $t_{retention,\ isorprene}$ = 3.721 (area 98.8 %). Isoprene and THF-d_8 were isolated via cryo-transfer from the NMR tube and the major peak can be ascribed to THF-d_8 with a $t_{retention,\ THF}$ = 5.777. All other signals are impurities in DMSO, which was used to prepare the GC sample.

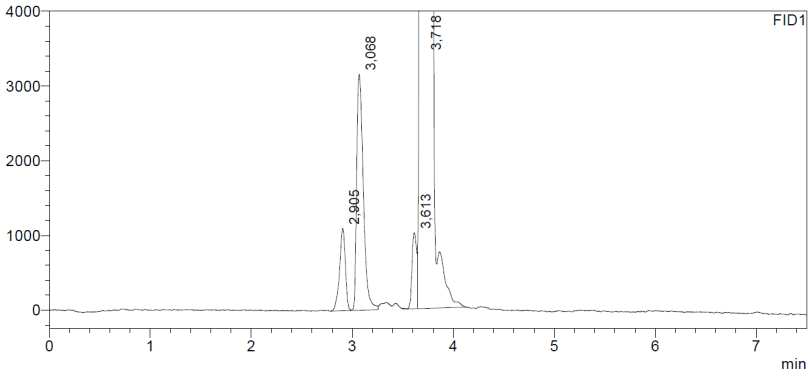

Figure S37: GC analysis of commercial isoprene with a $t_{retention,\ isorprene}$ = 3.718 (area 98.8 %). All other signals are impurities in DMSO, which was used to prepare the GC sample.

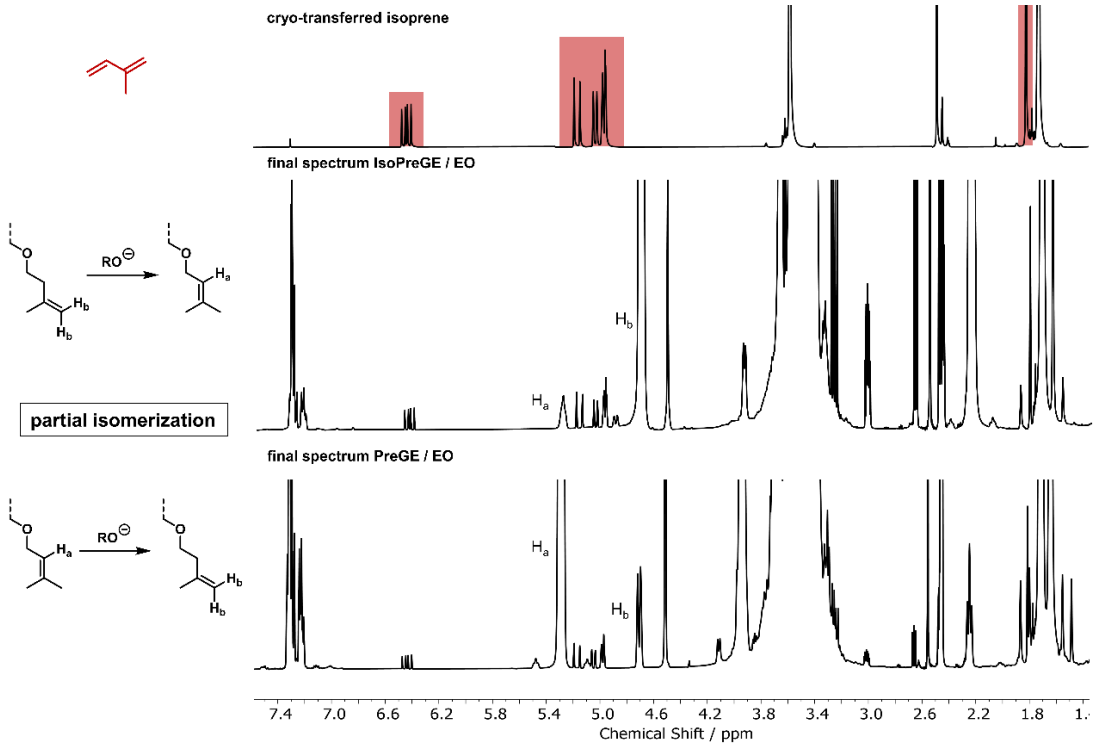

Figure S38: Overlay of ^{1}H NMR spectra (400 MHz, $CDCl_3$) of the spectrum of the cryo-transferred isoprene (top) and the final spectra of the *in situ* kinetic measurements of IsoPreGE (middle) with EO and PreGE with EO (bottom). *In situ* NMR kinetics mirror the formation of isoprene in trace amounts. The overlay also demonstrates a slight isomerization of the prenyl and isoprenly side chain to the respective isomer (H_a and H_b).

Kinetic data of the copolymerization of PreGE with EO

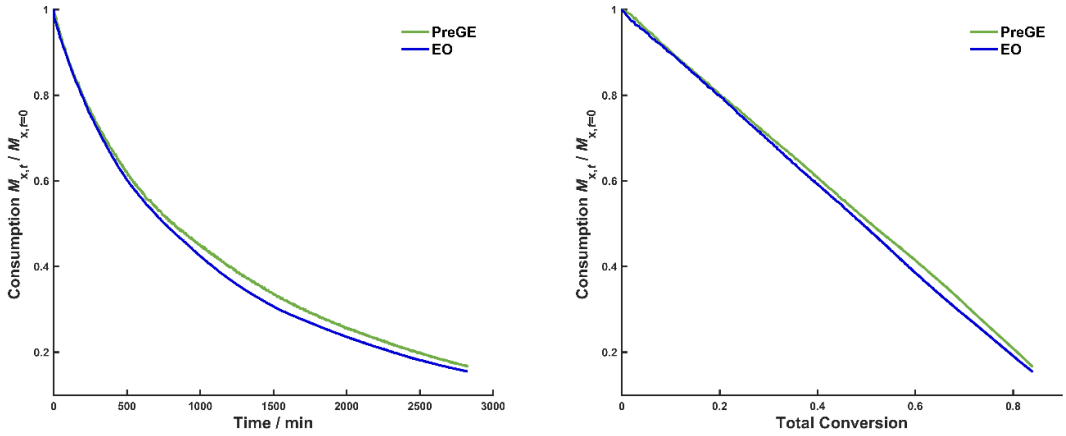

Figure S39: Time-conversion plot of the anionic copolymerization of IsoPreGE and with EO, determined via *in situ* ^{1}H NMR kinetics (left). Individual monomer conversion versus total monomer conversion (right).

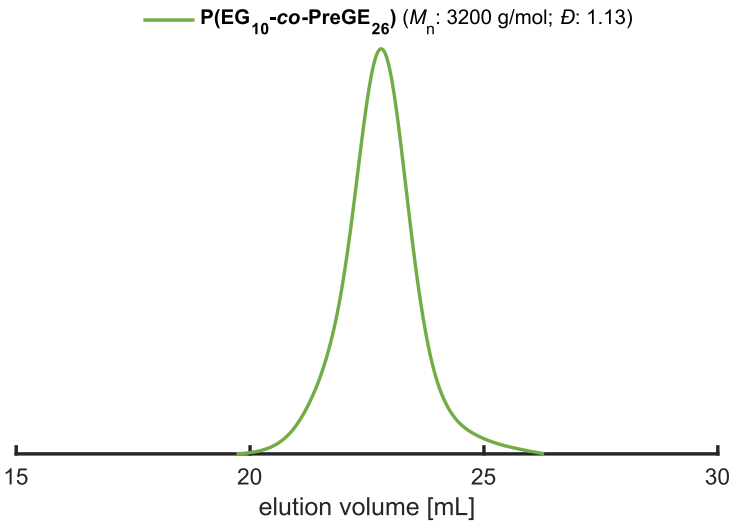

Figure S40: SEC elugram (RI detector, eluent: DMF, PEG calibration) of the P(EG_{10}-*co*-$PreGE_{26}$) copolymer synthesized from the *in situ* ^{1}H NMR copolymerization kinetics. SEC analysis: M_n = 3200 g·mol^{-1}, $Đ$ = 1.13.

Kinetic data of the copolymerization of IsoPreGE with EO

Note that the isoprene formation has additionally been observed during the copolymerization of IsoPreGE and EO. We conclude an elimination of isoprene (Scheme S2) from the glycidyl side chain occurring, which is confirmed in analogy to the PreGE/EO comonomer pair in the previous section (Figure S38).

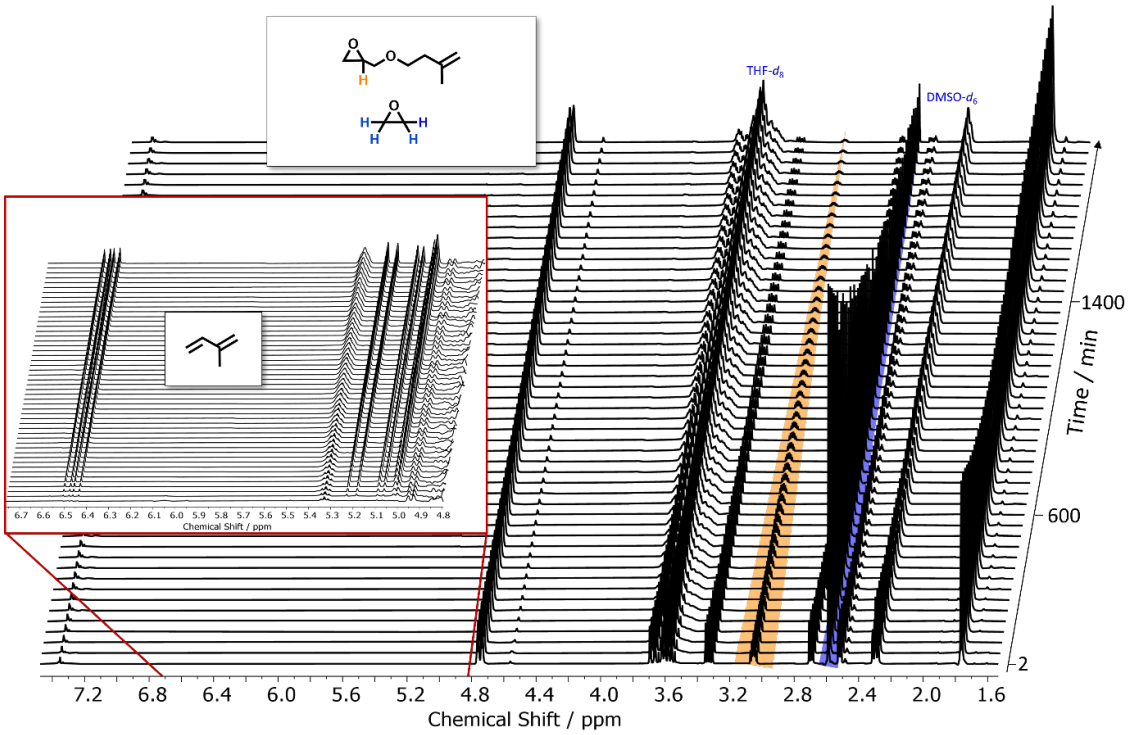

Figure S41: Selection of ^{1}H NMR spectra (400 MHz, THF-d_8 : DMSO-d_6= 5:1) for the *in situ* NMR kinetics of the statistical copolymerization of IsoPreGE with EO at 40 °C. Relevant epoxide signals for evaluation are highlighted in green at 3.05 ppm (IsoPreGE) and blue at 2.59 ppm (EO). Since spectra were recorded at 2 min intervals over a period of 32.9 h, only every 20th spectrum is displayed. The zoom-in section displays the appearance of new signals, which is ascribed to the isoprene formation during the copolymerization.

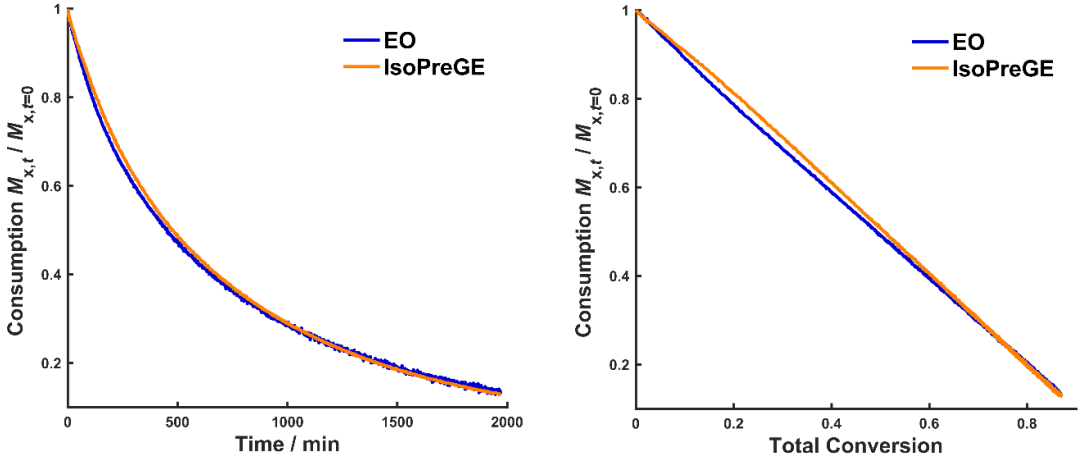

Figure S42: Time-conversion plot of the anionic copolymerization of IsoPreGE and with EO, determined via *in situ* ^{1}H NMR kinetics (left). Individual monomer conversion versus total monomer conversion (right).

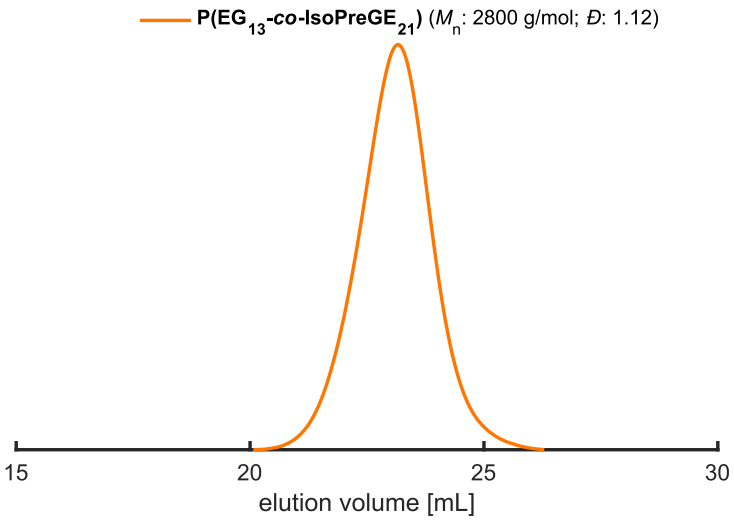

Figure S43: SEC elugram (RI detector, eluent: DMF, PEG calibration) of the P(EG_{13}-*co*-$IsoPreGE_{21}$) copolymer synthesized from the *in situ* ^{1}H NMR copolymerization kinetics. SEC analysis: M_n = 2800 g·mol^{-1}, $Đ$ = 1.12.

Kinetic data of the copolymerization of GeraGE with EO

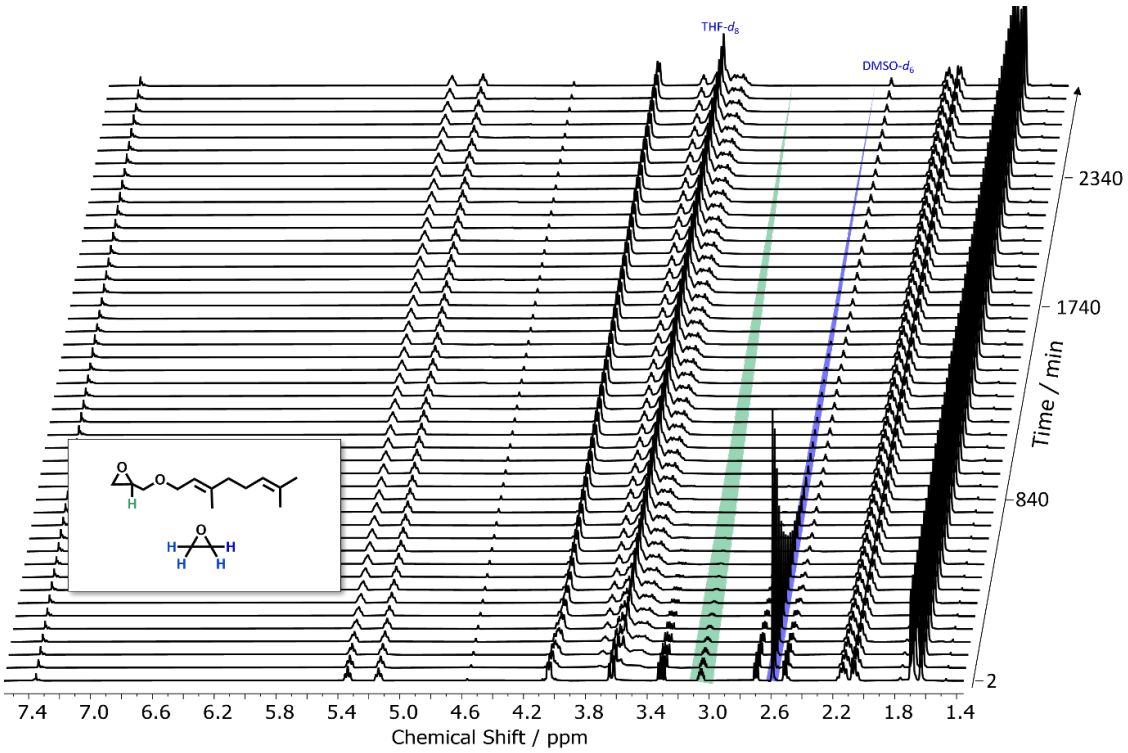

Figure S44: Selection of ^{1}H NMR spectra (400 MHz, THF-d_8 : DMSO-d_6= 5:1) for the *in situ* NMR kinetics of the statistical copolymerization of GeraGE with EO at 40 °C (top). Relevant epoxide signals for evaluation are highlighted in green at 3.05 ppm (GeraGE) and blue at 2.59 ppm (EO). Since spectra were recorded at 2 min intervals over a period of 46.0 h, only every 30th spectrum is displayed.

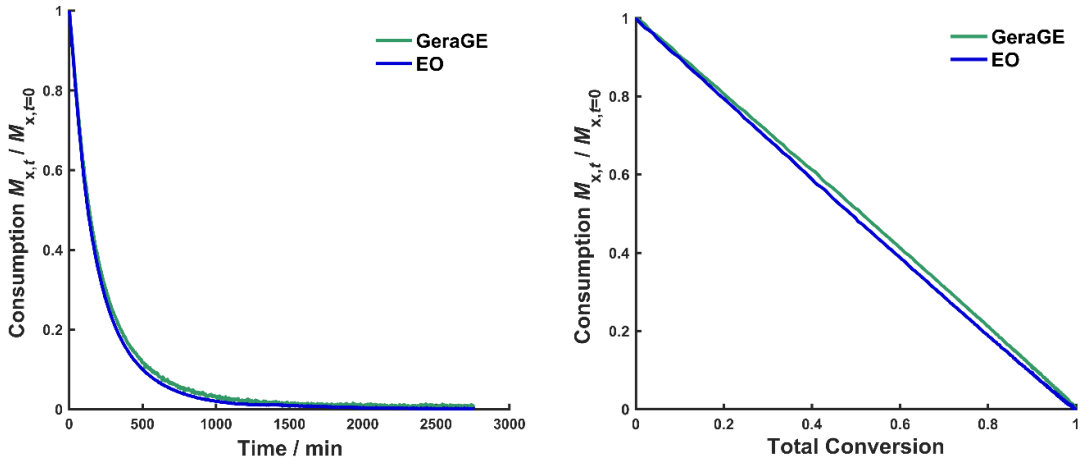

Figure S45: Time-conversion plot of the anionic copolymerization of GeraGE and with EO, determined via *in situ* ^{1}H NMR kinetics (left). Individual monomer conversion versus total monomer conversion (right).

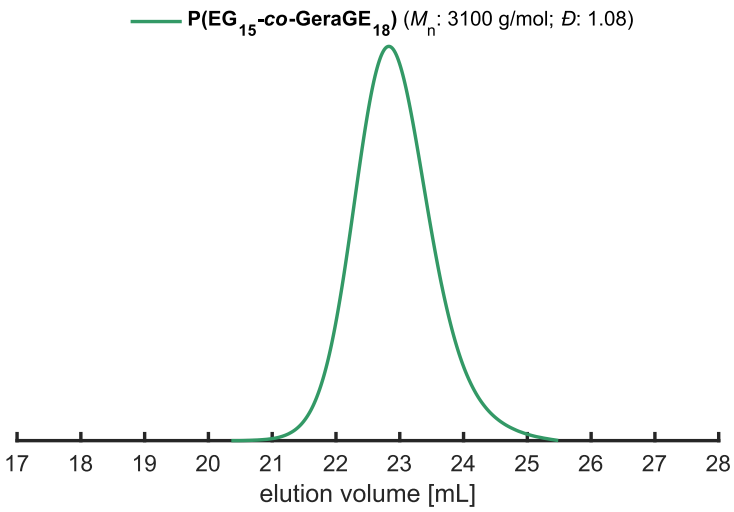

Figure S46: SEC elugram (RI detector, eluent: DMF, PEG calibration) of the P(EG_{15}-*co*-$GeraGE_{18}$) copolymer synthesized from the *in situ* ^{1}H NMR copolymerization kinetics. SEC analysis: M_n = 3100 g·mol^{-1}, $Đ$ = 1.08.

Kinetic data of the copolymerization of NerGE with EO

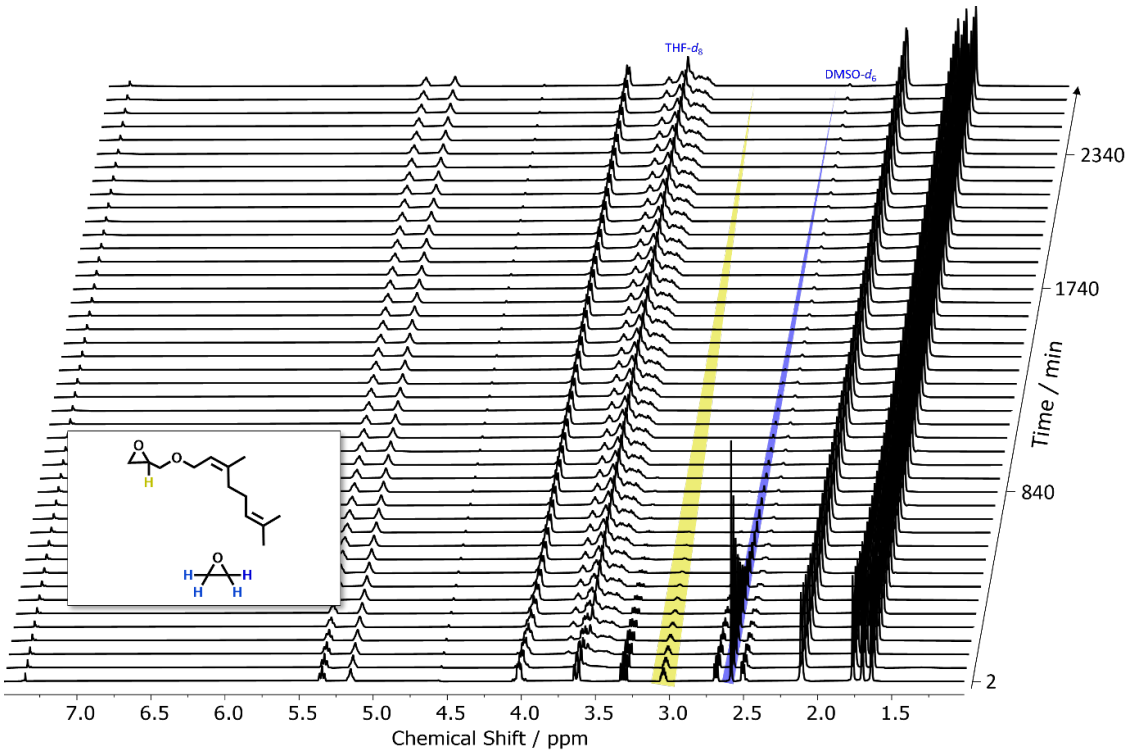

Figure S47: Selection of ^{1}H NMR spectra (400 MHz, THF-d_8 : DMSO-d_6= 5:1) for the *in situ* NMR kinetics of the statistical copolymerization of NerGE with EO at 40 °C. Relevant epoxide signals for evaluation are highlighted in yellow at 3.04 ppm (NerGE) and blue at 2.59 ppm (EO). Since spectra were recorded at 2 min intervals over a period of 44.6 h, only every 30th spectrum is displayed.

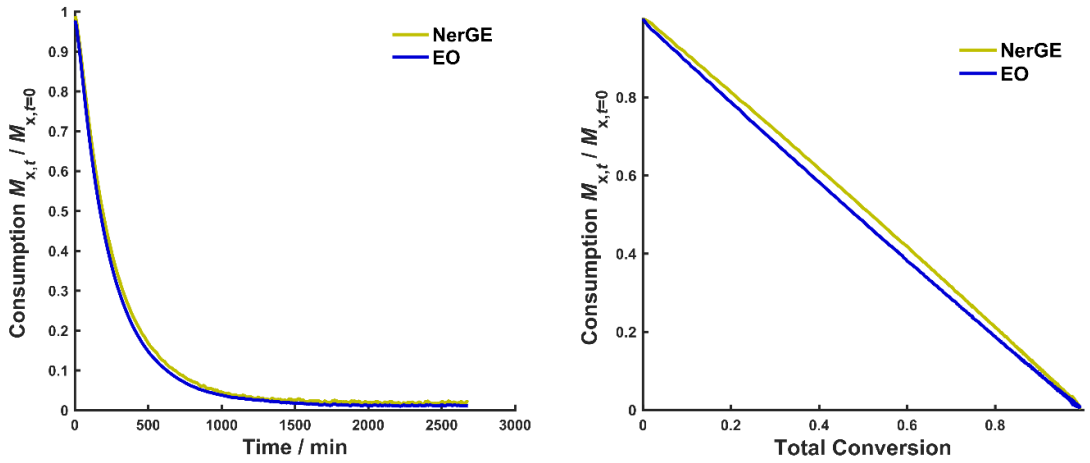

Figure S48: Time-conversion plot of the anionic copolymerization of NerGE and with EO, determined via *in situ* ^{1}H NMR kinetics (left). Individual monomer conversion versus total monomer conversion (right).

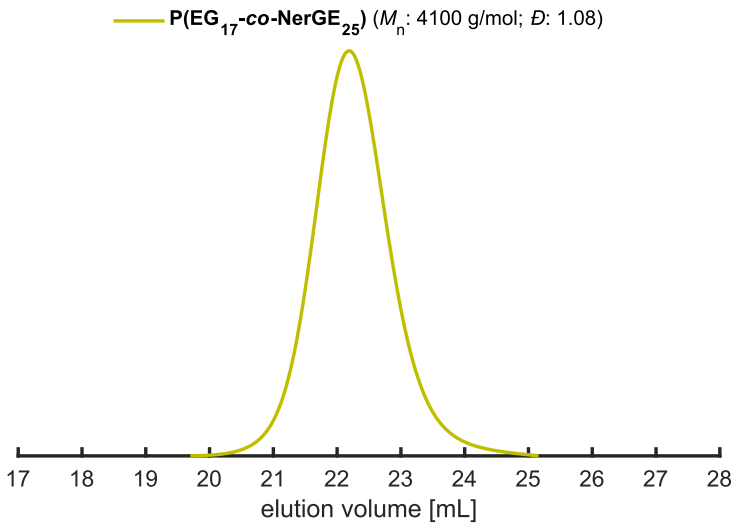

Figure S49: SEC elugram (RI detector, eluent: DMF, PEG calibration) of the P(EG_{17}-*co*-$NerGE_{25}$) copolymer synthesized from the *in situ* ^{1}H NMR copolymerization kinetics. SEC analysis: M_n = 4100 g·mol^{-1}, $Đ$ = 1.08.

Kinetic data of the copolymerization of DHPreGE with EO

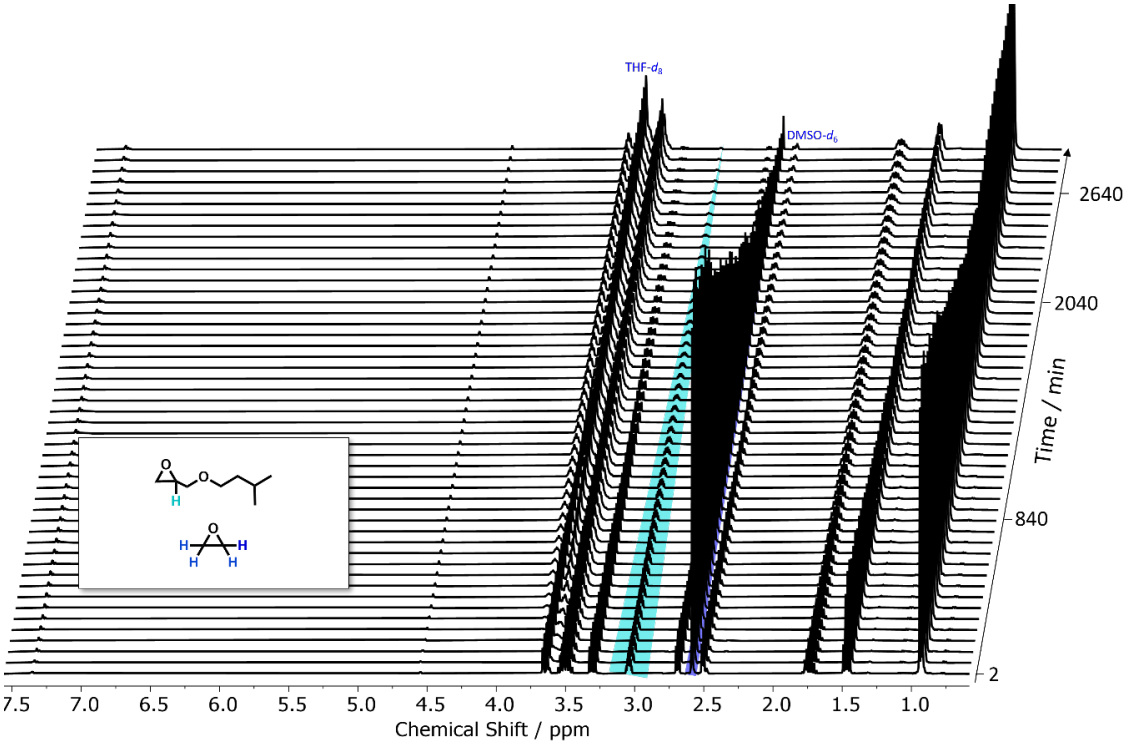

Figure S50: Selection of ^{1}H NMR spectra (400 MHz, THF-d_8 : DMSO-d_6= 5:1) for the *in situ* NMR kinetics of the statistical copolymerization of DHPreGE with EO at 40 °C. Relevant epoxide signals for evaluation are highlighted in cyan at 3.04 ppm (DHPreGE) and blue at 2.59 ppm (EO). Since spectra were recorded at 2 min intervals over a period of 48.4 h, only every 30th spectrum is displayed.

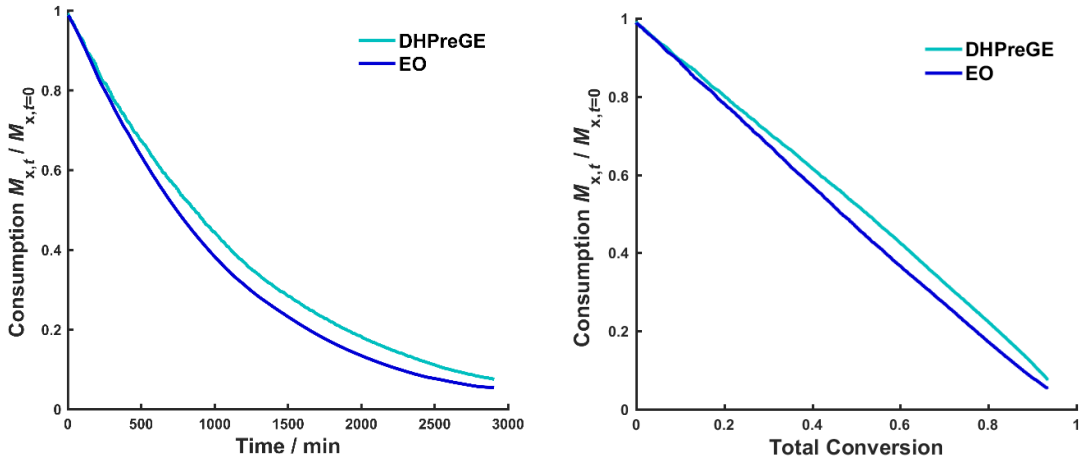

Figure S51: Time-conversion plot of the anionic copolymerization of DHPreGE and with EO, determined via *in situ* ^{1}H NMR kinetics (left). Individual monomer conversion versus total monomer (right).

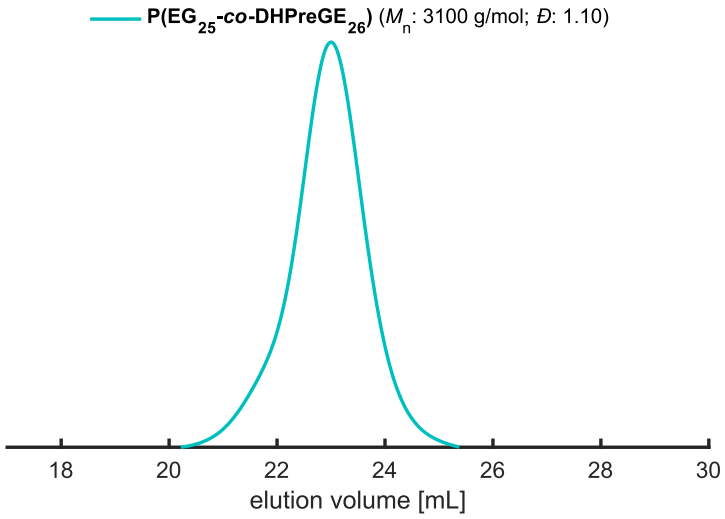

Figure S52: SEC elugram (RI detector, eluent: DMF, PEG calibration) of the P(EG_{25}-*co*-$DHPreGE_{26}$) copolymer synthesized from the *in situ* ^{1}H NMR copolymerization kinetics. SEC analysis: M_n = 3100 g·mol^{-1}, $Đ$ = 1.10.

Kinetic data of the copolymerization of THGeraGE with EO

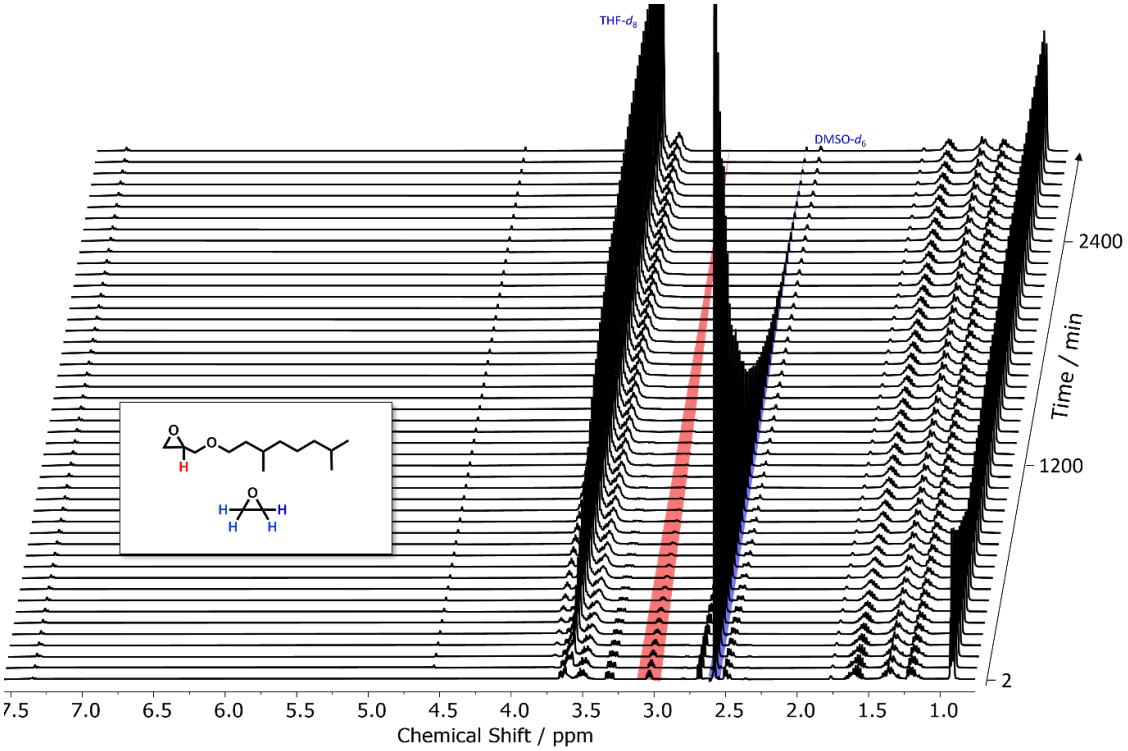

Figure S53: Selection of ^{1}H NMR spectra (400 MHz, THF-d_8 : DMSO-d_6= 5:1) for the *in situ* NMR kinetics of the statistical copolymerization of THGeraGE with EO at 40 °C. Relevant epoxide signals for evaluation are highlighted in red at 3.03 ppm (THGeraGE) and blue at 2.59 ppm (EO). Since spectra were recorded at 2 min intervals over a period of 48 h, only every 30th spectrum is displayed.

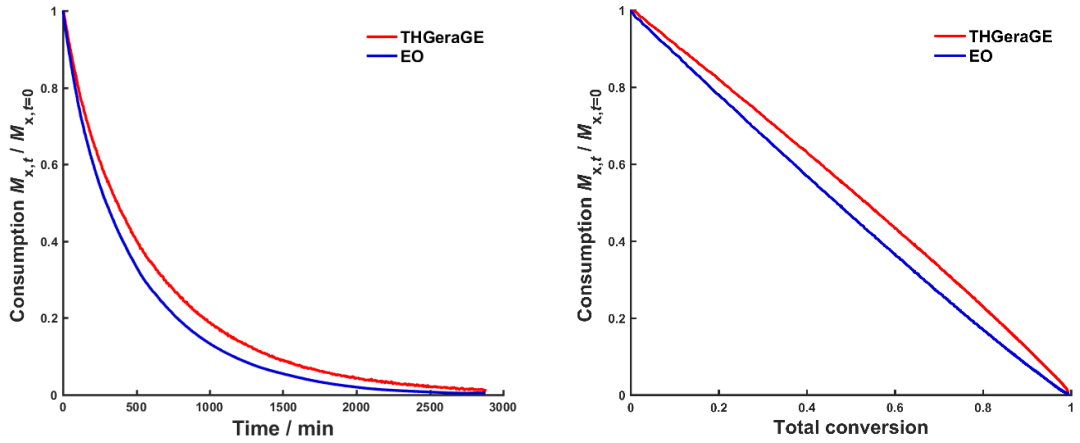

Figure S54: Time-conversion plot of the anionic copolymerization of THGeraGE and with EO, determined via *in situ* ^{1}H NMR kinetics (left). Individual monomer conversion versus total monomer conversion (right).

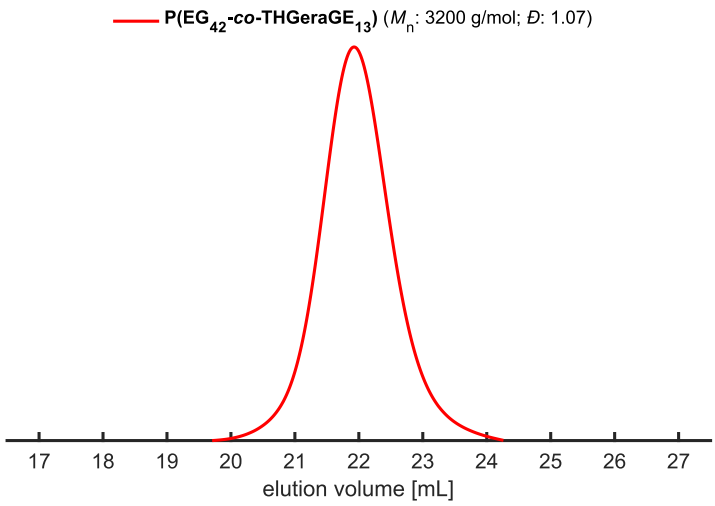

Figure S55: SEC elugram (RI detector, eluent: DMF, PEG calibration) of the P(EG_{42}-*co*-$THGeraGE_{13}$) copolymer synthesized from the *in situ* ^{1}H NMR copolymerization kinetics. SEC analysis: M_n = 3200 g·mol^{-1}, $Đ$ = 1.07.

Kinetic data of the copolymerization of HHFarGE with EO

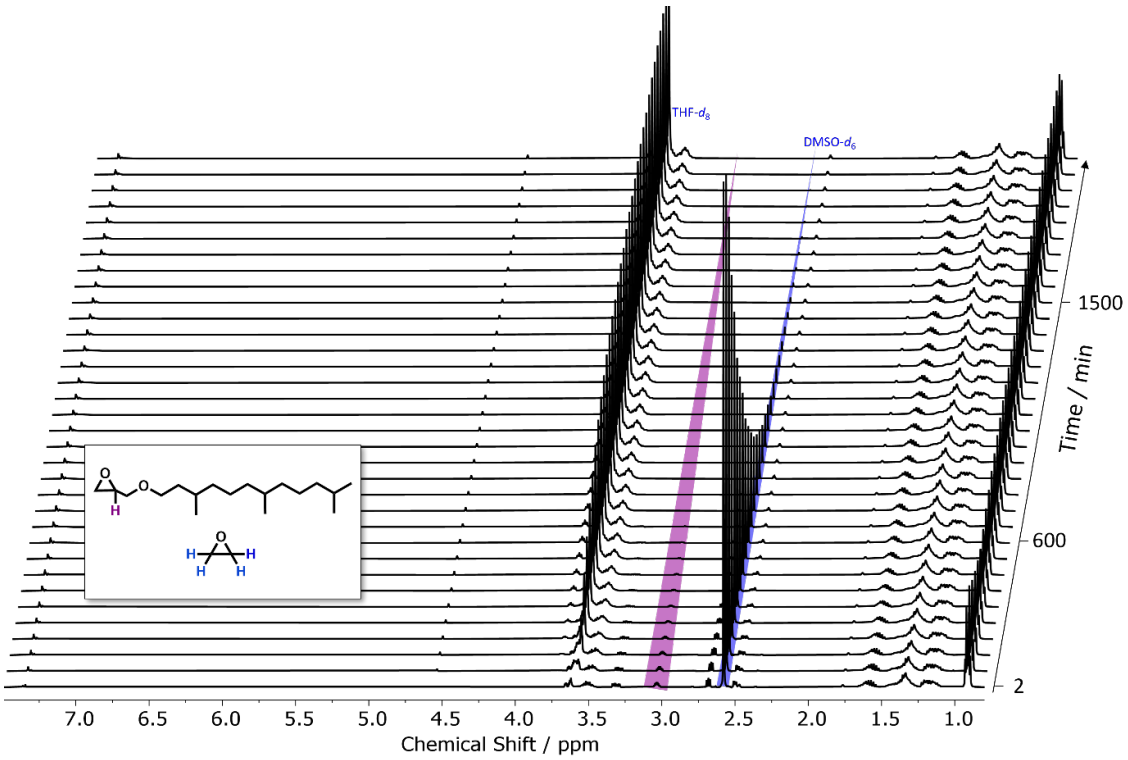

Figure S56: Selection of ^{1}H NMR spectra (400 MHz, THF-d_8 : DMSO-d_6= 5:1) for the *in situ* kinetics of the statistical copolymerization of HHFarGE with EO at 40 °C. Relevant epoxide signals for evaluation are highlighted in purple (HHFarGE) at 3.05 ppm and blue (EO) at 2.59 ppm. Since spectra were recorded every 2 min over a period of 34.0 h, only every 30th spectrum is displayed.

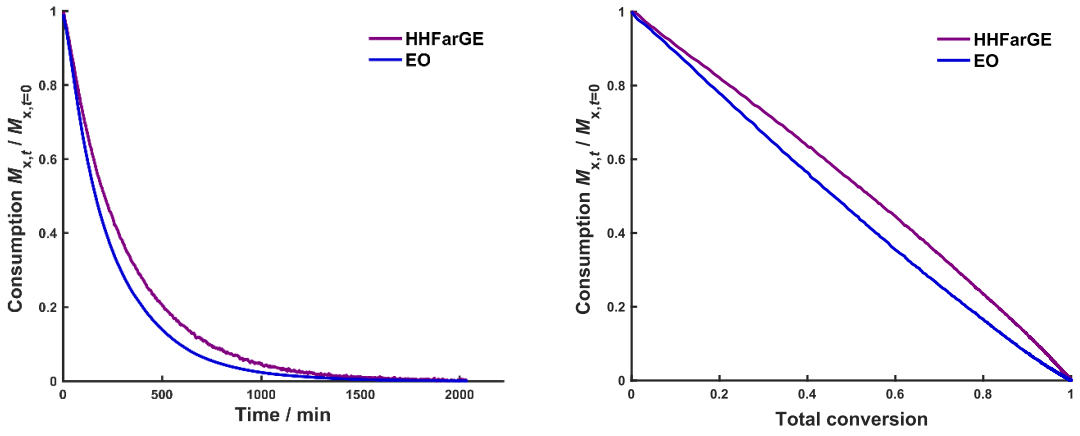

Figure S57: Time-conversion plot of the anionic copolymerization of HHFarGE and with EO, determined via *in situ* ^{1}H NMR kinetics (left). Individual monomer conversion versus total monomer conversion (right).

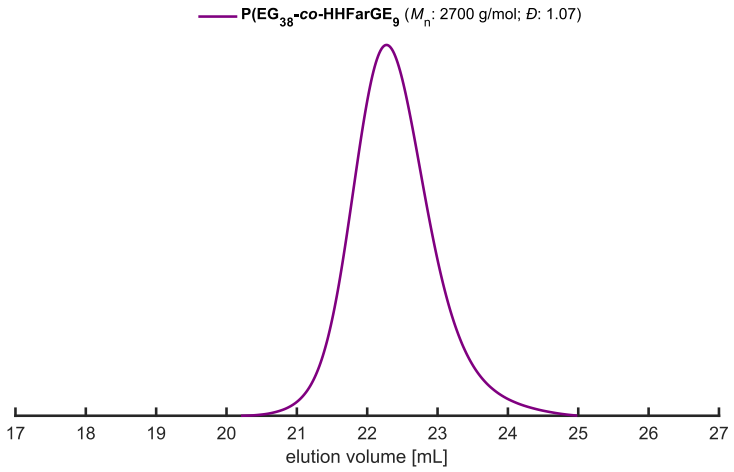

Figure S58: SEC elugram (RI detector, eluent: DMF, PEG calibration) of the P(EG_{38}-*co*-$HHFarGE_9$) copolymer synthesized from the *in situ* ^{1}H NMR copolymerization kinetics. SEC analysis: M_n = 2700 g·mol^{-1}, $Đ$ = 1.07.

Postpolymerization Functionalizations

Thiol-Ene Click

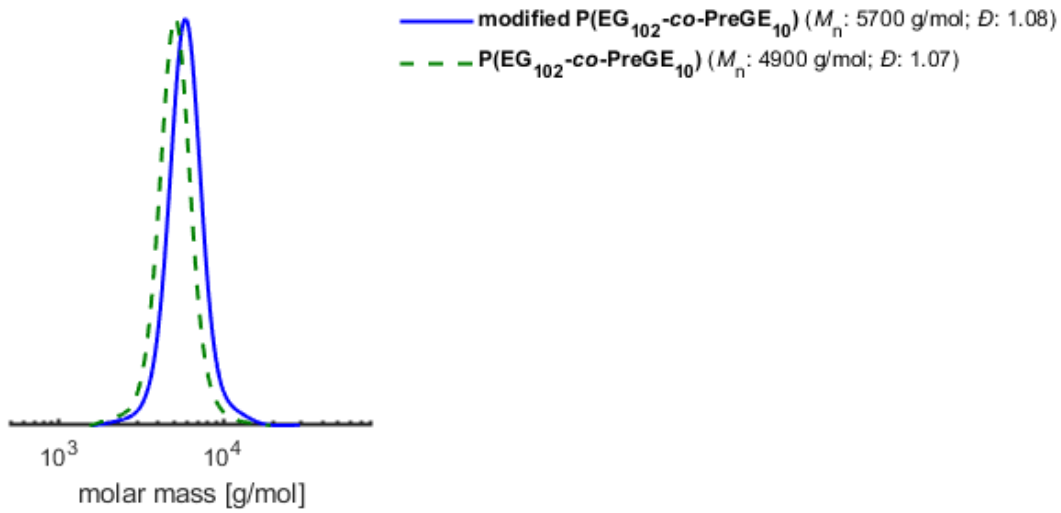

Figure S59: SEC traces of modified P(EG_{102}-*co*-$PreGE_{10}$) (blue) and its respective precursor polymer (green, dotted line). (Eluent: DMF, RI-Detector, PEG calibration).

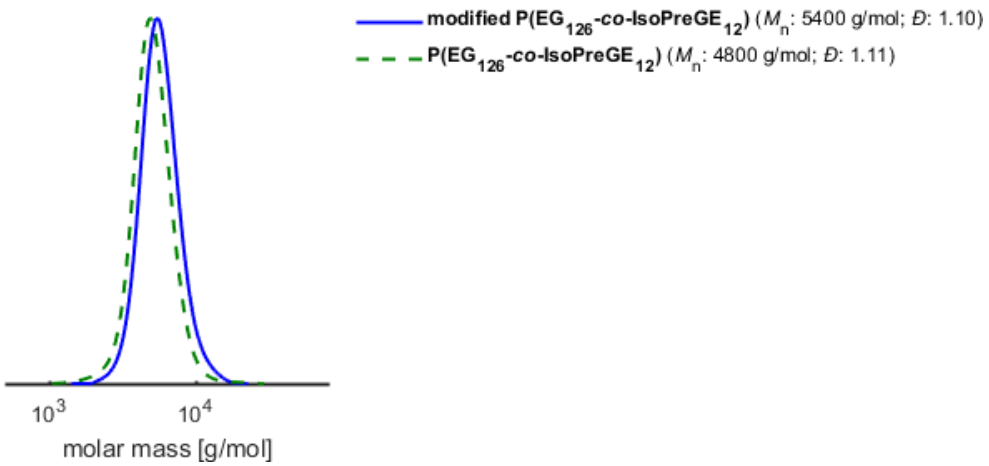

Figure S60: SEC traces of modified P(EG_{126}-*co*-$IsoPreGE_{12}$) (blue) and its respective precursor polymer (green, dotted line). (Eluent: DMF, RI-Detector, PEG calibration).

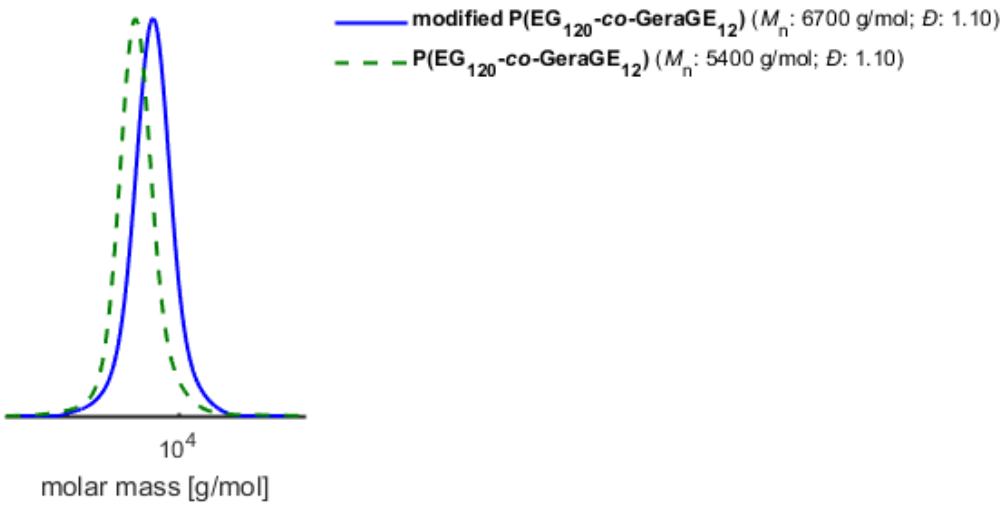

Figure S61: SEC traces of modified P(EG_{120}-*co*-$GeraGE_{12}$) (blue) and its respective precursor polymer (green, dotted line). (Eluent: DMF, RI-Detector, PEG calibration).

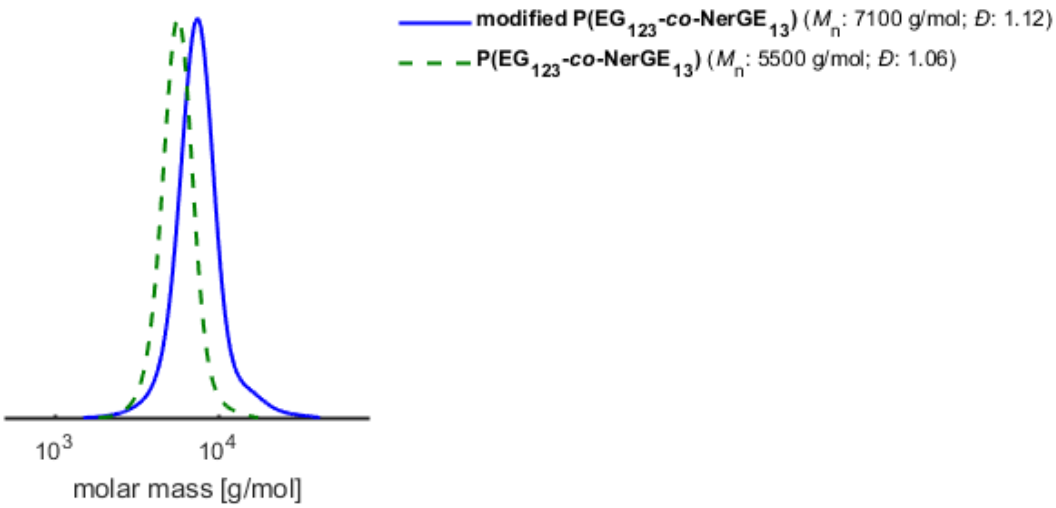

Figure S62: SEC traces of modified P(EG_{123}-*co*-$NerGE_{13}$) (blue) and its respective precursor polymer (green, dotted line) (Eluent: DMF, RI-Detector, PEG calibration).

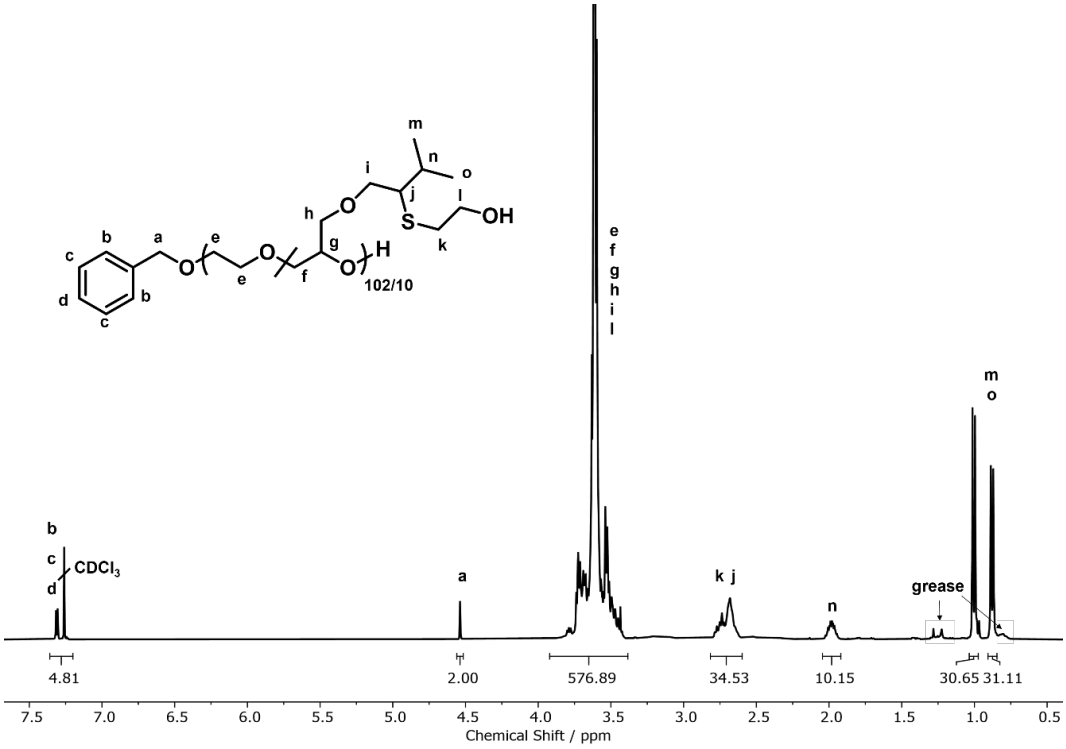

Figure S63: ^{1}H NMR spectrum of P(EG$_{102}$-*co*-PreGE$_{10}$) functionalized with 2-mercaptoethanol via Thiol-ene click reaction (400 MHz, CDCl$_3$).

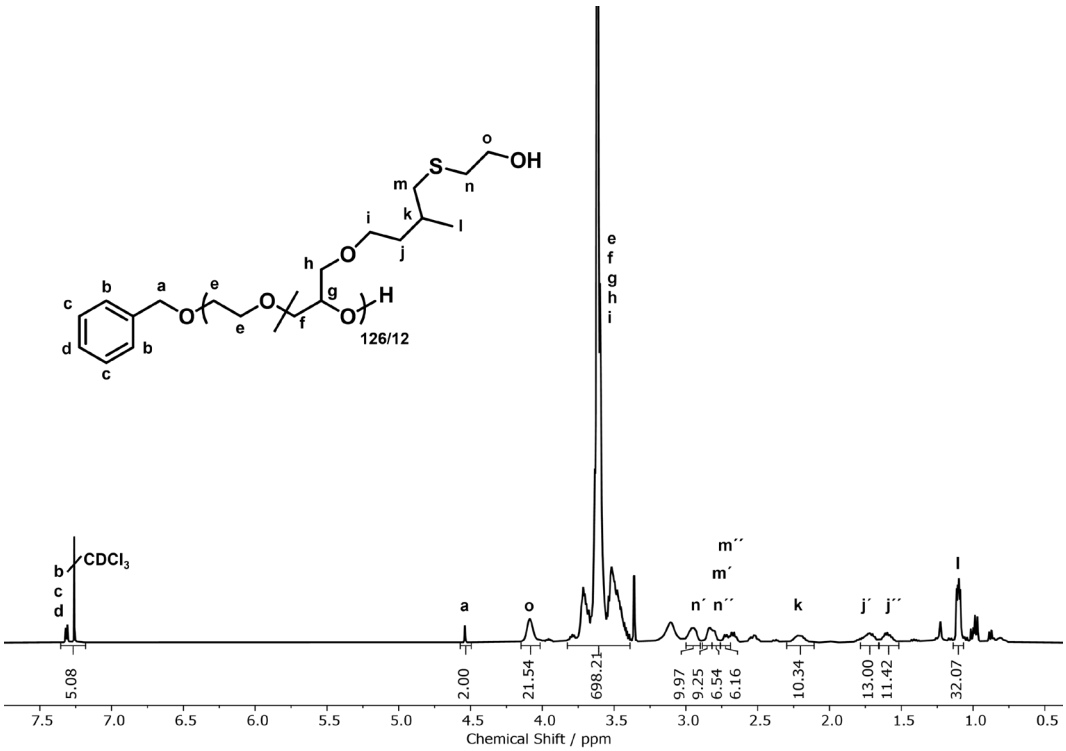

Figure S64: ^{1}H NMR spectrum of P(EG$_{126}$-*co*-IsoPreGE$_{12}$) functionalized with 2-mercaptoethanol via Thiol-ene click reaction (400 MHz, CDCl$_3$). Isoprenyl glycidyl ether partially isomerized to prenyl glycidyl ether during polymerization and was also functionalized. Signals are omitted for clarity.

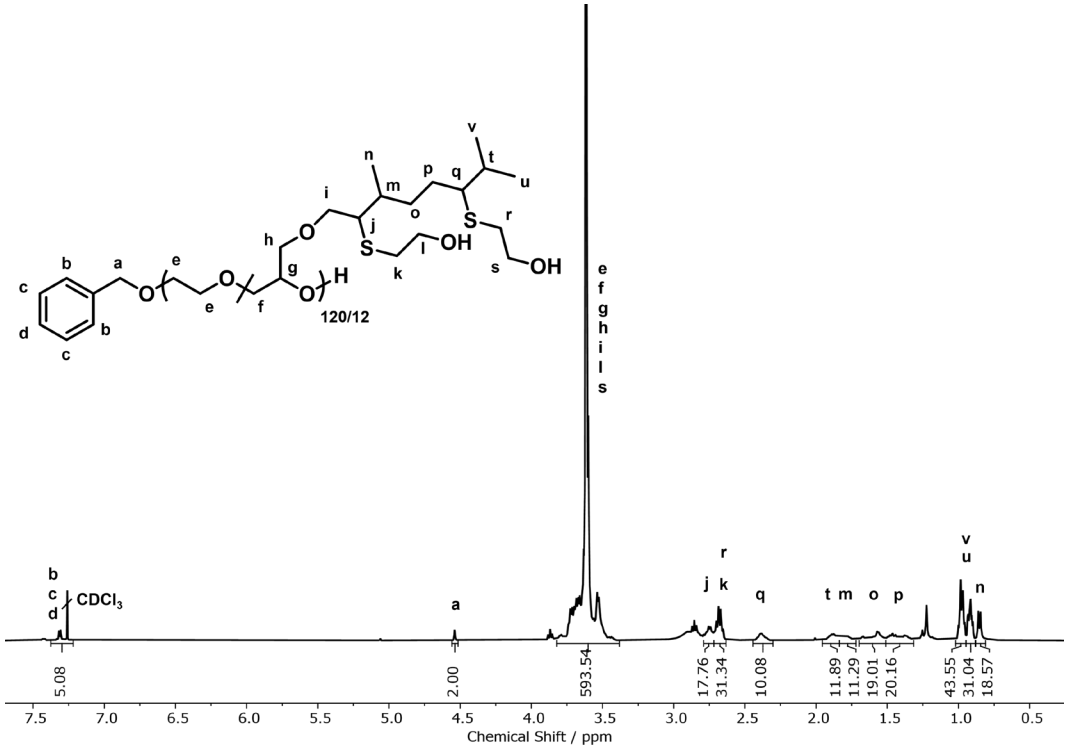

Figure S65: ^{1}H NMR spectrum of P(EG$_{120}$-*co*-GeraGE$_{12}$) functionalized with 2-mercaptoethanol via thiol-ene click reaction (400 MHz, $CDCl_3$).

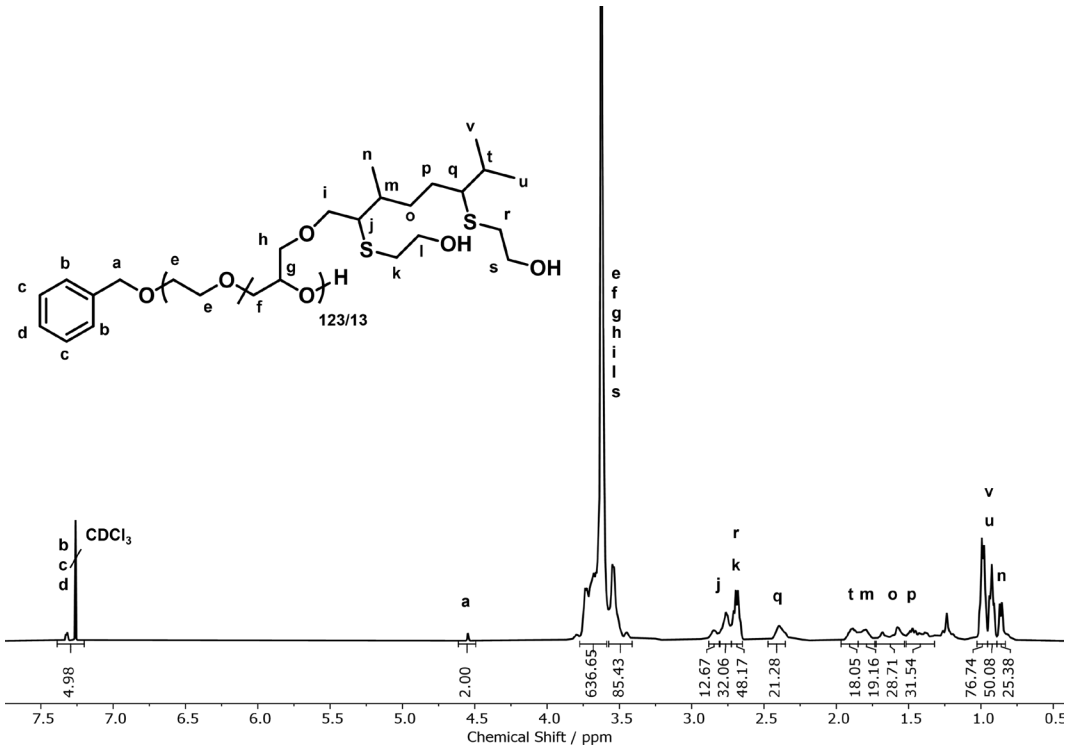

Figure S66: ^{1}H NMR spectrum of P(EG$_{123}$-*co*-NerGE$_{13}$) functionalized with 2-mercaptoethanol via thiol-ene click reaction (400 MHz, $CDCl_3$).

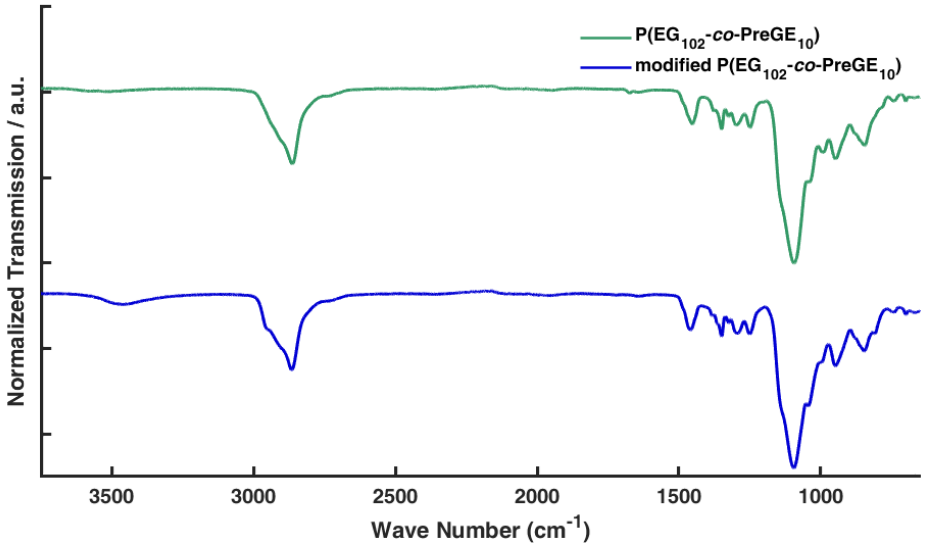

Figure S67: IR spectrum of P(EG_{102}-*co*-$PreGE_{10}$) functionalized with 2-mercaptoethanol via thiol-ene click reaction.

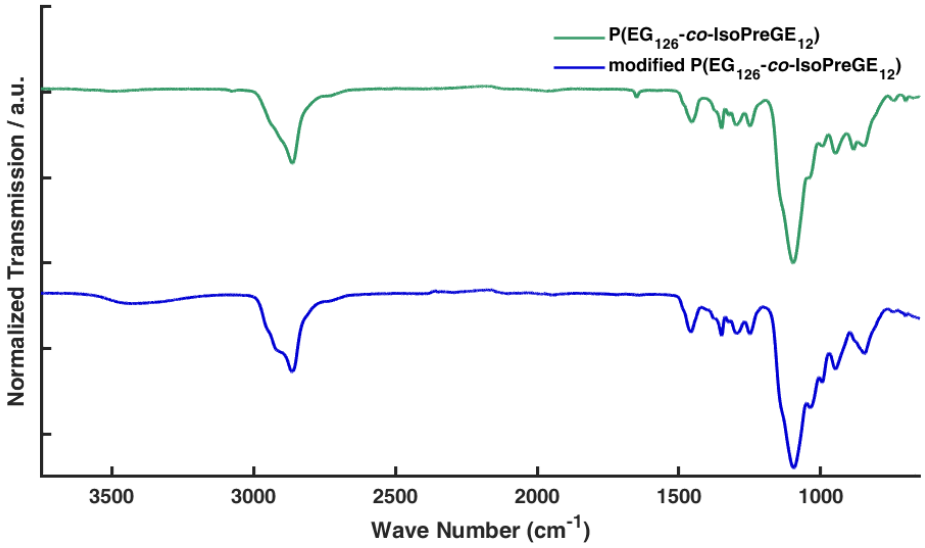

Figure S68: IR spectrum of P(EG_{126}-co-$IsoPreGE_{12}$) functionalized with 2-mercaptoethanol via thiol-ene click reaction.

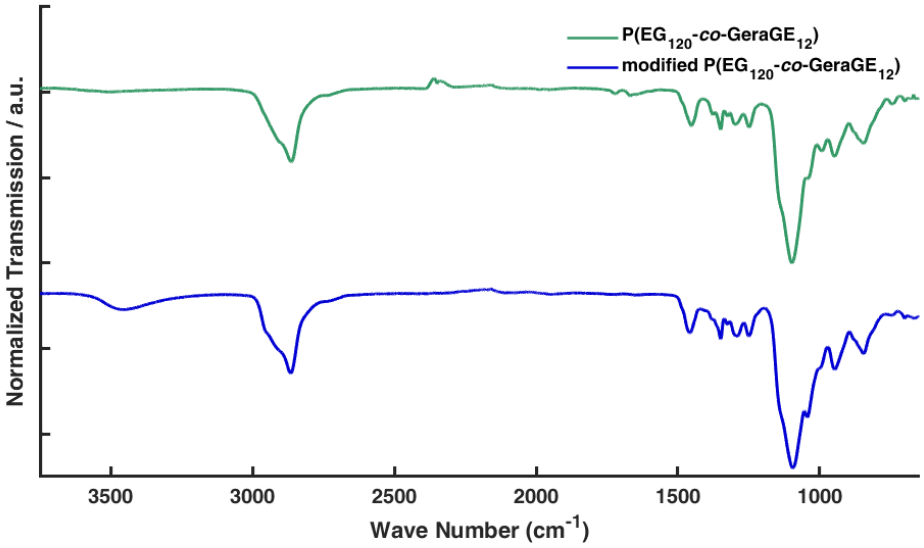

Figure S69: IR spectrum of P(EG_{120}-*co*-$GeraGE_{12}$) functionalized with 2-mercaptoethanol via thiol-ene click reaction.

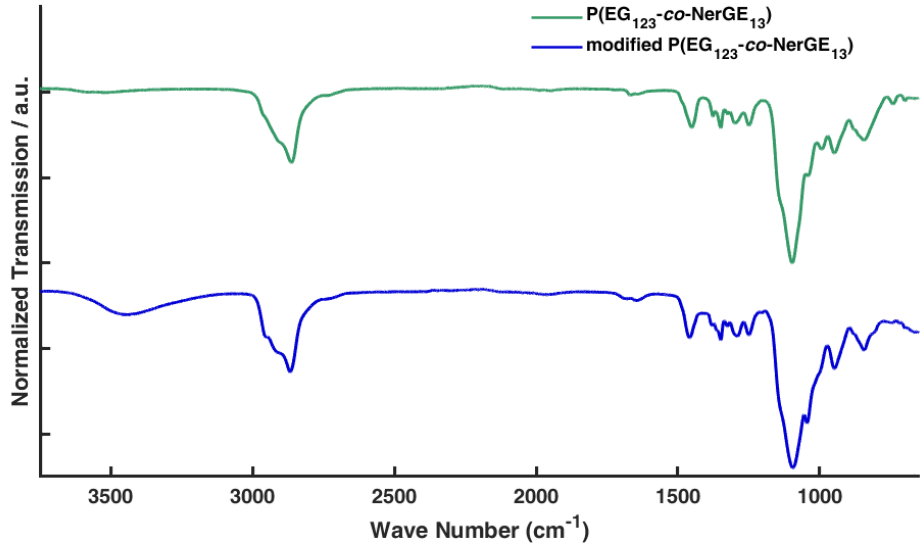

Figure S70: IR spectrum of P(EG_{123}-*co*-$NerGE_{13}$) functionalized with 2-mercaptoethanol via Thiol-ene click reaction.

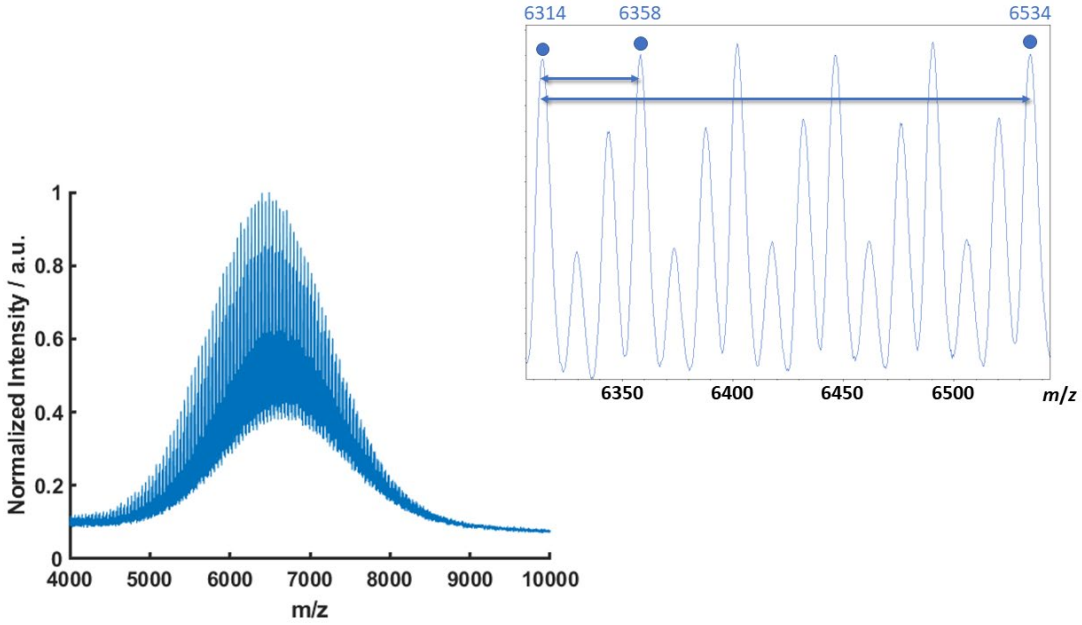

Figure S71: MALDI-ToF of P(EG_{102}-*co*-$PreGE_{10}$) functionalized with 2-mercaptoethanol via Thiol-ene click reaction. Small arrow denotes the mass difference of one EO unit with 44 g/mol. Large arrow denotes the mass difference of the functionalized PreGE unit with a mass difference of 220 g/mol. To be exact, 220 g/mol could also be a multiple of 44 g/mol.

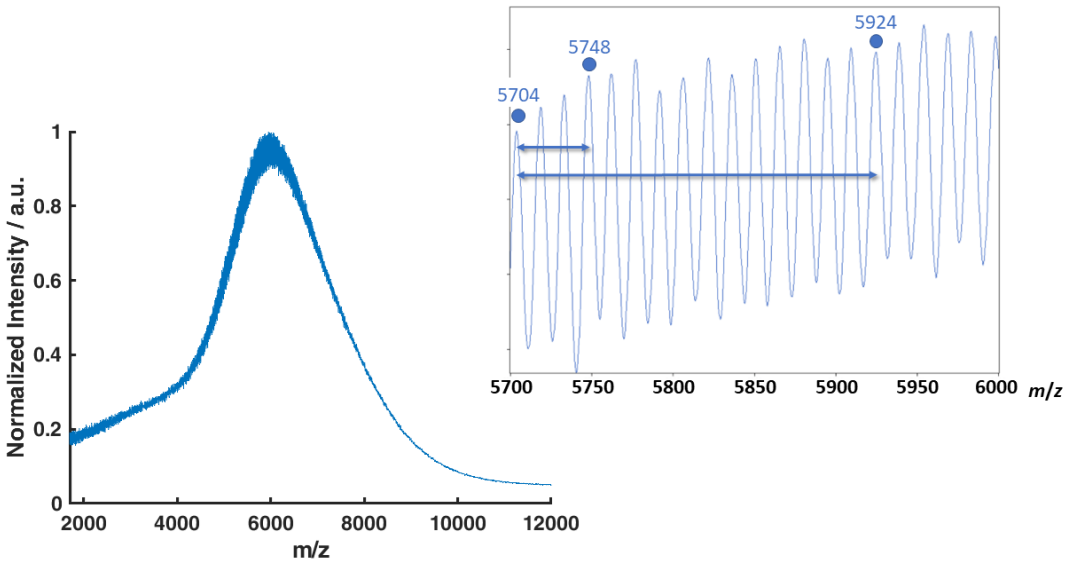

Figure S72: MALDI-ToF of P(EG_{126}-*co*-$IsoPreGE_{12}$) functionalized with 2-mercaptoethanol via Thiol-ene click reaction. Small arrow denotes the mass difference of one EO unit with 44 g/mol. Large arrow denotes the mass difference of the functionalized IsoPreGE unit with a mass difference of 220 g/mol. To be exact, 220 g/mol could also be a multiple of 44 g/mol.

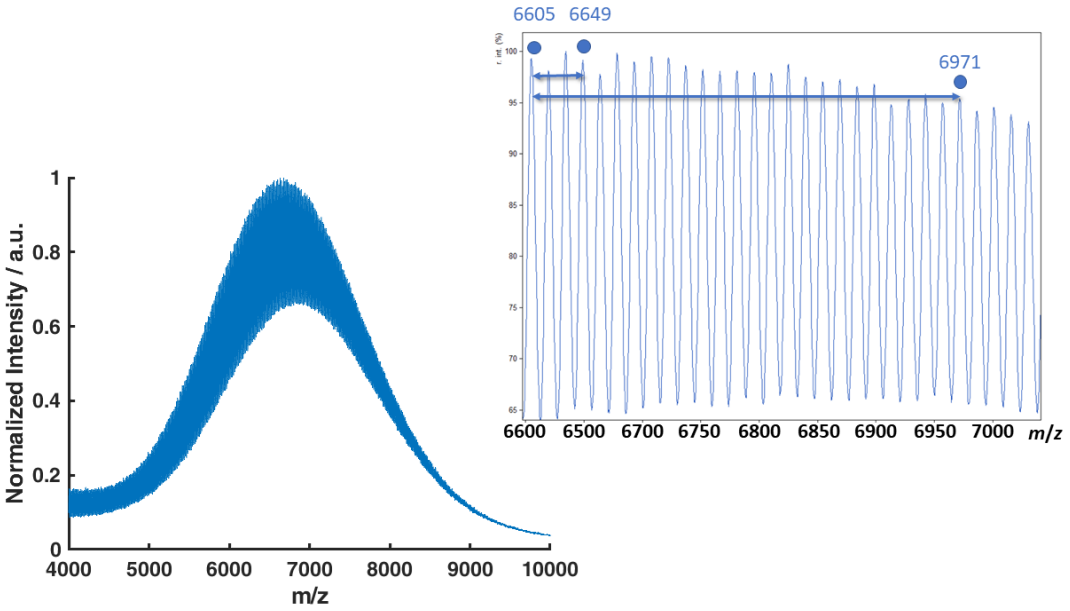

Figure S73: MALDI-ToF of P(EG_{120}-*co*-$GeraGE_{12}$) functionalized with 2-mercaptoethanol via Thiol-ene click reaction. Small arrow denotes the mass difference of one EO unit with 44 g/mol. Large arrow denotes the mass difference of the double functionalized GeraGE unit with a mass difference of 366 g/mol.

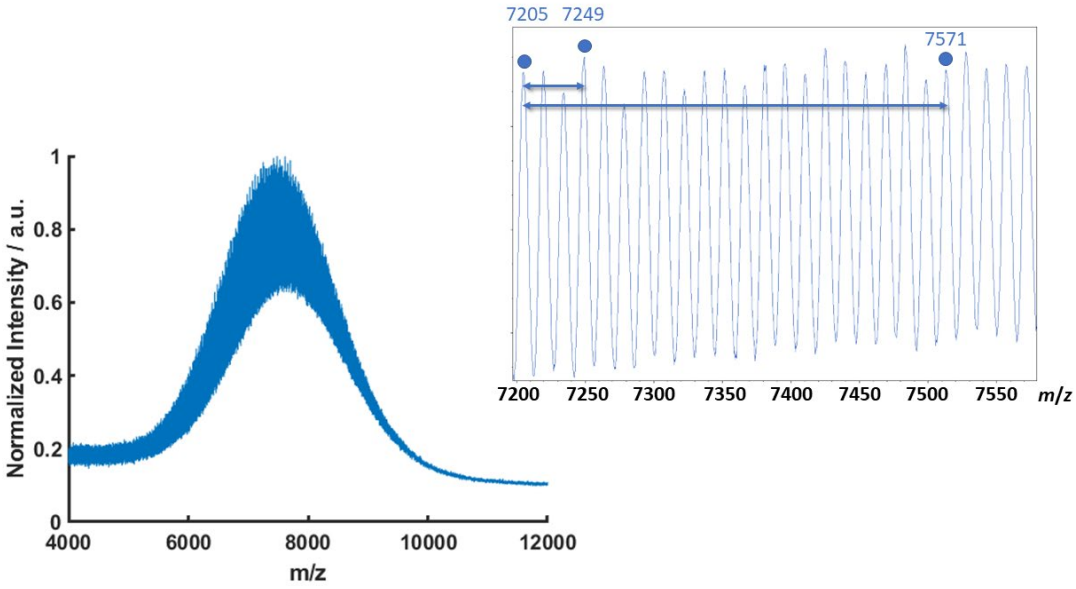

Figure S74: MALDI-ToF of P(EG_{123}-*co*-$NerGE_{13}$) functionalized with 2-mercaptoethanol via Thiol-ene click reaction. Small arrow denotes the mass difference of one EO unit with 44 g/mol. Large arrow denotes the mass difference of the double functionalized NerGE unit with a mass difference of 366 g/mol.

Hydrogenation

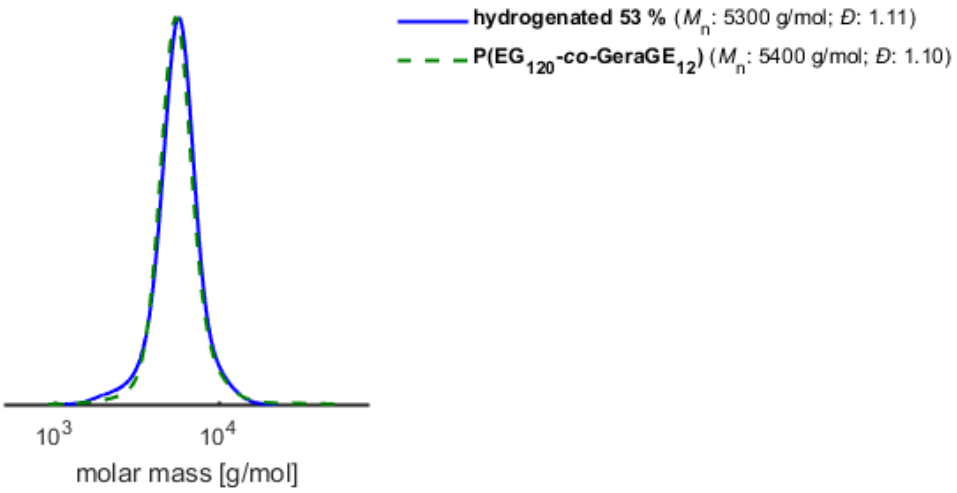

Figure S75: SEC traces of P(EG$_{120}$-*co*-GeraGE$_{12}$) with a degree of hydrogenation of 53 %. (Eluent: DMF, RI-Detector, PEG calibration).

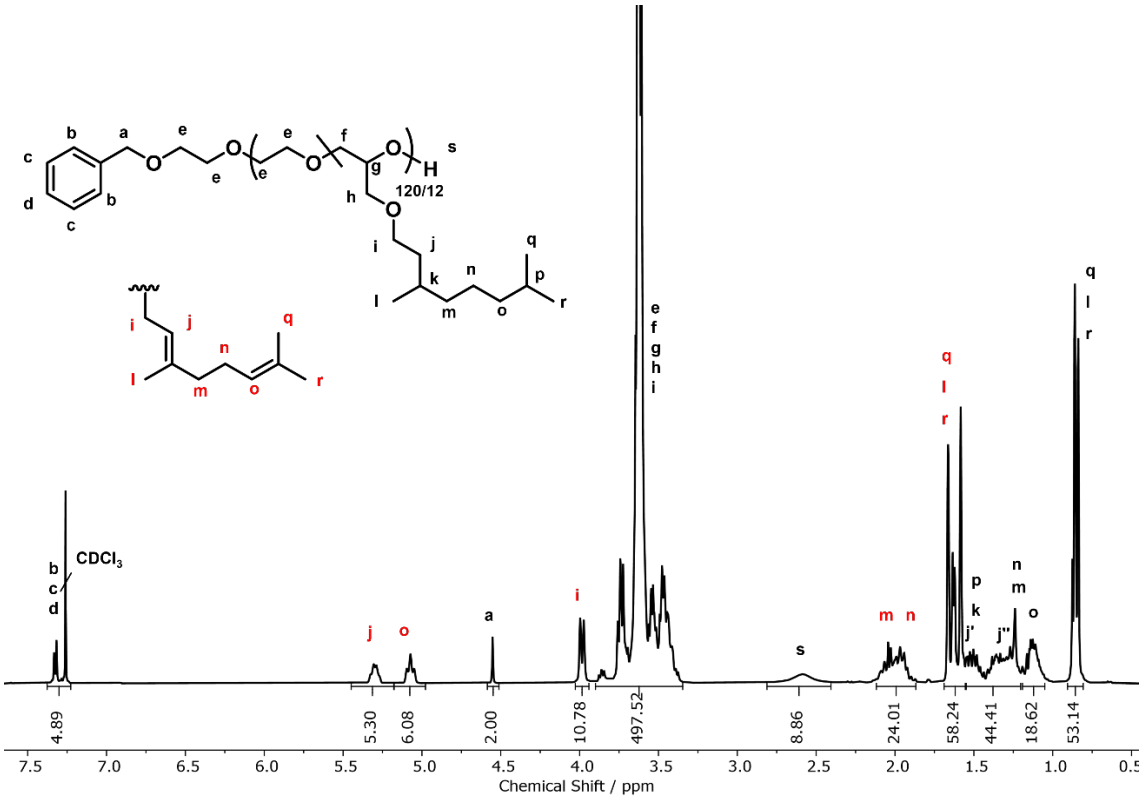

Figure S76: ^{1}H NMR spectrum of P(EG$_{120}$-*co*-GeraGE$_{12}$) hydrogenated with PADA (300 MHz, CDCl$_3$). The degree of hydrogenation is 53 %. Note that the electron-poor double bond is hydrogenated preferentially. Red letters denote atoms of residual not hydrogenated precursor polymer.

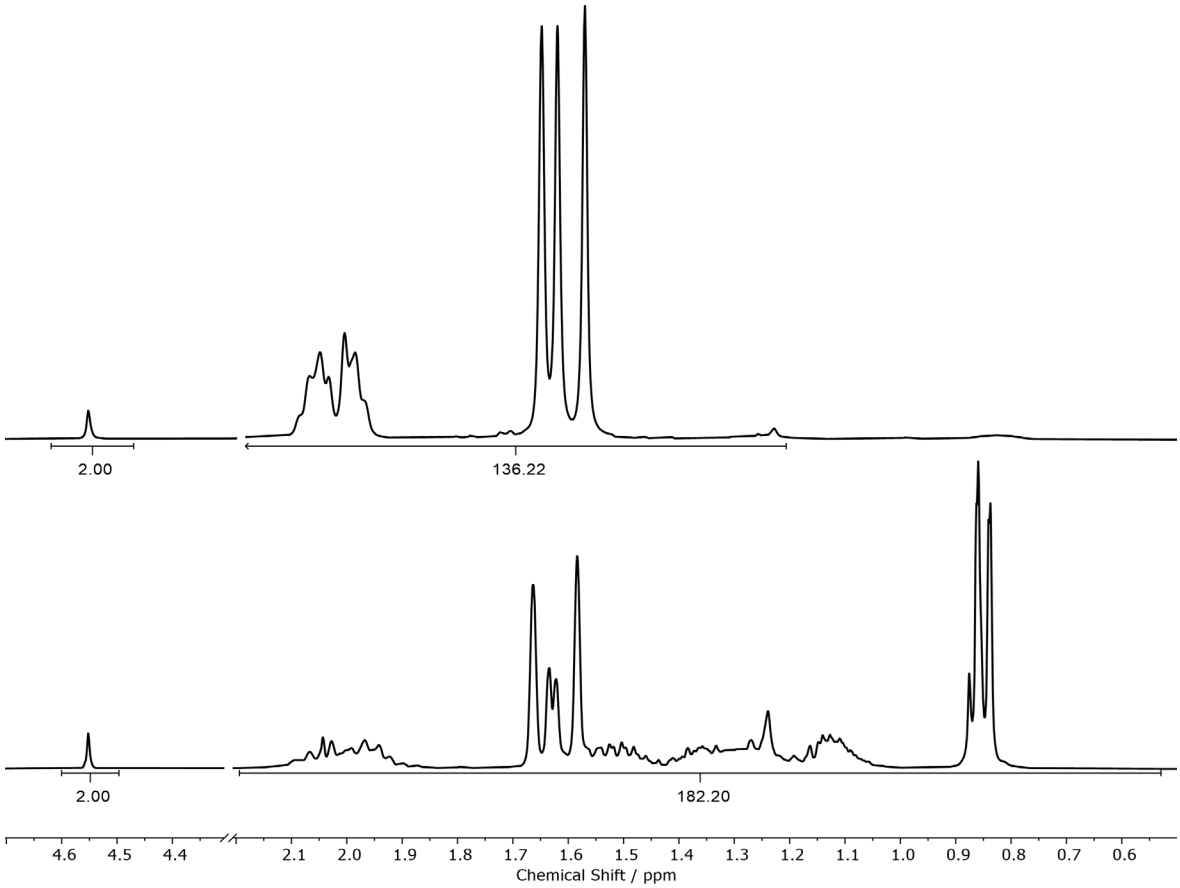

Figure S77: Zoom of the ^{1}H NMR spectrum of P(EG$_{120}$-*co*-GeraGE$_{12}$) before (top) and after (bottom) the hydrogenation. The spectrum shows the increase of observed protons after hydrogenation.

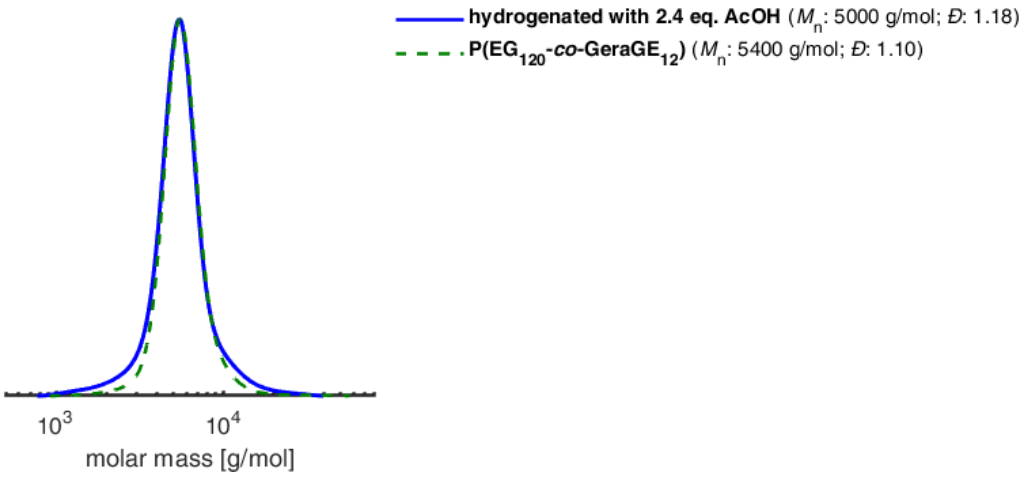

Figure S78: SEC traces of P(EG$_{120}$-*co*-GeraGE$_{12}$) before and after hydrogenation utilizing 2.4 eq. of acetic acid (standard: 2 eq., compare Figure S75). Higher amounts of acid result in an increase in dispersity and a small lower molecular weight shoulder.

Thermal Characterization of Polymers

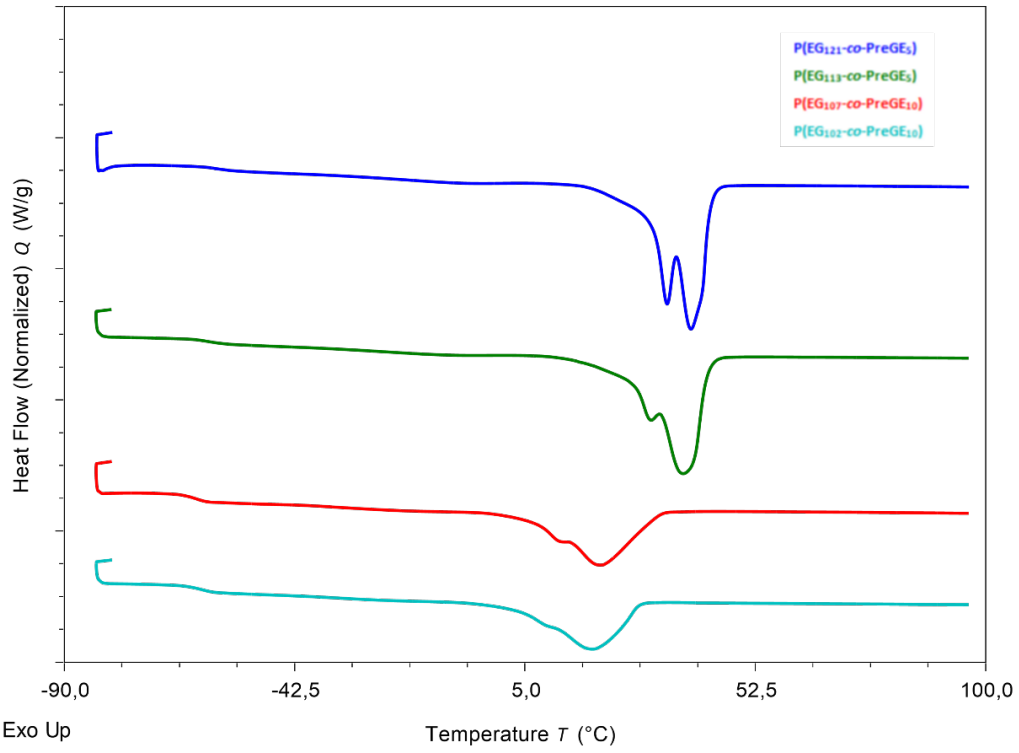

Figure S79: DSC thermograms of P(EG$_n$-*co*-PreGE$_m$) copolymers (second heating cycle, from -90 to 100 °C, 10 °C·min^{-1}).

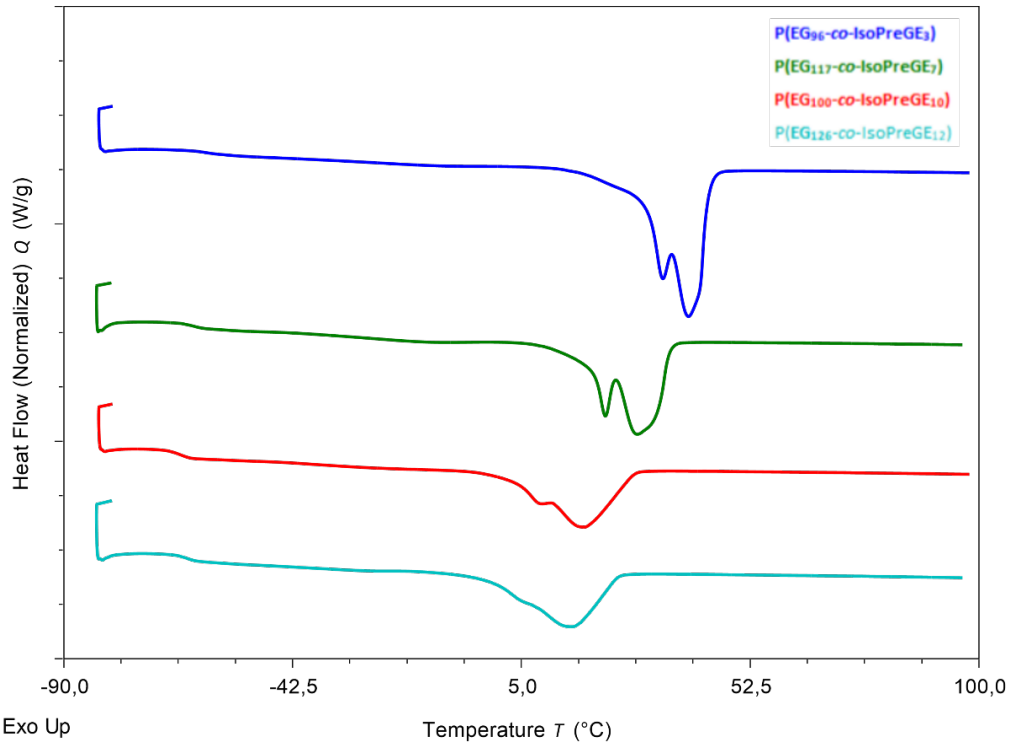

Figure S80: DSC thermograms of P(EG$_n$-*co*-IsoPreGE$_m$) copolymers (second heating cycle, from -90 to 100 °C, 10 °C·min^{-1}).

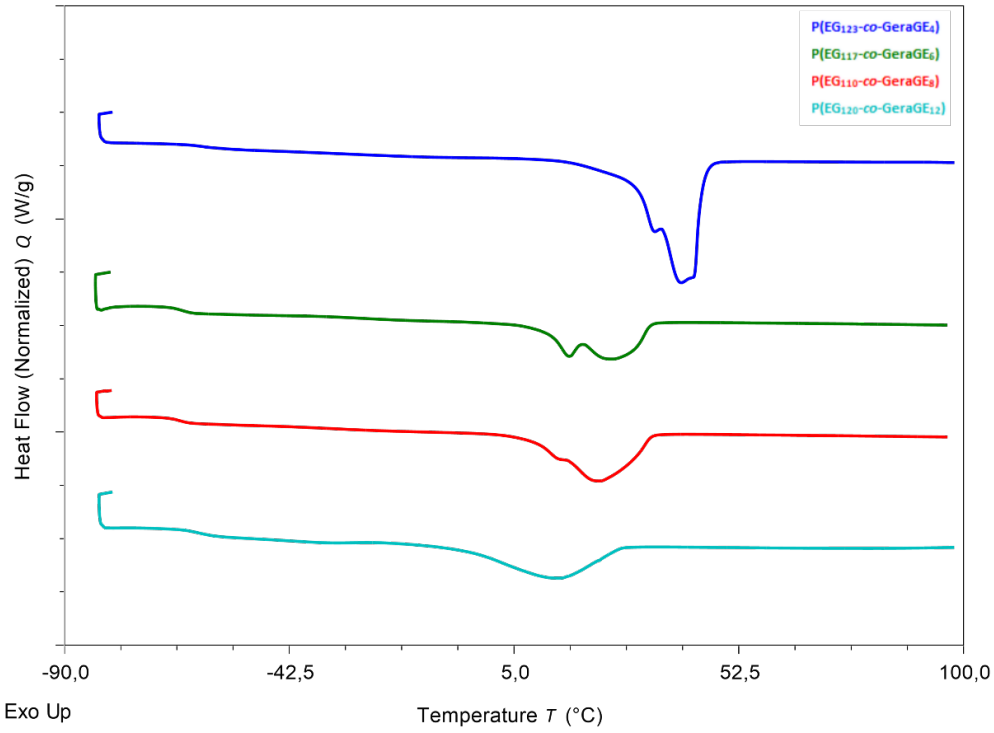

Figure S81: DSC thermograms of P(EG$_n$-*co*-GeraGE$_m$) copolymers (second heating cycle, from -90 to 100 °C, 10 °C·min^{-1}).

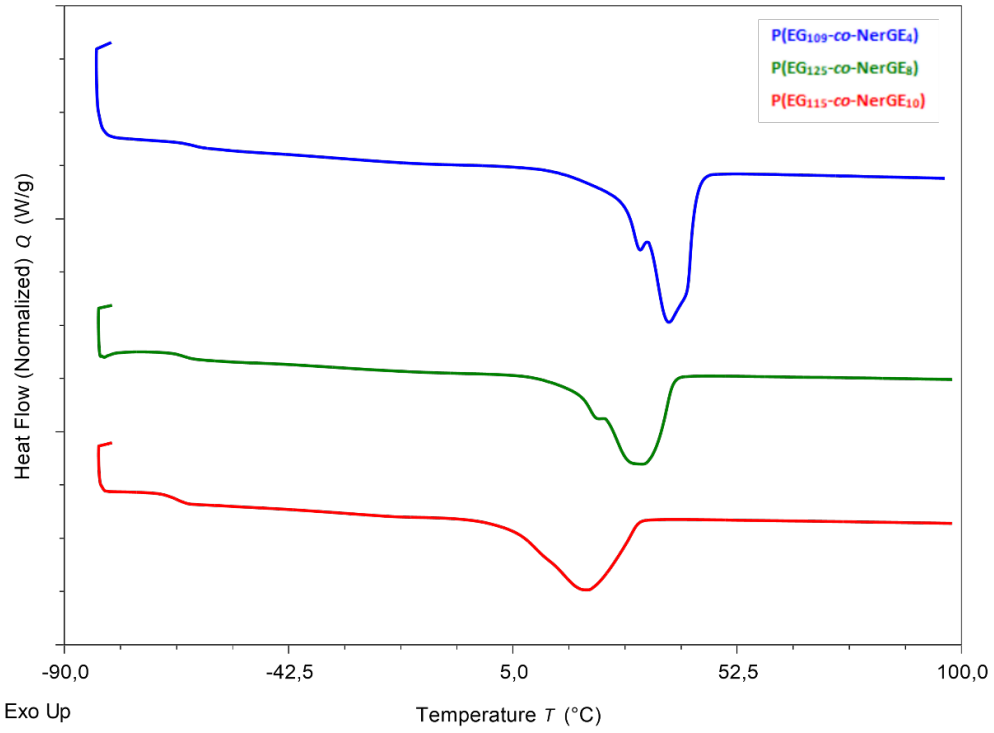

Figure S82: DSC thermograms of P(EG$_n$-*co*-NerGE$_m$) copolymers (second heating cycle, from -90 to 100 °C, 10 °C·min^{-1}).

References

(1) Mouzin, G.; Cousse, H.; Rieu, J.-P.; Duflos, A. A Convenient One-Step Synthesis of Glycidyl Ethers. *Synthesis* **1983** (02), 117–119. DOI: 10.1055/s-1983-30243.

(2) Schüttner, S.; Krappel, M.; Koziol, M.; Marquart, L.; Schneider, I.; Sottmann, T.; Frey, H. Anionic Ring-Opening Copolymerization of Farnesyl Glycidyl Ether: Fast Access to Terpenoid-Derived Amphiphilic Polyether Architectures. *Macromolecules* **2023**, *56* (17), 6928–6940. DOI: 10.1021/acs.macromol.3c00999.

(3) Holzmüller, P.; Gardiner, C.; Preis, J.; Frey, H. CO_2 -Based Polycarbonates with Low Glass Transition Temperatures Sourced from Long-Chain Terpenes. *Macromolecules* **2024**, *57* (11), 5358–5367. DOI: 10.1021/acs.macromol.4c00349.

(4) Herzberger, J.; Leibig, D.; Liermann, J. C.; Frey, H. Conventional Oxyanionic versus Monomer-Activated Anionic Copolymerization of Ethylene Oxide with Glycidyl Ethers: Striking Differences in Reactivity Ratios. *ACS Macro Lett.* **2016**, *5* (11), 1206–1211. DOI: 10.1021/acsmacrolett.6b00701.

(5) Steube, M.; Johann, T.; Plank, M.; Tjaberings, S.; Gröschel, A. H.; Gallei, M.; Frey, H.; Müller, A. H. E. Kinetics of Anionic Living Copolymerization of Isoprene and Styrene Using in Situ NIR Spectroscopy: Temperature Effects on Monomer Sequence and Morphology. *Macromolecules* **2019**, *52* (23), 9299–9310. DOI: 10.1021/acs.macromol.9b01790.

(6) Jaacks, V. A novel method of determination of reactivity ratios in binary and ternary copolymerizations. *Makromol. Chem.* **1972**, *161* (1), 161–172. DOI: 10.1002/macp.1972.021610110.

(7) Groves, J. T.; Ma, K. W. Carbon cluster compounds. Generation and reorganization of the homobullvalenyl cation, an 11-fold degenerate species. *J. Am. Chem. Soc.* **1977**, *99* (12), 4076–4082. DOI: 10.1021/ja00454a028.

(8) Schunicht, C.; Biffis, A.; Wulff, G. Microgel-supported Oxazaborolidines: Novel Catalysts for Enantioselective Reductions. *Tetrahedron* **2000**, *56* (12), 1693–1699. DOI: 10.1016/S0040-4020(00)00072-7.

(9) Hamersma, J. W.; Snyder, E. I. Diimide Reductions Using Potassium Azodicarboxylate. *J. Org. Chem.* **1965**, *30* (11), 3985–3988. DOI: 10.1021/jo01022a532.

(10) Wall, F. T. The Structure of Vinyl Copolymers. *J. Am. Chem. Soc.* **1941**, *63* (7), 1862–1866. DOI: 10.1021/ja01852a016.

(11) Beckingham, B. S.; Sanoja, G. E.; Lynd, N. A. Simple and Accurate Determination of Reactivity Ratios Using a Nonterminal Model of Chain Copolymerization. *Macromolecules* **2015**, *48* (19), 6922–6930. DOI: 10.1021/acs.macromol.5b01631.

(12) Hoffmann, R.; Minkin, V. I.; Carpenter, B. K. Ockham's razor and chemistry. *Bull. Soc. Chim. Fr.* **1996** (2), 117–130.

(13) Blankenburg, J.; Kersten, E.; Maciol, K.; Wagner, M.; Zarbakhsh, S.; Frey, H. The poly(propylene oxide-*co*-ethylene oxide) gradient is controlled by the polymerization method: determination of reactivity ratios by direct comparison of different copolymerization models. *Polym. Chem.* **2019**, *10* (22), 2863–2871. DOI: 10.1039/C9PY00500E.

(14) Hans, M.; Keul, H.; Moeller, M. Chain transfer reactions limit the molecular weight of polyglycidol prepared via alkali metal based initiating systems. *Polymer* **2009**, *50* (5), 1103–1108. DOI: 10.1016/j.polymer.2009.01.012.

(15) Guibé, F. Allylic protecting groups and their use in a complex environment part I: Allylic protection of alcohols. *Tetrahedron* **1997**, *53* (40), 13509–13556. DOI: 10.1016/S0040-4020(97)00524-3.

(16) Vatèle, J.-M. The prenyl group: a versatile hydroxy protecting group, removable chemoselectively under mild conditions. *Tetrahedron* **2002**, *58* (28), 5689–5698. DOI: 10.1016/S0040-4020(02)00539-2.

(17) Prosser, T. J. The Rearrangement of Allyl Ethers to Propenyl Ethers. *J. Am. Chem. Soc.* **1961**, *83* (7), 1701–1704. DOI: 10.1021/ja01468a035.

(18) Lee, B. F.; Kade, M. J.; Chute, J. A.; Gupta, N.; Campos, L. M.; Fredrickson, G. H.; Kramer, E. J.; Lynd, N. A.; Hawker, C. J. Poly(allyl glycidyl ether)-A versatile and functional polyether platform. *J. Polym. Sci., Part A: Polym. Chem.* **2011**, *49* (20), 4498–4504. DOI: 10.1002/pola.24891.

Chapter 6

Polymers of Biobased Oleyl Glycidyl Ether: Insights into Copolymerization with Ethylene Oxide, Postmodification, Thermal Properties, and Micellization Behavior

6 Polymers of Biobased Oleyl Glycidyl Ether: Insights into Copolymerization with Ethylene Oxide, Postmodification, Thermal Properties, and Micellization Behavior

Gregor M. Linden[1], [redacted]

[1]Department of Chemistry, Johannes Gutenberg University Mainz, Duesbergweg 10–14, 55128 Mainz, Germany.

Submitted to *Macromolecules*

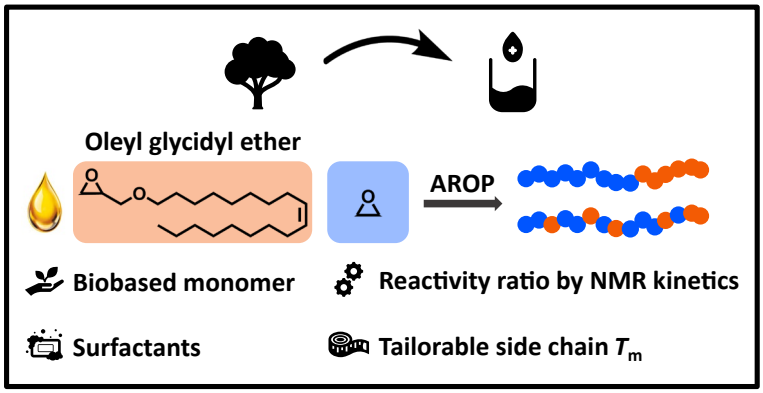

Abstract

Oleyl glycidyl ether (OlGE) is a highly hydrophobic monomer synthesized from a fatty alcohol and epichlorohydrin. When combined with hydrophilic monomethoxy poly(ethylene glycol) (mPEG) macroinitiators, well-defined, highly amphiphilic AB block copolymers are obtained via anionic ring-opening polymerization ($Đ \leq 1.08$). Surprisingly, an investigation of the copolymerization kinetics of OlGE and ethylene oxide revealed an almost ideally random copolymerization ($r_{EO} = 1.27$, $r_{OlGE} = 0.78$). Both statistical and block copolymers were investigated regarding their behavior in aqueous solution. The block copolymers featured two distinct melting temperatures (T_ms). Besides a melting transition of mPEG, a second T_m is attributed to the crystallization of the *cis*-alkenyl side chain of OlGE. Varying degrees of side chain hydrogenation of the POlGE homopolymer allowed tailoring of the T_m. The thiol-ene click reaction allowed subsequent functionalization. This work not merely highlights the prospect of novel surfactants, but it also emphasizes the potential for developing drug delivery systems featuring temperature-controlled release.

Introduction

Surfactants play a key role in numerous everyday applications, in which the compatibilization of components with different polarity is required. They typically alter the surface properties of water. These applications include surfactants, cosmetics, coatings, paints, biotechnology, water purification, and many others.[1,2] Polymer surfactants, due to their vast structural complexity, provide a means to tune and finely control these behaviors. Mostly, when discussing polymer surfactants, reference is made to block copolymers. However, the term 'surfactant' also includes polysoaps, which are random copolymers of hydrophilic and hydrophobic monomers, among many other architectural configurations. The domain of polymer surfactants is extensive, and comprehensive reviews are available.[1,3] The hydrophilic component of surfactants can either be charged, as seen in examples such as poly(acrylic acid),[4] quaternized arylamines,[5] and sulfonates,[6] or uncharged, as in saccharides,[7] polyoxazolines,[8] and poly(ethylene glycol) (PEG).[9] The industry provides a series of ethoxylated compounds as surfactants, such as Tween®, Myrj®, Span®, Triton X®, and Brij®.[10]

Fats and oils represent renewable feedstocks for the chemical industry. Their substantial production volume (208.1 Mt in 2019) enables the cost-efficient supply of a diverse range of linear alkyl and alkenyl alcohols from triglycerides.[11–15] The side product glycerol can be converted to epichlorohydrin and is equally commercially available as Epicerol® in a green process from Solvay. Glycerol is chlorinated twofold with HCl and after one elimination reaction, epichlorohydrin is

formed.[16–18] Epichlorohydrin can be utilized to introduce epoxide functionalities in molecules.[19] With a growing emphasis on the development of bio-based chemicals that do not affect the food chain,[20,21] it is crucial to underscore the effective utilization of triglycerides derived from non-edible oil plants as an alternative to using food crops.[22] Moreover, converting waste into chemicals proves to be significantly more economical when compared to biofuel or electricity production.[23] Ethylene oxide, the monomer used to produce PEG can be generated from bio-based sources using two primary methods: dehydration of bioethanol to produce ethylene, followed by oxidation[24,25] or electrosynthesis from bioethanol.[26] Another viable approach involves production from CO_2 and water.[27]

The field of drug solubilization via implementation of multifunctional polymeric micelles is highly active in research, focusing on the purposeful treatment of diseases. These systems effectively handle the limitations of free hydrophobic drugs such as low solubility, dose-limiting toxicity, and inadequate biodistribution.[28,29] The trigger to release drugs from external stimuli-responsive polymers can be changes in pH, temperature, magnetic fields, light, engineered sensitivities to enzymes, or radiofrequency.[30–32] The lower critical solution temperature of poly(*N*-isopropyl acrylamide) can be employed to trigger drug release during local hyperthermia.[33] Magnetically responsive nanoparticles (Fe_3O_4 or Fe_2O_3) can be incorporated into micelles or liposomes loaded with drugs while the drug release can be induced by an alternating external field.[34] Brazel *et al.* employed poly(EG)-*b*-poly(ε-caprolactone) micelles in combination with iron oxide nanoparticles. The release of doxorubicin was demonstrated to occur by melting of the crystalline core when subjected to external magnetic field-induced heating.[35] Block copolymers of PEG and glycidyl ethers with a hydrophobic chain have been synthesized and investigated for their use as cosurfactants,[36] and show low cytotoxicity for splenic immune cells.[37] ABA-type triblock copolymers of these structures can also be employed to prepare thermoresponsive hydrogels, capable of taking up Nile Red as a model for a hydrophobic drug. By variation of the alkyl side chain length, the T_m of the hydrophobic block was altered to 49 °C in pure water.[38]

Here we present the monomer oleyl glycidyl ether (OlGE), prepared from oleyl alcohol and epichlorohydrin. This monomer was utilized in anionic ring-opening polymerization (AROP), affording block copolymers, statistical copolymers, and homopolymers. Long-chain glycidyl ethers can modify the properties of highly water-soluble PEG, thereby allowing the fine-tuning of the physical characteristics of aqueous solutions.[9,39] Furthermore, mPEG-*b*-poly(alkyl glycidyl ether) surfactants were synthesized and the 'efficiency-boosting effect' was investigated. The polymers

increased the efficiency of medium- and longer-chain surfactants to stabilize water/oil interfaces.[36] Analogously, terpenoid-derived systems that cannot crystallize due to their branched structure were explored and showed comparable results.[40,41] OlGE is a potentially biorenewable and versatile platform for a variety of surfactants.

Experimental Section

Information regarding the reagents used, detailed monomer and polymer synthesis, as well as the analysis techniques employed, is available in the Supporting Information (SI).

Results and Discussion

Monomer Synthesis

The precursor oleyl alcohol is typically obtained through the hydrogenation of methyl oleate in industrial settings. Conventional industrial methods employ hydrogen gas and catalysts for the hydrogenation of methyl oleate. However, we opted for a more classical reduction method that employs lithium aluminum hydride ($LiAlH_4$, Scheme 1).[42] This choice was made to avoid the need for a high-pressure hydrogen gas apparatus. Methyl oleate is a byproduct of transesterification, a process that involves triglycerides commonly sourced from large quantities of bio-derived oils and fats.[12] Additionally, epichlorohydrin can be obtained from both petroleum-based resources and glycerol, which is a byproduct of biodiesel production and is available in abundance from fats and oils.[16,17] The combination of oleyl alcohol and green epichlorohydrin obtained by this pathway results in a completely bio-based monomer.

Oleyl glycidyl ether (OlGE) features a long hydrophobic side chain with a *cis* double bond at the C9 carbon atom. This prevents the side chain from crystallizing at room temperature and can serve as an anchoring point for post-polymerization modification if incorporated along the polymer backbone. The two-step reaction involves the reduction of methyl oleate followed by an etherification of the oleyl alcohol with epichlorohydrin (ECH) via phase transfer catalysis, as illustrated in Scheme 1. Hence, oleyl alcohol and epichlorohydrin underwent a two-phase reaction in the presence of a phase transfer catalyst under highly alkaline conditions, resulting in the formation of OlGE with yields of up to 71%. However, a known side reaction occurred during this process: the deprotonation of ECH with subsequent ring-opening led to 3-chloroallylalcohol. This alcohol is capable of reacting with ECH, leading to the formation of 3-chloroallyl glycidyl ether.[19] The byproduct was effectively removed using Kugelrohr distillation, facilitated by the significant difference in boiling points between the byproduct and OlGE.

All experimental details as well as the characterization are given in the SI.

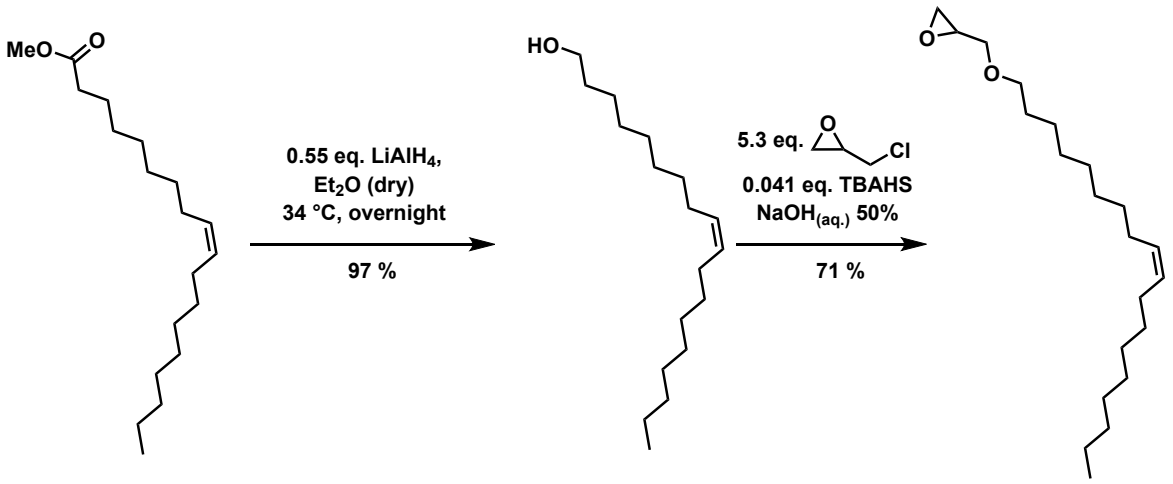

Scheme 1: Two-step reaction for the synthesis of the oleyl glycidyl ether monomer.

Synthesis of Oleyl Glycidyl Ether-Based Polymers

All polymers were synthesized using standard AROP techniques. Experimental details along with characterization are provided in the SI. For block copolymers, the monofunctional initiator monomethoxy poly(ethylene glycol) (mPEG) with molar masses of 2 000 g/mol (45 ethylene glycol units) and 5 000 g/mol (114 ethylene glycol units) was utilized. Prior to polymerization, mPEG was deprotonated to an extent of 90% using KO^{t}Bu with the aid of [18]crown-6 and subsequently, the dried monomer OlGE was added. After the polymerization, the active chain ends were terminated using acidified methanol, and the resulting polymer was purified by precipitation. POlGE homopolymers were synthesized in the same way, but potassium(2-benzyloxy)ethanolate was used as the initiator. Since POlGE homopolymers are not the primary focus of this study, they have been excluded in Scheme 2. In the case of statistical copolymers, CsOH·H_2O was employed as the deprotonating agent. This choice was made to maintain consistency in the experimental procedures between the copolymerization kinetics measurements (as described below) and the actual polymer synthesis. The procedure involved dissolving the cesium(2-benzyloxy)ethanolate initiator salt in dry DMSO and THF, after which dried OlGE was introduced into the reaction vessel. Subsequently, ethylene oxide was condensed to the custom-made anionic flask. Statistical copolymers with an overall number of both repeating units of 120 were targeted. Slight deviations stem from difficult measuring of liquefied EO at -80 °C, as small temperature increases led to a volume expansion of EO in the graduated ampule.

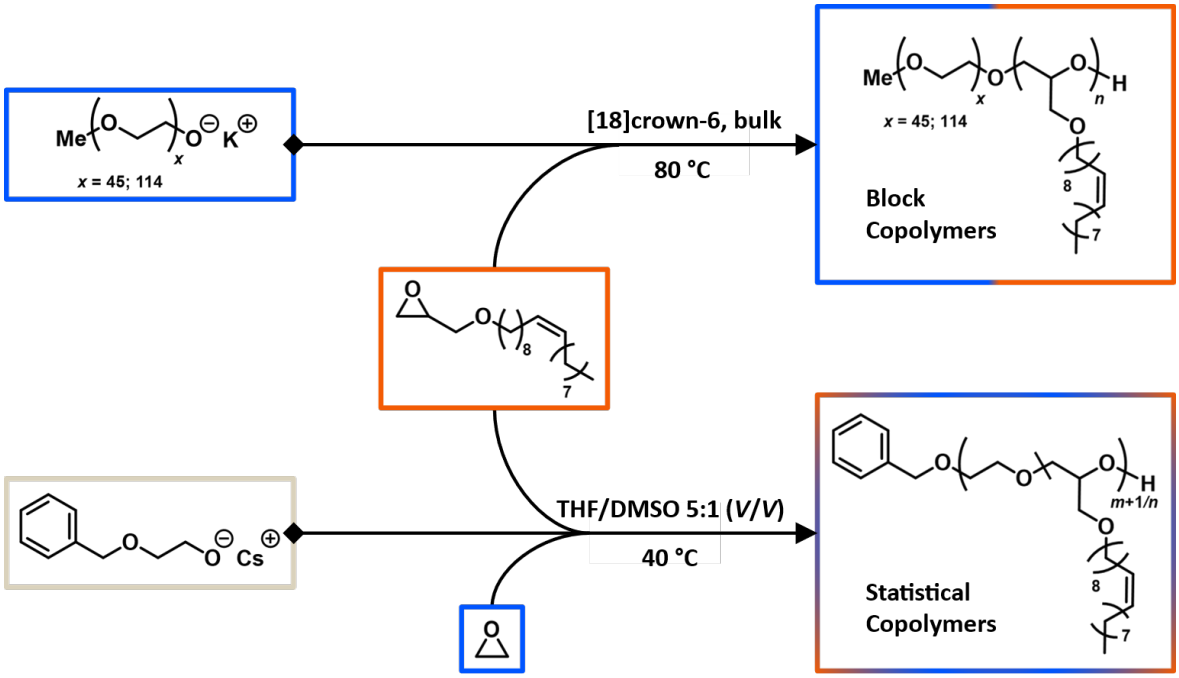

Scheme 2: Synthesis of block and statistical copolymers containing oleyl glycidyl ether by employing AROP techniques.

Table 1 presents a summary of the synthesized polymers, including their characterization data and the intended composition compared to the calculated composition. Notably, all polymers based on oleyl glycidyl ether exhibited narrow dispersities ranging from 1.06 to 1.11. The shift in the SEC traces towards higher molar masses supports the block copolymer formation. (Figures S5 and S6). Statistical copolymers showed slightly larger dispersities in the range of 1.11 to 1.15, although they still maintained a monomodal distribution, as illustrated in Figure S9. SEC analysis revealed an increase in molar mass for all polymers with the incorporation of higher amounts of OlGE. Variations are anticipated due to differences in the hydrodynamic volume behavior compared to the PEG calibration, which is particularly notable for POlGE homopolymers with their long side chains, leading to a bottlebrush-like structure (Figure S12). It is essential to recognize that the molar mass calculated from SEC should be considered a rough estimate given the relative nature of the method employed. The NMR spectra can be found in the SI (Figure S3, S4, S7, S8). Differences observed between the theoretical and achieved degree of polymerization can be attributed to contamination by small amounts of OlGE homopolymer, initiated by residual traces of water. These polymers were subsequently removed during the work-up process.

Table 1: Polymer characterization of the OlGE block copolymers, statistical copolymers, and homopolymers.

Polymer composition[a]	*n*(OlGE)[th]	*n*(EO)[th]	M_n(SEC)[b] (g/mol)	M_n(NMR)[a] (g/mol)	$Đ^b$
$mPEG_{45}$-*b*-$POlGE_{2.4}$	3	-	3000	2800	1.06
$mPEG_{45}$-*b*-$POlGE_{5.0}$	6	-	4300	3600	1.06
$mPEG_{45}$-*b*-$POlGE_{7.5}$	9	-	4500	4400	1.06
$mPEG_{45}$-*b*-$POlGE_{11.3}$	12	-	4800	5700	1.08
$mPEG_{114}$-*b*-$POlGE_{2.9}$	3	-	6400	5900	1.08
$mPEG_{114}$-*b*-$POlGE_{5.8}$	6	-	7700	6900	1.07
$mPEG_{114}$-*b*-$POlGE_{7.3}$	9	-	8200	7400	1.06
$mPEG_{114}$-*b*-$POlGE_{9.9}$	12	-	9100	8200	1.07
$P(EG_{123}$-*co*-$OlGE_7)$	6	114	7500	7800	1.14
$P(EG_{94}$-*co*-$OlGE_{13})$	12	108	7800	8500	1.15
$P(EG_{103}$-*co*-$OlGE_{35})$	30	90	16300	16000	1.12
$POlGE_{13}$	10	-	3400	4400	1.07
$POlGE_{25}$	25	-	5800	8300	1.11

[a]Determined *via* ^{1}H NMR analysis, [b]eluent THF, PEG calibration, RI detector, [th]theoretical.

Reactivity Ratios of OlGE/EO by *In Situ* ^{1}H NMR Copolymerization Kinetics

Knowledge of microstructure is crucial to understand polymer characteristics. Depending on the type of monomers and polymerization techniques employed, various microstructures can typically be achieved, ranging from random copolymers to nearly blocklike, tapered structures. These microstructures have a significant impact on various polymer properties such as thermal and mechanical properties, micellization, and solubility among others.[43,44] In our study, we investigated the copolymerization behavior via *in situ* ^{1}H NMR analysis. To this end, EO and OlGE were copolymerized at 40 °C in an NMR tube equipped with a Teflon stopcock, using a mixture of DMSO-d_6 and THF-d_8 at a 1:5 (*V*/*V*) ratio. Cesium 2-(benzyloxy)ethanolate was used as the initiator for the polymerization. Cesium was chosen as a counterion for all statistical copolymers, as it enhances the propagation rate compared to potassium and reduces the time required for the kinetic investigation experiment.[45] Experimental details are given in the SI. Monomer consumption was tracked by observing the monomer resonances at 2.68 ppm for OlGE and 2.58 ppm for EO during the copolymerization. Figure 1 displays a selection of stacked spectra.

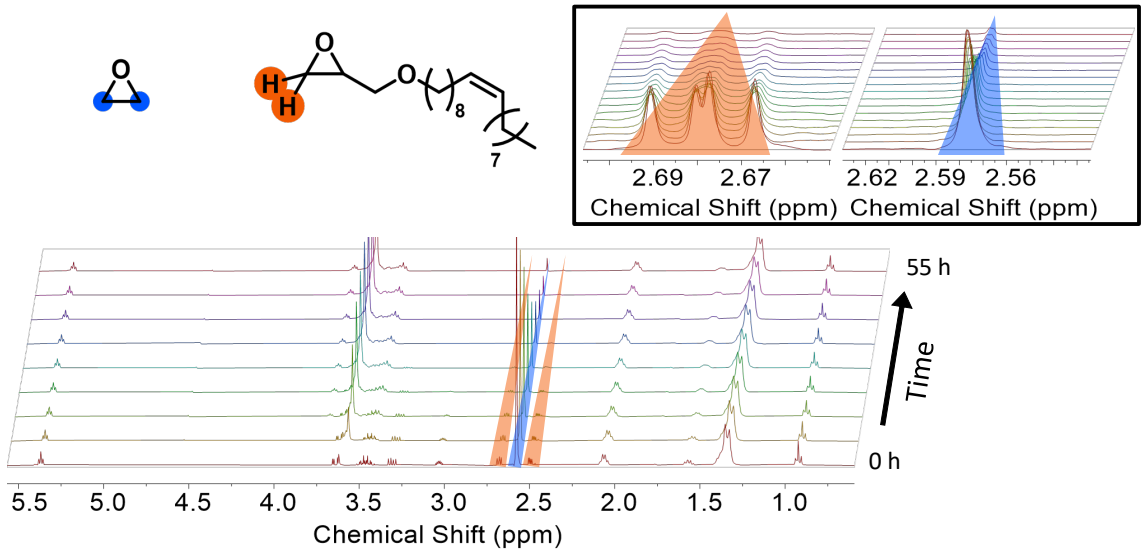

Figure 1: Stacked selection of ^{1}H NMR spectra of the copolymerization of OlGE and EO. Zoom-in shows the decrease of the OlGE (orange) and EO monomer signals (blue). Polymerization temperature 40 °C, solvent: DMSO-d_6 and THF-d_8 1:5 (*V*/*V*), 400 MHz. As spectra were collected every 2 min for 55 h, only every 200th spectrum is displayed.

Both monomers exhibited nearly complete conversion after 55 hours. The gradual decrease of the signals is illustrated in Figure 2, which shows the amount of unreacted monomer versus total conversion. Clearly, EO is incorporated more rapidly, while OlGE is consumed at a slightly lower rate. This already suggests that copolymerization is not ideally random.

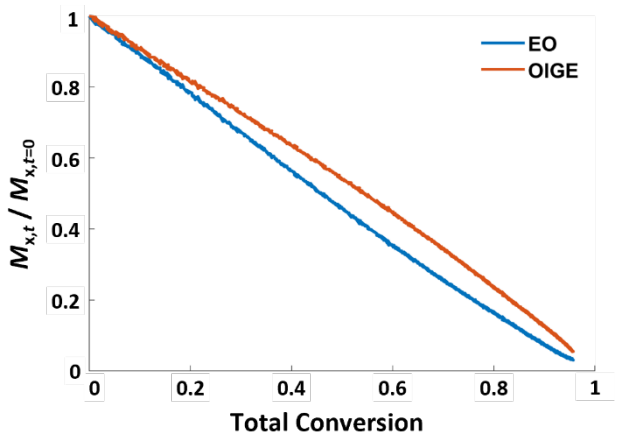

Figure 2: Unreacted monomer versus total conversion of the *in situ* ^{1}H NMR copolymerization kinetic study of EO with OlGE. Solvent: DMSO-d_6/THF-d_8 1:5 (*V*/*V*), 40 °C.

To determine reactivity ratios $r_{1,2}$ the data extracted from the kinetic experiment were fitted according to the Jaacks plot.[46–48] For this, the following Equation (1) was used.

$$\log\left(\frac{[\mathrm{M}_1]_t}{[\mathrm{M}_1]_0}\right) = r_1 \cdot \log\left(\frac{[\mathrm{M}_2]_t}{[\mathrm{M}_2]_0}\right) \quad (1)$$

In an ideal copolymerization, the following correlation is defined: $r_1 \cdot r_2 = 1$. Both reactivity ratios were determined with the results r_{EO}=1.27 and r_{OlGE}=0.78 (Figure S39). As the coefficient of determination R^2 was 0.99, an ideal or chain-end independent copolymerization can be concluded. The use of more complex terminal models such as the Meyer-Lowry method[49] should be avoided as long as the more simple, non-terminal model explains the data well. This principle was coined by Sir William Hamilton as "Ockham's Razor"[50] and its application to copolymerization kinetics was already described.[51] The fit is displayed in Figure S40, and the results are summarized in Table 2.

Table 2: Summary of different fitting models of the EO/OlGE copolymerization kinetic.

Method	Model	r_{EO}	r_{OlGE}	
Jaacks	Non-terminal, ideal	1.27 ± 0.01	0.78 ± 0.01	R^2 = 0.99
Meyer-Lowry	Terminal, non-ideal	1.32 ± 0.12	0.80 ± 0.14	NormRes = 0.38

The obtained reactivity ratios enable the simulation of the comonomer composition in the course of the copolymerization (Figure 3), which directly translates to the monomer gradient in the copolymer chains formed. As previously indicated in Figure 2, EO is initially incorporated with a slight preference during copolymerization. With increasing conversion, approaching full monomer conversion, more OlGE units are incorporated at the chain end. This subtle variation in reactivity ratios results in the enrichment of monomer units towards either the beginning or the terminus of the polymer chains, respectively. We would like to emphasize that this gradient is not pronounced, compared to other systems like the carbanionic copolymerization of isoprene and styrene.[48] This result is remarkable in view of the large steric bulk of the OlGE monomer in comparison to EO.

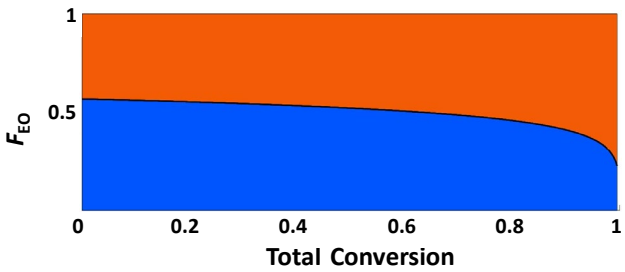

Figure 3: Simulated composition versus total conversion of the EO (blue)/OlGE (orange) comonomer pair for a hypothetical equimolar ratio.

Even though glycidyl ethers (GEs) exhibit a substituted epoxide functionality, usually the correlation $r_{EO} \approx r_{GE} \approx 1$ is valid.[37,52,53] This observation is counterintuitive, especially since propylene oxide copolymerizes with a much stronger gradient with EO, which is assigned to the methyl group

substitution.[54] Due to their ability to chelate the counterion and thereby activate the epoxide, glycidyl ethers show a transient "crown ether-effect".[55] Since the side chain contains additional oxygen atoms, glycidyl ethers react faster than the unsubstituted EO.[56–58] Bulky and/or inflexible side chains, in contrast, prevent sufficient chelation and also lead to hindered nucleophilic attack of an active chain end at the epoxide functionality, resulting in less favored incorporation.[40,58–60] This finding is confirmed by our study, as the bulky, apolar monomer is less prone to nucleophilic attack, translating to slower incorporation in the growing polymer chain.

Amphiphilic Nature and CMC Determination of OlGE Copolymers

The determination of the CMC is commonly achieved by employing pyrene as a fluorescent probe.[2,61] When pyrene transitions from a polar to an apolar environment, the emission spectrum experiences a pronounced shift towards higher values in the ratio of the I_3 and I_1 bands, correlated to the alteration in the polarity of the surrounding molecules. The experimental procedure used in this work is based on the method described by Zhu *et al*.[62] In short, pyrene was mixed with the respective polymer solution in a serial dilution. Then the fluorescence spectra of pyrene were measured at 23 °C, and I_3/I_1 was plotted against the logarithmic polymer concentration. A Boltzmann sigmoidal fit (Equation S1) was performed and the CMC was determined from the inflection point of the fit.[40,61] The graphs are shown in the SI (Figures S18-S24).

The Hydrophilic-Lipophilic Balance (HLB) is an empirical scale ranging from 1 to 20, employed to assess the utility of surfactants in various applications. Higher HLB values are indicative of surfactants with a greater affinity for polar environments, making them suitable for tasks such as solubilization and oil-in-water emulsification. Conversely, lower HLB values denote surfactants with a stronger preference for nonpolar environments, rendering them more appropriate for purposes such as water-in-oil emulsification and foam reduction. The HLB scale serves as a valuable tool for understanding the contrasting characteristics of surfactants.[63]

Table 3 gives an overview of the synthesized OlGE-containing polymers with their HLB values and the CMC determined by fluorometry. The sole water-soluble compound within the series of statistical copolymers was P(EG_{123}-*co*-$OlGE_7$), which exhibited a CMC of 24.5 mg/L. Of the four block copolymers obtained from $mPEG_{45}$, only two displayed aqueous solubility and had a CMC threshold of 23.8 mg/L. This observation is attributed to a significant increase in the weight percentage of the hydrophobic block due to the incorporation of additional 2.6 OlGE units, each with a high molar mass of 324 g/mol, in contrast to ethylene glycol units with a mass of only 44 g/mol each. A comparable outcome was noted in the case of block copolymers based on $mPEG_{114}$. The CMCs

exhibited a notable reduction from 73.4 to 25.4 mg/L, with just a slight 2.1 mg/L difference between $mPEG_{114}$-*b*-$POlGE_{7.3}$ and $mPEG_{114}$-*b*-$POlGE_{9.9}$. As reported by Lodge *et al.*, the CMC decreases exponentially, but is weakly dependent on the hydrophobic block length for longer blocks and is notably less dependent on the hydrophilic block length.[1,64] Noteworthy, all three varieties of copolymers exhibited a CMC threshold of approximately 25 mg/L. When contrasting our system with existing literature, the CMC of Brij® 98, a twentyfold ethoxylated oleyl alcohol, is reported to fall within the range of 7–29 mg/L.[65–68] Variations in CMC values for the same compound may arise from differences in measurement methods, among other factors.[69] Block copolymers of $mPEG_{114}$-*b*-poly(farnesyl glycidyl ether)$_m$ (m = 5 and 9) showed slightly lower CMCs of 53 and 15 mg/L, respectively.[40]

Table 3: Hydrophilic-lipophilic balances (HLBs) and critical micelle concentrations (CMCs) of the OlGE-containing copolymers.

Polymer	mol% (OlGE)	*w*% (OlGE)	HLB	CMC (mg/L)
$P(EG_{123}$-*co*-$OlGE_7)$	5.4	30	14.1	24.5
$P(EG_{94}$-*co*-$OlGE_{13})$	12.1	50	9.9	n.d.[a]
$P(EG_{103}$-*co*-$OlGE_{35})$	25.4	71	5.7	n.d.[a]
$mPEG_{45}$-*b*-$POlGE_{2.4}$	5.1	28	14.4	41.9
$mPEG_{45}$-*b*-$POlGE_{5.0}$	10.0	45	11.0	23.8
$mPEG_{45}$-*b*-$POlGE_{7.5}$	14.3	55	9.0	n.d.[a]
$mPEG_{45}$-*b*-$POlGE_{11.3}$	20.1	65	7.1	n.d.[a]
$mPEG_{114}$-*b*-$POlGE_{2.9}$	2.5	16	16.8	73.4
$mPEG_{114}$-*b*-$POlGE_{5.8}$	4.8	27	14.5	44.2
$mPEG_{114}$-*b*-$POlGE_{7.3}$	6.0	32	13.6	27.5
$mPEG_{114}$-*b*-$POlGE_{9.9}$	8.0	39	12.2	25.4

[a]Values could not be determined due to insufficient solubility in water.

Dynamic Light Scattering of OlGE Copolymers

Polymer solutions of the water-soluble copolymers were investigated by dynamic light scattering (DLS) to determine the hydrodynamic radius of the respective micelles and larger aggregates. Additionally, the results were compared to TEM observation of the aggregates. The polymer concentration was significantly above the CMC determined via fluorometry. The amplitude autocorrelation function was subjected to a biexponential fit (represented by equation S4), given that TEM images hinted at the presence of multiple types of aggregates for all copolymers. The diffusion coefficient of each measured angle was received from the relation $D=(\tau_R \cdot q^2)^{-1}$. This

diffusion coefficient was subsequently plotted versus q^2 to calculate the z-average diffusion coefficient for each specific aggregate. Additional details on the calculation of diffusion coefficients and hydrodynamic radii are described in the SI. A summary of the results obtained from DLS analysis is provided in Table 4. Among the statistical copolymers examined, P(EG_{123}-*co*-$OlGE_7$) was the only sample that could be analyzed, as the others were insoluble. The block copolymer $mPEG_{114}$-*b*-$POlGE_{9.9}$ was not analyzed by DLS, as a turbid solution was obtained. P(EG_{123}-*co*-$OlGE_7$) exhibited aggregates with an $R_{H,1}$ of 5.31 nm, corresponding to a single chain (micelle), as the comparable $mPEG_{114}$ unimer exhibited a hydrodynamic radius of 2 nm.[40] In contrast, the larger aggregates displayed a significantly greater $R_{H,2}$ of 107 nm. This discrepancy is attributed to chain folding, resulting in the formation of multicompartment micelles. This phenomenon has been discussed in previous studies.[70–72] The corresponding TEM micrograph equally indicates small circular structures as well as larger aggregates but with a smaller radius (Figure S25).

Block copolymers composed of $mPEG_{45}$ generally displayed larger $R_{H,1}$ values, despite having a significantly greater number of repeating units in comparison to the statistical copolymer. This observation implies the aggregation of multiple chains into micelles. When the size of the POlGE block is doubled, there is a notable four- to fivefold increase in the hydrodynamic radius of both aggregates. This finding aligns with the structures observed in the TEM micrographs (Figure 4, A and B).

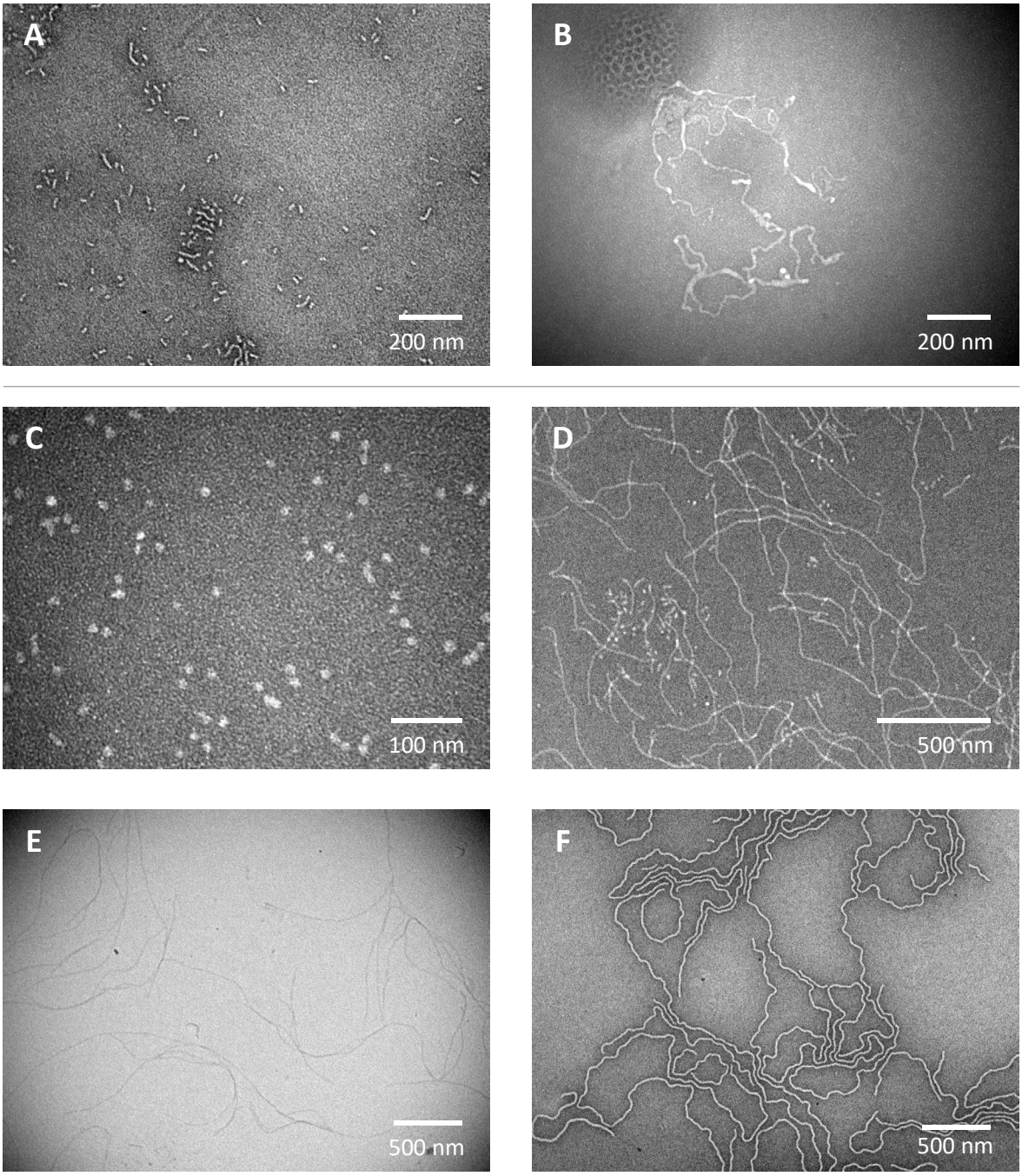

Figure 4: TEM micrograph of mPEG-*b*-POlGE$_n$ block copolymers in aqueous solution (0.1 g/L). A: mPEG$_{45}$-*b*-POlGE$_{2.4}$, B: mPEG$_{45}$-*b*-POlGE$_{5.0}$, The circular structure in the upper left corner is caused by irradiation damage. C: mPEG$_{114}$-*b*-POlGE$_{2.9}$, D: mPEG$_{114}$-*b*-POlGE$_{5.8}$, E: mPEG$_{114}$-*b*-POlGE$_{7.3}$, F: mPEG$_{114}$-*b*-POlGE$_{9.9}$. Samples were treated with 2% uranyl acetate solution as a negative stain. Original micrographs obtained by the software can be found in the SI (Figure S26–27).

The behavior of block copolymers containing mPEG$_{114}$ demonstrates subtle variations. While the hydrodynamic radius ($R_{H,1,2}$) for the POlGE$_n$ block (with n = 2.9 and 7.3, C and E) only experiences a slight increase as n increases, the block copolymer with n = 5.8 (D) exhibits a larger $R_{H,1,2}$ compared to the one with 7.3 OlGE monomer units. This outcome may seem unexpected, but it can be

attributed to the fact that due to the larger hydrophobic block, there are fewer chains present within the respective micelles, resulting in a reduced aggregation number. Consequently, the hydrodynamic radius does not increase as one might anticipate. The polymer $mPEG_{114}$-*b*-$POlGE_{2.9}$ reveals only small structures in the TEM micrograph, a finding that contrasts with the DLS analysis results indicating clustering in solution. The TEM micrograph of the block copolymer with the largest POlGE part, $mPEG_{114}$-*b*-$POlGE_{9.9}$ (F), displays well-resolved, fibrillar structures. Nevertheless, further analysis has been deferred to a later study. Original TEM micrographs can be found in the SI (Figures S25 – S27).

Table 4: DLS results of the investigated water-soluble OlGE copolymers. Index 1 denotes the smaller observed aggregates, whereas 2 denotes the larger observed aggregates.

Polymer	D_1 (10^{-7} $cm^2 \cdot s^{-1}$)	D_2 (10^{-7} $cm^2 \cdot s^{-1}$)	$R_{H,1}$ (nm)	$R_{H,2}$ (nm)
$P(EG_{123}$-*co*-$OlGE_7)$	4.64 ± 0.03	0.23 ± 0.01	5.3 ± 0.1	107 ± 5
$mPEG_{45}$-*b*-$POlGE_{2.4}$	2.54 ± 0.02	0.51 ± 0.05	9.7 ± 0.1	48 ± 4
$mPEG_{45}$-*b*-$POlGE_{5.0}$	0.51 ± 0.02	0.12 ± 0.01	48 ± 2	206 ± 5
$mPEG_{114}$-*b*-$POlGE_{2.9}$	1.41 ± 0.02	0.35 ± 0.01	17.5 ± 0.2	70 ± 1
$mPEG_{114}$-*b*-$POlGE_{5.8}$	0.55 ± 0.03	0.10 ± 0.01	45 ± 2	240 ± 20
$mPEG_{114}$-*b*-$POlGE_{7.3}$	1.12 ± 0.01	0.21 ± 0.01	21.9 ± 0.2	117 ± 7

Thermal Properties of Polymers Containing OlGE

PEG plays an important role as ointment base and tailoring the melting point slightly above human body temperature enables softening into a semi-solid during application and even spreading while lasting at the applied area.[9,73,74] The synthesized OlGE (co)polymers were investigated by differential scanning calorimetry (DSC) (Table 5). The thermograms are displayed in the SI (Figures S13 – S17). Detection of glass transition temperatures (T_gs) was performed with the second heating curve with a heating rate of 10 K/min. As OlGE has a long, flexible side chain, the T_g is shifted towards lower temperatures compared to PEG (< -60 °C).[9] Melting temperatures (T_ms) and melting enthalpies were determined with a 1 K/min heating rate. Reducing the heating/cooling rate to 1 K/min allowed for ordering of the side chains and prevention of recrystallization. Otherwise, a pronounced recrystallization was detected during the melting event in the measurements with a heating/cooling rate of 10 K/min (Figure S13). Substituted polyethers are typically amorphous materials. However, due to the elongated and linear structure of the side chain, POlGE displays a distinct T_m, despite the racemic monomer. This indicates a propensity for side chain crystallization.

The microphase separation driven by crystallization was previously described in literature with comparable side chains, albeit for polyacrylates or polyesters.[70,75,76]

Statistical P(EG-*co*-OlGE) Copolymers

The random incorporation of 5 mol% OlGE in P(EG-*co*-OlGE) copolymers (Table 5, entry 3) results in a notable reduction in crystallinity, as evidenced by the decrease of the melting enthalpy (ΔH_m) of PEG. For comparison, $mPEG_{114}$ (Table 5, entry 11), which closely resembles the polymer under investigation, was utilized. 12 mol% OlGE (Table 5, entry 4) further inhibited crystallization of the polyether backbone, and the material showed the PEG T_m already below room temperature. When 25 mol% OlGE was incorporated (Table 5, entry 5), the T_m (-41.7 °C) was solely dominated by the OlGE side chain.

mPEG-*b*-POlGE Block Copolymers

Block copolymers initiated by $mPEG_{45}$ showed decreasing ΔH_m with increasing POlGE block (Table 5, entry 6–10), again indicating partial miscibility of the two different blocks. Comparing entries 8 and 9, an unusual behavior appears: with an increasing amount of POlGE (entry 9), the T_m of both copolymer blocks decreased. This indicated a transition zone where both blocks were too small to crystallize. By further increase of the POlGE content, the T_m of the POlGE block increased again (entry 10), whereas the thermal properties of the PEG block remained unchanged. Very similar thermal behavior was observed for $mPEG_{114}$-*b*-POlGE block copolymers as well: both T_ms decreased with increasing POlGE content (entries 13 and 14), but with higher POlGE content the T_ms elevated again. This indicated that a more effective phase separation between the two polymers contributed to the rise in the T_ms (entry 15).

Table 5: Overview of the thermal properties of the OlGE (co)polymers.

Entry	Polymer	OlGE mol%	T_g[a] / °C	T_m[b] / °C	ΔH_m[b] / J/g
1	$POlGE_{13}$	100	n.d.	-27.8	32.2
2	$POlGE_{25}$	100	n.d.	-23.2	63.4
3	$P(EG_{123}$-*co*-$OlGE_7)$	5	n.d.	35.7	64.9
4	$P(EG_{94}$-*co*-$OlGE_{13})$	12	-81	12	46.5
5	$P(EG_{103}$-*co*-$OlGE_{35})$	25	-80	-41.7	30.3
6	$mPEG_{45}$	0	-60	– / 52.3	– / 164.7
7	$mPEG_{45}$-*b*-$POlGE_{2.4}$	3	-75	n.d. / 48.1	n.d. / 104.0
8	$mPEG_{45}$-*b*-$POlGE_{5.0}$	10	n.d.	-39.5 / 42.7	9.0 / 67.1
9	$mPEG_{45}$-*b*-$POlGE_{7.5}$	14	-78	-46.8 / 37.2	6.6 / 48.2
10	$mPEG_{45}$-*b*-$POlGE_{11.3}$	20	-79	-32.1 / 35.0	21.8 / 45.4
11	$mPEG_{114}$	0	-60	– / 61.9	– / 190.1
12	$mPEG_{114}$-*b*-$POlGE_{2.9}$	2	-79	n.d. / 57.4	n.d. / 133.8
13	$mPEG_{114}$-*b*-$POlGE_{5.8}$	5	-80	-50.5 / 53.7	4.2 / 108.5
14	$mPEG_{114}$-*b*-$POlGE_{7.3}$	6	-76	-58.0 / 51.9	0.8 / 89.8
15	$mPEG_{114}$-*b*-$POlGE_{9.9}$	8	n.d.	-41.3/ 53.3	10.2 / 88.9

[a]Heating rate 10 °C/min, second heating curve, [b]Heating rate 1 °C/min, second heating curve. In the case of block copolymers, the first T_m and ΔH_m denote the POlGE block crystallization, whereas the second denote the PEG block crystallization.

Post-Polymerization Modification

Hydrogenation *via* Diimide Reduction

Oleyl alcohol exhibits a T_m of 0–5 °C,[77] in contrast to its fully saturated alcohol counterpart, known as stearyl alcohol, showing a considerably higher T_m of 57 °C.[78] Accordingly, a similar correlation was expected for the respective GE monomers and the resulting polymers. The POlGE homopolymer exhibited a T_m of approximately -23 °C. To cover a broad range of side chain T_ms, particularly in the physiological range, we aimed at partial to complete hydrogenation as a post-polymerization modification. While copolymerization of saturated and unsaturated monomers is possible, the transfer of a solid monomer via a syringe entails additional effort and may represent a challenge. Moreover, elucidating the reactivity ratios of the GE monomers would be essential. Traditional hydrogenation in organic synthesis involves reacting the unsaturated substrate with hydrogen gas and a palladium catalyst. Although this method is widely used in industrial settings, it requires high pressures and involves handling highly explosive hydrogen, making it impractical in a

laboratory environment. Therefore, we turned to the reduction of the double bond using diimide reduction.[79–82] Potassium azodicarboxylate (PADA) was treated with acetic acid in pyridine to generate diimide. This compound transfers hydrogen to the *cis*-double bond of the OlGE side chain. The degree of hydrogenation was controlled by the amount of PADA equivalents used. In cases of high degrees of hydrogenation, PADA was employed in significant excess. Experimental details can be found in the SI. The decrease of the double bond resonance is visible in the ^{1}H NMR spectra of the hydrogenated polymer (Figure 5). We achieved a maximum degree of hydrogenation of 95% (H95%), which we refer to as fully hydrogenated. As the copolymers comprise a polyether structure lacking bonds susceptible to cleavage under hydrogenation conditions, SEC still showed monomodal distributions with only minor changes in M_n and $Đ$ (Figure S46). Statistical as well as block copolymers were hydrogenated for testing purposes. However, since the melting points of the hydrogenated OlGE monomer overlapped with the PEG part, the changes in thermal properties were uncertain: whether they are attributed to the higher T_m resulting from the hydrogenation of OlGE or a change in PEG crystallization. Therefore, only POlGE homopolymers were included in this study.

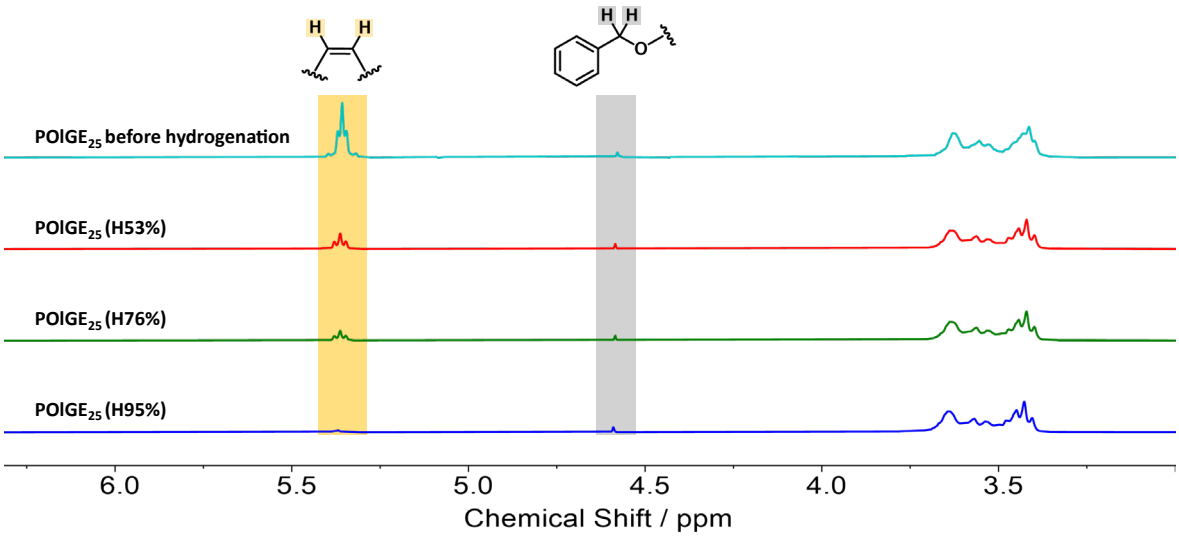

Figure 5: ^{1}H NMR spectra of POlGE$_{25}$ and the respective hydrogenated Polymers (400 MHz, $CDCl_3$). The value of H denotes the degree of hydrogenation. The intensity was locally normalized to the initiator benzyl group (gray).

To confirm the anticipated effect of hydrogenation concerning side chain crystallization, the thermal properties after hydrogenation were investigated by DSC (Figure S48). With an increasing degree of hydrogenation, the T_m of POlGE$_{25}$ rises above room temperature and reaches its peak at 51.9 °C when fully hydrogenated. Up to 53% of hydrogenation results in a significant increase of T_m, whereas the difference in T_m decreases with higher degrees of hydrogenation (entries 3 and 4). The

melting enthalpy increases only slightly, going from 63.4 to 75.2 J/g. This relatively small change occurs even though the hydrogenated side chains were expected to be hindered from crystallization due to the assumed miscibility of the saturated and unsaturated side chains. Here, the melting enthalpy is almost independent of the degree of hydrogenation, albeit the melting point increases by 75.1 °C in total. In summary, the hydrogenation experiments show that POlGE can be fully hydrogenated in a post-polymerization modification. With a T_m in the physiological range, copolymers containing OlGE repeating units possess potential for applications in drug delivery systems. Tailoring can be conveniently performed, as no copolymerization of high and low T_m monomers is necessary. Instead, one starting material is sufficient.

Table 6: Thermal properties of POlGE25 homopolymer before (H0%) and after hydrogenation at various degrees investigated by DSC.

Entry	Polymer[a]	T_m[b] / °C	ΔH_m[b] / J/g
1	$POlGE_{25}$ (H0%)	-23.2	63.4
2	$POlGE_{25}$ (H53%)	33.6	69.2
3	$POlGE_{25}$ (H76%)	43.7	73.0
4	$POlGE_{25}$ (H95%)	51.9	75.2

[a]The value of H denotes the degree of hydrogenation. [b]Heating rate 1 °C/min, second heating curve.

Not only does the double bond content provide the opportunity to customize thermal properties, but it also allows for the modification of the structure to meet specific requirements. It enables the incorporation of hydroxyl groups or other functional groups, which enables the tuning of hydrophobicity and facilitates further coupling with various other groups.[83–85]

Thiol-Ene Click

The addressability of the internal double bond of the side chains as a proof of concept reaction was demonstrated by a thiol-ene click reaction with thioglycol in a post-polymerization modification. As a model polymer, $mPEG_{114}$-*b*-$POlGE_{2.9}$ reacted with the thiyl radicals generated by irradiation of the photoinitiator 2,2-dimethoxy-2-phenylacetophenone (DMPA) in DCM.[86] Detailed experimental information is available in the SI.

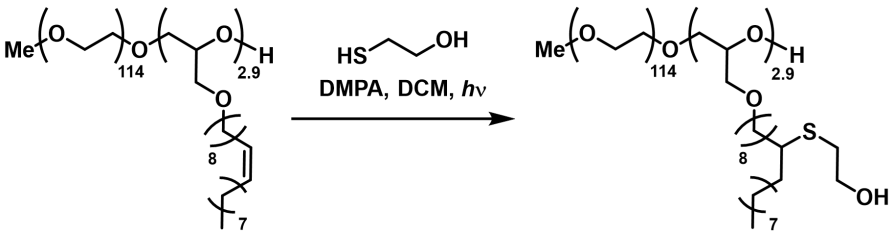

Scheme 3: Thiol-Ene Click reaction of mPEG$_{114}$-*b*-POlGE$_{2.9}$ with thioglycol. Note that two possible addition products can be present.

Complete conversion was confirmed by ^{1}H NMR by the disappearance of the double bond and allylic proton signal. The appearance of the methine and methylene group of the respective thioether further demonstrated the successful modification (Figure S42). SEC revealed a shift towards higher molar masses, again keeping the dispersity constant (Figure S43). DOSY NMR confirmed no residual thioglycol precursor after work-up by dialysis (Figure S44). MALDI-ToF MS analysis showed the new repeating unit with a molar mass of 402 g/mol (Figure S45).

Conclusion

OlGE was introduced as a biorenewable, apolar epoxide building block for the AROP copolymerization with EO. Investigation of the reactivity ratios revealed an ideal statistical copolymerization of OlGE (r_{OlGE} = 0.78) with EO (r_{EO} = 1.27), leading to an almost ideally random copolymer structure. This is a remarkable observation, considering the large steric bulk of the OlGE monomer in comparison to EO. In addition to statistical copolymers, utilization of two different mPEG macroinitiators yielded block copolymers. Capitalizing on block copolymers of POlGE with mPEG, amphiphilic polymers were successfully produced. The CMCs of mPEG-based block copolymers show a limit in the same range as the established surfactant Brij® 98. The water-soluble statistical copolymer also showed micelle formation, owing to the long hydrophobic side chain. TEM and DLS reveal the ability to form spherical and more elongated micellar aggregates, which can be explained by the arrangement of the sterically demanding, linear side chains. The utilization of OlGE allows the synthesis of bio-based surfactants from readily accessible starting materials. The bulk properties of the polymers showed two distinguishable T_ms, indicating partial miscibility of the EO and OlGE monomers, which are highly different in polarity. The *cis*-alkenyl side chain was successfully modified by a thiol-ene click reaction, demonstrating the accessibility and emphasizing the versatility of the hidden functionality. This grants coupling potential of the polymers to thiol-containing compounds, comparable to the PEGylation of proteins. Tailored hydrogenation of the double bond with PADA enables adjusting the material T_m, eradicating the mixing of monomers with high and low side chain T_m, respectively. The achieved range is suitable for developing

potential thermoresponsive drug delivery systems as it matches the human body temperature. In future drug delivery applications, active pharmaceutical ingredients could be released from micellar solutions if the T_m of the precisely adjusted side chain is reached.

In brief, our study shows that the bio-based novel monomer OlGE and its copolymerization can be employed to manufacture a wide range of structurally varied polymeric surfactants. This approach paves the way for replacing traditional petroleum-based surfactants and also unlocks the potential for generating diverse and sophisticated polymer architectures. Green, easily modifiable polymers towards the needs of the user with respect to melting temperatures or hydrophobicity can present a future platform for customized drug-delivery systems.

Acknowledgments

The authors thank [redacted] for SEC measurements, [redacted] for MALDI-TOF MS measurements. [redacted] are acknowledged for introduction to TEM measurements and [redacted] for experimental support. [redacted] is thanked for the thorough correction of the manuscript.

References

(1) Raffa, P.; Wever, D. A. Z.; Picchioni, F.; Broekhuis, A. A. Polymeric Surfactants: Synthesis, Properties, and Links to Applications. *Chem. Rev.* **2015**, *115* (16), 8504–8563. DOI: 10.1021/cr500129h.

(2) Alexandridis, P.; Lindman, B., Eds. *Amphiphilic block copolymers*:*Self-assembly and applications*, 1. ed., digital print; Elsevier, 2000.

(3) Schmolka, I. R. A review of block polymer surfactants. *J. Am. Chem. Soc.* **1977**, *54* (3), 110–116. DOI: 10.1007/BF02894385.

(4) Laruelle, G.; François, J.; Billon, L. Self-Assembly in Water of Poly(acrylic acid)-Based Diblock Copolymers Synthesized by Nitroxide-Mediated Polymerization. *Macromol. Rapid Commun.* **2004**, *25* (21), 1839–1844. DOI: 10.1002/marc.200400315.

(5) Gao, Z.; Varshney, S. K.; Wong, S.; Eisenberg, A. Block Copolymer "Crew-Cut" Micelles in Water. *Macromolecules* **1994**, *27* (26), 7923–7927. DOI: 10.1021/ma00104a058.

(6) Lienkamp, K.; Ruthard, C.; Lieser, G.; Berger, R.; Groehn, F.; Wegner, G. Polymerization of Styrene Sulfonate Ethyl Ester and Styrene Sulfonate Dodecyl Ester by ATRP: Synthesis and Characterization of Polymer Brushes. *Macromol. Chem. Phys.* **2006**, *207* (22), 2050–2065. DOI: 10.1002/macp.200600321.

(7) Koóš, M. Carbohydrate Surfactants. In *Encyclopedia of biophysics,* 1. ed.; Roberts, G. C. K., Ed.; Springer, 2013; p 237. DOI: 10.1007/978-3-642-16712-6_80.

(8) Lorson, T.; Lübtow, M. M.; Wegener, E.; Haider, M. S.; Borova, S.; Nahm, D.; Jordan, R.; Sokolski-Papkov, M.; Kabanov, A. V.; Luxenhofer, R. Poly(2-oxazoline)s based biomaterials: A comprehensive and critical update. *Biomaterials* **2018**, *178*, 204–280. DOI: 10.1016/j.biomaterials.2018.05.022.

(9) Herzberger, J.; Niederer, K.; Pohlit, H.; Seiwert, J.; Worm, M.; Wurm, F. R.; Frey, H. Polymerization of Ethylene Oxide, Propylene Oxide, and Other Alkylene Oxides: Synthesis, Novel Polymer Architectures, and Bioconjugation. *Chem. Rev.* **2016**, *116* (4), 2170–2243. DOI: 10.1021/acs.chemrev.5b00441.

(10) Hayes, D. G., Ed. *Biobased surfactants and detergents*:*Synthesis, properties, and applications*; Academic Press, 2019.

(11) Biermann, U.; Bornscheuer, U.; Meier, M. A. R.; Metzger, J. O.; Schäfer, H. J. Oils and fats as renewable raw materials in chemistry. *Angew. Chem. Int. Ed.* **2011**, *50* (17), 3854–3871. DOI: 10.1002/anie.201002767.

(12) Biermann, U.; Bornscheuer, U. T.; Feussner, I.; Meier, M. A. R.; Metzger, J. O. Fatty Acids and their Derivatives as Renewable Platform Molecules for the Chemical Industry. *Angew. Chem. Int. Ed.* **2021**, *60*, 20144–20165. DOI: 10.1002/anie.202100778.

(13) Noweck, K.; Grafahrend, W. Fatty Alcohols. In *Ullmann's Encyclopedia of Industrial Chemistry*; Wiley-VCH Verlag GmbH & Co. KGaA, 2000. DOI: 10.1002/14356007.a10_277.pub2.

(14) Baumann, H.; Bühler, M.; Fochem, H.; Hirsinger, F.; Zoebelein, H.; Falbe, J. Natural Fats and Oils—Renewable Raw Materials for the Chemical Industry. *Angew. Chem. Int. Ed. Engl.* **1988**, *27* (1), 41–62. DOI: 10.1002/anie.198800411.

(15) ISTA Mielke GmbH. *Oil World Annual 2020*, Hamburg, 2020.

(16) Solvay. *Solvay Epicerol® Earns Roundtable on Sustainable Biomaterials Certification*. https://www.solvay.com/sites/g/files/srpend221/files/tridion/documents/17_RSB%20Certificate_Final.pdf (accessed 2022-09-09).

(17) Bell, B. M.; Briggs, J. R.; Campbell, R. M.; Chambers, S. M.; Gaarenstroom, P. D.; Hippler, J. G.; Hook, B. D.; Kearns, K.; Kenney, J. M.; Kruper, W. J.; Schreck, D. J.; Theriault, C. N.; Wolfe, C. P. Glycerin as a Renewable Feedstock for Epichlorohydrin Production. The GTE Process. *Clean* **2008**, *36* (8), 657–661. DOI: 10.1002/clen.200800067.

(18) Meng, Y.; Taddeo, F.; Aguilera, A. F.; Cai, X.; Russo, V.; Tolvanen, P.; Leveneur, S. The Lord of the Chemical Rings: Catalytic Synthesis of Important Industrial Epoxide Compounds. *Catalysts* **2021**, *11* (7), 765. DOI: 10.3390/catal11070765.

(19) Gu, X.-P.; Ikeda, I.; Okahara, M. Stereoselective Formation of Allyl Ethers by Reaction of Epoxides with Organic Chlorides under Liquid-Solid Phase-Transfer Catalysis. *Bull. Chem. Soc. Jpn.* **1987**, *60* (2), 667–672. DOI: 10.1246/bcsj.60.667.

(20) Hill, J.; Nelson, E.; Tilman, D.; Polasky, S.; Tiffany, D. Environmental, economic, and energetic costs and benefits of biodiesel and ethanol biofuels. *Proc. Natl. Acad. Sci. U.S.A* **2006**, *103* (30), 11206–11210. DOI: 10.1073/pnas.0604600103.

(21) García-Franco, A.; Godoy, P.; La Torre, J. de; Duque, E.; Ramos, J. L. United Nations sustainability development goals approached from the side of the biological production of fuels. *Microb. Biotechnol.* **2021**, *14* (5), 1871–1877. DOI: 10.1111/1751-7915.13912.

(22) Thangaraj, B.; Solomon, P. R. Scope of biodiesel from oils of woody plants: a review. *Clean Energy* **2020**, *4* (2), 89–106. DOI: 10.1093/ce/zkaa006.

(23) Tuck, C. O.; Pérez, E.; Horváth, I. T.; Sheldon, R. A.; Poliakoff, M. Valorization of biomass: deriving more value from waste. *Science (New York, N.Y.)* **2012**, *337* (6095), 695–699. DOI: 10.1126/science.1218930.

(24) BASF. *Bioethanol*:*New catalyst geometry poised to re-shape the ethanol-to-ethylene conversion process*. https://chemicals.basf.com/global/en/Catalysts/hydrogenation-specialty/products-we-offer/alumina/Ethanol-to-Ethylene-E2E.html.

(25) Zhang, M.; Yu, Y. Dehydration of Ethanol to Ethylene. *Ind. Eng. Chem. Res.* **2013**, *52* (28), 9505–9514. DOI: 10.1021/ie401157c.

(26) Lucky, C.; Wang, T.; Schreier, M. Electrochemical Ethylene Oxide Synthesis from Ethanol. *ACS Energy Lett.* **2022**, *7* (4), 1316–1321. DOI: 10.1021/acsenergylett.2c00265.

(27) Li, Y.; Ozden, A.; Leow, W. R.; Ou, P.; Huang, J. E.; Wang, Y.; Bertens, K.; Xu, Y.; Liu, Y.; Roy, C.; Jiang, H.; Sinton, D.; Li, C.; Sargent, E. H. Redox-mediated electrosynthesis of ethylene oxide from CO_2 and water. *Nat. Catal.* **2022**, *5* (3), 185–192. DOI: 10.1038/s41929-022-00749-8.

(28) Jhaveri, A. M.; Torchilin, V. P. Multifunctional polymeric micelles for delivery of drugs and siRNA. *Front. Pharmacol.* **2014**, *5*, 77. DOI: 10.3389/fphar.2014.00077.

(29) Allen, T. M.; Cullis, P. R. Drug delivery systems: entering the mainstream. *Science (New York, N.Y.)* **2004**, *303* (5665), 1818–1822. DOI: 10.1126/science.1095833.

(30) LaVan, D. A.; McGuire, T.; Langer, R. Small-scale systems for in vivo drug delivery. *Nat. Biotechnol.* **2003**, *21* (10), 1184–1191. DOI: 10.1038/nbt876.

(31) Guo, X.; Szoka, F. C. Chemical approaches to triggerable lipid vesicles for drug and gene delivery. *Acc. Chem. Res.* **2003**, *36* (5), 335–341. DOI: 10.1021/ar9703241.

(32) Torchilin, V. Multifunctional and stimuli-sensitive pharmaceutical nanocarriers. *Eur. J. Pharm. Biopharm.* **2009**, *71* (3), 431–444. DOI: 10.1016/j.ejpb.2008.09.026.

(33) Meyer, D. E.; Shin, B. C.; Kong, G. A.; Dewhirst, M. W.; Chilkoti, A. Drug targeting using thermally responsive polymers and local hyperthermia. *J. Control. Release* **2001**, *74* (1-3), 213–224. DOI: 10.1016/s0168-3659(01)00319-4.

(34) Mura, S.; Nicolas, J.; Couvreur, P. Stimuli-responsive nanocarriers for drug delivery. *Nat. Mater.* **2013**, *12* (11), 991–1003. DOI: 10.1038/nmat3776.

(35) Glover, A. L.; Bennett, J. B.; Pritchett, J. S.; Nikles, S. M.; Nikles, D. E.; Nikles, J. A.; Brazel, C. S. Magnetic Heating of Iron Oxide Nanoparticles and Magnetic Micelles for Cancer Therapy. *IEEE Trans. Magn.* **2013**, *49* (1), 231–235. DOI: 10.1109/TMAG.2012.2222359.

(36) Schneider, K.; Verkoyen, P.; Krappel, M.; Gardiner, C.; Schweins, R.; Frey, H.; Sottmann, T. Efficiency Boosting of Surfactants with Poly(ethylene oxide)-Poly(alkyl glycidyl ether)s: A New Class of Amphiphilic Polymers. *Langmuir* **2020**, 9849–9866. DOI: 10.1021/acs.langmuir.0c01491.

(37) Verkoyen, P.; Dreier, P.; Bros, M.; Hils, C.; Schmalz, H.; Seiffert, S.; Frey, H. “Dumb” pH-Independent and Biocompatible Hydrogels Formed by Copolymers of Long-Chain Alkyl Glycidyl Ethers and Ethylene Oxide. *Biomacromolecules* **2020**, *21* (8), 3152–3162. DOI: 10.1021/acs.biomac.0c00576.

(38) Verkoyen, P.; Johann, T.; Blankenburg, J.; Czysch, C.; Frey, H. Polymerization of long chain alkyl glycidyl ethers: a platform for micellar gels with tailor-made melting points. *Polym. Chem.* **2018**, *9* (44), 5327–5338. DOI: 10.1039/C8PY01312H.

(39) Verkoyen, P.; Frey, H. Long-Chain Alkyl Epoxides and Glycidyl Ethers: An Underrated Class of Monomers. *Macromol. Rapid Commun.* **2020**, *41* (15). DOI: 10.1002/marc.202000225.

(40) Schüttner, S.; Krappel, M.; Koziol, M.; Marquart, L.; Schneider, I.; Sottmann, T.; Frey, H. Anionic Ring-Opening Copolymerization of Farnesyl Glycidyl Ether: Fast Access to Terpenoid-Derived Amphiphilic Polyether Architectures. *Macromolecules* **2023.** DOI: 10.1021/acs.macromol.3c00999.

(41) Krappel, M.; Schüttner, S.; Schneider, I.; Schweins, R.; Frey, H.; Sottmann, T. Amphiphilic, Bio-based Farnesyl Glycidyl Ether Block Copolymers: Aqueous Self-Assembly and Solubilization Enhancement. Submitted.

(42) Becker, H. G. O. *Organikum*:*Organisch-chemisches Grundpraktikum*, 21., neu bearb. und erw. Aufl.; Wiley-VCH, 2001.

(43) Matyjaszewski, K.; Gnanou, Y.; Leibler, L. *Macromolecular Engineering*:*4 volume*; Wiley, 2007. DOI: 10.1002/9783527631421.

(44) Tieke, B. *Makromolekulare Chemie*:*Eine Einführung*, 3. Aufl.; Wiley-VCH, 2014.

(45) Boileau, S.; Deffieux, A.; Lassalle, D.; Menezes, F.; Vidal, B. Reactivities of anionic species for the ring opening of ethylene oxide. *Tetrahedron Lett.* **1978**, *19* (20), 1767–1770. DOI: 10.1016/0040-4039(78)80039-2.

(46) Jaacks, V. Eine neuartige Methode zur Bestimmung von Copolymerisationsparametern. *Angew. Chem.* **1967**, *79* (9), 419. DOI: 10.1002/ange.19670790927.

(47) Jaacks, V. A Novel Method of Determination of Reactivity Ratios in Binary and Ternary Copolymerizations. *Makromol. Chem.* **1972**, *161* (1), 161–172. DOI: 10.1002/macp.1972.021610110.

(48) Steube, M.; Johann, T.; Plank, M.; Tjaberings, S.; Gröschel, A. H.; Gallei, M.; Frey, H.; Müller, A. H. E. Kinetics of Anionic Living Copolymerization of Isoprene and Styrene Using in Situ NIR Spectroscopy: Temperature Effects on Monomer Sequence and Morphology. *Macromolecules* **2019**, *52* (23), 9299–9310. DOI: 10.1021/acs.macromol.9b01790.

(49) Meyer, V. E.; Lowry, G. G. Integral and differential binary copolymerization equations. *J. Polym. Sci. A Gen. Pap.* **1965**, *3* (8), 2843–2851. DOI: 10.1002/pol.1965.100030811.

(50) Hoffman, R.; Carpenter, B. K.; Minkin, V. I. Ockham's Razor and Chemistry. *HYLE* **1997**, *3*, 3–28.

(51) Blankenburg, J.; Kersten, E.; Maciol, K.; Wagner, M.; Zarbakhsh, S.; Frey, H. The poly(propylene oxide-*co*-ethylene oxide) gradient is controlled by the polymerization method: determination of reactivity ratios by direct comparison of different copolymerization models. *Polym. Chem.* **2019**, *10* (22), 2863–2871. DOI: 10.1039/C9PY00500E.

(52) Mangold, C.; Wurm, F.; Obermeier, B.; Frey, H. "Functional Poly(ethylene glycol)": PEG-Based Random Copolymers with 1,2-Diol Side Chains and Terminal Amino Functionality. *Macromolecules* **2010**, *43* (20), 8511–8518. DOI: 10.1021/ma1015352.

(53) Tonhauser, C.; Alkan, A.; Schömer, M.; Dingels, C.; Ritz, S.; Mailänder, V.; Frey, H.; Wurm, F. R. Ferrocenyl Glycidyl Ether: A Versatile Ferrocene Monomer for Copolymerization with Ethylene Oxide to Water-Soluble, Thermoresponsive Copolymers. *Macromolecules* **2013**, *46* (3), 647–655. DOI: 10.1021/ma302241w.

(54) Deng, Y.; Ding, J.; Yu, G.; Mobbs, R. H.; Heatley, F.; Price, C.; Booth, C. Preparation and properties of *stat*-copoly-(oxyethylene-oxypropylene)-*block*-poly (oxyethylene): 1. Use of crown ether in the anionic copolymerization of propylene oxide and ethylene oxide. *Polymer* **1992**, *33* (9), 1959–1962. DOI: 10.1016/0032-3861(92)90500-V.

(55) Dreier, P.; Matthes, R.; Barent, R. D.; Schüttner, S.; Müller, A. H. E.; Frey, H. In Situ Kinetics Reveal the Influence of Solvents and Monomer Structure on the Anionic Ring-Opening Copolymerization of Epoxides. *Macromol. Chem. Phys.* **2022**, 2200209. DOI: 10.1002/macp.202200209.

(56) Lee, A.; Lundberg, P.; Klinger, D.; Lee, B. F.; Hawker, C. J.; Lynd, N. A. Physiologically relevant, pH-responsive PEG-based block and statistical copolymers with N,N-diisopropylamine units. *Polym. Chem.* **2013**, *4* (24), 5735–5742. DOI: 10.1039/C3PY00747B.

(57) Herzberger, J.; Fischer, K.; Leibig, D.; Bros, M.; Thiermann, R.; Frey, H. Oxidation-Responsive and "Clickable" Poly(ethylene glycol) via Copolymerization of 2-(Methylthio)ethyl Glycidyl Ether. *J. Am. Chem. Soc.* **2016**, *138* (29), 9212–9223. DOI: 10.1021/jacs.6b04548.

(58) Blankenburg, J.; Maciol, K.; Hahn, C.; Frey, H. Poly(ethylene glycol) with Multiple Aldehyde Functionalities Opens up a Rich and Versatile Post-Polymerization Chemistry. *Macromolecules* **2019**, *52* (4), 1785–1793. DOI: 10.1021/acs.macromol.8b02639.

(59) Herzberger, J.; Leibig, D.; Liermann, J. C.; Frey, H. Conventional Oxyanionic versus Monomer-Activated Anionic Copolymerization of Ethylene Oxide with Glycidyl Ethers: Striking Differences in Reactivity Ratios. *ACS Macro Lett.* **2016**, *5* (11), 1206–1211. DOI: 10.1021/acsmacrolett.6b00701.

(60) Niederer, K.; Schüll, C.; Leibig, D.; Johann, T.; Frey, H. Catechol Acetonide Glycidyl Ether (CAGE): A Functional Epoxide Monomer for Linear and Hyperbranched Multi-Catechol Functional Polyether Architectures. *Macromolecules* **2016**, *49* (5), 1655–1665. DOI: 10.1021/acs.macromol.5b02441.

(61) Aguiar, J.; Carpena, P.; Molina-Bolívar, J. A.; Carnero Ruiz, C. On the determination of the critical micelle concentration by the pyrene 1:3 ratio method. *J. Colloid Interface Sci.* **2003**, *258* (1), 116–122. DOI: 10.1016/S0021-9797(02)00082-6.

(62) Li, H.; Hu, D.; Liang, F.; Huang, X.; Zhu, Q. Influence factors on the critical micelle concentration determination using pyrene as a probe and a simple method of preparing samples. *R. Soc. Open Sci.* **2020**, *7* (3), 192092. DOI: 10.1098/rsos.192092.

(63) Griffin, W. C. Classification of surface-active agents by "HLB". *J. Soc. Cosmet. Chem.* **1949**, *1* (5), 311–326.

(64) Mok, M. M.; Thiagarajan, R.; Flores, M.; Morse, D. C.; Lodge, T. P. Apparent Critical Micelle Concentrations in Block Copolymer/Ionic Liquid Solutions: Remarkably Weak Dependence on Solvophobic Block Molecular Weight. *Macromolecules* **2012**, *45* (11), 4818–4829. DOI: 10.1021/ma300399c.

(65) Qiu, J.; Pintauer, T.; Gaynor, S. G.; Matyjaszewski, K.; Charleux, B.; Vairon, J.-P. Mechanistic Aspect of Reverse Atom Transfer Radical Polymerization of *n*-Butyl Methacrylate in Aqueous Dispersed System. *Macromolecules* **2000**, *33* (20), 7310–7320. DOI: 10.1021/ma000720q.

(66) Caritá, A. C.; Cavalcanti, R. R. M.; Oliveira, M. S. S.; Riske, K. A. Solubilization of biomimetic lipid mixtures by some commonly used non-ionic detergents. *Chem. Phys. Lipids* **2023**, *255*, 105327. DOI: 10.1016/j.chemphyslip.2023.105327.

(67) Ribeiro, M. E. N. P.; Moura, C. L. de; Vieira, M. G. S.; Gramosa, N. V.; Chaibundit, C.; Mattos, M. C. de; Attwood, D.; Yeates, S. G.; Nixon, S. K.; Ricardo, N. M. P. S. Solubilisation capacity of Brij surfactants. *Int. J. Pharm.* **2012**, *436* (1-2), 631–635. DOI: 10.1016/j.ijpharm.2012.07.032.

(68) Klammt, C.; Schwarz, D.; Fendler, K.; Haase, W.; Dötsch, V.; Bernhard, F. Evaluation of detergents for the soluble expression of alpha-helical and beta-barrel-type integral membrane proteins by a preparative scale individual cell-free expression system. *FEBS J.* **2005**, *272* (23), 6024–6038. DOI: 10.1111/j.1742-4658.2005.05002.x.

(69) Perinelli, D. R.; Cespi, M.; Lorusso, N.; Palmieri, G. F.; Bonacucina, G.; Blasi, P. Surfactant Self-Assembling and Critical Micelle Concentration: One Approach Fits All? *Langmuir* **2020**, *36* (21), 5745–5753. DOI: 10.1021/acs.langmuir.0c00420.

(70) Terashima, T. Controlled Self-Assembly of Amphiphilic Random Copolymers into Folded Micelles and Nanostructure Materials. *J. Oleo Sci.* **2020**, *69* (6), 529–538. DOI: 10.5650/jos.ess20089.

(71) Hibino, M.; Tanaka, K.; Ouchi, M.; Terashima, T. Amphiphilic Random-Block Copolymer Micelles in Water: Precise and Dynamic Self-Assembly Controlled by Random Copolymer Association. *Macromolecules* **2022**, *55* (1), 178–189. DOI: 10.1021/acs.macromol.1c02186.

(72) Nguyen, T. L.; Ishihara, K.; Yusa, S.-I. Separated Micelles Formation of pH-Responsive Random and Block Copolymers Containing Phosphorylcholine Groups. *Polymers* **2022**, *14* (3). DOI: 10.3390/polym14030577.

(73) PharmaCentral. *Polyethylene Glycol | Uses, Suppliers, and Specifications*. https://pharmacentral.com/product/polyethylene-glycol-pharmaceutical-excipient/.

(74) The Dow Chemical Company. *Formulating CARBOWAX™ SENTRY™ PEGs in ointment applications*. https://www.cphi-online.com/46/resourcefile/14/35/18/file.pdf.

(75) Hattori, G.; Takenaka, M.; Sawamoto, M.; Terashima, T. Nanostructured Materials via the Pendant Self-Assembly of Amphiphilic Crystalline Random Copolymers. *J. Am. Chem. Soc.* **2018**, *140* (27), 8376–8379. DOI: 10.1021/jacs.8b03838.

(76) Imai, S.; Ommura, Y.; Watanabe, Y.; Ogawa, H.; Takenaka, M.; Ouchi, M.; Terashima, T. Amphiphilic random and random block terpolymers with PEG, octadecyl, and oleyl pendants for controlled crystallization and microphase separation. *Polym. Chem.* **2021**, *12* (10), 1439–1447. DOI: 10.1039/D0PY01505A.

(77) Merck. *Safety data sheet*:*Oleyl alcohol*. https://www.sigmaaldrich.com/DE/de/sds/aldrich/369314?userType=anonymous (accessed 2023-12-08).

(78) Merck. *Safety data sheet*: *Stearyl alcohol*. https://www.sigmaaldrich.com/DE/de/sds/sial/phr1115?userType=anonymous (accessed 2023-12-08).

(79) Hamersma, J. W.; Snyder, E. I. Diimide Reductions Using Potassium Azodicarboxylate. *J. Org. Chem.* **1965**, *30* (11), 3985–3988. DOI: 10.1021/jo01022a532.

(80) Groves, J. T.; Ma, K. W. Carbon cluster compounds. Generation and reorganization of the homobullvalenyl cation, an 11-fold degenerate species. *J. Am. Chem. Soc.* **1977**, *99* (12), 4076–4082. DOI: 10.1021/ja00454a028.

(81) Wang, D.; Astruc, D. The golden age of transfer hydrogenation. *Chem. Rev.* **2015**, *115* (13), 6621–6686. DOI: 10.1021/acs.chemrev.5b00203.

(82) Schüttner, S.; Linden, G. M.; Hoffmann, E. C.; Holzmüller, P.; Frey, H. Poly(Terpenyl Glycidyl Ethers): Copolymerization with Ethylene Oxide, Properties, and Functionalization. Manuscript in preparation.

(83) Hoyle, C. E.; Lowe, A. B.; Bowman, C. N. Thiol-click chemistry: a multifaceted toolbox for small molecule and polymer synthesis. *Chem. Soc. Rev.* **2010**, *39* (4), 1355–1387. DOI: 10.1039/b901979k.

(84) Lowe, A. B. Thiol–ene “click” reactions and recent applications in polymer and materials synthesis: a first update. *Polym. Chem.* **2014**, *5* (17), 4820–4870. DOI: 10.1039/C4PY00339J.

(85) Lowe, A. B. Thiol-ene “click” reactions and recent applications in polymer and materials synthesis. *Polym. Chem.* **2010**, *1* (1), 17–36. DOI: 10.1039/B9PY00216B.

(86) Campos, L. M.; Killops, K. L.; Sakai, R.; Paulusse, J. M. J.; Damiron, D.; Drockenmuller, E.; Messmore, B. W.; Hawker, C. J. Development of Thermal and Photochemical Strategies for

Thiol–Ene Click Polymer Functionalization. *Macromolecules* **2008**, *41* (19), 7063–7070. DOI: 10.1021/ma801630n.

Supporting Information

Experimental Section

Reagents

The chemicals were sourced from commercial suppliers, such as *Sigma-Aldrich, TCI*, *Fluka*, and *Acros*, and were used without purification unless otherwise specified. The deuterated solvents were obtained from *Deutero GmbH* (Germany). Oleic acid methyl ester (99% purity) was procured from *Sigma-Aldrich*. Ethylene oxide (EO) was purchased from *Air Liquide*. Oleyl glycidyl ether (OlGE) was dried overnight using benzene under a high vacuum prior to polymerization. [18]Crown-6 was dried by azeotropic distillation under high vacuum, dissolved in a defined amount of dry benzene in a flame-dried Schlenk flask, and stored under argon. DMSO was stored over molecular sieves and added to the initiator salt using a syringe. Tetrahydrofuran (THF) was dried over a mixture of butyllithium and diphenylethylene, degassed, and stored under vacuum. The mixture was then transferred to the polymerization flask using cryogenic techniques. For online ^{1}H NMR kinetics, deuterated THF (THF-d_8) was dried over CaH_2 overnight and subsequently cryogenically transferred. DMSO-d_6 from a fresh bottle was used. Uranyl acetate solution for negative staining in transmission electron microscopy was purchased from *Polyscience*. The carbon-coated copper grids with 400 mesh (CF-400-Cu) were acquired from *Electron Microscopy Sciences*.

Instrumentation

Nuclear Magnetic Resonance (NMR) Spectroscopy

Standard 300 MHz NMR measurements were performed on a *Bruker Avance III HD 300* equipped with a 5 mm BBFO probe head with *z*-gradient and ATM. Standard 400 MHz NMR spectra were measured on a *Bruker Avance II 400* spectrometer with a 5 mm BBFO probe head with *z*-gradient and ATM. The spectra were referenced internally to the residual proton signal (^{1}H NMR) of the signal of the naturally occurring ^{13}C atom in the respective solvent (^{13}C NMR).

Two-dimensional- NMR Experiments, such as COSY, HSQC, DOSY, and HMBC, as well as *in situ* ^{1}H NMR copolymerization kinetics, were performed on a *Bruker Avance III 400* with a 5 mm BBO cryo probe head (BB/H+F), which was cooled with liquid nitrogen, with *z*-gradient, and ATM. All spectra were acquired at 23 °C unless stated otherwise and processed using *MestReNova* 14.3.32681.

Size Exclusion Chromatography (SEC)

SEC analysis using *N*,*N*-dimethylformamide (DMF) as the eluent was performed using an *Agilent 1100 series* SEC system. The system was equipped with UV (254 nm) and RI detectors, and a HEMA 300/100/40 Å column cascade was used. The measurements were conducted at a flow rate of 1 mL/min, with DMF as the eluent containing 1 g/mL lithium bromide at a temperature of 50 °C. SEC analysis with THF as the eluent was conducted using an MZ-Gel SD plus e5/e3/100 column cascade, *P100* pump, and *Waters 717 plus* injector. The SEC system was equipped with UV (254 nm) and refractive index (RI) detectors. The eluent flow rate was set to 1 mL/min. Toluene was used as the internal standard in both cases. The SEC calibration was performed using poly(ethylene glycol) standards provided by *Polymer Standard Service* (*PSS*). Data recording and processing were performed using *the PSS WinGPC UniChrom* software.

Matrix-assisted Laser Desorption Ionization Time-of-Flight (MALDI-ToF) Mass Spectrometry

MALDI-ToF analysis was performed using a *Bruker autoflex maX MALDI-ToF-MS/MS* instrument in linear or reflector mode. The analysis was conducted on a multi-target plate. *trans*-2-[3-(4-*tert*-Butylphenyl)-2-methyl-2-propenylidene] malononitrile (DCTB) or Dithranol (Dit) were used as the matrix. Potassium trifluoroacetate (KTFA) was used as a salt additive.

Differential Scanning Calorimetry (DSC)

DSC measurements were conducted using a *TA Instruments DSC 250* instrument equipped with a *Recovery Cooling System 90*. The measurements were conducted under a dry nitrogen flow at a rate of 20 mL/min. The instrument was calibrated using indium and *n*-octane as standards. Before analysis, all samples were dried by azeotropic distillation with benzene and weighed in aluminum pans with pinholes. The heating and cooling steps during the measurement were as follows.

1) Cool to -90 °C with 10 K/min, and hold for 5 min.
2) Heat to 100 °C with 10 K/min, and hold for 5 min.
3) Cool to -90 °C with 10 K/min, and hold for 5 min.
4) Heat to 100 °C with 10 K/min, and hold for 5 min.

Additionally, Steps 3 and 4 were repeated at a slower rate of 1 K/min in a separate run. All the reported physical values were extracted from the second heating cycle to ensure removal of the thermal history of the sample.

Transmission Electron Microscopy (TEM)

TEM images were acquired using an *FEI Tecnai G2 12 BioTwin* electron microscope operating at an acceleration voltage of 120 kV with a LaB6 cathode emitter. The microscope was equipped with two cameras: an on-axis *4kx4k Tietz CMOS* camera and a side-entry *MegaSYS 1kx1k CCD* camera.

Prior to imaging, carbon-coated copper grids with 400 mesh (CF-400-Cu) were hydrophilized using a plasma cleaner for one minute. Subsequently, 20 µL of the sample solution (0.1 g/L) was added to the grid and incubated for one minute. After the incubation period, excess liquid was removed by gently blotting the grid with filter paper. To enhance the contrast, 20 µL of uranyl acetate solution (2%) was added to the grid and blotted with filter paper after one minute.

Importantly, all the prepared grids were promptly investigated on the same day as their preparation to ensure the integrity and consistency of the sample during imaging.

CMC determination by fluorescence spectroscopy

Polymer solutions were prepared using stock solutions at concentrations of 1 g/L, 0.1 g/L, and 0.01 g/L, with Milli-Q® water as the solvent. Pyrene, dissolved in ethanol (Uvasol®), was introduced into empty graduated flasks, aiming for a final concentration of $7 \cdot 10^{-7}$ mol/L. The ethanol was subsequently evaporated, and the desired concentration was achieved by adding an appropriate volume of polymer stock solution along with Milli-Q® water. The flasks were gently agitated overnight on a laboratory shaker at room temperature to facilitate the equilibration of both pyrene and the micelles. Emission spectra were captured using a *Jasco FP-8200* spectrofluorometer with an excitation wavelength of 335 nm. The range covered 350–450 nm, with a data interval of 0.5 nm and a scanning rate of 20 nm/min. The excitation bandwidth was 2.5 nm, and the emission bandwidth was 2.5 nm. Quartz cells with a path length of 10 mm were employed for the solutions and were pre-treated with the corresponding polymer solution once. The data obtained from plotting the intensity ratio between the first (I_1) and third (I_3) vibronic bands in the fluorescence spectrum of pyrene against the logarithmic concentration of the polymer were analyzed using a Boltzmann sigmoidal fit (equation (S1)).[1]

$$\frac{I_3}{I_1} = \frac{A_1 - A_2}{1 + e^{(\log(c) - \log(\mathrm{CMC}))/dx}} + A_2 \qquad \text{(S1)}$$

A_1 represents the lower boundary, while A_2 represents the upper boundary of the sigmoid curve. The point of inflection denotes the logarithm of the CMC, and *dx* signifies the slope or steepness of the curve.

Monomer Synthesis

The monomer synthesis of oleyl glycidyl ether (OlGE) involved a two-step process that started with methyl oleate and led to the formation of oleyl alcohol. Subsequently, oleyl alcohol was subjected to phase-transfer catalysis using epichlorohydrin (ECH). Methyl oleate, with a purity of 99%, was purchased because commercially available oleyl alcohol of comparable quality could not be obtained at a reasonable cost.

Synthesis of oleyl alcohol from methyl oleate

The reduction of methyl oleate to oleyl alcohol was performed following a standard organic synthesis procedure.[2] A 250 mL three-necked round-bottom flask, equipped with a Dimroth cooler (metal cooling coil), mechanical stirrer, and a dropping funnel, was thoroughly dried using a heat gun and purged with dry nitrogen. Diethyl ether (Et_2O, 84 mL), which was dried over sodium and freshly distilled, was added to the flask. Powdered lithium aluminum hydride (LAH, 1.76 g, 46.4 mmol, 0.55 eq.) was gradually added to the flask. Methyl oleate (25.00 g, 84.3 mmol, 1 eq.) was mixed with 24 mL of dry Et_2O and placed in a dropping funnel. The methyl oleate-Et_2O mixture was slowly added dropwise to the LAH suspension, maintaining a slightly boiling Et_2O. After complete addition, 50 mL of dry Et_2O was added and the resulting mixture was stirred overnight. Subsequently, ice-cold water was added dropwise, and the precipitate was dissolved by adding 10% sulfuric acid (H_2SO_4). The aqueous phase was extracted thrice with 100 mL portions of petroleum ether. The combined organic phases were washed three times with brine and dried overnight with sodium sulfate. The solid was removed by filtration and the solvents were evaporated. Column chromatography was performed using a stepwise solvent gradient. The eluent mixture of cyclohexane/ethyl acetate ranged from 4/1 to 1/20 (V_{Cy}/V_{EtOAc}) and yielded 21.87 g (81.5 mmol) of colorless liquid as the sum of four columns, corresponding to a yield of 97%.

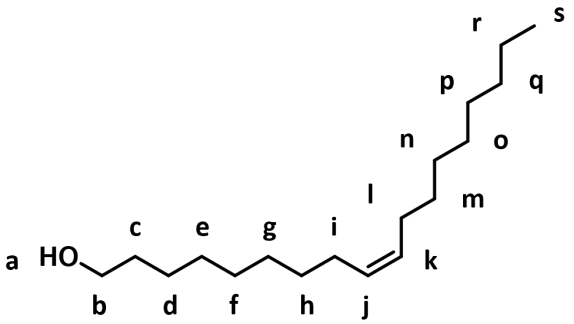

Yield: 97%

Purification by column chromatography, R_F=0.4, eluent 4/1 (V_{cy}/V_{EtOAc})

^{1}H NMR (400 MHz, $CDCl_3$) δ 5.39 – 5.26 (m, 2H, H_j, H_k), 3.60 (t, *J* = 6.7 Hz, 2H, H_b), 2.04 – 1.95 (m, 4H, H_i, H_l), 1.60 – 1.48 (m, 2H, H_c), 1.39 – 1.18 (m, 22H, H_{d-h}, H_{m-r}), 0.86 (t, *J* = 6.8 Hz, 3H, H_s).

^{13}C NMR (101 MHz, $CDCl_3$) δ 130.03 ($C_{J,K}$), 63.02 (C_B), 32.87 (C_C), 32.02 (C_Q), 29.87 ($C_{H,M}$), 29.54 (C_E), 29.73 – 29.28 ($C_{F,G,N,O,P}$), 27.30 ($C_{I,L}$), 25.87 (C_D), 22.79 (C_R), 14.20 (C_S).

Synthesis of oleyl glycidyl ether from oleyl alcohol

The following procedure was adapted from Mouzin *et al*.[3]

A 500 mL three-necked round-bottom flask equipped with a mechanical stirrer, dropping funnel, and plug was charged with oleyl alcohol (21.87 g, 81.5 mmol, 1 eq.), tetra-*n*-butylammonium hydrogen sulfate (1.134 g, 3.34 mmol, 0.041 eq.), and 50 *w*.-% aqueous NaOH (60.6 mL). Toluene (29.27 mL) was introduced, and the biphasic mixture was vigorously stirred while being cooled in an ice/water bath. Epichlorohydrin (22.85 mL, 432 mmol, 5.3 eq.) was added dropwise *using* a dropping funnel. Upon complete addition, the cooling bath was removed, and the reaction mixture was allowed to react overnight.

Subsequently, water (250 mL) was carefully added to the reaction mixture under ice cooling followed by brief stirring to dissolve the precipitate. The phases were separated, and the aqueous phase was subjected to three extractions with 200 mL of petroleum ether each. The combined organic phases were washed with brine until a neutral pH was reached and then dried using $MgSO_4$. Subsequent removal of the solvents and residual epichlorohydrin was achieved under high vacuum.

To purify the crude product and eliminate the side product, 3-chloroallyl glycidyl ether, fractional distillation was performed using a Kugelrohr apparatus at 140 °C (pressure: $5{\cdot}10^{-3}$ mbar). The fraction obtained at 185–198 °C was collected and further purified by column chromatography using a gradient eluent ranging from 50/1 to 8/1 (V_{Cy}/V_{EtOAc}). The final yield of the pure product from the four columns was determined to be 18.62 g (57.5 mmol), corresponding to a 71% yield.

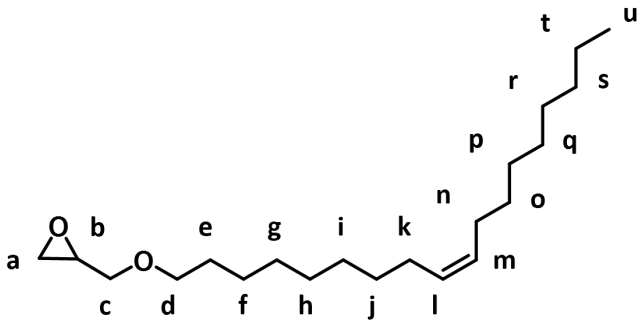

Yield: 71%

Purification by column chromatography, R_F=0.4, eluent 6/1 (V_{cy}/V_{EtOAc})

^{1}H NMR (400 MHz, $CDCl_3$) δ 5.37 – 5.27 (m, 2H, $H_{l,m}$), 3.68 (dd, *J* = 11.5, 3.1 Hz, 1H, $H_{c'}$), 3.53 – 3.40 (m, 2H, H_d), 3.36 (dd, *J* = 11.5, 5.8 Hz, 1H, $H_{c''}$), 3.16 – 3.08 (m, 1H, H_b), 2.81 – 2.72 (m, 1H, $H_{a'}$), 2.62 – 2.54 (m, 1H, $H_{a''}$), 2.06 – 1.92 (m, 4H, $H_{k,n}$), 1.62 – 1.51 (m, 2H, H_e), 1.36 – 1.21 (m, 22H, H_{f-j}, H_{o-t}), 0.86 (t, *J* = 6.7 Hz, 3H, H_u).

^{13}C NMR (101 MHz, $CDCl_3$) δ 129.95 ($C_{L,M}$), 71.79 (C_D), 71.55 (C_C), 50.96 (C_B), 44.37 (C_A), 32.01 (C_S), 29.86 ($C_{J,O}$), 29.80 (C_E), 29.67 – 29.34 ($C_{G,H,I,P,Q,R}$), 27.29 ($C_{K,N}$), 26.18 (C_F), 22.78 (C_T), 14.19 (C_U).

Polymerization Procedures

Synthesis of mPEG-*b*-POlGE block copolymers

The following procedure outlines the synthesis of block copolymers using monomethyl poly(ethylene glycol) (mPEG) initiators with molecular weights of 2000 and 5000 g/mol. The specific example described here is the synthesis of $mPEG_{114}$-*b*-$POlGE_{9.9}$.

In a flame-dried Schlenk flask equipped with a rubber septum and a neodymium magnetic stirring bar, mPEG (5000 g/mol, 650 mg, 0.13 mmol, 1 eq.) and KO^{t}Bu (13.1 mg, 0.117 mmol, 0.9 eq.) were dissolved in 8 mL of benzene, along with dry [18]crown-6 (61.9 mg, 0.234 mmol, 1.8 eq., 2 eq. towards KO^{t}Bu). The mixture was then heated at 60 °C under reduced pressure for approximately one hour. The solvent was then removed under high vacuum at room temperature. Once most of the solvent evaporated, the temperature was maintained at 60 °C overnight, forming the dried initiator salt.

The monomer (OlGE) was dried by azeotropic distillation using benzene. OlGE was mixed with 8 mL of benzene in a flame-dried Schlenk flask. The mixture was subsequently frozen with liquid nitrogen, and the solvent was removed under reduced pressure at room temperature overnight. The monomer was then heated to 60 °C under a high vacuum for 1 h to remove any residual benzene.

Next, OlGE (0.60 mL, 506 mg, 12 eq.) was added to the initiator salt at 80 °C and stirred overnight to initiate polymerization in bulk. The reaction was terminated by adding a mixture of 1 M hydrochloric acid (0.117 mmol, 0.9 eq., 1 eq. to KO^{t}Bu), and 1 mL of MeOH, followed by stirring for a few minutes. The polymer was then suspended in *n*-pentane at room temperature and frozen overnight. The resulting mixture was centrifuged, decanted, and suspended in fresh *n*-pentane, and the procedure was repeated. Subsequently, the polymer was dialyzed against MeOH using a dialysis tube with a molecular weight cut-off (MWCO) of 2000 g/mol to remove any potentially unreacted monomer as well as crown ether. The dialysis medium was exchanged after approximately 3 and 18 h. The workup procedures for the different polymers were varied and are summarized in Table S1. Polymers that were dissolved in solvents at or above room temperature did not precipitate sufficiently and needed to be deep-frozen.

Table S1: mPEG-*b*-POlGE block copolymers and their respective workup.

Polymer	Precipitation medium	MWCO dialysis tube
mPEG$_{45}$-*b*-POlGE$_{2.4}$	MeOH (RT), then freezer	1000 g/mol
mPEG$_{45}$-*b*-POlGE$_{5.0}$	MeOH (50 °C), then freezer	1000 g/mol
mPEG$_{45}$-*b*-POlGE$_{7.5}$	MeOH (50 °C), then freezer	1000 g/mol
mPEG$_{45}$-*b*-POlGE$_{11.3}$	*Dialysis against THF	1000 g/mol
mPEG$_{114}$-*b*-POlGE$_{2.9}$	*n*-Pentane (-18 °C)	2000 g/mol
mPEG$_{114}$-*b*-POlGE$_{5.8}$	*n*-Pentane (-18 °C)	2000 g/mol
mPEG$_{114}$-*b*-POlGE$_{7.3}$	*n*-Pentane (RT), then freezer	2000 g/mol
mPEG$_{114}$-*b*-POlGE$_{9.9}$	*n*-Pentane (RT), then freezer	2000 g/mol

After dialysis, the solvent was removed and the final product was dried under a high vacuum at 60 °C overnight, yielding 508 mg, which corresponded to a yield of 44%.

Synthesis of statistical P(EG-*co*-OlGE) copolymers

The synthesis of statistical copolymers using 2-(benzyloxy)ethanol as the initiator, with P(EG_{123}-*co*-$OlGE_7$) as a specific example, was conducted as follows. Please note that the procedure describes the use of ethylene oxide, a toxic and flammable gas which should be treated with caution.

In a flame-dried custom-made anionic flask equipped with a Teflon stopcock, rubber septum, and magnetic stirrer, $CsOH{\cdot}H_2O$ (24.8 mg, 0.148 mmol, 0.9 eq.) and 2-(benzyloxy)ethanol (25 mg, 0.164 mmol, 1 eq.) were dissolved in 8 mL of benzene. The mixture was heated at 60 °C under static vacuum for 1 h. Subsequently, the solvent was removed under vacuum and the residue was further heated at 60 °C overnight to obtain the dried initiator salt.

The monomer (OlGE) was dried by azeotropic distillation using benzene. OlGE was mixed with 8 mL of benzene in a flame-dried Schlenk flask. The mixture was then frozen with liquid nitrogen, and the solvent was removed under reduced pressure at room temperature overnight. The monomer was further heated to 60 °C under high vacuum for 1 h to remove any residual benzene.

Next, the initiator salt was dissolved in 0.83 mL of DMSO (dried over molecular sieves) and dry THF (4.17 mL) was condensed into a glass ampule using an ethanol/liquid nitrogen cooling bath. The condensed THF was then cryo-transferred to the anionic flask. The solvents were then mixed at room temperature and frozen in the cooling bath. Following this, OlGE (320 mg, 0.38 mL, 0.986 mmol, 6 eq.) was then added using a syringe. Ethylene oxide (EO) (0.83 mL at 80 °C, 18.73 mmol, 114 eq.) was condensed into a glass ampule and cryo-transferred to the anionic flask with the cooling bath. The resulting mixture was stirred at 40 °C for at least 72 h to ensure complete EO consumption during copolymerization.

After polymerization, the reaction was terminated by adding a mixture of 1 M hydrochloric acid (0.148 mmol, 0.9 eq., 1 eq. to $CsOH{\cdot}H_2O$) and 1 mL of MeOH. The solvents were roughly removed by a strong nitrogen flow through the anionic flask. The raw product was then dissolved in DCM and extracted thrice with water to remove DMSO. The resulting polymer was dialyzed against MeOH using a membrane with a molecular weight cut-off (MWCO) of 1000 g/mol, with the dialysis medium being exchanged after 3 and 18 h. The solvents were removed, and the polymer was dried at 60 °C under high vacuum, resulting in a yield of 883 mg, which corresponds to 77% yield.

Synthesis of POlGE homopolymers

The following procedure describes the synthesis of POlGE homopolymers using 2-(benzyloxy)ethanol as the initiator and $POlGE_{25}$ as an illustrative example.

In a flame-dried Schlenk flask equipped with a rubber septum and a neodymium magnetic stirring bar, 2-(benzyloxy)ethanol (15 mg, 98.6 µmol, 1 eq.) and KO^{t}Bu (10 mg, 88.7 µmol, 0.9 eq.) together with [18]crown-6 (46.9 mg, 0.177 mmol, 1.8 eq., 2 eq. to KO^{t}Bu) were dissolved in benzene (8 mL). The mixture was heated at 60 °C under static vacuum. After one hour, the solvents were removed *in vacuo* to yield the dried initiator salt. Azeotropic distillation with benzene was used to dry the OlGE monomer. First, a Schlenk flask equipped with a magnetic stirrer was heated in flame. Subsequently, more OlGE than required for the batch was mixed with benzene (8 mL). The benzene was subsequently removed under vacuum overnight, resulting in dried OlGE. OlGE (0.94 mL, 800 mg, 2.46 mmol) was transferred to the initiator salt at 80 °C under an Ar counterflow using a syringe. The polymerization was allowed to proceed for 18 h. Then, the polymerization was terminated using a mixture of 1 M hydrochloric acid (88.7 µmol, 1 eq. to KO^{t}Bu) and 1 mL MeOH. The mixture was dissolved in a small amount of DCM and precipitated using ice-cold MeOH. After centrifugation for at least 45 min, the solvent was decanted, and the procedure was repeated twice. Heating of the polymer at 60 °C yielded 650 mg, corresponding to 80% yield.

In situ ^{1}H NMR kinetical investigation of statistical copolymerization of EO and OlGE

A *Norell S-500-VT-7* sealable NMR tube with a Teflon stopcock was used to determine the reactivity ratios of EO and OlGE. The setup was similar to that described by Frey *et al.* described.[4] Preparation of the initiator salt (cesium 2-(benzyloxy)ethanolate) was done in a five-fold batch as described on page 8 The initiator salt was dissolved in the respective amount of DMSO-d_6, yielding an initiator stock solution. EO was condensed into the oven-dried NMR tube under static vacuum employing an acetone/nitrogen cooling bath. Next, THF-d_8 (which had been dried over CaH_2), dry OlGE, and one-fifth of the initiator stock solution were added while cooling under Ar counterflow. The mixture underwent three freeze-pump-thaw cycles to remove any remaining gas and was then cooled with liquid nitrogen before being inserted into the preheated NMR spectrometer at 40 °C. Sample spinning was turned off, and a spectrum was recorded before measuring the receiver gain. Online kinetic was conducted at 40 °C for 55 hours, with one scan every two minutes. Following the kinetic study, the copolymer underwent SEC analysis.

The distinctive chemical shift of the OlGE and EO epoxide functionality was observed to track the consumption of each respective monomer. The software *NIREVAL*, created by Frey *et al.*,[5] was utilized to analyze the normalized monomer consumption.

Post-polymerization procedures

Thiol-Ene Click

To modify the polymer $mPEG_{114}$-*b*-$POlGE_{2.9}$, the following steps were carried out. Firstly, 50 mg (8.33 µmol, 1 eq.) of the polymer was dissolved in DCM (0.3 mL) along with the photoinitiator 2,2-dimethoxy-2-phenylacetophenone (DMPA, 12.8 mg, 50 µmol, 6 eq.) in a 10 mL Schlenk tube with a magnetic stirring bar and rubber septum. Then, thioglycol (78.1 mg, 1 mmol, 120 eq., 40 eq. per double bond) was added to the mixture, and an additional 0.3 mL DCM was flushed into the tube. The mixture was subjected to three freeze-pump-thaw cycles and was then irradiated overnight under continuous stirring using a UV lamp with a wavelength of 254 nm at a 5 cm distance. Next, the mixture was diluted with DCM (10 mL) and extracted three times against water (15 mL) to remove any unreacted thioglycol. The organic phase was dialyzed (MWCO 2000 g/mol) against MeOH (1 L, solvent changed thrice). After the solvent was evaporated, and the polymer was exposed to high vacuum at 60 °C, the modified polymer (42 mg) was obtained in 84% yield.

Hydrogenation

For post-polymerization hydrogenation, the *in situ*-formed diimide was utilized. It was generated by the acidic decomposition of potassium azodicarboxylate (PADA):

Synthesis of potassium azodicarboxylate (PADA)

The described procedure was inspired by Ma and Groves.[6]

To synthesize PADA, 30 mL of a 40% aqueous potassium hydroxide solution was added to a 50 mL round-bottom flask with a magnetic stirrer. The flask was then placed into a water bath at 6 °C. Azodicarboxylate (4.84 g, 41.7 mmol) was added slowly over 2 hours. Afterward, the precipitate was filtered using a glass frit with filter paper and washed 20 times with ice-cold methanol. Finally, the product was dried in a desiccator for 1.5 days under vacuum, resulting in an intense yellow powder with a yield of 7.18 g, 37.0 mmol, or 89%.

Hydrogenation as post-polymerization modification

The utilization of PADA for generating diimide is a distinctive approach. In our study, we adjusted the synthesis methods previously reported by Groves and Ma,[6] as well as Snyder and Hamersma.[7] We also applied the method towards a similar system.[8]

Please note, that the *in situ* diimide generation may produce toxic hydrazine as a byproduct.

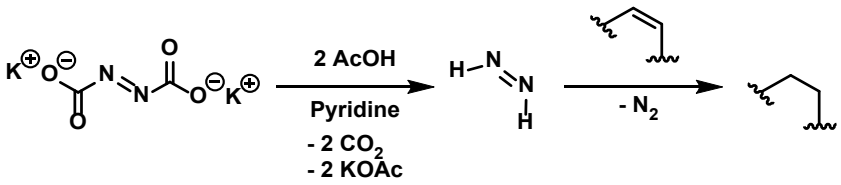

Scheme S1: Diimide generation of PADA by acidic decomposition, followed by polymer hydrogenation. Coupling products include gaseous carbon dioxide, nitrogen, and water-soluble potassium acetate.

Hydrogenation was subjected to the homopolymer $POlGE_{25}$ to achieve different degrees of hydrogenation. The procedure described here for the synthesis of $POlGE_{25}$ (H95%) (degree of hydrogenation 95%) was as follows: $POlGE_{25}$ (50 mg, 6.02 µmol, 1 eq.) was transferred into a flame-dried Schlenk tube equipped with a magnetic stirrer and a rubber septum using toluene. The solvent was removed *in vacuo* resulting in the azeotropically dried educt. The polymer was dissolved in 2.4 mL of pyridine, which had been previously dried over molecular sieves. To this solution, PADA (439 mg, 2.26 mmol, 375 eq., 15 eq. to the double bonds) was added. Additionally, 0.27 mL of glacial acetic acid, previously dried over P_4O_{10}, was mixed with 0.6 mL of dry pyridine. This acetic acid-pyridine mixture was then slowly added to the stirred polymer solution over 14 hours using a syringe pump, with the dead volume of the tube considered for precise proportion. After the complete addition, the mixture was further stirred for at least 2 hours until the colorless precipitate dissolved in water. The aqueous phase was then subjected to two extractions with chloroform (10 mL each), while the organic phase underwent three extractions with water (10 mL each) to remove any remaining salts. Next, the solvent was removed, and the resulting hydrogenated polymer was dried under high vacuum at 60 °C overnight to obtain the final product (47 mg) in 94% yield. To reach a hydrogenation level of 76% in $POlGE_{25}$ (H76%), three equivalents of PADA were needed per double bond. On the other hand, to achieve a hydrogenation level of 53% in $POlGE_{25}$ (H53%), 1.25 equivalents of PADA were required per double bond.

NMR Spectra of OlGE

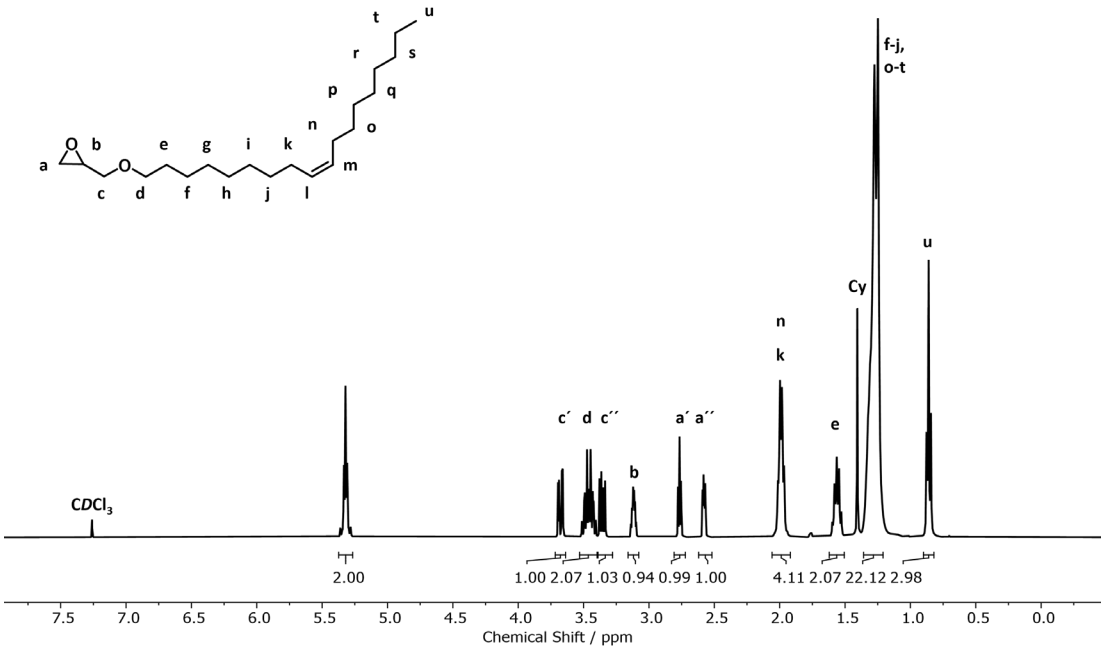

Figure S1: ^{1}H NMR of oleyl glycidyl ether (OlGE) ($CDCl_3$, 400 MHz).

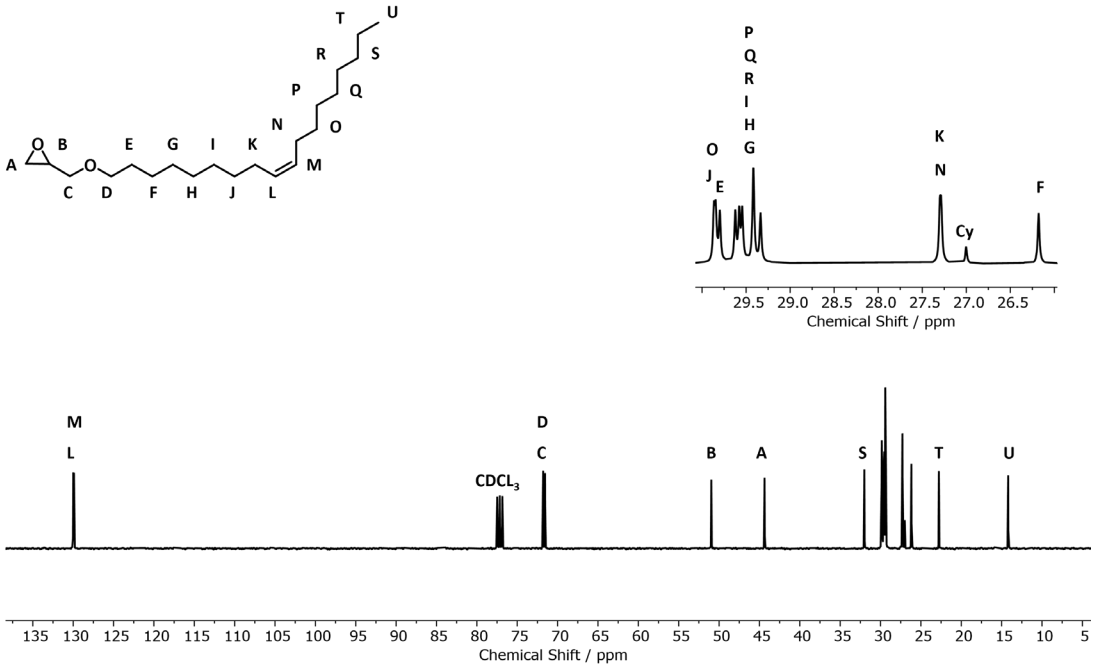

Figure S2: ^{13}C NMR of oleyl glycidyl ether (OlGE) (101 MHz, $CDCl_3$).

Characterization of Block copolymers of OlGE and EO

OlGE repeating units could not be calculated by integration of the initiator methoxy group due to the shift of the backbone into the highfield after copolymerization. Instead, the following equation was used to determine the OlGE repeating units (*n*(OlGE)) from the integral of the mPEG precursor and the integral of the synthesized polymer.

$$n(\mathrm{OlGE}) = \frac{I(\mathrm{mPEG})}{I(\mathrm{Backbone}) - 7} \tag{S2}$$

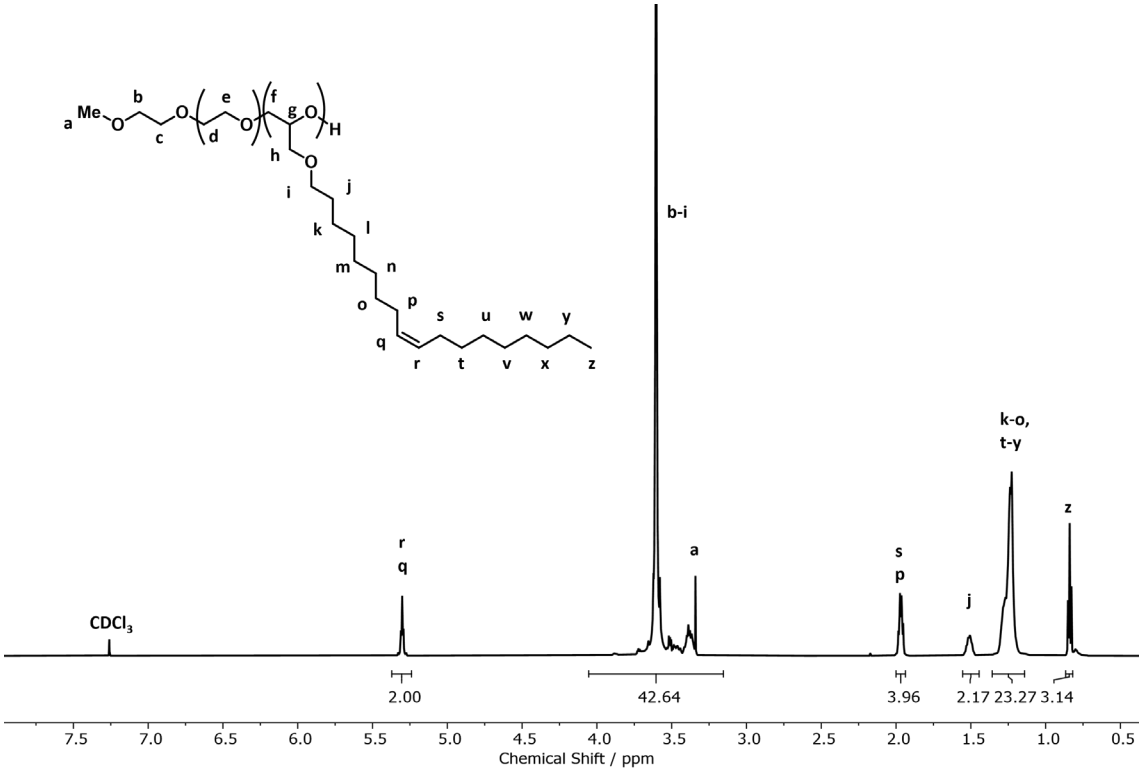

Figure S3: ^{1}H NMR of mPEG-*b*-POlGE (600 MHz, $CDCl_3$, 21 °C).

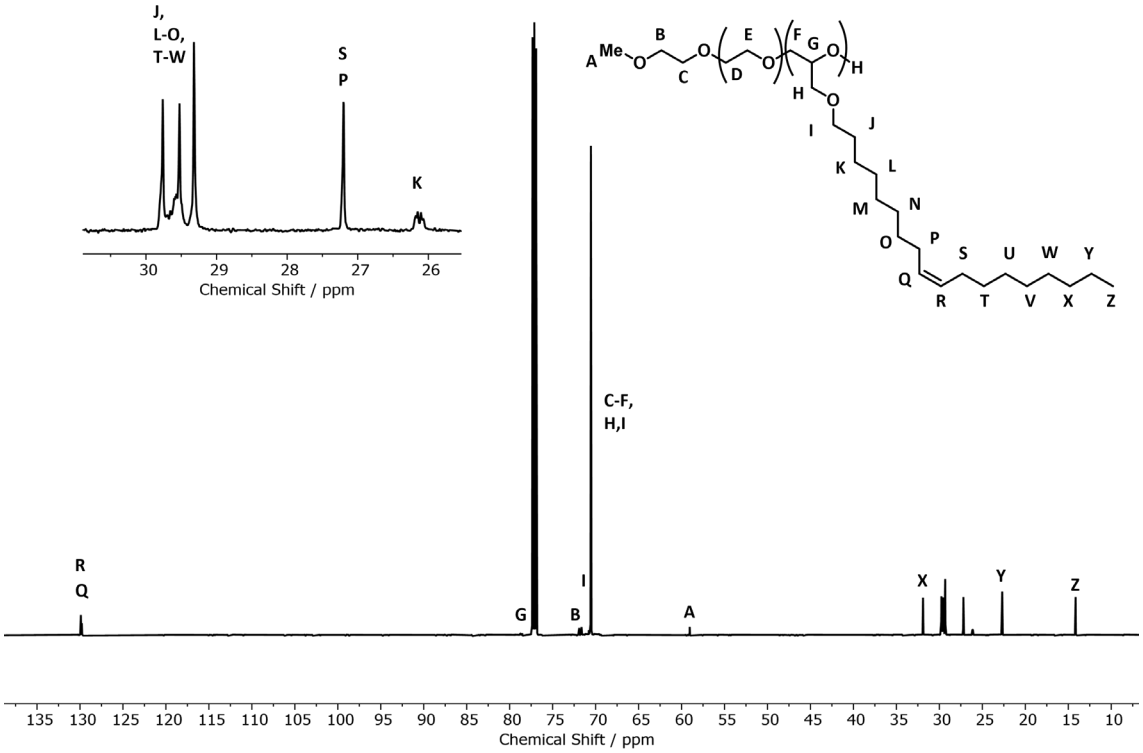

Figure S4: ^{13}C NMR of mPEG-*b*-POlGE (151 MHz, $CDCl_3$, 21 °C).

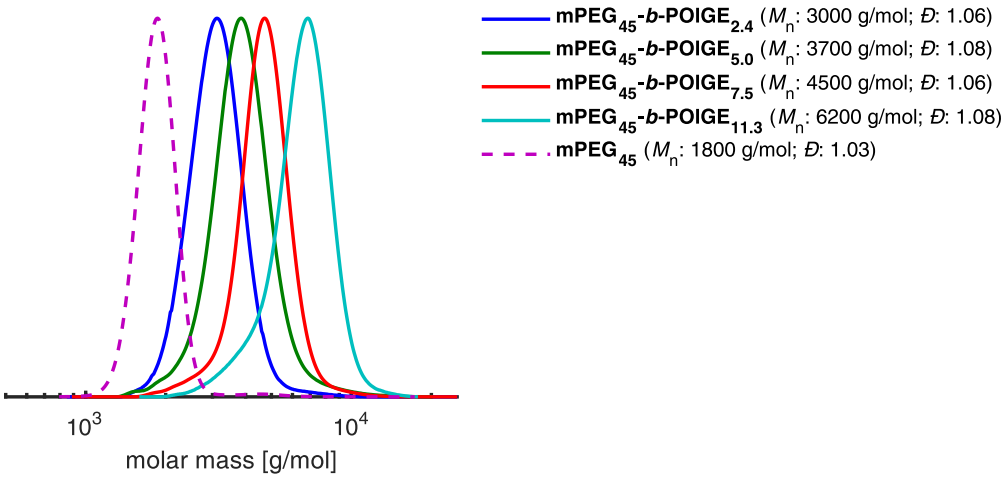

Figure S5: SEC traces of $mPEG_{45}$-*b*-POlGE (RI detector, eluent: THF, PEG calibration).

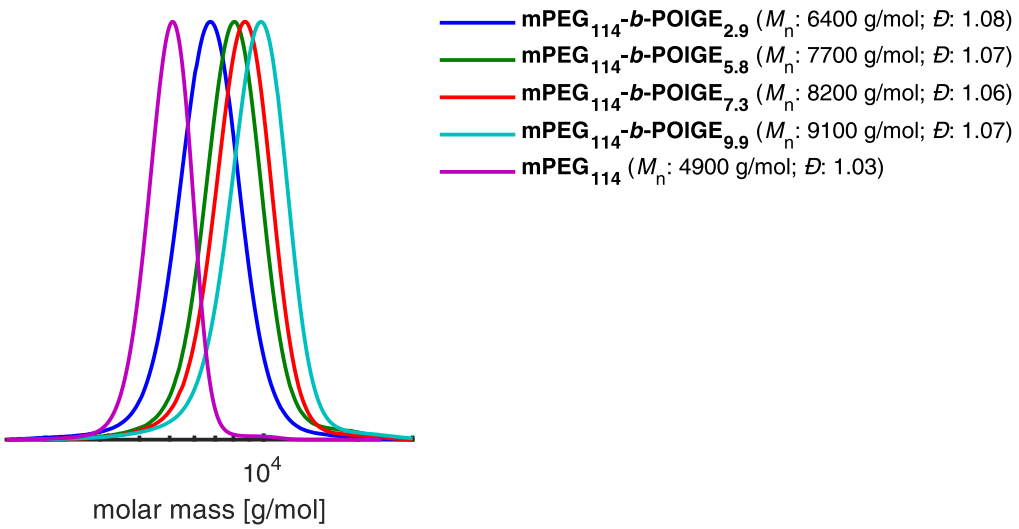

Figure S6: SEC traces of mPEG$_{114}$-*b*-POlGE (RI detector, eluent: THF, PEG calibration).

Characterization of statistical copolymers of OlGE and EO

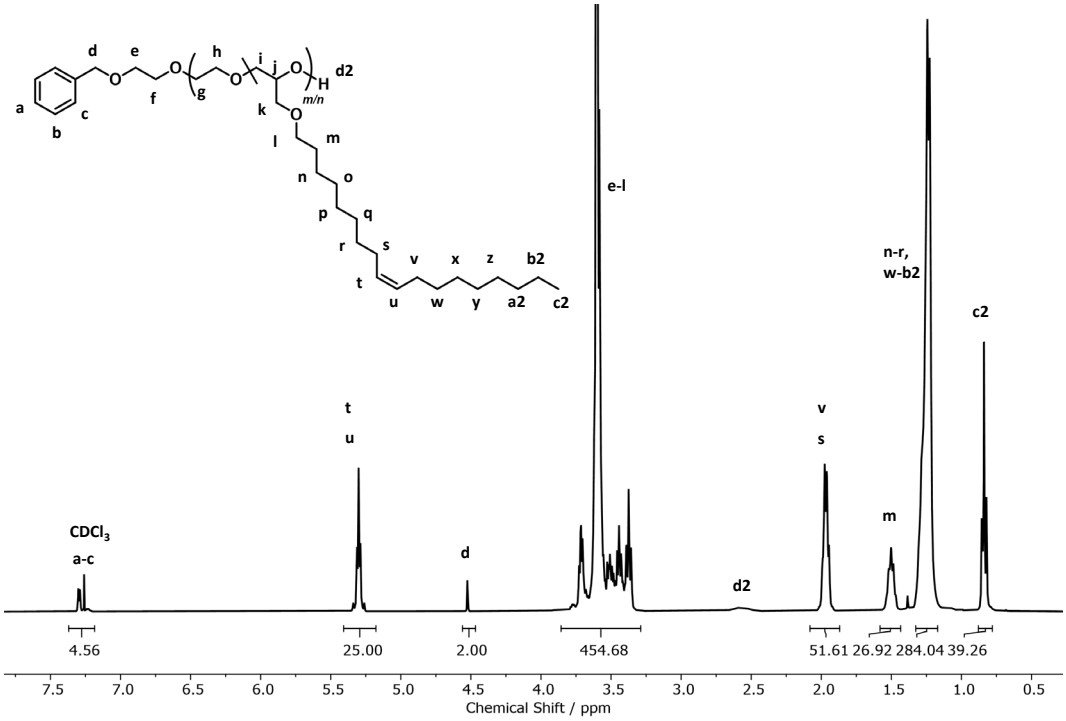

Figure S7: ^{1}H NMR of a statistical P(EG-*co*-OlGE) copolymer (400 MHz, $CDCl_3$).

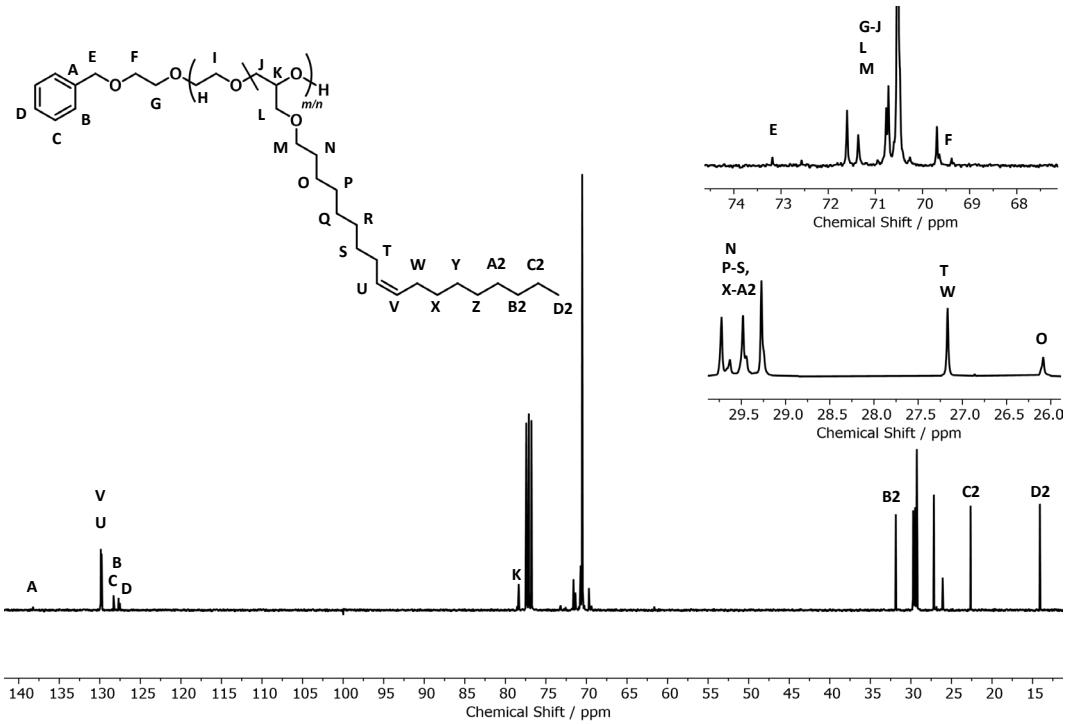

Figure S8: ^{13}C NMR of a statistical P(EG-*co*-OlGE) copolymer (101 MHz, $CDCl_3$).

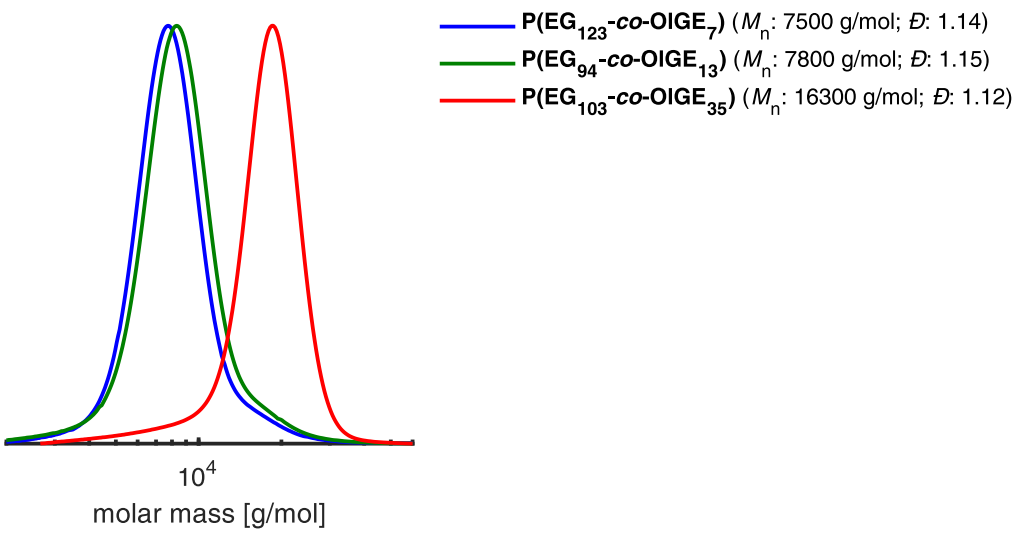

Figure S9: SEC traces of statistical P(EG-*co*-OlGE) copolymers (RI detector, eluent: THF, PEG calibration).

Characterization of Homopolymers of OlGE

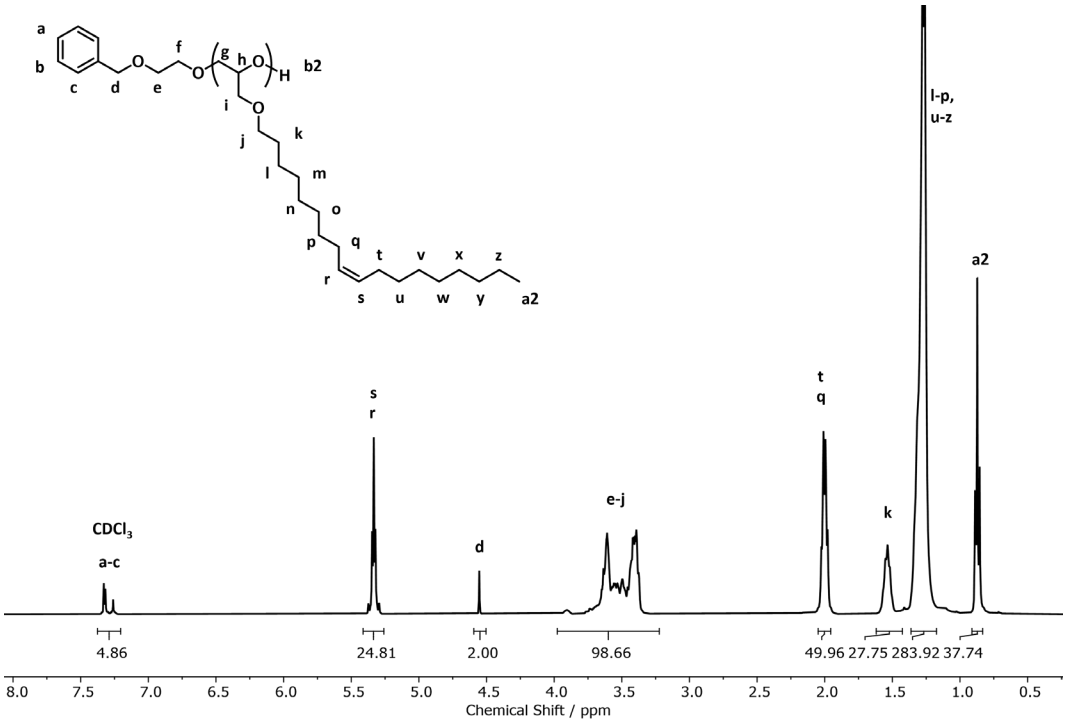

Figure S10: ^{1}H NMR of a POlGE homopolymer (400 MHz, $CDCl_3$).

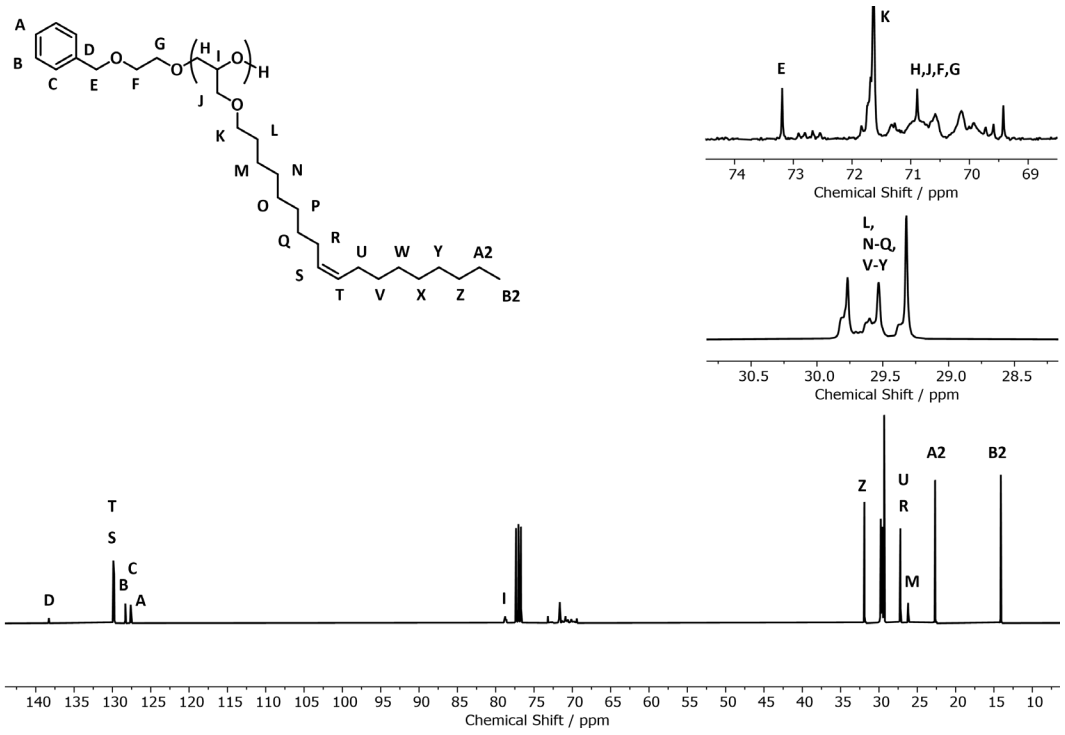

Figure S11: ^{13}C NMR of a POlGE homopolymer (101 MHz, $CDCl_3$).

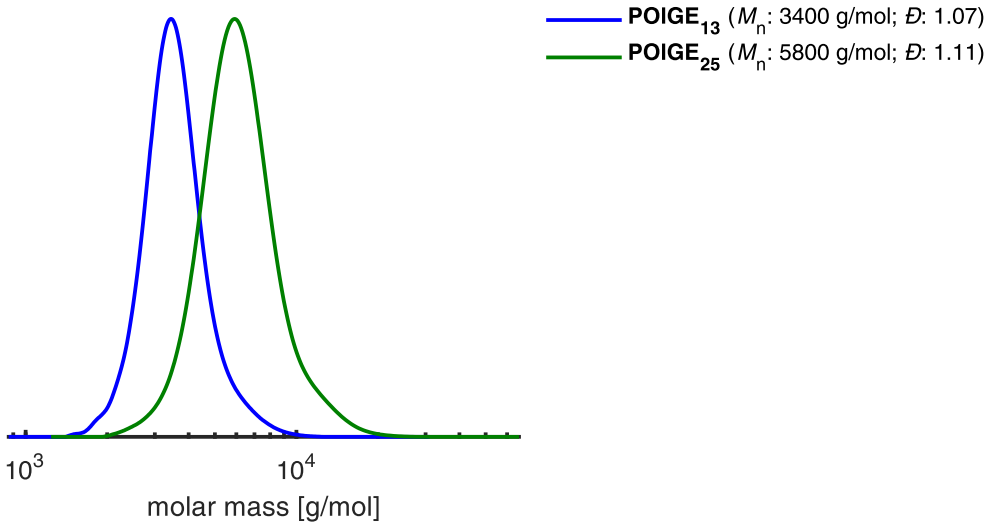

Figure S12: SEC traces of POlGE homopolymers (RI detector, eluent: THF, PEG calibration).

Thermal Characterizations of Polymers

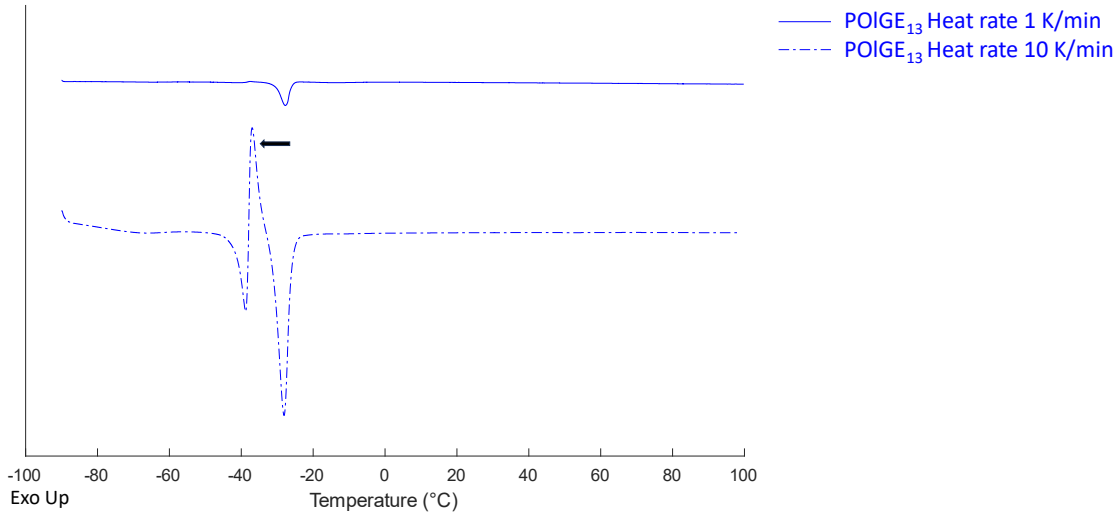

Figure S13: DSC thermograms of POlGE homopolymer measured at different heat and cool rates. Second heating curve. Black arrow marks a strong recrystallization peak at a heat rate of 10 K/min.

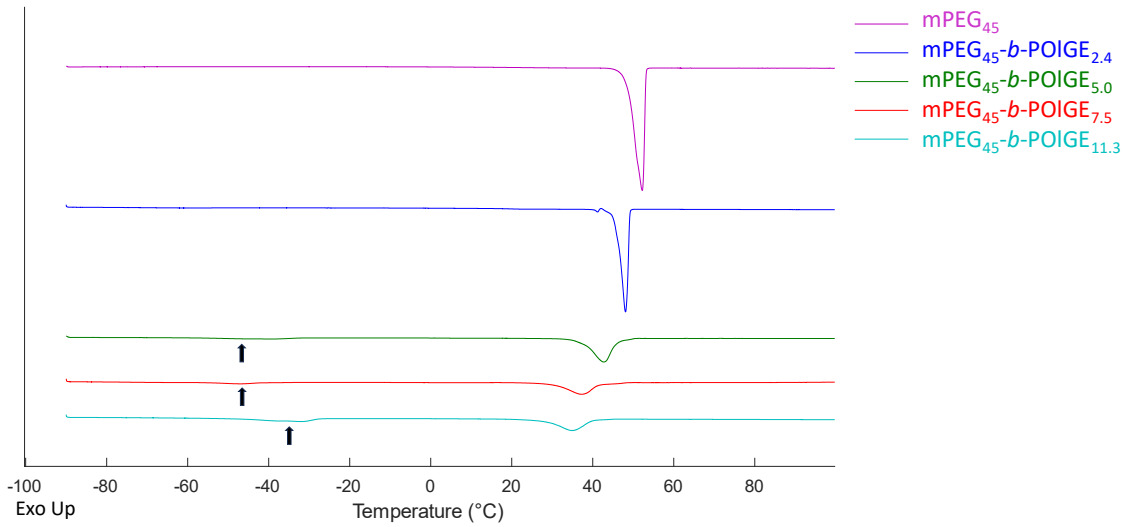

Figure S14: DSC thermograms of $mPEG_{45}$-based OlGE block copolymers and the precursor. Second heating curve, 1 K/min. Melting areas which are only visible in strong zoom are marked by black arrows.

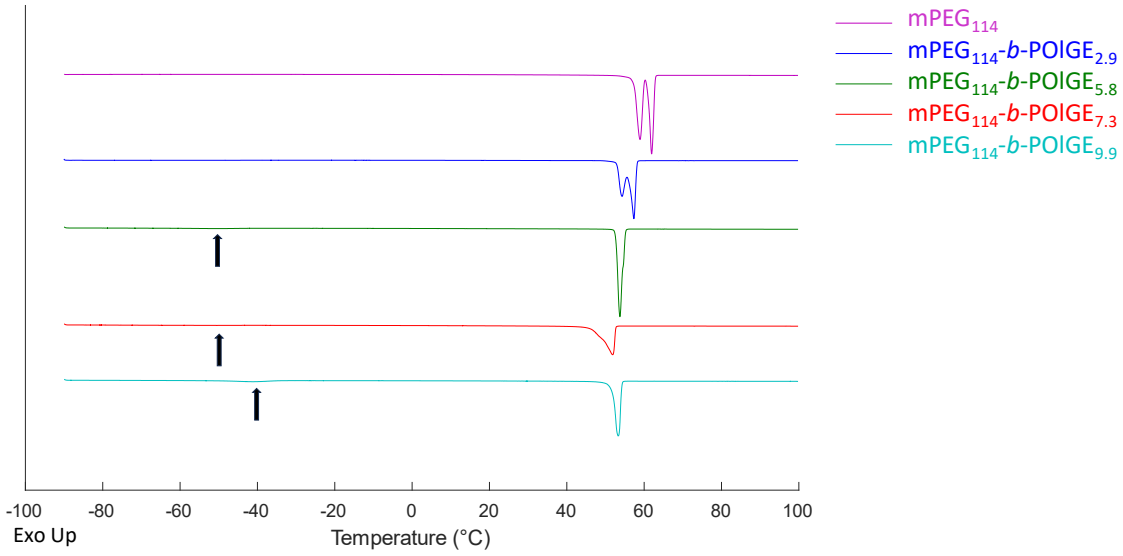

Figure S15: DSC thermograms of $mPEG_{114}$-based OlGE block copolymers and the precursor. Second heating curve, 1 K/min. Melting areas which are only visible in strong zoom are marked by black arrows.

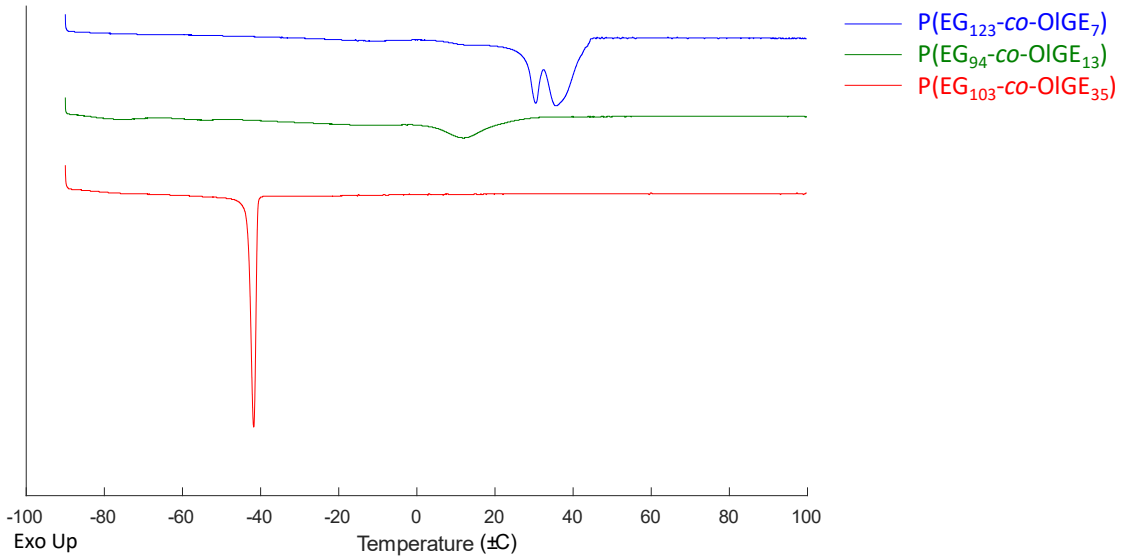

Figure S16: DSC thermograms of statistical EO/OlGE copolymers. Second heating curve, 1 K/min.

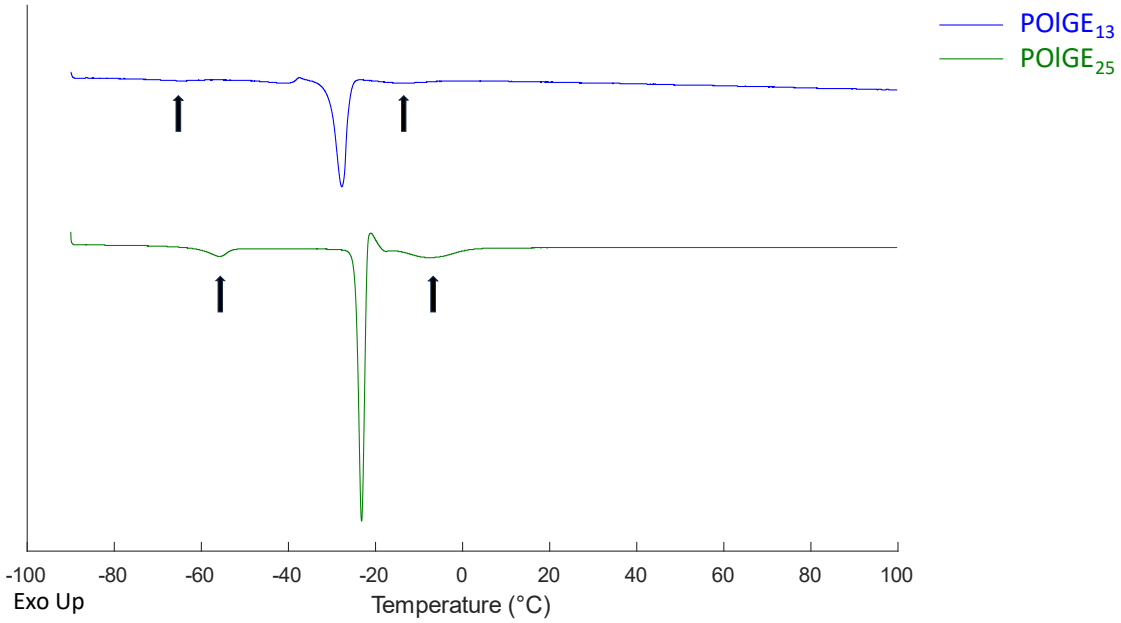

Figure S17: DSC thermograms of POlGE homopolymers. Second heating curve, 1 K/min. Melting areas which are only visible in strong zoom are marked by black arrows.

CMC determination by fluorescence spectroscopy

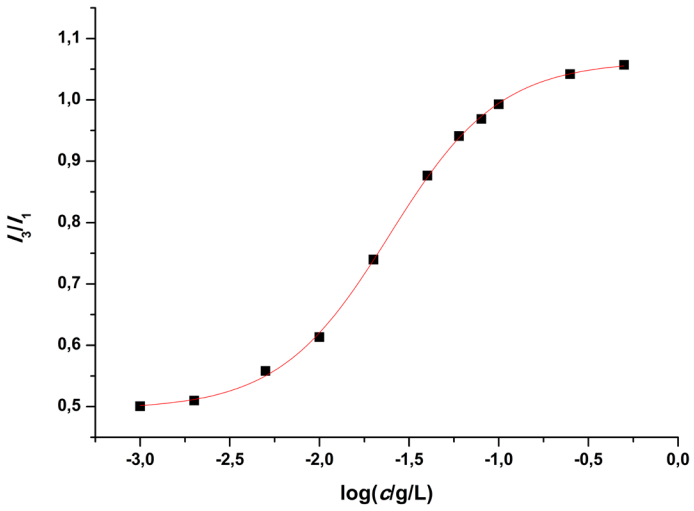

Figure S18: CMC determination of P(EG_{123}-*co*-$OlGE_7$) by fluorescence spectroscopy with pyrene as a probe. Black squares: data point, red line: fitting curve.

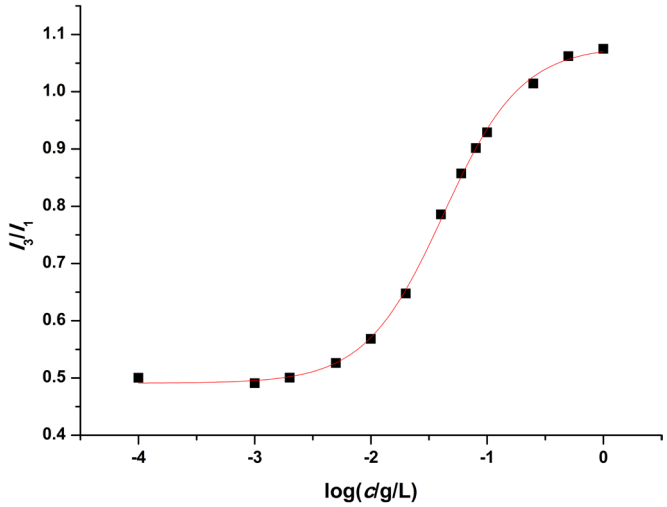

Figure S19: CMC determination of mPEG$_{45}$-*b*-POlGE$_{2.4}$ by fluorescence spectroscopy with pyrene as a probe. Black squares: data point, red line: fitting curve.

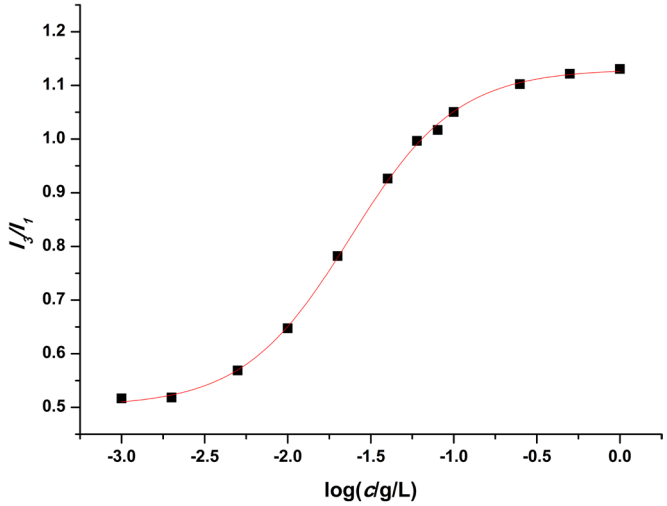

Figure S20: CMC determination of mPEG$_{45}$-*b*-POlGE$_{5.0}$ by fluorescence spectroscopy with pyrene as a probe. Black squares: data point, red line: fitting curve.

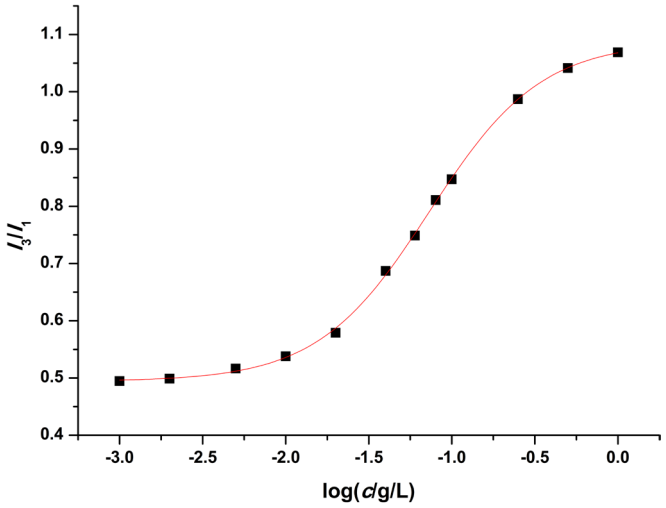

Figure S21: CMC determination of mPEG$_{114}$-*b*-POlGE$_{2.9}$ by fluorescence spectroscopy with pyrene as a probe. Black squares: data point, red line: fitting curve.

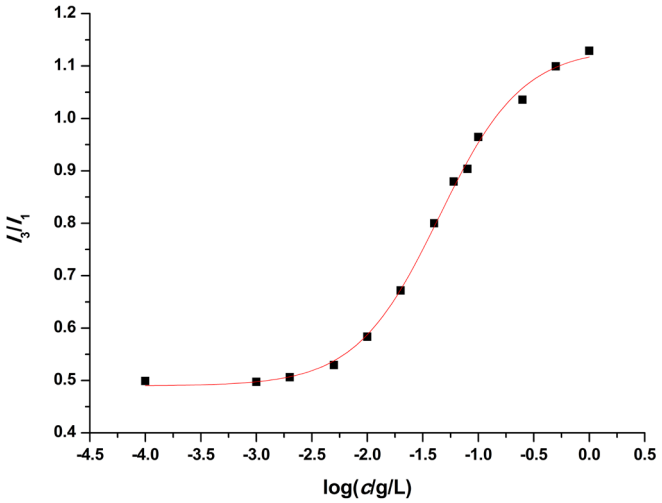

Figure S22: CMC determination of mPEG$_{114}$-*b*-POlGE$_{5.8}$ by fluorescence spectroscopy with pyrene as a probe. Black squares: data point, red line: fitting curve.

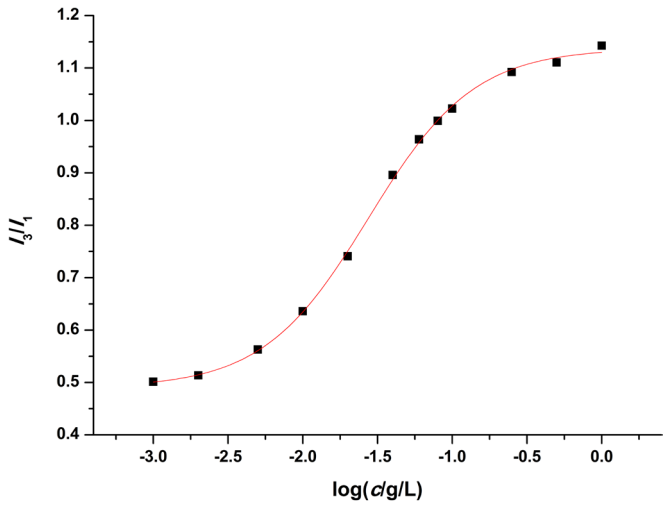

Figure S23: CMC determination of mPEG$_{114}$-*b*-POlGE$_{7.3}$ by fluorescence spectroscopy with pyrene as a probe. Black squares: data point, red line: fitting curve.

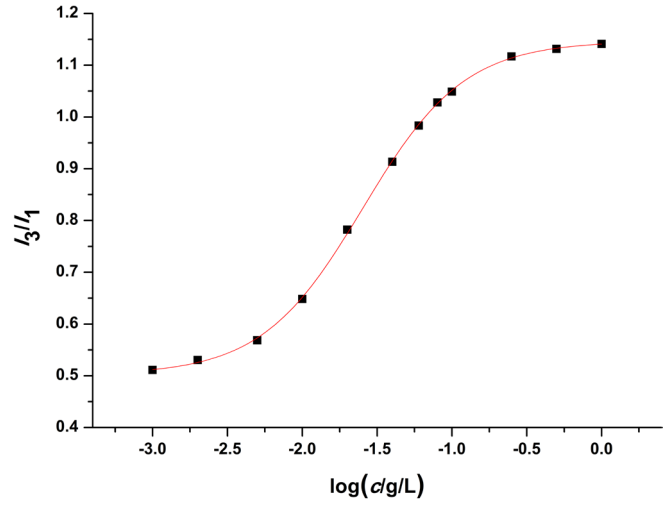

Figure S24: CMC determination of mPEG$_{114}$-*b*-POlGE$_{9.9}$ by fluorescence spectroscopy with pyrene as a probe. Black squares: data point, red line: fitting curve.

Transmission Electron Microscopy

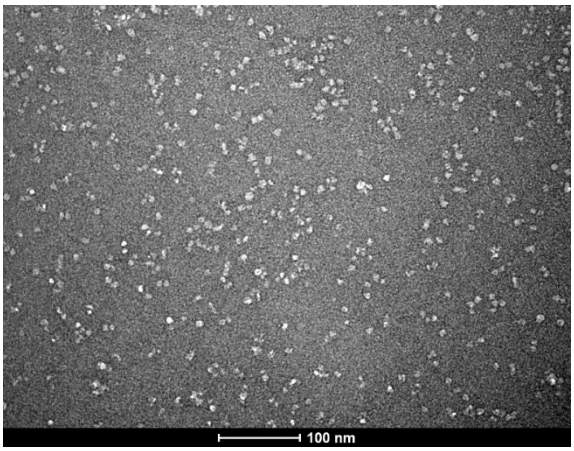

Figure S25: TEM micrograph of statistical P(EG_{123}-*co*-$OlGE_7$) copolymer in aqueous solution (0.1 g/L). Samples were treated with 2% uranyl acetate solution as negative stain.

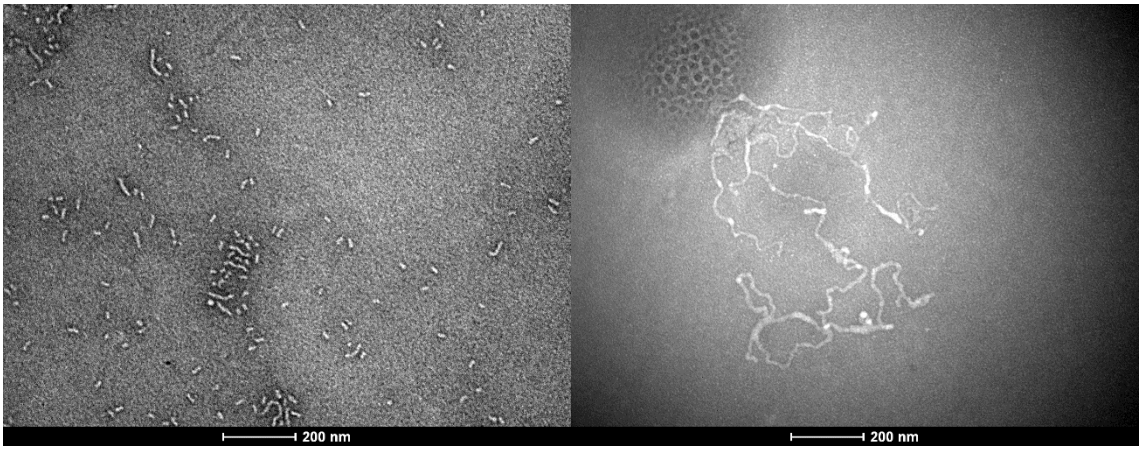

Figure S26: TEM micrograph of mPEG_{45}-*b*-$POlGE_n$ block copolymers in aqueous solution (0.1 g/L). Left: n=2.4, right: n=5.0. The circular structure in the upper left corner is caused by irradiation damage. Samples were treated with 2% uranyl acetate solution as negative stain.

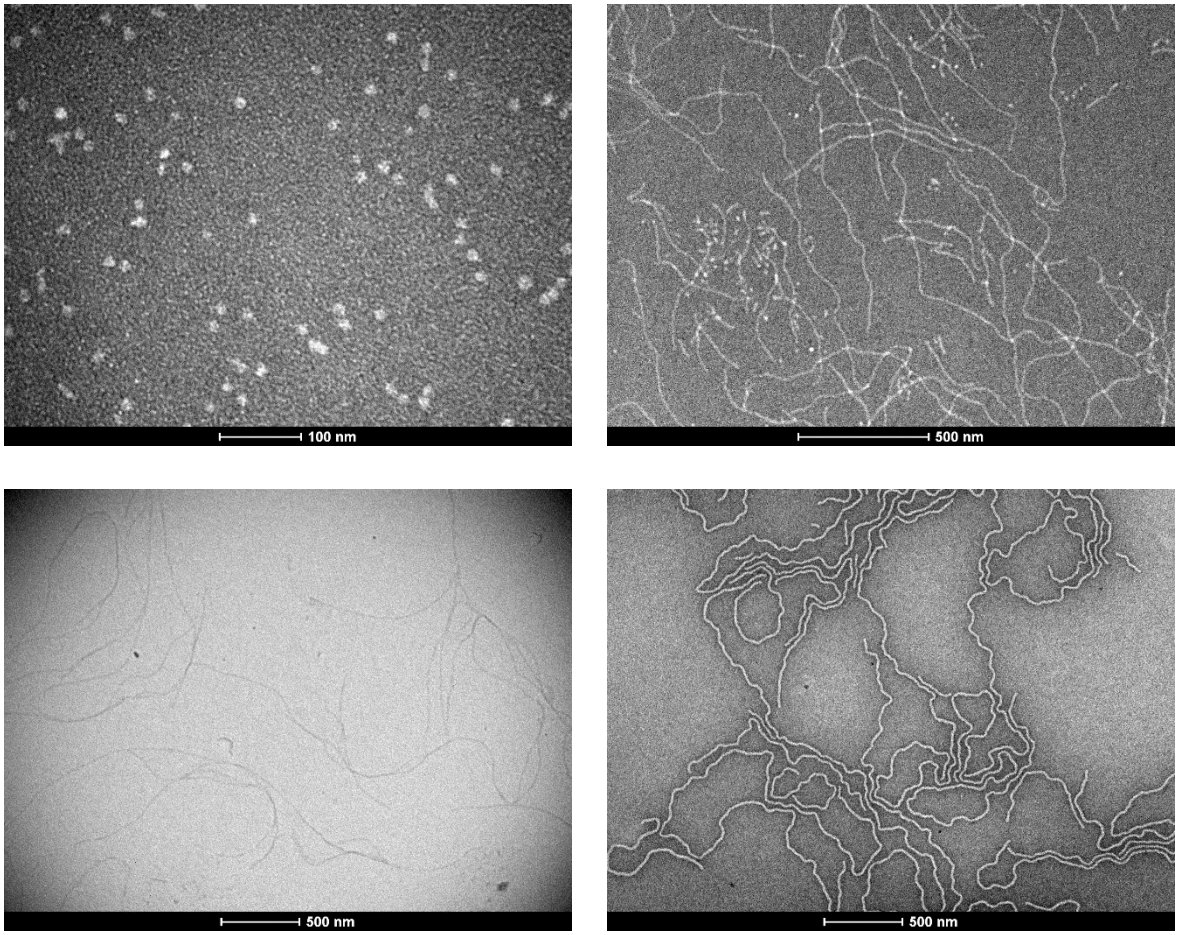

Figure S27: TEM micrograph of mPEG$_{114}$-*b*-POlGE$_n$ block copolymers in aqueous solution (0.1 g/L). Top left: *n*=2.9, top right: *n*=5.8. Bottom left: *n*=7.3, bottom right: *n*=9.9. Samples were treated with 2% uranyl acetate solution as negative stain.

Dynamic Light Scattering

Cylindrical quartz glass cuvettes were thoroughly cleaned with hot acetone before usage to ensure they were free of any dust particles. Temperature control was maintained using a *Huber Pilot One* thermostat manufactured by *Peter Huber Kältemaschinenbau AG*. The measurements were conducted at a temperature of 25 °C, with a polymer concentration of 0.3 g/L. To eliminate any dust contaminants from the polymer solution, the solutions were filtered through a *Millex*-HV filter (0.45 µm, 13 mm). The filtering process was carried out within a dust-free laminar flow box. The measurements were executed across an angular range from 30° to 150° in 10° increments. The laser was from Thorlabs and had a wavelength of 632.8 nm. The respective scattering vector *q* can be defined using the following equation, considering the refractive index of water n, the scattering angle θ and the wavelength λ:

$$q = \frac{4\pi n}{\lambda}\sin(\theta/2) \tag{S3}$$

The amplitude autocorrelation functions $g^{(1)}(q,\tau)$ were fitted using the following biexponential function:

$$g^{(1)}(q,\tau) = A + B \cdot \exp\left(-\frac{\tau}{\tau_{\mathrm{R},1}}\right) + C \cdot \exp\left(-\frac{\tau}{\tau_{\mathrm{R},2}}\right) \tag{S4}$$

With time τ, baseline A, amplitudes B and C, as well as the characteristic relaxation times of the respective modes τ_R. The diffusion coefficient of each measured angle is received from the relation $D=(\tau_R \cdot q^2)^{-1}$. Graphing D in relation to q^2 yielded z-average D from the coordinate section. Applying the Stokes-Einstein equation gives the hydrodynamic radius R_H:

$$R_{\mathrm{H}} = \frac{k_{\mathrm{B}}T}{6\pi\eta D} \tag{S5}$$

With the Boltzmann constant k_B, absolute temperature T in K, and the dynamic viscosity of water η.

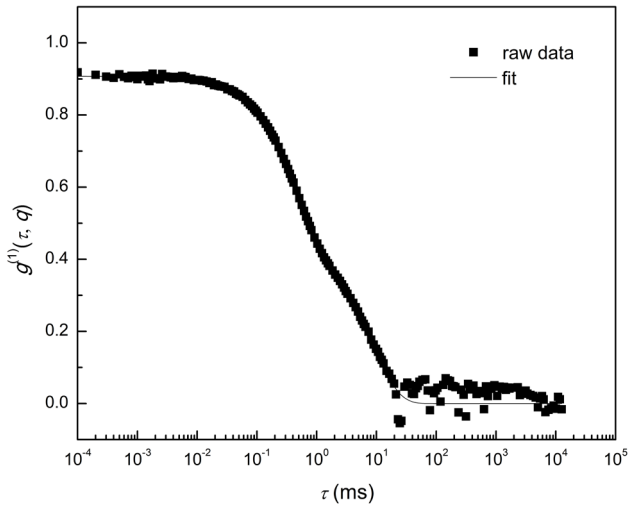

Figure S28: Auto correlation function of P(EG_{123}-*co*-$OlGE_7$) at a scattering angle of 30° plotted against τ.

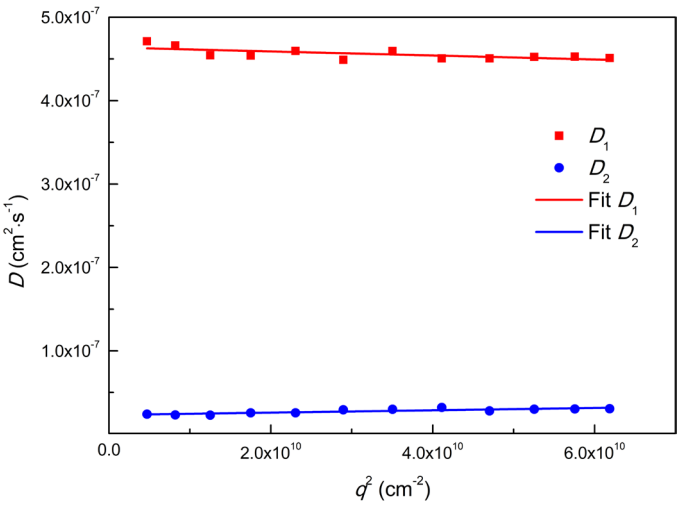

Figure S29: Diffusion coefficient plotted against the square of the scattering vector of the polymer P(EG_{123}-*co*-$OlGE_7$).

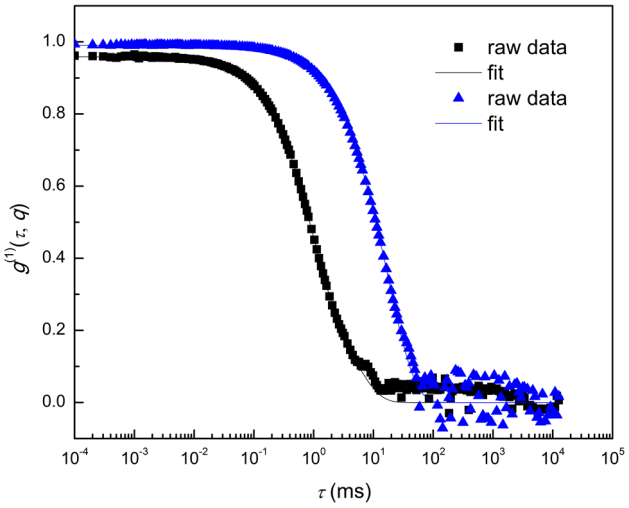

Figure S30: Auto correlation function of mPEG_{45}-*b*-$POlGE_{2.4}$ (black squares) and mPEG_{45}-*b*-$POlGE_{5.0}$ (blue triangles) at a scattering angle of 30° plotted against τ.

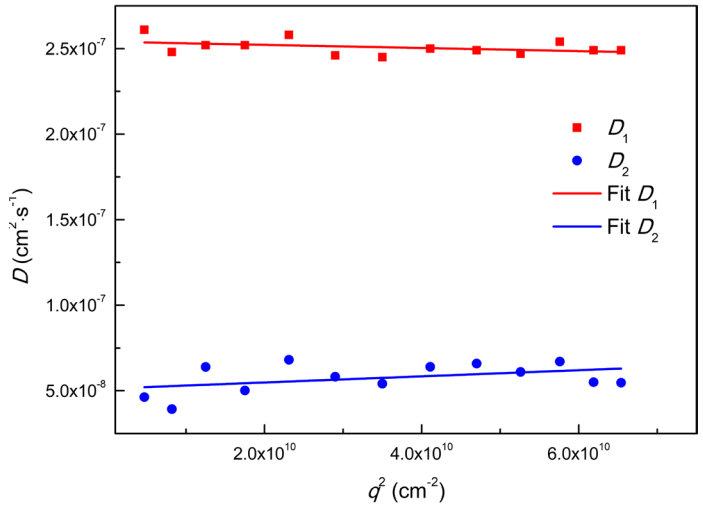

Figure S31: Diffusion coefficient plotted against the square of the scattering vector of the polymer mPEG$_{45}$-*b*-POlGE$_{2.4}$.

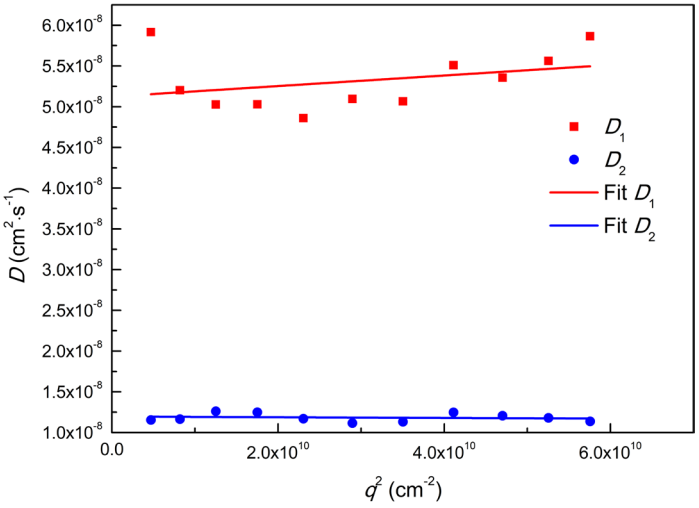

Figure S32: Diffusion coefficient plotted against the square of the scattering vector of the polymer mPEG$_{45}$-*b*-POlGE$_{5.0}$.

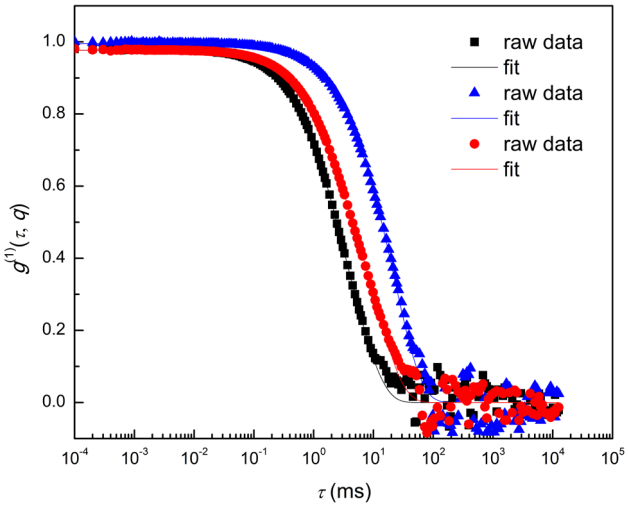

Figure S33: Auto correlation function of mPEG$_{114}$-*b*-POlGE$_{2.9}$ (black squares), mPEG$_{114}$-*b*-POlGE$_{5.8}$ (blue triangles) and mPEG$_{114}$-*b*-POlGE$_{7.3}$ (red circles) at a scattering angle of 30° plotted against *τ*.

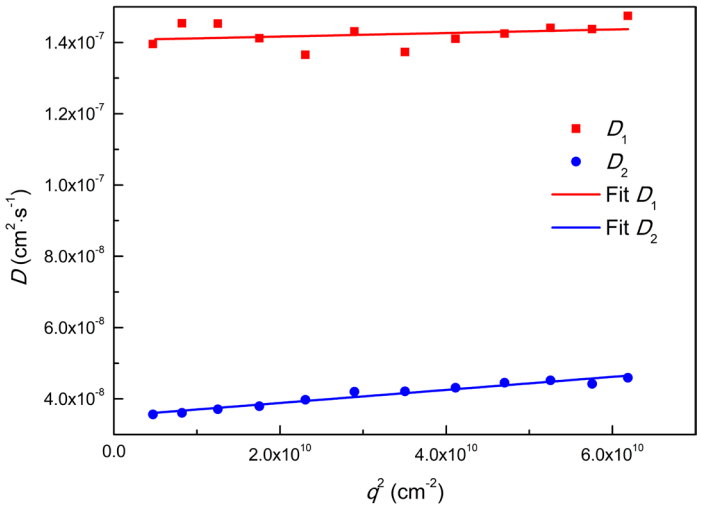

Figure S34: Diffusion coefficient plotted against the square of the scattering vector of the polymer mPEG$_{114}$-*b*-POlGE$_{2.9}$.

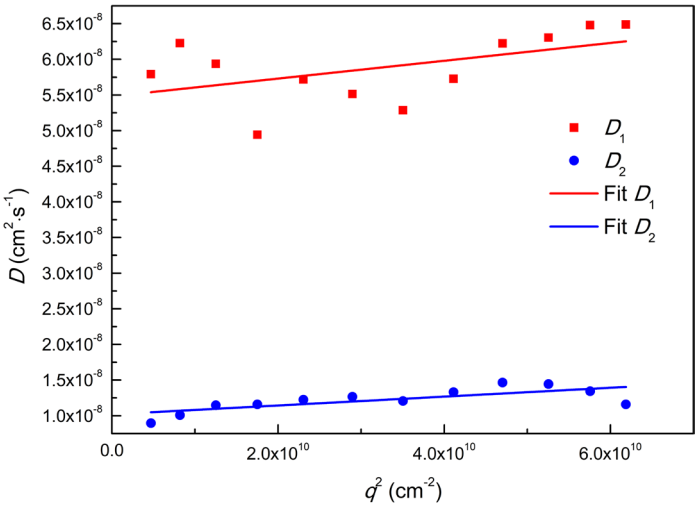

Figure S35: Diffusion coefficient plotted against the square of the scattering vector of the polymer mPEG$_{114}$-*b*-POlGE$_{5.8}$.

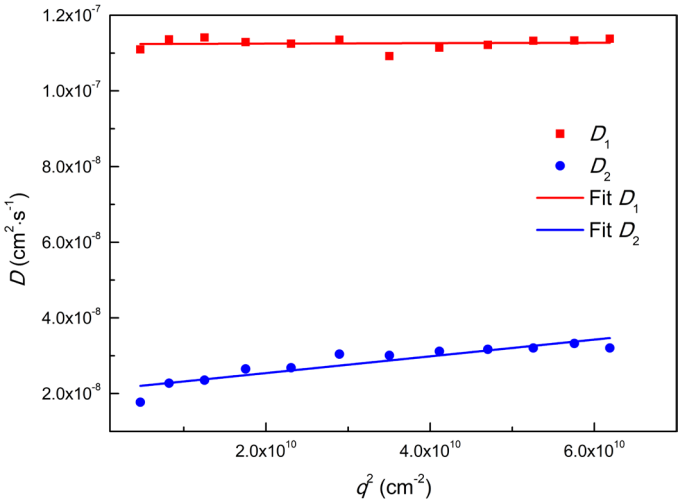

Figure S36: Diffusion coefficient plotted against the square of the scattering vector of the polymer mPEG$_{114}$-*b*-POlGE$_{7.3}$.

In Situ ^{1}H NMR Copolymerization Kinetics of OlGE and EO

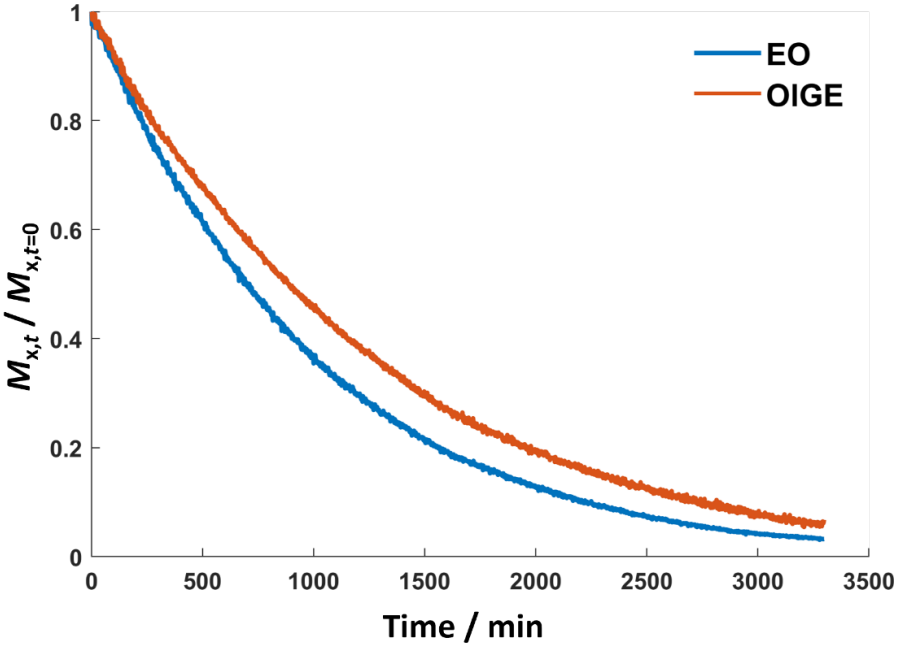

Figure S37: Time-conversion plot of the *in situ* ^{1}H NMR copolymerization kinetic study of EO with OlGE. (Solvent: DMSO-d_6/THF-d_8 1:5 (*V*/*V*), 40 °C.

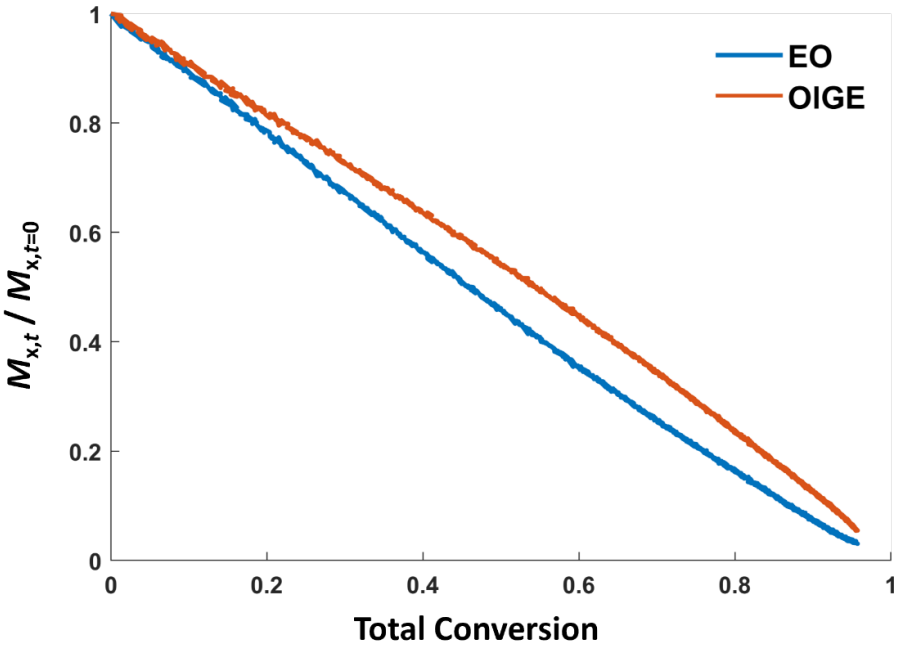

Figure S38: Individual versus total conversion of the *in situ* ^{1}H NMR copolymerization kinetic study of EO with OlGE. (Solvent: DMSO-d_6/THF-d_8 1:5 (*V*/*V*), 40 °C.

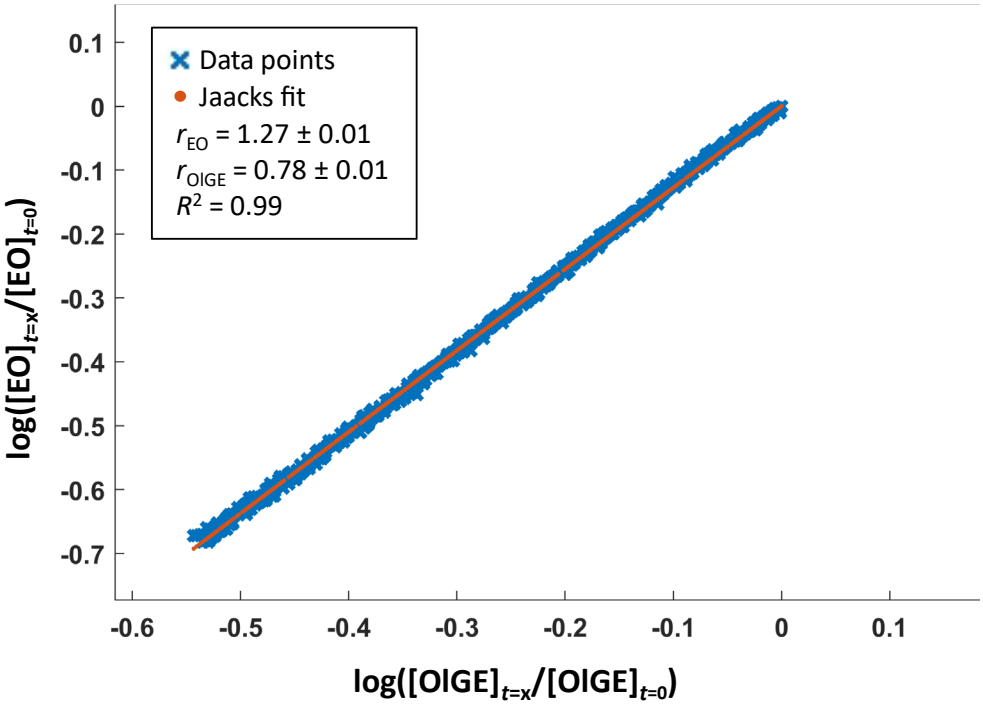

Figure S39: Jaacks fit of the *in situ* ^{1}H NMR copolymerization kinetic study of EO with OlGE. (Solvent: DMSO-d_6/THF-d_8 1:5 (*V*/*V*), 40 °C. Conversion threshold 75% to ensure significant signal to noise ratio of the epoxide functionalities.

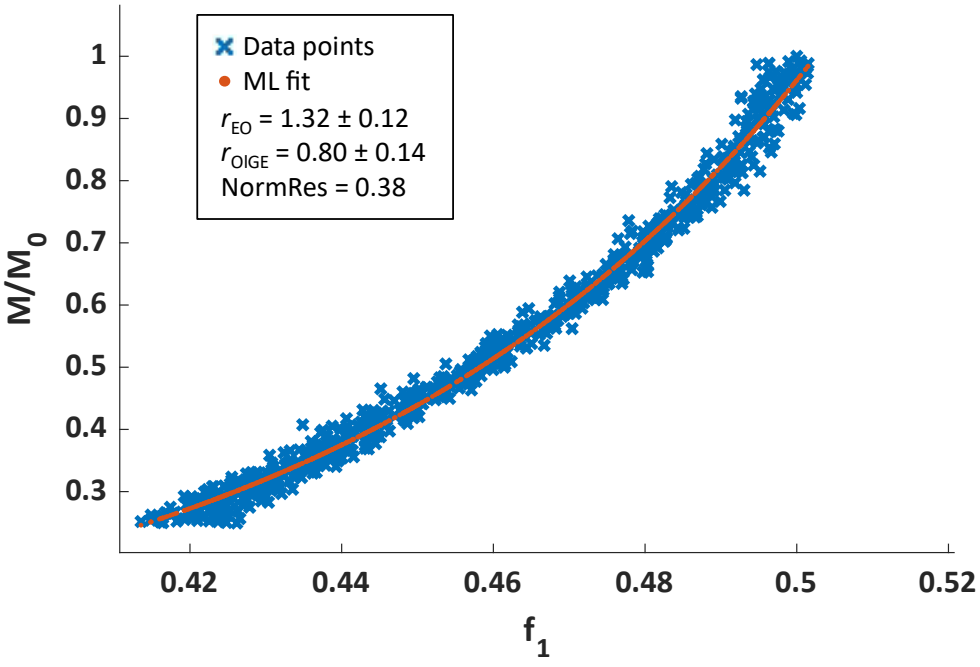

Figure S40: Meyer-Lowry fit of the *in situ* ^{1}H NMR copolymerization kinetic study of EO with OlGE. (Solvent: DMSO-d_6/THF-d_8 1:5 (*V*/*V*), 40 °C. Conversion threshold 75% to ensure significant signal to noise ratio of the epoxide functionalities.

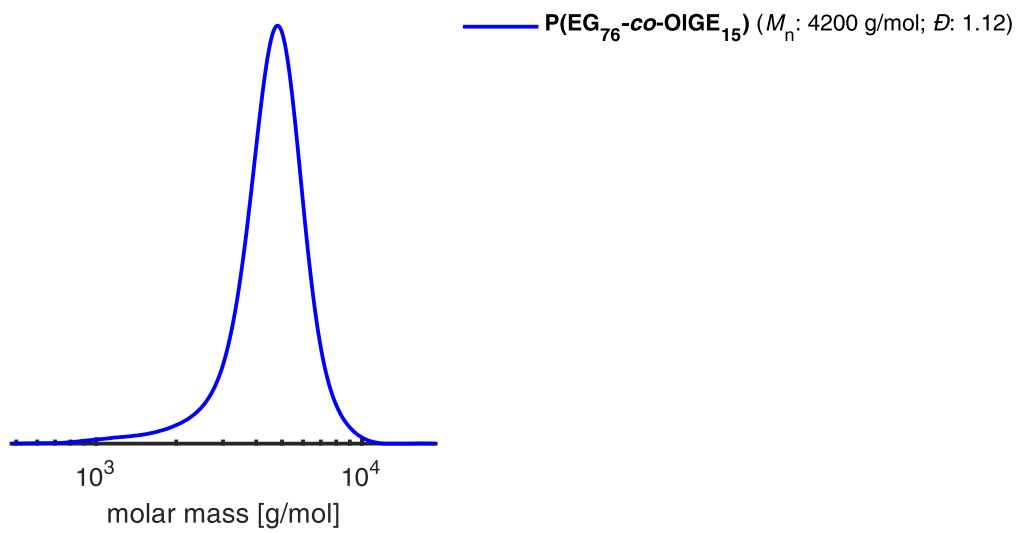

Figure S41: SEC trace of the P(EG$_{76}$-*co*-OlGE$_{15}$) copolymer synthesized during the *in situ* ^{1}H NMR kinetic study (RI detector, eluent: DMF, PEG calibration).

Post-polymerization Functionalization

Thiol-Ene Click

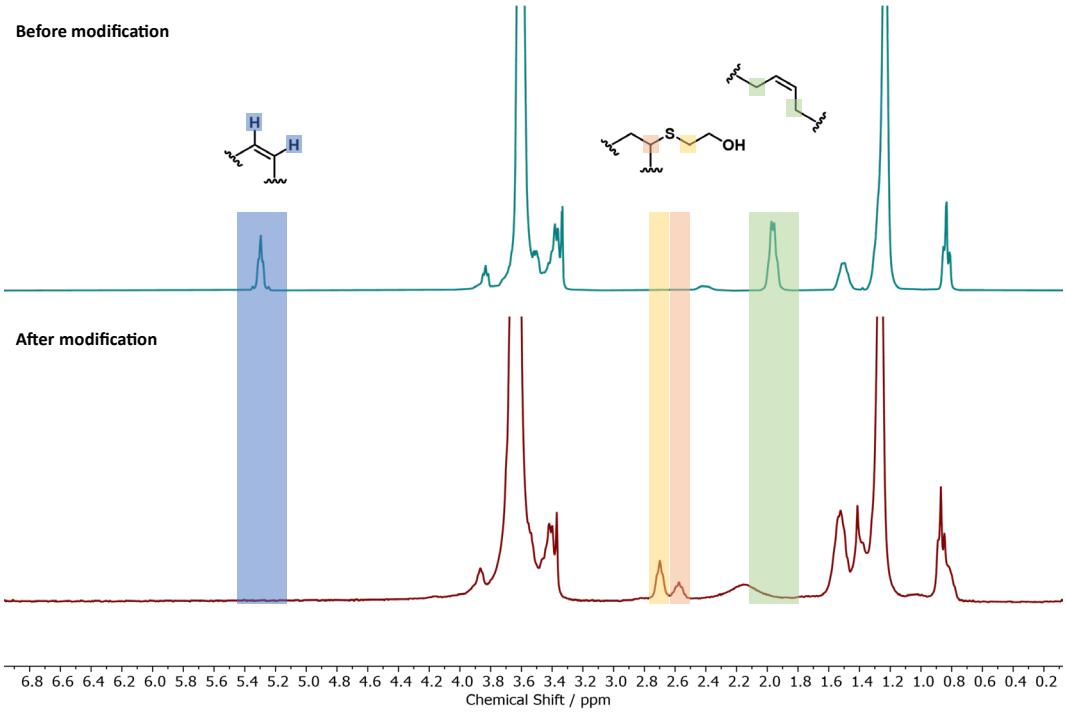

Figure S42: ^{1}H NMR of mPEG$_{114}$-*b*-POlGE$_{2.9}$ before and after modification via thiol-ene click (300 MHz, $CDCl_3$).

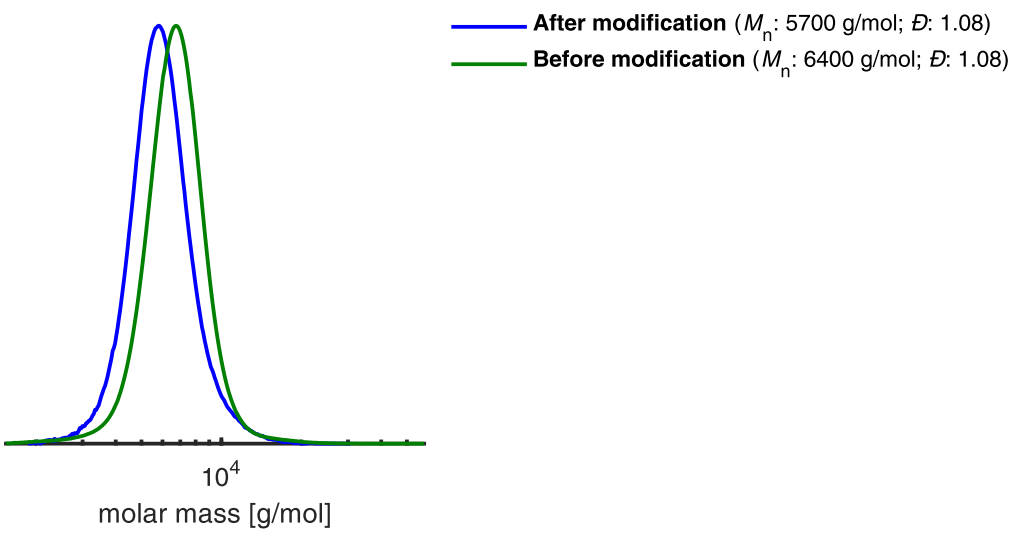

Figure S43: SEC traces of the polymer mPEG$_{114}$-*b*-POlGE$_{2.9}$ before (green) and after modification (blue) *via* thiol-ene click. Note that the apparent molecular weight decreases upon modification with thioglycol (eluent: THF, RI detector, PEG calibration).

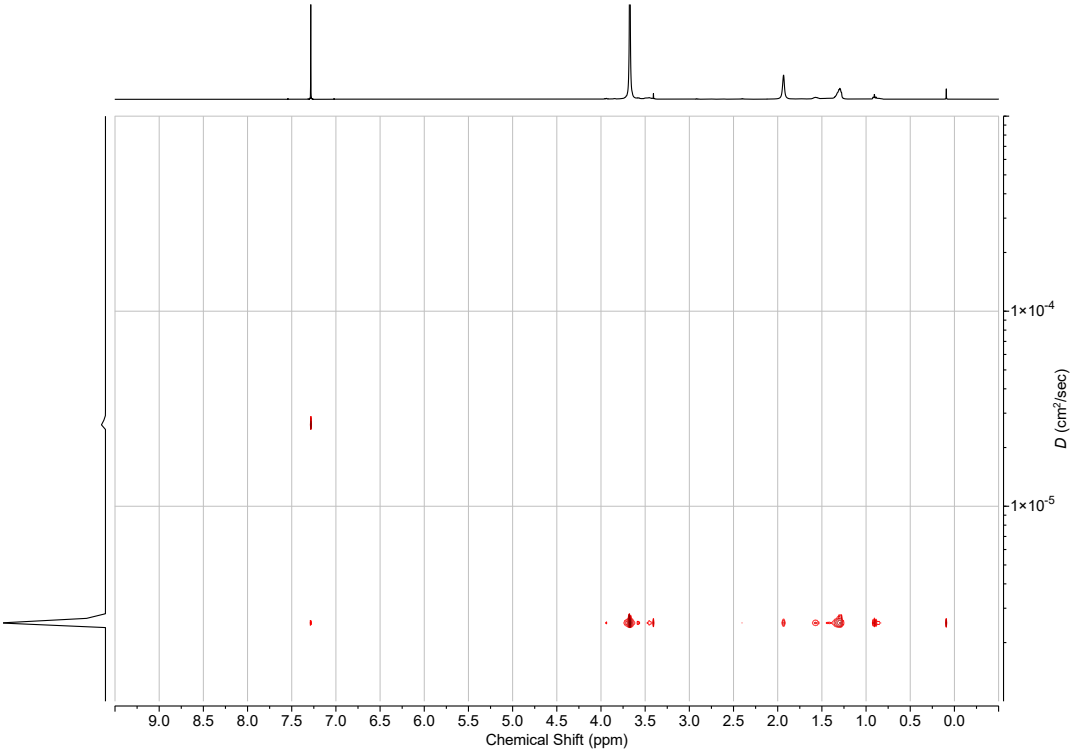

Figure S44: DOSY of modified mPEG$_{114}$-*b*-POlGE$_{2.9}$ with thioglycol (400 MHz, $CDCl_3$).

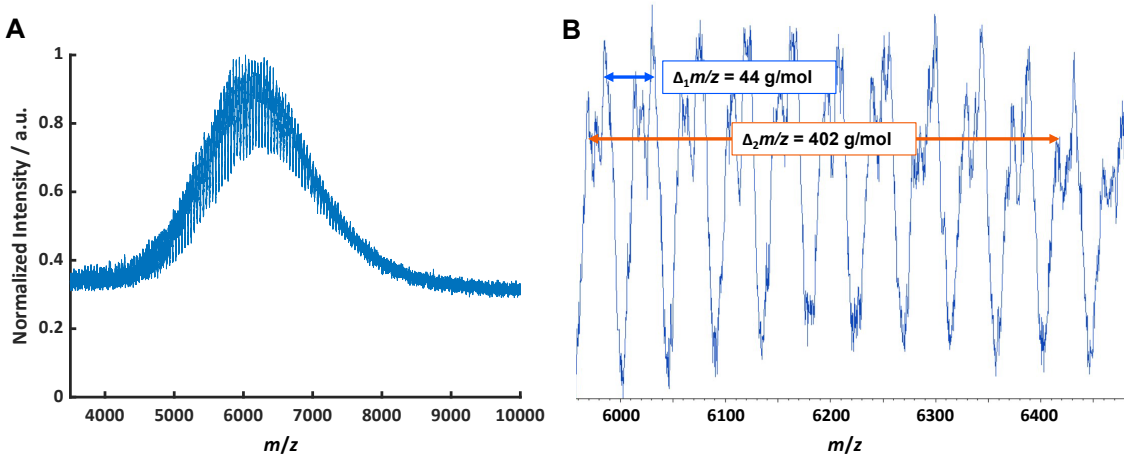

Figure S45: MALDI-ToF of mPEG$_{114}$-*b*-POlGE$_{2.9}$ functionalized with thioglycol (KTFA, linear mode, matrix: DCTB). Long arrow denotes the mass difference of the functionalized OlGE. Small arrow denotes the mass difference of the EO repeating unit. Note that the OlGE repeating unit (324 g/mol) was not found.

Hydrogenation via diimide from PADA

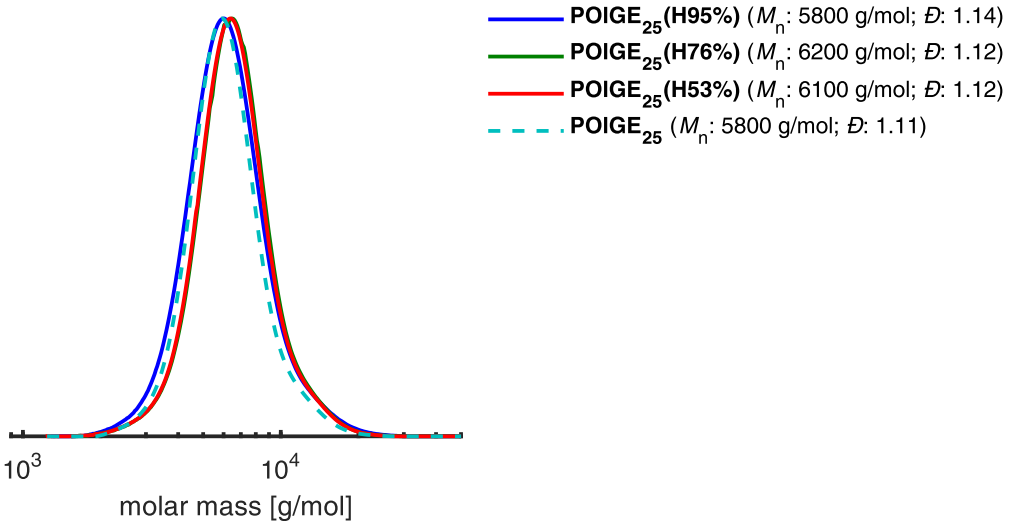

Figure S46: SEC trace of POlGE$_{25}$ and the respective hydrogenated Polymers (eluent: THF, RI detector, PEG calibration). The value of H denotes the degree of hydrogenation.

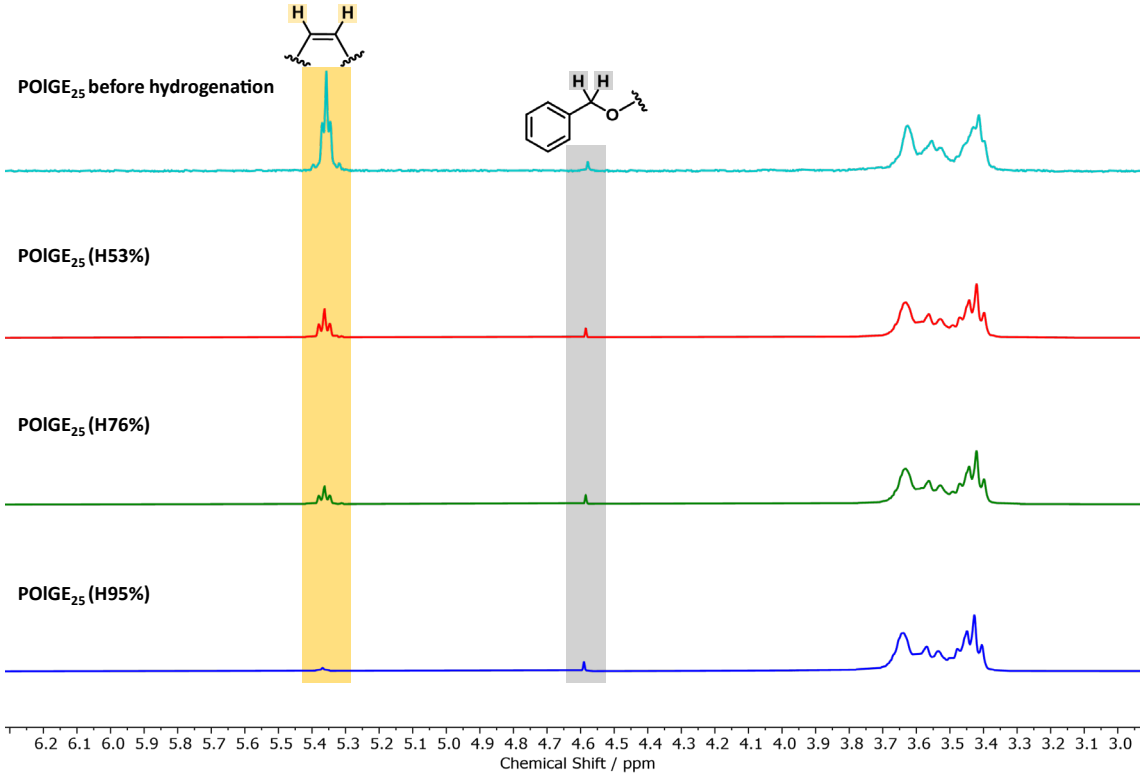

Figure S47: ^{1}H NMR spectra of POlGE$_{25}$ and the respective hydrogenated Polymers (400 MHz, $CDCl_3$). The value of H denotes the degree of hydrogenation.

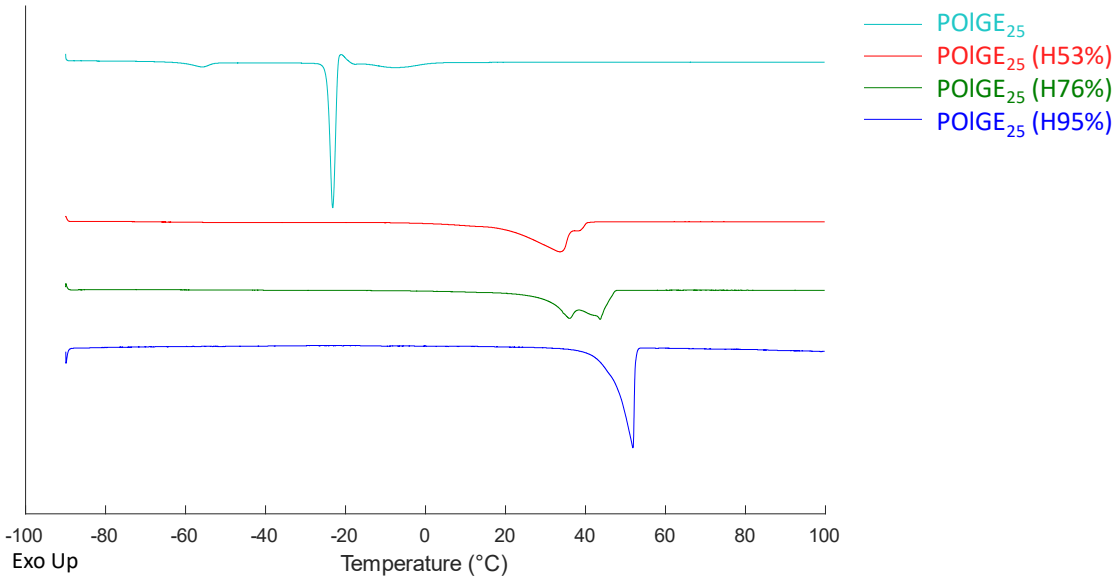

Figure S48: DSC thermograms of POlGE (partially) hydrogenated homopolymers and the respective precursor. Second heating curve, 1 K/min.

References

(1) Schüttner, S.; Krappel, M.; Koziol, M.; Marquart, L.; Schneider, I.; Sottmann, T.; Frey, H. Anionic Ring-Opening Copolymerization of Farnesyl Glycidyl Ether: Fast Access to Terpenoid-Derived Amphiphilic Polyether Architectures. *Macromolecules* **2023.** DOI: 10.1021/acs.macromol.3c00999.

(2) Becker, H. G. O. *Organikum*:*Organisch-chemisches Grundpraktikum*, 21., neu bearb. und erw. Aufl.; Wiley-VCH, 2001.

(3) Mouzin, G.; Cousse, H.; Rieu, J.-P.; Duflos, A. A Convenient One-Step Synthesis of Glycidyl Ethers. *Synthesis* **1983**, *1983* (02), 117–119. DOI: 10.1055/s-1983-30243.

(4) Herzberger, J.; Leibig, D.; Liermann, J. C.; Frey, H. Conventional Oxyanionic versus Monomer-Activated Anionic Copolymerization of Ethylene Oxide with Glycidyl Ethers: Striking Differences in Reactivity Ratios. *ACS Macro Lett.* **2016**, *5* (11), 1206–1211. DOI: 10.1021/acsmacrolett.6b00701.

(5) Steube, M.; Johann, T.; Plank, M.; Tjaberings, S.; Gröschel, A. H.; Gallei, M.; Frey, H.; Müller, A. H. E. Kinetics of Anionic Living Copolymerization of Isoprene and Styrene Using in Situ NIR Spectroscopy: Temperature Effects on Monomer Sequence and Morphology. *Macromolecules* **2019**, *52* (23), 9299–9310. DOI: 10.1021/acs.macromol.9b01790.

(6) Groves, J. T.; Ma, K. W. Carbon cluster compounds. Generation and reorganization of the homobullvalenyl cation, an 11-fold degenerate species. *J. Am. Chem. Soc.* **1977**, *99* (12), 4076–4082. DOI: 10.1021/ja00454a028.

(7) Hamersma, J. W.; Snyder, E. I. Diimide Reductions Using Potassium Azodicarboxylate. *J. Org. Chem.* **1965**, *30* (11), 3985–3988. DOI: 10.1021/jo01022a532.

(8) Schüttner, S.; Linden, G. M.; Hoffmann, E. C.; Holzmüller, P.; Frey, H. Poly(Terpenyl Glycidyl Ethers): Copolymerization with Ethylene Oxide, Properties, and Functionalization. Manuscript in preparation.

Outlook

Outlook

The copolymerization of epoxides presents an invaluable pathway for synthesizing innovative, customizable polyethers. Simultaneous, *i.e*. statistical copolymerization opens access to a vast variety of possible structures relevant to many areas of application, depending on monomer selection and reactivity ratios. This thesis discusses multiple examples, where copolymerization is controlled by the structures of the monomers and the reaction conditions. A particular focus has been placed on the role of solvent polarity and other parameters.

Bio-based monomers, such as those derived from fatty alcohols and terpenoids, offer significant potential to replace fossil-based monomers, creating new sustainable materials. These monomers, when copolymerized with ethylene oxide, tend to form random copolymers, making them excellent candidates for multifunctional poly(ethylene glycol) (PEG) derivatives. Anionic ring-opening polymerization is a living polymerization method, characterized by the absence of termination reactions. Therefore, the reactivity ratios provide insight into monomer incorporation and the resulting compositional gradient along the polymer chains.

Advanced online techniques enable the investigation of reactivity ratios in greater detail. Although many reactivity ratios have been reported since the 1960s, they are not aligned with the latest technological advancements. In the last decades, many experimental methods have advanced, making the *in situ* observation of monomer conversion possible. The copolymerization conditions are still too unheeded, even though they can influence the reactivity ratios. Besides, choosing the right copolymerization model is important to avoid erroneous results, but many authors still use outdated models. Nonetheless, the required inert conditions and potentially gaseous monomers in anionic ring-opening polymerization increase experimental effort. Future research needs to consider the influence of the reaction conditions. Systematic variation of the reaction conditions (degree of deprotonation, solvent, different monomers, etc.) can illuminate the impact of the combined factors. This enables the determination of more accurate reactivity ratios, which aids in understanding the influence of reaction conditions. The copolymerization of ethylene oxide with glycidyl methyl ether results in almost ideally random copolymers, while the copolymerization with propylene oxide yields gradient copolymers. The reaction conditions slightly alter reactivity ratios and understanding the influence of the conditions is essential to predict copolymer properties. This especially applies to copolymers for biomedical applications, where structural precision is crucial.

Decarbonizing the chemical industry will be the defining goal of the century. Societal demands for readily available, cheap, and renewable resources must be fulfilled to reduce greenhouse gas

emissions below the preindustrial level. Bio-based monomers will play a key role in polymer technology, they can provide a large variety of especially hydrophobic compounds. Terpenyl glycidyl ethers from terpenoids are already available, and their structural diversity allows them to be used in manifold applications. As such, they could be used in surfactants to solubilize apolar compounds or serve as sustainable alternatives in drug delivery systems. With nearly equal reactivity ratios, terpenyl glycidyl ethers and ethylene oxide enable the synthesis of gradient copolymers via continuous monomer addition during polymerization. This approach allows for a diverse range of innovative, sustainable materials, ranging from random, over gradient, to block copolymers. The comonomer content modifies the aqueous solubility of PEG, offering a potential lever to adjust drug release profiles. Postpolymerization reactions can further serve to tailor these materials for specific applications. Fatty alcohols are another promising resource for glycidyl ethers. In contrast to terpenoids, they exhibit linear side chains. The saturated, long-chain derivatives crystallize at room temperature. By tuning the melting point of the apolar segment in these block copolymers, they can form thermoresponsive micelles, enabling controlled drug release from the micellar core at a specific temperature in the patient. Nature also provides unsaturated alcohols that can be converted to glycidyl ethers. The side chains can be altered by postpolymerization modification of the double bonds, similar to the terpenyl glycidyl ethers.

Future research has the potential to revolutionize sustainable material development by integrating bio-based monomers and advancing copolymerization techniques. This progress will not only reduce environmental impact but also pave the way for innovative applications across diverse industries.

Appendix

A1: Isomerization of poly(ethylene glycol): A strategy for the evasion of immune recognition

[redacted] G. M. Linden[1], [redacted]

Affiliations:

[1]Department of Chemistry, Johannes Gutenberg University, Mainz; 55128 Mainz, Germany

[2]University Medical Centre, Johannes Gutenberg University; 55101 Mainz, Germany

[*]Corresponding author. Email: [redacted]

[redacted] contributed equally to this work.

Submitted to *Science*

Abstract:

PEGylation, the conjugation of poly(ethylene glycol) (PEG) to bioactive peptide drugs or nanocarriers, is a key strategy in nanomedicine to extend the circulation time of therapeutics in the bloodstream based on the stealth-effect of PEG. However, the growing prevalence of anti-PEG antibodies in the population can lead to pronounced immune responses upon drug administration and accelerated blood clearance of PEGylated drugs, resulting in the loss of the stealth-effect. We introduce the randomized PEG (rPEG) technology designed to mitigate the antigenicity of PEG while preserving its core benefits. This approach is based on an ideally random introduction of hydrophilic side chains along the PEG backbone. This effectively diminishes antigen recognition by anti-PEG antibodies. However, all relevant pharmaceutical properties of PEG are preserved.

Introduction

PEGylation, the conjugation of poly(ethylene glycol) (PEG) to proteins, small molecules or lipids, is a crucial strategy for the delivery of peptide and protein drugs (*1, 2*). It is frequently used in liposomal formulations (*3, 4*) and in PEGylated lipids as solubilizing and crucial stabilizing components of lipid nanoparticles, e.g. SARS-CoV-2 vaccines (*5, 6*). Presently, over 40 PEGylated therapeutics are on the market or in clinical phase III, with market introduction pending (*7*). It is appropriate to state that PEGylation represents a key technology of current nanomedicine. The non-ionic PEG provides a hydrophilic shield that protects conjugates from recognition by the patient's immune system, commonly referred to as "stealth-effect". It effectively increases the size of the biomolecule, consequently reducing clearance from the bloodstream (*8*). The investigation of PEG-coated nanocarriers additionally revealed the impact of PEG on the composition of the protein corona formed at the particles, which is important to prevent non-specific cellular uptake (*9*). However, whereas it was initially believed that PEG is immunologically inert, it has become evident in recent decades that an increasing number of individuals have developed anti-PEG antibodies (APAs), extensively boosted by PEG lipid-containing SARS-CoV-2 lipid nanoparticles (LNPs) used for mRNA vaccinations (*10–12*). The induction of APAs in humans may not only result from PEGylated therapeutics but could also arise from exposure to PEG present in food, cosmetics and other common sources. The potential antigenicity of PEG has been confirmed by the existence of APAs in healthy individuals who have never received PEGylated therapeutics systemically (*13, 14*). A recent study revealed that 83% of individuals in a typical western population are positive for either anti-PEG IgG or IgM (*15*).

The presence of APAs results in the recognition and accelerated blood clearance of PEGylated therapeutics up to complement activation-related pseudo allergy and anaphylactic shocks in severe

cases. A phase III clinical study regarding anti-coagulation factor IXa RNA PEG-conjugated aptamer had to be interrupted since anaphylactic reactions in 0.6% of the patients were observed, most likely caused by the pre-existence of APAs in the bloodstream (*16*). Recent clinical works regarding Pegaspargase have shown that the presence of APAs permits the prediction of allergic reactions and failure of rechallenge, emphasizing the clinical relevance of APA-Fabs for the success of treating leukemia in this case (*17*). Based on these concerns, the search for PEG replacement structures has intensified in recent years. Several alternatives based on polymer classes other than polyethers, *i.e*. polysarcosine, polyoxazolines and polymethacrylates have been discussed (*7, 8, 18*). However, it is important to note that antigenicity was also observed for some homopolymers of polymer classes other than PEG (*19, 20*) due to the flexibility of the adaptive immune system.

In contrast to the aforementioned approaches, the presented study targets the 'PEG alternative dilemma' via a fundamentally different PEG isomerization approach. Our strategy aims to preserve the wide spectrum of beneficial properties of PEG, while diminishing its immunological drawbacks by the introduction of statistical heterogenicity, retaining precise control over the chain length. Additionally, we aim at a PEG-based alternative that could be seamlessly integrated into existing PEG manufacturing and PEGylation processes.

Tackling APAs by introducing 'synthetic point mutations' to PEG via isomerization

Recently, crystal-structures of two types of APAs that bind to the PEG backbone (*21*) or the methoxy end group of mPEG (*22*) were determined for the first time. In both cases, an open ring-like substructure of the APA Fab paratope recognizes ethylene glycol (EO) units of PEG via multiple van der Waals and polar interactions. While the backbone-specific APA binds 16 EO units, seven units and the methoxy residue at the chain end are recognized by the investigated end group-specific APA. Inspired by these observations, we hypothesized that an interruption of the periodic and linear PEG structure by randomly distributed branching points should significantly alter the interaction of the APA with the PEG epitope. This random disruption of the regular PEG structure may be viewed as an introduction of 'synthetic point mutations' along the polyether backbone. In this context, we chose methoxy methylene side chains as branching points to preserve the carbon-hydrogen-oxygen ratio of PEG while altering the underlying architecture of the polyether (**Fig. 1A**).

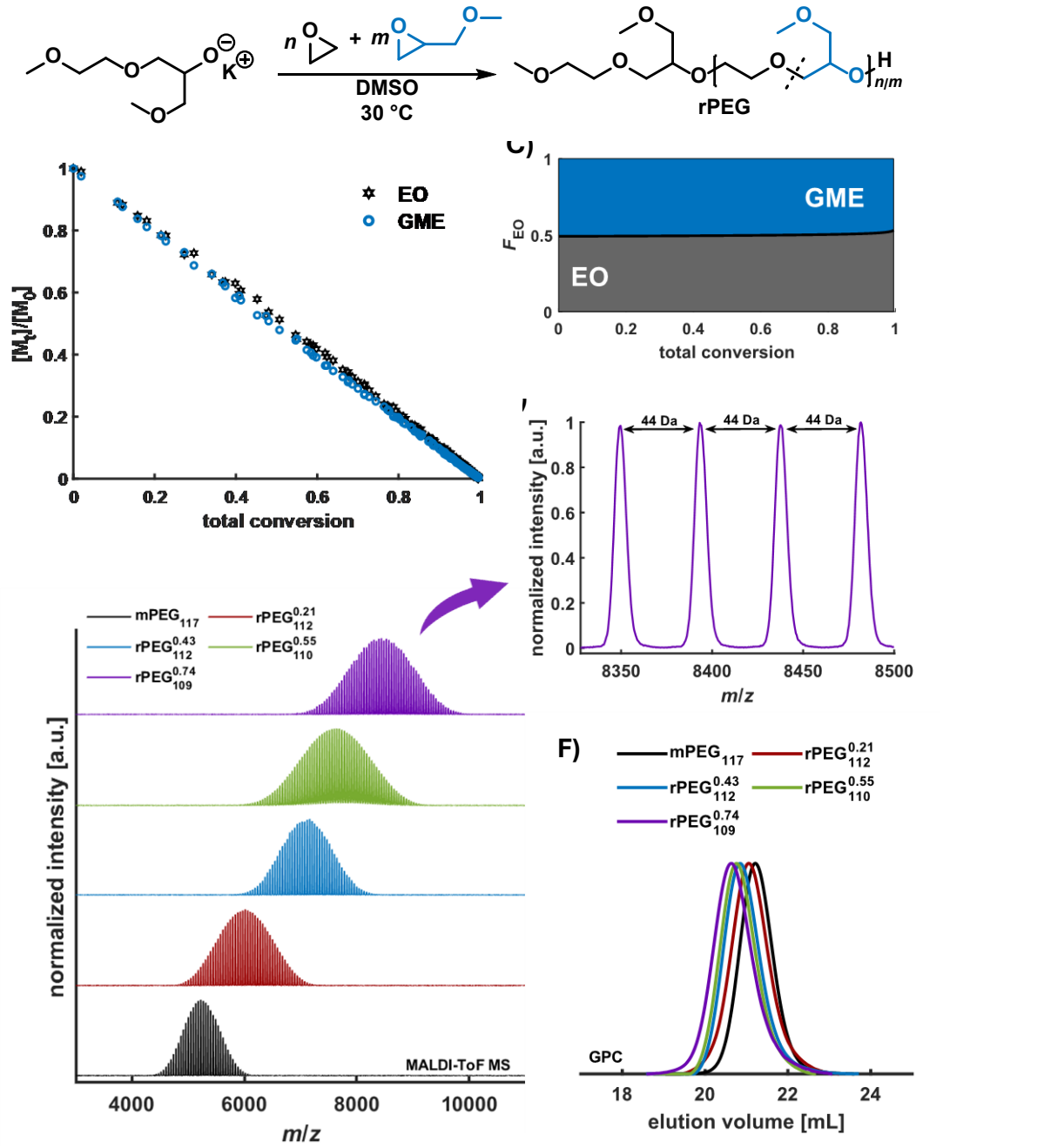

Figure 1. Synthesis and characterization of rPEGs. (A) Applied synthesis strategy for rPEG by copolymerization; (B) comonomer consumption ($[M_t]/[M_0]$) vs. total conversion obtained from in-situ ^{1}H NMR kinetics in DMSO-d_6; (C) molar-based composition diagram of rPEG (50 mol% GME) derived from the in-situ ^{1}H NMR kinetics data in DMSO-d_6; (D) stacked MALDI ToF mass spectra of investigated rPEGs; (E) zoom-in of $rPEG^{0.74}_{105}$ MALDI ToF MS; (F) stacked GPC traces of investigated rPEGs.

The repeating unit can be introduced via the epoxide monomer glycidyl methyl ether (GME). As GME is a formal dimer of EO ($C_{2n}H_{4n}O_n$; n = 1 (EO), 2 (GME)), all copolymers of EO and GME represent constitutional isomers of PEG, independent of their monomer composition. We assumed that these randomized PEG (rPEG) structures hold potential as a highly suitable non-antigenic alternative to PEG, albeit preserving the polyether backbone and the beneficial physicochemical properties of PEG. The random incorporation of EO and GME units into the polymer backbone is an

essential parameter to decrease the occurrence of EO-rich epitope segments in the polyether chains. In principle, the incorporation of GME repeating units can be achieved via copolymerization of EO and GME. Noteworthy, anionic homo- and copolymerization of GME has rarely been investigated to date due to synthetic challenges and impurities (**scheme S2**), resulting in ill-defined polymers that are not suitable for pharmaceutical applications. PGME homopolymers were either obtained as oligomers (*23*) or with high dispersity (*24*). EO-GME copolymer structures are accessible using an activated monomer mechanism (*24*) albeit resulting in ill-defined materials with poor end group fidelity and non-tolerable traces of the aluminum catalyst in the products. It is important to note that for a polymer to be regarded as a viable alternative to PEG, it must meet the standard specifications of pharmaceutical-grade PEG. Specifically, it must possess high purity and a dispersity (M_w/M_n) lower than 1.10. High end group fidelity (>99%) is critical for the subsequent conjugation of the polymers to proteins, nanocarriers or surfaces.

Via utilization of analytically pure GME (>99%) (**fig. S1, S4 and S5**) and anionic ring-opening (co)polymerization (AROP) of EO and GME (**Fig. 1A**), the first successful synthesis of well-defined rPEGs was accomplished, circumventing the abovementioned synthetic challenges (**scheme S2**). AROP was selected as polymerization method of choice, as it represents the standard polymerization technique for pharmaceutical grade PEG, characterized by the absence of toxic side products or catalysts, high end-group fidelity and the ability to precisely control molar masses due to quantitative conversion of the epoxide monomers (*25*). The method is also utilized in the industrially established synthesis of pharmaceutical-grade PEG. Therefore, it is the key for the potential synthesis of a polyether-based PEG alternative in existing PEG production facilities.

In the AROP of epoxides, the choice of solvent is a crucial reaction parameter because it has a direct influence on the copolymerization kinetics and the resulting microstructure of the copolymer (*26*). Therefore, in a first optimization step, we elucidated the incorporation of EO and GME into the polymer backbone by following the mean composition at all chain positions during the copolymerization. This was achieved by performing *in-situ* ^{1}H NMR kinetics measurements in various non-protic solvents suitable for AROP of monosubstituted epoxides (**fig. S8 – S39 and tables S1 and S2**). In the case of DMSO-d_6, an almost linear decrease of comonomer consumption with progressing conversion (**Fig. 1B**) for both comonomers is observed. This demonstrates that the incorporation of EO and GME units occurs in an ideally random manner ($r_{EO} \approx r_{GME} \approx 1$) (**Fig. 1C**) independent of temperature and degree of deprotonation (**figs. S15 – S18, S24 – S26**). In the case of less polar solvents, a slightly preferred incorporation of GME over EO was observed, resulting in soft gradient microstructures (**figs. S19 – S23, S27 – S31**). As a random distribution of GME along

the polymer backbone is preferred to statistically minimize the occurrence of EO-rich segments, we chose DMSO as a suitable solvent for the optimization of the rPEG synthesis on multi-gram scale.

To ensure systematic comparability of the side groups´ influence on the physicochemical properties and their behavior in the bioassays, copolymers in analogy to 5000 g mol^{-1} mPEG were synthesized. This translates to a constant degree of polymerization of 114, while varying the GME content, leading to higher molar masses that depend on the introduced GME content. In this context, we designed and utilized the potassium salt of 1-methoxy-3-(2-methoxyethoxy)propan-2-ol (MMEPOK) as initiator (**Fig. 1A**) for the synthesis of the rPEG samples to lock a 'synthetic point mutation' at the second repeating unit of each polymer chain (**supplementary text**). The design of the initiator structure was derived from preliminary enzyme-linked immunosorbent assay (ELISA) experiments of PGME samples with differing initiator molecules (**fig. S40**). We further designed and conducted an additional purification protocol via semi-preparative high-performance liquid chromatography (HPLC) (**supplementary text**) to obtain rPEG samples in high purity which is an essential requirement for potential pharmaceutical applications (**fig. S43, table S5**). Additionally, the purification protocol was applied using a commercial mPEG sample to allow for comparison between mPEG and rPEG in the following studies. Hence, rPEGs with varying molar compositions of 21 – 74 mol% GME and molecular weights of 6.0 – 8.4 kg mol^{-1} were synthesized and purified (**tables S3 and S4**). All isomeric rPEGs and mPEG were analyzed by ^{1}H NMR spectroscopy (**fig. S44**) and MALDI ToF MS. The latter reveals one distinct distribution which is assigned to the potassium-ionized and methoxy-initiated species ($[rPEG + K]^{+}$) carrying an alcohol group at the *ω*-chain end exclusively (**Fig. 1D and 1E, figs. S45 and S46**). This confirms the purity and high end group fidelity of the synthesized rPEGs. It is important to note that due to the isomeric character of the rPEGs, only a single distribution with intervals of 44 *m*/*z* is observed, despite the copolymer structure. Additionally, all synthesized rPEGs show monomodal distributions and dispersity <1.10 (GPC) independent of their molar comonomer composition (**Fig. 1F, fig. S47**). Therefore, from a synthetic point of view, the requirements of rPEGs as a PEG alternative are fully met.

Preservation of stealth properties

The application of PEG alternatives in polymer-protein conjugates and in lipid-nucleic acid formulations under physiological conditions necessitates sufficient solubility of the polymer in aqueous solutions significantly above body temperature. Since the formation of a hydration shell is crucial for the stealth effect and therefore shielding of the active pharmaceutical ingredient (API) or nanoparticle, a collapse of the PEGylation alternative in aqueous solutions must be prevented.

Therefore, we investigated the thermo-responsive behavior of the synthesized rPEG samples in PBS buffer via turbidimetry. In the measurements, the cloud point temperatures (T_{cp}), marking phase separation of polymers and the solvent of the rPEGs with varying amounts of GME were determined at a concentration of 2 mg mL^{-1} (**Fig. 2A, table S6**). The investigation shows that no cloud point is observed up to a molar GME content of 43% in the rPEG samples. The observed T_{cp}s at a transmittance of 50% for rPEG$^{0.55}_{110}$ and rPEG$^{0.74}_{105}$ at 86 °C and 75 °C, respectively, demonstrate that even for high content of GME no coil-globule transition is to be expected at physiological temperatures. Additionally, T_{cp}s for rPEG$^{0.74}_{105}$ at varying polymer concentrations (0.5-10.0 mg mL^{-1}) were investigated showing merely a slight decrease of the T_{cp} up to 71 °C (10.0 mg mL^{-1}) with increasing polymer concentration (**Fig. 2B, table S6**).

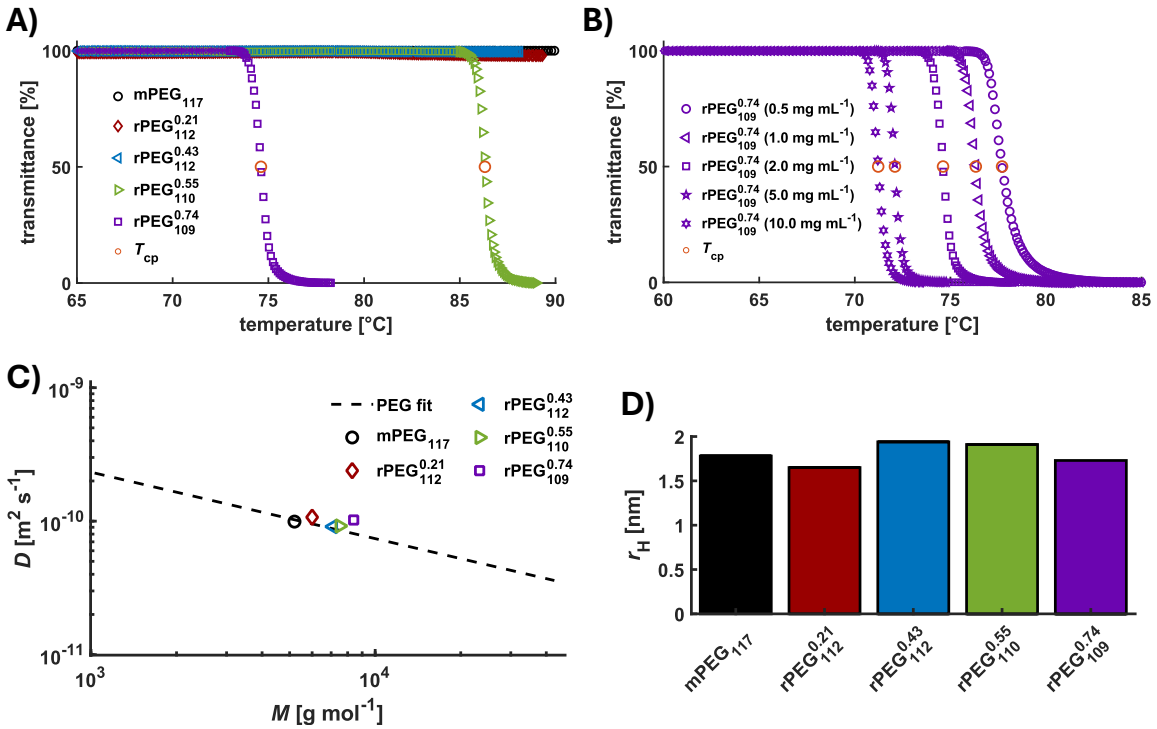

Figure 2. Physicochemical properties of rPEGs. (A) Stacked turbidimetry plots (heating curves) (2.0 mg mL^{-1}) of mPEG$_{117}$ and rPEG samples in PBS buffer; (B) stacked turbidimetry plots (heating curves) of rPEG$^{0.74}_{105}$ at different concentrations in PBS buffer; (C) diffusion coefficients in dependence of the molecular weight for mPEG and rPEG samples in D_2O obtained via DOSY NMR; dashed line shows PEG fit determined from different well-defined PEG samples; (D) comparison of hydrodynamic radii of mPEG and rPEG samples based on the obtained diffusion coefficients from DOSY experiments.

Pursuing, we utilized diffusion-ordered NMR spectroscopy (DOSY NMR) in D_2O (**figs. S48 – S52**) to evaluate the influence of the methoxy methylene side chains on the properties of rPEGs in solution. The obtained data (**table S7**) was referenced to a PEG fit (**fig. S53)** to elucidate differences of the rPEG samples to conventional PEG. In this context, the rPEG samples exhibit slight deviations from the expected PEG fit values, whereas the mPEG$_{117}$ sample aligns closely with the fit (**Fig. 2C)**. This confirms that the methoxy end group of the investigated samples has no significant influence on

the diffusion of the polymers in the investigated molar mass range. Calculation of the hydrodynamic radii (r_H) from the diffusion data (**supplementary text**) reveals unexpected behavior. Despite the significant increase in molar mass with higher content of GME, the r_H of the rPEG samples remains comparable to that of the mPEG reference (**Fig. 2D, table S7)**. In comparison, a PEG sample with the same molecular weight as $rPEG_{105}^{0.74}$ (r_H = 1.73 nm) possesses a r_H of ≈2.23 nm based on the determined PEG fit (**fig. S53**). From these observations, we conclude that the primary contribution to the hydrodynamic radius of the rPEG polymer coil derives from the hydration of the backbone, while the methoxy methylene side groups play a rather minor role.

In summary, the study of the thermoresponsiveness and hydrodynamic radii of rPEGs in buffer solution and D_2O, respectively, show similar results as for PEG, hinting towards comparable shielding capability for drug or protein conjugates and nanoparticles.

Sustainment of cell viability

Further, we investigated the cell viability and the activation of human leukocytes via flow cytometry to assess the behavior of rPEGs in biomedical applications. It was shown in earlier studies that the PGME homopolymer and other glycidyl ether-based polyethers show excellent biocompatibility in cell viability tests (*23, 27*). To establish biocompatibility for the series of rPEGs, we incubated peripheral blood mononuclear cells (PBMCs) of four healthy donors with rPEGs and $mPEG_{117}$ in a broad concentration range (5.0, 1.0 and 0.1 mg mL^{-1}) for 16 h. Cytokine release in the supernatants was measured to evaluate immunomodulatory effects of rPEGs. rPEGs exhibit high cell viability for all cell types at all investigated concentrations (**Fig. 3A, fig S59**).

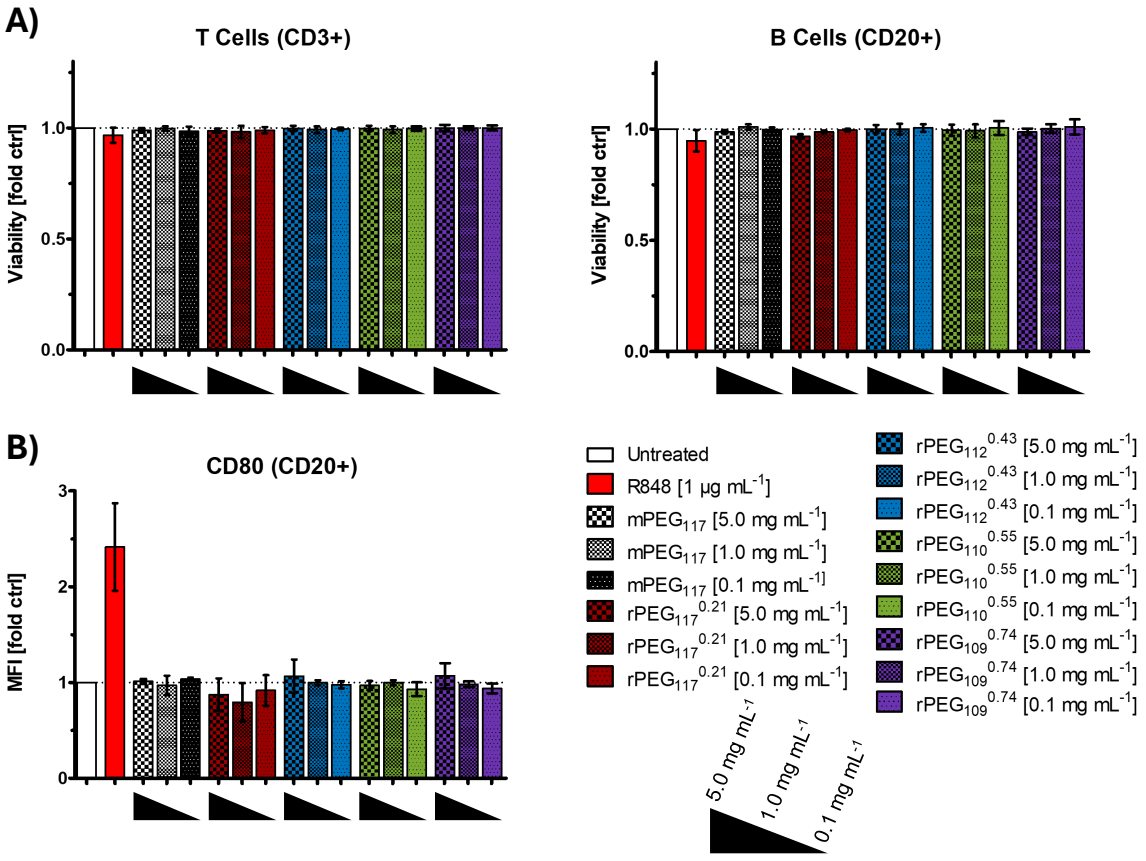

Figure 3. PBMC Cell viability & B cell activation in the presence of $mPEG_{117}$ and rPEGs. (A) Cell viability of human leukocytes; (B) CD80 expression on B Cells (CD20 positive) as a biomarker for immunomodulatory effects; determined via flow cytometry at different concentrations (5.0, 1.0 and 0.1 mg mL^{-1}).

No influence on the viability of B cells, T cells, neutral killer cells (NK) and monocytes is observed for rPEGs. At the highest concentration of 5 mg mL^{-1} some rPEG samples show a slight effect on dendritic cells (DC) and the remaining polymorphonuclear leukocytes, but their viability remains above 75% (fold ctrl) (**fig S59**). This effect can be attributed to the high polymer concentration and heterogeneity of human donors. A reduction of the cell viability with increasing GME content is not observed. The CD80 and CD86 expressions on B cells remain at a basal level (**Fig. 3B. fig. S60)** Therefore, it can be established that rPEG does not activate resting B cells. A possible influence of pre-existing APAs is not observed. Given the significant variability in immune activity among individual donors, cytokine release data permits only relative assessments. To account for this variability, cytokine levels were normalized to the positive control (R848) of each respective donor (**supplementary text**). The relative cytokine release sustains near zero and never increased above 0.05-fold R848 control (**fig. S61, tables S10– S14**). To conclude, all investigated rPEGs are non-cytotoxic and do not feature a notable immune-modulatory effect for clinically relevant concentrations. Thus, rPEG appears to be suitable for utilization in *in vivo* experiments and addition preclinical studies.

Suppression of antibody recognition

Based on the reactivity ratios determined in DMSO-d_6 ($r_{EO} \approx r_{GME} \approx 1$), calculations and simulations with different molar compositions were performed (**supplementary text**) to illustrate the random distribution of the 'synthetic point mutations' along the rPEG chains (**Figs. 4A and 4B, figs. S54 – S56**). The targeted chemical heterogeneity within the polymer sample is evident from the simulation, as each distinct chain possesses a different sequence of repeating units (**Fig. 4B**). The methoxy methylene groups as 'synthetic point mutations' are randomly distributed in the polyether backbone, and the statistical diversity within each chain within one sample is tremendously high. As an example, for a copolymer with 114 monomer units, among which 23 monomer units are GME (20 mol%), the number of possible chain isomers with different monomer sequences is $7.3 \cdot 10^{23}$. This illustrates that the induction of polymer-specific antibodies targeting a regular chain segment should be highly hampered or even impossible. The calculations show that a decrease in the molar fractions of longer, merely EO containing segments with increasing GME amount occurs (**Fig. 4A**). This is confirmed by the simulations (**Fig. 4B, figs. S54 – S56**) where the probability of finding at least one repeating pattern of 16 or more consecutive EO repeating units (highlighted in orange) in a rPEG chain decreases from 46% for $rPEG_{114}^{0.20}$ to below 0.1% in the case of $rPEG_{114}^{0.50}$ (**table S8**). Besides the decrease in consecutive EO units, the increased spatial requirement of rPEGs and the random distribution of methoxy methylene side chains should additionally impede or even disable interaction with APAs according to the specific "lock and key principle". In addition, GME is utilized as a racemic mixture, which introduces additional symmetry inhomogeneities of the individual chains within one sample.

To investigate our hypothesis regarding APAs, we tested the effect of a varied concentration of synthetic point mutations (0 to 74 mol% GME) on the binding capability of backbone- and end group-specific APAs via competitive ELISA. The concentration-dependent interaction between the APA and polyether is detected by a decrease of fluorescence intensity. In summary, the backbone-specific APA ELISA results confirm the effect of the incorporation of methoxy methylene groups along the PEG backbone on the APA recognition, in alignment with the simulations.

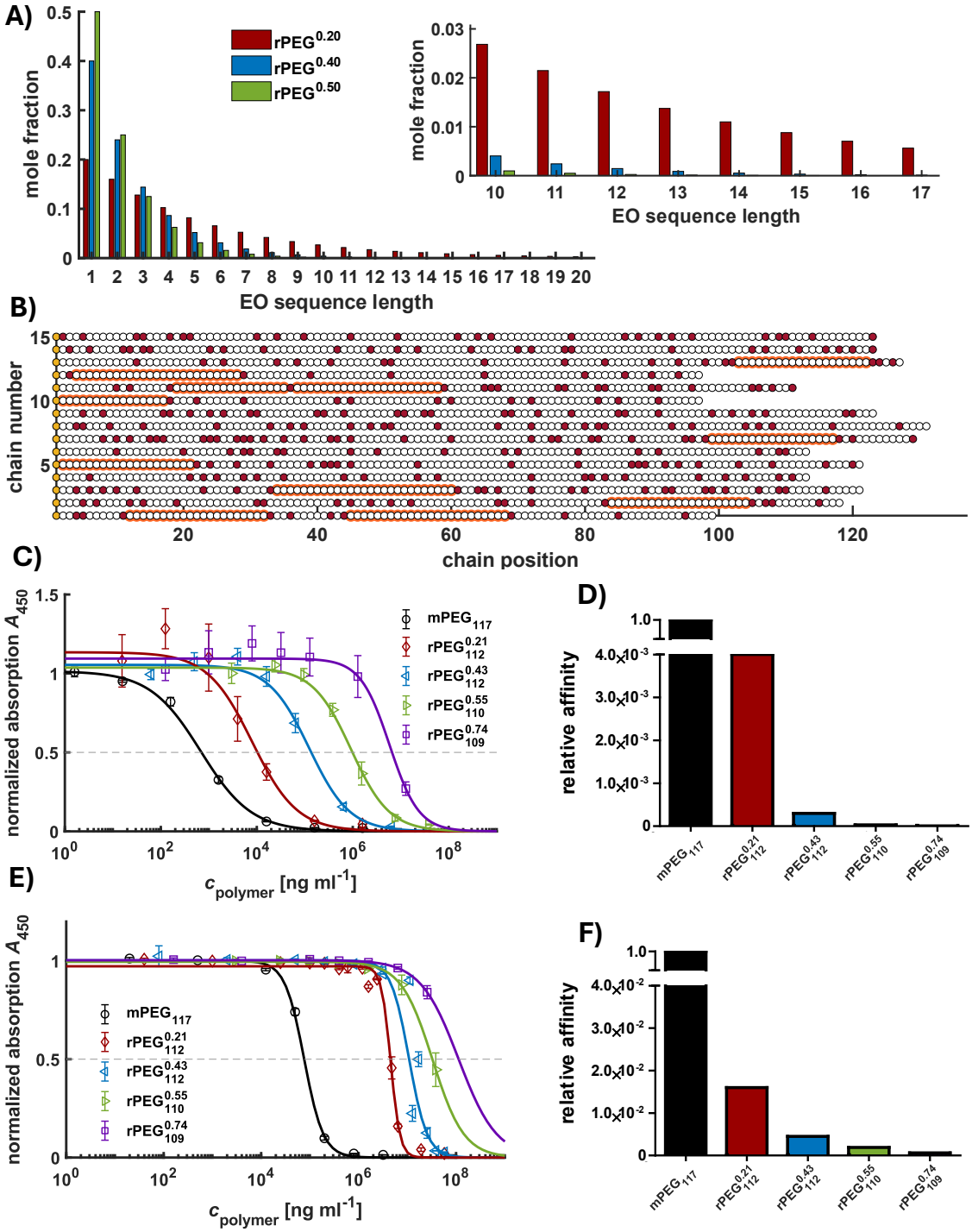

Figure 4. Calculation and influence of 'synthetic point mutations'. (A) Mole fractions of EO sequence lengths for different comonomer compositions; (B) section of 15 chains from the simulation (10^4 chains) of EO (white) and GME (red) repeating unit distribution at different chain positions of $rPEG^{0.20}_{114}$; repeating patterns with 16 consecutive EO repeating units are highlighted in orange; yellow circles represent the initiator; (C) backbone-specific APA ELISA of investigated rPEGs and $mPEG_{117}$; the dashed grey line represents the EC_{50} value; (D) relative affinity of backbone-specific APA for investigated rPEGs and $mPEG_{117}$ based on EC_{50} values obtained from backbone-specific APA ELISA; (E) end group-specific APA ELISA of investigated rPEGs and $mPEG_{117}$; the dashed grey line represents the EC_{50} value; (F) relative affinity of end group-specific APA for investigated rPEGs and $mPEG_{117}$ based on EC_{50} values obtained from backbone-specific APA ELISA.

A major increase of the EC_{50} value is observed with increasing GME content. Comparing the relative affinities ($1/EC_{50}$) of the APA towards $mPEG_{117}$ and rPEGs (**Fig. 4C and 4D, table S9**) underlines the significance of the diminished antigenicity. With incorporation of 21 – 74 $mol\%_{GME}$ within the polyether, its affinity drops to $0.4 – 4.6 \cdot 10^{-6}$% relative to $mPEG_{117}$, respectively. Following the simulations, the random nature of 'synthetic point mutation' incorporation in the PEG chains reduces the length of undisrupted PEG segments, thereby minimizing the probability of forming a PEG epitope. Nevertheless, binding of the APA is still observed at very high rPEG concentrations. We consider two possible explanations for this behavior: (i) an interaction of less than 16 consecutive EO units may already cause weak binding; (ii) the initial interaction between APA and PEG is based on van der Waals interactions before trapping the polymer by a conformational change (*21*). At polymer concentrations as high as tested, an unspecific aggregation or entanglement of polymer and APA could cause a decrease in binding affinity to the competitive PEG coated on the ELISA plate wells. Considering the overall polymer portion of PEGylated therapeutics, antigenic concentrations of rPEGs in the performed studies are magnitudes higher than those of PEG in current clinical applications. While the introduction of pendant methoxy methylene groups strongly reduces the antigenicity of rPEGs towards backbone-specific APAs, this assay does not provide information regarding end group-specific APA interactions. In principle, each GME repeating unit contains a methoxy group which could theoretically be detected by the end group-specific APAs.

Compared to the backbone-specific APA, the EC_{50} value of $mPEG_{117}$ in the end group-specific APA assay is shifted to higher concentrations, indicating an overall lower polymer affinity. In accordance with the backbone-specific APA ELISA, a notable shift of EC_{50} values of all rPEGs in relation to $mPEG_{117}$ is observed (**Fig. 4E**). The relative APA affinity drops to $1.6 – 6 \cdot 10^{-2}$% (**Fig. 4F, table S9**). While the EC_{50} value of $rPEG_{112}^{0.21}$ significantly differs from $mPEG_{117}$, a further increase of the GME content has a minor impact on the APA binding relative to $rPEG_{112}^{0.21}$. This can be explained with the two different binding domains of the end group-specific APA. The APAs' end group binding domain cannot contribute to the overall binding, as all rPEGs are furnished with a blocked α-chain end (**Fig. 1A**). Consequently, merely the domain that interacts with PEG_7 sequences along the polymer backbone can mediate binding. Since the change in affinity is significantly affected by blocking of the end group binding domain, this appears to be the primary binding site for the end group-specific APA. The results further confirm that the methoxy groups of the side chains do not enable binding of the end group-specific APAs, in stark contrast to a methoxy end group.

Summary

The increasing abundance of anti-PEG antibodies (APA) in the population leads to undesired immune responses to PEGylated drugs as well as PEG-based formulations and causes accelerated blood clearance. This has become an increasingly severe issue over the years, since it renders the stealth effect of PEG ineffective. Recently, this issue has increased drastically, as the containment of the global COVID-19 pandemic strongly relied on PEGylated lipids for the transport of mRNA vaccines. We introduce the concept of random polyether copolymers that are structural PEG isomers, i.e., randomized PEGs (rPEG), containing 'synthetic point mutations' as a key alternative to PEG for applications in therapeutic nanomedicine.

Detailed *in situ* ^{1}H NMR kinetics experiments revealed an ideally random introduction of sterically demanding branching points in PEG by random copolymerization of EO and the comonomer glycidyl methyl ether (GME). The highly hydrophilic rPEGs demonstrate drastically reduced recognition by both backbone and end group-selective anti-PEG antibodies in competitive enzyme-linked immunosorbent assays (ELISA). Simulations and calculations regarding the microstructure of such copolymers further support the experimental ELISA results. A wide structural diversity, due to the statistical copolymerization process, is present in rPEG samples, despite the precise control of chain length and high end group fidelity.

The presented rPEG strategy can rely on existing PEG technology at every stage, allowing for the use of established PEG GxP manufacturing processes and supply chains. Versatile conjugation chemistry has been established for PEG for more than three decades and is, in principle, fully transferrable to rPEG. On the other hand, the possibility of separating medical and pharmaceutical application of PEG from its widespread use in everyday products, e.g., surfactants, by use of rPEGs is relevant to avoid severe immune responses in individuals. We firmly believe that the statistical variation approach bears universal potential in different areas, ranging from bioconjugation to PEGylated nanocarriers such as LNPs, for the treatment of chronic diseases.

References and Notes

1. Y. Gao, M. Joshi, Z. Zhao, S. Mitragotri, PEGylated therapeutics in the clinic. *Bioengineering & translational medicine*. **9**, e10600 (2024), doi:10.1002/btm2.10600.

2. J. M. Harris, R. B. Chess, Effect of pegylation on pharmaceuticals. *Nature reviews. Drug discovery*. **2**, 214–221 (2003), doi:10.1038/nrd1033.

3. M. Hamidi, A. Azadi, P. Rafiei, Pharmacokinetic consequences of pegylation. *Drug delivery*. **13**, 399–409 (2006), doi:10.1080/10717540600814402.

4. N. J. Butcher, G. M. Mortimer, R. F. Minchin, Drug delivery: Unravelling the stealth effect. *Nature nanotechnology*. **11**, 310–311 (2016), doi:10.1038/nnano.2016.6.

5. N. Pardi, M. J. Hogan, F. W. Porter, D. Weissman, mRNA vaccines - a new era in vaccinology. *Nature reviews. Drug discovery*. **17**, 261–279 (2018), doi:10.1038/nrd.2017.243.

6. L. Schoenmaker *et al.,* mRNA-lipid nanoparticle COVID-19 vaccines: Structure and stability. *International journal of pharmaceutics*. **601**, 120586 (2021), doi:10.1016/j.ijpharm.2021.120586.

7. G. Pasut, S. Zalipsky, Eds., *Polymer-protein conjugates*, *From PEGylation and beyond* (Elsevier, Amsterdam, 2020).

8. E. M. Pelegri-O'Day, E.-W. Lin, H. D. Maynard, Therapeutic protein-polymer conjugates: advancing beyond PEGylation. *Journal of the American Chemical Society*. **136**, 14323–14332 (2014), doi:10.1021/ja504390x.

9. S. Schöttler, G. Becker, S. Winzen, T. Steinbach, K. Mohr, K. Landfester, V. Mailänder, F. R. Wurm*,* Protein adsorption is required for stealth effect of poly(ethylene glycol)- and poly(phosphoester)-coated nanocarriers. *Nature nanotechnology*. **11**, 372–377 (2016), doi:10.1038/nnano.2015.330.

10. Y. Ju *et al.,* Anti-PEG Antibodies Boosted in Humans by SARS-CoV-2 Lipid Nanoparticle mRNA Vaccine. *ACS nano*. **16**, 11769–11780 (2022), doi:10.1021/acsnano.2c04543.

11. A. Remmel, COVID vaccines and safety: what the research says. *Nature*. **590**, 538–540 (2021), doi:10.1038/d41586-021-00290-x.

12. J. de Vrieze, Pfizer's vaccine raises allergy concerns. *Science (New York, N.Y.)*. **371**, 10–11 (2021), doi:10.1126/science.371.6524.10.

13. B.-M. Chen, Y.-C. Su, C.-J. Chang, P.-A. Burnout, K.-H. Chuang, C.-H. Chen, T.-L. Cheng, Y.-T. Chen, J.-Y. Wu, S. R. Roffler, Measurement of Pre-Existing IgG and IgM Antibodies against Polyethylene Glycol in Healthy Individuals. *Analytical chemistry*. **88**, 10661–10666 (2016), doi:10.1021/acs.analchem.6b03109.

14. Q. Yang, T. M. Jacobs, J. D. McCallen, D. T. Moore, J. T. Huckaby, J. N. Edelstein, S. K. Lai, Analysis of Pre-existing IgG and IgM Antibodies against Polyethylene Glycol (PEG) in the General Population. *Analytical chemistry*. **88**, 11804–11812 (2016), doi:10.1021/acs.analchem.6b03437.

15. M. F. S. Deuker, V. Mailänder, S. Morsbach, K. Landfester, Anti-PEG antibodies enriched in the protein corona of PEGylated nanocarriers impact the cell uptake. *Nanoscale horizons*. **8**, 1377–1385 (2023), doi:10.1039/D3NH00198A.

16. A. M. Lincoff *et al.,* Effect of the REG1 anticoagulation system versus bivalirudin on outcomes after percutaneous coronary intervention (REGULATE-PCI): a randomised clinical trial. *Lancet (London, England)*. **387**, 349–356 (2016), doi:10.1016/S0140-6736(15)00515-2.

17. Y. Liu *et al.,* Antibodies Predict Pegaspargase Allergic Reactions and Failure of Rechallenge. *Journal of clinical oncology: official journal of the American Society of Clinical Oncology*. **37**, 2051–2061 (2019), doi:10.1200/JCO.18.02439.

18. K. Knop, R. Hoogenboom, D. Fischer, U. S. Schubert, Poly(ethylene glycol) in drug delivery: pros and cons as well as potential alternatives. *Angewandte Chemie (International ed. in English)*. **49**, 6288–6308 (2010), doi:10.1002/anie.200902672.

19. J. Humphries, N. L. Fletcher, S. E. Sonderegger, C. A. Bell, K. Kempe, K. J. Thurecht, Mitigating the Effects of Persistent Antipolymer Immune Reactions in Nanomedicine: Evaluating Materials-Based Approaches Using Molecular Imaging. *ACS nano* (2024), doi:10.1021/acsnano.4c07317.

20. P. H. Kierstead, H. Okochi, V. J. Venditto, T. C. Chuong, S. Kivimae, J. M. J. Fréchet, F. C. Szoka, The effect of polymer backbone chemistry on the induction of the accelerated blood clearance in polymer modified liposomes. *Journal of controlled release: official journal of the Controlled Release Society*. **213**, 1–9 (2015), doi:10.1016/j.jconrel.2015.06.023.

21. J. T. Huckaby, T. M. Jacobs, Z. Li, R. J. Perna, A. Wang, N. I. Nicely, S. K. Lai, Structure of an anti-PEG antibody reveals an open ring that captures highly flexible PEG polymers. *Communications chemistry*. **3**, 124 (2020), doi:10.1038/s42004-020-00369-y.

22. M.-T. T. Nguyen *et al.,* Structural determination of an antibody that specifically recognizes polyethylene glycol with a terminal methoxy group. *Communications chemistry*. **5**, 88 (2022), doi:10.1038/s42004-022-00709-0.

23. M. Weinhart, I. Grunwald, M. Wyszogrodzka, L. Gaetjen, A. Hartwig, R. Haag, Linear poly(methyl glycerol) and linear polyglycerol as potent protein and cell resistant alternatives to poly(ethylene glycol). *Chemistry, an Asian journal*. **5**, 1992–2000 (2010), doi:10.1002/asia.201000127.

24. S. S. Müller, C. Moers, H. Frey, A Challenging Comonomer Pair: Copolymerization of Ethylene Oxide and Glycidyl Methyl Ether to Thermoresponsive Polyethers. *Macromolecules*. **47**, 5492–5500 (2014), doi:10.1021/ma501280k.

25. J. Herzberger, K. Niederer, H. Pohlit, J. Seiwert, M. Worm, F. R. Wurm, H. Frey, Polymerization of Ethylene Oxide, Propylene Oxide, and Other Alkylene Oxides: Synthesis, Novel Polymer Architectures, and Bioconjugation. *Chemical reviews*. **116**, 2170–2243 (2016), doi:10.1021/acs.chemrev.5b00441.

26. P. Dreier, R. Matthes, R. D. Barent, S. Schüttner, A. H. E. Müller, H. Frey, In Situ Kinetics Reveal the Influence of Solvents and Monomer Structure on the Anionic Ring-Opening Copolymerization of Epoxides. *Macro Chemistry & Physics*. **224** (2023), doi:10.1002/macp.202200209.

27. R. Matthes, H. Frey, Polyethers Based on Short-Chain Alkyl Glycidyl Ethers: Thermoresponsive and Highly Biocompatible Materials. *Biomacromolecules*. **23**, 2219–2235 (2022), doi:10.1021/acs.biomac.2c00223.

28. M. Steube, T. Johann, M. Plank, S. Tjaberings, A. H. Gröschel, M. Gallei, H. Frey, A. H. E. Müller, Kinetics of Anionic Living Copolymerization of Isoprene and Styrene Using in Situ NIR Spectroscopy: Temperature Effects on Monomer Sequence and Morphology. *Macromolecules*. **52**, 9299–9310 (2019), doi:10.1021/acs.macromol.9b01790.

29. F. Merah-Mourah, S. O. Cohen, A. Haziot, A Two-Stage Flow Cytometry Strategy to Distinguish Single Cells from Doublets in Heterogeneous Cell Mixtures and Improve Cell Cluster Identification: Application to Human Monocyte Subpopulations. *Current Protocols*. **1**, e229 (2021), doi:10.1002/cpz1.229.

30. O. Sedlacek, O. Janouskova, B. Verbraeken, R. Hoogenboom, Straightforward Route to Superhydrophilic Poly(2-oxazoline)s via Acylation of Well-Defined Polyethylenimine. *Biomacromolecules*. **20**, 222–230 (2019), doi:10.1021/acs.biomac.8b01366.

31. G. Odian, Ed., *Principles of Polymerization, Fourth Edition* (John Wiley & Sons Incorporated, ed. 4, 2004).

32. J. Blankenburg, E. Kersten, K. Maciol, M. Wagner, S. Zarbakhsh, H. Frey, The poly(propylene oxide-*co*-ethylene oxide) gradient is controlled by the polymerization method: determination of reactivity ratios by direct comparison of different copolymerization models. *Polym. Chem.* **10**, 2863–2871 (2019), doi:10.1039/C9PY00500E.

33. B. S. Beckingham, G. E. Sanoja, N. A. Lynd, Simple and Accurate Determination of Reactivity Ratios Using a Nonterminal Model of Chain Copolymerization. *Macromolecules*. **48**, 6922–6930 (2015), doi:10.1021/acs.macromol.5b01631.

34. V. Jaacks, A novel method of determination of reactivity ratios in binary and ternary copolymerizations. *Makromol. Chem.* **161**, 161–172 (1972), doi:10.1002/macp.1972.021610110.

35. A. A. Solov'yanov, K. S. Kazanskii, The kinetics and mechanism of anionic polymerization of ethylene oxide in ether solvents. *Polymer Science U.S.S.R.* **14**, 1186–1195 (1972), doi:10.1016/0032-3950(72)90162-1.

36. A. Duda, S. Penczek, Determination of the Absolute Propagation Rate Constants in Polymerization with Reversible Aggregation of Active Centers. *Macromolecules*. **27**, 4867–4870 (1994), doi:10.1021/ma00096a002.

Acknowledgments:

[redacted] thank the ERC for important financial support in the context of the ERC Advanced Grant “RandoPEGMed”. [redacted] thanks SFB 1066 for financial support.

Funding:

German Research Foundation, grant from CRC 1066, project TP Q6 ([redacted])

European Research Council, ERC Advanced Grant for the project *RandoPEGmed*, Project 101055434 ([redacted])

Author contributions:

Conceptualization: [redacted]

Methodology: [redacted]

Investigation: [redacted]

Visualization: [redacted]

Funding acquisition: [redacted]

Project administration: [redacted]

Supervision: [redacted]

Writing – original draft: [redacted]

Writing – review & editing: [redacted]

Competing interests: [redacted] are co-owners of Patent No. [redacted] which relates to the rPEG technology described in this manuscript. All authors may benefit from potential licensing agreements or future revenue associated with this patent. Therefore, this patent may be considered a competing interest, as the authors have an economic interest in the commercialization of the research findings presented in this manuscript.

Data and materials availability: All data are available in the main text or the supplementary materials.

Supplementary Materials

Materials and Instrumentations

Experimental Procedures

Supplementary Text

Scheme S1 to S2

Figs. S1 to S66

Tables S1 to S14

References (*28*–*36*)

1. Materials and Instrumentation

1.1. Reagents and Equipment

All chemicals and solvents were purchased from Acros Organics, Roth, TCI, Sigma-Aldrich, Fisher Scientific. BLDpharm and Fluka, unless otherwise noted. Deuterated solvents were received from Deutero GmbH. Ethylene Oxide was acquired from Air Liquide. THF was flashed over basic aluminum oxide before usage. Glycidyl methyl ether was dried over CaH_2 and cryo-transferred before polymerizations.

1.2. NMR spectroscopy

^{1}H and ^{13}C NMR spectra were recorded on a Bruker Avance III HD 400 spectrometer with 400 and 100 MHz, respectively, and referenced internally to residual proton signals of the deuterated solvent. All spectra were acquired at 23 °C. Spectra were processed and analyzed utilizing the *MestReNova 14.3.3-33362* software.

in-situ ^{1}H NMR kinetics: Polymerization kinetics were conducted on a *Bruker Avance III HD* (400 MHz) with a 5 mm nitrogen-cooled BBO-cryoprobe-head (BB+H+F) with *z*-gradient, automated tune and match (ATM) and autosampler SampleXPress 60. All spectra were acquired at temperatures stated in **Table S1** and **Table S2**. Spectra were referenced to the residual protons of the used solvents. Data were processed with *MestReNova 14.3.3-33362* software. For kinetics in anisole (non-deuterated), lock was turned off. Shim was performed with TopShim (gradient shim) using the protons of the anisole methoxy group. Sample spinning was turned off and one spectrum was recorded to acquire the receiver gain. Afterwards, one spectrum was recorded every two minutes. The respective resonances of the monomers were used to track the consumption (δ(EO) = 2.26–2.31 ppm, δ(GME) = 2.35–2.43 ppm). To analyze the normalized monomer consumption, the software *NIREVAL* was used (*28*).

Diffusion-ordered NMR spectroscopy (DOSY NMR): Polymer samples were measured in D_2O at a concentration of 1 mg mL^{-1}. DOSY measurements were conducted on a *Bruker Avance III HD* (400 MHz) with a 5 mm nitrogen-cooled BBO-cryoprobe-head (BB+H+F) with *z*-gradient, automated tune and match (ATM) and autosampler SampleXPress 60. A total of 8 scans were acquired. The time domain consisted of 64 data points. The diffusion delay was set to 0.2 s. Additionally, the duration of each gradient pulse was 2500 µs. All spectra were acquired at 23 °C. Spectra were referenced to the residual protons of the used solvents. Spectra were processed and analyzed utilizing the *MestReNova 14.3.3-33362* software.

1.3. Gel permeation chromatography (GPC)

Measurements were conducted using an Agilent 1100 series HPLC system, which included a degasser, isocratic pump (G1310A), autosampler (G1313A), column oven (G1316A), and detectors for refractive index (RI) (G1310A) and variable wavelength (VWD) (G1314A). Separations were carried out employing a four-column set-up (*MZ-Analysentechnik GmbH*) connected sequentially:

i) HEMA-40 guard column (40 Å pore size, 10 µm particle size, 50x8.0 mm)
ii) HEMA-40 analytical column (40 Å pore size, 10 µm particle size, 300x8.0 mm)
iii) HEMA-100 analytical column (100 Å pore size, 10 µm particle size, 300x8.0 mm)
iv) HEMA-300 analytical column (300 Å pore size, 10 µm particle size, 300x8.0 mm)

The eluent consisted of DMF (Fisher Chemical) with 1 mg mL^{-1} anhydrous LiBr (Acros Organics), delivered at a flow rate of 1 mL min^{-1}. Both, the column oven and RI detector cell were maintained at 50 °C. Calibration was performed using well-defined poly(ethylene glycol)s from PSS (PSS Standards Kit) with molar mass values (M_p) ranging from 106 to 42700 g mol^{-1}. Samples were dissolved in DMF (with 1 mg mL^{-1} anhydrous LiBr) at a concentration of 1 mg mL^{-1} with the addition of 1 drop of toluene. Injection of 100 µL of the stock solutions was carried out via the autosampler, with a measurement duration of 45 min. Elution times were referenced using toluene as an internal standard. RI traces were analyzed using the *PSS WinGPC Unichrom V8.31* software.

1.4. MALDI-TOF Mass Spectrometry (MS)

MALDI-TOF MS measurements were carried out at a Bruker autoflex maX MALDI-TOF/TOF using a smartbeam-II solid state laser with a wavelength of 337 nm. Spectra were recorded using the software *Bruker flexControl 3.4* and analyzed using *Bruker flexAnalysis 3.4* and *Bruker polytools 1.31*. The potassium salt of triflouroacetic acid (KTFA) and *trans*-2-[3-(4-*tert*-butylphenyl)-2-methyl-2-propenylidene]malononitrile (DCTB) were utilized as ionization salt and matrix, respectively. For sample preparation, the polymers were dissolved in chloroform at 10 mg mL^{-1}. 20 µL of this solution were combined with 20 µL of a 10 mg mL^{-1} solution of the matrix in chloroform. 5 µL of a 0.1 M solution of the salt in methanol were added and 1 µL of the resulting mixture was spotted onto a MTP 384 ground steel target plate. The solvents were allowed to evaporate completely before the measurement. All measurements were performed in linear mode.

1.5. High-performance liquid chromatography (HPLC)

Analytical Protocol: The HPLC system consisted of an Agilent Technologies 1260 Infinity system with a 1260 Quat pump, a 1260 ALS autosampler, a 1260 VWD UV−vis variable-wavelength spectrophotometric detector, a Softa 1300 evaporative light scattering detector (ELSD), a PSS

TCC6000 column thermostat and a solvent degasser. The UV detector was operated at a wavelength of 254 nm. The ELSD was operated with a spray chamber temperature of 30 °C, a drift tube temperature of 60 °C and an air pressure of 3.0 bar. The column oven temperature was set to 30 °C. A flowrate of 1 mL min^{-1} was applied. For analysis, a PerfectSil 300 (C_4, 5 µm particle size, 250 × 4.6 mm (L × ID) column from MZ-Analysentechnik GmbH was used. The mobile phases consisted of MeOH (HiPerSolv Chromanorm (HPLC gradient grade) and H_2O (LiChrosolv® Merck Chemicals, LC-MS grade). Samples were dissolved in H_2O at a concentration of 1 mg mL^{-1}, filtered through a Rotilabo® syringe filter (PTFE, pore size 0.45 µm). 25-50 µL of the stock solution was injected and analyzed by RP-HPLC with a MeOH/H_2O gradient:

i) 0-5 min: isocratic at 60% MeOH
ii) 5-15 min: linear gradient from 60 to 100% MeOH
iii) 15-20 min: isocratic at 100% MeOH

Subsequently, the starting gradient was restored within 1 min and a 20 min reconditioning time at 60% MeOH was allowed before further analysis. ELSD elugrams were analyzed using the *PSS WinGPC Unichrom V8.31* software.

Semi-preparative Protocol: The HPLC system consisted of an Agilent Technologies 1260 Infinity system with a 1260 Quat pump, a 1260 ALS autosampler, a 1260 VWD UV−vis variable-wavelength spectrophotometric detector, a solvent degasser and a fraction collector (ADVANTEC CHF122SC). The UV detector was operated at a wavelength of 254 nm. A flowrate of 10 mL min^{-1} was applied. A PerfectSil 300 (C_4, 5 µm particle size, 250 × 20 mm (L × ID) column from MZ-Analysentechnik GmbH was used. The mobile phases consisted of MeOH (HiPerSolv Chromanorm (HPLC gradient grade) and H_2O (LiChrosolv® Merck Chemicals, LC-MS grade). Samples were dissolved in H_2O at a concentration of 200 mg mL^{-1}, filtered through a Rotilabo® syringe filter (PTFE, pore size 0.45 µm). 500 µL of the stock solution was injected and purified by RP-HPLC with a MeOH/H_2O gradient:

i) 0-10 min: isocratic at 60% MeOH
ii) 10-30 min: linear gradient from 60 to 100% MeOH
iii) 30-60 min: isocratic at 100% MeOH

Subsequently, the starting gradient was restored within 1 min and a 40 min reconditioning time at 60% MeOH was allowed before further purification runs. Each fraction consisted of a volume of 30 mL. Product fractions were visualized via consecutive tapping of six drops of each fraction on a silica gel TLC plate (Sigma Aldrich), subsequent staining with potassium permanganate solution and heating of the plate.

1.6. Turbidimetric Measurements

Turbidimetric measurements were performed with a *JASCO* UV-Vis Spectrometer (V730) at a light wavelength of 600 nm and a heating rate of 1 K min^{-1} using the software *JASCO Spectra Manager Ver.2*. Polymers were dissolved in PBS buffer solution (pH = 7.4) at various concentrations. Pure PBS buffer solution was utilized as a reference value of 100% transmittance and was measured prior to each experiment. All measurements were performed in a quartz glass cuvette from Hellma Analytics with a light path of 10 mm. Cloud point temperatures (T_{cp}) were determined at a transmittance of 50 %. Raw data was normalized to maximum and minimum values of the respective heating curves.

1.7. Enzyme-linked Immunosorbent Assay (ELISA)

Competitive backbone-specific anti-PEG antibody ELISA: The assessment of anti-PEG antibody affinity for the respective polymer involved performing assays on mPEG (20 kDa)-BSA coated 96-well plates. The LifeDiagnostics anti-PEG-ELISA Kit, including TMB staining solution, stop-solution, anti-PEG antibody HRP-conjugate and dilution buffer was utilized. Absorption measurements were conducted with a BMG Labtech FLUOstar Omega multi-mode reader at a wavelength of 450 nm and all samples were measured in triplicates. The data acquired was analyzed utilizing both Omega Software and OriginPro 8. To create samples of varying concentrations, 10 mg of polymer was dissolved in dilution buffer and aliquots were prepared through a dilution series. The anti-PEG antibody (9 µL) was dissolved in 12 mL of dilution buffer. The wash buffer concentrate (50 mL) was diluted with MilliQ water to yield 1 L of wash buffer. In the assay process, 50 µL of each polymer solution was added to the coated 96-well plate, followed by 50 µL of the anti-PEG antibody solution. The samples were incubated for 1 h at 25 °C with shaking at 300 rpm. After discarding the solution, each well underwent six washes with 300 µL of wash buffer. Excess wash buffer was removed by gently tapping the plate on the bench. Subsequently, 100 µL of TMB staining solution was added to each well, followed by a 20 min incubation at 25 °C with shaking at 300 rpm. The reaction was quenched by adding 100 µL of stop-solution to each well and immediate absorption measurements were taken. The determined absorbance values were normalized to visualize the percentage of maximal binding. The sample concentrations were transformed to a function of $\log_{10}$. The sigmoidal fits were calculated using the following equation with *A*2 representing the upper limit *A*1 the lower limit c the inflection point and d the hill slope.

$$y = A1\,\frac{A2 - A1}{1 + 10^{(c-x)d}} \qquad \textbf{(S1)}$$

Competitive end group-specific anti-PEG antibody ELISA: The assessment of anti-mPEG antibody affinity for the respective polymer involved performing assays on mPEG (20 kDa)-BSA coated 96-well plates. The LifeDiagnostics anti-mPEG-ELISA Kit was utilized. Additionally, the mPEG (20 kDa)-BSA coated 96-well plate from the anti-PEG-ELISA Kit of LifeDiagnostics was used. Absorption measurements were conducted with a BMG Labtech FLUOstar Omega multi-mode reader at a wavelength of 450 nm and all samples were measured in triplicates. The data acquired was analyzed utilizing both Omega Software and OriginPro 8.

To create samples of varying concentrations, 10 mg of polymer was dissolved in dilution buffer and aliquots were prepared through a dilution series. The anti-mPEG antibody (9 µL) was dissolved in 12 mL of dilution buffer. The wash buffer concentrate (12.5 mL) was diluted with MilliQ water to yield 250 mL of wash buffer. In the assay process, 50 µL of each polymer solution was added to the coated 96-well plate, followed by 50 µL of the anti-mPEG antibody solution. The samples were incubated for 1 h at 25 °C with shaking at 300 rpm. After discarding the solution, each well underwent six washes with 300 µL of wash buffer. Excess wash buffer was removed by gently tapping the plate on the bench. Subsequently, 100 µL of TMB staining solution was added to each well, followed by a 20 min incubation at 25 °C with shaking at 300 rpm. The reaction was quenched by adding 100 µL of stop-solution to each well and immediate absorption measurements were taken. The determined absorbance values were normalized to visualize the percentage of maximal binding. The sample concentrations were transformed to a function of $\log_{10}$. The sigmoidal fits were calculated using **equation S1**.

1.8. Cell viability assays

Cell viability and immune cell immunophenotypes were analyzed using fluorescence-activated cell sorting (FACS). mPEG and rPEGs were purified by semi-preparative HPLC to ensure endotoxin-free samples and lyophilized prior to analysis. The viability of primary immune cells and expression of activation markers CD80 and CD86 were determined using human PBMCs. PBMC isolation was performed under sterile conditions using a laminar flow bench. Fluorescent-dye labeled antibodies for flow cytometric analysis were purchased from Thermo Fisher Scientific, BD Bioscience or BioLegend. Human whole blood (CPD-stabilized, citrate-phosphate buffer) of healthy donors was received from the transfusion central of the University Medical Centre of the Johannes Gutenberg University Mainz. The PBMCs were isolated using the common density gradient technique. In detail 20 mL Histopaque-1077 (1.077 g mL^{-1}, Sigma Aldrich) were carefully under-layered with a mixture of 10 mL blood pre-diluted in 10 mL DPBS in 50 mL tubes. Afterward, the tubes were centrifuged (20 min, room temperature, 700 g) with break switched off. The plasma phase and the PBMC

interphase were separately retrieved. The Plasma was heat-inactivated for at least 30 min at 56 °C, centrifuged (10 min, 4 °C, 1500 g) and stored at 4 °C until further usage. The PBMCs of two tubes from one donor (total blood volume 20 mL) were combined in a new 50 mL tube, which was then filled up to 50 mL with DBPS. The mixture was centrifuged (10 min, 4 °C, 600 g) and the supernatant was discarded. The cell pellet was resuspended in fresh DPBS and again filled up to 50 mL with DPBS. This washing procedure was performed five times. Afterwards, the PBMCs were resuspended in RPMI-1640 culture medium (+100 U/mL penicillin, +100 U/mL streptomycin, +50 µM 2-mercaptoethanol, +2 mM L-glutamine) at a concentration of 5×10^6 cells mL^{-1}. Aliquots of 0.450 mL were transferred into FACS tubes. mPEG and rPEG formulations were dissolved in DPBS and added to final concentrations of 5.0, 1.0 and 0.1 mg mL^{-1} to the cell suspensions. Additionally, resiquimod (R848, 0.1 µg mL^{-1}) was prepared in parallel as a positive control to assess immunostimulatory effects. After 16 h of incubation (37 °C, 7.5% CO_2), the samples were centrifuged (10 min, 4 °C, 300 g) and 100 µL aliquots of supernatants were collected and stored at -20 °C for cytokine analysis. Each cell pellet was resuspended in 1 mL human FACS buffer (DPBS, 2 mM EDTA, 0.5 vol-% fetal calf serum), then all samples were centrifuged (10 min, 4 °C, 300 g) and the supernatants were discarded. Afterward, the Fc receptors were blocked for 10 min at 4 °C using 5 µL human FcR blocking reagent (Miltenyi Biotec) to prevent non-specific binding. Lineage and immune activation markers were detected using fluorescence-label antibodies specific for CD80 (PerCP-eFluor710), CD15 (APC), CD20 (V450), CD11b (BV510), CD1c (BV605), CD3 (BV711), CD86 (PE), CD14 (PE-eFluor610) and CD56 (PE-Cy7) for 20 min at 4 °C. The samples were washed twice with 1 mL human FACS buffer. The cells were resuspended in 0.5 mL human FACS buffer and stored at 4 °C until measurement (maximum 3 hours). 0.5 mL of the viability dye solution (30 nM, Sytox™ Green™) was added 15 min before the measurement of each donor. Each sample was stored on ice until immanent flow cytometric measurements using an Attune NxT acoustic focusing cytometer (Lasers: BRVK, Instrument model: 4486521, Thermo Fisher Scientific) with Attune Nxt Software v3.2.1526.0. The raw data was evaluated with Attune NxT software v3.1.1 according to the gating strategy depicted in **Fig. S57**. The exclusion of doublets was applied after the lineage gating to improve the detection of low numbers of small cells in the heterogeneous cell mixture (*29*). Cell viability as well as CD80 and CD86 mean fluorescence intensity (MFI) were normalized to the untreated control for each respective donor. The mean values and the standard deviation were visualized using GraphPad Prism 5.

1.9. Human Inflammatory Cytokine Cytometric Bead Array (CBA)

The contents of interferon-γ (INF-γ), tumor necrosis factor-α (TNF-α), interleukin-1β (IL-1β), interleukin-6 (IL-6) and interleukin-10 (IL-10) were determined using a BD Bioscience Cytometric

Bead Array Flex Kit with minor adjustments according to the manufacturer's protocol. A standard calibration containing all five cytokines was prepared in CBA buffer (DPBS +1.0 vol-% fetal calf serum) comprising 2500, 1250, 625, 312.5, 156, 80, 40, 20, 10 and 0 pg mL^{-1}. A capture bead master mixture was prepared by mixing 0.2 µL/sample of each capture bead with 10 µL/sample CBA buffer. 10 µL of each sample were added to 10 µL master bead mixture and incubated for one hour, in the dark at room temperature. Afterward, 10 µL of the detection reagent master mixture (0.2 µL/sample of each detection reagent in 10 µL/sample CBA buffer) were added and incubated for two hours, in the dark at room temperature. 1 mL of CBA buffer was added to the samples. The tubes were centrifuged (5 min, 4 °C, 300 g) and the supernatants were carefully discarded. 200 µL CBA buffer were added to each sample just before the measurement. The MFI values of each bead were recorded using an Attune NxT acoustic focusing cytometer (Lasers: BRVK, Instrument model: 4486521, Thermo Fisher Scientific) with Attune Nxt Software v3.2.1526.0. The FCS 3.0 files were evaluated using FCAP Array (v1.0.1). The standard calibration curves were calculated with a five-parameter logistic fit function and the respective cytokine concentrations were determined. The concentrations were normalized to the R848 positive control (PBMCs incubated for 16 h with 1 µg mL^{-1} R848) for each respective donor. The mean values and the standard deviation were visualized using GraphPad Prism 5.

$$y = D\ \frac{A - D}{1 + \left(x - \frac{E}{C}\right)^{B}} \qquad \textbf{(S2)}$$

2. Experimental Procedures

2.1. Synthesis of 1-chloro-3-methoxy-propan-2-ol

A 1 L three-necked flask equipped with neodym stirrer bar, reflux condenser and dropping funnel was charged with MeOH (306 g, 388 mL, 9.57 mol) and sulfuric acid (98%, 7 mL, 125 mmol). The flask was immersed in an oil bath and epichlorohydrin (295 g, 250 mL, 3.19 mol) was added dropwise through the dropping funnel to the solution under vigorous stirring. After complete addition of epichlorohydrin, the reaction was heated to reflux and stirred overnight under reflux. The reaction mixture was cooled to room temperature and $BaCO_3$ (37.0 g, 187 mmol) was added under vigorous stirring. After 1 h of stirring, excess MeOH was evaporated under reduced pressure. 1-Chloro-3-methoxy-propan-2-ol (320 g, 2.60 mol, 81%) was obtained as colorless liquid after fractional distillation (T_b = 83-87 °C (85 mbar)) of the residue. ^{1}H and ^{13}C NMR spectra can be found in **Figure S2** and **Figure S3**, respectively.

^{1}H NMR (400 MHz, DMSO-d_6) δ [ppm]: 5.26 (d, J = 5.3 Hz, 1H), 3.87 – 3.71 (m, 1H), 3.61 (dd, J = 11.0, 4.5 Hz, 1H), 3.51 (dd, J = 11.0, 5.6 Hz, 1H), 3.33 (dd, 2H), 3.26 (s, 3H).

^{13}C NMR (100 MHz, DMSO-d_6) δ [ppm]: 73.53 (CH_2), 68.93 (CH), 58.51 (CH_3), 47.12 (CH_2).

2.2. Synthesis of glycidyl methyl ether (GME)

1-Chloro-3-methoxy-propan-2-ol (320 g, 2.57 mol) was added to a three-necked flask equipped with mechanical stirrer, thermometer and reflux condenser. Diethyl ether (320 mL) was added and the solution was cooled to 0 °C with an ice bath under stirring. Sodium hydroxide (123 g, 3.08 mol) was added portion wise to the solution under vigorous stirring while the temperature was kept below 15 °C. The reaction mixture was allowed to reach room temperature over 4 h. The reaction mixture was filtered through a G2 frit and the filter was washed four times with diethyl ether (160 mL each). The combined organic phases were dried over $MgSO_4$ (96 g) and filtered through a pleated filter. The filter was washed with diethyl ether (160 mL). Diethyl ether was evaporated under reduced pressure. Glycidyl methyl ether (156 g, 1.77 mol, 69%) was obtained as a colorless liquid after fractional distillation (T_b = 72-74 °C (300 mbar)) of the residue. ^{1}H and ^{13}C NMR spectra can be found in **Figure S4** and **Figure S5**, respectively.

^{1}H NMR (400 MHz, DMSO-d_6) δ [ppm]: 3.63 (dd, J = 11.4, 2.6 Hz, 1H), 3.28 (s, 3H), 3.16 (dd, J = 11.4, 6.5 Hz, 1H), 3.12 – 3.04 (m, 1H), 2.72 (dd, J = 5.1, 4.2 Hz, 1H), 2.53 (dd, J = 5.1, 2.7 Hz, 1H).

^{13}C NMR (100 MHz, DMSO-d_6) δ [ppm]: 72.90 (CH_2), 58.27 (CH_3), 50.14 (CH), 43.27 (CH_2).

2.3. Synthesis of 1-methoxy-3-(2-methoxyethoxy)propan-2-ol (MMEPOH)

A flame-dried two-necked Schlenk flask equipped with stirrer bar, septum and reflux condenser was charged with 2-methoxy ethanol (33.6 g, 36.0 mL, 442 mmol) under argon. The flask was immersed in an ice-bath. Sodium (2.84 g, 124 mmol) was added portion wise to the alcohol under stirring and argon. The reaction mixture was allowed to reach room temperature. After complete reaction of the sodium, the solution was heated to 55 °C and GME (9.31 g, 9.50 mL, 106 mmol) was slowly added via syringe pump (1 mL h^{-1}) under argon. The reaction mixture was stirred overnight, cooled to room temperature and neutralized by the addition of aqueous 2 M HCl solution. After evaporation of water and excess 2-methoxy ethanol under reduced pressure, 1-methoxy-3-(2-methoxyethoxy)propan-2-ol (12.03 g, 73.2 mmol, 69%) was obtained after fractional distillation (T_b =60 °C (5 10^{-2} mbar)) of the residue. ^{1}H and ^{13}C NMR spectra can be found in **Figure S6** and **Figure S7,** respectively.

^{1}H NMR (400 MHz, DMSO-d_6) δ [ppm]: 4.79 (d, J = 5.2 Hz, 1H), 3.76 – 3.60 (m, 1H), 3.54 – 3.46 (m, 2H), 3.46 – 3.39 (m, 2H), 3.39 – 3.16 (m, 10H).

^{13}C NMR (100 MHz, DMSO-d_6) δ [ppm]: 74.26 (CH_2), 72.63 (CH_2), 71.28 (CH_2), 69.92 (CH_2), 68.38 (CH), 58.41 (CH_3), 58.09 (CH_3).

2.4. Synthesis of polyether copolymers (rPEG)

Caveat: Ethylene oxide is a highly flammable and toxic gas; it must be handled by trained researchers and staff!

The following synthesis protocol was applied for rPEG samples $rPEG_{112}^{0.21}$, $rPEG_{112}^{0.43}$ and $rPEG_{110}^{0.55}$. The EO and GME ratio varied depending on the targeted GME content. In the case of $rPEG_{109}^{0.74}$, two sequential comonomer addition steps were performed, each with half of the total EO and GME amounts. The second addition was performed after full conversion of both comonomers of the first addition.

Potassium *tert*-butoxide (KO*t*Bu) (21.0 mg, 191 µmol) was dissolved in stabilizer-free THF and small quantities of Millipore water and transferred into a flame-dried and argon flushed flask equipped with a teflon stopcock and a septum. MMEPOH (32.0 mg, 195 µmol) was dissolved in benzene and transferred into the flask. High vacuum ($1 \cdot 10^{-3}$mbar) was applied to the flask and the solvents were removed at 30 °C. The resulting initiator salt was further dried under high vacuum at 60 °C overnight. The initiator salt was dissolved in dry DMSO (10 mL). After freezing the resulting solution at -80 °C, CaH_2-dried glycidyl methyl ether (GME) (97.9 mg, 1.00 mL, 11.1 mmol) was added to the

flask via syringe. Ethylene oxide (EO) (48.9 mg, 500 µL, 11.1 mmol) was added to the flask via cryo-transfer from a graduated ampoule. The cooling bath was removed, and the reaction mixture was allowed to reach room temperature. The resulting solution was stirred for 1 d at 30 °C under static high vacuum. The flask was ventilated and DMSO was evaporated under reduced pressure. The residue was redissolved in diethyl ether (17 mL) and toluene (2 mL) and acetic acid (34.0 µL) was added under stirring. After 15 min the reaction mixture was filtered through a dense layer of celite. $rPEG_{110}^{0.55}$ (1.44 g, 96%) was obtained as a yellow-colored viscous liquid after evaporation of the solvents and excess acetic acid under reduced pressure. ^{1}H NMR spectra of all synthesized rPEGs can be found in **Figure S44**.

^{1}H NMR (D_2O, 400 MHz) δ [ppm]: 3.85-3.45 (m, polyether backbone), 3.36 (s, OCH_3).

2.5. *in-situ* ^{1}H NMR kinetics

The following procedure was applied for all kinetics. This exemplary procedure describes the copolymerization of EO with GME in anisole at 55 °C with a degree of deprotonation of 90 %. Measurements in DMSO and toluene were performed using the respective deuterated solvents. Reactivity ratios and reaction rates were determined from *in situ* ^{1}H NMR measurements.

Preparation of the initiator salt solution: In a flame-dried Schlenk flask equipped with a rubber septum and a stirring bar, 2-(benzyloxy)ethanol (44.7 mg, 294 µmol, 1 eq.) and KO^{t}Bu (29.7 mg, 0.264 mmol, 0.9 eq.) were dissolved in benzene (8 mL, dried over MS 4 Å). For kinetics utilizing [18]crown-6, a dry benzene solution, using 2 equivalents per potassium cation was added. The mixture was heated under static vacuum for 1 h at 60 °C. The solvents were removed *in vacuo* overnight at 60 °C, yielding the dry, partially deprotonated initiator salt. Subsequently, anisole (2.22 mL, dried over CaH_2) was added. The mixture was heated for 1 h at 60 °C and allowed to cool to room temperature.

Preparation of the polymerization mixture: EO was cryo-transferred into an oven-dried *Norell S-500-VT-7* sealable NMR tube with a Teflon stopcock using an acetone/liquid N_2 bath and static vacuum. Under argon counterflow, glycidyl methyl ether (50.0 µL, 587 µmol, 10 eq., dried twice over CaH_2) and one-fifth of the initiator salt solution was added. The mixture was degassed by applying three freeze-pump-thaw cycles using the acetone/liquid N_2 bath. Then, the NMR tube was transferred into the preheated NMR device. After the kinetics study, the solvents were removed by applying a nitrogen stream to the solution.

Caveat: We experienced seldom break of the NMR tube if subjected to liquid nitrogen. We strongly recommend only using an acetone/liquid N_2 bath for cooling. Ethylene oxide is a highly flammable and toxic gas; it must be handled by trained researchers and staff!

3. Supplementary Text

3.1. Sample description

The samples composition is described with

$$\mathrm{rPEG}^{f}_{DP}$$

where *f* is the molar fraction of GME in the sample and *DP* the total degree of polymerization. All samples carry a methoxy and hydroxy group at the *α*- and *ω*-group, respectively.

3.2. Calculation of incorporated GME content and achieved degree of polymerization

The calculation of the GME content and total degree of polymerization (DP_{total}) in the rPEG samples is not feasible via end group analysis from their respective ^{1}H NMR spectrum because of the overlap of methoxy groups deriving from the initiator and the methoxy methylene side groups. Therefore, the GME content was determined by a combination of MALDI ToF MS and ^{1}H NMR spectroscopy. First, the number average molecular weight ($M_{\mathrm{n,MALDI}}$) and the ratio ($I_{\mathrm{backbone}}/I_{\mathrm{MeO}}$) of the integrals of backbone signals (I_{backbone}) from 3.90 to 3.45 ppm to methoxy groups signals (I_{MeO}) from 3.45 to 3.25 ppm was determined via MALDI ToF MS and ^{1}H NMR spectroscopy, respectively. Based on the relationship

$$\left(\frac{I_{\mathrm{backbone}}}{I_{\mathrm{MeO}}}\right) = \frac{5 \cdot DP_{\mathrm{GME}} + 4 \cdot DP_{\mathrm{EO}}}{3 \cdot DP_{\mathrm{GME}} + 3} \qquad \textbf{(S3)}$$

and

$$DP_{\mathrm{total}} = DP_{\mathrm{GME}} + DP_{\mathrm{EO}} = \frac{M_{\mathrm{n,MALDI}} - M_{\mathrm{initiator\,group}} - M_{\mathrm{end\,group}}}{44.05 \cdot \left(\frac{100 - mol\%_{\mathrm{GME}}}{100}\right) + 88.11 \cdot \left(\frac{mol\%_{\mathrm{GME}}}{100}\right)} \qquad \textbf{(S4)}$$

DP_{GME} and therefore the molar content of GME ($mol\%_{\mathrm{GME}}$) and DP_{total} of the sample can be determined by choosing values that fit the experimental data. It is important to note that the GME and EO repeating unit of the initiator is included in DP_{GME} and DP_{EO}, respectively. The obtained values can be found in **Table S3** and **Table S4**.

3.3. Determination of diffusion coefficients and hydrodynamic radii

To determine the diffusion coefficient (*D*) of the investigated polymer samples, the decay of the polymer backbone signal between 3.85-3.35 ppm in the DOSY NMR (**Fig. S48 – S52**) was integrated and the resulting data points were fitted with a three-parameter fit,

$$I = B + F \cdot e^{-gD} \quad \textbf{(S5)}$$

wherein *I* is the intensity of the signal, *g* is the gradient strength, *D* is the diffusion coefficient and *B* and *F* are fit-dependent values. From the obtained *D*, the hydrodynamic radii (r_H) were calculated utilizing the rearranged Stokes-Einstein equation

$$r_{\mathrm{H}} = \frac{k_B T}{6\pi\eta D} \quad \textbf{(S6)}$$

wherein k_B is the Boltzmann constant, *T* the applied temperature and η the viscosity of the solvent at *T*. **Table S7** shows an overview of the obtained *D* and r_H. The obtained values were compared to the expected values of the PEG fit (**Fig. S53**).

3.4. Determination of retention times and purification of rPEGs and mPEG via HPLC

An analytical reversed-phase (RP) HPLC method (**Fig. S41**) was applied to analyze the dependence of the mPEG and rPEG samples' properties on the interaction with the hydrophobic column material. Herein, the retention time of a sample depends on both the molecular weight and the polarity of the polymer sample. Therefore, it is possible to estimate the polarity of the rPEG samples by comparing their retention times relative to the one of mPEG (*30*). In the case of the rPEG samples, a trend is observed. The increase of GME content results in increasing retention times (**Fig. S41**, **Table S5**) which can be attributed to both the increase in molecular weight and a decrease in polarity of the rPEG samples. This is in accordance with the observed cloud points of the turbidimetry measurements (**Table S6**).

In similarity to the analytical results, product fractions obtained from the semi-preparative purification depended on the comonomer composition, molecular weight and polarity of the samples (**Fig. S43**). Repetitions of the purification runs using the same conditions resulted in identical purity profiles and GME contents of the samples (**Fig. S46**).

3.5. ELISAs of PGME with different α-end groups and selection of initiator

The influence of methoxy methylene groups of PGME on the interaction of end group-specific APAs was assessed via ELISA. Therefore, PGME homopolymers without terminal methoxy groups (BisOH-PGME), with an α-methoxy group followed by two EO repeating units MeO-$(EO)_2$-PGME and with

an α-methoxy group followed by three EO repeating units (MeO-$(EO)_3$-PGME) were compared. mPEG (2 kg mol^{-1}) was utilized as a reference. As presented in **Fig. S40**, the end group-specific APA exhibits no affinity for BisOH-PGME and MeO-$(EO)_2$-PGME in the tested concentration range. A binding is visible for MeO-$(EO)_3$-PGME and its affinity is 10.8 times lower than for mPEG. Based on these results, MMEPOH was chosen as initiator (**Fig. 1A**) to allow a direct comparison of all rPEG samples and prevent the formation of an epitope at the α-chain end because of the statistical nature of the monomer incorporation. MMEPOH consists of a methoxy group followed by one EO and one GME repeating unit resembling the polymer backbone and the isomeric character of rPEG.

3.6. Calculation of EO Sequences in rPEGs

Calculations were performed based on the following fundamentals (*31*). The copolymerization of two monomers M_1 and M_2 can be divided in four propagation reactions

$$M_1^* + M_1 \rightarrow M_1^*$$

$$M_1^* + M_2 \rightarrow M_2^*$$

$$M_2^* + M_1 \rightarrow M_1^*$$

$$M_2^* + M_2 \rightarrow M_2^*$$

where M_1^* and M_2^* represent the polymer chain end with an active chain end of an ultimate M_1 and M_2 unit, respectively. The consumption rate is described by

$$\frac{d[M_1]}{dt} = k_{11}[M_1^*][M_1] + k_{21}[M_2^*][M_1] \quad \textbf{(S7)}$$

$$\frac{d[M_2]}{dt} = k_{12}[M_1^*][M_2] + k_{22}[M_2^*][M_2] \quad \textbf{(S8)}$$

where k_{11}, k_{21}, k_{12}, k_{22} are the rate constants. Combining the equations with the reactivity ratios r_1 and r_2 which are defined as

$$r_1 = \frac{k_{11}}{k_{12}} \quad \textbf{(S9)}$$

$$r_2 = \frac{k_{22}}{k_{21}} \quad \textbf{(S10)}$$

respectively, one obtains the copolymerization composition equation

$$\frac{d[M_1]}{d[M_2]} = \frac{[M_1](r_1[M_1] + [M_2])}{[M_2]([M_1] + r_2[M_2])} \quad \textbf{(S11)}$$

Based on mole fractions, the copolymerization composition equation can be expressed as

$$F_1 = \frac{r_1 f_1^2 + f_1 f_2}{r_1 f_1^2 + 2 f_1 f_2 + r_2 f_2^2} \quad \textbf{(S12)}$$

or

$$\frac{F_1}{F_2} = \frac{f_1(r_1 f_1 + f_2)}{f_2(r_2 f_2 + f_1)} \quad \textbf{(S13)}$$

where f_1 and f_2 are the mole fractions of monomers M_1 and M_2 in the feed, respectively, and F_1 and F_2 are the mole fractions of M_1 and M_2 in the copolymer, respectively. In the case of a random copolymerization ($r_1 = r_2 = 1$) no composition drift is obtained because $f_1 = F_1$ and $f_2 = F_2$ over the whole range of the copolymerization. This allows a simplified calculation of the mole fraction of a sequence of M_1 units $N_{1,x}$ over the whole polymer chain with

$$N_{1,x} = (p_{11})^{(x-1)} p_{12} \quad \textbf{(S14)}$$

Where p_{11} and p_{12} are the probability of forming a M_1M_1 and M_1M_2 dyad, respectively, and x is the sequence length from 1 to infinity. p_{11} and p_{12} are defined as

$$p_{11} = \frac{r_1}{r_1 + ([\mathrm{M_2}]/[\mathrm{M_1}])} \quad \textbf{(S15)}$$

$$p_{12} = \frac{[\mathrm{M_2}]}{r_1[\mathrm{M_1}] + [\mathrm{M_2}]} \quad \textbf{(S16)}$$

3.7. Analysis of microstructure based on simulations

To provide an insight into chemical composition distribution, more precisely the consecutive EO repeating units in the rPEGs, simulations were performed. Hence, four polymerizations were conducted *in silico*. For this purpose, the rationale of a living anionic polymerization was taken as a foundation which implies the absence of chain termination or chain transfer reactions and a Poisson distribution of the chain lengths. The copolymerization reaction can be described by the four rate constants: The homo-propagation rate constants k_{11} and k_{22} as well as the cross-propagation rate constants k_{12} and k_{21}. The copolymerization kinetics was assumed to be perfectly random, implying

$$k_{11} = k_{22} = k_{12} = k_{21} \quad \textbf{(S17)}$$

As a result, it was assumed in the simulations that EO and GME monomers possess the same probability to be incorporated into the chain. For each polymerization, 10^4 chains were simulated. The simulations were run with a targeted quantitative conversion and an overall degree of polymerization of 114. Molar ratios of 20 up to 50% of GME with a stepwise increase by 10 mol% were presumed. In **Table S8** the four simulated polymerizations and the respective proportional

occurrence of hektakaidekads (16 consecutive EO units) are listed. To visualize the results of the simulations, 15 exemplary chains for each respective GME content are shown in **Fig. 2, Fig. S54 – S56.**

3.8. Calculation of possible GME unit distributions in individual chains

The number of possible combinations (*P*) of 23 GME units (*k*) in a polymer with a total chain length (*n*) of 114 repeating units can be calculated by

$$P = \binom{n}{k} = \frac{n!}{k!\,(n-k)!} = \frac{114!}{23!\,(114-23)!} = 7.3 \cdot 10^{23} \quad \textbf{(S18)}$$

3.9. *in-situ* ^{1}H NMR kinetics

Rate constants of EO and GME: We investigated the copolymerization of EO and GME in the solvents DMSO-d_6, toluene-d_8, and anisole by *in-situ* ^{1}H NMR kinetics studies. EO and GME were copolymerized in the respective solvents in an NMR tube with a sealable Teflon stopcock. Copolymerizations were conducted with the potassium salt of 2-(benzyloxy)ethanol at two different degrees of deprotonation (*dod*) 50% and 90%.

$$dod = \frac{\text{base eq.}}{\text{hydroxyl group}} \cdot 100\% \quad \textbf{(S19)}$$

The *dod* denotes how much base equivalent was added per hydroxyl group of the initiator alcohol to prepare the initiator salt. From the slope of the pseudo-first-order plots of the copolymerization (**Fig. S8 – S13**) obtained from the monomer integrals in the ^{1}H NMR spectra the resulting apparent rate constant of EO ($k_{app,EO}$) was determined based on **equation S29**. This allows the comparison of the reaction rate in different solvents at a constant initiator concentration. Copolymerization in DMSO showed a linear behavior in the pseudo-first-order plots (**Fig S8**). In anisole, a slight induction period was present at the beginning of the copolymerization with both *dod*s (**Fig. S9**, enlargement in **Fig. S10**). In toluene (**Fig. S11**), the induction period is only observed at a *dod* of 50% (enlargement in **Fig. S12**). At the beginning of the copolymerization, the reaction rate increases which can be explained by the dissolution of aggregates, leading to more reactive active species in the copolymerization system. The slope increases slowly after the initial period, comparable to the copolymerization in anisole. A pronounced induction period is observed in DMSO (*dod*: 50%, **Fig. S13**) if a bifunctional initiator was utilized. This induction period slows down the overall reaction due to the relatively slow reaction rate at the beginning of the copolymerization. After the induction period, the reaction rate was comparable to the monofunctional initiator conditions (**Fig. S8 and**

S13). We want to emphasize that the reaction rates of EO in the copolymerization cannot be treated as the homopolymerization reaction rates. Determination of the propagation constant k_p ($[k_p]$ = L mol^{-1} s^{-1}) is not possible, as the aggregation number is unknown. The reaction rate is slightly influenced by a change of *dod* from 50% to 90% in DMSO. Polymerization in anisole occurs twice as fast as in toluene at a *dod* of 50%. However, at a *dod* of 90%, $k_{app,EO}$ in toluene is ≈1.8 times higher than in anisole. Addition of [18]crown-6 further increases the reaction rate by a factor of ≈1.9 compared to the run without [18]crown-6.

Reactivity ratios of EO and GME: Determination of the reactivity ratios (*r*) can be performed by various methods, such as differential and integral methods. Herein, ideal models ($r_1 \cdot r_2 = 1$) which are chain end independent (such as BSL, Jaacks, Ideal Integrated) should be applied if the models adequately describe the data (*32, 33*). The Jaacks method (34) is given by the equation

$$\log\left(\frac{[\mathrm{M}_1]_t}{[\mathrm{M}_1]_0}\right) = r_1 \cdot \log\left(\frac{[\mathrm{M}_2]_t}{[\mathrm{M}_2]_0}\right) \quad \textbf{(S20)}$$

We decided to present the results using the Jaacks method as it is comprehensible and can be readily recalculated. By plotting $\log([M_1]_t/[M_1]_0)$ versus $\log([M_2]_t/[M_2]_0)$, r_1 can be derived from the slope. With the relation $r_1 \cdot r_2 = 1$, both reactivity ratios can be calculated.

Reactivity ratios of the EO/GME comonomer pair were investigated at two different degrees of deprotonation, using the monofunctional 2-(benzyloxy)ethanol (BnO) or 3-ethoxypropane-1,2-diol (EPD). The summarized results can be found in **Table S2**. The results were obtained using the *NIREVAL* software (*1*). **Fig. S15** shows the reactivity ratios in dependence on the *dod*. In DMSO, they do not change significantly. Furthermore, the results indicate a fully random copolymer, as both reactivity ratios are almost one. In anisole, and especially in toluene, the reactivity ratios diverge significantly. This divergence becomes slightly more pronounced when the degree of deprotonation is increased. The difference in reactivity ratios directly affects the polymer composition. While the resulting difference may seem small, **Fig. S16** demonstrates that polymerization in toluene results in a slight gradient microstructure. In contrast, copolymerization in DMSO yields an almost ideal random microstructure. To determine if the reactivity ratios from the DMSO experiment can be applied to toluene, [18]crown-6 was added to reduce the chelation of GME to the potassium counterion. The reaction condition with a *dod* of 90% in toluene was chosen because of the highest difference in reactivity ratios. Unexpectedly, the reactivity ratios converged just slightly (**Fig. S15,** red squares). This finding suggests that the role of the solvent in the copolymerization in DMSO is not yet fully understood. The determined reactivity ratios can be found in **Table S2** and the resulting

GPC curves in **Fig. S32 to Fig. S39**. The use of EPD as a bifunctional initiator yielded the same reactivity ratios as BnO (**Table S2**, entry 8). The copolymer composition was simulated for all experiments and is shown in **Fig. S25 to S31**. In summary, the reaction rates in apolar solvents like toluene and anisole, although slower overall, demonstrate that such solvents remain viable alternatives to DMSO, particularly when specific circumstances make DMSO unsuitable. The faster copolymerization in toluene compared to anisole further underscores the importance of solvent choice. Our results also reveal that increasing the *dod* from 50% to 90% with a monofunctional initiator significantly accelerates copolymerization rates, except in DMSO, where a minor influence is observed.

Derivation of the pseudo-first-order plot:

$$-\frac{\mathrm{d[M]}}{\mathrm{d}t} = k_\mathrm{p} * [\mathrm{I}] * [\mathrm{M}] \quad \textbf{(S21)}$$

$$k_\mathrm{app} = k_\mathrm{p} * [\mathrm{I}] \quad \textbf{(S22)}$$

$$-\frac{\mathrm{d[M]}}{\mathrm{d}t} = k_\mathrm{app}[\mathrm{M}] \quad \textbf{(S23)}$$

$$-\mathrm{d[M]}\frac{1}{[\mathrm{M}]} = k_\mathrm{app}\,\mathrm{d}t \quad \textbf{(S24)}$$

$$-\int_{[\mathrm{M}]_0}^{[\mathrm{M}]_t} \frac{1}{[\mathrm{M}]}\mathrm{d[M]} = k_\mathrm{app}\int_0^t \mathrm{d}t \quad \textbf{(S25)}$$

$$\int \frac{1}{x} = \ln(x) \quad \textbf{(S26)}$$

$$-(\ln([\mathrm{M}]_t) - \ln([\mathrm{M}]_0)) = k_\mathrm{app} * t \quad \textbf{(S27)}$$

$$-\ln\left(\frac{[\mathrm{M}]_t}{[\mathrm{M}]_0}\right) = k_\mathrm{app} * t \quad \textbf{(S28)}$$

$$\ln\left(\frac{[\mathrm{M}]_0}{[\mathrm{M}]_t}\right) = k_\mathrm{app} * t \quad \textbf{(S29)}$$

The Initiator concentration [I] consists of deprotonated and protonated initiator species and assuming all initiator reacts, this equals the concentration of the growing polymer chain ends. It is important to note, that the apparent rate constant k_{app} cannot be converted to k_p by the relation

$k_{\mathrm{p}} = \frac{k_{\mathrm{app}}}{[\mathrm{I}]}$, if the degree of association (or aggregation) is unknown (*8, 9*). If $\ln\left(\frac{[\mathrm{M}]_0}{[\mathrm{M}]_t}\right)$ is plotted versus *t*, the slope yields k_{app}.

4. Scheme S1 to S2

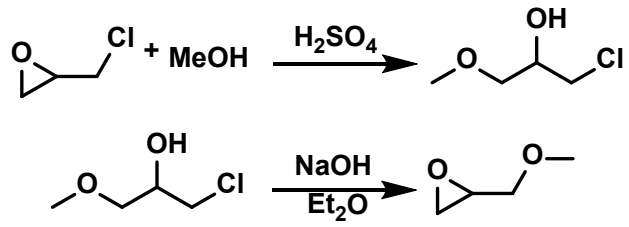

Scheme S1. Synthesis of glycidyl methyl ether.

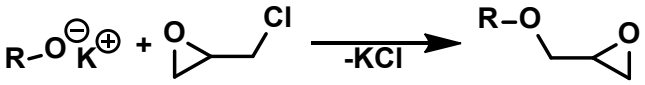

Scheme S2. Occurring chain termination reaction in the presence of epichlorohydrin in the polymerization mixture.

5. Figs. S1 to S66

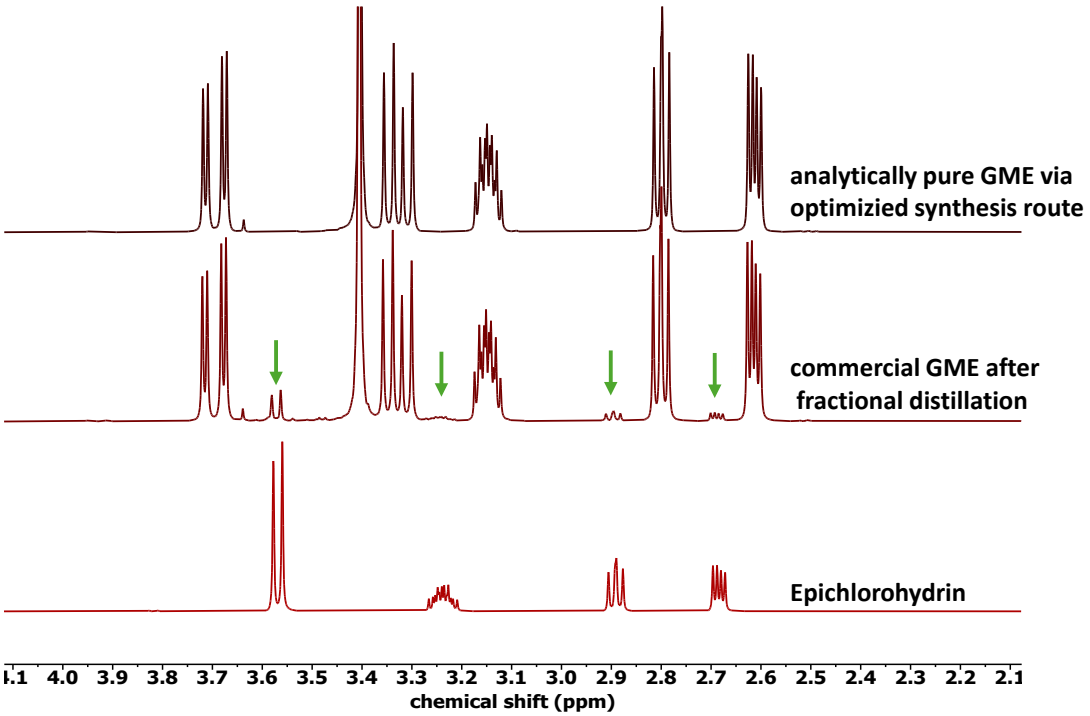

Figure S1. Stacked ^{1}H NMR spectra ($CDCl_3$, 400 MHz) of synthesized GME (top), commercial GME after fractional distillation (middle) and epichlorohydrin (bottom); traces of non-removable epichlorohydrin impurities are indicated via green arrows.

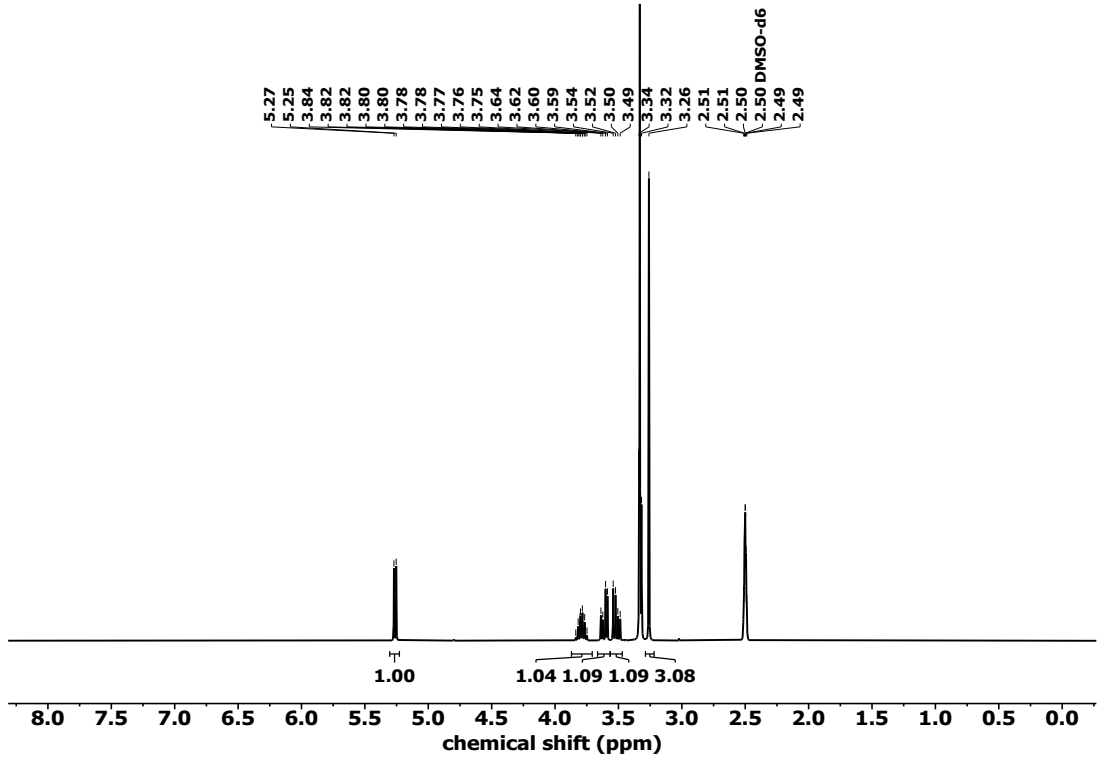

Figure S2. ^{1}H NMR spectrum (DMSO-d_6, 400 MHz) of 1-chloro-3-methoxy-propan-2-ol; Integration of signal at 3.33 ppm (dd) is not possible because of resonance from water traces in DMSO-d_6.

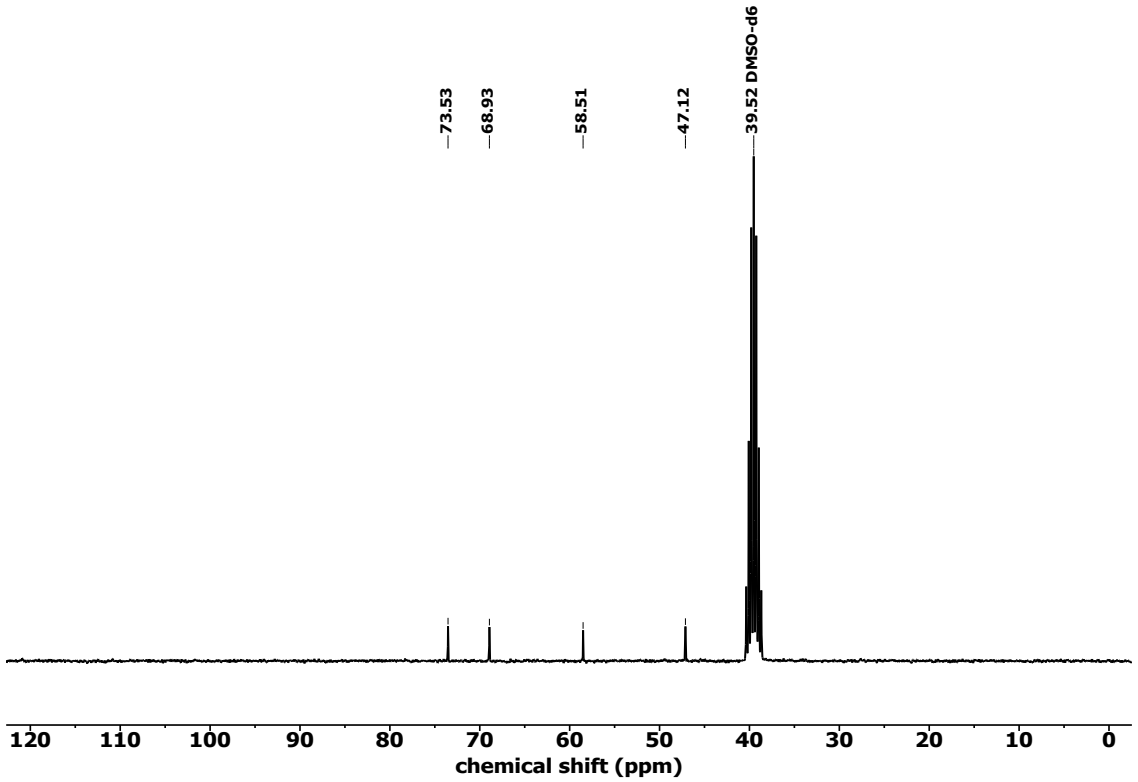

Figure S3. ^{13}C NMR spectrum (DMSO-d_6, 100 MHz) of 1-chloro-3-methoxy-propan-2-ol.

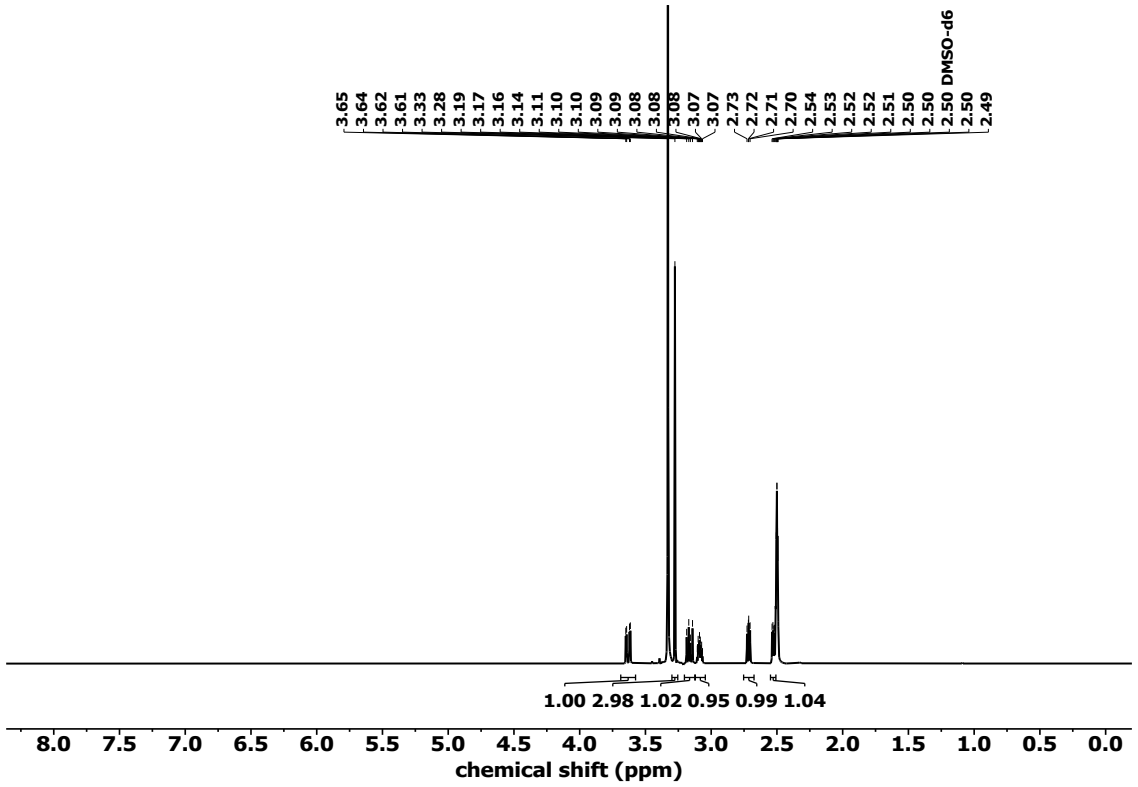

Figure S4. ^{1}H NMR spectrum (DMSO-d_6, 400 MHz) of glycidyl methyl ether.

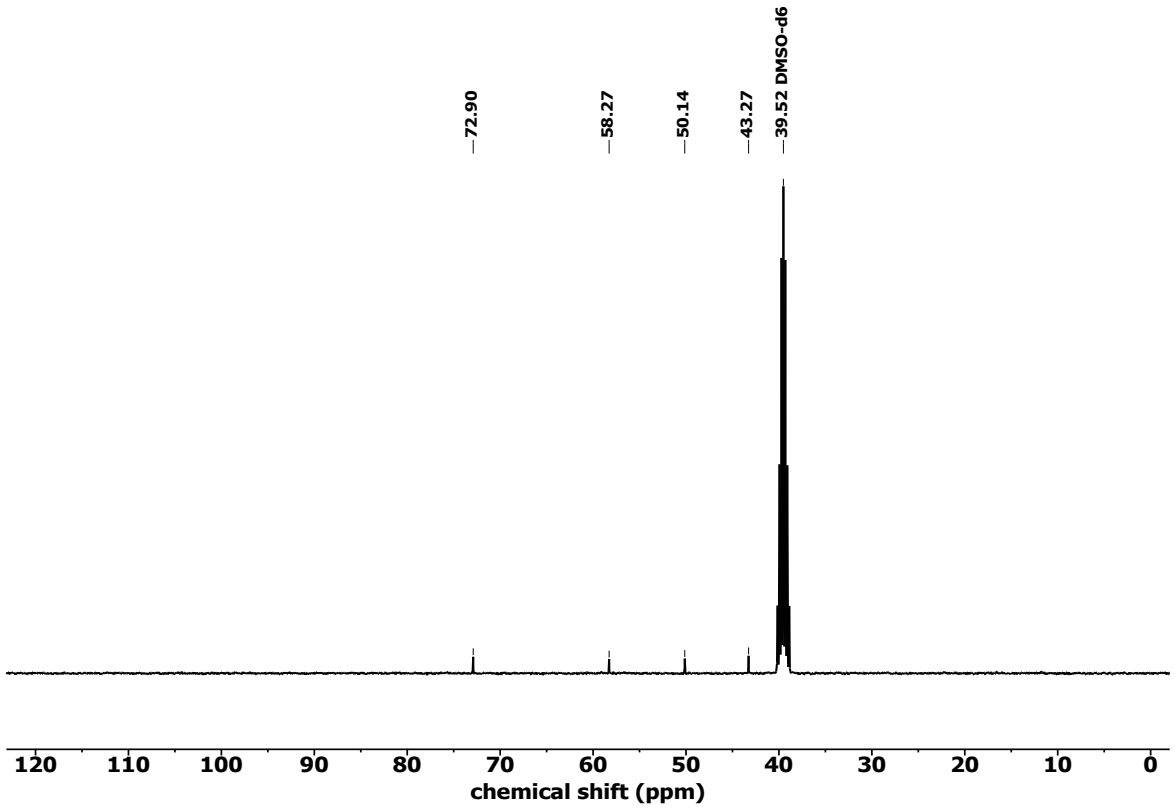

Figure S5. ^{13}C NMR spectrum (DMSO-d_6, 100 MHz) of glycidyl methyl ether.

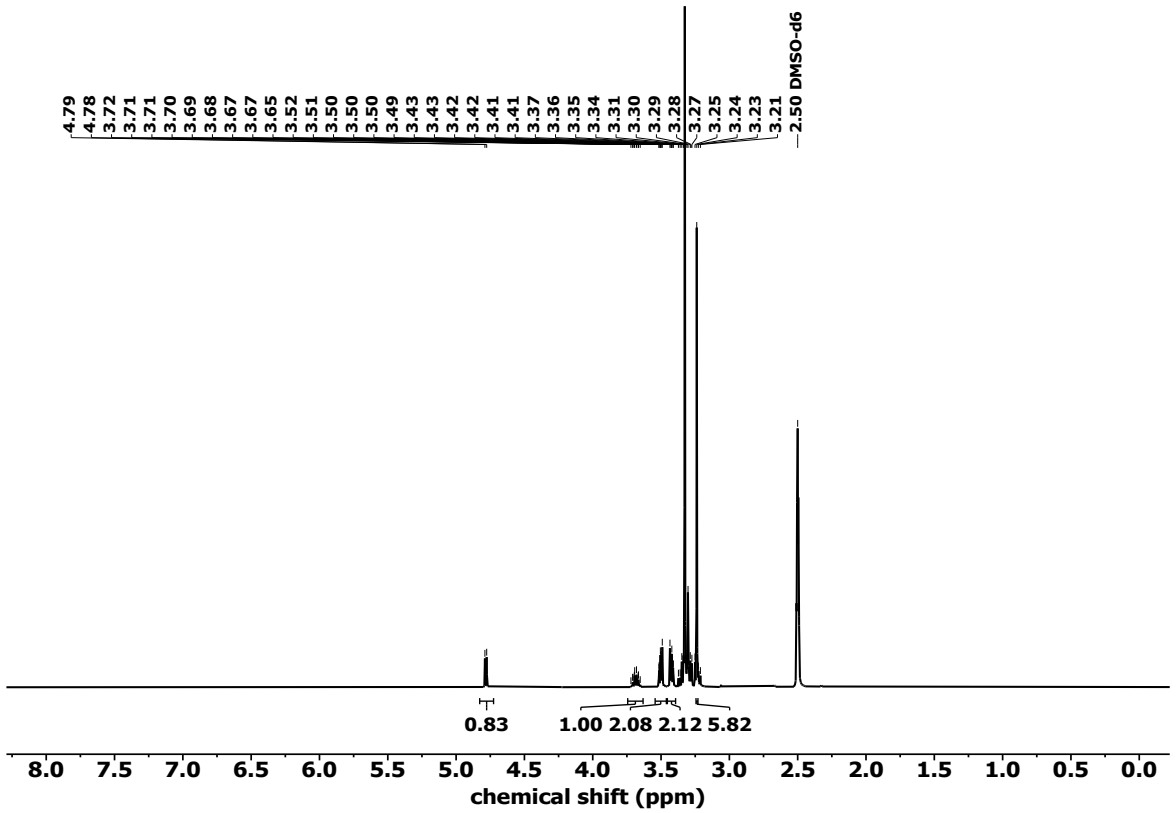

Figure S6. ^{1}H NMR spectrum (DMSO-d_6, 400 MHz) of 1-methoxy-3-(2-methoxyethoxy)propan-2-ol; Integration of signal at 3.38-3.26 ppm (m) is not possible because of resonance from water traces (3.33 ppm) in DMSO-d_6.

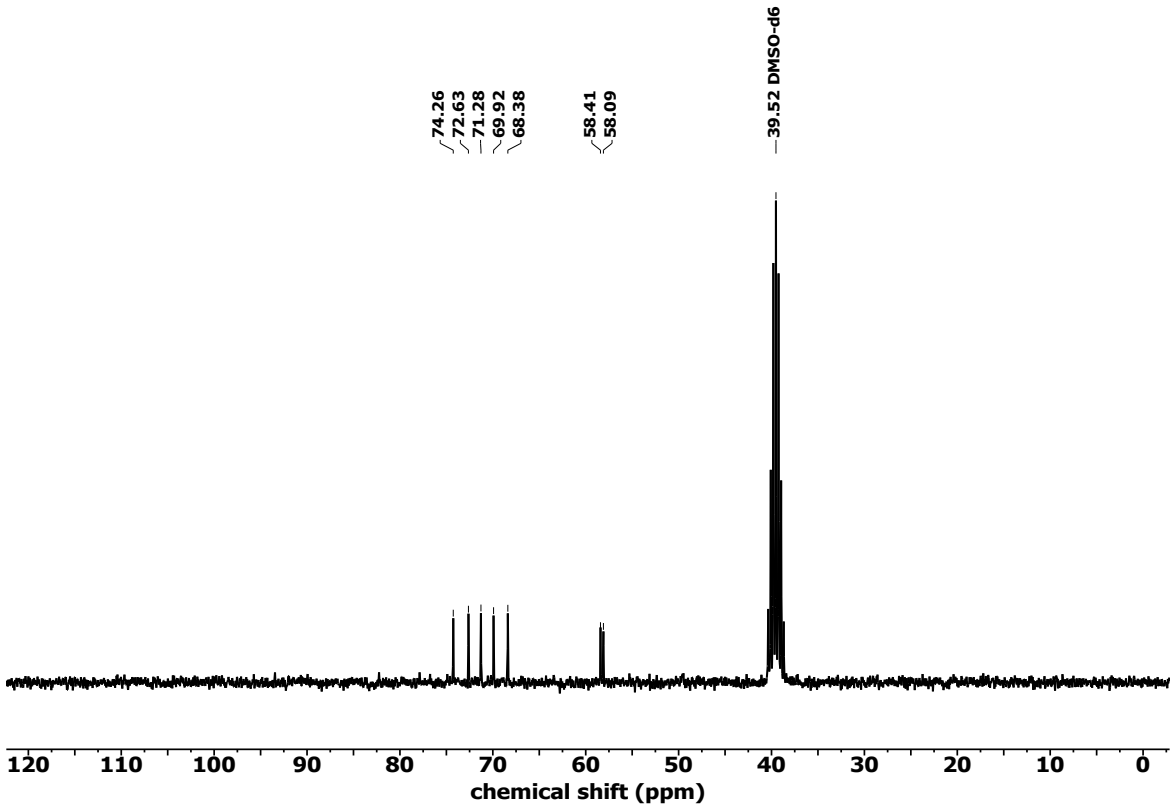

Figure S7. ^{13}C NMR spectrum (DMSO-d_6, 100 MHz) of 1-methoxy-3-(2-methoxyethoxy)propan-2-ol.

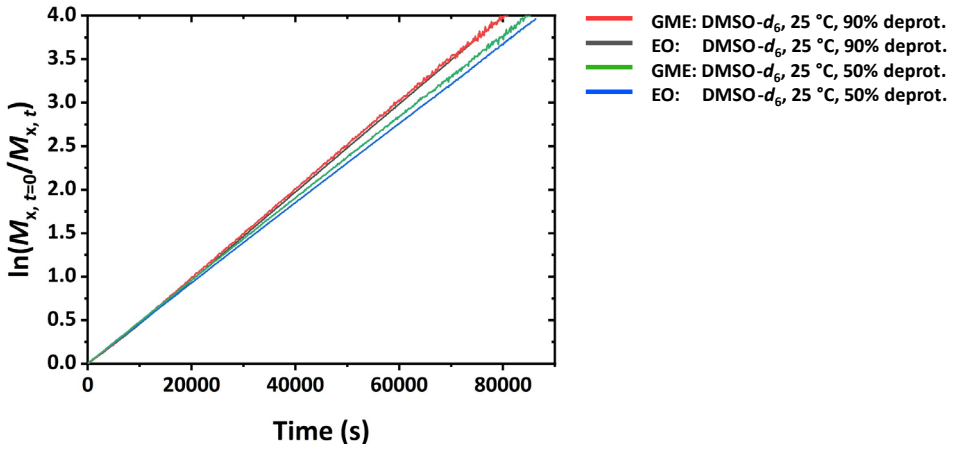

Figure S8. Pseudo-first-order plot of the copolymerization of EO with GME from **Table S1**. Green and blue: entry 1. Red and black: entry 2.

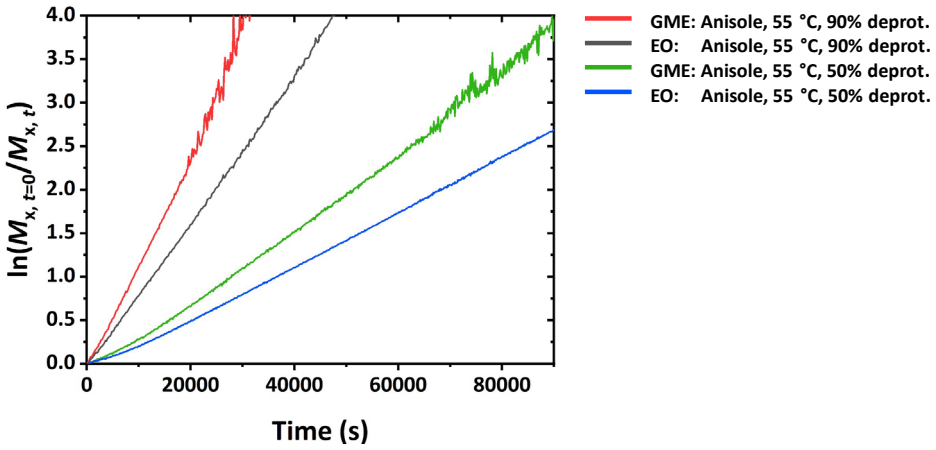

Figure S9. Pseudo-first-order plot of the copolymerization of EO with GME from **Table S1**. Green and blue: entry 3. Red and black: entry 4.

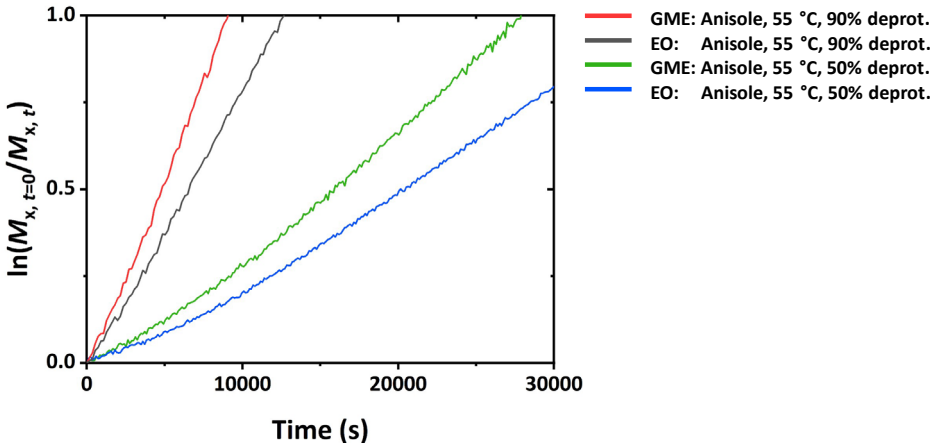

Figure S10. Enlargement of the pseudo-first-order plot of the copolymerization of EO with GME from **Table S1**. Green and blue: entry 3. Red and black: entry 4. The graphs follow nonlinear behavior at the beginning of the copolymerization, indicating an induction period.

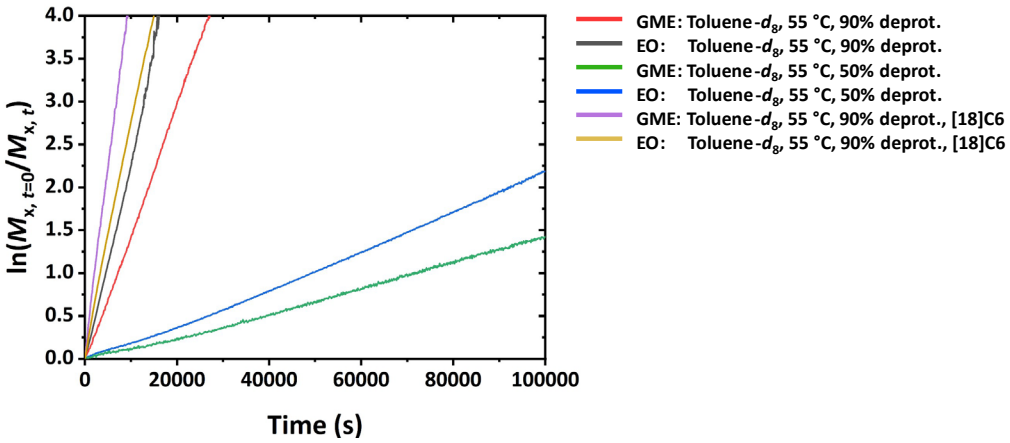

Figure S11. Pseudo-first-order plot of the copolymerization of EO with GME from **Table S1**. Green and blue: entry 5. Red and black: entry 6. Purple and yellow: entry 7.

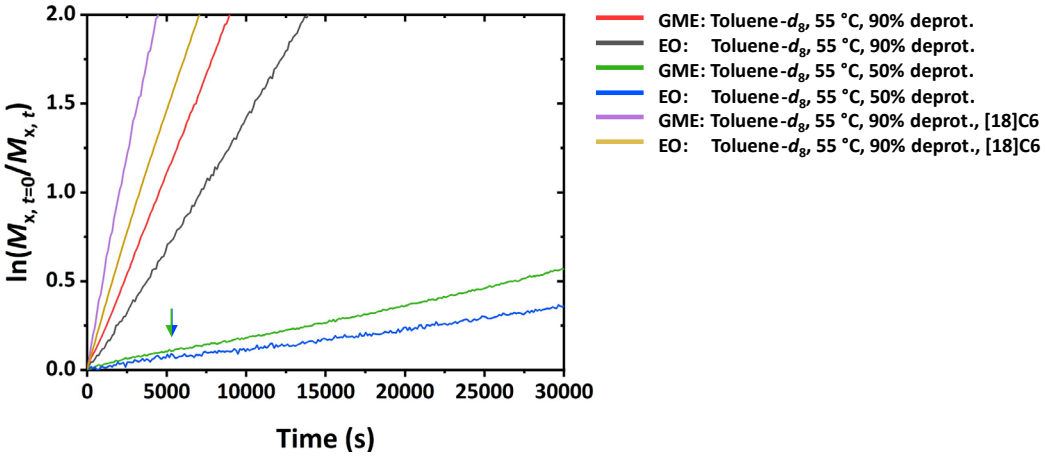

Figure S12: Enlargement of the pseudo-first-order plot of the copolymerization of EO with GME from **Table S1**. Green and blue: entry 5. Red and black: entry 6. Purple and yellow: entry 7. Green-blue arrow marks the end of the time range with an increased reaction rate due to the dissolution of aggregates and/or overheating.

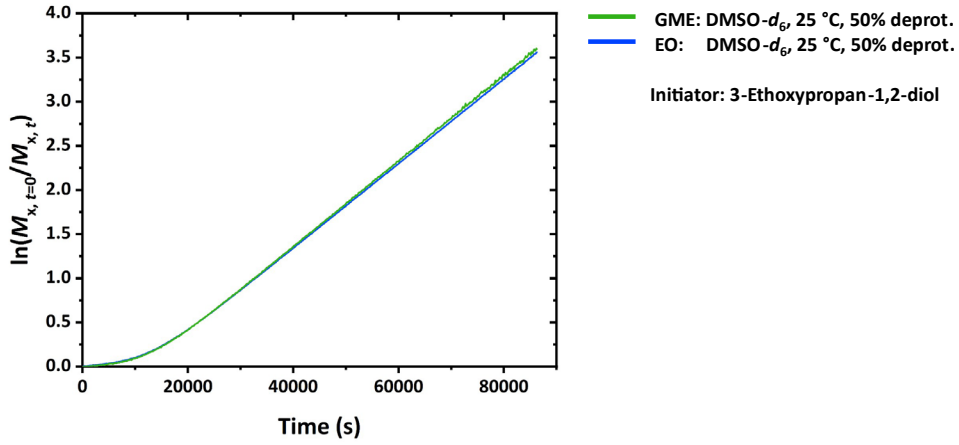

Figure S13: Pseudo-first-order plot of the copolymerization of EO with GME from **Table S1**, entry 8. Active chain end concentration: $3.60 \cdot 10^{-2}$ mol/L.

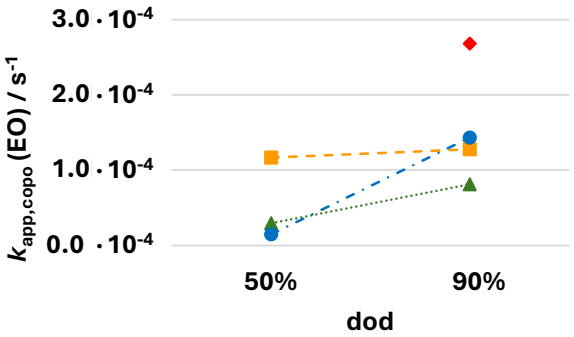

Figure S14. Apparent reaction rates of EO in the copolymerization with GME. The values for experiments in DMSO were adjusted to fit the initiator concentrations of the anisole and toluene experiments. *dod*: degree of deprotonation. Orange squares ■: DMSO, 25 °C. Green triangles ▲: anisole, 55 °C. Blue circles ●: toluene, 55 °C. Red upside square ◆: toluene, 55 °C, [18]crown-6 addition. The values can be found in **Table S1**.

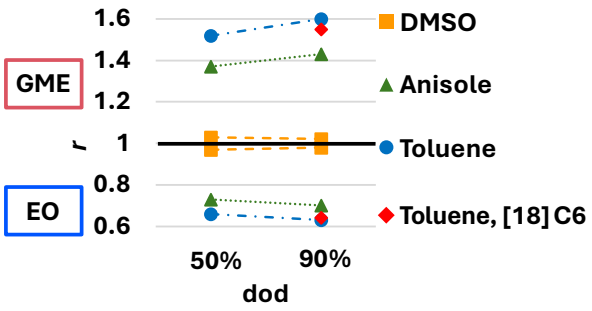

Figure S15. Reactivity ratios of the P(EO-*co*-GME) copolymers. DMSO experiments were conducted at 25 °C, anisole and toluene experiments at 55 °C. *dod*: degree of deprotonation. The values can be found in **Table S2**.

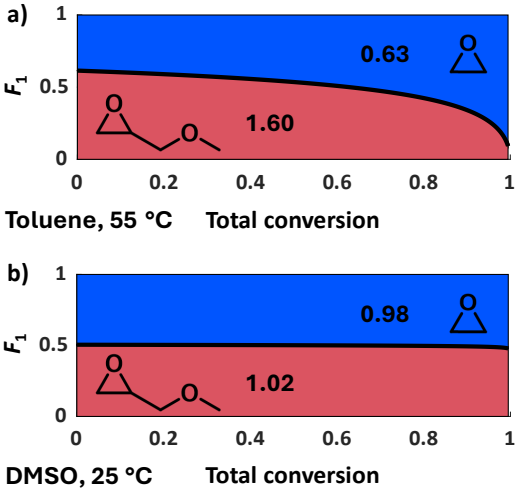

Figure S16. Simulated polymer composition at the denoted polymerization conditions with an equimolar monomer feed and a degree of deprotonation of 90%.

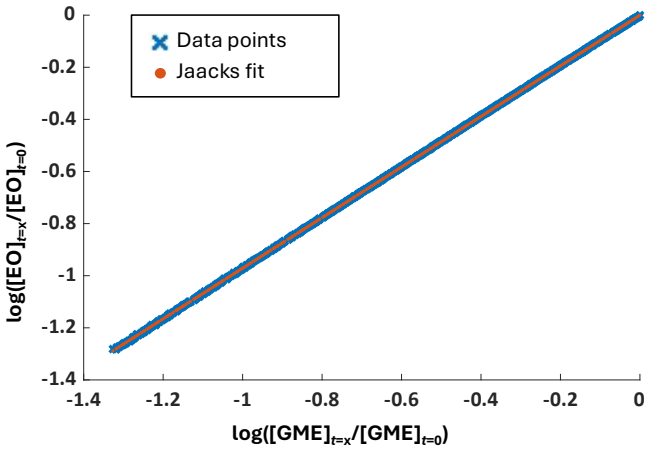

Figure S17. Jaacks fit of the copolymerization of EO and GME from **Table S2**, entry 1.

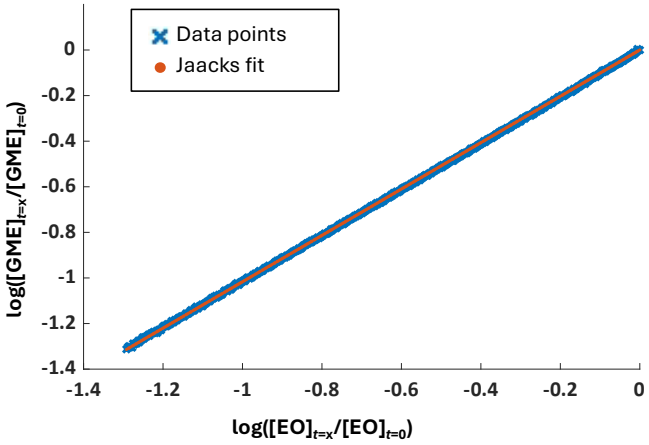

Figure S18. Jaacks fit of the copolymerization of EO and GME from **Table S2**, entry 2.

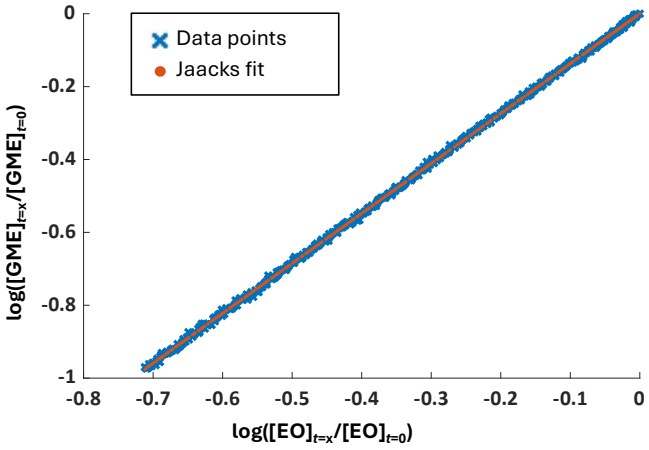

Figure S19. Jaacks fit of the copolymerization of EO and GME from **Table S2**, entry 3. Fit was applied over the whole copolymerization until a conversion of 85%, due to a declining signal-to-noise ratio.

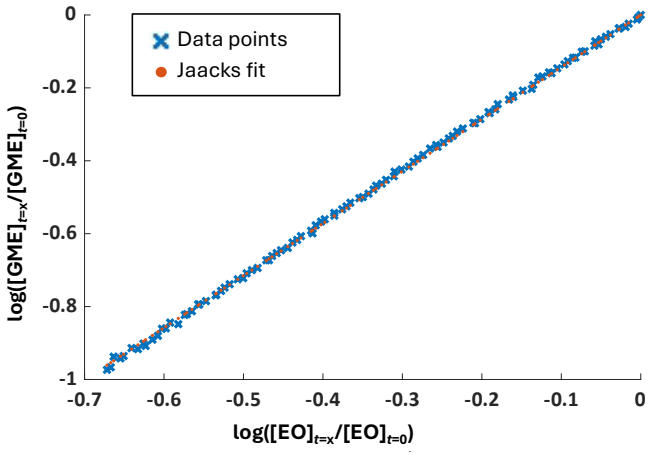

Figure S20. Jaacks fit of the copolymerization of EO and GME from **Table S2**, entry 4. Fit was applied over the whole copolymerization until a conversion of 84%, due to a declining signal-to-noise ratio.

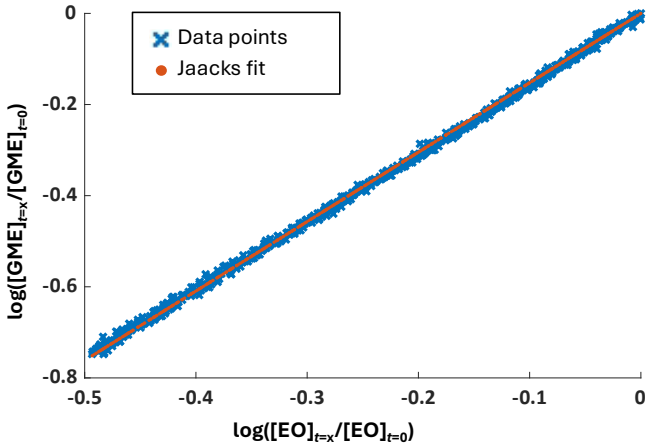

Figure S21. Jaacks fit of the copolymerization of EO and GME from **Table S2**, entry 5. Fit was applied over the whole copolymerization until a conversion of 75%, due to a declining signal-to-noise ratio.

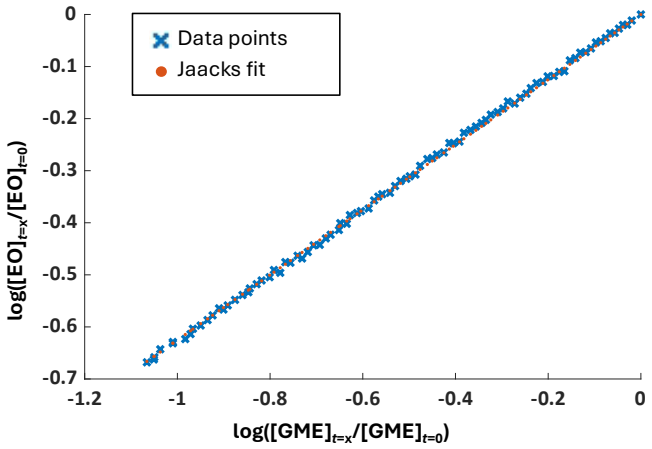

Figure S22. Jaacks fit of the copolymerization of EO and GME from **Table S2**, entry 6. Fit was applied over the whole copolymerization until a conversion of 85%, due to a declining signal-to-noise ratio.

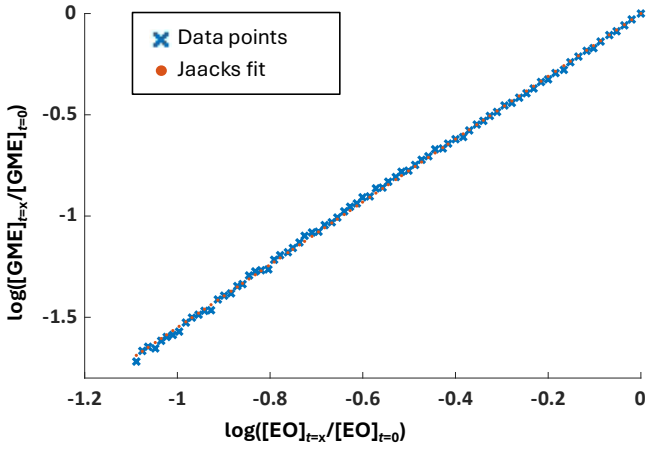

Figure S23. Jaacks fit of the copolymerization of EO and GME from **Table S2**, entry 7.

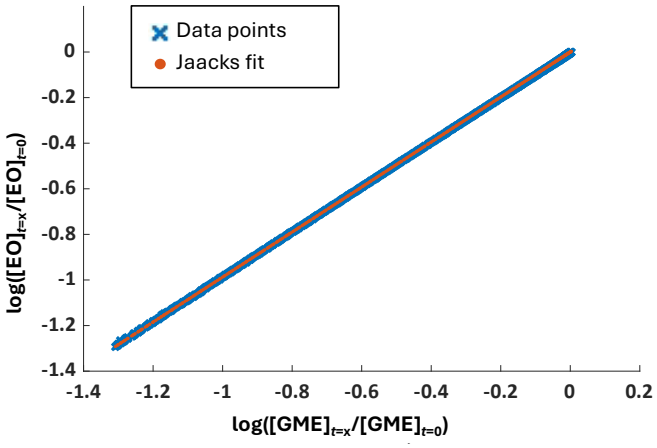

Figure S24. Jaacks fit of the copolymerization of EO and GME from **Table S2**, entry 8. Fit was applied over the whole copolymerization.

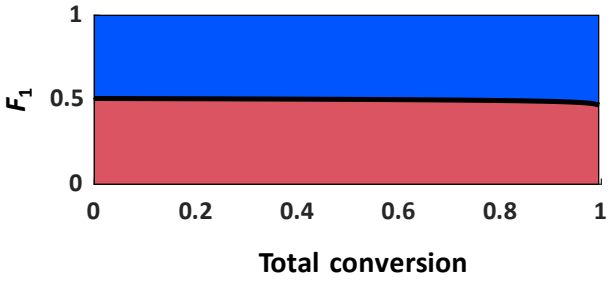

Figure S25. Composition plot of the *in situ* ^{1}H NMR copolymerization kinetic study of EO (blue) with GME (red) with an equimolar monomer ratio (Solvent: DMSO-d_6, 25 °C, *dod*: 50%) with *r*(GME) = 1.03, *r*(EO) = 0.97.

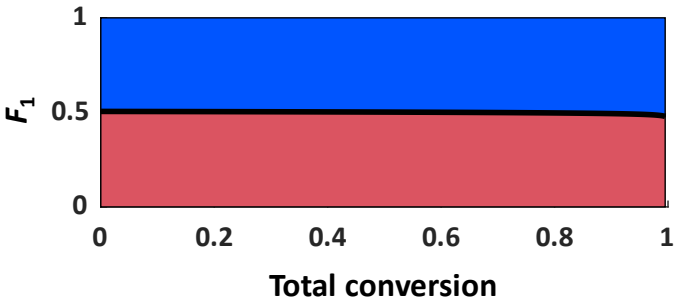

Figure S26. Composition plot of the *in situ* ^{1}H NMR copolymerization kinetic study of EO (blue) with GME (red) with an equimolar monomer ratio (Solvent: DMSO-d_6, 25 °C, *dod*: 90%) with *r*(GME) = 1.02, *r*(EO) = 0.98.

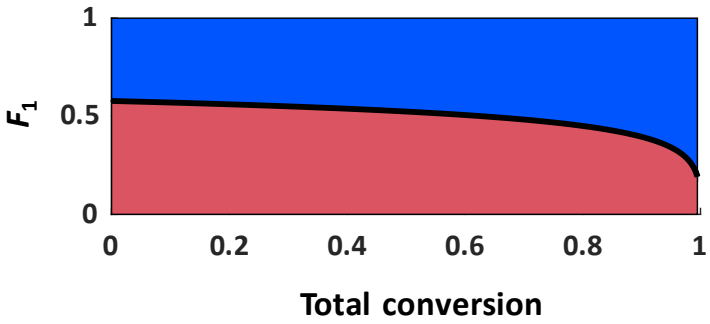

Figure S27. Composition plot of the *in situ* ^{1}H NMR copolymerization kinetic study of EO (blue) with GME (red) with an equimolar monomer ratio (Solvent: anisole, 55 °C, *dod*: 50%) with *r*(GME) = 1.37, *r*(EO) = 0.73.

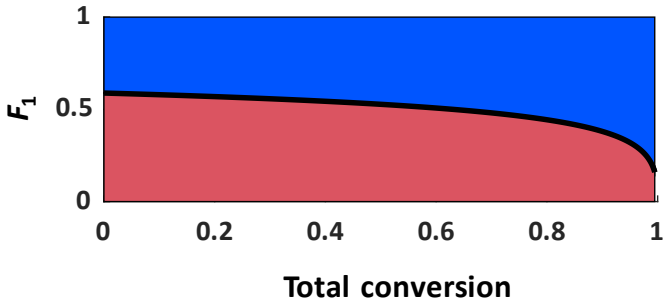

Figure S28. Composition plot of the *in situ* ^{1}H NMR copolymerization kinetic study of EO (blue) with GME (red) with an equimolar monomer ratio (Solvent: anisole, 55 °C, *dod*: 90%) with *r*(GME) = 1.43, *r*(EO) = 0.70.

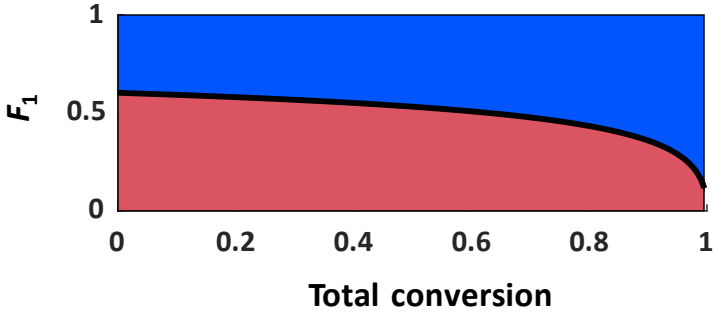

Figure S29. Composition plot of the *in situ* ^{1}H NMR copolymerization kinetic study of EO (blue) with GME (red) with an equimolar monomer ratio (Solvent: toluene-d_8, 55 °C, *dod*: 50%) with *r*(GME) = 1.52, *r*(EO) = 0.66.

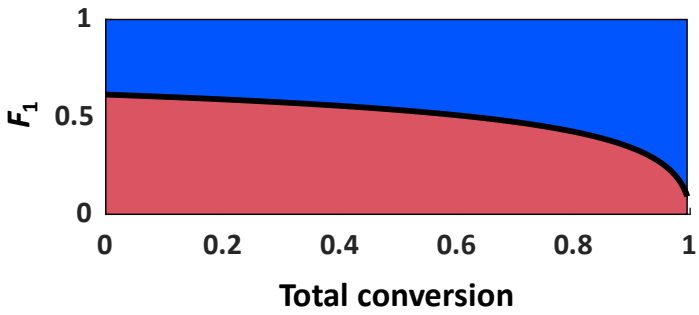

Figure S30. Composition plot of the *in situ* ^{1}H NMR copolymerization kinetic study of EO (blue) with GME (red) with an equimolar monomer ratio (Solvent: toluene-d_8, 55 °C, *dod*: 90%) with *r*(GME) = 1.60, *r*(EO) = 0.63.

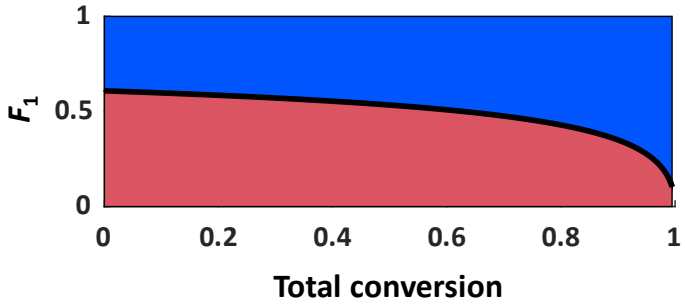

Figure S31. Composition plot of the *in situ* ^{1}H NMR copolymerization kinetic study of EO (blue) with GME (red) with an equimolar monomer ratio (Solvent: toluene-d_8, 55 °C, *dod*: 90%) with *r*(GME) = 1.55, *r*(EO) = 0.64.

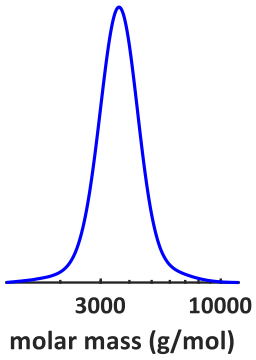

Figure S32. GPC elugram of the polymer obtained after ^{1}H NMR kinetics. Initiator: 2-(benzyloxy)ethanol, solvent: DMSO-d_6, degree of deprotonation: 50%, temperature: 25 °C.

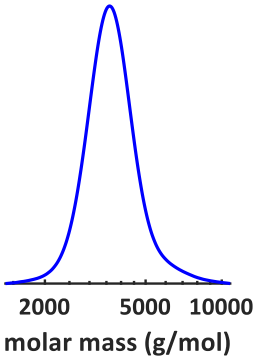

Figure S33. GPC elugram of the polymer obtained after ^{1}H NMR kinetics. Initiator: 2-(benzyloxy)ethanol, solvent: DMSO-d_6, degree of deprotonation: 90%, temperature: 25 °C.

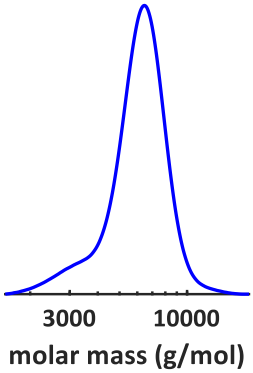

Figure S34. GPC elugram of the polymer obtained after ^{1}H NMR kinetics. Initiator: 3-ethoxypropane-1,2-diol, solvent: DMSO-d_6, degree of deprotonation: 50%, temperature: 25 °C.

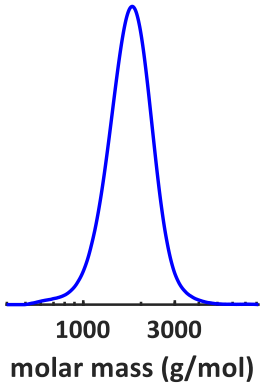

Figure S35. GPC elugram of the polymer obtained after ^{1}H NMR kinetics. Initiator: 2-(benzyloxy)ethanol, solvent: anisole, degree of deprotonation: 50%, temperature: 55 °C.

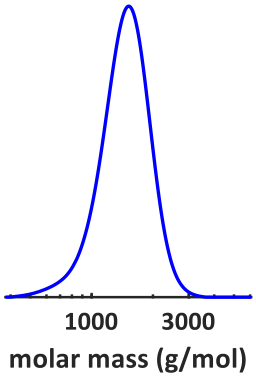

Figure S36. GPC elugram of the polymer obtained after ^{1}H NMR kinetics. Initiator: 2-(benzyloxy)ethanol, solvent: anisole, degree of deprotonation: 90%, temperature: 55 °C.

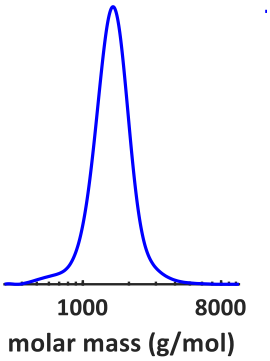

Figure S37. GPC elugram of the polymer obtained after ^{1}H NMR kinetics. Initiator: 2-(benzyloxy)ethanol, solvent: toluene-d_8, degree of deprotonation: 50%, temperature: 55 °C.

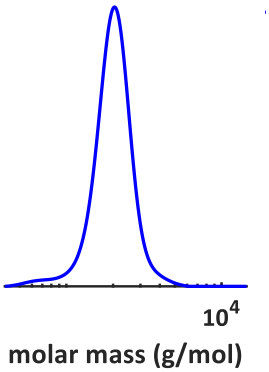

Figure S38. GPC elugram of the polymer obtained after ^{1}H NMR kinetics. Initiator: 2-(benzyloxy)ethanol, solvent: toluene-d_8, degree of deprotonation: 90%, temperature: 55 °C.

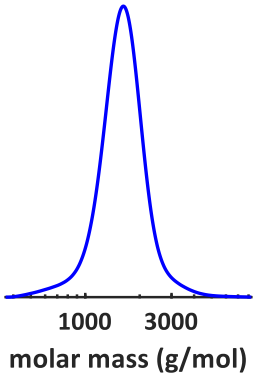

Figure S39. GPC elugram of the polymer obtained after ^{1}H NMR kinetics. Initiator: 2-(benzyloxy)ethanol, solvent: toluene-d_8, degree of deprotonation: 90%, temperature 55 °C, addition of 2 eq. of [18]crown-6 per potassium equivalent.

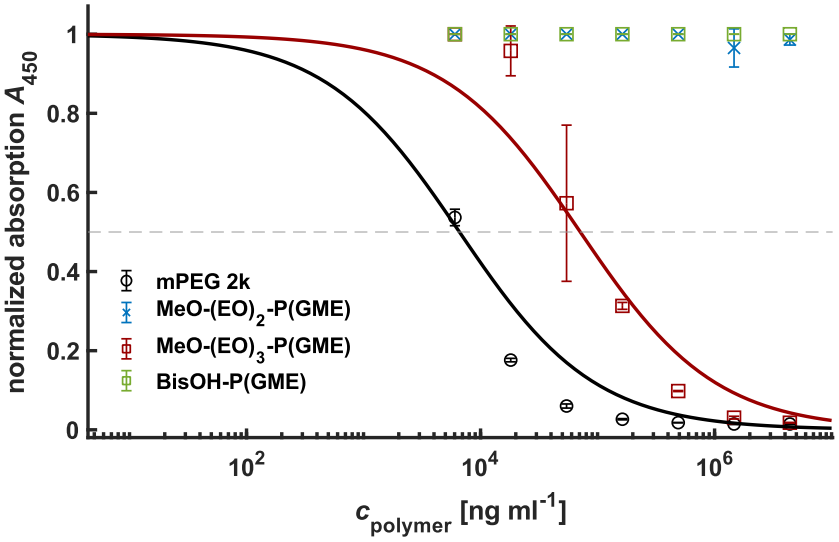

Figure S40. Influence of consecutive EO units at the initiator on the interactions of PGME with end group-specific APA.

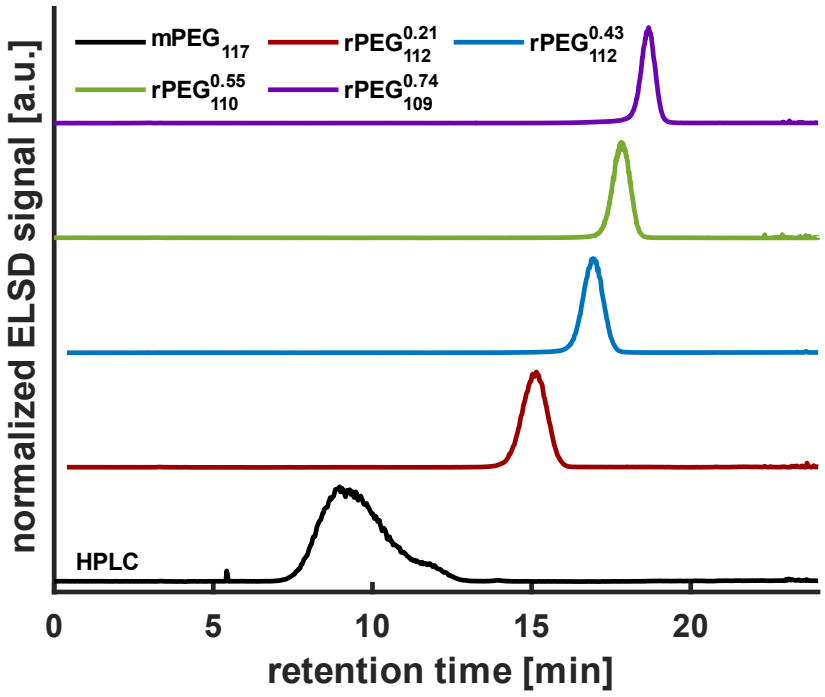

Figure S41. Stacked HPLC elugrams of investigated $mPEG_{117}$ and rPEG samples.

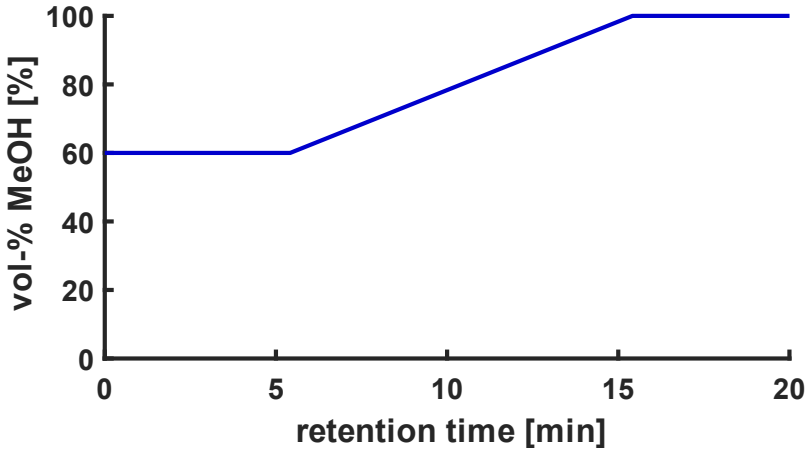

Figure S42. Applied solvent gradient conditions for mPEG and rPEG samples via analytical HPLC.

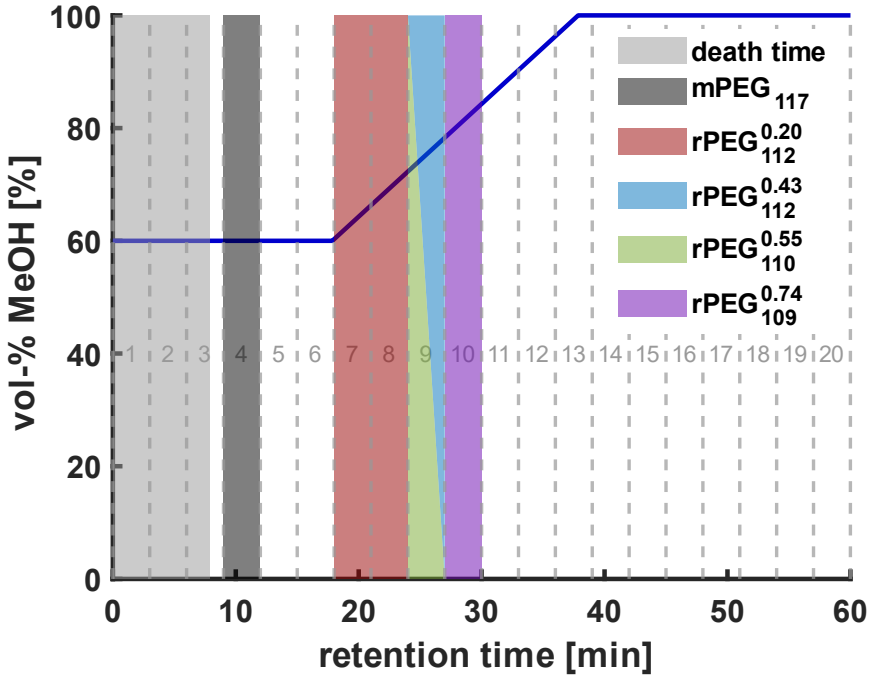

Figure S43. Applied solvent gradient conditions for mPEG and rPEG samples purification via semipreparative HPLC (blue graph); death time and product fractions of each sample are highlighted.

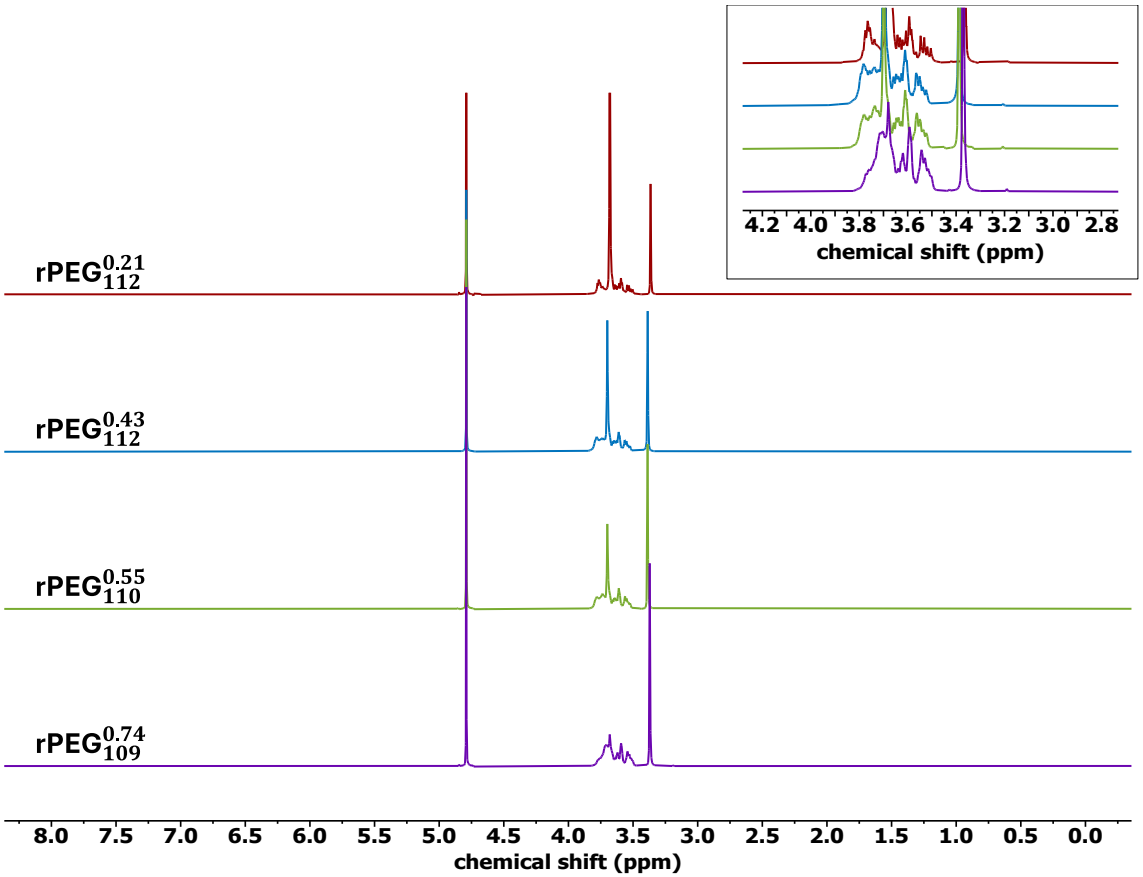

Figure S44. Stacked ^{1}H NMR spectra (D_2O, 400 MHz) of investigated rPEG samples.

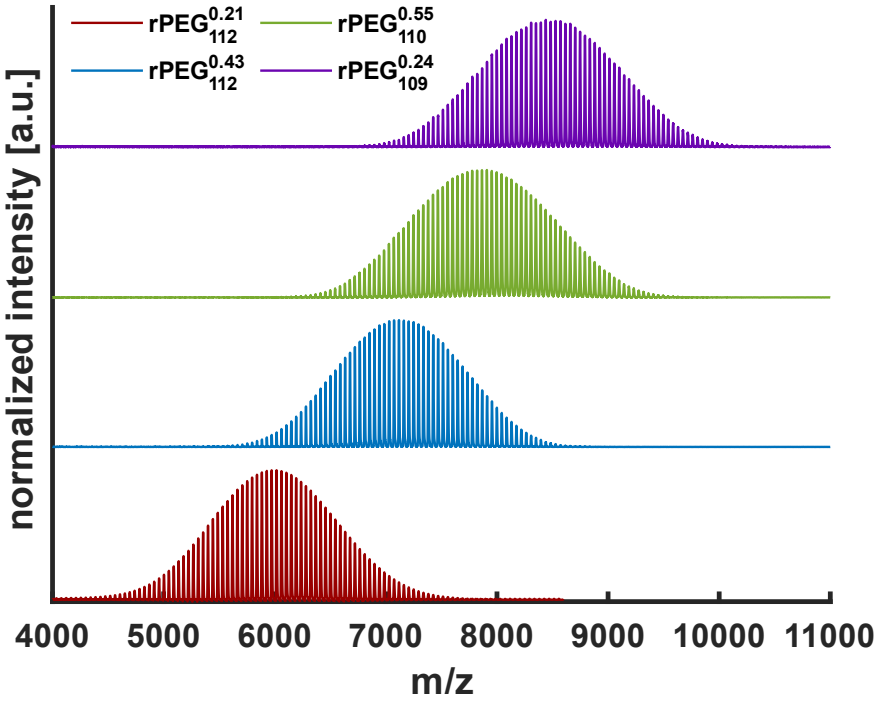

Figure S45. Stacked MALDI ToF mass spectra of synthesized rPEGs before HPLC purification.

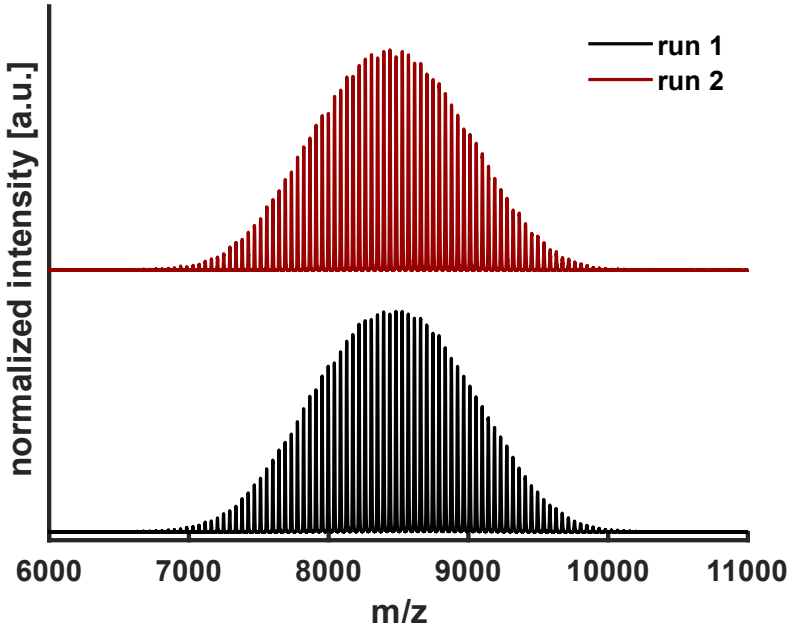

Figure S46. Stacked MALDI ToF mass spectra of purified $rPEG_{109}^{0.74}$ after different runs.

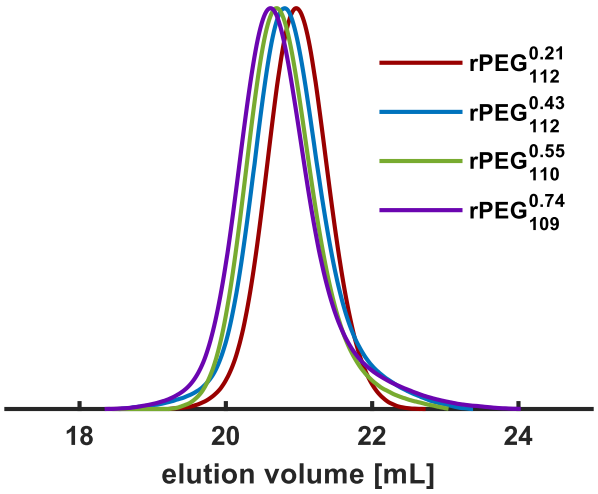

Figure S47. Stacked GPC elugrams of rPEG samples before HPLC purification.

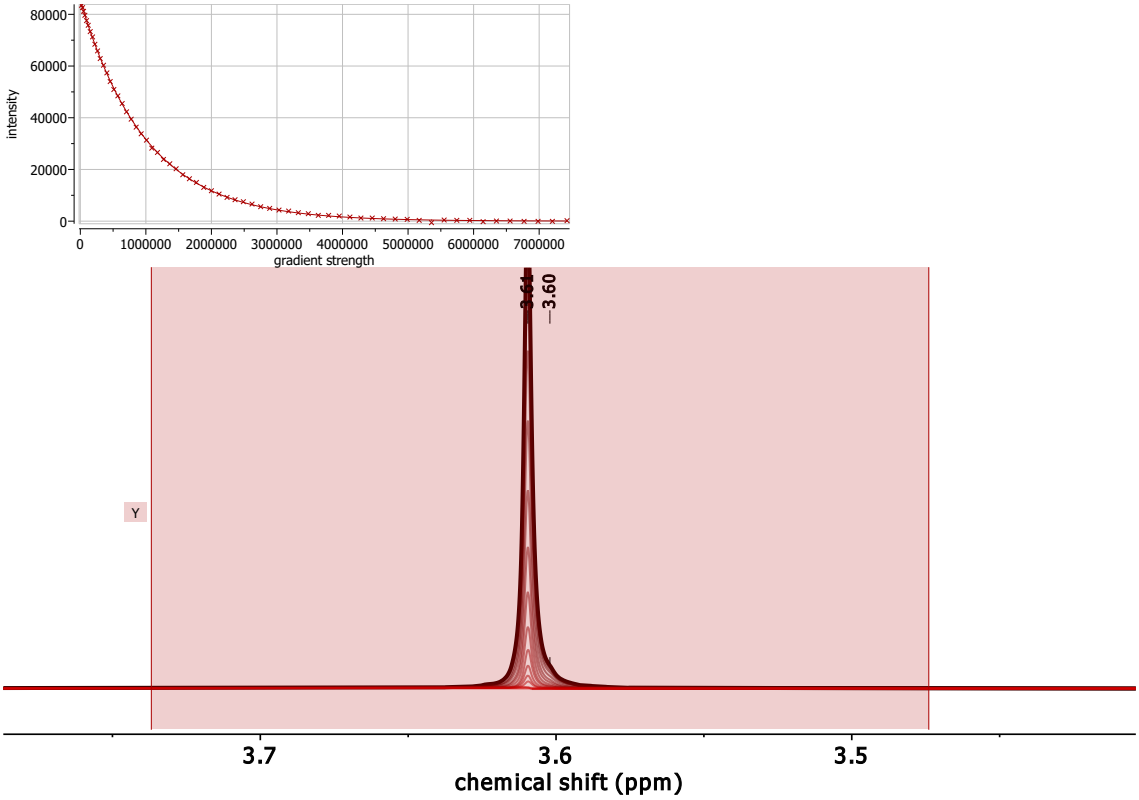

Figure S48. DOSY NMR (400 MHz, D_2O) of $mPEG_{117}$.

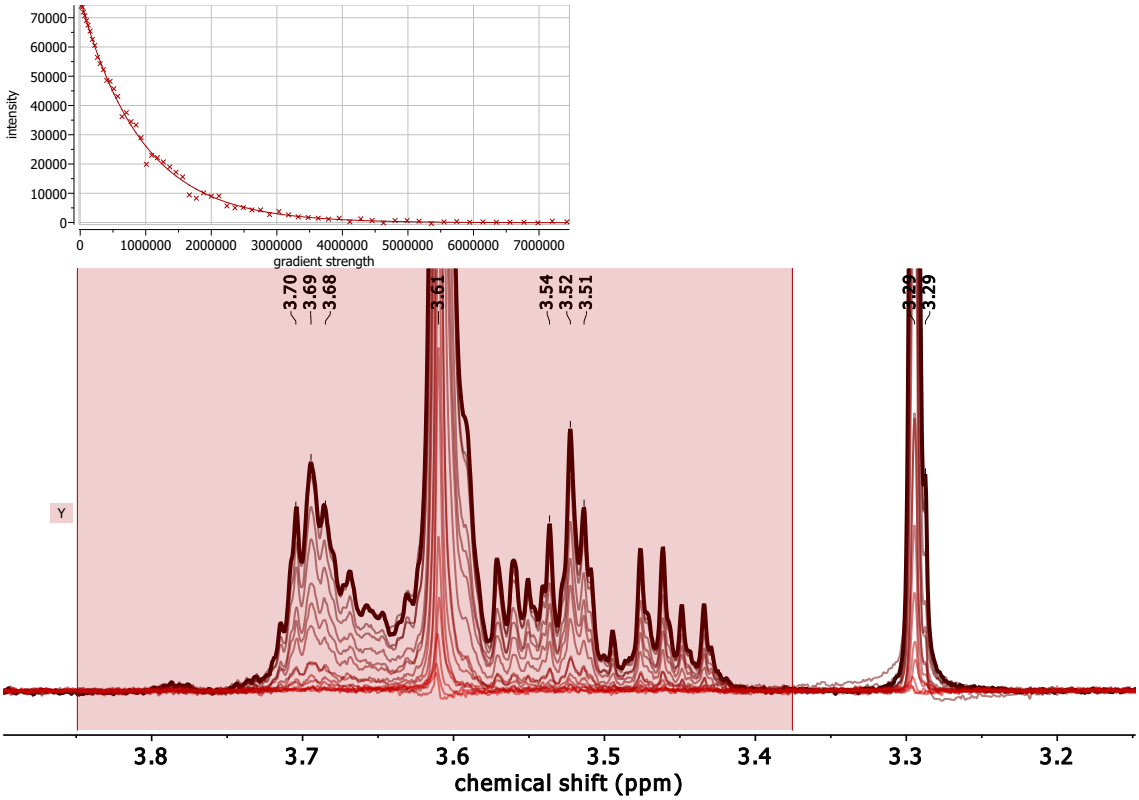

Figure S49. DOSY NMR (400 MHz, D_2O) of $rPEG_{112}^{0.21}$.

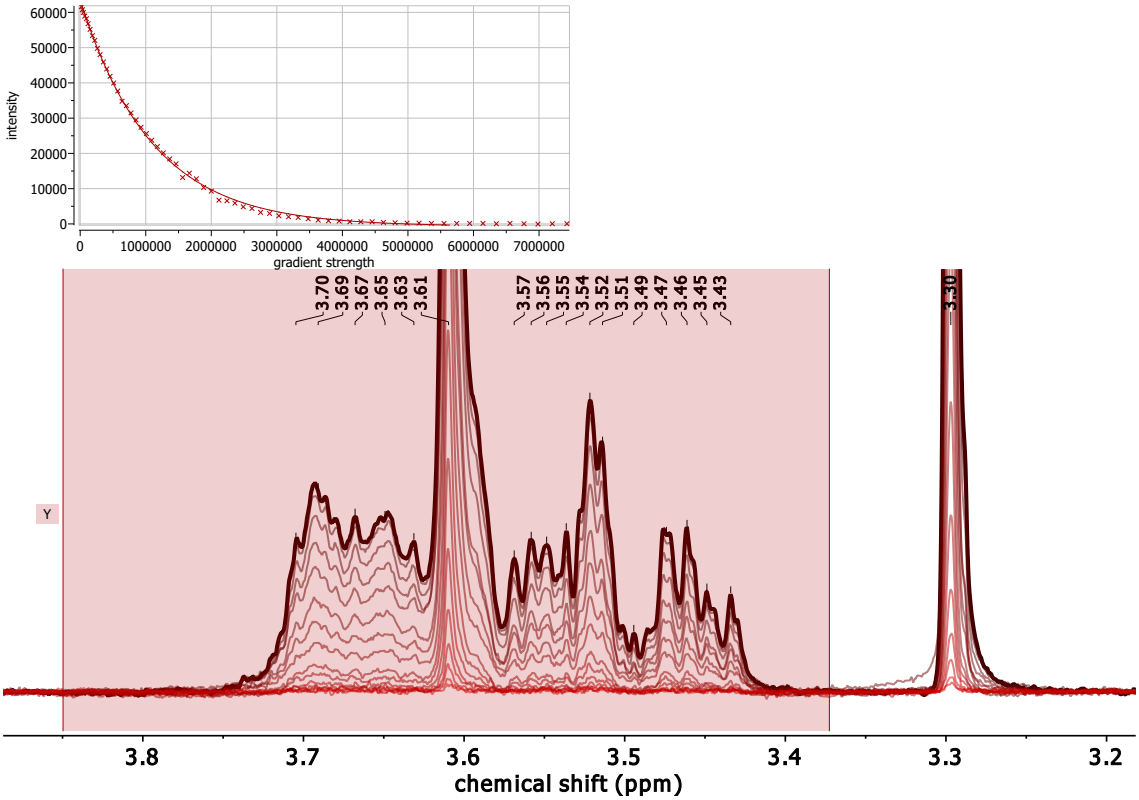

Figure S50. DOSY NMR (400 MHz, D_2O) of $rPEG_{112}^{0.43}$.

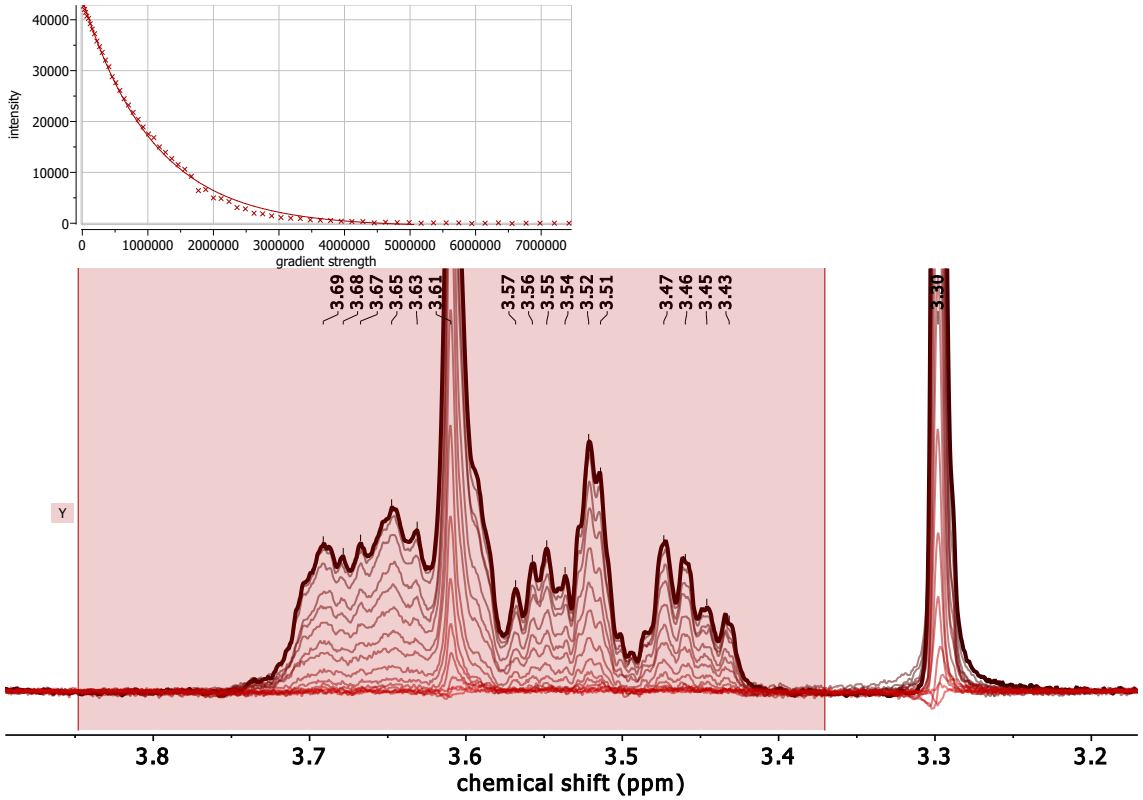

Figure S51. DOSY NMR (400 MHz, D_2O) of $rPEG_{110}^{0.55}$.

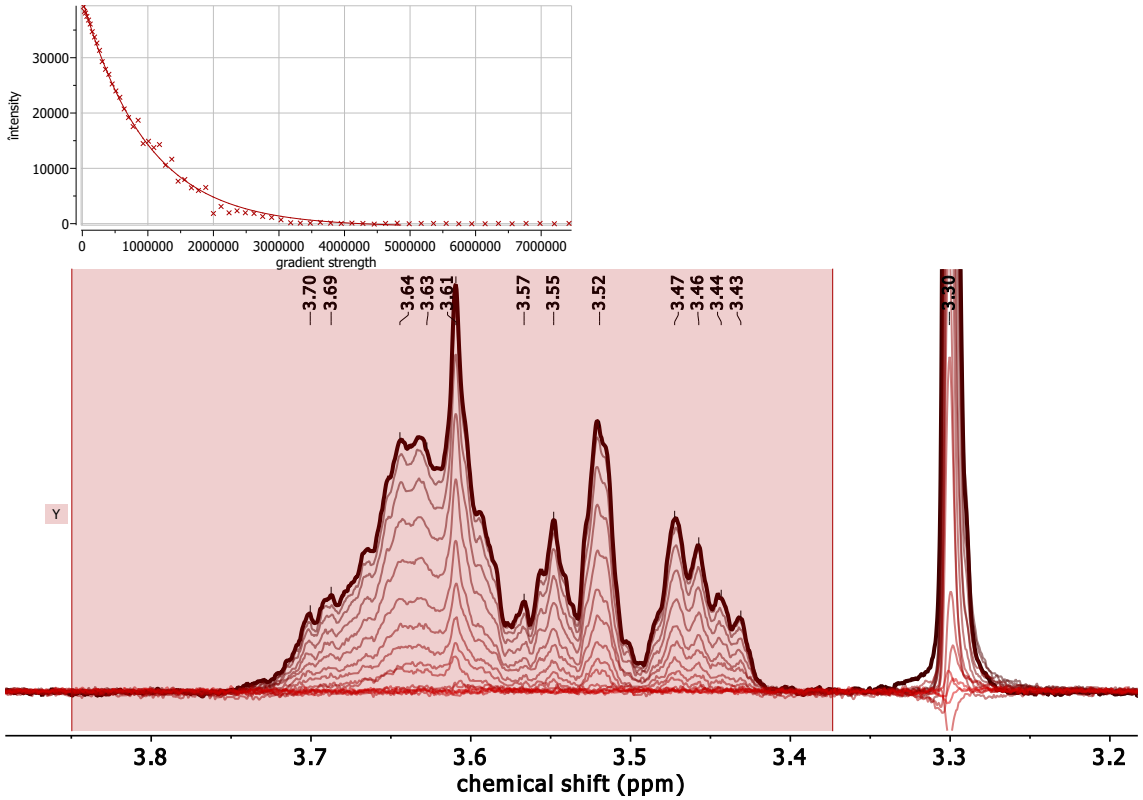

Figure S52. DOSY NMR (400 MHz, D_2O) of $rPEG_{109}^{0.74}$.

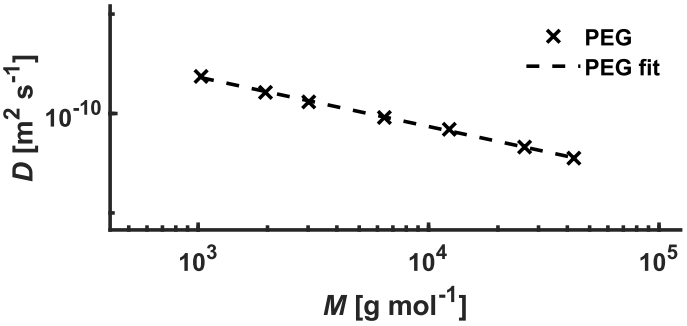

Figure S53. Diffusion coefficient (*D*) of PEG samples with different molecular weights from *PSS* and resulting fit.

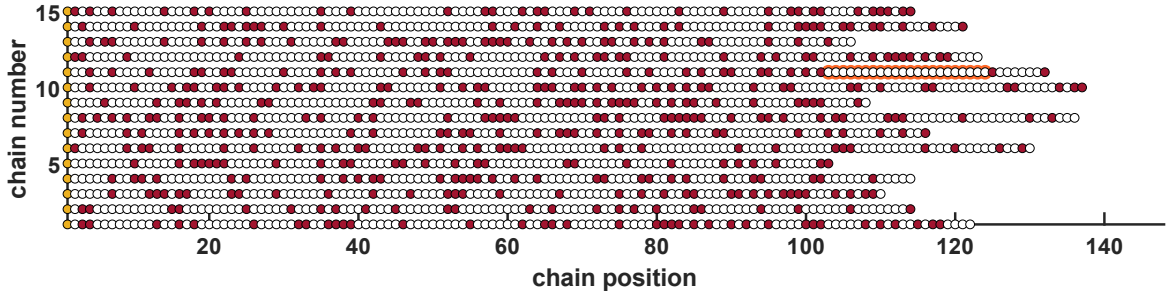

Figure S54. Section of 15 chains from the simulation (10^4 chains) of EO (white) and GME (red) repeating unit distribution at different chain positions of $rPEG_{114}^{0.30}$; repeating patterns with 16 consecutive EO repeating units are highlighted in orange; yellow circles represent the initiator.

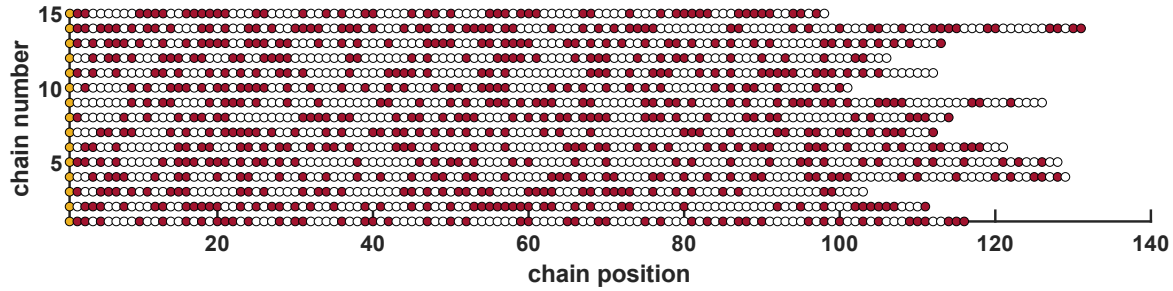

Figure S55. Section of 15 chains from the simulation (10^4 chains) of EO (white) and GME (red) repeating unit distribution at different chain positions of $rPEG_{114}^{0.40}$; yellow circles represent the initiator.

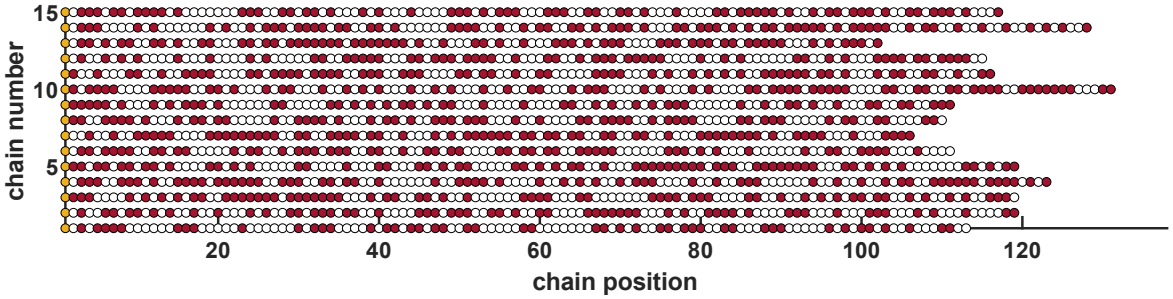

Figure S56. Section of 15 chains from the simulation (10^4 chains) of EO (white) and GME (red) repeating unit distribution at different chain positions of $rPEG_{114}^{0.50}$; yellow circles represent the initiator.

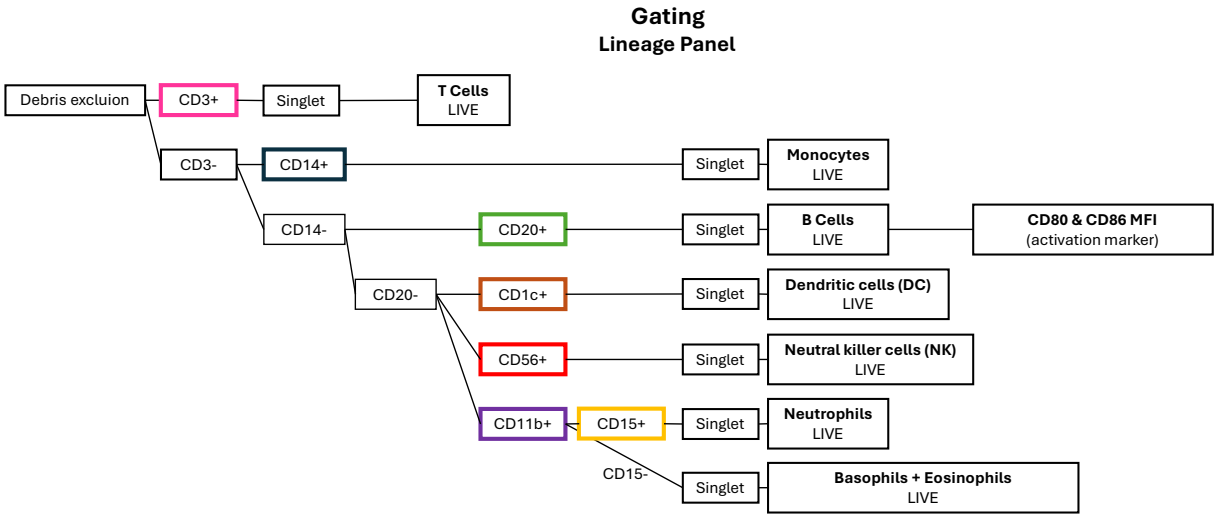

Figure S57. Schematic gating strategy applied to the flow cytometry evaluation. First cell debris was excluded, then the cell types were distinguished based on differential expression of lineage markers. Cell duplets were excluded and the viability of each singlet cell population was determined with Sytox™ Green™.

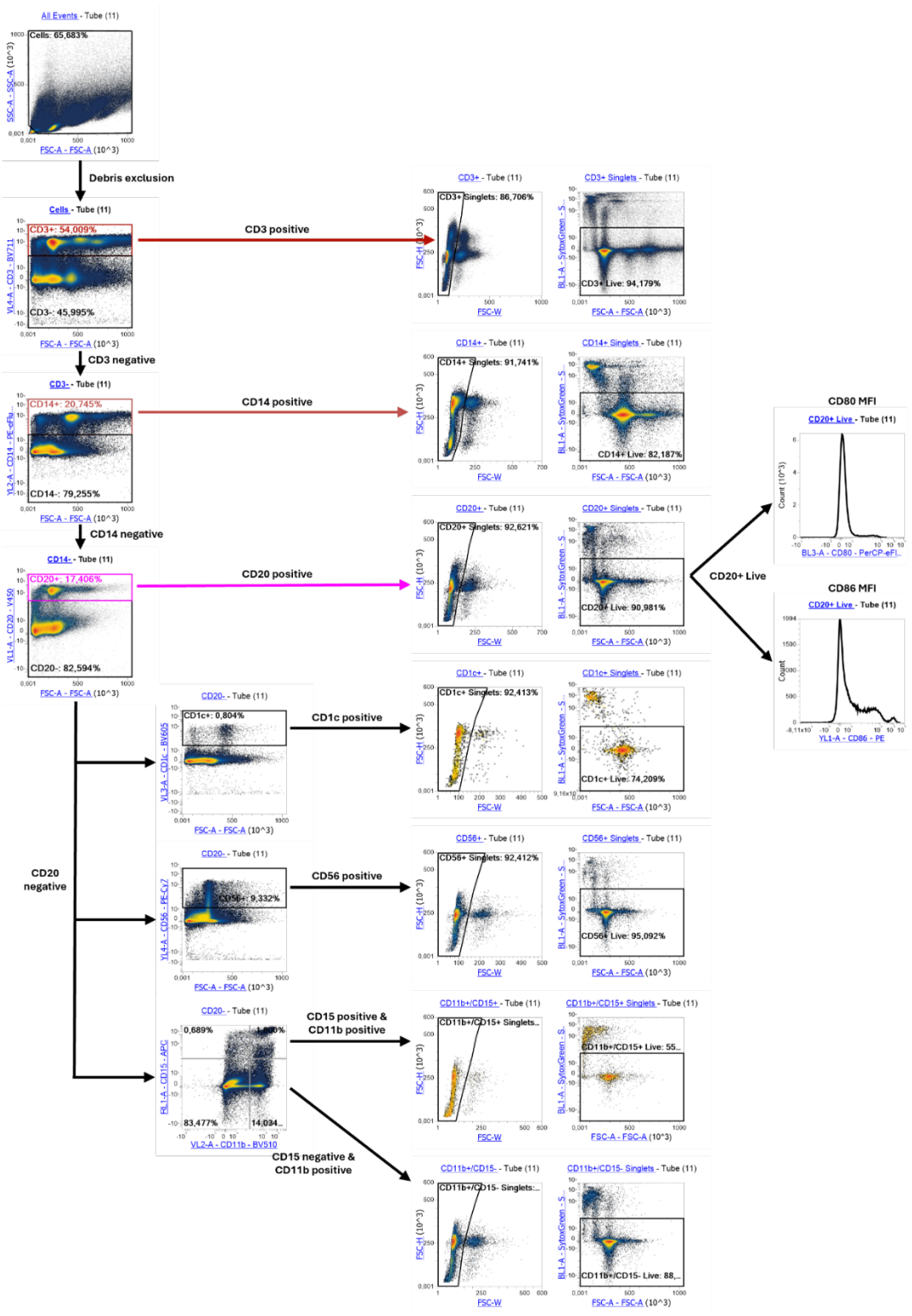

Figure S58. Exemplary gating strategy applied to the untreated control of donor 6 for flow cytometry evaluation. First cell debris were excluded, then the cell types were distinguished by detecting cell type-specific surface markers. Cell duplets were excluded and the viability of each singlet cell population was measured with Sytox™ Green™. For viable B cells ($CD20^+$ Live) the MFI of the activation markers CD80 and CD86 were determined.

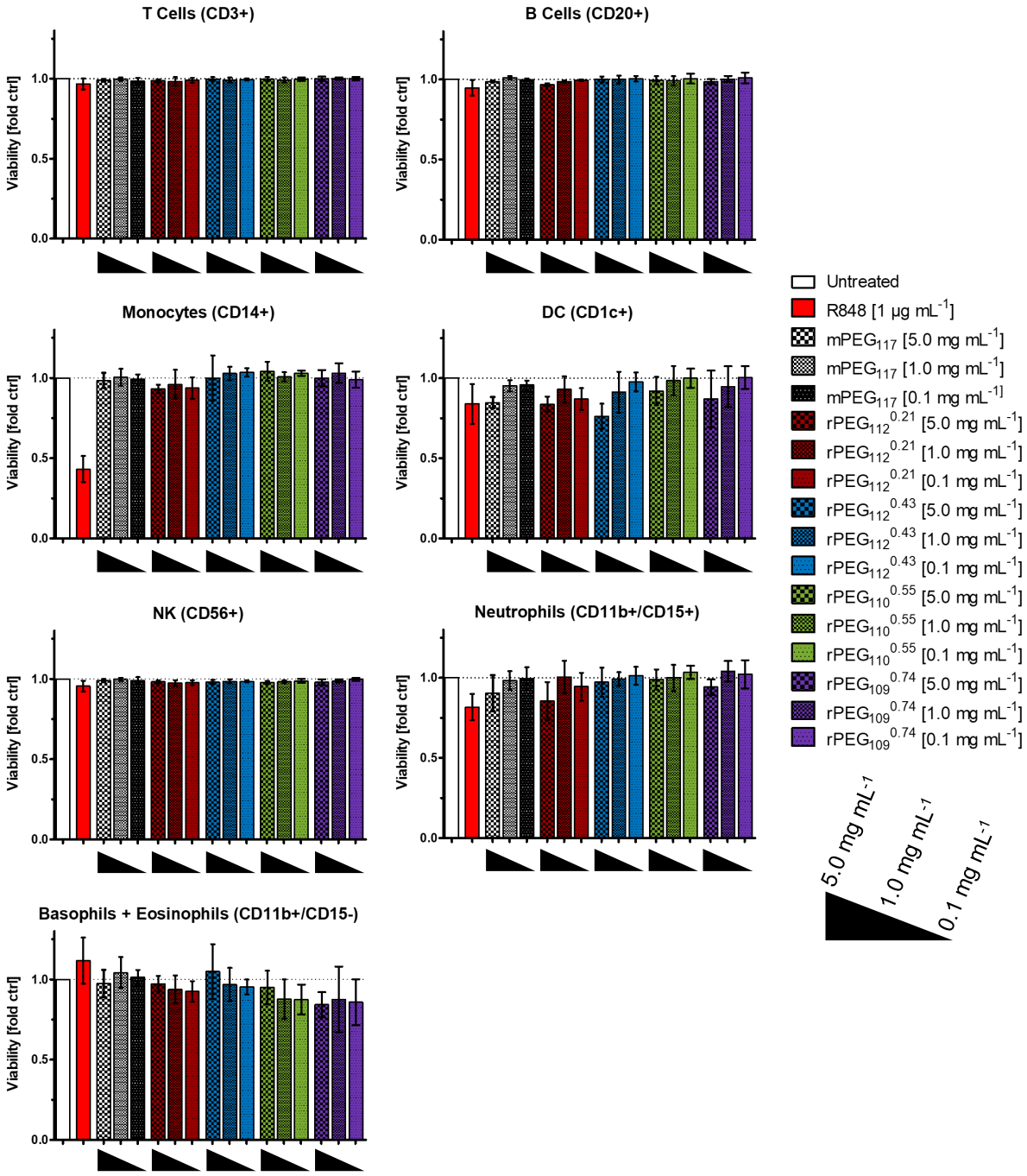

Figure S59. Normalized viability of human T cells, B cells, monocytes, dendritic cells (DC), neutral killer cells (NK), neutrophils and the remaining Basophils + Eosinophils. Determined with flow cytometry. The PBMC were isolated with density gradient centrifugation from whole blood of healthy donors (*N* = 4). Afterward, the PBMCs were incubated with the respective mPEG & rPEG samples for 16 hours.

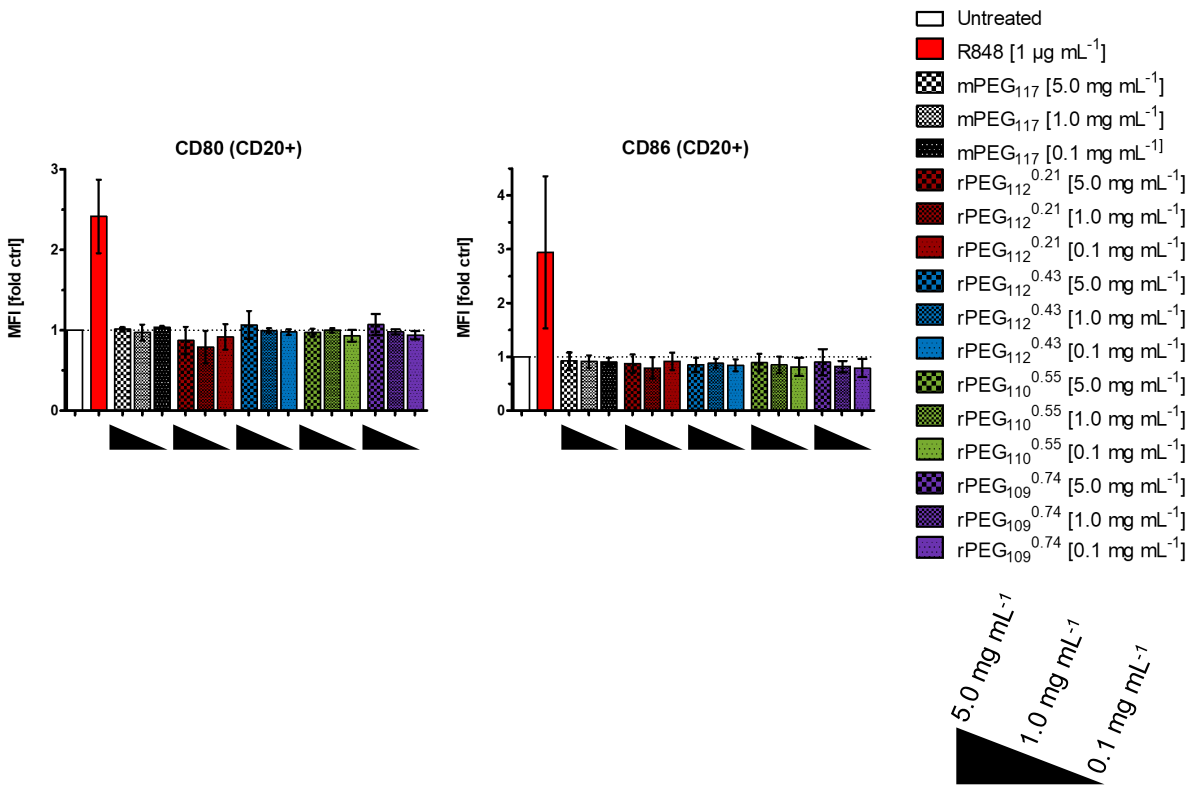

Figure S60. Analysis of immunomodulatory effects. Normalized mean fluorescence intensity (MFI) of CD80 and CD86 for viable CD20 positive cells (B cells). The PBMC were isolated with density gradient centrifugation from whole blood of healthy donors (*N* = 4). Afterward, the PBMCs were incubated with the respective formulations for 16 hours. As positive control, R848 was added to a final concentration of 1 µg mL^{-1} before incubation.

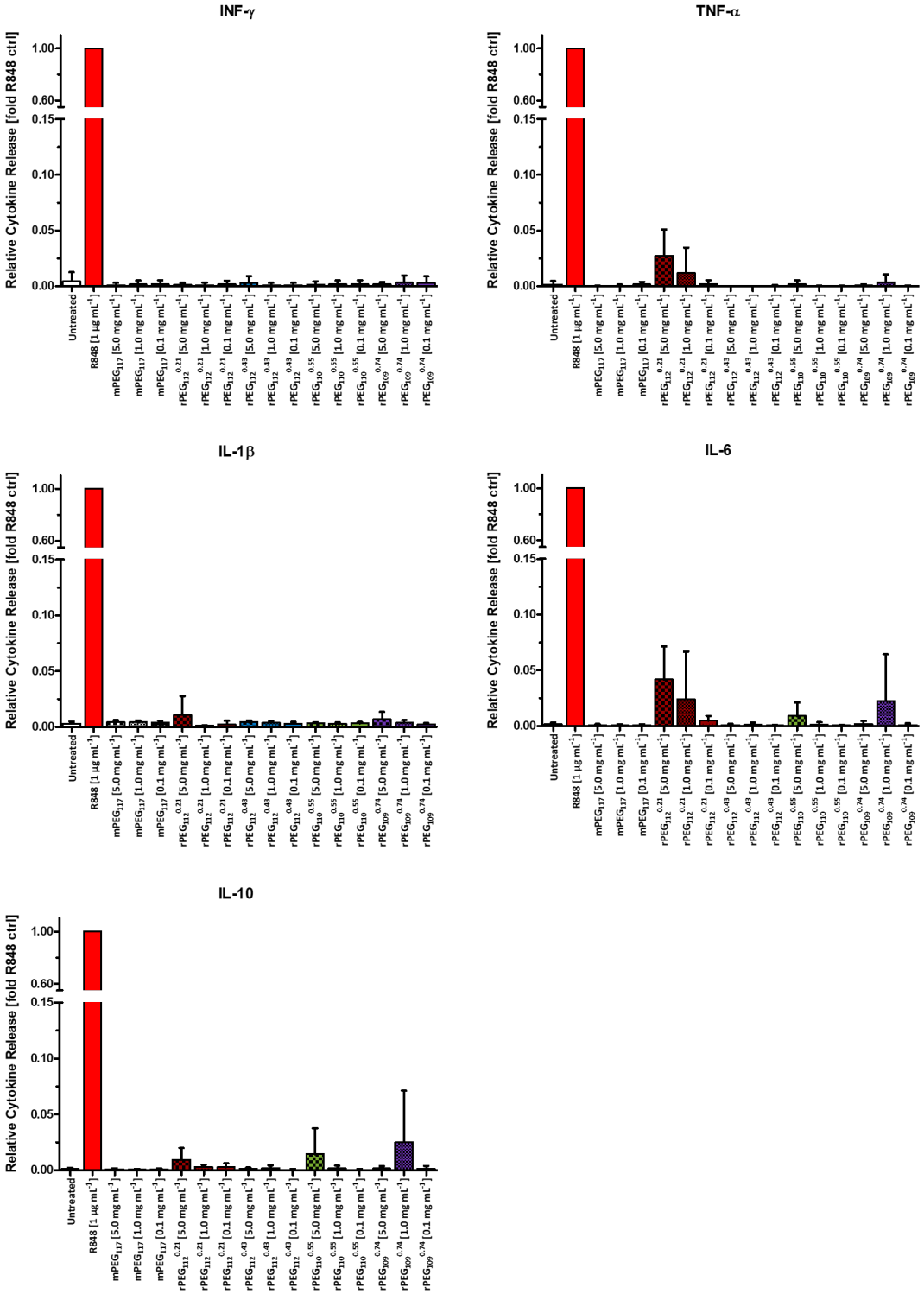

Figure S61. Relative cytokine release after 16 hours of incubation. Cytokine concentrations are given in pg mL^{-1} according to an external standard calibration. To account for this variability, cytokine levels were normalized to each donor's positive control (R848). All polymer samples were measured with $N = 4$ whereas the untreated and the R848 control were measured with $N = 8$.

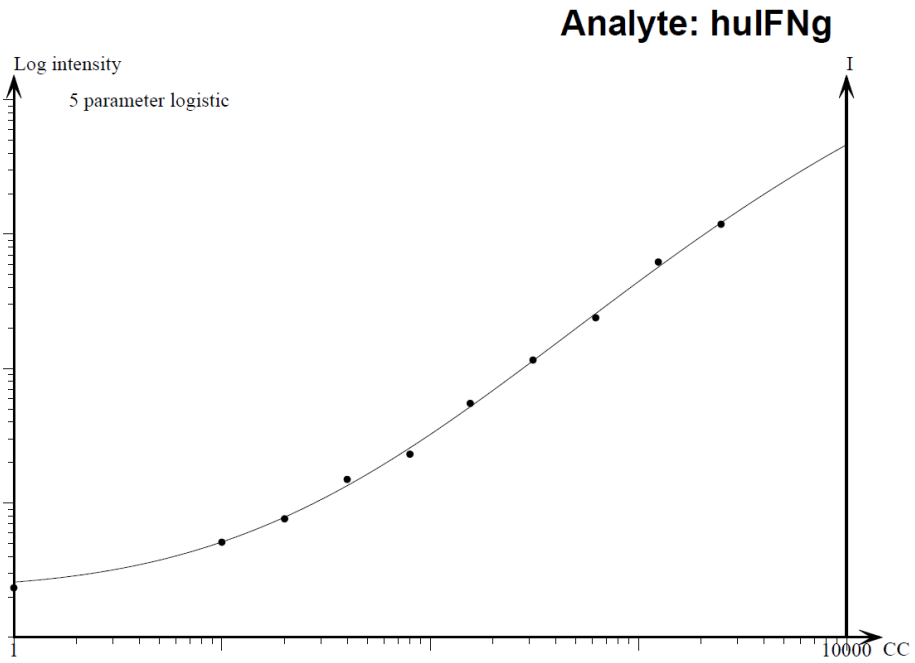

Figure S62. IFN-γ standard calibration curve.

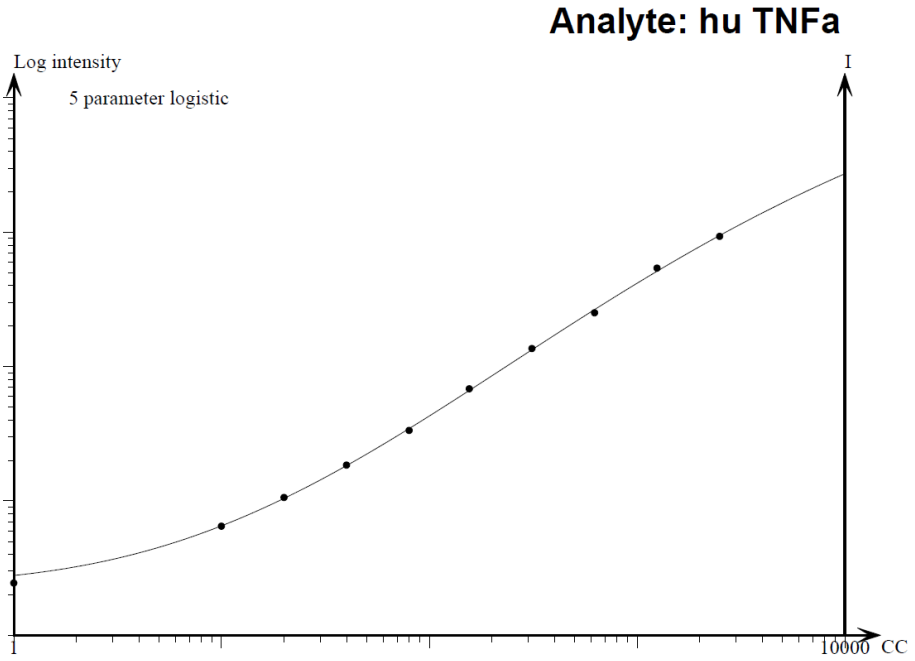

Figure S63. TNF-α standard calibration curve.

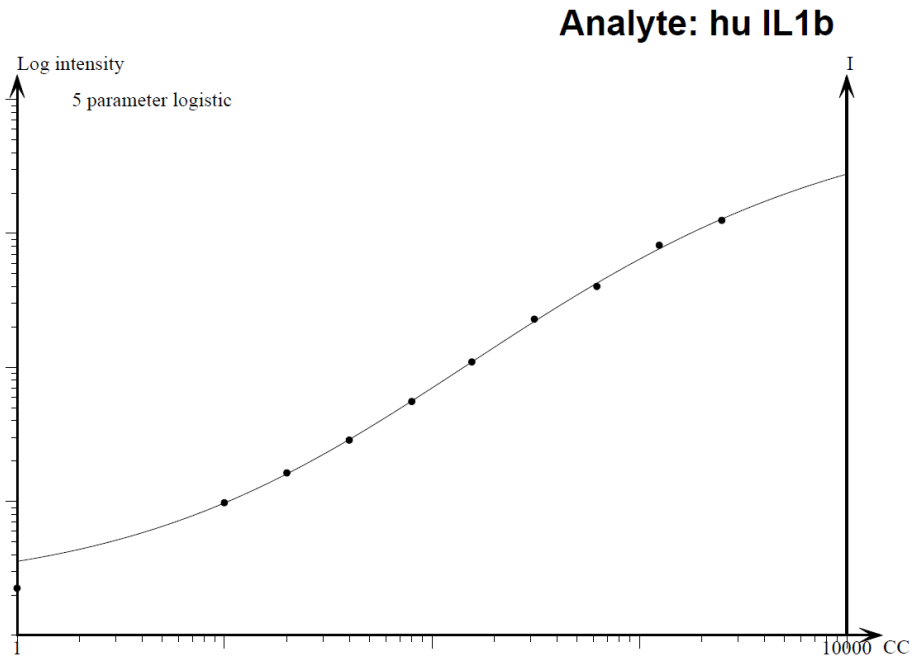

Figure S64. IL-1β standard calibration curve.

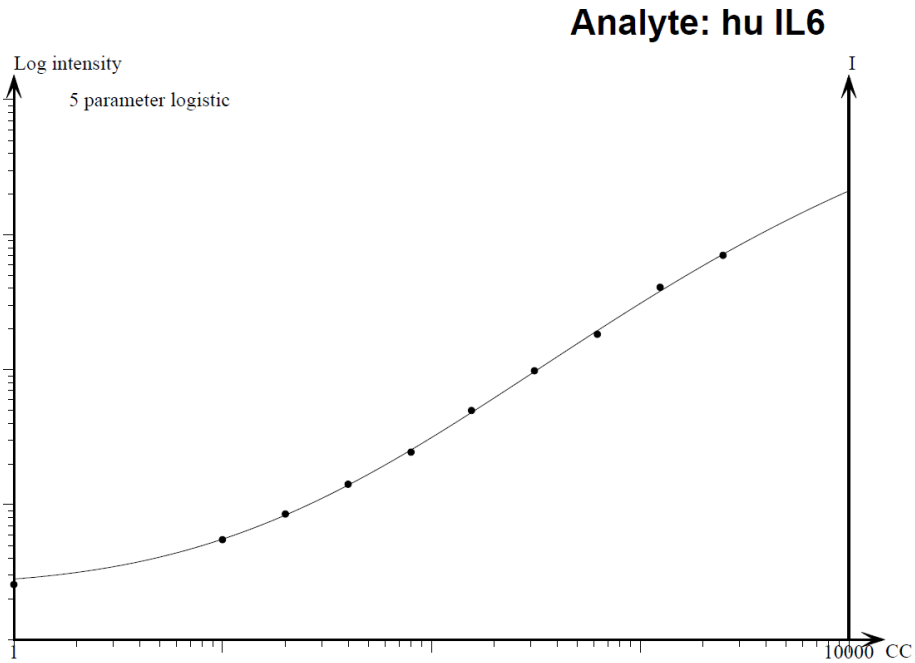

Figure S65. IL-6 standard calibration curve.

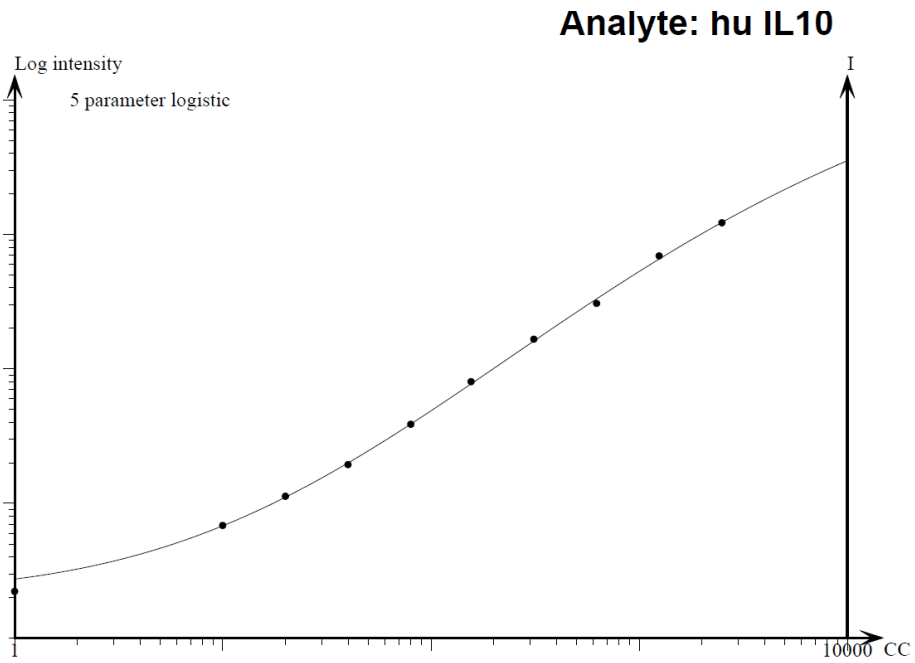

Figure S66. IL-10 standard calibration curve.

6. Tables S1 to S14

Table S1. Apparent rate constants of EO in the copolymerization with GME and 2-(benzyloxy)ethanol as initiator. Fit was applied for the linear regime in the pseudo-first-order plots.

Entry	Solvent	T [°C]	dod*	$[I]^{\dagger}$ / 10^{-2} [mol L^{-1}]	$k_{app,copo}$ (EO) [s^{-1}]	R^2
1	DMSO	25	50%	3.80	1.17E-04§±0.01	>0.99
2	DMSO	25	90%	3.80	1.28E-04§±0.01	>0.99
3	Anisole	55	50%	9.66	2.99E-05±0.01	>0.99
4	Anisole	55	90%	9.66	8.10E-05±0.01	>0.99
5	Toluene	55	50%	9.66	1.46E-05±0.01	>0.99
6	Toluene	55	90%	9.66	1.43E-04±0.01	>0.99
7‡	Toluene	55	90%	9.66	2.68E-04±0.01	>0.99
8	DMSO	25	50%	3.60¶	4.78E-05±0.01	>0.99

*) Degree of deprotonation; †) theoretical chain end concentration; ‡) addition of 2 eq. of [18]crown-6 per potassium cation, §) multiplied by a factor of (9.66/3.80) to be comparable to the [I] of the anisole and toluene experiments; ¶) 3-ethoxy-1,2-propanediol was used as initiator.

Table S2. Copolymerization kinetics of GME and EO with potassium 2-(benzyloxy)ethoxide as initiator.

Entry	Solvent	T [°C]	dod*	$[I]^{\dagger}$ / 10^{-2} [mol L^{-1}]	r_{GME}	r_{EO}	R^2	$Đ^{\S}$
1	DMSO	25	50%	3.80	1.03±0.01	0.97±0.01	>0.99	1.06
2	DMSO	25	90%	3.80	1.02±0.01	0.98±0.01	>0.99	1.07
3	Anisole	55	50%	9.66	1.37±0.01	0.73±0.01	>0.99	1.09
4	Anisole	55	90%	9.66	1.43±0.01	0.70±0.01	>0.99	1.08
5	Toluene	55	50%	9.66	1.52±0.01	0.66±0.01	>0.99	1.10
6	Toluene	55	90%	9.66	1.60±0.01	0.63±0.01	>0.99	1.10
7‡	Toluene	55	90%	9.66	1.55±0.01	0.64±0.01	>0.99	1.10
8	DMSO	25	50%	3.60¶	1.01±0.01	0.99±0.01	>0.99	1.10

*) Degree of deprotonation; †) theoretical chain end concentration; ‡) addition of 2 eq. of [18]crown-6; §) determined by GPC (eluent: DMF, PEG calibration, RI detector); ¶) active chain ends of 3-ethoxy-1,2-propanediol.

Table S3. Overview of characterizations of synthesized rPEG samples before HPLC purification.

Sample	$DP_{calc.}$	$DP_{MALDI+NMR}$	GME_{calc} [%]	GME_{NMR} [%]	$M_{n,calc.}$ [kg mol^{-1}]	$M_{n,MALDI}$ [kg mol^{-1}]	$M_{n,GPC}$ [kg mol^{-1}]	$Đ_{GPC}$
$rPEG_{112}^{0.21}$	114	112	20	21	6.0	6.0	5.6	1.04
$rPEG_{112}^{0.43}$	114	113	40	43	7.2	7.1	5.7	1.08
$rPEG_{110}^{0.55}$	114	114	50	57	7.7	7.9	6.0	1.06
$rPEG_{109}^{0.74}$	114	108	80	78	9.2	8.5	6.0	1.10

Table S4. Overview of characterizations of mPEG and rPEG samples after HPLC purification.

Sample	$DP_{calc.}$	$DP_{MALDI+NMR}$	GME_{calc} [%]	GME_{NMR} [%]	$M_{n,calc.}$ [kg mol^{-1}]	$M_{n,MALDI}$ [kg mol^{-1}]	$M_{n,GPC}$ [kg mol^{-1}]	$Đ_{GPC}$
$mPEG_{117}$	114	117	0	0	5.0	5.2	4.9	1.04
$rPEG_{112}^{0.21}$	114	112	20	21	6.0	6.0	5.2	1.06
$rPEG_{112}^{0.43}$	114	112	40	43	7.2	7.1	5.6	1.05
$rPEG_{110}^{0.55}$	114	110	50	55	7.7	7.5	5.9	1.04
$rPEG_{109}^{0.74}$	114	109	80	74	9.2	8.4	6.2	1.07

Table S5. Overview of HPLC data for investigated rPEGs.

Sample	$t_{e,max}$ [min]	$purity_{ELSD}$ [%a]
$mPEG_{117}$	8.9	>99
$rPEG_{112}^{0.21}$	15.1	>99
$rPEG_{112}^{0.43}$	16.9	>99
$rPEG_{110}^{0.55}$	17.6	>99
$rPEG_{109}^{0.74}$	18.7	>99

Table S6. Turbidimetric measurements of the cloud point temperatures (T_{cp}) of investigated rPEG samples with varying molar GME contents in PBS buffer.

Sample	concentration [mg mL^{-1}]	T_{cp} at 90 % transmittance [°C]	T_{cp} at 50 % transmittance [°C]	T_{cp} at 0 % transmittance [°C]
$mPEG_{117}$	2.0	-*	-*	-*
$rPEG_{112}^{0.21}$	2.0	-*	-*	-*
$rPEG_{112}^{0.43}$	2.0	-*	-*	-*
$rPEG_{105}^{0.55}$	2.0	85.9	86.3	89.0
$rPEG_{109}^{0.74}$	2.0	74.1	74.6	78.4
$rPEG_{109}^{0.74}$	0.5	77.0	77.7	84.8
$rPEG_{109}^{0.74}$	1.0	75.8	76.3	81.4
$rPEG_{109}^{0.74}$	5.0	71.7	72.1	74.9
$rPEG_{109}^{0.74}$	10.0	70.8	71.2	73.7

*) no decrease in transmittance observed.

Table S7. Diffusion coefficient (*D)* and calculated hydrodynamic radii (r_H) of investigated rPEG samples.

Sample	D [m^2 s^{-1}]	r_H [nm]
$mPEG_{117}$	9.92 10^{-11}	1.8
$rPEG_{112}^{0.21}$	1.07 10^{-10}	1.7
$rPEG_{112}^{0.43}$	9.10 10^{-11}	1.9
$rPEG_{110}^{0.55}$	9.21 10^{-11}	1.9
$rPEG_{109}^{0.74}$	1.02 10^{-10}	1.7

Table S8. Analysis concerning the occurrence of at least one hektakaidekads (16 EO units) within the 10^4 simulated rPEG chains with varying GME ratios (20 to 50 mol%).

Polymer	mol% GME [%]	probability of hektakaidekads [%]
$rPEG_{114}^{0.20}$	20	46.0
$rPEG_{114}^{0.30}$	30	10.1
$rPEG_{114}^{0.40}$	40	0.99
$rPEG_{114}^{0.50}$	50	0.09

Table S9. ELISA results for mPEG and rPEG samples.

Sample	$EC_{50,backbone}$ [ng ml^{-1}]	relative $affinity_{backbone}$	$EC_{50,end\ group}$ [ng ml^{-1}]	relative $affinity_{end\ group}$
$mPEG_{117}$	$3.31\ 10^1$	1	$6.95\ 10^4$	1
$rPEG_{112}^{0.21}$	$8.00\ 10^3$	$4.14\ 10^{-3}$	$4.35\ 10^6$	$1.60\ 10^{-2}$
$rPEG_{112}^{0.43}$	$1.28\ 10^5$	$2.58\ 10^{-4}$	$1.54\ 10^7$	$4.50\ 10^{-3}$
$rPEG_{110}^{0.55}$	$1.04\ 10^6$	$3.18\ 10^{-5}$	$3.64\ 10^7$	$1.91\ 10^{-3}$
$rPEG_{109}^{0.74}$	$7.10\ 10^6$	$4.66\ 10^{-6}$	$1.10\ 10^8$	$6.23\ 10^{-4}$

Table S10. Interferon-gamma (INF-γ) concentrations determined by CBA analysis.

Donor	INF-γ [pg mL^{-1}]							
	1	2	3	4	5	6	7	8
Untreated	0	1	0	36	0	3	4	0
R848 [1 µg mL^{-1}]	1374	1931	1744	1678	1255	1621	277	1481
$mPEG_{117}$ [5.0 µg mL^{-1}]	0	0	0	7	-†	-†	-†	-†
$mPEG_{117}$ [1.0 µg mL^{-1}]	0	0	0	12	-†	-†	-†	-†
$mPEG_{117}$ [0.1 µg mL^{-1}]	0	0	0	12	-†	-†	-†	-†
$rPEG_{112}^{0.21}$ [5.0 µg mL^{-1}]	-*	-*	-*	-*	0	1	1	1
$rPEG_{112}^{0.21}$ [1.0 µg mL^{-1}]	-*	-*	-*	-*	0	1	2	0
$rPEG_{112}^{0.21}$ [0.1 µg mL^{-1}]	-*	-*	-*	-*	0	2	2	0
$rPEG_{112}^{0.43}$ [5.0 µg mL^{-1}]	0	0	0	20	-†	-†	-†	-†
$rPEG_{112}^{0.43}$ [1.0 µg mL^{-1}]	0	0	0	7	-†	-†	-†	-†
$rPEG_{112}^{0.43}$ [0.1 µg mL^{-1}]	0	0	0	7	-†	-†	-†	-†
$rPEG_{110}^{0.55}$ [5.0 µg mL^{-1}]	0	0	0	10	-†	-†	-†	-†
$rPEG_{110}^{0.55}$ [1.0 µg mL^{-1}]	0	0	0	11	-†	-†	-†	-†
$rPEG_{110}^{0.55}$ [0.1 µg mL^{-1}]	0	1	0	11	-†	-†	-†	-†
$rPEG_{108}^{0.74}$ [5.0 µg mL^{-1}]	0	8	0	5	-†	-†	-†	-†
$rPEG_{108}^{0.74}$ [1.0 µg mL^{-1}]	0	0	0	21	-†	-†	-†	-†
$rPEG_{108}^{0.74}$ [0.1 µg mL^{-1}]	0	0	0	20	-†	-†	-†	-†

*) Sample was contaminated during the cell culture and discarded.

†) A second assay was deemed unnecessary due to success of the initial test.

Table S11. Tumor necrosis factor-alpha (TNF-α) concentrations determined by CBA analysis.

Donor	TNF-α [pg mL^{-1}]							
	1	2	3	4	5	6	7	8
Untreated	4	25	8	100	1	1	5	3
R848 [1 µg mL^{-1}]	12104	12937	10143	11766	6947	7763	7005	7602
$mPEG_{117}$ [5.0 µg mL^{-1}]	1	5	3	7	-†	-†	-†	-†
$mPEG_{117}$ [1.0 µg mL^{-1}]	2	5	2	19	-†	-†	-†	-†
$mPEG_{117}$ [0.1 µg mL^{-1}]	0	7	5	62	-†	-†	-†	-†
$rPEG_{112}^{0.21}$ [5.0 µg mL^{-1}]	-*	-*	-*	-*	48	114	195	454
$rPEG_{112}^{0.21}$ [1.0 µg mL^{-1}]	-*	-*	-*	-*	319	3	7	11
$rPEG_{112}^{0.21}$ [0.1 µg mL^{-1}]	-*	-*	-*	-*	1	2	4	52
$rPEG_{112}^{0.43}$ [5.0 µg mL^{-1}]	2	4	0	9068‡	-†	-†	-†	-†
$rPEG_{112}^{0.43}$ [1.0 µg mL^{-1}]	2	6	1	5	-†	-†	-†	-†
$rPEG_{112}^{0.43}$ [0.1 µg mL^{-1}]	0	9	0	12	-†	-†	-†	-†
$rPEG_{110}^{0.55}$ [5.0 µg mL^{-1}]	2	5	3	80	-†	-†	-†	-†
$rPEG_{110}^{0.55}$ [1.0 µg mL^{-1}]	2	7	1	5	-†	-†	-†	-†
$rPEG_{110}^{0.55}$ [0.1 µg mL^{-1}]	2	6	2	17	-†	-†	-†	-†
$rPEG_{108}^{0.74}$ [5.0 µg mL^{-1}]	0	1350‡	0	25	-†	-†	-†	-†
$rPEG_{108}^{0.74}$ [1.0 µg mL^{-1}]	1	3	0	162	-†	-†	-†	-†
$rPEG_{108}^{0.74}$ [0.1 µg mL^{-1}]	2	2	0	11	-†	-†	-†	-†

*) Sample was contaminated during the cell culture and discarded.

†) A second assay was deemed unnecessary due to success of the initial test.

‡) Excluded outliner.

Table S12. Interleukin-1 beta (IL-1β) concentrations determined by CBA analysis.

Donor	IL-1β [pg mL^{-1}]							
	1	2	3	4	5	6	7	8
Untreated	3	5	3	3	15	23	43	12
R848 [1 µg mL^{-1}]	1212	1411	466	778	14349	13632	11554	10659
$mPEG_{117}$ [5.0 µg mL^{-1}]	4	4	3	3	-†	-†	-†	-†
$mPEG_{117}$ [1.0 µg mL^{-1}]	4	4	3	4	-†	-†	-†	-†
$mPEG_{117}$ [0.1 µg mL^{-1}]	3	4	3	3	-†	-†	-†	-†
$rPEG_{112}^{0.21}$ [5.0 µg mL^{-1}]	-*	-*	-*	-*	25	20	48	383
$rPEG_{112}^{0.21}$ [1.0 µg mL^{-1}]	-*	-*	-*	-*	31	8	11	10
$rPEG_{112}^{0.21}$ [0.1 µg mL^{-1}]	-*	-*	-*	-*	5	9	18	72
$rPEG_{112}^{0.43}$ [5.0 µg mL^{-1}]	4	5	3	44‡	-†	-†	-†	-†
$rPEG_{112}^{0.43}$ [1.0 µg mL^{-1}]	4	4	3	2	-†	-†	-†	-†
$rPEG_{112}^{0.43}$ [0.1 µg mL^{-1}]	3	3	2	2	-†	-†	-†	-†
$rPEG_{110}^{0.55}$ [5.0 µg mL^{-1}]	4	4	2	3	-†	-†	-†	-†
$rPEG_{110}^{0.55}$ [1.0 µg mL^{-1}]	3	4	2	2	-†	-†	-†	-†
$rPEG_{110}^{0.55}$ [0.1 µg mL^{-1}]	3	3	2	2	-†	-†	-†	-†
$rPEG_{108}^{0.74}$ [5.0 µg mL^{-1}]	3	23	3	2	-†	-†	-†	-†
$rPEG_{108}^{0.74}$ [1.0 µg mL^{-1}]	3	3	2	5	-†	-†	-†	-†
$rPEG_{108}^{0.74}$ [0.1 µg mL^{-1}]	3	3	2	2	-†	-†	-†	-†

*) Sample was contaminated during the cell culture and discarded.

†) A second assay was deemed unnecessary due to success of the initial test.

‡) Excluded outliner.

Table S13. Interleukin-6 (IL-6) concentrations determined by CBA analysis.

Donor	IL-6 [pg mL^{-1}]							
	1	2	3	4	5	6	7	8
Untreated	11	70	20	242	58	112	117	787
R848 [1 µg mL^{-1}]	98783	113245	114487	103224	41024	38029	29742	298497
$mPEG_{117}$ [5.0 µg mL^{-1}]	21	124	65	195	-†	-†	-†	-†
$mPEG_{117}$ [1.0 µg mL^{-1}]	33	97	24	209	-†	-†	-†	-†
$mPEG_{117}$ [0.1 µg mL^{-1}]	17	88	24	202	-†	-†	-†	-†
$rPEG_{112}^{0.21}$ [5.0 µg mL^{-1}]	-*	-*	-*	-*	240	1159	2172	17191
$rPEG_{112}^{0.21}$ [1.0 µg mL^{-1}]	-*	-*	-*	-*	3597	111	125	699
$rPEG_{112}^{0.21}$ [0.1 µg mL^{-1}]	-*	-*	-*	-*	83	100	111	3288
$rPEG_{112}^{0.43}$ [5.0 µg mL^{-1}]	116	250	36	92779‡	-†	-†	-†	-†
$rPEG_{112}^{0.43}$ [1.0 µg mL^{-1}]	27	414	25	140	-†	-†	-†	-†
$rPEG_{112}^{0.43}$ [0.1 µg mL^{-1}]	16	104	19	132	-†	-†	-†	-†
$rPEG_{110}^{0.55}$ [5.0 µg mL^{-1}]	183	730	97	2773	-†	-†	-†	-†
$rPEG_{110}^{0.55}$ [1.0 µg mL^{-1}]	18	504	13	165	-†	-†	-†	-†
$rPEG_{110}^{0.55}$ [0.1 µg mL^{-1}]	14	79	16	139	-†	-†	-†	-†
$rPEG_{108}^{0.74}$ [5.0 µg mL^{-1}]	25	126369‡	68	541	-†	-†	-†	-†
$rPEG_{108}^{0.74}$ [1.0 µg mL^{-1}]	66	559	18	8815	-†	-†	-†	-†
$rPEG_{108}^{0.74}$ [0.1 µg mL^{-1}]	16	91	17	283	-†	-†	-†	-†

*) Sample was contaminated during the cell culture and discarded.

†) A second assay was deemed unnecessary due to success of the initial test.

‡) Excluded outliner.

Table S14. Interleukin-10 (IL-10) concentrations determined by CBA analysis.

Donor	IL-10 [pg mL^{-1}]							
	1	2	3	4	5	6	7	8
Untreated	2	4	4	9	3	1	1	1
R848 [1 µg mL^{-1}]	5539	4615	5291	3421	2094	930	593	358
$mPEG_{117}$ [5.0 µg mL^{-1}]	2	5	5	7	-†	-†	-†	-†
$mPEG_{117}$ [1.0 µg mL^{-1}]	3	6	2	5	-†	-†	-†	-†
$mPEG_{117}$ [0.1 µg mL^{-1}]	2	5	3	5	-†	-†	-†	-†
$rPEG_{112}^{0.21}$ [5.0 µg mL^{-1}]	-*	-*	-*	-*	7	5	3	9
$rPEG_{112}^{0.21}$ [1.0 µg mL^{-1}]	-*	-*	-*	-*	8	2	1	2
$rPEG_{112}^{0.21}$ [0.1 µg mL^{-1}]	-*	-*	-*	-*	3	1	1	3
$rPEG_{112}^{0.43}$ [5.0 µg mL^{-1}]	8	10	2	5352‡	-†	-†	-†	-†
$rPEG_{112}^{0.43}$ [1.0 µg mL^{-1}]	2	21	2	9	-†	-†	-†	-†
$rPEG_{112}^{0.43}$ [0.1 µg mL^{-1}]	2	6	2	4	-†	-†	-†	-†
$rPEG_{110}^{0.55}$ [5.0 µg mL^{-1}]	14	20	12	167	-†	-†	-†	-†
$rPEG_{110}^{0.55}$ [1.0 µg mL^{-1}]	2	24	2	8	-†	-†	-†	-†
$rPEG_{110}^{0.55}$ [0.1 µg mL^{-1}]	2	4	2	4	-†	-†	-†	-†
$rPEG_{108}^{0.74}$ [5.0 µg mL^{-1}]	2	2421‡	5	13	-†	-†	-†	-†
$rPEG_{108}^{0.74}$ [1.0 µg mL^{-1}]	10	18	3	320	-†	-†	-†	-†
$rPEG_{108}^{0.74}$ [0.1 µg mL^{-1}]	2	4	2	17	-†	-†	-†	-†

*) Sample was contaminated during the cell culture and discarded.

†) A second assay was deemed unnecessary due to success of the initial test.

‡) Excluded outliner.

A2: Polymerization of Epoxides at a Static Oil-Alkaline Water Interface

[redacted], Gregor M. Linden[2], [redacted]

[1]Membrane Technology Group, Centre for Membrane Separations, Adsorption Catalysis and Spectroscopy for Sustainable Solutions (cMACS), KU Leuven Celestijnenlaan 200F, Leuven, 3001, Belgium.

[2]Department of Chemistry, Johannes Gutenberg University Mainz, Duesbergweg 10-14, 55128, Mainz, Germany.

Published in: *Macromol. Rapid Commun.* **2024**, e2400423, DOI: 10.1002/marc.202400423

Supporting Information is available from the publisher.

The following publication is reprinted with permission by [redacted] Linden, G. M.; [redacted]; [redacted] Polymerization of Epoxides at a Static Oil-Alkaline Water Interface. *Macromol. Rapid Commun.* **2024**, e2400423. DOI: 10.1002/marc.202400423. Copyright © 2024 Wiley-VCH GmbH

RESEARCH ARTICLE

Macromolecular Rapid Communications
www.mrc-journal.de

Polymerization of Epoxides at a Static Oil-Alkaline Water Interface

Rhea Verbeke, Gregor M. Linden, Philip Dreier, Christopher Kampf, and Holger Frey*

'On-water' catalysis entails the significant enhancement of a chemical reaction by water, even when those reactions are known to be water-sensitive. Here, the findings about the anionic ring opening polymerization of epoxides at the static interface between oil and alkaline water are shared. Unexpectedly, high molar mass fractions are observed with the interfacial system presented herein, albeit at very low conversions (< 5%). Styrene oxide, a notably unreactive epoxide, is chosen as the model compound to investigate the influence of several reaction parameters (i.e., pH, type of the initiator salt, polymerization time, interfacial area, solvent, shaking) on the polymerization. Poly(styrene oxide) (PSO) with an M_n of 5300 g mol^{-1} is observed via MALDI-ToF MS, with species of at least 8000 g mol^{-1}. The feasibility of expanding the system to (cyclic) aliphatic and aromatic epoxides, and glycidyl ethers is also explored. The system appears to promote polymerization of epoxides that position at the interface, in such a way that initiation and propagation can occur. A mechanistic interpretation of the interfacial polymerization is suggested. The surprising results obtained in this work urge to revisit the role of water in ionic polymerizations.

1. Introduction

The unique physical and chemical properties of water have attracted long-term attention to its use as a green solvent for organic synthesis.[1] When organic reactions are conducted "on-water", i.e., when insoluble reactants are stirred in an aqueous suspension, a significant impact in terms of rate acceleration and selectivity can be obtained under very simple conditions.[2–4] "On-water" catalysis has been observed for many classes of organic reactions, such as Diels-Alder cycloadditions, Wittig reactions, and nucleophilic substitution reactions.[3] The unique role of water in the nucleophilic ring-opening of three-membered heterocycles, such as epoxides, has also been highlighted.[5–9]

The heterogeneity of the system is a prerequisite to observing these catalytic effects.[2,10] The interface can occur at the macroscale, i.e., a static interface between two immiscible liquids, or at the micro/nanoscale in emulsions.[11] The exact reasons underlying the observed rate accelerations remain unclear due to the limited information available about the molecular properties at the interface, which vastly differ from bulk properties.[12] However, several suggestions have been made, such as enforced hydrophobic interactions, ions channeling over the oil-water interface, and the unique structure of water at the interface.[4,10,13–16] Especially the broken water symmetry at the interface, resulting in dangling hydroxyl groups into the hydrophobic phase which can undergo hydrogen bonding with the reagents in the transition state, has been suggested as a crucial factor for some reactions.[10,17]

The enabling properties of interfaces have also been exploited in polymer synthesis, e.g., for the production of Nylon, reverse osmosis membranes, and microcapsules.[18–20] The biphasic system allows the separation of reactive monomers in two phases, that react at the interface to form a thin polymer film.[21] Reaction initiators, catalysts, or oxidizing/reducing agents can also be present.[22] Different chemistries, solvents, and types of polymerization reactions at liquid-liquid interfaces have been explored, including radical polymerizations and polyadditions.[11,22,23] Ionic polymerizations have been less studied under interfacial conditions due to their sensitivity to water and other impurities.[11] Indeed, both anionic and cationic polymerizations are traditionally executed under strictly anhydrous conditions to avoid termination of the propagating chain by water. As a result, very narrow distributions with control over molar mass can be achieved, as exemplified by the well-defined polyether architectures obtained via the anionic ring-opening polymerization (AROP) of epoxides.[24]

However, cationic and anionic polymerizations can occur under specific conditions in aqueous media, as reviewed by Charleux et al.[25] Several studies have also reported the successful ROP of epoxides in the presence of water, either in miniemulsion,[26] with water as an additive,[27] with phosphate-buffered saline as a solvent,[28] or with octanol as the initiator

R. Verbeke, G. M. Linden, P. Dreier, C. Kampf, H. Frey
Department of Chemistry
Johannes Gutenberg University Mainz
Duesbergweg 10–14, 55128 Mainz, Germany
E-mail: rhea.verbeke@kuleuven.be
R. Verbeke
Membrane Technology Group
Centre for Membrane Separations
Adsorption Catalysis and Spectroscopy for Sustainable Solutions (cMACS)
KU Leuven Celestijnenlaan 200F, Leuven 3001, Belgium

The ORCID identification number(s) for the author(s) of this article can be found under https://doi.org/10.1002/marc.202400423

DOI: 10.1002/marc.202400423

 © 2024 Wiley-VCH GmbH

ADVANCED SCIENCE NEWS
www.advancedsciencenews.com

Macromolecular Rapid Communications
www.mrc-journal.de

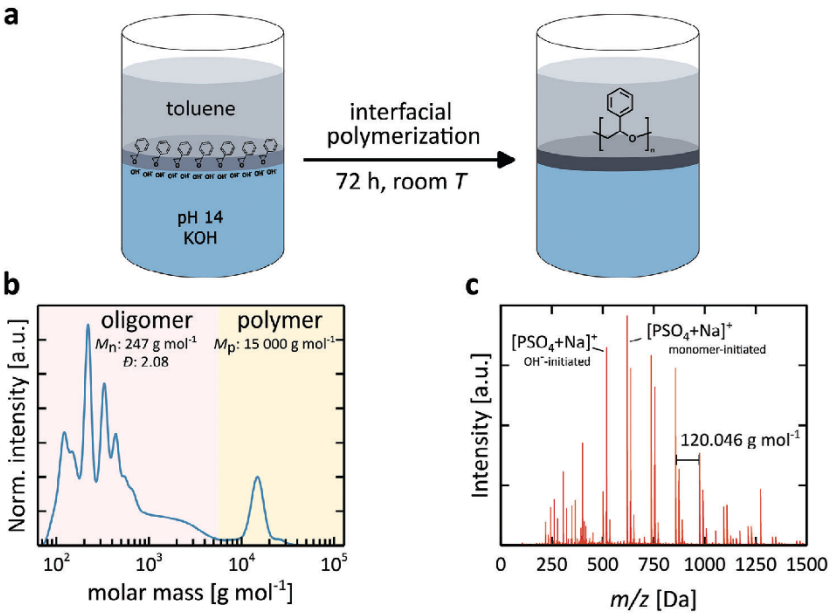

Figure 1. a) Interfacial synthesis of poly(styrene oxide) at a static oil-alkaline water interface. The reference conditions are 1 M styrene oxide in toluene, on water at pH 14 (KOH) for a reaction time of 72 h and at an interfacial area of 50 cm^2. The interface is static and undisturbed throughout the experiment. b) SEC traces (THF, PS calibration, UV-detector), consisting of a low and a high molecular weight fraction, denoted as "oligomer" and "polymer", respectively. The shown M_n (number-average molar mass) and dispersity ($Đ$) of the oligomer fraction are based on integration over the red area (background color). The shown M_p (molar mass at highest peak) for the polymer fraction is based on the peak in the yellow area (background color). c) ESI mass spectrum of poly(styrene oxide), in which both monomer (SO)-initiation and hydroxide ion initiation are visible. Signals from PSO with four repeating units (PSO$_4$) ionized with Na$^+$ are shown.

and phosphazene base and triethyl borane as co-catalysts.[29] Molar masses up to 2500 g mol^{-1} could be achieved, indicating that propagation occurred to some extent under protic conditions. In addition, interfacial polymerization at an oil-water interface between multifunctional epoxides and tertiary amines was recently introduced to synthesize thin polyether films to achieve nanofiltration membranes.[30] Even when no amine was present and the pH of the aqueous solution was increased, polymerization occurred.[31] These studies further allude to the potential of "on-water" catalysis for ionic polymerizations.

Here, we share our findings on the occurrence of epoxide ring-opening polymerizations at the static interface between an immiscible solvent and alkaline water, without the need for any surfactants or additives, resulting in high and low molar mass fractions. Several reaction parameters and epoxides are investigated, with styrene oxide as a non-polar model compound. While a better molecular understanding of interfacial phenomena is needed to explain the surprising findings, this work further supports the exciting potential of heterogeneous conditions to enable ionic polymerizations.

2. Results and Discussion

2.1. Reference System with SO as Monomer

The feasibility of conducting an epoxide AROP at a static (i.e., avoiding stirring) oil-alkaline water interface was demonstrated in this work by the homopolymerization of styrene oxide (SO), a notably unreactive epoxide.[32,33] SO was dissolved in toluene and subsequently added to an aqueous solution of pH 14 (KOH) and allowed to react for 72 h at room temperature (**Figure 1a**). Visually, a colorless swirl was observed at the interface (Figure S1, Supporting Information). This colorless precipitate was not observed for any of the control experiments at neutral pH, with and without SO (i.e., toluene on top of pure Milli-Q water, and SO in toluene on top of Milli-Q water) (Table S1-r1,2, Supporting Information).

The colorless precipitate was collected and investigated via NMR spectroscopy, SEC, and ESI-MS. While the conversion was low (< 5%), different analytics confirmed the presence of poly(styrene oxide) (PSO). The ^{1}H NMR spectrum shows a broad signal between 3.25 and 4.75 ppm, originating from the formed polyether backbone, compared to the SO monomer (Figures S2 and S3, Supporting Information). SEC demonstrates the presence of both low molar mass (oligomeric) and high molar mass (polymeric) species, as highlighted by the red and yellow areas, respectively, in Figure 1b. The different peak maxima in the oligomer region indicate the apparent degree of polymerization (DP). Based on a polystyrene standard, the $Đ$ of the oligomeric fraction (integrated over the red area) equals 2.08 with a number-average molar mass (M_n) of 300 g mol^{-1} (**Table 1**-r 1). Strikingly, the polymeric fraction (integrated over the yellow area) has a narrow dispersity ($Đ$ of ca. 1.1), and an M_p (molar mass at the highest peak in the yellow area) of 15 000 g mol^{-1}. Note that

 © 2024 Wiley-VCH GmbH

ADVANCED SCIENCE NEWS
www.advancedsciencenews.com

Macromolecular Rapid Communications
www.mrc-journal.de

Table 1. Overview of synthesized polymers (i.e., poly(styrene oxide), poly(phenyl glycidyl ether), and poly(dodecyl/tetradecyl glycidyl ether) under different reaction conditions. The dispersity ($Đ$) and the number-average molar mass (M_n) of the oligomer fraction, and the molar mass at the highest peak (M_p) of the polymer fraction are based on SEC (THF, PS calibration, UV-detector). "Shaken" indicates the system was shaken at 600 rpm. All other experiments consisted of a static interface. *N.A. = not applicable.*

Run	Epoxide	Conc. [mol L^{-1}]	Solvent	pH, initiator	Time [h]	Area [cm^2]	$M_{n,oligomer}$ [g mol^{-1}]	$Đ_{oligomer}$ [-]	$M_{p,polymer}$ [g mol^{-1}]
1	SO	1	Toluene	pH 14 (KOH)	72	50	300	2.08	15 000
2	SO	1	Cyclohexane	pH 14 (KOH)	72	2	300	1.91	15 000
3	SO	1	*n*-Hexane	pH 14 (KOH)	72	2	300	1.52	14 900
4	SO	1	Chloroform	pH 14 (KOH)	72	2	400	2.02	14 900
5	SO	1	Dichloromethane	pH 14 (KOH)	72	2	300	1.89	15 100
6	SO	1	Toluene	pH 13 (KOH)	72	2	400	1.84	14 700
7	SO	1	Toluene	pH 14 (NaOH)	72	50	300	2.05	14 800
8	SO	1	Toluene	pH 14 (LiOH)	72	50	300	1.66	15 400
9	SO	0.1	Toluene	pH 14 (KOH)	72	50	300	1.33	15 800
10	SO	1	Toluene	pH 14 (KOH)	72	2	300	2.09	14 900
11	SO	1	Toluene	pH 14 (KOH)	24	50	300	1.90	15 700
12	SO	1	Toluene	pH 14 (KOH)	100	50	200	1.96	14 600
13	SO	1	Toluene	pH 14 (KOH)	72	Shaken	266	1.54	15 700
14	PhGE	1	Toluene	pH 14 (NaOH)	72	2	400	1.85	N.A.
15	DDTDGE	1	Toluene	pH 14 (NaOH)	72	2	N.A.	N.A.	16 200

the narrow dispersity is broader in reality due to tailing to lower elution volumes of the high molar mass oligomeric fraction. As this shoulder is omitted during SEC data analysis, an artificial underestimation of the $Đ$ is obtained and hence $Đ$ of the polymer fraction is not displayed here. For the same reason, only the M_p of the polymer fraction will be shown throughout this work. The oligomeric fraction was further investigated by ESI-MS. Oligomers, ranging from 2 to 14 repeating units, and cationized by H^+, Na^+, and/or K^+, were detected. Both hydroxide-initiated and monomer-initiated distributions were present (Figure 1c). A hypothetical reaction mechanism for SO-initiation of PSO via chain transfer reaction is shown in Figure S4 (Supporting Information). The peaks in each distribution are separated by 120.1 Da, i.e., the molar mass of SO. Thus, ESI-MS further substantiates the presence of PSO, initiated by either hydroxide ions or by the SO monomer itself.

To investigate how polymerization is affected by the environment, different solvents (i.e., *n*-hexane, cyclohexane, chloroform, and dichloromethane) were investigated as an alternative for toluene, and their SEC traces were analyzed. Polymerization occurred for all solvents and the conversions were again < 5%. Note that SEC is a relative method, hence only relative conclusions can be drawn when comparing the observed oligomeric and polymeric species per sample. The SEC traces were normalized to the polymer peak for a more accurate comparison. Pristine spectra can be found in Figure S5 (Supporting Information). In toluene, cyclohexane, and *n*-hexane, a similar M_p of the polymer fraction is observed (Table 1-r 1,2,3). However, significantly more polymer is formed in toluene than in cyclohexane and *n*-hexane, as suggested by the lower intensity of the oligomer peak (**Figure 2a**). Toluene thus appears to be a good solvent for the interfacial polymerization of SO, possibly due to more favorable interactions with the SO units. The toluene-water interface also appears to be more diffuse,[34] and toluene can form hydrogen bonds with water.[35] The lower interfacial tension of toluene with water and higher solubility in water (and vice versa), compared to *n*-hexane and cyclohexane (Table S2, Supporting Information), does not appear to cause termination, hinting in the direction of a shielding effect of the reactive alkoxide. Microscale details about interfacial phenomena (e.g., molecular ordering and the presence of charges at the interface) probably also contribute to the observed differences, but are not yet elucidated.[12]

When using chloroform and DCM instead of toluene, the interfacial system reverses with the organic phase down and the aqueous phase up (Figure 2b). Polymerization was successful for all solvents, with a similar M_p of the polymer fraction and overall conversions again below 5% (Table 1-r 1,4,5). Compared to toluene, the use of chloroform results in a shift toward higher molar masses, with limited oligomer formation, and starting at a higher molar mass (Figure 2b). In contrast, the use of DCM results in significantly more oligomer than polymer formation, suggesting propagation is hindered more significantly, provided that termination is reversible. As DCM and chloroform are both very good solvents for PSO and have similar properties, such as density, interfacial tension with water, and solubilities in water (Table S2, Supporting Information), the origin of the observed differences can possibly be found at the orientation of molecules at the interface. For chloroform-water interfaces, a net out-of-plane dipole moment has been observed, resulting in a movement of hydroxide ions to the interface.[36] For a DCM-water interface, both negative and positive ions accumulate further and closer to the Gibbs surface, respectively.[36] However, here a pH 14 solution is used, resulting in orders of magnitude more hydroxide ions, making accurate comparison with literature cumbersome. Modeling of interfaces with alkaline water would be helpful to further elucidate the occurring phenomena and explain the observed experimental data.

© 2024 Wiley-VCH GmbH

ADVANCED SCIENCE NEWS
www.advancedsciencenews.com

Macromolecular Rapid Communications
www.mrc-journal.de

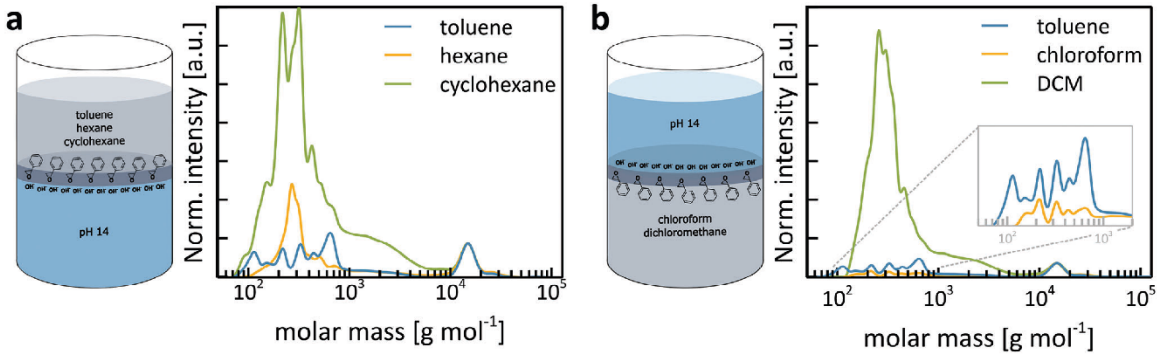

Figure 2. SEC traces (THF, PS calibration, UV-detector) of poly(styrene oxide) made with different organic solvents, normalized to the polymer peak. a) Comparison of toluene (run 1) with cyclohexane (run 2) and hexane (run 3). b) Comparison of toluene with chloroform (run 4) and dichloromethane (run 5). Please note the reversal of the phases for the latter two conditions.

It is remarkable that for all the tested conditions the high molar mass fraction elutes at a similar elution volume during SEC experiments, resulting in similar M_p values. To further investigate this high molar mass fraction, SEC fractionation was conducted on PSO synthesized at a DCM-pH 14 interface (**run 5**). The obtained fractions were subsequently analyzed by MALDI-ToF MS (**Figure 3a**). A regular interval of the molar mass of SO (i.e., 120.1 g mol^{-1}) is visible in the MALDI-ToF MS spectra for all fractions (Figure 3b). Similar to ESI-MS, the series of peaks can be assigned to PSO, initiated by hydroxide ions or by the SO monomer, and cationized either by K^+ or by Ag^+ (from AgTFA, the salt additive used for the MALDI ToF measurement). Strikingly, poly(styrene oxide) (PSO) with an M_n of 5300 g mol^{-1} was observed, with species of at least 8000 g mol^{-1}, confirming for the first time the possibility of synthesizing high molar mass PSO via interfacial polymerization (Figure 3b, inset). Even though the interfacial system investigated in this work is not presented as a novel synthesis method for PSO, it is noteworthy that the obtained molar masses largely exceed those accessible for PSO synthesized via conventional AROP (e.g., $M_{p,SEC}$ = 2000 g mol,$^{-1}$[37] $M_{n,SEC}$ = 1700 – 4800 g mol^{-1},[38] $M_{n,SEC}$ = 1680 g mol^{-1}[39]). Note that the MALDI-ToF MS signal intensity significantly decreases with increasing molar mass, which is possibly related to a decrease in ionization efficiency.[40] Hence, signals originating from the polymers observed at lower elution volumes via SEC were not observed. Nevertheless, the different characterization techniques confirm the occurrence of SO polymerization at an oil-alkaline water interface, resulting in PSO of at least 8000 g mol^{-1}.

2.2. Investigation of System Parameters

To better understand the constraints and the polymerization mechanism of this new interfacial system, different synthesis parameters (i.e., pH, salt initiator, time, interfacial area, shaking) were explored, with toluene as the organic phase. More specifically, their effect on the initiation and propagation steps of the chain growth polymerization of SO was investigated by analyzing the SEC traces that were normalized to the polymer peak. Pristine spectra can be found in Figure S6 (Supporting Information). As SEC is a relative method, the obtained values for the molar mass should be interpreted with caution and not be seen as absolute numbers. Note that the total reaction yields for all conditions were low (< 5%, lower mg-scale), limiting the number of charac-

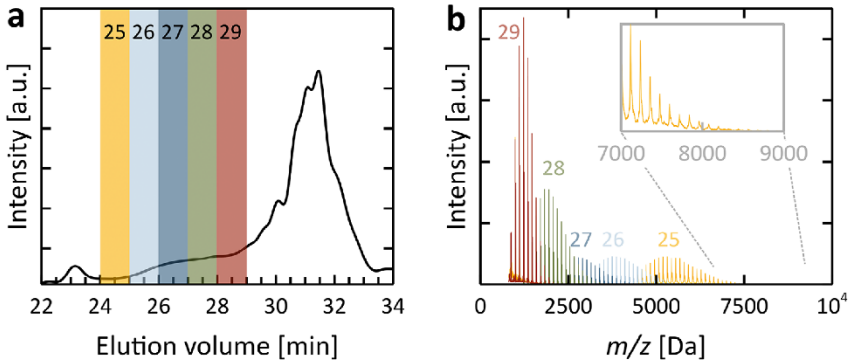

Figure 3. a) SEC traces (THF, PS calibration, UV-detector) of poly(styrene oxide) (run 5). b) MALDI-ToF mass spectra of the different fractions obtained via SEC, indicated by the corresponding numbers. The inset shows the high molar mass fractions.

© 2024 Wiley-VCH GmbH

ADVANCED SCIENCE NEWS
www.advancedsciencenews.com

Macromolecular Rapid Communications
www.mrc-journal.de

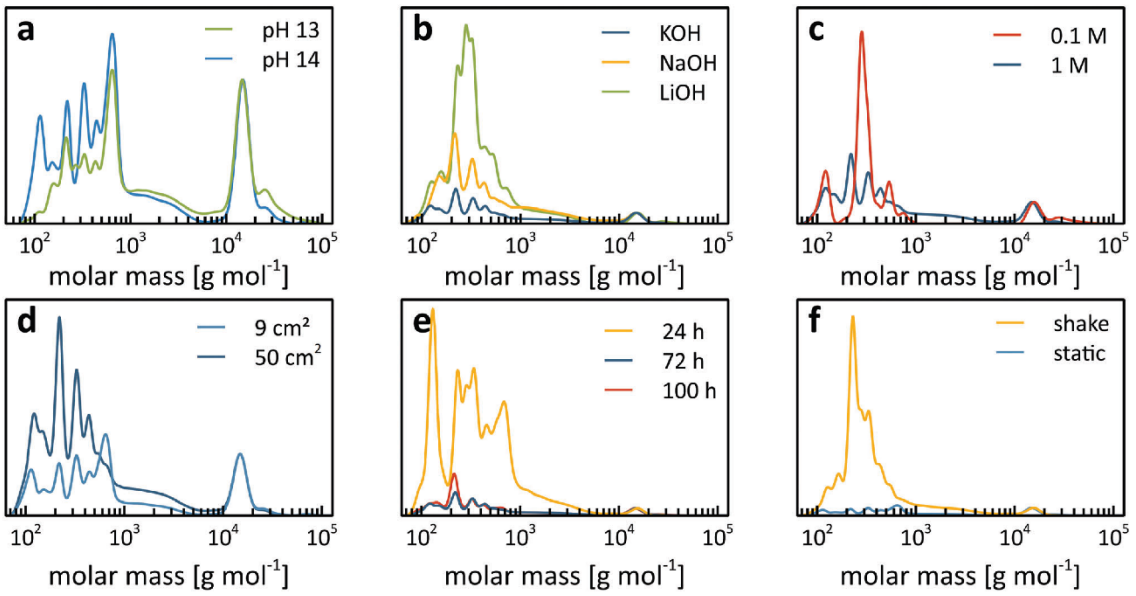

Figure 4. SEC traces (THF, PS calibration, UV-detector) of different poly(styrene oxide) samples made under different interfacial conditions, normalized to the polymer peak. The reference conditions are 1 M styrene oxide in toluene, on the water at pH 14 (KOH) for a reaction time 72 h and for the interfacial area of 50 cm^2 under static conditions (dark blue). Variations in a) pH, b) initiator salt, c) concentration, d) interfacial area, and e) reaction time, and by f) shaking at 600 rpm are shown, while keeping the other parameters constant. [Correction added on 5 October 2024, after first online publication: figure 4 was updated.]

terization techniques that could be applied. In addition, it was not possible to determine the polymer molar mass via ^{1}H NMR spectroscopy as the water-initiated fraction with the respective glycol has a chemical shift within the backbone region. While this is also the case for the SO-initiated fraction, the chemical shift related to the double bond could not be detected, most probably due to the low yield.

It is important to stress that the pH plays a critical role, as no SO polymerization is observed at pH values below 13 (Table S1-r3,4, Supporting Information). The white deposition at the interface (Figure S1, Supporting Information for run 1) is not observed at, e.g., pH 10 (Figure S7, Supporting Information). This pH-dependency suggests that a threshold hydroxide concentration (i.e., $[OH^-]$ = 0.1 M) is required for initiation to occur (Table 1-r6). SEC traces also show that a higher oligomer than polymer fraction is present at pH 14, compared to pH 13, suggesting that more initiation occurred at higher hydroxide initiator concentrations, similar to conventional AROP (**Figure** 4a). These results suggest that hydroxide ions are readily available at the interface to initiate the polymerization, either directly or via H-abstraction of the SO monomer (suggested mechanism in Figure S4, Supporting Information). Fundamental research on the molecular structure of water at the interface between an oil and (neutral pH) water already pointed toward a negative interfacial charge, even though the exact origin of this charge is still under debate. Plausible possibilities are the partitioning of hydroxide ions to the interface or the charge transfer between water molecules at the interface.[17,41–47] The occurrence of epoxide AROP in the interfacial system used in this work, where the aqueous phase possesses a high pH, further alludes to the presence of hydroxide ions at the interface.

In addition to pH, different counterions of the alkaline initiator (i.e., KOH, NaOH, and LiOH) were tested at pH 14. Oligomerization and polymerization are observed for all initiators (Figure 4b and Table 1-r 1,7,8), including also for LiOH. This is in stark contrast with the conventional oxyanionic polymerization of epoxides, where typically ring opening, albeit no further polymerization occurs with LiOH.[24] However, in the interfacial system, significantly more oligomers are formed with LiOH compared to NaOH and KOH. The counterion thus indeed affects the interfacial polymerization kinetics, but to a lesser extent than in conventional systems.

Interestingly, when decreasing the SO concentration by a factor of 10 (i.e., from 1 to 0.1 M), the M_n of the polymer fraction slightly shifts from 15 000 to 15 800 g mol^{-1} (Figure 4c and Table 1-r 1,9). However, based on the SEC traces, a relatively higher oligomer than polymer fraction was observed for the lower monomer concentration, as expected. This result additionally suggests that the interfacial area is not saturated with monomer under the tested conditions. Indeed, when decreasing the interfacial area from 50 to 2 cm^2, while keeping the SO concentration constant, relatively less oligomer with respect to polymer is formed (Figure 4d and Table 1-r 1,10). This can be explained by a higher areal concentration (i.e., concentration/area) for the smaller area, which is in line with the results observed for the SO concentration series. When shortening the synthesis time from 72 to 24 h, a significant increase in the oligomer fraction is observed. In contrast, lengthening the reaction time from 72 to

 © 2024 Wiley-VCH GmbH

ADVANCED SCIENCE NEWS
www.advancedsciencenews.com

Macromolecular Rapid Communications
www.mrc-journal.de

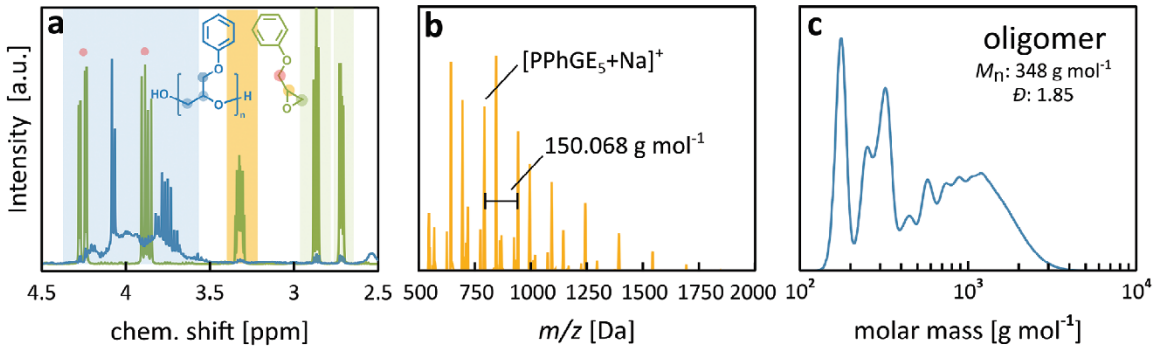

Figure 5. Interfacial polymerization of phenyl glycidyl ether at a toluene-alkaline water interface under the reference conditions (run 14). a) ^{1}H NMR spectra of the PhGE monomer before and after polymerization. Full spectra can be found in the Supporting Information. b) ESI mass spectrum. PPhGE with five repeating units, ionized with Na^{+} and initiated by OH^{-}, is indicated as an example. c) SEC traces (THF, PS calibration, UV-detector) of the oligomer fraction. No polymer fraction was observed.

100 h did not seem to largely influence the SEC traces, suggesting that a limiting polymer yield is reached after a certain time (Figure 4e and Table 1-r 1,11,12).

To investigate whether a static interface is required to achieve polymerization, the system was also shaken at 600 rpm for 72 h. In contrast to conventional emulsion polymerization but in line with typical "on water" conditions,[2] no additives or surfactants were used. Both low and high molar mass fractions were observed for the disturbed system (Table 1-r13). However, the SEC traces indicate that the formed polymeric fraction is significantly smaller than the oligomeric fraction in the shaken system, compared to the static system (Figure 4f). These findings could suggest that undisturbed molecular orientation and ordering in the interfacial region is beneficial to achieve a high degree of polymerization.

2.3. Expanding the System to Other Epoxides

Besides SO, other epoxide monomers with different physical properties (Table S3, Supporting Information), including phenyl glycidyl ether (PhGE), cyclohexene oxide (CHO), epoxy dodecane (EDD), and a commercially available mixture of dodecyl glycidyl and tetradecyl glycidyl ethers (DDTDGE) were investigated separately for their potential to polymerize at an oil-water interface under the reference conditions (i.e., 1 M epoxide in toluene, water at pH 14 (KOH), 72 h, and a static interface). Polymerization only occurred for PhGE and DDTDGE.

Polymerization of PhGE is confirmed by ^{1}H NMR spectroscopy, SEC, and ESI-MS. A broad polyether backbone signal in the ^{1}H NMR spectrum is observed between 3.5 and 4.2 ppm after interfacial polymerization (**Figure 5a**, full spectra in Figures S8 and S9, Supporting Information). ESI-MS also confirms the presence of PPhGE, with a repeating unit of 150.1 Da (i.e., the molar mass of the PhGE monomer), up to twelve repeating units (Figure 5b, full spectrum in Figure S10, Supporting Information). Multiple distributions are present, amongst which those initiated by hydroxide ions or by PhGE itself. A more detailed explanation of the different distributions and a suggestion of the corresponding adducts are given in the Supporting Information (Figure S11 and Table S4, Supporting Information). The SEC traces show a broad distribution of the low molar mass fraction (Table 1-r14 and Figure 5c). Surprisingly, and in stark contrast to SO, no high molar mass fraction is observed for PhGE, which could indicate that the presence of a glycidyl ether group alters its interfacial orientation to a different extent in comparison to other epoxide monomers, such as alkene oxides. Possibly, the higher polarity of the head group of PhGE compared to SO causes a higher affinity for the aqueous phase, which could result in slower propagation and thus in a lower DP.

To further investigate the influence of the (a)polarity of the head and tail moieties of the epoxide on the polymerization, DDTDGE was used as the epoxide, which contains a glycidyl ether but also a long (i.e., C_{12} or C_{14}) alkyl chain, under the reference interfacial protocol. The highly apolar alkyl chains were hypothesized to compensate for the polar glycidyl ether group, hence distributing the molecule more toward the organic phase and allowing propagation to continue. Indeed, a high molar mass fraction (M_n = 16 200 g mol^{-1}) is observed in the SEC traces, without oligomer formation (Table 1-r15, Figure S12, Supporting Information). Note that the signal in the low molar mass region originates from the DDTDGE monomer itself. Polymerization was also confirmed via ^{1}H NMR spectroscopy by the increased signal originating from the polyether backbone formed, compared to the monomer signals (Figures S13 and S14, Supporting Information). In contrast, interfacial polymerization of CHO and EDD under the reference conditions was not successful (Table S1-r5,6, Supporting Information). While the reason for CHO is most probably its low intrinsic reactivity due to its 1,2-substitution pattern, as known from conventional polyether synthesis,[48] the absence of EDD polymerization is more surprising. Provided that DDTDGE polymerized, the absence of EDD polymerization might be because of its lower affinity for the interface due to its more apolar head group, inhibiting initiation. However, as no high molar mass PhGE was observed, the right orientation of the epoxide monomer at the interface that enables initiation and allows propagation appears to be of crucial importance to attaining high molar mass species. More detailed studies specifically investigating the orientation of epoxide monomers

© 2024 Wiley-VCH GmbH

ADVANCED SCIENCE NEWS
www.advancedsciencenews.com

Macromolecular Rapid Communications
www.mrc-journal.de

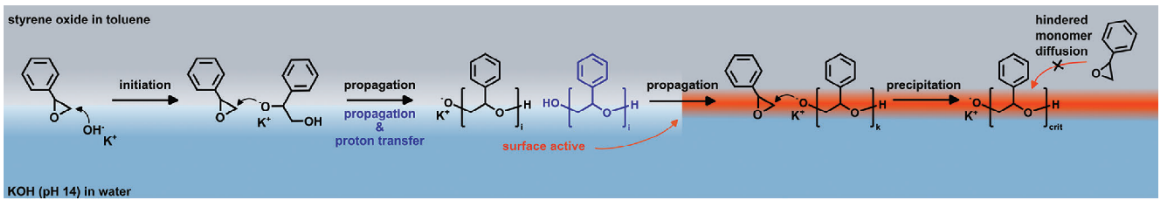

Figure 6. The suggested mechanism of the polymerization of styrene oxide at a toluene-alkaline water interface with hydroxide ions as the initiator. Initiation occurs at the interface, followed by propagation. Oligomers of a certain DP_i are obtained which have surface-active properties and hence stabilize the interface. This facilitates propagation. Eventually, at a certain critical DP (DP_{crit}), the polymer precipitates and monomer diffusion toward the active chain end is significantly hindered.

and the growing chains at an oil-water interface are needed to fully elucidate the surprising observations in this work.

2.4. Suggested Mechanism

Based on the experimental data and inspired by a previous model developed for the anionic polymerization of PhGE in miniemulsion with surfactants,[26] a mechanistic interpretation for epoxide homopolymerization at a static oil-water interface is suggested here in brief (**Figure 6** for OH^--initiation). The epoxides will have a well-defined orientation at the oil-water interface. A balance between the apolar nature of the tail and the polarity of the head of the epoxide monomer seems imperative to obtain the right orientation to allow for initiation and propagation. The initiation occurs at the interface, via a reactive alkoxide for hydroxide initiation or via a chain transfer reaction. These anions most probably are stabilized at the interface by ion-pair formation with the counterion of the salt employed (e.g., K^+ of KOH). The formed ion-pair appears sufficiently stable to allow for propagation until (reversible) protonation occurs by water. The OH-terminated short oligomers will have a relatively high affinity for the interface. The interface then becomes more hydrophobic and can accommodate a higher epoxide concentration, favoring propagation. However, at a certain DP, the solubility limit is reached, and the polymer will precipitate, hindering monomer diffusion toward the active chain end and significantly slowing down propagation. Note that termination by protonation of the active alkoxide is not suggested here as a probable cause of termination, as proton exchange is a key feature of epoxide AROP.[24]

This mechanistic hypothesis is supported by the fact that for almost all tested conditions, including different epoxides and different solvents, the M_p of the polymer fraction fluctuated between 14 600–16 000 g mol^{-1}, even though comparison of the observed M_p values should be done with caution as SEC remains a relative method. Furthermore, it is noteworthy that higher DPs are not achieved with excellent solvents such as DCM and chloroform, in which the solubility of PSO is significantly higher. More detailed investigations, combining experiments with modeling, should be conducted to take into account nano-scale phenomena at interfaces, such as molecular ordering and the presence of electrical charges.[12,44,46]

3. Conclusion

In this work, we share our observations regarding the occurrence of the AROP of epoxides at a static oil-alkaline water (pH $\geq$ 13) interface with several initiator salts (i.e., KOH, NaOH, and LiOH). For styrene oxide, a low molar mass fraction and an unexpectedly high molar mass fraction were observed for all tested conditions. Importantly, PSO of at least 8000 g mol^{-1} was confirmed via MALDI-ToF MS. When changing the reaction parameters (i.e., initiator salt, polymerization time, interfacial area, solvent, and shaking), the overall reaction conversion remained below 5% for all experiments, but the relative amount of the formed polymer with respect to the oligomer fraction changed, based on SEC traces. It appears that a static system (i.e., no stirring) and higher areal concentrations of the epoxide monomer result in a relatively higher polymer than oligomer fraction. Similar SEC traces are observed when increasing the reaction time from 72 h to 100 h, suggesting a limiting polymer yield is reached after a certain time. No polymerization was observed when lowering the pH below 13, suggesting that a threshold hydroxide concentration is mandatory for initiation to occur. In addition, polymerization occurred when using NaOH and KOH, and strikingly also with LiOH, which is in stark contrast to conventional AROP, where Li counterions lead to a tight ion pair, disabling polymerization. The structure and polarity of the epoxide and its orientation at the interface also appeared to influence the achievable degree of polymerization. While more detailed information on interfacial phenomena is required to truly understand the system, the surprising observation that AROP is feasible at an oil-alkaline water interface challenges the common belief that water rapidly terminates and disables such reactions, and further supports the counter-intuitive but exciting opportunities static interfaces may provide for polymer synthesis, for instance to achieve elusive polymer structures.

4. Experimental Section

Reagents: All solvents (i.e., toluene, cyclohexane, *n*-hexane, dichloromethane, and chloroform) were purchased from Sigma-Aldrich, Fisher Chemical (Pittsburgh, PA, USA), and Honeywell (Morris Plaines, NJ, USA) and used without further purification. Milli-Q water (resistivity 18.2 MΩ·cm @ 25 °C) was used. All reagents were purchased from Thermo Fisher Scientific, Sigma-Aldrich, Acros Organics (Pittsburgh, PA, USA), and Alfa Aesar (Kandel, Germany). Deuterated solvents were obtained from Deutero GmbH (Kastellaun, Germany).

Instrumentation—NMR: ^{1}H NMR spectra were recorded at 400 MHz using a Bruker Avance II HD 400 spectrometer at 23 °C, equipped with a 5 mm BBFO-Smartprobe (z-gradient), an automated tuning and matching device, and a SampleXPress 60 autosampler. The spectra are referenced internally to the residual proton signal of the deuterated solvent (CD_2Cl_2).

Instrumentation—ESI: High-resolution mass spectra were obtained using a G6545A Q-ToF (Agilent GmbH, Waldbronn, Germany) with a dual

© 2024 Wiley-VCH GmbH

ADVANCED SCIENCE NEWS
www.advancedsciencenews.com

Macromolecular Rapid Communications
www.mrc-journal.de

AJS electrospray ion source (Dual AJS ESI). MS parameters were as follows: a mass range between 80–2000 *m/z*, a scan rate of 1 spectrum s^{-1}, a nebulizer pressure of 25 psig, a capillary voltage of 3500 V, a fragmentor at 50 V, a skimmer at 45 V, a dry gas temperature of 275 °C, a dry gas flow rate of 10 L min^{-1}, a sheath gas temperature of 350 °C, and a sheath gas flow rate of 10 L min^{-1}. Analysis was performed in positive mode and via direct injection. Mass calibration was performed on the day of measurement using an external standard. The mass accuracy of the measurement results is better than 5 ppm.

Instrumentation—SEC: Size-exclusion chromatography (SEC) measurements were performed at 30 °C with THF as the mobile phase (flow rate 1 mL min^{-1}) on an SDV column set (10^3, 10^5, and, 10^6 Å) for the DDTDGe samples and for all other samples on a SECcurity2 GPC System with an MZ-Gel SDplus column set (100, 10^3, and 10^5 Å) from Polymer Standards Service, Mainz (PSS). Polymer concentrations were ca. 1 mg mL^{-1}. Calibration was carried out with polystyrene standards (PSS, Mainz): 1 240 000, 552 000, 304 000, 130 000, 66 000, 34 800, 19 700, 8 680, 3 500, 1 306, and 682 Da. For the SO-based and PhGE-based samples, a UV-detector was used, while for the DDTDGe-based samples, a RI detector was used. The SO monomer and the PhGE monomer eluted before the respective oligomers (Figures S15 and S16, Supporting Information, respectively) and were hence excluded from the reported spectra and the calculations. Note that for some SO-based samples, the SEC traces were normalized to the polymer peak (i.e., the intensity of the polymer peak was set to one and the intensity of the oligomer fraction was scaled accordingly) to make a comparison between the oligomer and polymer fractions more apparent.

Instrumentation—MALDI ToF MS: MALDI-ToF spectra were collected on a Bruker MALDI-ToF MS Autoflex Max in the linear modus. Trans-2-[3-(4-tert-Butylphenyl)−2-methyl-2-propenyliden] malononitrile (DCTB) was used as a matrix, and AgTFA or KTFA as a salt additive.

Experimental Procedures: Solutions of different pH values (i.e., pH 10, pH 12, pH 13, and pH 14) with LiOH, KOH, or NaOH were prepared in Milli-Q water. Solutions of different epoxides (SO, PhGE, DDTDGE, EDD, and CHO) at 0.1 or 1 M were prepared in toluene, chloroform, dichloromethane, hexane, or cyclohexane. For interfacial polymerization to occur, the organic solution was gently added with a pipette onto the aqueous phase in a closed container of different sizes (i.e., diameters of 1.7 cm (area of 2.3 cm^2) and 8 cm (area of 50.3 cm^2)) and allowed to react statically. One experiment was also conducted without a static interface by shaking at 600 rpm. After the designated reaction time (24, 72, or 100 h), polymer deposition was observed under some conditions. The precipitated polymer at the interface was collected with a pipette, dissolved in $CHCl_3$, and washed three times with Milli-Q water, with a centrifugation step of 10 min at −10 °C and 4500 rpm in between each wash cycle. After the last centrifugation cycle, most of the water was removed with a pipette. The remaining $CHCl_3$ and water were removed via a rotary evaporator, and the sample was subsequently analyzed with NMR spectroscopy, SEC, and ESI MS. A Kugelrohr short-path distillation was conducted on the sample made with DDTDGe to remove unreacted monomers and dimers. Several other control experiments were executed (i.e., toluene on top of pure Milli-Q water, 1 M SO in toluene on top of Milli-Q water) to investigate whether the colorless interface was also observed if no polymerization occurred.

Supporting Information

Supporting Information is available from the Wiley Online Library or from the author.

Acknowledgements

R.V. thanks the Research Foundation Flanders for her postdoctoral fellowship (1216222N). Ulrike Kemmer-Jones is thanked for her support. Dominik Schulz and Elena Berger-Nicoletti are thanked for the MALDI-ToF MS measurements. Sarah Vangrunderbeeck is thanked for her support with the ESI data interpretation.

Conflict of Interest

The authors declare no conflict of interest.

Data Availability Statement

The data that support the findings of this study are available from the corresponding author upon reasonable request.

Keywords

epoxide homopolymerization, interfacial anionic polymerization, on-water catalysis, poly(styrene oxide)

Received: June 5, 2024
Revised: July 18, 2024
Published online:

[1] M. Cortes-Clerget, J. Yu, J. R. A. Kincaid, P. Walde, F. Gallou, B. H. Lipshutz, *Chem. Sci.* **2021**, *12*, 4237.
[2] S. Narayan, J. Muldoon, M. G. Finn, V. V. Fokin, H. C. Kolb, K. B. Sharpless, *Angew. Chemie – Int. Ed.* **2005**, *44*, 3275.
[3] A. Chanda, V. V. Fokin, *Chem. Rev.* **2009**, *109*, 725.
[4] D. C. Rideout, R. Breslow, *J. Am. Chem. Soc.* **1980**, *102*, 7816.
[5] S. Bonollo, D. Lanari, L. Vaccaro, *European J. Org. Chem.* **2011**, https://doi.org/10.1002/ejoc.201001693.
[6] Z. Yan, C. Du, G. Luo, J. Deng, *React. Chem. Eng.* **2021**, *6*, 2159.
[7] Y. Zheng, J. Zhang, *ChemPhysChem* **2010**, *11*, 65.
[8] N. Azizi, M. R. Saidi, *Org. Lett.* **2005**, *7*, 3649.
[9] I. Vilotijevic, T. F. Jamison, *Science* **2007**, *317*, 1189.
[10] A. Manna, A. Kumar, *J. Phys. Chem. A.* **2013**, *117*, 2446.
[11] K. Piradashvili, E. M. Alexandrino, F. R. Wurm, K. Landfester, *Chem. Rev.* **2016**, *116*, 2141.
[12] M. F. Ruiz-Lopez, J. S. Francisco, M. T. C. Martins-Costa, J. M. Anglada, *Nat. Rev. Chem.* **2020**, *4*, 459.
[13] R. N. Butler, A. G. Coyne, *J. Org. Chem.* **2015**, *80*, 1809.
[14] Y. Jung, R. A. Marcus, *JACS* **2007**, *6*, 73.
[15] J. B. F. N. Engberts, *Pure Appl. Chem.* **1995**, *67*, 823.
[16] F. O. Laforge, P. Sun, M. V. Mirkin, *J. Am. Chem. Soc.* **2006**, *128*, 15019.
[17] J. G. Davis, B. M. Rankin, K. P. Gierszal, D. Ben-Amotz, *Nat. Chem.* **2013**, *5*, 796.
[18] X. Lu, M. Elimelech, *Chem. Soc. Rev.* **2021**, *50*, 6290.
[19] Y. Zhang, D. Rochefort, *J. Microencapsul.* **2012**, *29*, 636.
[20] G. B. Kauffman, *J. Chem. Educ.* **1988**, *65*, 803.
[21] F. Zhang, J. bing Fan, S. Wang, *Angew. Chemie – Int. Ed.* **2020**, *59*, 21840.
[22] M. J. T. Raaijmakers, N. E. Benes, *Prog. Polym. Sci.* **2015**, *63*, 86.
[23] J. H. Xin, H. Y. Fan, B. B. Guo, H. C. Yang, C. Y. Zhu, C. Zhang, Z. K. Xu, *Chem. Commun.* **2023**, *59*, 13258.
[24] J. Herzberger, K. Niederer, H. Pohlit, J. Seiwert, M. Worm, F. R. Wurm, H. Frey, *Chem. Rev.* **2016**, *116*, 2170.
[25] B. Charleux, Y. Ganachaud, *Macromolecular Engineering: Precise Synthesis, Materials Properties, Applications*, **2007**, pp. 605–642.
[26] C. Maitre, F. Ganachaud, O. Ferreira, J. F. Lutz, Y. Paintoux, P. Hémery, *Macromolecules* **2000**, *33*, 7730.
[27] H. Morinaga, Y. Ujihara, N. Yuto, D. Nagai, T. Endo, *J. Polym. Sci. Part A Polym. Chem.* **2011**, *49*, 5210.
[28] B. R. Spears, M. A. Marin, J. R. Montenegro-Burke, B. C. Evans, J. McLean, E. Harth, *Macromolecules* **2016**, *49*, 2022.

 © 2024 Wiley-VCH GmbH

ADVANCED SCIENCE NEWS
www.advancedsciencenews.com

Macromolecular Rapid Communications
www.mrc-journal.de

[29] D. D. Harrier, D. Guironnet, *Polym. Chem.* **2022**, *13*, 2459.
[30] R. Verbeke, W. Arts, E. Dom, M. Dickmann, W. Egger, G. Koeckelberghs, A. Szymczyk, I. F. J. Vankelecom, *J. Memb. Sci.* **2019**, *582*, 442.
[31] R. Verbeke, M. Seynaeve, M. Bastin, D. Davenport, S. Eyley, W. Thielemans, G. Koeckelberghs, M. Elimelech, I. Vankelecom, *J. Memb. Sci.* **2020**, *612*, 118438.
[32] R. E. Parker, N. S. Isaacs, *Chem. Rev.* **1959**, *59*, 737.
[33] L. Schechter, J. Wynstra, R. Kurkjy, *Ind. Eng. Chem.* **1957**, *49*, 1107.
[34] A. M. Tikhonov, *JETP Lett.* **2018**, *108*, 102.
[35] T. Zhu, P. Ning, Z. Chen, *J. Mol. Liq.* **2021**, *326*, 115213.
[36] D. K. Hore, D. S. Walker, L. Mackinnon, G. L. Richmond, *J. Phys. Chem. C* **2007**, *111*, 8832.
[37] F. Heatley, G. E. Yu, M. D. Draper, C. Booth, *Eur. Polym. J.* **1991**, *27*, 471.
[38] Z. Grobelny, M. Matlengiewicz, J. Jurek-Suliga, S. Golba, K. Skrzeczyna, D. Kwapulińska, *Polym. Bull.* **2017**, *74*, 4763.
[39] A. Yahiaoui, M. Belbachir, *J. Appl. Polym. Sci.* **2006**, *100*, 1681.
[40] D. C. Schriemer, L. Li, *Anal. Chem.* **1997**, *69*, 4169.
[41] S. Pullanchery, S. Kulik, B. Rehl, A. Hassanali, S. Roke, *Science* **2021**, *374*, 1366.
[42] P. Creux, J. Lachaise, A. Graciaa, J. K. Beattie, A. M. Djerdjev, *J. Phys. Chem. B.* **2009**, *113*, 14146.
[43] H. Fang, W. Wu, Y. Sang, S. Chen, X. Zhu, L. Zhang, Y. Niu, W. Gan, *RSC Adv.* **2015**, *5*, 23578.
[44] J. Nauruzbayeva, Z. Sun, A. Gallo, M. Ibrahim, J. C. Santamarina, H. Mishra, *Nat. Commun.* **2020**, 5285.
[45] F. G. Moore, G. L. Richmond, *Acc. Chem. Res.* **2008**, *41*, 739.
[46] A. P. Carpenter, R. M. Altman, E. Tran, G. L. Richmond, *J. Phys. Chem. B.* **2020**, *124*, 4234.
[47] R. Vaécha, S. W. Rick, P. Jungwirth, A. G. F. De Beer, H. B. De Aguiar, J. S. Samson, S. Roke, *J. Am. Chem. Soc.* **2011**, *133*, 10204.
[48] M. Kucera, Mechanism and Kinetics of Addition Polymerizations, in: *Compr. Chem. Kinet*, Elsevier, Amsterdam, **1991**.

© 2024 Wiley-VCH GmbH

A3: Anionic polymerization of phenyl-substituted isoprene derivatives: polymerization behaviour and cyclization-enabled fluorescence

[redacted], Gregor M. Linden[1], [redacted]

[1]Department of Chemistry, Johannes Gutenberg University Mainz, Duesbergweg 10-14, 55128, Mainz, Germany.

[2]Max Planck Graduate Center, Forum Universitatis 2, 55122 Mainz, Germany

Published in: *Polym. Chem.* **2024**, *15*, (31), 3204–3213, DOI: 10.1039/D4PY00601A

Supporting Information is available from the publisher.

The following publication is reproduced with permission from the Royal Society of Chemistry under the Creative Commons Attribution 3.0 Unported Licence.

Polymer Chemistry

ROYAL SOCIETY OF CHEMISTRY

PAPER

View Article Online
View Journal | View Issue

Cite this: *Polym. Chem.*, 2024, **15**, 3204

Anionic polymerization of phenyl-substituted isoprene derivatives: polymerization behaviour and cyclization-enabled fluorescence†

Moritz Rauschenbach,[a] Laura Stein,[a] Gregor M. Linden,[a] Ramona Barent,[a,b] Katja Heinze [a] and Holger Frey *[a]

Received 3rd June 2024,
Accepted 9th July 2024

DOI: 10.1039/d4py00601a

rsc.li/polymers

1,3-Dienes are important monomers for living anionic polymerization. However, phenyl-substituted diene monomer structures have been rarely investigated. Based on DFT calculations and ^{13}C NMR spectroscopy, a discrepancy in the reactivity of the two monomers 1-phenyl isoprene (1PhI) and 4-phenyl isoprene (4PhI) in anionic polymerization is expected. Starting from a Wittig reaction including an optimized extraction procedure, disubstituted 1,3-dienes were obtained that resulted in polymers with different degrees of 1,3-incorporation. The polymers have been characterized by ^{1}H NMR spectroscopy and using different SEC conditions. Molecular weights of up to 48.8 kg mol^{-1} with narrow dispersities ($Đ \leq 1.13$) were achieved. The addition of the modifier THF led to an initial increase of vinyl units as well as a loss of control over the polymerization of 4PhI. Increasing the THF concentration further resulted in a rather unusual decrease of the vinyl units and ended with more than 80% 1,4-units in pure THF. Copolymerizations with styrene (S) and isoprene (I), respectively, were tracked *via in situ* ^{1}H NMR kinetics. The observed ideally random copolymerizations of I and 1PhI as well as the gradient copolymers with S were further investigated *via* the synthesis of copolymers with a targeted M_n of 40 kg mol^{-1}. In a subsequent reaction step, the homopolymers were cyclized using trifluoromethyl sulfonic acid inducing fluorescence properties. The different microstructures and substitution patterns of the original polymers differ in both emission maxima and quantum yields.

Introduction

Living anionic polymerization introduced by Michael Szwarc in 1956 offers excellent control over molecular weights and the dispersity $Đ$ of polymers.[1,2] It has been widely used for the polymerization of 1,3-dienes, such as 1,3-butadiene and isoprene, to generate polydiene materials for synthetic rubber. The elastic properties of these polydienes after crosslinking notably depend on their microstructure. Therefore, the main target of early studies of anionic polymerization of 1,3-dienes was the optimization of reaction parameters (*e.g.*, initiator, solvent, further additives, and temperature) to obtain a high *cis*-1,4-content.[3]

The copolymerization of 1,3-dienes, such as 1,3-butadiene (B) and isoprene (I), with styrene (S) affords a variety of possible polymer architectures.[4,5] ABA triblock copolymers have attracted attention as thermoplastic elastomers (TPEs). This architecture relies on a flexible, low T_g polydiene midblock B (*e.g.*, polyisoprene) and two outer polystyrene A blocks that act as crosslinks after cooling and vitrification.[6] In 1966, Holden and Milkovich reported that the statistical copolymerization of isoprene and styrene in apolar solvents like cyclohexane results in block-like gradient copolymers that were later designated as "tapered".[7] The addition of a small quantity of THF with respect to the lithium-ion concentration leads to a change of the reactivity ratios and the respective monomer gradient. By varying the THF concentration, the incorporation of both monomers can be tuned to achieve ideally random incorporation, and even complete reversal of the molar composition is possible, as shown by detailed online NIR kinetics recently.[8] However, the addition of THF as a "modifier" at the same time also influences the incorporation mode of isoprene (increasing the extent of 3,4-addition) and therefore has an undesired impact on the elastic properties. As described in many studies, an increase of the number of 1,2- and 3,4-units in polydienes is observed when increasing the polarity of the system.[8–11]

Only a few studies have been reported for phenyl-substituted butadiene derivatives.[12,13] As an example, the 1-phenyl-

[a]*Department of Chemistry, Johannes Gutenberg University, Duesbergweg 10-14, 55128 Mainz, Germany. E-mail: hfrey@uni-mainz.de*
[b]*Max Planck Graduate Center, Forum Universitatis 2, 55122 Mainz, Germany*
†Electronic supplementary information (ESI) available. See DOI: https://doi.org/10.1039/d4py00601a

This journal is © The Royal Society of Chemistry 2024

View Article Online
Polymer Chemistry Paper

1,3-butadiene (PhB) monomer has been polymerized *via* either anionic or catalytic approaches.[14–17] It can be considered as a β-substituted styrene or as a 1-phenyl-substituted 1,3-butadiene.[18] This combination of two very established monomers provides an intriguing perspective. Suzuki *et al.* systematically investigated the anionic polymerization of PhB regarding its copolymerization with butadiene and styrene as well as the microstructure with respect to various parameters.[12,19–22] ^{1}H NMR studies of the resulting microstructure of PhB in different solvents revealed distinct behaviour compared to established dienes. The addition of aliquots of THF enhanced the formation of the vinylic microstructure. However, a 1,4-dominated microstructure was obtained when polymerization was performed in THF, confirmed by NMR analysis based on the chemical shifts of the aromatic protons of oligomeric structures in deuterated THF. The authors concluded that the negative charge is localized in the α-position of the phenyl ring to form the most stable anion as the active chain end. This explains why poly(1-phenyl butadiene) (PPhB) polymerized in THF shows predominantly 1,4-units.[21]

The phenyl-substituted polybutadienes showed a glass transition temperature (T_g) of around 30 °C.[17] It is worth mentioning that the T_g is in between those of the structurally similar polyisoprene ($T_g \leq -65$ °C)[23] and polystyrene (T_g = 100 °C).[11] Han *et al.* reported catalytic polymerization with a 3,4-content of 94%, resulting in a T_g of 82 °C, indicating a high dependency on the respective microstructure.[24] In a cationic polymerization approach, phenyl butadiene underwent cyclization as a side-reaction. Fundamental studies report on the targeted cationic cyclization post-polymerization of polydienes to obtain an unsaturated polycyclic species.[25–28] More recently, the cyclisation reaction was adapted to P(PhB) to maximize the T_g. Depending on the microstructure, the T_g of the cyclized material can reach nearly 200 °C, which is among the highest T_gs reported for aliphatic hydrocarbon polymers.[29] Additionally, cyclized poly(phenylbutadiene) (*cyc*P(PhB)) showed fluorescence.

Herein, we report the copolymerization of "phenyl isoprenes" with styrene and isoprene. For isoprene, the attachment of the phenyl ring can take place either at the 1- or the 4-position, resulting in a 1,2- or a 1,3-disubstituted 1,3-diene structure. While the 4-phenyl isoprene (4PhI) has been briefly described with respect to its anionic polymerization,[30] to the best of our knowledge, the 1-phenyl isoprene (1PhI) has not been employed for anionic polymerization to date. In this work, we compare 1PhI and 4PhI on a theoretical basis using density functional theory (DFT) as well as ^{13}C NMR spectroscopy to predict their reactivity in anionic polymerization. We use styrene and isoprene, respectively, for comparison. Both phenyl isoprene monomers are investigated in depth regarding their behaviour in anionic polymerization and are also copolymerized with both isoprene and styrene. For the determination of reactivity ratios, online ^{1}H NMR spectroscopy was employed. We monitored the anionic copolymerization with the structurally related monomers styrene and isoprene in cyclohexane, respectively. Finally, polymer cyclization is explored according to literature procedures, aiming at fluorescent, high T_g materials based on the reported monomers.[17,24,29,31]

Results and discussion

Synthesis of phenyl-substituted isoprene derivatives

1PhI and 4PhI were synthesized *via* a one-step Wittig reaction starting from commercially available aldehyde and ketone structures, respectively. For the synthesis of 1PhI, using the potassium *tert*-butoxide monomer, yields exceeding 75% were achieved. However, the stronger base sodium hexamethyldisilyl amine (NaHMDS) is required to achieve similar yields for the ketone benzylidene acetone. A straightforward method was established for the separation of triphenylphosphine oxide including precipitation, centrifugation and subsequential distillation. The details are given in the ESI.†

Since 1PhI and 4PhI can be viewed as β-substituted styrene derivatives, we estimate the reactivity of both monomers in analogy to previously described methods. ^{13}C NMR spectroscopy was utilized to estimate the reactivity of *para*-substituted styrene derivatives by Hirao *et al.*[32] The β-carbon shift identifies the electron charge density of the reactive vinyl bond. Increasing the polarization of the reacting carbon–carbon bond leads to increased reactivity. Therefore, it is in good agreement with the monomer reactivity in anionic polymerization. If 1PhI and 4PhI are viewed as styrene derivatives, the chemical shift of C1 as assigned in Scheme 1 was identified. Thus, 4PhI (δ = 117.45 ppm, $CDCl_3$) is expected to be much more reactive compared to styrene (δ = 113.36 ppm, $CDCl_3$), while 1PhI (δ = 113.02 ppm, $CDCl_3$) should be slightly less reactive in anionic copolymerization in apolar media.

Furthermore, DFT calculations of both monomers were conducted to obtain further theoretical insights. Fig. 1 shows the relative electron densities of both 1PhI and 4PhI in comparison with the values calculated for isoprene (differences shown in brackets). Focusing on the free methylene groups, which are most likely to be attacked by nucleophilic reagents, 4PhI (−0.176e) exhibits a lower charge at this position compared to 1PhI (−0.193e). Hence, the nucleophilic attack as part of the propagation is prone to occur, supporting the expectation based on ^{13}C NMR spectroscopy. Nevertheless, the electron densities of the reactive double bond show just a minor deviation from the 3,4-double bond in isoprene, which is

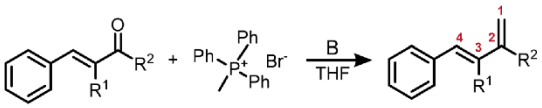

1PhI: $R^1 = CH_3$; R^2 = H; B = KO*t*Bu
4PhI: R^1 = H; $R^2 = CH_3$; B = NaHDMS

Scheme 1 Synthesis route to the phenyl-substituted isoprene derivatives.

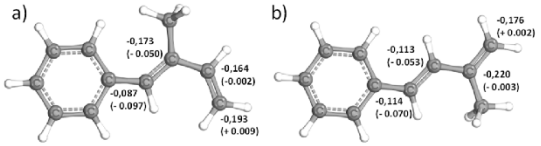

Fig. 1 3D visualization of (a) 1PhI and (b) 4PhI, respectively, with the corresponding partial charges of the dienic carbon atoms calculated using DFT. In brackets, the deviations from the calculated electron densities of isoprene are given.[59,60]

assumed to be the one reacting in the anionic polymerization. This could be interpreted in terms of a fast crossover reaction in both directions.

Homopolymerization of PhIs with *sec*-BuLi in cyclohexane

Both monomers 1PhI and 4PhI can be interpreted as a structural combination of styrene and isoprene. To investigate whether their behaviour in the anionic polymerization resembles that of S or I, a series of homopolymers with increasing M_n has been synthesized. All polymerizations were carried out in cyclohexane, using *sec*-butyl lithium as an initiator at room temperature. Subsequently, the homopolymers were characterized *via* SEC, ^{1}H NMR spectroscopy and DSC. Table 1 summarizes all characterization data of the obtained polymers, which possessed molecular weights in good agreement with the targeted values in a range of 4.6–48.8 kg mol^{-1} (SEC, eluent THF, and PS calibration) with low dispersities ($Đ \leq 1.13$). The SEC-determined molecular weights are strongly dependent on the calibration standard employed.

The microstructures of both P(1PhI) and P(4PhI) were investigated by ^{1}H NMR spectroscopy in analogy to previously reported studies.[12,17] The spectra (Fig. 2) show the olefinic signals used for the determination of the microstructures. The signals were assigned according to the reported microstructure of P(1-phenyl butadiene).[12] The sharp signals of P(4PhI) indicate a highly defined composition, which is supported by the integration, showing 94% 1,4-units. This is consistent with the microstructure of polyisoprene obtained under these conditions.[33] In comparison, the ^{1}H NMR spectrum of P(1PhI) displays broad signals with a microstructure consisting of 66% 1,2-units. This result can be explained by a sterically hindered 1,4-addition reaction, as previously suggested for 1,1-disubstituted 1,3-dienes.[34]

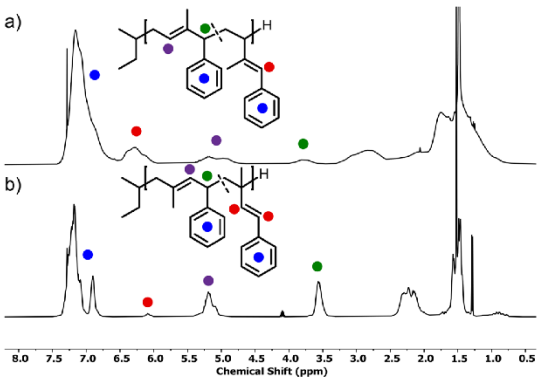

Fig. 2 ^{1}H NMR spectra ($CDCl_3$, 400 MHz) of (a) P(1PhI) and (b) P(4PhI).

The SEC traces shown in Fig. 3 confirm the good control of the polymerization for both monomers, resulting in narrow, monomodal distributions. A high degree of agreement was observed between the targeted molecular weights and the results based on PI calibration, which can be taken as an indirect confirmation of the predominant 1,4-microstructure. In contrast, the prevalence of the 1,2-microstructure in P(1PhI) samples underlines why PS calibration yields values that exhibit closer proximity to theoretical predictions.

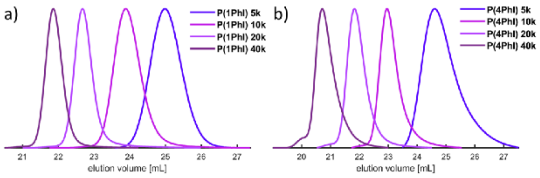

Fig. 3 SEC traces of the synthesized homopolymers with increasing targeted M_n from (a) 1-phenyl isoprene and (b) 4-phenyl isoprene.

Table 1 Overview of the homopolymers synthesized *via sec*-butyllithium initiated polymerization in cyclohexane

Entry	M	M_n^{targ} (kg mol^{-1})	M_n[a] (kg mol^{-1})	M_n[b] (kg mol^{-1})	$Đ$	1,4-PhI[c] (%)	1,2-PhI[c] (%)	T_g (°C)
1	1PhI	5	3.6	4.6	1.06	42	58	62
2		10	6.5	8.5	1.05	34	66	69
3		20	13.6	18.4	1.04	35	65	65
4		40	24.0	32.4	1.02	37	63	69
5	4PhI	5	3.8	4.7	1.13	85	15	47
6		10	10.7	13.6	1.07	94	6	47
7		20	22.6	30.0	1.09	94	6	48
8		40	48.8	64.8	1.11	94	6	48

[a] Determined by SEC (THF, PI calibration, and RI detector). [b] Determined by SEC (THF, PS calibration, and RI detector). [c] Determined from the olefinic region of the ^{1}H NMR spectra (400 MHz, $CDCl_3$).

 This journal is © The Royal Society of Chemistry 2024

Addition of polar additives

The polymerization of 1,3-dienes is known to depend on several parameters (*e.g.*, chain end and monomer concentration, temperature, solvent, *etc.*) in terms of the regio-isomeric composition of the resulting polymers.[8,35–38] The polarity of the solvent is a key parameter, since it determines the coordination of the chain end to the lithium ion.[39] In numerous studies, it was shown that the addition of aliquots of THF in the polymerization of 1,3-dienes increases the content of vinylic units.[8,9,40] Furthermore, the addition of THF accelerates propagation kinetics. This effect has been observed in both isoprene and styrene, where propagation reaches a maximum before further addition of THF decelerates propagation.[41,42]

For 1-phenyl butadiene, it was reported that upon addition of a few aliquots of THF, the ratio of 1,2-units increases.[12] Further increasing the content of THF and polymerization in pure THF led to a maximum of 90% 1,4-content. In a similar fashion, we conducted the polymerization of 1PhI and 4PhI in cyclohexane with 2 and 20 equivalents of THF with respect to the lithium-ion concentration. Furthermore, we carried out the polymerization reaction in pure THF at −78 °C. It should be noted that common dienes, such as myrcene and isoprene, are not capable of polymerizing under these conditions.[43,44] As listed in Table 2, the addition of THF has an impact on the resulting microstructure as the ratio of vinyl units increases. In line with previous observations for PhB, in pure THF, more than 80% 1,4-units were formed. A tentative explanation might be given by the reactivity of the chain end and the resulting propagation rates. Strohmann *et al.* reported experiments with *tert*-butyl lithium and THF in a ratio of 1 : 2, revealing remarkable aggregation, leading to an increase in reactivity compared to the ratios 1 : 1 and 1 : 2.5.[45] Consequently, the polymerization rate is enhanced by small amounts of THF, promoting the formation of vinylic units. The faster kinetics may also explain the broad distribution observed for entry 12. Carrying out the polymerization of 4PhI with 2 equivalents of THF with respect to the BuLi concentration did not result in dispersities lower than 1.4, as illustrated in Fig. S16.† Further increasing the polarity supports the formation of the most stable anion. For both 1PhI and 4PhI, the charge will be delocalized in the aromatic ring as demonstrated for PhB.[21,22] Therefore, one observes the predominant formation of 1,4-units with increasing polarity of the system, as obvious from a comparison of the respective ^{1}H NMR spectra (Fig. 4).

As expected, DSC measurements of the resulting polymers show a clear correlation between the glass transition and the respective microstructure. For example, 1PhI polymerized in THF with a high 1,4-content exhibited a lower T_g of 50 °C compared to 67 °C when polymerized in cyclohexane due to its more flexible backbone compared to P1PhI synthesized in cyclohexane, which is dominated by a 1,2-microstructure (Fig. S14†). As shown by the values in Table 2, the T_gs for the P1PhI samples prepared in different systems shift to higher temperature with increasing solvent polarity. P4PhI polymerized in either cyclohexane or THF always resulted in a high 1,4-content. Therefore, as shown in Fig. S15,† the T_gs of both samples are in the same range of 50–56 °C. A higher 1,2-content can raise the T_g to 73 °C.

In situ ^{1}H NMR: copolymerisation with styrene as a comonomer

Living poly(1PhB) chain ends were not sufficiently reactive to initiate the polymerization of butadiene or styrene in THF. Reaching a maximum of 35% block efficiency, only bimodal

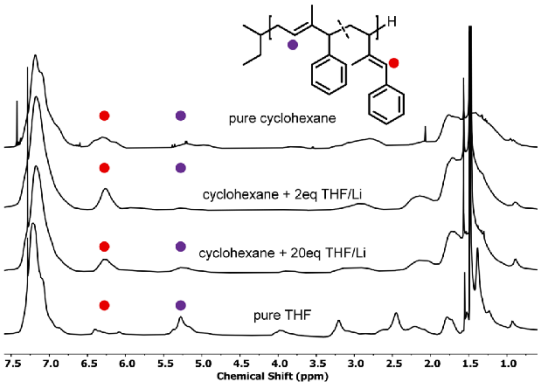

Fig. 4 Stacked ^{1}H NMR spectra of P(1PhI) polymerized with increasing concentrations of THF, resulting in microstructures with shifting ratios.

Table 2 Data of the polymer samples obtained when investigating the impact of THF on the polymerization of PhI monomers in cyclohexane

Entry	M	M_n^{targ} (kg mol^{-1})	M_n [b] (kg mol^{-1})	$\frac{[THF]}{[Li]}$	$Đ$	1,4-PhI[c] (%)	1,2-PhI[c] (%)	T_g (°C)
1	1PhI	10	7.8	0	1.05	34	66	67
9		10	10.3	2	1.07	12	88	62
10		10	11.1	20	1.08	33	67	53
11[a]		10	9.6	Pure	1.06	85	15	50
5	4PhI	10	13.9	0	1.09	94	6	56
12		10	7.1	2	1.44	n.d.	n.d.	73
13		10	8.7	20	1.15	56	44	63
14[a]		10	9.9	Pure	1.08	82	18	50

[a] Polymerization at −78 °C. [b] Determined by SEC (THF, PS calibration, and RI detector). [c] Calculation using the respective olefinic signals of the ^{1}H NMR spectra.

View Article Online
Paper Polymer Chemistry

distributions were reported. However, reverse monomer addition resulted in monomodal SEC traces, confirming that all living chain ends initiated 1PhB.[20]

To investigate the statistical copolymerization behaviour of both monomers with styrene and isoprene, respectively, we conducted real-time ^{1}H NMR spectroscopy to evaluate the reactivity ratios. First, copolymerization reactions of styrene with 1PhI and 4PhI, respectively, were conducted. During the statistical copolymerization, individual monomer peaks were traced to determine monomer conversion. Due to the absence of termination and transfer reactions in classical anionic polymerization, monitoring of the integrals can also be used to determine the relative position along the growing chains.[46,47] The stacked ^{1}H NMR spectra for the copolymerization of styrene and 1PhI are shown in Fig. 5 and in Fig. S18† for 4PhI. The monomer concentrations plotted as a function of time and total conversion, respectively, show preferential consumption of the phenyl isoprenes over styrene in both cases.

The collected data were used to calculate the reactivity ratios r_{PhI} and r_S, as listed in Table 3. They define the ratio between the rate of homopolymerization and the rate of the crossover reaction. Using the non-terminal model of Jaacks, the values were determined.[48] Based on these evaluated parameters, plots of the relative comonomer position along the chain were generated. As illustrated in Fig. 6(b) and (c), for both systems, a pronounced gradient is observed. The steeper gradient for the 4PhI system confirms 4PhI to be more reactive, supporting the hypothesis derived from the β-C-shift.

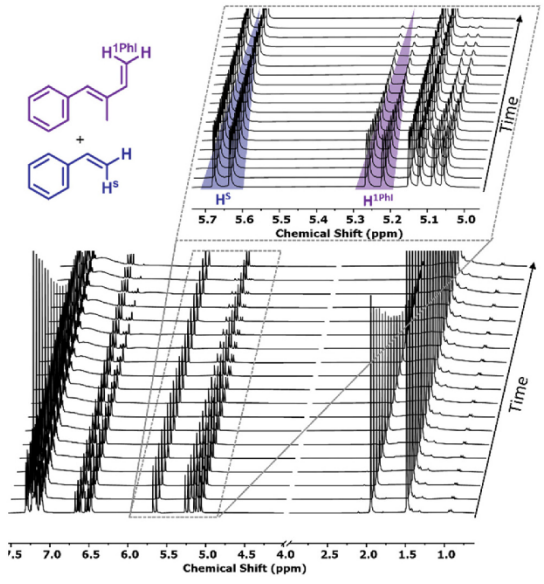

Fig. 5 Stacked ^{1}H NMR spectra (400 MHz, C_6D_{12}) of the copolymerization of styrene/1PhI as a function of time. The zoomed-in region shows the peaks tracked for the evaluation of the respective comonomer consumption.

Table 3 Evaluated reactivity ratios of the copolymerization of styrene with 1PhI and 4PhI, respectively, using the Jaacks model. For comparison, the reactivity ratios of dienes and styrene are given as well

Diene	r_{diene}	r_S
1-Phenyl isoprene	3.38	0.30
4-Phenyl isoprene	9.20	0.109
Isoprene[49]	11	0.049
β-Myrcene[50]	36	0.028
β-Farnesene[51]	27	0.037
cis-Ocimene[52]	1.015	0.985
trans-Ocimene[52]	0.62	1.52
Vinylcyclohexene[53]	0.39	2.56

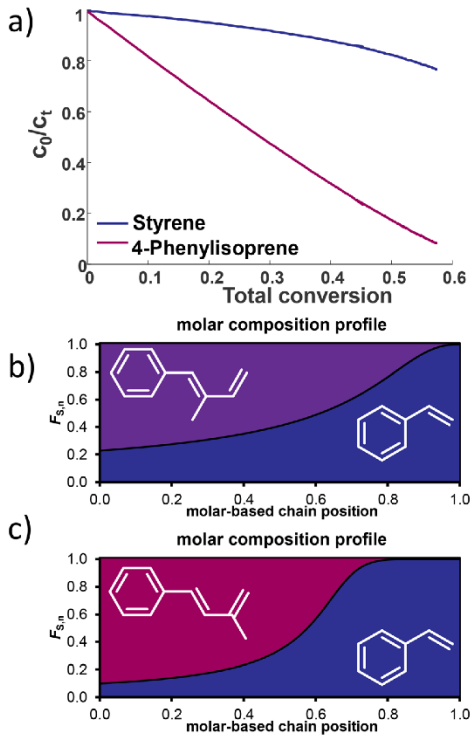

Fig. 6 (a) Monomer conversion for the copolymerization of S and 4PhI. Calculated molar composition profiles of S and (b) 1PhI and (c) 4PhI, respectively.

However, in contrast to the abovementioned assumption, 1PhI is also consumed faster, although the carbon shift indicated the opposite. This demonstrates that these simple considerations cannot be applied to diene systems. Reactivity ratios calculated using the terminal model of the Meyer–Lowry fit are given in the ESI.†

In comparison with the reactivity ratios observed for the copolymerization of styrene with isoprene (substituted in the 2-position) and myrcene (Table 3), the di-substituted 1PhI and 4PhI display a less pronounced gradient. Nevertheless, it is

This journal is © The Royal Society of Chemistry 2024

worth noting that the 1,2-disubstituted 1PhI demonstrates higher reactivity ratios compared to previously reported 1,2-disubstituted dienes (*i.e.*, *trans*- and *cis*-ocimene and 1-vinyl cyclohexene).[52,53] To the best of our knowledge, 4PhI is the first 1,3-disubstituted 1,3-diene that has been investigated regarding its copolymerization kinetics with styrene.

In situ ^{1}H NMR kinetics with isoprene as a comonomer

In analogy to the investigation of copolymerization with styrene, we also studied *in situ* ^{1}H NMR kinetics for copolymerization with isoprene (I). Due to the diene nature of both monomers, the respective peaks overlapped, as shown in the stacked spectra as a function of time in Fig. S21 and S22.† From the obtained data, the plots of the comonomer concentrations *vs.* the total conversion and against time are given in Fig. 7 and in the ESI.† To our surprise, the copolymerization of 4PhI with I did not result in plausible results, neither for the Jaacks nor for the Meyer–Lowry fit, when carried out in an equimolar ratio. Repeating the copolymerization under the same conditions or with a ratio of 70 : 30 did not improve the given results, which are illustrated in the ESI.† Using the Meyer–Lowry fit, in all cases the reactivity ratios were calculated to exceed 1, as summarized in Table S3.† In comparison, the obtained data do not reflect the theoretical Jaacks fit. Nevertheless, the stacked NMR spectra in Fig. S22† indicate a faster consumption of isoprene compared to 4PhI.

The Jaacks fit was successfully used for 1PhI and isoprene, confirming the almost ideally random copolymerization with reactivity ratios of r_I = 1.155 and r_{1PhI} = 0.865. The cross-over reaction seems to be independent of the monomer. This might be explained by the similar electron densities calculated using DFT. A comparison with the known reactivity ratios using myrcene as another diene is given in Table 4.

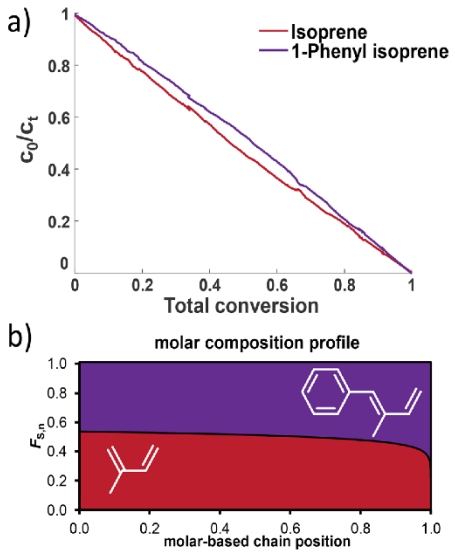

Fig. 7 (a) Monomer conversion in the copolymerization of I and 1PhI and (b) the molar composition profile of the copolymer of I and 1PhI.

Table 4 Reactivity ratios of the copolymerization of isoprene and reported 1,3-dienes

Monomer A	r_A	r_I
1PhI	0.865	1.155
4PhI	n.d.	n.d.
β-Myrcene[50]	4.4	0.23

Copolymerization with isoprene and styrene

The determined reactivity ratios may lead to unique material properties. Therefore, the copolymerizations were conducted on a larger scale (Fig. 8). A rather high molecular weight of 40 kg mol^{-1} was targeted to induce phase separation despite the gradient structure (Table 5). In all cases, monomodal distributions with a low dispersity ($Đ$ < 1.11) were obtained. The stacked ^{1}H NMR spectra in Fig. S28† show the characteristic signals of the monomers. The gradient structure in the anionic copolymerization of I and S can be visually tracked through the gradual colour change with monomer conversion. This results in a decreasing concentration of the colorless polydienyl chain ends and a gradually increasing concentration of orange polystyryl chain ends. For both copolymerization reactions with isoprene, an immediate coloration of the solution was observed after initiation. Throughout the polymerization, no colour change was observed. Therefore, as shown before, a significant number of polyphenylisoprenyl chain ends were present from the beginning. To lend further support to the completely random distribution of 1PhI throughout the chain when copolymerized with isoprene, we observed only one glass transition at 3 °C. The copolymer P(I-*co*-4PhI) exhibits a broad softening regime rather than a defined glass transition.

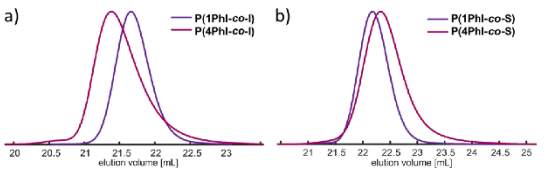

Fig. 8 SEC traces of the copolymerization of 1PhI and 4PhI with (a) isoprene and (b) styrene.

Table 5 Summarized data of the copolymerization of phenyl isoprenes with isoprene or styrene as a comonomer

Entry	Monomer (A)	Monomer (B)	M_n^{targ} (kg mol^{-1})	$M_{n,SEC}$[a] (kg mol^{-1})	$Đ$	T_g (°C)
15	1PhI	I	40	33.8	1.04	3
16	1PhI	S	40	35.6	1.05	67
17	4PhI	I	40	37.9	1.09	−10
18	4PhI	S	40	29.7	1.11	61

[a] Determined by SEC (THF, PS calibration, and RI detector).

Further drying in a high vacuum and the change of the heating rate did not clarify the inflection point. The soft gradients of the styrenic copolymers prevented phase segregation, resulting in merely one T_g >60 °C.

Cyclization to enhance thermal properties and prepare fluorescent materials

The synthesized homopolymers show lower T_gs compared to polystyrene (T_g = 100 °C).[11] However, since the phenyl rings are all adjacent to double bonds, cationic cyclization can be performed to alter the thermal properties. As already presented for butadiene-derived structures, the trifluoromethanesulfonic acid-initiated modification influences the thermal properties of these polymers drastically.[16,17,24,29,31,54–56] Consequently, the cyclized P(PhI) structures are expected to exhibit strongly increased rigidity and thus high T_g values. The selected polymers (entries 4 and 8 of Table 1) with a targeted molecular weight of 40 kg mol^{-1} were cyclized using CF_3SO_3H in cyclohexane at room temperature (Scheme 2). After drying, amber-coloured powders were obtained. Since the samples remained soluble in a variety of solvents after the intramolecular cyclization, they were investigated by SEC and NMR analyses. The SEC traces shown in Fig. 9 and S33† present the expected shift to a higher elution volume. The SEC traces (Fig. S33†) show a signal for the flow rate marker toluene, indicating the presence of a polymer rather than degradation to small molecules. This discovery was described by Han *et al.* and attributed to the compression of the polymer chain and an increase in hydrodynamic radii.[29] DSC measurements verified the expected increase of the T_g values (Table 6). The cyclization effect on the T_g values is stronger for *cyc*P(1PhI), with T_g reaching 180 °C after cyclization. The T_g of *cyc*P(4PhI) was determined to be 131 °C.

In agreement with the reported *cyc*P(PhB) of Ma and coworkers, we observed that the cyclized P(PhI) samples show fluorescence when irradiated with UV light (Fig. 9).[17] This observation is most likely explained by a clusterization-trig-

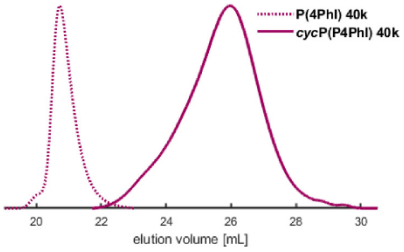

Fig. 9 SEC traces of the cyclized P4PhI in comparison with the initial polymer (entry 8, Table 1).

Table 6 Summarized data of the changed material properties after the cyclization reaction

Entry	Entry of the precursor	Polymer	M_n[a] (kg mol^{-1})	$Đ$	T_g (°C)
19	4	P1PhI	3.2	1.63	187
20	8	P4PhI	2.9	1.45	131

[a] Determined by SEC (THF, PS calibration, and RI detector).

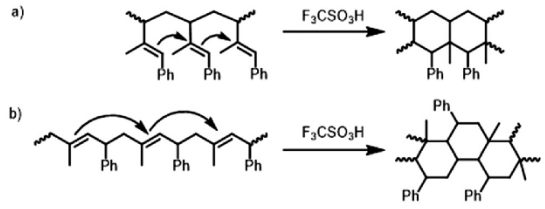

Scheme 2 Proposed mechanism for the cyclization of the predominant microstructures of (a) P1PhI and (b) P4PhI in analogy to the literature.[24]

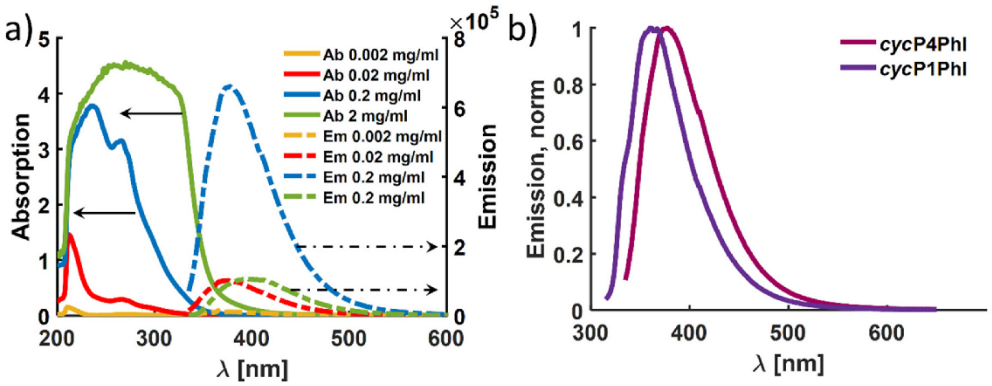

Fig. 10 (a) Absorption (solid) and emission (dashed) spectra of cyclized P4PhI at different concentrations in toluene (λ_{exc} = 330 nm) and (b) normalized emission spectra of *cyc*P1PhI and *cyc*P4PhI in toluene (c = 0.2 mg mL^{-1}, $\lambda_{exc,cycP1PhI}$ = 310 nm and $\lambda_{exc,cycP4PhI}$ = 330 nm).

 This journal is © The Royal Society of Chemistry 2024

gered emission.[57] To quantify the photochemical properties dependent on presumed clusterization, absorption and emission properties were determined using four different concentrations (2, 0.2, 0.02, and 0.002 mg mL^{-1}). The main questions raised were (i) whether the introduction of the methyl group leads to a shift in the emission maximum compared to the *cyc*P(PhB) polymer due to different ordering and (ii) whether the differing initial microstructures of P1PhI and P4PhI might result in distinct emission properties. In Fig. 10a, the emission spectra of the solutions of *cyc*P(P4PhI) with decreasing dilution are shown (λ_{exc} = 330 nm). Due to the high optical density and therefore self-absorption, the sample with the highest concentration shows a significantly reduced emission intensity compared to the other concentrations under the same conditions. At the same time, the emission maximum shifts from 375 nm to 395 nm (Table S4†). In contrast to previously reported interpretation clusterization-triggered emission,[57] we propose that the emission maximum shifts apparently and its intensity decreases due to inner filter effects with increasing concentration. Going from *cyc*P1PhI to *cyc*P4PhI, a presumed impact of the initial microstructure is observable with the emission maximum shifting from 360 nm to 377 nm (Fig. 10b). The absolute quantum yields of both samples in the solid state were determined using an integrating sphere. In both cases, the observed self-absorption decreases the overall quantum yield. As it is higher for *cyc*P4PhI (4.1%) than for *cyc*P1PhI (2.9%), *cyc*P4PhI is a more efficient candidate for utilization in organic light-emitting diodes (OLEDs).

Experimental

Terminology

(*E*)-(2-Methylbuta-1,3-dien-1-yl)benzene and (*E*)-(3-methylbuta-1,3-dien-1-yl)benzene are abbreviated as 1PhI and 4PhI, respectively.

Instrumentation

SEC measurements were performed using an Agilent 1100 Series system equipped with a SDV column set from PSS (SDV 103, SDV 105, and SDV 106). Tetrahydrofuran (THF) was used as the mobile phase (flow rate: 1 mL min^{-1}) and as the solvent. The calibration standards polystyrene and polyisoprene were provided by PSS. Measurements were performed at 30 °C with both RI and UV (275 nm) detectors and toluene was used as a reference. The data analysis was carried out using PSS WinGPC UniChrom (V 8.31, Build 8417) software provided by PSS Polymer Standards Service GmbH. NMR spectra were recorded on a Bruker Avance 400 spectrometer at 400 MHz for ^{1}H NMR and 103 MHz for ^{13}C NMR. The determination of glass transition temperatures (T_g) was performed on a DSC 250 (TA Instruments) differential scanning calorimeter. Two heating cycles and one cooling cycle were conducted at a rate of 10 °C min^{-1}. A detailed description of the DSC measurements and the description of the photochemical measurements are given in the ESI.†

Monomer and polymer synthesis

Both novel monomers 1PhI and 4PhI were synthesized in a one-step Wittig reaction. Alterations to published procedures are given in the ESI† together with a detailed description of the polymerization conditions.

Real-time ^{1}H NMR

The measurements were conducted on a 400 MHz Bruker Avance spectrometer. All spectra are referenced internally to the residual proton signal of deuterated cyclohexane-d_{12}. The polymerization mixtures were prepared in an argon-filled glove box. Monomers and solvents were purified over calcium hydride and trioctyl aluminum in the case of the monomers. The measurements were performed in a conventional NMR tube sealed with a rubber septum.

Prior to initiation, a first spectrum was recorded and equilibrated to a temperature of 25 °C. Following the initiation using 30 μL of *sec*-butyl lithium (0.65 M in cyclohexane), the NMR experiment was started, in which every 30 s, a scan was performed over a period of 6 to 7 hours. By tracking the decrease of the respective monomer signals, determination of the reactivity ratios was achieved using NIREVAL software designed by our group.[58]

Cyclization

The cyclization reaction was performed according to the literature. Into a solution of 200 mg P(4PhI) dissolved in 25 mL cyclohexane, trifluorosulfonic acid (0.2 mL, 2 eq. per double bond in every repeating unit) was added. The dark solution was quenched after 1 hour using a 1 wt% aqueous sodium carbonate solution. After washing with water, the polymer was precipitated in methanol and dried under vacuum.

Conclusion

In this work, the anionic polymerization of two isoprene derivatives, *i.e.*, 1-phenyl isoprene and 4-phenyl isoprene, was introduced. 4PhI was investigated in more detail than in earlier reports, and 1PhI has not been described to date. The difference in the substitution pattern of 1,3-dienes was expected to result in different reactivities, as already indicated by their β-C-shifts and by DFT calculations. Butyl lithium-initiated polymerizations allowed for the synthesis of polymers with narrow molar mass distributions and good control over the molecular weights in a range of 4.6 to 48.8 kg mol^{-1}. ^{1}H NMR spectroscopy revealed the expected differences in the microstructures. This was further modified using THF, leading to unusual behaviour caused by the attached phenyl ring. Online NMR kinetics uncovered a preference for the phenyl-substituted isoprene over styrene, despite the initial theoretical results predicting reduced reactivity of 1PhI. Nevertheless, these predictions are in line with the data obtained from kinetics with isoprene, which showed random incorporation for 1PhI/I. DSC measurements of the respective compositions further revealed merely one glass transition. In a post-polymer-

ization cyclization reaction, soluble materials with distinct photophysical properties were obtained. The characterization revealed an apparent dependency of the fluorescence maximum on the different microstructures of the starting materials due to self-absorption. As those materials also present a pronounced increase in rigidity, as indicated by the drastic increase of the glass transition temperature, they could be considered intriguing building blocks for block copolymers with an intramolecularly crosslinked high T_g block.

Author contributions

Moritz Rauschenbach: conceptualization, data curation, investigation, methodology, validation, visualization, and writing. Gregor Linden, Ramona Barent, and Laura Stein: investigation, data curation, and methodology. Holger Frey: conceptualization, supervision, and writing – review and editing.

Data availability

The data supporting this article have been included as part of the ESI.†

Conflicts of interest

There are no conflicts to declare.

Acknowledgements

The authors acknowledge A. H. E. Müller for valuable discussions and for critically reviewing the results of the online NMR kinetics. We thank the Deutsche Forschungsgemeinschaft DFG for funding *via* INST 247/1018-1 FUGG to Katja Heinze.

References

1 M. Szwarc, *Nature*, 1956, **178**, 1168–1169.
2 A. Hirao, R. Goseki and T. Ishizone, *Macromolecules*, 2014, **47**, 1883–1905.
3 N. Hadjichristidis and A. Hirao, *Anionic Polymerization*, Springer, Tokio, 2013.
4 F. S. Bates, M. A. Hillmyer, T. P. Lodge, C. M. Bates, K. T. Delaney and G. H. Fredrickson, *Science*, 2012, **336**, 434–440.
5 K. Ntetsikas, V. Ladelta, S. Bhaumik and N. Hadjichristidis, *ACS Polym. Au*, 2022, **3**, 158–181.
6 W. Wang, W. Lu, A. Goodwin, H. Wang, P. Yin, N. G. Kang, K. Hong and J. W. Mays, *Prog. Polym. Sci.*, 2019, **95**, 1–31.
7 G. Holden and R. Milkovich, US Patent 3265765, 1966.
8 M. Steube, T. Johann, H. Hübner, M. Koch, T. Dinh, M. Gallei, G. Floudas, H. Frey and A. H. E. Müller, *Macromolecules*, 2020, **53**, 5512–5527.
9 D. A. H. Fuchs, H. Hübner, T. Kraus, B. J. Niebuur, M. Gallei, H. Frey and A. H. E. Müller, *Polym. Chem.*, 2021, **12**, 4632–4642.
10 L. Shaw and L. R. Hutchings, *Polym. Chem.*, 2020, **11**, 7020–7025.
11 A. H. E. Müller and K. Matyjaszewski, *Controlled and Living Polymerizations: From Mechanisms to Applications*, Wiley-VCH Verlag, Weinheim, 2010.
12 T. Suzuki, Y. Tsuji and Y. Takegami, *Macromolecules*, 1978, **11**, 639.
13 T. Suzuki, Y. Tsuji, Y. Takegami and H. J. Harwood, *Macromolecules*, 1979, **12**, 234.
14 S. Pragliola, M. Cipriano, A. C. Boccia and P. Longo, *Macromol. Rapid Commun.*, 2002, **23**, 356–361.
15 J. Lin, F. Wang, C. Zhang, H. Liu, D. Li and X. Zhang, *RSC Adv.*, 2021, **11**, 23184–23191.
16 Y. Jiang, X. Kang, Z. Zhang, S. Li and D. Cui, *ACS Catal.*, 2020, **10**, 5223–5229.
17 H. Bai, L. Han, W. Li, C. Li, S. Zhang, X. Wang, Y. Yin, H. Yan and H. Ma, *Macromolecules*, 2021, **54**, 1183–1191.
18 Y. Qi, Z. Liu, S. Liu, L. Cui, Q. Dai, J. He, W. Dong and C. Bai, *Catalysts*, 2019, **9**, 97.
19 T. Suzuki, Y. Tsuji, Y. Watanabe and Y. Takegami, *Macromolecules*, 1980, **13**, 849–852.
20 Y. Tsuji, T. Suzuki, Y. Watanabe and Y. Takegami, *Macromolecules*, 1981, **14**, 1194–1196.
21 T. Suzuki, Y. Tsuji, Y. Watanabe and Y. Takegami, *Polym. J.*, 1979, **11**, 651–660.
22 Y. Tsuji, T. Suzuki, Y. Watanabe and Y. Takegami, *Polym. J.*, 1981, **13**, 1099–1110.
23 J. M. Widmaier and G. C. Meyer, *Macromolecules*, 1981, **14**, 450–452.
24 Y. Cai, J. Lu, D. Zuo, S. Li, D. Cui, B. Han and W. Yang, *Macromol. Rapid Commun.*, 2018, **39**, 1800298.
25 R. K. Agnihotri, D. Falcon and E. C. Fredericks, *J. Polym. Sci., Part A-1: Polym. Chem.*, 1972, **10**, 1839–1850.
26 A. Priola, M. Bruzzone, F. Mistrali and S. Cesca, *Angew. Makromol. Chem.*, 1980, **88**, 1–19.
27 R. Y. Asami, K.-I. Hasegawa and T. Onoe, *Polym. J*, 1976, **8**, 43–52.
28 J. Lal, *Polymer*, 1998, **39**, 6183–6186.
29 Y. Cai, J. Lu, G. Jing, W. Yang and B. Han, *Macromolecules*, 2017, **50**, 7498–7508.
30 J. Li and J. He, *ACS Macro Lett.*, 2015, **4**, 372–376.
31 Q. Lv, C. K. Yu, Q. Yin, J. Lu and B. Han, *J. Macromol. Sci., Part A: Pure Appl.Chem*, 2020, **57**, 388–397.
32 T. Ishizone, A. Hirao and S. Nakahama, *Macromolecules*, 1993, **26**, 6964–6975.
33 H. Hsieh and R. Quirk, *Anionic polymerization: principles and practical applications*, Dekker, New York, 1996.
34 S. Uchida, K. Togii, S. Miyai, R. Goseki and T. Ishizone, *Macromolecules*, 2020, **53**, 10107–10116.
35 A. Forens, K. Roos, C. Dire, B. Gadenne and S. Carlotti, *Polymer*, 2018, **153**, 103–122.

 This journal is © The Royal Society of Chemistry 2024

36 T. A. Antkowiak, A. E. Oberster, A. F. Halasa and D. P. Tate, *J. Polym. Sci., Part A-1: Polym. Chem.*, 1972, **10**, 1319–1334.
37 W. Gebert, J. Hinz and H. Sinn, *Makromol. Chem.*, 1971, **144**, 97–115.
38 D. J. Worsfold and S. Bywater, *Macromolecules*, 1978, **11**, 582–586.
39 H. Hsieh, D. J. Kelley and A. V. Tobolsky, *J. Polym. Sci.*, 1957, **26**, 240–242.
40 C. A. Uraneck, *J. Polym. Sci., Part A-1: Polym. Chem.*, 1971, **9**, 2273–2281.
41 S. Bywater and D. J. Worsfold, *Can. J. Chem.*, 1962, **40**, 1564–1570.
42 M. Morton and L. J. Fetters, *J. Polym. Sci., Part A: Gen. Pap.*, 1964, **2**, 3311–3326.
43 J. Bareuther, M. Plank, B. Kuttich, T. Kraus, H. Frey and M. Gallei, *Macromol. Rapid Commun.*, 2021, **42**, 2000513.
44 A. Garton, R. P. Chaplint and S. Bywater, *Eur. Polym. J.*, 1976, **12**, 697–700.
45 J. Kleinheider, T. Schrimpf, R. Scheel, T. Mairath, A. Hermann, K. Knepper and C. Strohmann, *Chem. – Eur. J.*, 2024, **30**, e202304226.
46 A. Natalello, M. Werre, A. Alkan and H. Frey, *Macromolecules*, 2013, **46**, 8467–8471.
47 T. Johann, D. Leibig, E. Grune, A. H. E. Müller and H. Frey, *Macromolecules*, 2019, **52**, 4545–4554.
48 V. Jaacks, *Makromol. Chem.*, 1972, **161**, 161–172.
49 S. P. Wadgaonkar, M. Wagner, L. A. Baptista, R. Cortes-Huerto, H. Frey and A. H. E. Müller, *Macromolecules*, 2023, **56**, 664–677.
50 C. Hahn, M. Rauschenbach and H. Frey, *Angew. Chem., Int. Ed.*, 2023, **62**, e202302907.
51 E. Grune, T. Johann, M. Appold, C. Wahlen, J. Blankenburg, D. Leibig, A. H. E. Müller, M. Gallei and H. Frey, *Macromolecules*, 2018, **51**, 3527–3537.
52 E. Grune, J. Bareuther, J. Blankenburg, M. Appold, L. Shaw, A. H. E. Müller, G. Floudas, L. R. Hutchings, M. Gallei and H. Frey, *Polym. Chem.*, 2019, **10**, 1213–1220.
53 C. Wahlen, J. Blankenburg, P. Von Tiedemann, J. Ewald, P. Sajkiewicz, A. H. E. Müller, G. Floudas and H. Frey, *Macromolecules*, 2020, **53**, 10397–10408.
54 K. Liu, F. Zhang, M. Sun, F. Xie, S. Ying, Z. Yang, C. Zhou, J. Xia, A. Li, K. Liu, F. Zhang, M. Sun, F. Xie, S. Ying, Z. Yang, C. Zhou, J. Xia and A. Li, *Macromol. Chem. Phys.*, 2020, **221**, 2000161.
55 A. Nakahara, K. Satoh and M. Kamigaito, *Macromolecules*, 2009, **42**, 620–625.
56 A. Nakahara, K. Satoh, H. Saito and M. Kamigaito, *J. Polym. Sci., Part A: Polym. Chem.*, 2012, **50**, 1298–1307.
57 H. Zhang, Z. Zhao, P. R. McGonigal, R. Ye, S. Liu, J. W. Y. Lam, R. T. K. Kwok, W. Z. Yuan, J. Xie, A. L. Rogach and B. Z. Tang, *Mater. Today*, 2020, **32**, 275–292.
58 M. Steube, T. Johann, M. Plank, S. Tjaberings, A. H. Gröschel, M. Gallei, H. Frey and A. H. E. Müller, *Macromolecules*, 2019, **52**, 9299–9310.
59 A. E. Reed, R. B. Weinstock and F. Weinhold, *J. Chem. Phys.*, 1998, **83**, 735.
60 T. Y. Nikolaienko, L. A. Bulavin and D. M. Hovorun, *Comput. Theor. Chem.*, 2014, **1050**, 15–22.

This journal is © The Royal Society of Chemistry 2024

Curriculum Vitae

Curriculum Vitae

List of publications